

BIRLA CENTRAL LIBRARY

PILANI (Rajasthan)

Class No:- 629.133

Book No:- S192A

Accession No. 51467

REQUEST

IT IS EARNESTLY DESIRED THAT THE BOOK BE HANDLED WITH CARE AND BE NOT MARKED, UNDERLINED OR DISFIGURED IN ANY OTHER WAY, OTHERWISE IT WILL HAVE TO BE REPLACED OR PAID FOR BY THE BORROWER IN THE INTEREST OF THE LIBRARY

LIBRARIAN

AIRPLANE STRUCTURAL ANALYSIS
AND
DESIGN

GALCIT AERONAUTICAL SERIES

AERODYNAMICS OF THE AIRPLANE. By *Clark B. Millikan*. Cloth, 6×9 , 181 pages, 125 illustrations.

THE AIRPLANE AND ITS COMPONENTS. By *William R. Sears*. Cloth, 6×9 , 75 pages, 34 illustrations.

AIRPLANE STRUCTURAL ANALYSIS AND DESIGN. By *Ernest E. Sechler* and *Louis G. Dunn*. Cloth, 6×9 , 412 pages, 231 illustrations.

MATRIX AND TENSOR CALCULUS WITH APPLICATIONS TO MECHANICS, ELASTICITY, AND AERONAUTICS. By *Aristotle D. Michal*. Cloth, 6×9 , 132 pages, 15 illustrations.

Other volumes in preparation

AIRPLANE STRUCTURAL ANALYSIS AND DESIGN

BY
ERNEST E. SECHLER, P.H.D.

*Professor of Aeronautics
California Institute of Technology*

AND
LOUIS G. DUNN, P.H.D.

*Associate Professor of Aeronautics
California Institute of Technology*

GALCIT AERONAUTICAL SERIES

NEW YORK
JOHN WILEY & SONS, INC.

LONDON: CHAPMAN & HALL, LIMITED

COPYRIGHT, 1942

BY

ERNEST E. SECHLER AND LOUIS G. DUNN

All Rights Reserved

*This book or any part thereof must not
be reproduced in any form without
the written permission of the publisher.*

FOURTH PRINTING, AUGUST, 1952

PRINTED IN THE UNITED STATES OF AMERICA

EDITORS' PREFACE

In the nearly thirteen years since the Guggenheim Aeronautical Laboratory at the California Institute of Technology was established, a large number of scientific and engineering problems in various fields related to aeronautics have been investigated under its auspices. The results of this activity have appeared in the form of numerous technical papers. However, it has been felt for some time that certain of the subjects dealt with at the laboratory deserved more systematic treatment. It has also been suggested that aeronautical texts based on the staff's experience in training aeronautical engineers and scientists might be of some value. Accordingly, about two years ago an agreement was made by the undersigned editors with John Wiley and Sons, Inc., for the publication of a series of volumes, covering these two fields, to be known as the GALCIT * series. A start was then made on the preparation of material for certain of the monographs of this series, but the press of work associated with national emergency defense activities and the rapidly changing nature of the GALCIT'S academic courses made progress very slow.

In the spring of 1940 the Lockheed Aircraft Corporation requested the California Institute to cooperate in its expansion program by giving a course of aeronautical training to a large group of graduate non-aeronautical engineers. This program was undertaken during the following summer, when it appeared that the material presented, being somewhat more general than that given in the regular GALCIT post-graduate courses, might fill a rather important gap in the aeronautical training literature. The lecture notes were accordingly worked over into volumes dealing with various aspects of aeronautical engineering. This book is one of the series.

Acknowledgment must be made of the cooperation extended by the Lockheed Aircraft Corporation which released much of the information originally issued for use in the training course, and whose stimulus was

* The rather unwieldy title "Guggenheim Aeronautical Laboratory, California Institute of Technology" has been abbreviated to the more convenient "GALCIT." This notation has been widely used in aeronautical circles and is employed throughout the present work.

responsible for the preparation of the initial lecture notes on which the volumes are based. The Douglas Aircraft Company was also most cooperative in furnishing valuable material for incorporation in these books.

THEODORE VON KÁRMÁN
CLARK B. MILLIKAN
Editors

June, 1942

AUTHORS' PREFACE

In selecting the material to be presented in this volume, the authors have made no attempt to establish hard and fast rules for the design of aircraft structural components. Rather, they have presented most of the recognized design criteria and, where such data were available, have included experimental evidence as to the exactness of these criteria.

The treatment of the standard structural problems has been held to an absolute minimum since it was felt that the large number of textbooks now available on applied mechanics cover this phase of design satisfactorily. Since this is true, it will be found that a large portion of this work is made up of controversial material which is presented merely as the present best state of knowledge in the hopes that it will inspire research men and research organizations to lay out research programs designed to fill the gaps in these design criteria.

The authors gratefully acknowledge the permission given by the Matériel Division of the U. S. Army Air Corps to use in this volume a great deal of material from Air Corps Technical Report 4313 and, in addition, they express their appreciation to Professor J. S. Newell of the Massachusetts Institute of Technology who was co-author of the above Technical Report with one of the authors of this book. The authors are happy to acknowledge their indebtedness to the National Advisory Committee for Aeronautics and to the large number of aircraft manufacturers who made available extremely valuable research data. They are also grateful to the many members of the staff and of the graduate school of GALCIT who have given valuable suggestions as to the subject matter to be presented and who have aided in preparing the manuscript. Especial credit is given to Mr. C. K. Newby for his aid in preparing the numerous illustrations.

ERNEST E. SECHLER
LOUIS G. DUNN

California Institute of Technology
June, 1942

* For this printing, Problems have been added as an appendix.

CONTENTS

PART I

PRELIMINARY CONSIDERATIONS IN DESIGN

CHAPTER	PAGE
1. THE AIRPLANE LAYOUT	1
2. APPLIED AND DESIGN LOADS	42

PART II

METHODS OF STRUCTURAL ANALYSIS

3. STRESS-STRAIN RELATIONSHIPS FOR STABLE STRUCTURES	78
4. TRUSS AND FRAME ANALYSIS	124
5. THE PROBLEM OF INSTABILITY	154
6. THE ULTIMATE STRENGTH OF STIFFENED FLAT SHEET	203
7. PLATES UNDER NORMAL PRESSURE.	283
8. THE ANALYSIS OF CYLINDRICAL STRUCTURES	309

PART III

APPLIED STRESS ANALYSIS

9. WINGS AND CONTROL SURFACES	342
10. FUSELAGE ANALYSIS	370
11. ENGINE MOUNTS, LANDING GEARS, AND FITTINGS	386
PROBLEMS	397
AUTHOR INDEX	405
SUBJECT INDEX	407

INTRODUCTION

The first problem confronting the designer of the structural parts of an airplane is that of determining just what loads are to be expected on his structure and how these loads are to be distributed. Over a period of years, the governmental agencies, who have in their power the approval of commercial and military aircraft, have established certain rules and regulations which they felt covered the various loading conditions of each particular type of airplane. The rules for commercial aircraft are briefly discussed in Part I and, since these regulations are subject to constant revision, the designer should always use the latest revision rather than blindly following the load and load factor requirements as outlined therein.

The second need of the designer is to have made available to him design methods for structural components subjected to any given combination of loads. Part II is concerned chiefly with this phase of the problem. Well-known methods of beam and truss analysis are merely outlined and the basic equations are given. A great deal of empirical data is also included for which there is no present theoretical justification. However, in all cases, these empirical design criteria are accompanied by such experimental data as are available in order that the designer may judge for himself the probable limits of accuracy of the methods.

Part III of this work gives a short discussion of methods of analysis of various structural types used for the major structural items of a modern metal airplane. Advantages and disadvantages of each method are pointed out in order to aid the designer in making a choice as to the type of construction best suited to the type of airplane under consideration and to the available plant facilities, and the type of analysis applicable to the chosen construction method.

PART I
PRELIMINARY CONSIDERATIONS IN DESIGN

CHAPTER 1
THE AIRPLANE LAYOUT

1-1. Design Procedures

In designing an airplane, it is first necessary to know its type and size and the purpose for which it is to be designed. These items, in general, are determined by the requirements of the prospective purchaser who, when he contacts a manufacturer, usually has in mind a definite type of airplane which he wishes to have engineered and constructed. In a commercial airplane, for example, his specifications may begin with a general description of the airplane as follows:

(a) Specifications.

The airplane described herein shall be a two-engine, cantilever mid-wing, all-metal monoplane with retractable landing gear. The airplane shall be designed and constructed primarily for use in airline operation and shall be suitable for night and instrument flying.

A flight station for a pilot and co-pilot operating side by side shall be provided in the forward portion of the fuselage, the pilot being on the left side. The flight station shall be isolated from the passenger compartment by a bulkhead with a door.

A passenger compartment shall be provided aft of the flight station providing comfortable seats for fourteen passengers, seven on each side, and a folding seat for a stewardess. The seat provided for the stewardess shall be located at the main door and shall be arranged to fold out of the way.

The passenger seats shall be upholstered and shall incorporate a combination back and seat adjustment, affording maximum comfort. Each seat shall be provided with an approved type safety belt conforming to the requirements of the U. S. Civil Aeronautics Authority. There shall be fourteen shatterproof glass windows in the passenger cabin, seven windows on each side providing best practicable vision from each passenger seat.

Provision for mail and baggage, including hold-down straps, shall be provided in the fuselage nose, forward of the pilots' compartment, and in three spaces

under the flight station and cabin floor. All baggage compartments shall be accessible from the left-hand side.

A lavatory compartment shall be provided, located aft of the passenger compartment. Two windows shall be provided in this compartment, one on each side. A bulkhead complete with door and lock shall isolate this area from the passenger compartment.

The airplane shall be licensed for a gross weight of not less than 17,500 lb. and a useful load of not less than 30 per cent of the gross weight.

The weight empty shall include the complete airplane with all equipment and supplies required in these specifications ready in all respects for air transport operation. The weight empty as outlined above shall be determined by actually weighing the airplane.

The airplane, engines, and accessories shall satisfy all the requirements stated herein as well as the necessary requirements of the U. S. Civil Aeronautics Authority for an approved "Type Certificate," etc.

Following the general description in the specifications, are such items as performance guarantees, specifications of flying qualities, materials, workmanship, finish, maintenance and service requirements. The majority of specifications list the engine and the engine accessory weights.*

The specifications for military aircraft, or aircraft for any other purpose will, in general, follow a trend similar to the above specifications. At times aircraft manufacturing companies themselves will write a set of specifications consistent with the needs which have been previously determined through an extensive survey of the airline operating companies.

It should be clearly understood that it is not always possible for the designer to meet all the requirements of a given set of specifications. In fact, it is not at all uncommon to find certain minimum requirements unattainable and it is then necessary to compromise. The extent to which compromises can be made must be left to the judgment of the designer. However, it must be kept in mind, that, to achieve a design most adaptable to the specified purpose of the airplane, sound judgment must be exercised in considering the value of the necessary modifications and compromises.

The first task of the designer should be to familiarize himself thoroughly with the specifications of the airplane upon which the design is to be based. Also, if the airplane may be sold to more than one purchaser, all available information should be obtained as to possible changes in the design which might have to be made in the future. There should be no thought of making a general-purpose airplane, suitable for any purchaser or any use, because that is an impossibility. However, it is fre-

* The above specifications have been obtained from material furnished through the courtesy of the Lockheed Aircraft Corporation.

quently possible to arrange a design so as to simplify future changes without sacrificing either structural or aerodynamic efficiency or taking a weight penalty.

As the next step the designer should familiarize himself with all existing airplanes of the same general type as that proposed. If possible, it is advisable to collect all comments both positive and negative of pilots, passengers, maintenance groups, and operators using this existing equipment. The designer should not blindly copy any existing design just because it happens to be available; this hampers progress; but, on the other hand, not to take advantage equally of others' successes and of their mistakes is inefficient.

(b) Preliminary Weight Estimate. The degree of success attained in estimating the weight of a new design depends largely on experience combined with data on previous airplanes and a knowledge of the proposed types of construction. The first preliminary estimate usually is founded upon the calculations involving the useful load consisting of crew, passengers, fuel, oil, and cargo. The performance data of the specifications give the desired range, speed, and payload. This information enables the designer to estimate roughly the necessary fuel and oil, the only unknowns in the useful load. Since the useful load ranges from 25 to 40 per cent of the airplane's design gross weight, depending upon the purpose of the airplane and upon the type and amount of equipment installed, the approximate design gross weight can be found by dividing the useful load by the assumed percentage.

In the preliminary estimate it is convenient to consider first a subdivision of the total gross weight into main groups. The weight empty of a multi-engined airplane may be broken down in a very preliminary fashion by the following percentages of the design gross weight:

Wing	13.0 - 17.0%
Tail	1.5 - 2.5
Fuselage	8.0 - 13.0
Main landing gear	5.0 - 8.0
Tail wheel	0.5 - 0.8
For tricycle gear:	
Main landing gear	4.0 - 7.0
Nose wheel	1.5 - 2.5
Power plant:	15.0 - 27.0
Engines	10.0 - 20.0
Engine accessories	1.0 - 2.0
Power plant controls	0.1 - 0.4
Propellers	2.0 - 4.0
Starting system	0.3 - 0.9
Lubricating system	0.3 - 0.6
Fuel system	1.5 - 2.5

Instruments	0.5 - 1.2
Surface controls	1.0 - 2.0
Furnishings	4.0 - 10.0
Weight per passenger	90.0 - 215.0 lb.
Communicating equipment	2.0 - 3.0%
Electrical equipment	2.0 - 3.0
Possible useful load (food and water)	0.3 - 0.6
Weight per passenger	3.5 - 9.0 lb.
De-icer installation	0.06%
Residual fuel and oil	30 lb. per engine

It is evident from the given data that the rather wide variation in the possible weights makes it desirable to entrust the weight estimation to the judgment of experienced personnel.

With the above information at hand, it is possible to make a preliminary calculation of the required wing- and tail-surface areas. These calculations will, in general, be carried out by the senior members of the aerodynamics and design departments. They will also furnish a rough sketch of the airplane's profile, and a plan view showing the location of passengers, cargo, and fuselage equipment. In addition, the sketch outlines the shape and locations of the wings, nacelles, tail surfaces, propellers, fuel and oil tanks. The locations of these items are first laid out to conform with the requirements of the specifications, structure, clearances, available space, and U. S. Civil Aeronautics Authority or military regulations.

If the power plant is not covered in the specifications, a tentative selection of engines will be made to meet the required power loading based on the preliminary weight estimate. As the design progresses a more exact analysis becomes possible through a further breakdown of the main groups. The methods which have been developed for the detail analysis are discussed in section 1-2.

(c) Performance. Performance calculations are necessary at several stages of the design to insure that the performance requirements as set forth in the specifications are either being met or approached. After the completion of the first preliminary weight estimate from which a tentative wing area is determined and after the selection of a power plant, a set of preliminary performance calculations are made. Since these calculations are of necessity based on empirical formulas established by past experience, and are also based upon the judgment of the designer, they are useful only to indicate whether the performance specifications can be met at all.

These preliminary calculations may include the following performance characteristics:

1. Maximum velocity at critical altitude
2. Operating velocity at critical altitude

3. Maximum range at specified altitude
4. Absolute ceiling with partial engine operation
5. Take-off over 50-ft. obstacle
6. Landing speed

As the design progresses more exact performance data are obtained, either through suitable wind tunnel tests or by more refined methods of calculation or both. A further discussion on performance is given in section 2-1.

(d) Wind Tunnel Tests. That phase of the design which is concerned with the performance characteristics of the airplane belongs to the field of aerodynamics. However, since the magnitude of the external loads are determined by the airplane's performance characteristics it might be well to consider briefly the methods by which performance characteristics are determined.

When the general dimensions and layout of the airplane are reasonably well established by the methods discussed above, it is necessary to obtain a more accurate estimate of the performance characteristics of the airplane. This can be accomplished by one of two methods: (a) The designer may proceed purely on the basis of his present and future calculations and hope that when the airplane is completed and test flown, his calculations will not be too far in error. (b) He may carry out suitable wind tunnel tests on a scale model of the airplane and obtain the desired results within normal engineering accuracy.

In general, experience has shown that the second method is more satisfactory. This fact is borne out by the wide use of wind tunnel tests in modern aircraft design. Until recently all wind tunnel tests were conducted on models without power or running propellers, but with the rapid rise in engine powers in recent years, the corrections, necessary because of the effect of power when added to the power-off wind tunnel results (in order to obtain corresponding full-scale characteristics), have become more of an uncertainty than existed in the past. Prior to this condition there existed suitable empirical correction factors for the effect of power; these factors have been found through experience to be no longer adequate. Consequently there has been a growing tendency towards power-on wind tunnel tests for all basic airplane designs.

From the wind tunnel tests it is possible to obtain the lift, drag, and propulsive properties of the full-scale airplane. This information enables the designer to calculate all flight speeds, rates of climb, ceiling, landing and take-off distances, etc. It should be kept in mind that the accuracy of the performance characteristics as obtained from wind tunnel tests is governed by the validity of the necessary extrapolations, corrections, and adjustments of the original data to cover the full-scale airplane. For this reason it requires the ability of an experienced person

for the proper handling of this material in its interpretation and its actual use. The performance items which have a direct bearing on the structural design of the airplane are discussed in section 1-5.

(e) The Mock-Up. The construction of the mock-up, which is essentially a full-scale reproduction of a certain section of the proposed design, is started immediately after the first preliminary three-view drawings of the airplane are completed. The extent of the mock-up is a very flexible quantity; it may vary from a reproduction of the cockpit and a section of the wing to the complete airplane. The relation of the completeness of the mock-up to the airplane as a whole is dependent on the type of airplane, i.e., the more complicated the design and installation problems the more comprehensive will be the required mock-up.

The essential requirements for the material used in the mock-up are that it should lend itself to ease of fabrication, and that it must be sufficiently rigid to withstand the loads imposed upon the structure by the necessary installations and crew. Plywood is commonly used.

The purpose of the mock-up is primarily to facilitate installation, accommodation, and accessibility problems. In the design of an airplane certain items, which will be discussed in some detail in the following paragraphs, have through past experience been found to be extremely difficult to determine on the drawing board.

The cockpit of the airplane is, in general, reproduced with all necessary installations such as controls, instrument panels, windows, and seats. It is then possible to ascertain whether the pilot has sufficient room to perform his various duties, whether the window arrangement meets the required degree of visibility, whether all controls are conveniently located, and whether the instrument board is free from glare, etc.

Controls and control cables of the engines and movable surfaces are installed as far as is practicable. In large airplanes the congestion of control cables becomes a very serious problem. This is particularly true of the cables which lie ahead of the main spar. In the mock-up it is then possible to determine the most convenient location for the individual cables and it also is possible to check the satisfactory operation of the controls.

Conduit lines and ducts generally are completely installed. These items usually require cutouts of considerable magnitude in the main structure of the wing and fuselage and it is therefore desirable to determine their locations on the mock-up in order to insure "the least amount of destruction" to the main structure.

For a commercial airplane it is customary to build at least a section of the cabin with complete seating arrangement, sleeping berth, and the necessary items essential to the comfort of the passenger. These can then be examined in regard to required space, accessibility, comfort, and ease of operation.

In military aircraft, armament, which includes such items as machine guns, bomb racks, bomb hoists, and bomb-releasing mechanisms, may be installed. The firing angles of the machine guns and the satisfactory operation and installation of the bombing equipment are determined from these installations. The designer may sometimes install the complete movable control surfaces on the mock-up to facilitate in the design of the operating mechanism.

The above discussion is in no way a complete picture of the various functions for which a mock-up is useful, but it should serve to give a general idea of its advantages in time-saving and in the solution of the difficulties involved in installation problems. As the design progresses and compromises become necessary the mock-up will be modified to conform to the changes in design. The mock-up will also aid in determining the feasibility of such changes and compromises as may be felt to be necessary.

1-2. Second Weight Breakdown

A final weight-empty estimate results from a number of preliminary estimates, each based on additional information available as the design progresses. With the preliminary weight estimate at hand, as discussed in section 1-1(b) and with the first completed three-view drawing showing as much of the equipment and construction as practicable, a more accurate weight estimate is possible. In the following discussion of the methods developed to attain greater accuracy, each group will be considered separately.

(a) **The Wing Group.** First in order is the wing group, which includes the wing panels, ailerons, flaps, struts, wires, fairings, attaching bolts, etc. The weight of a wing is one of the most difficult of the various items to estimate because it is influenced by a large number of factors, of which the major ones are:

1. Gross (design) weight of the airplane
2. Wing area
3. Aspect ratio
4. Design load factor
5. Thickness and chord at the root
6. Taper ratio (root chord/tip chord)
7. Wing span and thickness ratio (root thickness/tip thickness)
8. Type of structure
 - a. Biplane or monoplane
 - b. Landing gear
 - c. Flotation gear
 - d. Arresting and catapult gear
 - e. Armament

In a paper by Lipp (reference 1·1) formulas have been devised which attempt to give the effects of most of the above items on the weight of a modern, all-metal monoplane wing. Lipp attacked the problem by dividing it into two parts: (1) the effects of aerodynamic loads and (2) the effects of dead loads. In calculating the material necessary to resist the air loads, it was found convenient to consider (1) material that resists bending of the wing, (2) shear material, and (3) ribs and other members that resist direct pressure. The nomenclature used in the Lipp analysis follows:

- u = total wing structural weight
 - $u_1 \cdots u_n$ = component parts of u
 - x = distance of station from tip
 - b = span
 - S_c = design stress in spar cap material
 - S_s = design stress in shear webs
 - S'_c = design compression stress in ribs
 - $k_1 \cdots k_3$ = dimensionless constants
 - $K_1 \cdots K_3$ = coefficients having dimensions of pounds per cubic inch
 - t = thickness of wing at x
 - f = design load factor
 - w_x = running lift load (pounds per inch)
 - W = gross weight of airplane
 - W_1 = W minus u
 - W_2 = non-structural dead weight in wing
 - m = root thickness/tip thickness
 - n = root chord/tip chord
 - $r = 2l/b$ = length of unloaded tip/semi-span
- Subscript T refers to tip and R refers to root of wing

The assumptions made by Lipp in computing the air load bending material were: (1) The skin plus the stiffeners can be replaced by an "effective thickness" of skin having the same cross-sectional area. (2) The perimeter of the airfoil equals a constant times the chord. (3) The wing is a full cantilever type so there are no end loads and the only stresses are caused by bending loads. (4) The running load (w_x) caused by the lift is proportional to the chord. This gives a trapezoidal lift distribution which approximates that used by the Civil Aeronautics Authority. (5) The total lift is equal to the gross weight of the airplane.

By a rational beam theory analysis it can be shown that the weight of the material resisting the bending loads due to lift is given by an equation of the form

$$u_1 = \frac{K_1 W b^2 f m}{S_s t_R (n+1)(m-1)^3} \left\{ \left[\frac{3}{2} - 2m + \frac{m^2}{2} + \log m \right] + \frac{(n-1)}{3(m-1)} \left[-\frac{11}{6} + 3m - \frac{3m^2}{2} + \frac{m^3}{3} - \log m \right] \right\} \quad [1.1]$$

In calculating the weight of the material which resists the air-load shear, i.e., the weight of the shear webs, it was assumed that torsion of the wing merely redistributes weight among the spars without changing the total web weight. The area of the cross section of the web material is considered to be equal to the total shear at the particular wing section divided by the design shear stress. Again by beam theory analysis, the weight of the material resisting the aerodynamic shear loads is calculated as

$$u_2 = \frac{K_2 W b (n+2) f}{S_s (n+1)} \quad [1.2]$$

In addition to the effects of bending and shear, it is logical to add the effect of direct air pressure on the structure. Ribs transmit the air force to the spar webs and also serve to hold the shape of the wing. Therefore, the ribs form the largest part of the pressure material. The stresses involved are caused by direct air loads and the shear forces transmitted to the spars. The assumptions made in calculating the pressure material are:

1. For the direct crushing material.
 - a. The rib weight is proportional to the wing thickness at any section times the area of the horizontal section through the rib.
 - b. The area of the horizontal section through the rib is proportional to the applied pressure times the wing surface supported by the rib.
2. For the shear transfer material.
 - a. The rib weight is proportional to the wing chord times the area of a vertical section through the rib.
 - b. The area of the vertical section through the rib is proportional to the applied pressure times the rib spacing times the chord, or is proportional to the applied pressure times the area over which it acts.
 - c. The average wing chord is proportional to the average wing thickness for all wings.
 - d. The ratio of the crushing stress to the shear stress in one wing is proportional to the same ratio in another wing.

Considering all the above factors, the weight of the pressure-resisting material is given by

$$u_3 = \frac{K_3 W f t_R (m + 1)}{2m S'_c} \quad [1.3]$$

Dead weights in the wing can be classified in two groups according to their structural or non-structural character. The first of these groups, structure, is distributed along the span in approximately the same manner as the aerodynamic load and can be easily included in the calculations by substituting

$$W_1 = W - u(\text{estimated}) \quad [1.4]$$

into equations 1.1 and 1.2 instead of W . This is possible because the structural weight in a wing will tend to reduce the bending and shear stresses introduced by the aerodynamic loadings. This substitution would seem at first glance to introduce difficulties into the problem since u is unknown. However, u is small compared to W (less than 15 per cent) so that a reasonable error in estimating u will result in a much smaller error in the final answer, and, if the final value for u differs much from the estimated value it is a simple matter to make the necessary corrections.

Non-structural items such as engines and fuel are largely concentrated near the wing root. These weights are assumed to be distributed as follows: (1) The resultant center of gravity of the highly concentrated loads is found (small scattered loads being neglected). (2) A rectangular distribution is drawn having the same total weight as the dead loads and extending roughly over the region of application of the concentrated dead loads.

The weight of the material to resist the bending stresses induced by these dead loads is given by

$$u_4 = -\frac{K_1 W_2 f b^2 m}{2 S_c t_R (m-1)^3} \left\{ - (m-1)(1+rm-r) + \frac{(1-r)}{2} (m-1)^2 + \right. \\ \left. + \frac{(1+rm-r)^2}{1-r} \log \left(\frac{m}{1+rm-r} \right) \right\} \quad [1.5]$$

and the weight of the material to resist the shearing stresses set up by the dead loads is

$$u_5 = -\frac{1.5 K_2 W_2 f b (1-r)}{S_s} \quad [1.6]$$

Note that K_1 and K_2 are the same as those used in equations 1.1 and 1.2. Minus signs are used since dead loads are opposed to the air

loads. This cannot be carried too far, however, since heavy dead weights if far outboard may cause the landing loads to become critical. Effects of the dead loads on the web weights are neglected.

By plotting the actual wing weight factor, i.e., u/Wf , against the wing span for a large number of airplanes an empirical curve is obtained

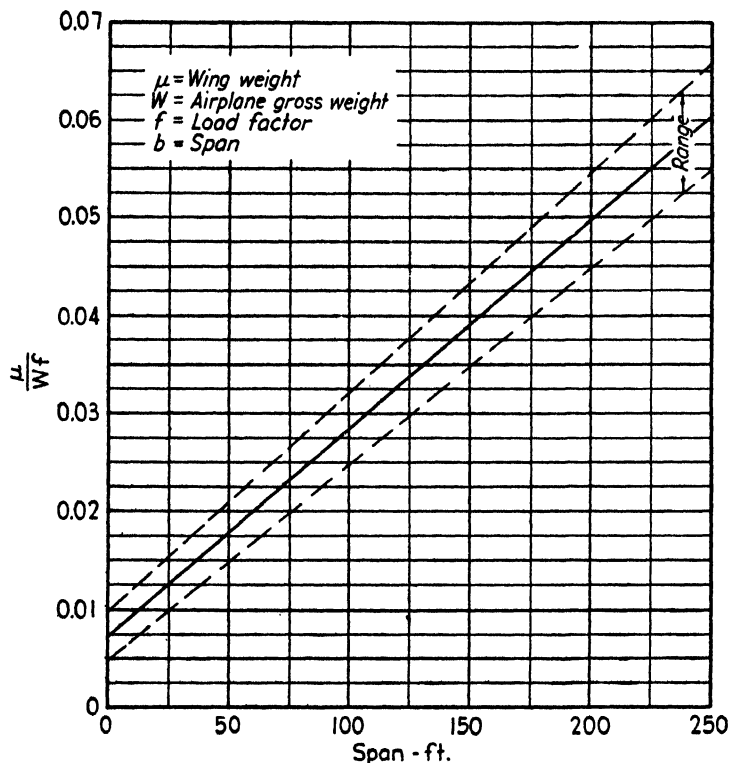


FIG. 1-1. Variation of wing weight with span.

which does not pass through the origin. This indicates that there is a certain portion of the wing weight which is independent of span. Therefore a final term is added to the weight equation which is of the form

$$u_6 = 0.0075Wf \quad [1.7]$$

and the total wing weight is therefore given by

$$u = u_1 + u_2 + u_3 + u_4 + u_5 + u_6 \quad [1.8]$$

and the empirical curve for determining u is given in Fig. 1-1. The limits between which present-day airplanes lie is also indicated in this figure. The lower range line represents wings having a large amount of distributed dead weight outboard and a light, efficient structural design.

In the preliminary stages of weight estimating, Fig. 1-1 will be sufficient. For more accurate calculations, the constants K_1 , K_2 , and K_3 are determined by means of data collected from an actual wing which is as structurally similar as possible. Then, using these values for the constants and substituting the new wing data in the equations for $u_1 \cdots u_6$, the weight of the new design may be calculated.

(b) **The Tail Group.** The weights of the various tail surfaces are dependent upon a number of items similar to those discussed above for

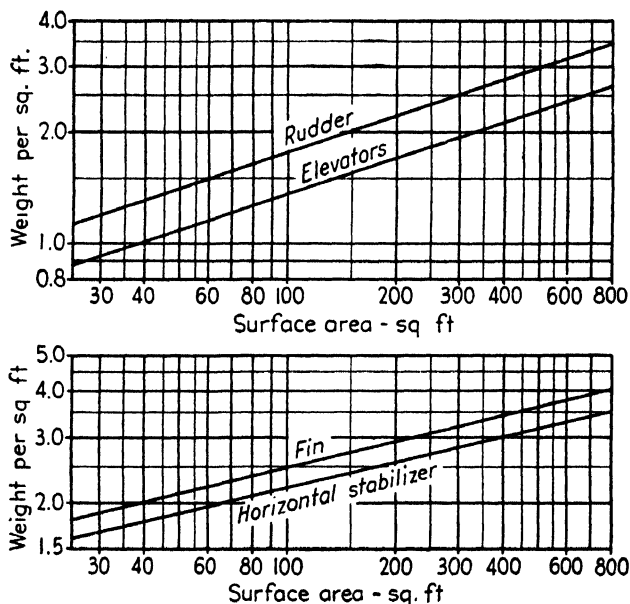


FIG. 1-2. Tail-surface weights.

the wing. Type of construction is somewhat more important for these surfaces because frequently mixed types of construction are employed. For example, it is common practice to make the fixed surfaces all metal using a type of construction similar to that used for the wings, and, for balance reasons, to make the movable surfaces fabric-covered. In addition to these factors, tail-surface weights are greatly influenced by the amount of aerodynamic, static, and dynamic balance. The inauguration of multiple vertical surfaces has presented additional weight problems over and above those present when only one fin and rudder were being used.

No detailed analysis similar to the Lipp wing analysis for the elements of the tail group is available; however, the average weight trends for the

various members are shown in Fig. 1·2 which was made up by the Douglas Aircraft Company on the basis of the study of a large number of modern airplane designs and the actual weight breakdown of these designs.

(c) **The Fuselage.** In general the fuselage structures of commercial aircraft are lighter in weight than the military type. This decrease is

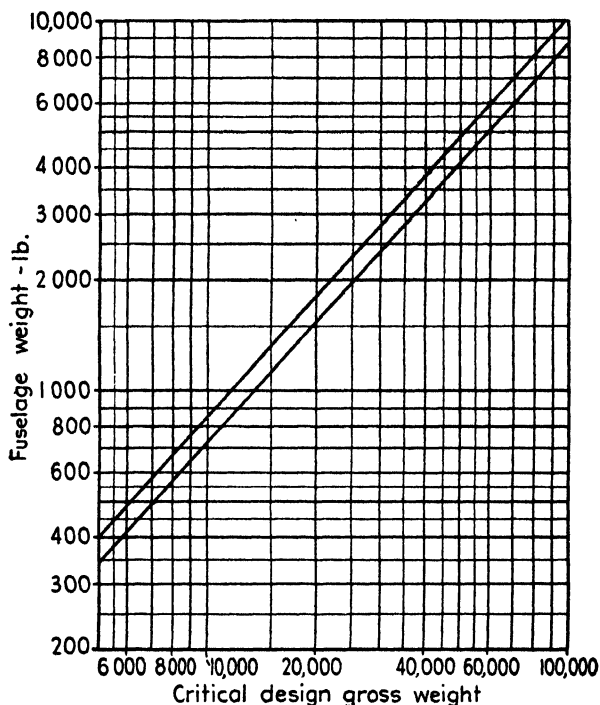


FIG. 1·3. Fuselage weight curve.

caused by lower design factors and fewer complicated features such as gun mounts, bomb bays, and bomb doors. In estimating the fuselage structural weight, such relationships as percentage of gross weight, weight per inch length, weight per square foot of the side projected area, or weight per square foot of lateral area may be compared and the most reasonable or coherent value accepted. The weight calculated from the fuselage surface area usually proves to be the most accurate for such items as skin and doublers and lengthwise stringers. In order to eliminate tedious calculations in using this method, perimeters of the fuselage are calculated at various stations along its length and the plating area is calculated upon the basis that the sections between these stations are frustums of a cone, or that the forward 10 per cent and the aft 25 per

cent are conical sections. To aid in this calculation the following equations are given:

$$\text{Area of a cone} = \frac{1}{2}p \sqrt{\left(\frac{p}{2\pi}\right)^2 + h^2} \quad [1.9]$$

$$\text{Area of a frustum of a cone} = \frac{1}{2}(p_1 + p_2) \sqrt{\left(\frac{p_1 - p_2}{2\pi}\right)^2 + h^2} \quad [1.10]$$

where p = base perimeter of the cone,

p_1 = larger perimeter of the frustum,

p_2 = smaller perimeter of the frustum,

h = height of the cone or frustum, i.e., a distance between stations at which the perimeters were calculated.

The general trend of fuselage weights is shown in Fig. 1.3. In the more refined estimates, the fuselage may be broken down into subgroups, each item being plotted against some dimension or area or some similar reference parameter (see Fig. 1.4). A list of possible subgroups follows.

- Skin and doublers
- Side stringers
- Top and bottom stringers
- Nose wheel provisions
- Frames and bulkheads
- Flooring and floor supports
- Doors, hatches, auxiliary exits, and their frames
- Windows, and their frames
- Nose installation
- Pilot's enclosure
- Tail cone
- Tail stubs (if integral with the fuselage)
- Emergency tail skid or provision for tail wheel
- Bomb-bay structure and doors
- Miscellaneous installation provisions
- Cabin sealing for pressure installations
- Provision for flotation in fuselage
- Miscellaneous remaining items

(d) Landing Gear. For conventional gears (two main wheels and a tail wheel), the weight of the main landing gear, not including the tail wheel, is divided into two parts in order to make a more accurate weight estimate. The first part is the chassis structural weight (R) consisting of the structural members which carry the primary stresses and which are affected by airplane gross weight, load factor, and landing-gear length. The remaining part (P) includes the wheels, tires, tubes, and retracting mechanisms. These latter items are affected primarily by

the gross weight and are not so much a function of the load factors and the gear length.

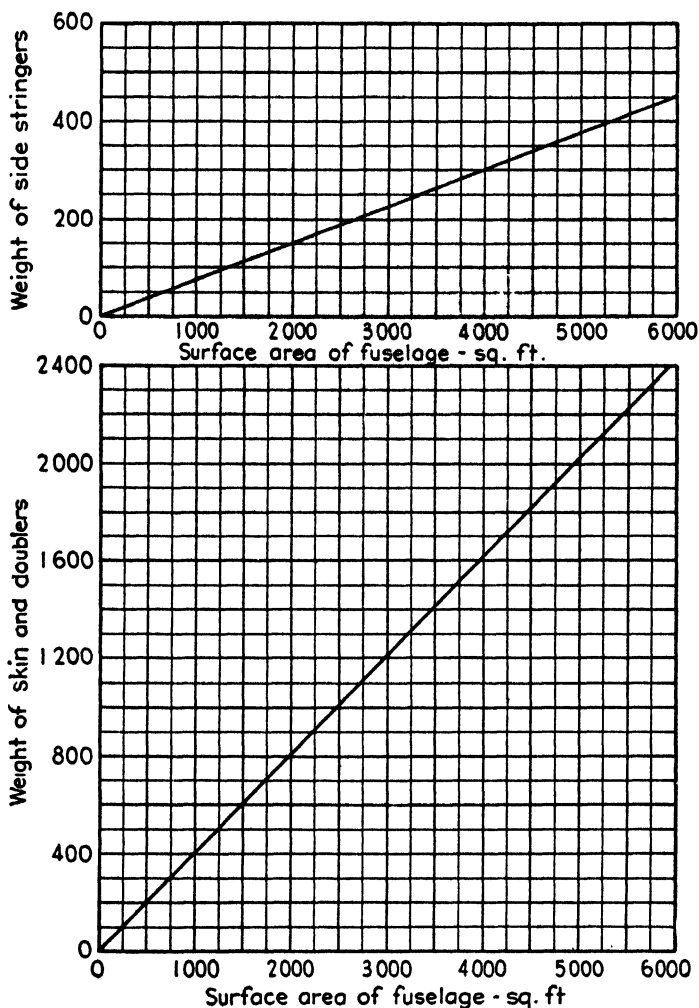


FIG. 1.4. Fuselage weight breakdown.

From a consideration of the actual data from a number of models, it has been found that the following formulas give a reasonable estimate of the two weights discussed above:

$$R = 0.0003WfL$$

$$P = 0.035W$$

[1.11]

where R = main chassis structural weight,
 W = airplane's design gross weight,
 f = critical design load factor,
 L = distance in feet from the ground line (tire and oleo statically deflected) to the midpoint between supporting fittings (point where bending moment is taken out),
 P = weight of wheels, tires, and retracting mechanism.

For the main gear in a tricycle gear system (two main wheels and a nose wheel) insufficient data is available for any more accurate estimate

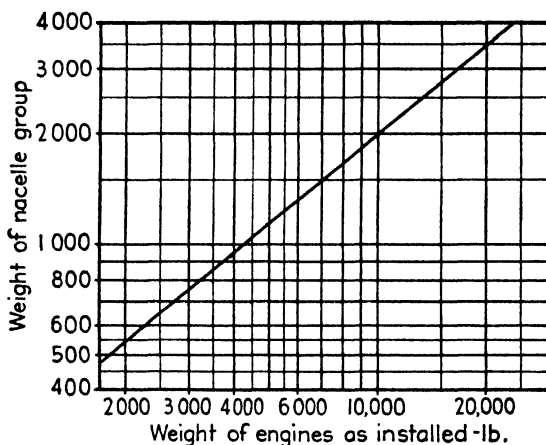


FIG. 1-5. Nacelle weights.

than is given by the percentages of gross weight indicated in section 1-1(b).

For the tail and nose wheel, the percentages given in section 1-1(b) are as accurate as any data now available.

(e) Nacelles. The weight of the nacelles is obviously dependent upon the size and, consequently, upon the weight of the engines. Figure 1-5 shows the weight of the nacelle group plotted against the as-installed engine weight for a large range of power plant weights. Items which may cause variation of the nacelle weights from this figure are: (1) Position of the nacelle on the wing. (2) Whether or not the landing gear is to be housed in the nacelle. (3) Whether or not the nacelle is to be used as a part of the wing structure and as such carries part of the stresses coming in from the wing loading conditions. In this case a reasonable balance must be made between what is strictly speaking wing weight and what should legitimately be charged to the nacelle weight.

(f) Power Plant (less Fuel System). The most important item in the power plant weight is that of the engines as installed. The engine's dry

weight determined at the completion of the acceptance test includes the following:

Supercharger	Propeller cones and attaching nuts
Integral pumps	Integral provisions for controllable pitch propeller
Magnetos and ignition system	Intercylinder baffles
Spark plugs	Such oil and grease as remain after draining and external washing
Carburetors	
Integral preheaters	
Radio shielding	

The as-installed weight of the engine as received from the manufacturer, cleaned and ready for installation in the airplane, with all items listed under dry weight and deducting those items listed under engine equipment, is the weight listed by airplane manufacturers on the weight reports.

For a multi-engined airplane, experience has shown that the weight of the power plant, less fuel system, equals approximately 2.2 lb. per normal rated horsepower. It has been found to be divided as follows:

	LB. PER RATED HORSEPOWER
Engines—as installed	1.46
Engine accessories	0.15
Power plant controls	0.03
Propellers	0.45
Starting system	0.06
Lubricating system	0.05
Total power plant less fuel system	2.20

All the above discussion is based on present-day, air-cooled, radial engines. In line, air-cooled engines will be similar, but for liquid-cooled engines, the manufacturer should be consulted for actual weights since there is insufficient data available to make any general statements regarding the weight breakdown.

(g) **Fuel System.** The fuel system weight has been separated from the power plant weight because the fuel capacity is dependent upon the desired range of the airplane as well as upon the installed horsepower. For ordinary wing tanks, the piping, valves, etc., weigh approximately 0.05 lb. per normal rated horsepower. The weight of the tanks and their supports is a function of the capacity of the tanks, and curves have been drawn up in Fig. 1-6 showing the average weight of such tanks in both military and commercial airplanes. The weight of the tanks in military aircraft must obviously be increased over the value given in this graph if they are armored or made otherwise bulletproof.

Integral tanks will eliminate the weight of the separate tanks and their support but will add some weight to the wing structure owing to the necessity of completely sealing the structure in that region. Whenever possible, comparison should be made with existing airplanes, but for a first approximation it will be conservative to consider that the

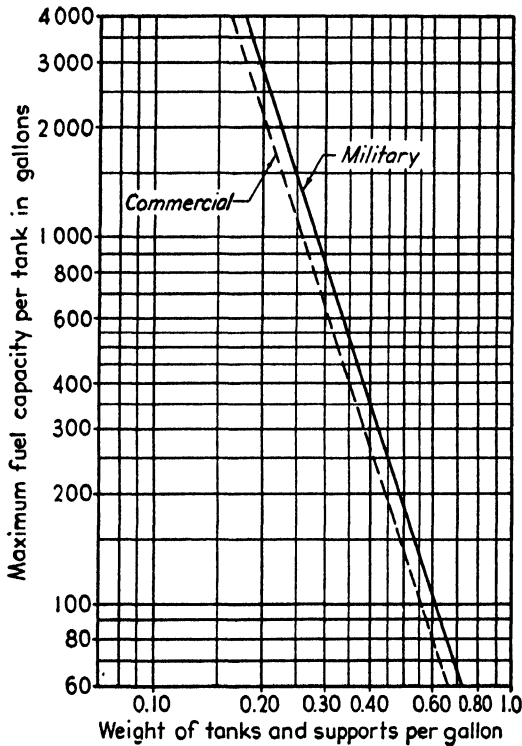


FIG. 1-6. Weight of fuel tanks.

integral tank will weigh 50 per cent of the value given in Fig 1-6 for separate tanks.

(h) Instruments. The required instruments are usually listed in the specifications. If they are not, they may be divided into three subgroups, namely, auto pilot, flight instruments, and engine instruments. The weight of the auto pilot ranges from 100 to 175 lb., depending upon the size of the airplane. The flight instruments' weight depends upon the amount of equipment specified and the number of duplicated instruments. The weight of this subgroup ranges from 50 to 150 lb. Engine instruments weigh from 20 to 60 lb. per engine depending upon the installation. The above weights include tubing, wiring, and supports.

For a more accurate weight estimation of these groups, the weights of each individual instrument as obtained from the manufacturer should be added up, and a small weight should be added for lines, brackets, wiring, etc. A reasonably complete list of instruments and their weights is given in reference 1-2.

(i) **Surface Controls.** In studying the weight variations of the surface controls in various airplanes, it is observed that the larger airplanes having side-by-side wheel-column control contain some items which

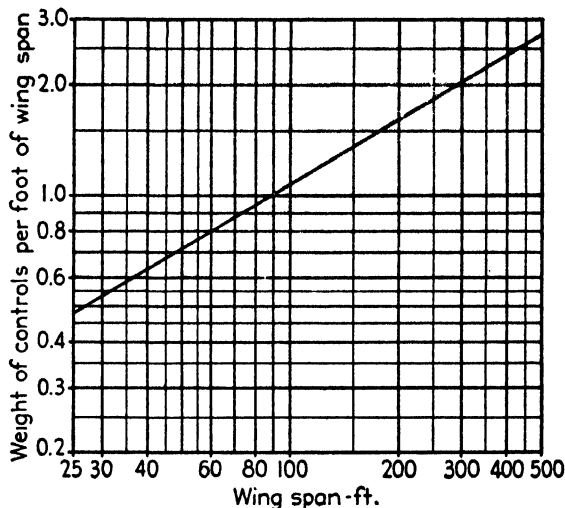


FIG. 1-7. Weight of control systems (high-wing airplanes).

always remain about the same weight (unless the specifications call for unusual and elaborate arrangements which must be handled separately). These items are as follows:

Control column (pilot and second pilot)	45-55 lb.
Control column support and locks	5-7 lb.
Rudder pedals (pilot and second pilot)	20-25 lb. each
Pedal supports and stops	2-3 lb. each

Regarding the aileron, elevator, rudder, and flap controls, it is reasonable to assume that their weight is a function of the wing span. Graphs showing this relationship are shown in Figs. 1-7 and 1-8. The weights of the tab and booster control systems must obviously depend upon the loads which they must carry and this in turn is a function of the areas of the surfaces upon which they operate. Figure 1-9 gives the relationship between tab and booster control weight as a function of the tail-surface area.

(j) **Furnishings.** The furnishing group requires more attention in t preliminary estimate since it is highly variable and depends largely up the customer's needs either actual or imagined. The most satisfacto method of making the weight estimate for the furnishings group is

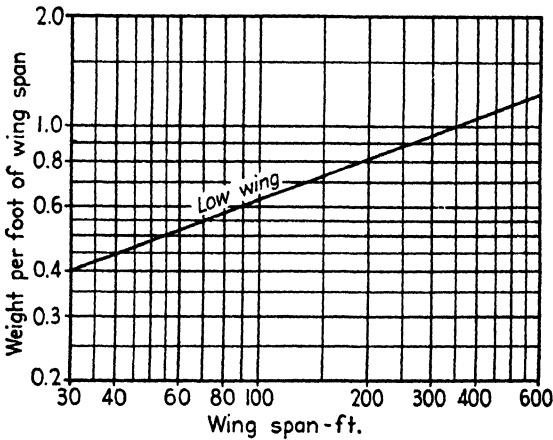


FIG. 1-8. Weight of control systems (low-wing airplanes).

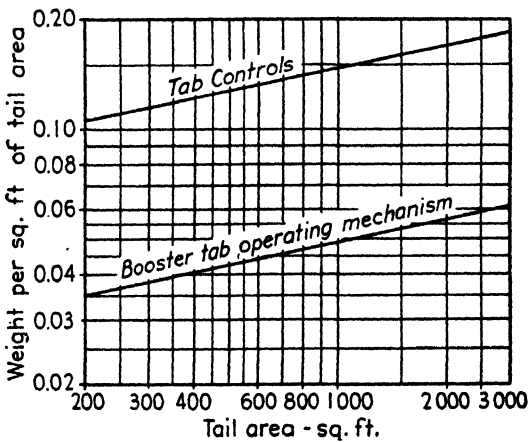


FIG. 1-9. Weight of tab control systems.

sketch the cabin arrangement and then consider each item individually. A table of weights giving the weight per square foot of the various materials used in this group is given in reference 1-2.

(k) **Communicating Equipment.** The amount and type of communicating equipment depends upon the Civil Aeronautics Authority or Service requirements which, in turn, are dependent upon the purpose of the airplanes and upon additional requirements which may be added to

the specification. Unit weights of each piece of equipment may be obtained from the manufacturers. For typical commercial passenger airplanes the weight of this item may vary from 100 lb. (absolute minimum equipment) to 600 lb.

(l) **Electrical Equipment.** Radio and electrical appliances determine the electrical power requirements. Such items are those of the generators (25-40 lb. each) and the batteries (35-90 lb. each) assuming a 12-volt d-c. system. The remaining items, making up a total of approximately 2.5 per cent of the gross weight, consist largely of wiring and conduits and are distributed rather uniformly throughout the airplane.

If auxiliary power units delivering 110 volts are used, the total weight for large aircraft may be appreciably reduced because of a great saving in transmission wire weights. However, very little information on this system is available and each installation must be considered separately.

(m) **De-Icer Installation.** Assume the weight of the de-icer equipment equal to approximately 0.06 per cent of the design gross weight.

(n) **Possible Useful Load.** This group consists of food stores (emergency rations) and water. Sometimes these items are included in useful load, hence the name, possible useful load.

The above is a breakdown of the weights which are necessarily fixed for any given airplane type. The other weight item to be considered is the useful load which will be treated in detail in section 1-4. This discussion has been made since the items under the weight-empty classification are, to a large extent, fixed as to weight and position when the airplane has been built whereas the items under useful load are variable as to both weight and position and therefore seriously affect the balance computations.

1-3. Arrangement

It has wisely been said that a number of the external dimensions of an airplane are determined purely by the fact that the outside dimension must at least be as large as the inside dimension. In other words certain necessary arrangements of the airplane contents are more or less fixed and the airplane is essentially built around the contents. It is therefore well to consider at this point the items over which the designer has some control as to size and location and those over which little or no control is possible. For purposes of discussion a commercial transport has been used; however, it must be realized that designers of military airplanes are faced with as many, or more, similar problems.

The preliminary weight estimate, as discussed in section 1-1(b), has been based on the first three-view drawing of the airplane. After that

the designer will be ready to start on a series of arrangement drawings, each of which will have to be modified as the design progresses. The number of these changes will nevertheless be considerably reduced if proper consideration is given to the items mentioned in the following sections.

The three-view drawing consists of a side, front elevation, and plan view of the proposed airplane drawn to scale. This drawing will be the basis for the detail design of the airplane, and like all other drawings should show as much detail as is consistent with clearness.

The following sections include the main items which must be considered in order to satisfy the detail requirements for the arrangement layout. In general, three things must be considered for each item mentioned, namely, its weight, its location, and its relationship to other items of equipment, personnel, or structure. Section 1-3(e) contains a typical list of the fixed equipment for a particular airplane.

Since the Civil Aeronautics Authority and the Services have their own restrictions regarding the location of certain items in aircraft and the safety devices which must be installed, the designer should familiarize himself with the regulations applicable to his design and follow them implicitly. If he feels that the regulations are wrong, his job is to give his opinion to the chief engineer and then to follow the regulations until they have been changed or until approval has been obtained to waive the regulations in the given case. It might be remarked here that to accomplish such a change or waiver is a long, time-consuming process.

(a) **Balance Considerations.** Since the location of the center of gravity of the airplane with relation to the center of lift of the lifting surfaces is very important from an aerodynamic standpoint, one of the primary considerations which must be kept in mind during the arrangement study is the effect the position of each part may have on the center of gravity location of the completed airplane. The major weight items may be broken down into two main subgroups.

(1) *Weight empty.* This includes the weight of

Wings	Furnishings
Tail	Instruments
Fuselage	Surface controls
Power plant	Electrical equipment
Landing gear	Communicating equipment

This group has been discussed in detail in section 1-2 and will again be mentioned in section 1-4. It is necessary only to mention here that the sole item in this group which can be appreciably moved in order to obtain correct balance is the wing group and, in multi-engined airplanes, the power plant which is attached to the wing. The wings can either be

bodily shifted in their position relative to the fuselage or the attachment of the wing and fuselage can remain fixed and the wings can be swept backward or forward thus giving an effective change in the location of the average total lifting force relative to the center of gravity.

(2) *Useful load.* This includes the weight of the payload (passengers and cargo), fuel and oil, and crew members.

This group is the most flexible, and therefore the most troublesome from a balance standpoint. The number of passengers may vary from zero to the complete passenger load, and their position is highly variable since it is psychologically undesirable to assign seats to passengers and to insist that they remain fixed in any given seat during flight. The same is true of the cargo to a somewhat lesser extent since, once it is located, its position will not change in flight. The fuel and oil will diminish in weight and, unless carefully controlled, the center of gravity of the fuel and oil supply may change appreciably, and thus affect balance considerations. The crew members are usually fixed in number and the movement of at least the pilot and the second pilot is restricted. More detailed considerations of these problems will be discussed in section 1-4.

(b) **Comfort Considerations.** The emphasis placed on considerations of the comfort of the crew and passengers on an airplane is largely a function of the proposed length of the longest non-stop flight. Conditions which go unnoticed or can be ignored for a flight of an hour or two may become very irritating before the end of much longer flights. The major items to be considered will be discussed briefly below.

(1) *Noise level.* For commercial transport airplanes the noise in the cabin should be kept down to a level that will not seriously restrict ordinary conversation and particular attention should be paid to the elimination of the higher frequency sounds which may become very annoying after a period of time. Chief noise sources are the power plant and propeller, the ventilating system, and external fittings on the airplane. Since most of the important noise sources are outside the cabin, the main problem is to keep these noises from entering the cabin or, if they do enter to absorb them as rapidly as possible. Prevention of the noise entering the fuselage is accomplished by two methods: first, by eliminating any openings connecting the outside with the inside of the fuselage and second, prevention of a noise source being set up in the cabin due to vibration in the structure caused by some external force.

Absorption of the sound which does enter is carried out by approved soundproofing methods utilizing as far as possible the sound-absorption properties of seats, wall and floor coverings.

(2) *Propeller location and clearance.* The location of the propellers on an airplane is a very important factor from the standpoint of comfort.

The maximum propeller noise lies in the plane of rotation and the noise level drops off very fast as one leaves the plane of rotation in either direction. It is therefore advisable to keep any openings which eventually lead into the fuselage, such as air intake ducts and the like, out of this plane of rotation and, if possible, put quantities of sound-absorption material in this region. Requirements have been set up by the Civil Aeronautics Authority and the Services which make it necessary to keep the pilots out of a region given by a conical angle of 5 degrees from the plane of rotation of any or all propellers, and it is usually considered good practice as well not to put passengers in this region. The logical item to put in this volume is, then, either the lavatories in which noise level restrictions are not serious (except in so far as the noise may be retransmitted back into the cabin) or, even better, the baggage or cargo compartment which, due to the character of its contents, provides considerable sound absorption.

The minimum distance of the propeller tips from any structural element such as the side of the fuselage is also very important. If the tips of the rotating propeller are too close to the fuselage side a severe vibration may be set up in the fuselage skin which may act as a sound and vibration source into the interior. This interaction has sometimes been so severe as actually to cause structural fatigue failure of the skin in that region due to the intense vibrations of the sheet covering. In general, it is advisable to keep at least 12 in. between the propeller tips and the nearest adjacent structure and more space is desirable.

(3) *Vibration.* Again the propeller and engines are the chief sources of vibration. There are, as well, aerodynamic sources such as tail buffeting, because the tail surfaces are partly in the propeller slipstream or are in the wake of some other part of the airplane which causes a turbulent disturbance of the air. These causes can usually be eliminated by external changes in the aerodynamic shape of the airplane, but the propeller and engine vibration are essentially fixed quantities. A new type of dynamic suspension engine mount has helped considerably to reduce the amount of power plant vibration that is transmitted to the remaining structure. Vibration-damping material placed at or near the attachment of the wing to the fuselage is also advantageous.

One of the main things to watch in any sheet-metal structure is the tendency of large plate areas to get in resonance with some fluctuating energy source. No matter how carefully each sheet panel may be designed, there is always the possibility that a few panels in every airplane (they may be completely different panels in the next airplane of the same type) may go into resonance at some speed of the airplane or at some value of the engine r.p.m. The best way of eliminating such

trouble is to coat the inside surface of all panels with some material with a high damping coefficient. If this method leads to too large a weight increase, the offending panels can be broken up by light stiffener sections which should be placed so as to divide the panel in unequal, odd-shaped areas which will not go into resonance at some higher harmonic of the panel frequency.

(4) *Vision.* At one time it was thought that vision was one of the primary considerations in the arrangement of an airplane. For military airplanes this is still true and it is also very important that the pilots in a commercial transport have good vision. However, from a passenger standpoint it is of secondary importance. For passenger visibility, the high-wing monoplane is obviously the best. However, such considerations as increased length of landing gear and its attendant increase in weight, difficulties of obtaining sufficient head room in the cabin, and other such items so far overshadow the vision problem that such constructions are seldom used, or if used, have been established by considerations other than that of giving the passengers complete and unobstructed vision. In fact, it is usually only the passenger on his first or second flight over a given portion of the country who is much interested in what he is flying over, and there are sufficient places in an airplane with good downward vision to accommodate such a person.

It must again be repeated however, that the pilot's vision must be unrestricted and must not be hampered, particularly at night, by reflections from his windshields. This is a very troublesome problem and must usually be solved in the mock-up since it is impossible to handle such problems satisfactorily on the drafting board or in the design room.

(5) *Heating and ventilating.* In an airplane, as in any confined space containing a number of people, heating and ventilation must be considered. It is therefore necessary to provide first, a source of uncontaminated air and second, a source of heat.

The source of uncontaminated air must be located so that fumes from the engines and their exhaust cannot possibly enter the system, and it should also be located so that the dynamic pressure due to the forward velocity of the airplane can be utilized to force the air through the ventilation system. Two logical points on the airplane which satisfy these requirements are the nose of the fuselage and the leading edge of the wing. Taking air in at the nose of the fuselage encounters difficulties because the air ducts tend to run through the region occupied by a large number of controls and may further be complicated by a nose wheel installation. Also, since the source of heat for this air is the engines, considerable ducting or piping must be used to get the air to and from

the engines in the wing, or to get the heat from the engines into the ventilation system.

The other method, taking the air in at the leading edge, some distance outside the propeller slipstream (to prevent propeller de-icing fluid from entering the system) usually provides a simpler air heating and ducting arrangement. It has, however, the possible disadvantage that, if the intake is not carefully made, serious aerodynamic interference may arise.

Since a large part of the time the passengers spend in an airplane will be at high altitudes where the temperature is very low, it will be necessary to heat the air before it is put into the cabin. As mentioned before, the main source of heat is in the exhaust system of the power plant. Electrical heating has been suggested, but the large current drain necessary makes a prohibitive load on an already heavily overloaded electrical system. Two methods of utilizing the heat in the exhaust gases have been used. The first is actually to pass the hot exhaust gases around some form of heat exchange unit through which the ventilating air passes. This has the major disadvantage that leaks in the system allow exhaust gases to pass directly into the cabin ventilation systems which, to say the least, is undesirable. The second system uses the exhaust gases as a heat source in a liquid boiler and the heated liquid then passes through the ventilation system heat exchange unit. The disadvantage of this system is the additional weight; however, with modern types of flash boilers, containing very little liquid, this weight can be reduced to a minimum.

In laying out the airplane it is necessary to make space provisions for the ducts and piping necessary for the ventilation distribution system. It must also be realized that this system may be a noise source, either because it furnishes a possible opening to outside noises, or because fans or other noise sources are present in the system itself. It is also necessary to introduce regulators into the system so that the amount of air and of heat may be varied by one of the crew members. Since the power and heat sources are dependent upon the airplane's velocity and the engine exhausts, respectively, when on the ground it is necessary to provide some ventilation from an outside source. This is usually furnished by an air-conditioning system contained in a truck and means of attaching this system and proper interconnecting ducting must be provided.

(c) Operating Considerations. It is obvious that provision must be made for loading and unloading the airplane's passengers. However, certain problems arise during this simple operation that may be overlooked by the designer. For an airplane with a tricycle gear, it is possible for enough passengers to congregate near a rear door to put the center of gravity of the airplane behind the rear wheels, and cause the

airplane to drop by the tail. This obviously must be prevented. Another problem that must be considered is that of providing space for overcoats near the passenger loading door. The passengers may want these as they leave the ship but they will not need them in flight; therefore sufficient space must be provided so that winter wraps for all the passengers may be stored. Ease in loading and unloading baggage and express should be carefully considered because any difficulty in this operation would lead to unnecessary delay on the ground.

The location of the pilot and second pilot is obvious. In larger crews including a navigator and an engineer, the location of each crew member should be such as to permit exchange of information readily. Telephone communication is, of course, necessary but, in addition, provision should be made for the interchange of written messages with a minimum of effort. Stewards and stewardesses should be located where they can command a view of the outer cabin. The buffet and food and water supplies should be so arranged that the stewardess can serve meals to all the passengers with a minimum of effort. The space in which the stewardess has to work is very limited; therefore, great care must be taken so that there will be little lost motion or time in serving food to passengers and crew.

Airplane maintenance is one of the large items in the cost of operating an airline or in the cost of operating Service airplanes. The designer of the airplane can cause the maintenance engineer a great deal of unnecessary trouble if he does not realize during the layout process that all important elements in an airplane must be inspectable, removable, repairable, and replaceable with the minimum of effort on the part of the ground crew. This means that easily reached and quickly removable access doors must be installed where internal inspection is necessary, and that the use of quickly detachable assemblies should be carefully considered. The degree of importance of an airplane part determines how often it must be inspected and consequently determines the amount of time that the designer should give to designing ways and means of making inspection and maintenance as simple as possible.

Safety features which must be considered include a wide range of items from adjustable seats for the pilots to prevent fatigue and consequent loss in efficiency, to de-icing equipment for the wings, tail surfaces, ailerons, and propellers. A few other items to be considered are:

- (1) Fire extinguisher apparatus at all vulnerable points such as the inside of the engine cowlings. These extinguishers are to be operated either directly by a fire or by a crew member in connection with a suitable fire warning system.

- (2) Emergency exits in passengers' and pilots' cabins. The number of these is determined by regulation.

(3) Safety locks on all doors in the airplane.

(4) Warning signals for flap, tab, and landing-gear positions, etc.

(d) Manufacturing Considerations. It must be kept in mind by the designer that, no matter how good a design may be, if it cannot be economically manufactured by the company considering the design, it is useless to that company. From this standpoint, certain arrangements which might otherwise appear attractive, may have to be changed owing to limitations in shop space, shop tool equipment, or the available sources of supply. If the proposed order is large enough, a large expenditure may be justified to correct some of these limitations. However, for small orders, the designer should give considerable thought to keeping his design suitable to the available manufacturing facilities of his company.

(e) Fixed Equipment. It will be impossible in a text such as this to give a detailed discussion of all the items which must be considered under the fixed equipment group. All that will be done is to list the things for which space must be provided and their general location in order that the designer will have at least an approximate check list for reference purposes. In the classification which follows, a large transport has been considered and the operating crew has been assumed to be composed of a pilot and second pilot, an engineer, a navigator, and a radio operator. For a smaller transport having only a pilot and second pilot, there is very little reduction in the number of instruments and controls and therefore space must be provided in the pilots' compartment for most of the articles listed below. Of course such items as desks and chairs for the engineer, navigator, and radio operator are obviously eliminated in a ship having only a pilot and second pilot; however the instrumentation and controls are essentially the same.

1. Pilots' section

a. Instruments

Air-speed indicator	Clock
Altimeters	Landing-gear position indicator
Bank-and-turn indicator	Flap-position indicator
Rate-of-climb indicator	Marker-beacon indicator
Artificial horizon	Compass indicator
Directional gyro	Air-temperature indicator
Compass	Instrument board

b. Controls

Flight controls

Aileron	Aileron trim tab
Rudder	Rudder trim tab
Elevator	Elevator trim tab
Flap controls	Landing-gear retraction control
Auto pilot	

Engine controls

Throttle

Propeller pitch control

Miscellaneous equipment and controls

Parachute flare release

Electrical controls

Dump valve

Running lights

Fire extinguisher

Passing lights

Telephone

Instrument lights

Loud speaker

Landing lights, etc.

Cabin warning-lamp control

Flight-log container

Brake controls

Map container

Remote controls for radio

2. Engineer

a. Instruments

Air speed

Exhaust-gas-analyzer indicators

Altimeter

De-icer pressure gage

Tachometers

Hydraulic system pressure gage

Engine synchronizer

Vacuum gage

Manifold pressure

Auxiliary power plant instruments

Oil temperature

Auxiliary power plant controls

Oil pressure

Electrical system volts

Oil quantity

Electrical system amps.

Fuel pressure

Electrical system watts

Fuel quantity

Cabin water-temperature indicator
and control

Thermocouple indicator

Cabin air-temperature indicator and
control

Outside air temperature

Carburetor air temperature

Cabin steam-temperature indi-
cator and controlCabin boiler water-level indicator
and control

b. Controls

Throttle

Tank-selector valves

Mixture

Refuel valves and pump

Carburetor air

Fire extinguishers

Carburetor air heat

Dump valve

Oil temperature

Auto pilot oil pressure

Cowl flap control

De-icer air pressure

Auxiliary power plant selector

Starting

Supercharger

Electrical

Cross-feed valves

c. Miscellaneous

Desk

Loudspeaker

Chair

Maintenance manual

Writing materials

Wiring diagrams

Telephone

3. Navigator

Chart table	Telephone and loudspeaker
Chair	Instruments
Navigation equipment	Air speed
Drafting machine	Altitude
Sextant	Air temperature
Nautical almanac	Clock
Books	Aperiodic compass
Charts	Drift meter
Computers	Ground-speed meter
Vision for dead reckoning	Radio-compass indicator
Vision for celestial observation	

4. Radio operator**a. Miscellaneous**

Chair	Typewriter
Desk	Telephone and loudspeaker
Writing materials	

b. Radio equipment

Variable frequency transmitter
Variable frequency receiver
Beacon receiver
Combination short- and long-wave receiver for standby use with battery
High-frequency transmitter airport control
High-frequency receiver airport control
Cone of silence and approach marker receiver
Instrument landing-glide path and loop receiver
Facsimile keyer and printer
Headphones and microphones
Trailing-wire antenna and retracting mechanism
Trailing-wire-antenna tuning unit
Shielded loop antenna

5. Crew accommodations**a. Captain's cabin**

Desk	Bed
Lavatory facilities	Wardrobe

b. Crew cabin

Bunks	Lockers
Lavatory facilities	

6. Passenger accommodations**a. Stateroom**

Seats	Luggage storage
Beds	Wash basin
Toilet	Appointments
Bedding storage	

- | | |
|------------------------------------|--|
| b. Main cabin | |
| Seats, convertible to berths | Floor covering |
| Bedding | Luggage stowage facilities |
| Appointments | Bedding stowage facilities |
| c. Lounge | |
| Cards | Bar |
| Magazines | Bar equipment |
| Cigarettes | Tables |
| Ash trays | Chairs |
| d. Dining room | |
| Linens | Storage for equipment |
| Silver | Tables |
| Dishes | Chairs |
| e. Galley facilities | |
| Food storage facilities | Sink and drain |
| Refrigerator | Steam or electric cooker |
| Refuse container | Cupboards and shelves |
| Hot plates | Hot-and-cold-water facilities |
| Food preparation facilities | |
| f. Dressing room facilities | |
| Chemical toilets | Wash basin |
| Toilet paper | Soap dispensers |
| Mirrors | Vanity tables |
| Towel holder | Dressing sets |
| First-aid containers | Sanitary napkin dispenser |
| g. Miscellaneous | |
| Sickness containers | Reading material |
| Coat hangers | Writing material |
| Ash trays | Removable tables |
| Safety belts | Rugs and carpets |
| Safety belt signal | Windows and curtains |
| 7. Cargo accommodations | |
| Loading facilities | Bins for small parcels |
| Lining | Mail lockers |
| Tie downs | Checking facilities |
| 8. Power plant | |
| Engines | Accessories |
| Propellers | Fuel and refueling system, tanks and lines |
| Starting system | Power plant controls |
| Oil system tanks and lines | |
| 9. Electrical system | |
| Generators | Junction boxes |
| Wiring | Auxiliary power plants |
| Switches | Lamps |
| Conduit | Motors, etc. |

10. Cabin heating and ventilating

Ducts	Water lines
Boilers	Blowers, recirculating
Radiators	Controls
Reservoirs	Pumps
Steam lines	

11. Cabin supercharging system

Ducts	Cabin regulators
Cabin superchargers	Cabin supercharger drive

12. Miscellaneous

Handling equipment	De-icing equipment
Cabin fireproofing	Electrical connections
Cabin fire extinguishers	Heat and ventilating connections

(f) **Summary.** The above impressive list should indicate that the arrangement of the contents of an airplane is no easy task. It takes the combined efforts of the aerodynamicists, structural engineers, and detail designers, all working under the critical eye of the head of the weight group to arrive at a solution that will be more or less satisfactory to all concerned. The use of the mock-up also becomes immediately apparent since an attempt to make a location layout on a drawing board for all of the items indicated is doomed to failure at the start. Little has been said about Service aircraft, but the problems are similar and just as difficult although the items requiring consideration are of a different character. In general, it can be said that the personnel of a military aircraft cannot expect the comfort and luxury which is provided in a transport, and more attention can be paid to the problems of armament, bomb racks, and other military equipment. It must, however, be realized that the efficiency of the crew on a military airplane can very easily be greatly lowered if they are not made reasonably comfortable, particularly in long flights.

1-4. Weight and Balance

Having obtained the information discussed in the previous section, the designer is then ready to make up the weight and balance estimate of the airplane. The side and plan view of the three-view drawing is utilized for this purpose and the centers of gravity of all items are spotted on one or both of these figures. Suitable reference axes are then chosen, Fig. 1-10, from which all horizontal and vertical distances are measured.

Tables similar to Table 1-1 are then filled out, the final result of this tabulation giving the horizontal and vertical location of the center of

gravity of the airplane. It is not, however, sufficient to determine this location for only one condition, say the completely loaded condition, because what is of primary importance to the aerodynamicist and the designer are the fore-and-aft limits of the center of gravity travel for

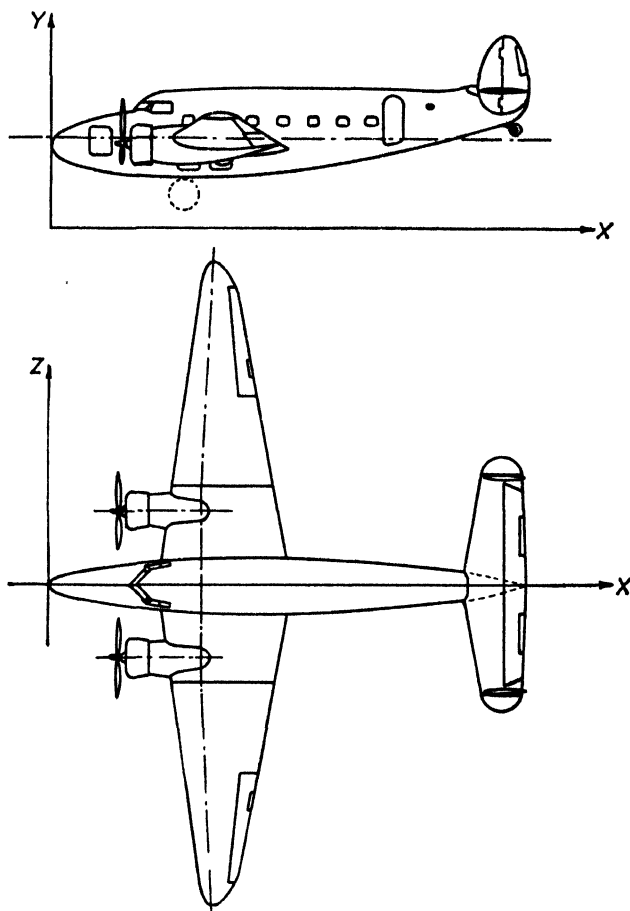


FIG. 1-10. Assumed axes for balance calculation.

all possible loading conditions. If this travel is too great for arbitrary loading arrangements, it may be necessary to specify such arrangements as: (1) order in which fuel tanks should be emptied or filled, (2) amount of cargo in each of the cargo compartments for various numbers of passengers being carried, (3) amount of ballast necessary to keep the center of gravity within the proper limits under certain loading conditions. A detailed discussion of some of the most important considerations follows.

(a) **Stability Range.** The first important item to consider before attempting to fit the useful load into the balance picture is the stability range of the airplane. The estimation of this range, a function of the aerodynamics department, is determined from wind tunnel tests and data obtained from previously flown airplanes of the same type. Stability, control, and maneuverability, because of their close relationships to the airplane balance, require the center of gravity travel to be limited to a prescribed range.

As an example, assume the stability range of a given airplane when landing with the wheels and flaps down, to be from 15 to 30 per cent of

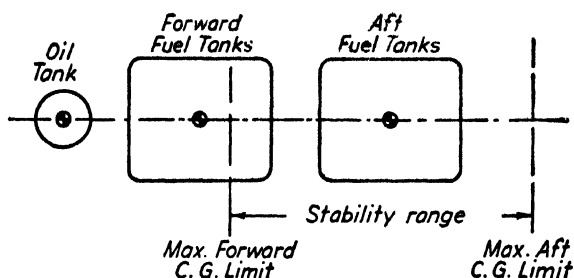


FIG. 1-11. Fuel tank arrangement.

the mean aerodynamic chord (m.a.c.) In other words, the maximum forward center of gravity (nose-heavy condition) can be no farther forward than 15 per cent of the length of the m.a.c. measured aft of the leading edge of the m.a.c. In a similar fashion, the maximum aft center of gravity cannot exceed 30 per cent of the m.a.c. Once this range has been established, the designer can proceed with the balance study by investigating the most advantageous order of filling and emptying the fuel tanks.

(b) **Fuel and Oil.** Probably the relationship between fuel consumption and balance can best be explained by observing a simple example. The locations of the stability range limits, fuel tank centers of gravity, and oil tank center of gravity are shown in Fig. 1-11.

For the sake of explanation let us assume that the airplane which contains these tanks is inclined to be nose heavy when carrying the desired useful load less fuel and oil. From the diagram, obviously it would be most advantageous to fill the tanks from rear to front and empty the tanks from front to rear, since fuel in the rear tanks will offset the weight of the front fuel and oil which are both on the forward side of the maximum forward center of gravity position. To visualize more clearly how various loadings are calculated to bring the resulting centers of gravity to the extremes of the allowable center of gravity travel, let

us consider these limits to be the fulcrums of levers carrying the various weights of the airplane. In order to satisfy the stability requirements, the airplane must balance upon either one or the other of these fulcrums, or at some point between them.

Ordinarily, the tanks to be emptied last will carry a 45-minute emergency fuel reserve. After the first balance results have been completed, the tendency of the airplane to be either nose heavy or tail heavy will be noted and this reserve fuel will be assigned to the tank which will offset the worst case. At this point it should be clear that the ideal position for the center of gravity of the front and rear fuel should be well within the forward and aft center of gravity limits. As a matter of fact, to have all the centers of gravity of the fuel tanks located midway between the limits would be the ideal situation, because additional fuel would better the balance by the greatest amount for either a nose-heavy or tail-heavy condition.

(c) Critical Fuel and Oil Loads. Once the order of fuel consumption has been decided, the next step is to determine what condition during the consumption of fuel will give the most forward center of gravity and the most aft centers of gravity when balancing about each respective fulcrum. In addition to the consideration of fuel, the location and weight of the oil must be included in the calculations. The Civil Aeronautics Authority requires at least 1.0 gal. of oil for each 20 gal. of fuel to be carried in our present transports. This ratio may vary with future engines and the Army and Navy usually specify their own ratio.

If we return to Fig. 1-11 and again assume that the tanks fill from rear to front and empty from front to rear, the most nose-heavy balance is possible either when the fuel and oil tanks are filled; or, when the forward tanks are empty, the aft tanks have only the reserve fuel and the oil tanks are filled to one-half capacity. It is reasonable to assume that no more than one-half the oil will remain when all the fuel except the reserve has been consumed. From the diagram it is obvious that the most tail-heavy case will be caused by empty oil tanks, empty forward tanks, and only the 45-minute reserve fuel remaining in the rear tanks.

To determine which condition of fuel and oil is critical for the nose-heavy balance, assume the airplane's center of gravity is at the forward limit with fuel and oil tanks filled to capacity. Then consider that the fuel is consumed from the forward tanks and the aft tanks except the reserve in the aft tanks, and that the oil has been reduced to one-half the total capacity. With these new conditions, the center of gravity travel is calculated. If it is forward, the case with the tanks empty is critical and should be used to compute all nose-heavy conditions. If the

center of gravity has traveled aft, the case with the tanks full is critical and should be used instead.

For preliminary calculations, it may be assumed that the fuel consumption of the engines is 0.5 lb. per hp. per hr. at 60 per cent power. A gallon of fuel weighs 6 lb. and a gallon of oil weighs 7.5 lb.

(d) Crew. In a large transport airplane, the crew may consist of two pilots, one radio operator, one stewardess, and one porter. In large military bombers it may number six or more. The crew can consist of pilot, co-pilot, radio operator, front gunner, bomber, and possibly two rear gunners. In commercial aircraft, the crew for balance purposes is assumed to weigh 170 lb. each, except the stewardess, whose weight is 130 lb. The airlines actually weigh their crew in order to take advantage of additional payload if the amount is less than the above total. Each member of the crew of a military airplane is considered to weigh 200 lb. which includes parachute and flying equipment.

(e) Passengers. All passengers flying in commercial airplanes are assumed to weigh 170 lb. each for balance purposes. However, the airlines receive each passenger's weight and thus are able to know more accurately the actual gross weight of the airplane. Each passenger is allowed 40 lb. of baggage, but here again each piece is actually weighed and recorded in the gross weight of the airplane.

At present, the airlines object strenuously to assigning passengers definite seats. As a result, it is necessary to consider the worst possible passenger seating arrangement when calculating balance extremes. One of the reasons that passengers are required to be out of the dressing rooms and in their seats when landing is that the airplane's stability range when landing is decreased. For this condition, then, various seating arrangements must be considered in the balance calculations. On the other hand, when cruising, the passengers are allowed freedom of motion and not only may take up arbitrary seating arrangements, but also may congregate in any dressing rooms which may be provided. In a large airplane recently under consideration, there were two dressing rooms having a total capacity of nine persons in the aft part of the fuselage. Obviously filling both dressing rooms to capacity would happen only on rare occasions. However, the Civil Aeronautics Authority ruled that there was that possibility and that the balance calculations should consider the case in which the dressing rooms were filled to capacity and the remaining passengers filled the rear seating space in the cabin. This ruling imposed a considerable penalty on the main cargo load. In order to remove this penalty and to meet the stability requirements, it was necessary to move the men's dressing room to a location

forward of the cabin and to restrict the capacity of the women's dressing room to three persons. In this case, the center of gravity travel caused by taking the three persons out of the rear dressing room equaled the decrease in allowable center of gravity range in landing, making a very efficient design.

(f) **Buffet Supplies.** Buffet supplies consist of the food and equipment to serve the necessary meals and drinks in flight. For a typical transport carrying fourteen persons, the following supplies are required in the specifications:

BUFFET SUPPLIES—STANDARDS

Item	Weight in Pounds
Food trays—7	6.30
Dishes—1-lb. per set	7.00
Three 2-quart thermos bottles	11.30
Blankets—5 (assumed)	8.80
Pillows—10 (assumed)	6.00
Silverware—7-place	1.90
Stewardess' bag	32.00
Wash water—3 gallons	24.90
Coat hangers—14	1.80

This total for buffet supplies may vary considerably depending upon the type of service for which the airplane is designed. For an airplane where most of the flights are short, there will probably be little need for much in the way of food supplies. For trips that may cross the United States with only one or two stops, the meal problem becomes one of great importance and the proper design of buffet equipment may save considerable weight. On a trancontinental trip making a number of stops, a large amount of food may be carried during one part of the trip and little or none on the next part. The effect of this on the balance and the center of gravity location must be considered by the designer.

(g) **Cargo.** The cargo compartments of most transports are located about the cone of the propeller and aft of the passenger cabin. The front compartment is restricted to the former location because Civil Aeronautics Authority regulations state that the cabin or the pilots' compartment shall not be in the cone of the propeller. It is also a logical location for soundproofing reasons as previously discussed. Other cargo compartments may be located in the belly of the fuselage aft of the wing trailing edge. When a number of small cargo compartments are grouped together, the capacities of each are multiplied by their individual horizontal distance from a reference line. A summation of the moments divided by the total capacity of the group gives the location of

the resultant center of gravity aft of the reference line. All cargo loads are considered acting at this point because any fraction of the total cargo is divided among the various compartments of the group in proportion to their capacities.

At this stage in the design, sufficient information has been obtained to make possible a graph showing the maximum and minimum allowable cargo in the front cargo compartment with no cargo in the rear. This graph should look similar to the one sketched in Fig. 1-13. The curve for the minimum allowable front cargo is calculated as follows.

Compute the total weight and resultant center of gravity of the weight empty, buffet supplies, and critical fuel for the tail-heavy condition. To

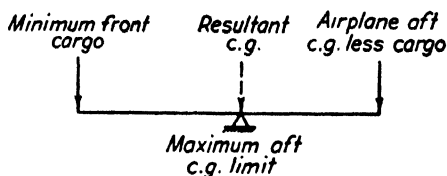


FIG. 1-12. Cargo balance.

this total, add the passengers seated in the rearmost row of seats in the cabin and compute a new total weight and resultant center of gravity. If the resultant center of gravity lies forward of the aft limit, no minimum front cargo is necessary. If, however, the resultant center of gravity lies aft of the aft limit, front cargo will be required to bring the final resultant center of gravity forward of the aft limit. If this limit is assumed to be a fulcrum, and the airplane is balanced upon it, it is a simple matter to calculate the minimum front cargo required (Fig. 1-12).

By this method, the first point on the curve is calculated. By adding passengers to the seats in the second row from the rear of the cabin and computing a new total weight and resultant center of gravity, the second point of the curve can be plotted. By continuing the process, the complete curve will result.

The curve for the maximum allowable front cargo is calculated in a similar manner. The total weight and resultant center of gravity of the weight empty, crew, and fuel is computed, with the fuel supply for the critical nose-heavy condition. Then add passengers seated in the front row of seats in the cabin and compute a new weight and center of gravity position. If the resultant center of gravity lies forward of the forward limit, minimum ballast or cargo will be necessary in the rear compartment. However, if the center of gravity lies aft of the forward limit, front cargo may be added until the resultant center of gravity reaches the forward limit. The maximum value gives the first point on

the maximum front cargo curve. More passengers are added from front to rear until the whole curve is drawn.

The most desirable minimum allowable front cargo loading for various numbers of passengers is shown in Fig. 1-13. Here the curve giving the amount of passenger baggage for the various numbers of passengers is tangent to the curve of minimum allowable front cargo. This condition is advantageous in the event of no cargo, because passenger baggage will usually be available and therefore ballasting will be unnecessary. However, ballasting would be necessary if the cargo curve had passed through

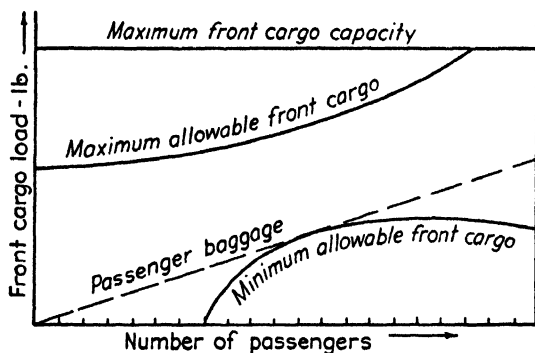


FIG. 1-13. Allowable limits on cargo load.

the passenger baggage line. The maximum front cargo curve should be fairly high so early splitting of the cargo load will be unnecessary and there should be a reasonable gap between the two curves.

If not limited by capacity, the maximum cargo that can be carried in the rear compartment for each number of passengers, after the front compartment is filled to capacity, is the difference between the minimum allowable front cargo and the maximum capacity of the front cargo compartment (Fig. 1-13) multiplied by the distance of the front cargo center of gravity to the aft limit and divided by the distance of the aft limit to the rear cargo center of gravity.

(h) Adjusting the Center of Gravity Limits. If the maximum and minimum front cargo curves are found to be out of reason, they may be altered by (1) rearranging items in the fuselage, (2) moving the engines forward or aft, (3) moving the complete wing with relation to the fuselage, and (4) sweeping the wings.

Rearranging the items within the fuselage is the simplest method if the required change is not too great. Moving the engines fore and aft is in the same category if sufficient room remains behind the engines for an aft movement or the nacelles are not so long as to prohibit moving the

engines forward because of unreasonable stresses, etc. The intersection of the propeller cones with the fuselage must also be considered.

Moving the complete wing with respect to the fuselage offers no difficulties in the early stages of design, but later may cause a rearrangement of fuselage frames. A certain distance must be maintained between the wing and the tail, and if the wing position is changed, the fuselage weight will change.

The final decision of moving items or sweeping the wing to arrive at the desired cargo loading, will depend upon how many items must be relocated and the complications involved. Suppose it is desirable to lower the minimum front cargo curve at its peak F pounds. Then the total necessary moment decrease will be F pounds times the distance of the front cargo center of gravity to the maximum aft limit, L . This moment decrease may be obtained by moving an item of weight W located in the fuselage a forward distance, d , in which

$$d = \frac{FL}{W}$$

(i) **Summary.** It might well be said that the balance criterion is the most important single item in determining the arrangement of the useful load in an airplane. It may alter the desired seating arrangements, it may change the location of the cargo compartments, and may even alter the entire external shape of the airplane. It is for this reason, that the designer must give a great deal of attention to the accurate determination of the center of gravity limits, considering all possible (not only probable) arrangements that the useful load may take.

There is an additional balance condition that must not be neglected, although it is not concerned with stability in flight. For an airplane with a tricycle type of landing gear, a calculation of the aft center of gravity location must be made to see that it does not fall behind the center of the main wheels' ground reaction and thus cause the airplane to drop by the tail. For this case, it is assumed that the rear seats are full and the aisle is full of passengers crowding towards the exit, the fuel is in the critical aft position, and the pilot and second pilot are not in the pilots' compartment.

REFERENCES FOR CHAPTER 1

- 1-1. J. E. LIPP, "Estimation of Wing Weight," *J. Aero. Sci.*, Vol. 5, No. 12, October 1938.
- 1-2. F. K. TEICHMANN, *Airplane Design Manual*, Pitman, 1939.

CHAPTER 2

APPLIED AND DESIGN LOADS

2-1. Performance and Design Data

The performance of the airplane is in general the concern of the aerodynamicist; however, certain performance characteristics of the airplane bear directly upon the work of the stress analyst in so far as they determine the load factors for which the airplane is designed. Only the performance data of which a knowledge is required in the load factor calculations will be briefly discussed in this section. The detailed methods of performance calculations will not be touched upon as they are covered in aerodynamics courses.

The nomenclature employed and the given definitions are in accordance with those given in Civil Aeronautics Authority Manuals, CAR 04 and CAM 04.

Indicated air speed, V_i . For stress analysis purposes all air speeds are expressed as indicated air speeds. The "indicated" air speed is defined as the speed which would be indicated by a perfect air-speed indicator, namely, one which would indicate true air speed at sea level under standard atmosphere conditions. The relation between the actual air speed V_a and the indicated air speed V_i is given by the equation:

$$V_i = \sqrt{\frac{\rho_a}{\rho_0}} V_a$$

where V_i = indicated air speed

V_a = actual air speed

ρ_0 = standard air density at sea level

ρ_a = density of air in which V_a is attained.

Design level speed, V_L . The design level speed is the speed of the airplane in level flight corresponding to the design power for continuous operation reduced to equivalent indicated air speed (f.p.s.) at sea level in standard air. If the estimated value of V_L is less than the value of V_L as finally determined from flight tests, either V_L or P , the design power, must be revised to show correspondence. If V_L is raised to correspond with P , it is necessary to revise the structural analysis. If P is revised,

the reduced value must be entered on the aircraft operation limitations placard as the maximum allowable (except take-off) horsepower.

Design gliding speed, V_g . The design gliding speed, V_g (indicated f.p.s.), with power off shall not be less than $V_L + K_g(V_M - V_L)$, except that it need not be greater than either $V_L + 100$ m.p.h. or $1.5 V_L$, whichever is the lower where

$$K_g = 0.08 + \frac{1850}{W + 3000}$$

W = gross weight of the airplane

V_M = terminal velocity with power off

V_M can be estimated from the formula:

$$V_M = 29 \left(\frac{W}{S_D} \right)^{1/4} \text{ (f.p.s.)}$$

S_D = estimated total drag area in square feet

K_g shall not be less than 0.15

Stalling speed, V_{sf} . The stalling speed of an airplane with high lift devices is given by the equation

$$V_{sf} = \left[\frac{W}{\rho/2(SC_{L_{\max}})} \right]^{1/2} \quad [2.1]$$

where $C_{L_{\max}}$ = maximum lift coefficient with flaps.

Where high lift devices are not employed, the stalling speed V_{sf} can be calculated from the above equation using the appropriate maximum lift coefficient. V_f is the indicated air speed at which maximum operation of high lift devices is assumed. The value of V_f shall not be less than $2V_{sf}$.

Design maneuvering speed, V_p , is the indicated air speed at which maximum operation of the control surfaces is assumed. V_p can be calculated from the equation

$$V_p = V_{sf} + K_p(V_L - V_{sf}) \quad [2.2]$$

V_p need not be larger than V_L .

Where

$$K_p = 0.15 + \frac{5400}{W + 3300}$$

K_p need not be greater than 1.0, but shall not be less than 0.5. The equation for V_p is intended to provide for the following factors:

1. The maneuvering speed cannot be less than the minimum speed of level flight.

2. Assuming that the size of the control surfaces is governed by the necessity for adequate control at the minimum speed, the formula provides for a reduction of the unit loading on the larger control surface area required for low stalling speeds.

3. The high speed is included in the formula to provide for an increase of the unit loading on the control surface area with an increase in high speed.

4. K_p is an empirical factor which provides for the more severe maneuvers likely to be experienced by small airplanes. This factor has been chosen in such a manner as to make the control surface loadings for average airplanes agree approximately with those known to be satisfactory from past experience.

In addition to the above speeds a knowledge of certain design data is necessary; a brief discussion of this data is given in the following paragraphs.

Design weight. The design gross weight of the airplane is the maximum weight at which it is licensed to fly. Usually this weight condition will be critical for most of the airplane's structure; with the exception of certain portions of the airplane, such as engine mounts, nacelles, and the forward portion of the fuselage, for which the inertia loads remain substantially constant while the airplane as a whole becomes lighter from the consumption of fuel and oil. These items may be designed by the gust load factors for the minimum weight condition. The *minimum weight* is defined as the weight empty with standard equipment, plus minimum crew, plus fuel of 0.25 lb. per maximum horsepower (except take-off), plus a full load of oil.

Effective wing area. Based upon wind tunnel tests on complete models the *design effective wing area* is taken as that of the complete wing without any deduction for that portion blanketed by the fuselage or nacelles. For the blanketed portions the wing outline is taken as though it were continuous.

Design wing loading. The design wing loading is defined as the design weight of the airplane divided by the *design effective wing area*.

Rated horsepower. Engines, as supplied by the manufacturer, are usually rated in three ways:

1. A maximum rating for continuous operation.
2. A take-off rating which is the power that can be developed for a short time without harmful effects on the engine. This time is generally sufficient to cover the time required for take-off.
3. An emergency rating for continuous operation when one or more engines has failed. (This applies, of course, to multi-engined airplanes only.)

The wing load factors are calculated on the basis of the maximum rating for continuous operation.

Design power loading. Design power loading is defined as the gross weight of the airplane divided by the design power. The design power being the power which corresponds to the design level speed.

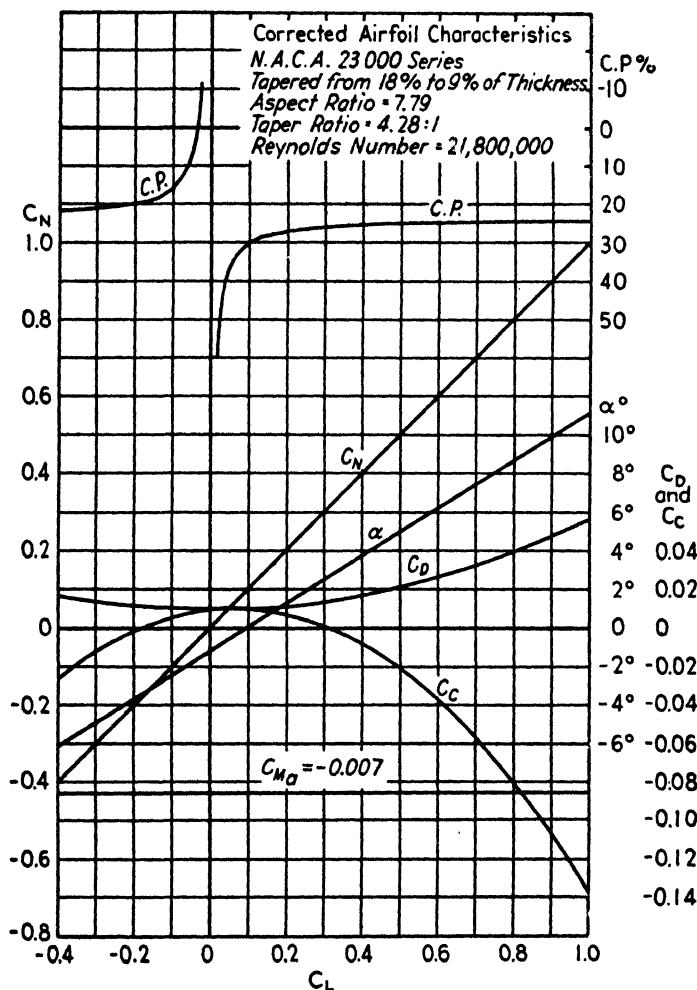


FIG. 2-1. Corrected airfoil characteristics.

Mean aerodynamic chord is an imaginary chord on which all the wing area may be considered concentrated without changing the lift or moment of the air forces on the airplane.

The center of gravity of an airplane is a variable which may travel within the stability limits as determined by actual flight tests. In

designing the airplane it is necessary to use limiting locations determined from the wind tunnel tests. Generally these limits are arbitrarily extended in both directions to insure that the full range determined from the flight tests will be covered by the analysis.

In addition to the performance and design data discussed above a knowledge of the corrected airfoil characteristics for the particular design is necessary. By way of illustration a typical set of airfoil characteristics is shown in Fig. 2·1.

2-2. Loads and Load Factors

The airplane will, during its lifetime, be subjected to an infinite number of combinations of loads. These loads are essentially of two kinds, namely, flight loads which arise from a sudden change in flight attitude and those which arise from landing conditions. The former may occur through intentional maneuvers executed by the pilot or by encountering a "sharp-edged" gust during level flight; in either case the resulting force on the airplane is caused by a sudden change in flight attitude.

No single combination of loads, i.e., lift drag, thrust, ground reactions, will be critical for all of the airplane's structural elements. It is therefore necessary to investigate the flight and landing conditions which will include all the critical loadings for the structure. It is not possible to predict with exact certainty the worst load conditions which will be imposed upon the airplane's structure. However, our knowledge of aerodynamics enables us to limit the necessary investigations to a number of standard conditions. The Civil Aeronautics Authority has published in bulletins CAR 04 and CAM 04, rules by which the external loads resulting from each of these standard conditions can be calculated. These rules cover all the necessary requirements for commercial airplanes; however, the Army and Navy have additional requirements which must be met in the design of military aircraft. Although these published rules contain certain arbitrary assumptions and empirical formulas, they have through past experience been proved to be adequate and satisfactory.

(a) **Acceleration Forces.** The external forces resulting from an acceleration of the airplane can be readily illustrated if we consider the lifting forces acting on the airplane and the weight of the airplane as concentrated forces, Fig. 2·2. During unaccelerated level flight the vector sum of all the forces acting on the airplane will be exactly equal to zero, i.e.,

$$L - W = 0$$

In this case, the airplane as regards the external forces may be considered as being in static equilibrium.

Now if upon the airplane is impressed a force of a magnitude nL ($n > 1$) the condition of equilibrium will no longer exist and an acceleration will occur in the direction of the force nL . According to d'Alembert's principle, every state of motion may be considered at any instant as a state of equilibrium provided appropriate inertia forces are introduced. Newton's first law states that the force acting on a mass is equal to the mass times the acceleration. Instead of this we can say that the force impressed is in equilibrium with the inertia force which is defined as the product of the mass and the negative acceleration. Therefore, our problem of accelerated motion can be treated as one of static equilibrium provided we introduce the proper inertia forces. The equation of equilibrium then becomes

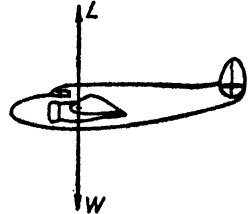


FIG. 2-2.

$$nL = W + \frac{W}{g} a \quad [2.3]$$

where a corresponds to the negative acceleration and g is the acceleration of gravity. Now since L is equal to W , it follows that

$$n = 1 + \frac{a}{g} \quad [2.4]$$

(b) Load Factors. The term a/g is generally referred to as the load factor increment and n as the limit load factor for the wing.

The *load factor* can be defined as that multiplying factor by which the steady flight forces are multiplied to obtain the equivalent static effect of dynamic forces acting during acceleration of the airplane. The *limit load factor* is the maximum load factor which is to be expected in any normal maneuver. A factor of safety is introduced to give a material safety factor and to provide some factor of ignorance. Usually this factor of safety is 1.5, except in the cases of joints, fittings, and castings where higher factors are required. The limit load factor multiplied by the factor of safety is generally referred to as the *design load factor*, i.e.,

$$n' = \text{design load factor} = \text{F.S.} \times n \quad [2.5]$$

As previously stated the external flight loads, or similarly, the load factors arise from the effect of maneuvering (controlled by the pilot), or from the effects of gusts in rough air. Basically the results are the same, namely, to change suddenly the attitude of the airplane without decreas-

ing its speed to correspond to the changed attitude. To assure a clear understanding of this latter statement consider the lifting force on the wing given by the equation

$$L = \frac{\rho}{2} C_L V^2 S$$

Since C_L is a linear function of the effective angle of attack of the airplane, throughout the normal flight range, it means that if the attitude of the airplane is suddenly changed in such a manner that the effective angle of attack increases, C_L will increase correspondingly. Now, if there is no decrease in the speed V , the total lifting force L will increase in amount corresponding to the increase in C_L , thus causing an acceleration of the airplane. The load factor n will be equal to the ratio of C_L , corresponding to the changed flight attitude, to the value of C_L necessary to maintain level flight at the velocity V .

If the lifting forces were to be calculated on the assumption that an instantaneous change in flight attitude can be attained, load factors as high as 30 and even greater would be necessary in designing the airplane's structure. In practice we do not have instantaneous changes, for the following reasons:

1. The human being can only stand acceleration, without injury, corresponding to wing loads of approximately twelve times the weight of the airplane and even loads of five to six times the weight of the airplane are quite uncomfortable.

2. The rapidity with which a maneuver can be executed is a function of the maneuverability of the airplane. Large airplanes are generally not required to execute violent maneuvers and are protected from the imposition of heavy loads by the inadequacy of the control surfaces to produce large, sudden changes in flight attitude. Military aircraft are designed for wing loads which are considerably higher than those of commercial airplanes; this is necessary because of the greater maneuverability required in military aircraft. However, in all cases the airplane is protected from loads higher than those for which it is designed, by the intentional limitations of the control surfaces and also by the pilot's knowledge of the purpose for which the airplane has been designed and the maneuvers which can safely be executed.

In the rules set forth by the Civil Aeronautics Authority the above facts have been properly taken into account. These rules are based on years of practical experience combined with extensive tests in which the actual accelerations in flight were measured by means of accelerometers placed as near as possible to the center of gravity of the airplane. The degree of success which has been achieved in the past through the

application of these rules in the design of airplanes is sufficient proof of the adequacy of these rules.

(c) **Forces on the Airplane Wing in Flight.** Inasmuch as the airfoil characteristics are always given in absolute (non-dimensional) coefficients we shall consider the coefficients first. For stress analysis purposes it is convenient to resolve all forces normal and parallel to the basic wing chord. The given force coefficients will be, the lift coefficient, C_L , normal to the relative wind; the drag coefficient, C_D , parallel to the relative wind; and the moment coefficient, C_M , about some definite point on the wing chord. The magnitudes of the coefficients are func-

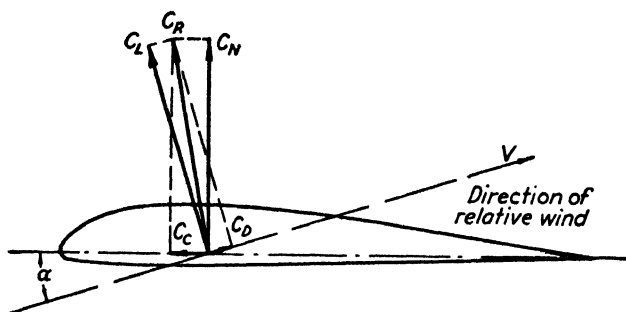


FIG. 2-3. Airfoil force characteristics.

tions of the angle of attack α . Resolving these coefficients normal and parallel to the wing chord, Fig. 2-3, we have

$$C_N = C_L \cos \alpha + C_D \sin \alpha$$

$$C_C = -C_L \sin \alpha + C_D \cos \alpha$$

$$C_R = (C_N^2 + C_C^2)^{1/2} = (C_L^2 + C_D^2)^{1/2}$$

where C_N = the force coefficient normal to the wing chord, positive upward;

C_C = the force coefficient parallel to the wing chord, positive rearward;

C_R = the resultant force coefficient.

If the spars and drag truss are not perpendicular and parallel to the wing chord, the resultant force coefficient, C_R , may be resolved parallel to the spars and the drag truss respectively, giving C'_N and C'_C , which are not necessarily perpendicular to each other.

For design purposes it is satisfactory to assume that $C_L = C_N = C'_N$. The total lift force on the wing is then given by $C_L \cdot Sq$ (or $C_N \cdot Sq$ or $C'_N \cdot Sq$) and the total force parallel to the wing chord by $C_C \cdot Sq$, where S is the

effective wing area in square feet and q is the dynamic pressure ($q = \rho V^2/2$). The total twisting moment of the lift forces on a wing is given by $C_M S q c$, where c is the wing chord. The moment coefficient, C_M , must be given about some definite point on the wing chord. Usually it

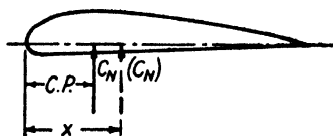


FIG. 2-4.

is given about the aerodynamic center. The aerodynamic center (a.c.) may be defined as that location on the wing chord about which the moment of the air forces is substantially independent of C_L , that is, the product of C_N times the distance

to the aerodynamic center in percentage of the wing chord is equal to a constant.

For any point x along the chord, Fig. 2-4, the moment coefficient is given by the equation

$$C_{M_x} = C_N(x - \overline{CP}) \quad [2.6]$$

where \overline{CP} is the center of pressure position. \overline{CP} and x are given in per cent of the chord. If x is taken as the distance from the leading edge to the aerodynamic center and assuming $x = 0.25$, then

$$\overline{CP} = 0.25 - \frac{C_M}{C_N}$$

where C_M is the moment coefficient about the quarter chord point. (+ C_M gives a moment such as to cause an increase in the angle of attack.)

2-3. Methods of Calculating the Required Load Factors

The methods which have been adopted by the Civil Aeronautics Authority for determining the load factors resulting from the various flight conditions are contained in the Civil Air Regulations CAR 04 and in Civil Aeronautics Authority Manual CAM 04.

In order to familiarize the student with the methods of calculation, and also to clarify why the particular condition is considered critical, a number of the more important conditions will be discussed in detail. Since the regulations may change from time to time, it is recommended that the student refer to the above bulletins for the latest regulations and also for a more complete discussion of the various regulations.

(a) **Gust Load Factor.** The limit gust load factors arise from a sudden change in flight attitude when an airplane flies into sharp-edged up or down air currents acting normal to the flight path. To appreciate more fully the effects of these conditions it is necessary to consider the effect

of changes in the angle of attack on the lift coefficient, C_L . In the design range of angles of attack, C_L is a linear function of the angle of attack, α . As previously stated, the effect of a sudden change in angle of attack without any change in speed (at least momentarily) is to increase the total air load on the wing by the ratio of the respective values of C_L . For example, if C_L at A, Fig. 2·5, represents the lift coefficient necessary to maintain level flight at the speed V , and C_L at B represents the lift coefficient after a sharp-edged gust, KU , has caused a sudden change, $\Delta\alpha$, in the angle of attack, without a decrease in V , then the

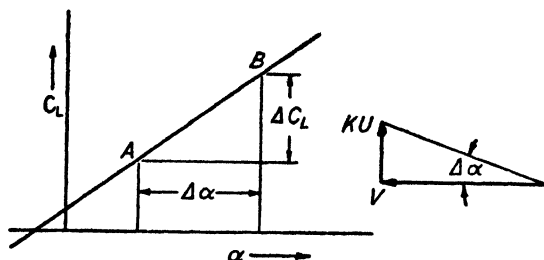


FIG. 2·5. Effect of gust on C_L .

total air load increase is given by $(C_L \text{ at } B)/(C_L \text{ at } A)$. Since for small angles, the angle in radians is approximately equal to the tangent, we have

$$\Delta\alpha = \frac{KU}{V}$$

and

$$\Delta C_L = m\Delta\alpha = \frac{KU m}{V}$$

where m is the slope of the lift curve, C_L per radian, corrected for aspect ratio. The limit load factor increment, Δn , is given by the equation

$$\Delta n = \frac{\Delta C_L}{C_L} = \frac{KU m}{V} \cdot \frac{\rho V^2 S}{2W} = \frac{\rho KUVSm}{2W} = \frac{KUVSm}{575W} \quad [2\cdot7]$$

where U = gust velocity in feet per second,
 V = indicated air speed in miles per hour,
 K = gust reduction factor (reference 2·2, Fig. 11a),
 W = gross weight of airplane in pounds,
 S = design effective wing area in square feet.

Extensive tests have been conducted on commercial airplanes to determine the maximum gust velocities which may be encountered in

where n_I is the higher value determined from:

$$\Delta n_{Ia} = \frac{KUV_L Sm}{575W}$$

$$\Delta n_{Ib} = \left[0.77 + \frac{32,000}{W + 9200} \right] \left[\frac{3.25}{(W/P)^{0.435}} \right]$$

where K = gust reduction factor,
 U = gust velocity = 30 f.p.s.,
 S = effective wing area in square feet,
 W = gross weight in pounds,
 P = power corresponding to V_L .

In calculating Δn_{Ib} two further limiting conditions are, that W/P need not be less than 12 and shall not be greater than 24.

To provide for flight conditions critical for the front spar or its equivalent, the aerodynamic characteristics C_N , \overline{CP} , and C_C shall be determined as follows:

$$C_{N_I} = \frac{n_I W}{q_L S} \quad (q_L = \text{dynamic pressure corresponding to } V_L)$$

C'_C = value corresponding to C_{N_I} , or a value equal to $-0.20 C_{N_I}$, whichever is the greater negatively.

\overline{CP}' = most forward position of the center of pressure between $C_L = C_{N_I}$ and $C_{L_{\max}}$. When C_{N_I} exceeds $C_{L_{\max}}$ the \overline{CP} curve shall be extended accordingly.

The value of C_N required to produce the limit load factor at the high speed of the airplane will usually be considerably less than that corresponding to $C_{L_{\max}}$. Condition I is designed to be critical for the front spar in bending and compression. For this reason, arbitrary values of C'_C and \overline{CP} are assigned, which ordinarily represent a pull-up to the limit load factor at a speed lower than V_L .

Condition I₁—Positive high angle of attack—modified. The smaller of the two values of C_C specified in Condition I and the most rearward \overline{CP} position between $C_L = C_{N_I}$ and $C_{L_{\max}}$ (Fig. 2·7) shall also be investigated when Condition I is critical for the rear spar (or its equivalent) or if any portion of the front spar (or its equivalent) is likely to be critical in tension. Only the wings and wing bracing need be investigated for this condition. (Balancing loads on the tail are not required and their effect on the fuselage is not considered.)

(c) **Condition II—Negative High Angle of Attack.** The previous condition provides for the effects of a sudden increase in angle of attack. It is equally important to investigate the effects of a sudden decrease in angle of attack. The decrease in angle of attack may be sufficiently large to carry the wing past the angle of zero lift into the range of negative lift, such that the air load on the wing becomes a “down” load. From our previous discussion of inertia forces it is obvious that these

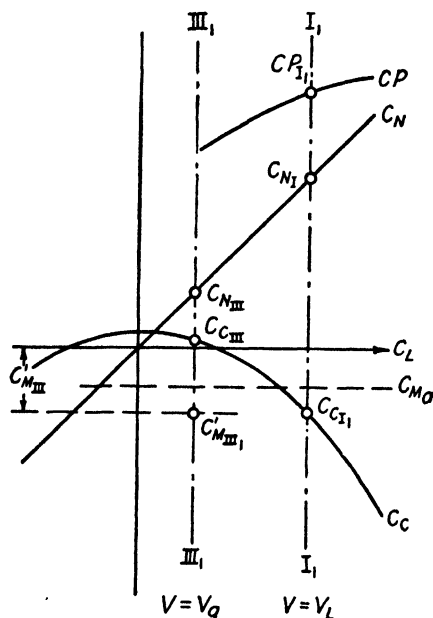


FIG. 2-7. Regions covered by Conditions I_1 and III_1 .

forces will act upward and since they may become greater than the weight of the airplane it is necessary to provide for such conditions. Since the maneuvering loads are always lower than those which are likely to be imposed by gusts, it is sufficient to consider only the load factors due to a 30 ft. per sec. down gust when flying at the speed V_L . The load factor and coefficients are obtained from the following equations:

$$n_{II} = 1 - \Delta n_{I_a}$$

where Δn_{I_a} is taken from Condition I.

$$C_{N_{II}} = \frac{n_{II} W}{q_L S}$$

C_c = actual value corresponding to $C_{N_{II}}$

Note: When C_c is positive or has a negative value smaller than 0.02, it may be assumed zero.

$$C_M = \text{actual value corresponding to } C_{NII}$$

The coefficients are graphically illustrated in Fig. 2-6 (Condition II).

(d) Condition III—Positive Low Angle of Attack. This condition represents an upward acceleration of the airplane at its design gliding speed V_g . As in Condition I, the applied load factor is considered to be produced by either a gust or a maneuver. As the speed V_g is the speed at which the airplane will be flown least, and not at all in very turbulent air, the gust load factor formula is based on a gust of 15 ft. per sec. and the arbitrary value of the limit acceleration required is less than that for Condition I. The load factors and coefficients are obtained from the following equations:

$$n_{III} = 1 + \Delta n_{III} \quad (\text{shall not be less than } 2.0)$$

where Δn_{III} is the higher value obtained from the following:

$$\Delta n_{IIIa} = \frac{KUV_g S}{575W} m$$

where $U = 15$ ft. per sec.

$$\Delta n_{IIIb} = \Delta n_{Ib} \quad (\Delta n_{Ib} \text{ is determined in Condition I})$$

$$C_{NIII} = \frac{n_{III} W}{q_g S} \quad (q_g = \text{dynamic pressure corresponding to } V_g)$$

C_c = actual value corresponding to C_{NIII} . (When C_c is positive or has a negative value smaller than 0.02 it may be assumed zero.)

C_M = the actual value corresponding to C_{NIII} .

The coefficients to be used are graphically illustrated in Fig. 2-8.

Condition III₁—Positive low angle of attack—modified. If the moment coefficient of the airfoil section at zero lift has a positive value, or a negative value smaller than 0.06, the effects of displaced ailerons on the moment coefficient shall be accounted for in Condition III for that portion of the span incorporating ailerons. To cover this point it will be satisfactory to combine 75 per cent of the loads acting in Condition III with the loads due to a moment coefficient of $-0.08 - C_{MIII}$ acting over that portion of the wing only which incorporates ailerons. The design dynamic pressure for the additional moment forces shall be equal

to $0.75 q_g$. Only the wings and wing bracing need be investigated for this condition. (That is, balancing loads on the tail and their transfer through the fuselage need not be investigated.)

(e) **Condition IV—Negative Low Angle of Attack.** This condition allows for the effects of a sudden decrease in angle of attack while flying at the speed V_g . Experience has shown that it is sufficient only to con-

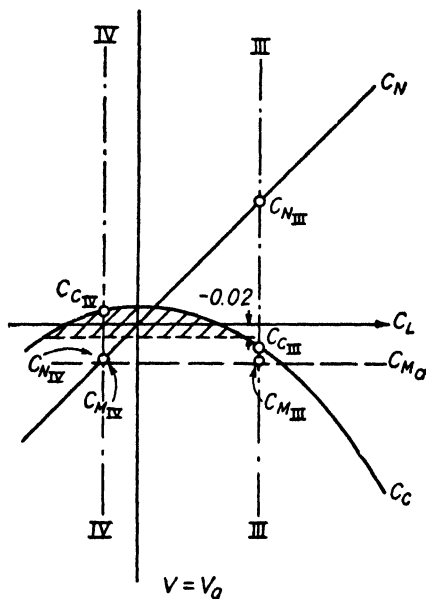


FIG. 2-8. Regions covered by Conditions III and IV.

sider the effects of a 15 ft. per sec. gust. The load factors are determined from the following equations:

$$n_{IV} = 1 - \Delta n_{III_a}$$

where Δn_{III_a} is taken from Condition III.

$$C_{N_{IV}} = \frac{n_{IV} W}{q_g S}$$

C_c = actual value corresponding to $C_{N_{IV}}$

When C_c is positive or has a negative value smaller than 0.02 it may be assumed to be zero.

C_M = the actual value corresponding to $C_{N_{IV}}$

The coefficients are graphically illustrated in Fig. 2-8.

In addition to the above conditions it is necessary to investigate two special conditions, namely, Condition V—inverted flight, and Condition VI—gliding at the limited diving speed V_g .

(f) **Symmetrical Flight Conditions—With Flaps Down.** When flaps or similar high lift devices are used on wings, the design conditions must be modified to account for their use in flight. These modifications are based on the intended use of the flaps and the aerodynamic characteristics of the wing. The following conditions are considered the minimum required to cover a suitable range of symmetrical flight loadings *in cases where the flaps are used only at relatively low air speeds.*

(1) *Condition VII—Positive gust with flaps down.* The design speed for this condition is V_f which is the restricted speed with flaps down. V_f may not be less than $2V_{sf}$, where V_{sf} is the stalling speed of the airplane with flaps down.

Gust velocity, $U = 15$ f.p.s.

$$n_{VII} = 1 + \Delta n_{VII} \quad (\text{minimum value} + 2.0)$$

$$\Delta n_{VII} = \frac{KUV_f S_m}{575W}$$

$$C_{N_{VII}} = \frac{n_{VII} W}{q_f S}$$

C_c = actual value corresponding to $C_{n_{VII}}$

C_M = actual value corresponding to $C_{n_{VII}}$

Note: The most critical deflection of the flap must be investigated, generally maximum throw.

(2) *Condition VIII—Negative gust with flaps down.* This condition provides for the effects of down gust of 15 ft. per sec. at the speed V_f .

$$n_{VIII} = 1 - \Delta n_{VII} \quad (\text{with no lower limiting value})$$

$$C_{N_{VIII}} = \frac{n_{VIII} W}{q_f S}$$

C_C and C_M correspond to the values for $C_{N_{VIII}}$

(3) *Condition IX—Dive with flaps down.* This condition is a check for the maximum rearward chord loads on the wing structure. The maximum deflection of the flap is used, and the load factor and the magnitude and distribution of normal, chord and moment forces over

the wing correspond to the angle of attack at which the greatest rearward chord loads are produced.

- a. Speed = V_f with no gust factor
- b. $C_{C_{IX}}$ = maximum rearward chord coefficient with flaps down
- c. $C_{N_{IX}}$ = value of C_N corresponding to $C_{C_{IX}}$
- d. $n_{IX} = \frac{C_{N_{IX}} q_f}{W/S}$
- e. $C_{M_{IX}}$ = value corresponding to $C_{N_{IX}}$

Only the wings and wing bracing need be investigated for this condition. That is, balancing loads on the tail and their effect on the fuselage need not be computed.

It is also necessary to investigate a number of conditions in which the wing loads are unsymmetrical, e.g., it is assumed that the load on one half of the span is different from that on the other. For a detailed discussion of these conditions the student is referred to the Civil Aeronautics Authority manuals.

(g) Minimum Weight Requirement. Up to this point all the design conditions have been based on the gross weight of the airplane. It is also necessary to investigate certain portions of the structure, which carry fixed weights, for the effect of gusts when the airplane is flying light; because under light load conditions the effect of gusts is more severe. (*Note:* the increment of load factor due to gust is inversely proportional to the wing loading.) The light load conditions in particular design engine mounts and the front portions of fuselages. On large airplanes where most of the fuel is carried in the wings it is generally necessary to investigate the fuselage for some intermediate weight conditions in which the fuselage is carrying its maximum load, while the weight of the airplane as a whole is less than the gross weight because of the fuel which has been consumed.

The minimum design weight (which gives the highest possible gust load factors) is defined as the weight empty of the airplane with standard equipment, plus crew, plus fuel of 0.25 lb. per normal rated horsepower, plus a full load of oil.

(h) Distinction between Wing Load Factor and Dead Weight Factor. All the lift load factors previously determined are *wing load factors*. They represent the ratio between the wing forces actually necessary to sustain the airplane, and the forces built up on the wings when the angle of attack is changed without a corresponding change in speed. If the resultant air forces on the airplane passed through the center of gravity

of the airplane, there would be no tendency toward rotation, except that induced by unbalanced moment from thrust and drag. Actually there is nearly always a tendency for the airplane to rotate about the center of gravity which must be balanced by loads on the horizontal tail. To keep the summation of vertical forces equal to zero the force at the center of gravity must balance the effect of the wing load plus tail load. If all these values are expressed in terms of the airplane weight, then the balancing force at the center of gravity is the dead weight, or inertia load factor.

Since the *moment about the center of gravity* determines the vertical load on the horizontal tail, and thus the dead weight load factor, the location of the center of gravity is important. On a transport airplane the center of gravity travel may be anywhere within the stability range as determined by flight tests. It is generally sufficient to investigate the extreme forward and aft center of gravity travel. For analysis purposes one must rely on wind tunnel data if available, or make a conservative estimate of the center of gravity limits. Even when wind tunnel results are available it is a general practice to allow for limits two or three per cent in either direction outside the indicated stability range. The importance of the location of the center of gravity becomes clearer when all the forces acting on the airplane are taken into account. This point will be considered further in the computations for balancing loads on the tail.

(i) Balancing of the Airplane. The basic design conditions must be converted into conditions representing the external loads applied to the airplane, before a complete stress analysis can be made. This process is known as balancing the airplane and represents a complete static condition in which the fundamental equations $\Sigma V = 0$, $\Sigma H = 0$, and $\Sigma M = 0$ must be satisfied. It is a momentary condition of equilibrium. Actually there are both angular and linear accelerations acting to change the velocity and attitude of the airplane, but as previously stated it is customary to represent a dynamic condition, for analysis purposes, as a static condition by assigning to each item of mass in the airplane the appropriate inertia forces.

If the direction of the resultant air forces on the airplane is not through the center of gravity, there will be an angular acceleration tending to rotate the airplane. An exact analysis would require the computation of this angular acceleration and its application to each item of mass in the airplane. Instead of this laborious method it is customary to eliminate the angular inertia forces by providing the necessary moment with a load on the tail surfaces. This is convenient, since the balancing load can be thought of either as an aerodynamic force on the tail surfaces or as a summation of the required balancing inertia forces. In a gust

condition it is probable that angular inertia loads resist most of the unbalanced couple added by the gust, whereas in a steady pull-up condition the tail load is mostly a balancing air load from the tail surfaces.

The following general assumptions are made in balancing the airplane:

1. Full "power on" is assumed for conditions at V_L (I and II). For conditions at V_g (III and IV) the propeller thrust is assumed to be zero.
2. It is assumed that the applied load factors specified for the basic flight conditions are *wing* load factors. A solution is therefore made for

n_1 = Applied wing load factor	x_{2F} = Horizontal distance from fwd. C.G. to A.C.
n_2 = Net load factor (n_{2F} = C.G. fwd. n_{2A} = C.G. aft)	x_{2A} = Horizontal distance from aft C.G. to A.C.
n_3 = Tail load factor	x_3 = Horizontal distance from A.C. to 20% of mean tail chord
n_{x1} = Applied chord load factor	h_2 = Vertical distance from A.C. to C.G.
n_{x2} = Net chord load factor	h_4 = Vertical distance from A.C. to line of propeller thrust
n_{x4} = Propeller thrust factor	
m_1 = Moment factor	

Load factors and distances are positive upward and rearward, moments are positive clockwise

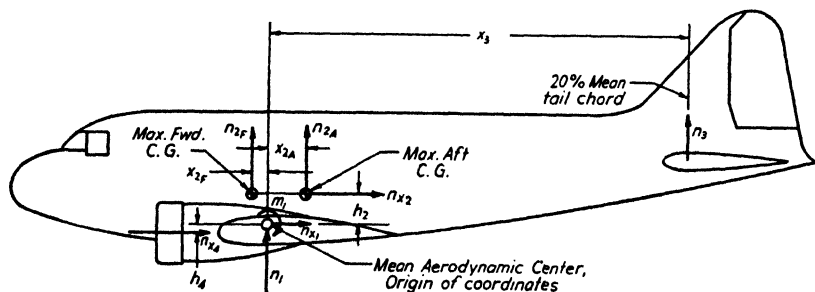


FIG. 2-9. Assumed force system for flight conditions.

the *net* load factor acting on the entire airplane. The net load factor is then used in connection with each item or group of items in the analysis of the fuselage. For balancing purposes the net load factor can be assumed to act at the center of gravity of the airplane. When the center of gravity is variable, as on a transport airplane, the fore and aft limits must be determined and the load factors for the limiting conditions must be computed.

3. In balancing the airplane we are concerned primarily with tail loads. Assuming that it is possible for the stabilizer and elevator loads to be acting in opposite directions, the Civil Aeronautics Authority recommends that the center of pressure of the loads on the horizontal tail be placed at *20 per cent of the mean chord of the entire tail surface*. This arbitrary location is also considered as the point of application of the inertia forces resulting from angular accelerations, thus simplifying the balancing process.

4. The simplifying assumptions are made so that the external forces act at only four points on the airplane. The forces consist of: (a) wing

lift, wing drag, and wing moment acting at the mean aerodynamic center; (b) the weight of the airplane and parasite drag of the airplane acting at the center of gravity; (c) the thrust of the propeller acting at the center line of thrust; * (d) the tail force acting up or down at 20 per cent of the mean tail chord; (e) the chord load acting at the tail surface may be neglected.

A tabular form as shown below is used to simplify the computation of the balancing loads for the various flight conditions.

In the calculations for the tail load factor moments must be taken about the center of gravity of the airplane since both the tail coefficient and the net load factor through the center of gravity are unknown.

In using Fig. 2·9 and Table 2·1 the following assumptions and conventions should be employed:

1. If known distances or forces are opposite in direction from those shown in Fig. 2·9, a negative sign should be prefixed before inserting in the computations. The direction of unknown forces will be indicated by the sign of the value obtained from the equations. A negative value of n_3 indicates a down load on the tail. For conditions of positive acceleration the solution should give a negative value for n_2 , as the inertia load will be acting downward. The convention for m_1 corresponds to that used for moment coefficients, that is, when the value of C_M is negative, m_1 should also be negative, indicating a diving moment.

2. All distances should be divided by the mean aerodynamic chord before being used in the computations.

The following explanatory notes refer by number to the items appearing in Table 2·1.

- (3) The wing loading, W/S , should be based on the design wing area.
- (5) n_1 = limit load factor required for the condition being investigated.
- (8) C_c are the values obtained in the load factor calculations.
- (10) The propeller thrust, F_{pr} , should be determined from the following equation for conditions at V_L .

$$F_{pr} = \eta 375 HP_a / V_a \quad (\text{propeller thrust in pounds})$$

where V_a = actual air speed in miles per hour

HP_a = actual horsepower

η = propeller efficiency

- (11) C'_M are the values obtained in the load factor calculations.

* If the line of propeller thrust is within three degrees of the same angle as the reference line of the fuselage the difference is neglected.

TABLE 2-1
BALANCING COMPUTATIONS

No.	Item	$V_L = \text{m.p.h.}$		$V_g = \text{m.p.h.}$	
		I	II	III	IV
(1)	$W = \text{gross weight, lb.}$				
(2)	$q = 0.00256V^2$				
(3)	$s = (1)/S$				
(4)	$q/s = (2)/(3)$				
(5)	$n_1 = \text{applied wing load factor}$				
(6)	$C_N = (5)/(4)$				
(7)	C_L corresponding to C_N				
(8)	C_C				
(9)	$n_{x_1} = (8) \times (4)$				
(10)	$n_{x_4} = F_{pr}/(1)$				
(11)	$C_m = \text{design moment coefficient}$				
(12)	$m_1 = (11) \times (4)$				
(13)	$n_3 = \text{tail load factor}$				
(14)	$n_2 = - (5) - (13) = \text{net load factor}$				
(15)	$n_{x_2} = - (9) - (10) = \text{chord load factor}$				
(16)	$T = (1) \times (13) = \text{tail load}$				
(17)	$C_{mt} = \text{moment coefficient of airplane less tail}$				
(18)	$\Delta C_m = (17) - (11)$				
(19)	$\Delta m_1 = (18) \times (4)$				
(20)	$\Delta n_3 = (19)/(x_3 - x_2)$				
(21)	$\Delta T = (1) \times (20)$				
(22)	$T' = (16) + (21)$				

- (13) The net tail load factor, n_3 , is found by a summation of moments about the center of gravity, Fig. 2·9, from which the following equations, for the fore and aft center of gravity positions, are obtained:

$$n_3 = \frac{1}{x_3 + x_{2_F}} [m_1 - n_{x_1}h_2 - n_1x_{2_F} - n_{x_4}(h_4 + h_2)]$$

and

$$n_3 = \frac{1}{x_3 - x_{2_A}} [m_1 - n_{x_1}h_2 + n_1x_{2_A} - n_{x_4}(h_4 + h_2)]$$

Items 1 to 16 of Table 2·1 cover the determination of the balancing loads, without considering the moment which may be contributed by the fuselage and nacelles. The following explanatory notes refer by number to items appearing in Table 2·1 which provide for the determination of tail loads when the fuselage moment effects are taken into account.

- (17) C_{mt} is the total moment coefficient about the center of gravity of the airplane less tail, as determined from a wind tunnel test. Item 18 provides for cases in which test results are not available.
- (18) ΔC_m is the increment in moment coefficient due to the fuselage and nacelle moments, also based on design wing area and mean aerodynamic chord. When test data is not available, ΔC_m can be assumed equal to -0.01 .
- (22) T' is the tail load considering fuselage and nacelle moment effects.

The above explanatory notes apply only when the setup as shown in Fig. 2·9 is used. When the value of C_{mt} is obtained from wind tunnel tests, the tail loads T' may be used in design. However, if the -0.01 moment increment is used, the design balancing load should be taken as either item (16) or (22) whichever is the more severe.

2-4. Control Surfaces

In the preceding sections methods have been discussed for calculating flight loads on the wings, flight balancing loads on the tail surfaces and the inertia (or dead weight) factors to be applied to all the weights in the airplane to satisfy the equations of equilibrium $\Sigma V = 0$, $\Sigma H = 0$, and $\Sigma M = 0$. The balancing load on the tail was assumed to act at the 20 per cent point on the mean chord of the horizontal tail. In order

to design the tail surfaces it is still necessary to determine the proportion of load on elevator and stabilizer and the direction in which it acts on each. Further, the tail surfaces must be investigated for loads imposed by the pilot in maneuvering, for the effects of gusts in flight, and for the effects of gusts in any direction when the ship is parked or taxiing on the ground.

(a) **Balancing Loads in Flight.** The limit load acting on the horizontal tail surface is the maximum balancing load calculated from flight conditions I, II, III, IV, VII, or VIII. The distribution of load is according

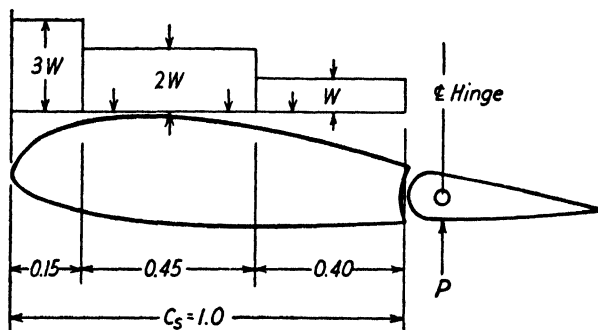


FIG. 2-10. Stabilizer load distribution.

to Fig. 2-10. The elevator load, P , is taken as 40 per cent of the total tail load, T , with the load directed opposite to that on the stabilizer. This means that the stabilizer load would be 140 per cent of the net tail load. However, there are cases where 40 per cent of the balancing load on the tail corresponds to an elevator load much higher than the pilot could apply. In such a case the limit load on the elevator, P , is reduced to that corresponding to 150 lb. exerted by the pilot on the controls. The load on the stabilizer is still $T + P$. (Note that there is no reduction of load on the stabilizer except that due to the reduction in load P on the elevator.)

Figure 2-10 represents the distribution of load on an average strip of chord of the horizontal surface.

For loads on the fixed surface,

$$w = \frac{\text{total load on fixed surface}}{1.75 \times \text{area of fixed surface}}$$

A constant value of C_N is assumed along the span. The above loading designs the forward portion of the stabilizer and the structure transmitting the stabilizer torque to the fuselage.

(b) **Maneuvering Loads.** Horizontal tails must also be designed for *limit* unit loads not less than those corresponding to pull-up speed V_p and the following normal force coefficients:

$$C_N = -0.55 \text{ downward}$$

$$C_N = +0.35 \text{ upward}$$

$$V_p = V_{sf} + K_p(V_L - V_{sf})$$

$$V_{sf} = \text{stalling speed with flaps down in miles per hour} \\ = 19.77(s/C_{L_{\max}})^{1/2}$$

$$C_{L_{\max}} = \text{maximum lift coefficient for the wing with flaps down}$$

$$V_L = \text{maximum level flight high speed in miles per hour}$$

$$K_p = 0.15 + \frac{5400}{W_g + 3300} \text{ but shall not be less than } 0.5$$

$$W_g = \text{gross design weight.}$$

The *average limit unit down load* over the entire surface is

$$-\bar{w} = -0.55q_p \text{ and the average limit up load } +\bar{w} = 0.35q_p.$$

$$q_p = 0.002558V_p^2 = \text{dynamic pressure at pull-up speed, } V_p \text{ in miles per hour.}$$

Where the unit loads obtained by the above equations give elevator torques in excess of those corresponding to a 200-lb. load on the controls

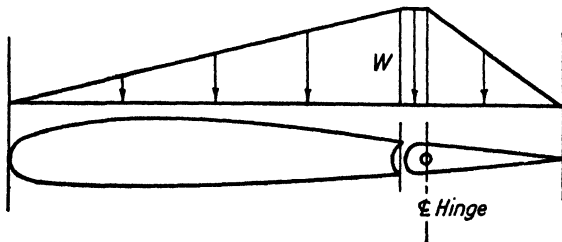


FIG. 2-11. Maneuvering load distribution.

in the cockpit they may be reduced to those which do correspond to the above control load, except in no case shall the average unit load be less than 15 lb. per sq. ft. The distribution for this loading condition is according to Fig. 2-11.

(c) **Effect of Tabs on Elevators.** When tabs are installed on the elevators, either to trim the ship or to aid the pilot in moving the surfaces, their effect must be accounted for. Under such conditions the minimum limit load over the entire horizontal surfaces shall not be less than that corresponding to the torque applied on the elevator when the pilot exerts

a force of 200 lb. in addition to the maximum aiding effect from the trim tab when fully deflected with relation to the elevator. When the tabs aid the pilots the loads are computed as follows:

1. Determine the normal coefficient, (C_N) for the *tab fully deflected*, assuming the deflection and angle of attack of the elevator to be zero. (See N.A.C.A. *Technical Report 360*.)

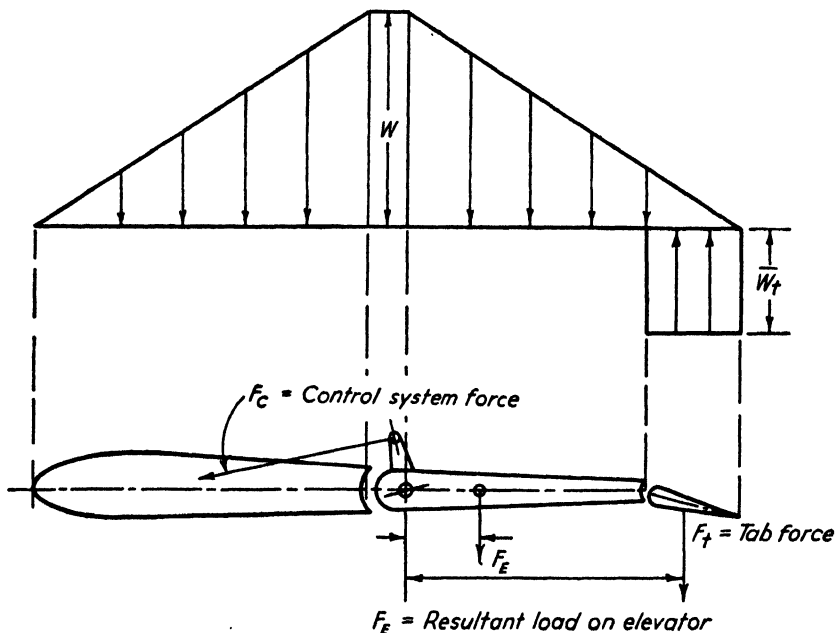


FIG. 2-12: Load distribution with tabs aiding the pilot.

2. Determine the applied unit load, w , on the tab corresponding to the normal force coefficient, C_N , and the high speed of the airplane in level flight, V_L .

$$w = C_N q L$$

The load distribution is assumed uniform over the tab.

3. Determine the loading which when distributed over the elevator in accordance with Fig. 2-12 will balance the sum of the hinge moments produced by the tab load and a force of 200 lb. applied by the pilot. The loading over the main surface aft of the hinge line is assumed triangular while that over the tab is uniform and in the opposite direction.

Figure 2-13 shows the loading over the elevator when the tab and elevator are deflected in the same direction. Because of the effect of the tab on the surface in front of it this condition will usually design the

ribs forward of the tab, and may be critical for the elevator torque member. The loads for this condition are obtained as follows:

1. For all portions of the movable surface except the area between the hinge line and the tab, assume the usual distribution of Fig. 2-11, with an unknown value of unit loading, w , at the hinge line.

2. For that portion of the movable surface included between the hinge line and the trailing edge of the tab, assume a uniform distribution. The unit load is w , the same value as at the hinge line.

3. Compute the moment about the main hinge line in terms of w , and equate this value to the moment produced by a 200-lb. load applied in the cockpit by the pilot, to solve for the unknown value of w .

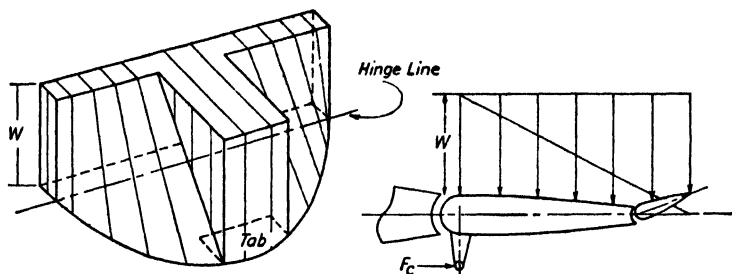


FIG. 2-13. Load distribution with tabs opposing the pilot.

Note: All the foregoing values have been given in terms of *limit* loads. *Design* loads are 1.5 times *limit* loads.

(d) Vertical Tail Surfaces. (1) *Maneuvering loads.* When the propeller axes are in the plane of symmetry the vertical surfaces are designed for an average normal force coefficient, $C_N = 0.45$ and for speed, V_p ; hence the average $\bar{w} = 0.45q_p$. The load distribution is the same as that of Fig. 2-11.

If the *propeller axes are not in the plane of symmetry* the vertical surfaces must be investigated for the following conditions: (a) The design speed shall not be less than the maximum speed in level flight with any engine inoperative. (b) The *limit* load need not be greater than that corresponding to a 200-lb. force applied by the pilot except that in no case may it be less than 12 lb. per sq. ft.

(2) *Flight gust on vertical tail.* The following gust condition shall be assumed for the vertical tail:

Gust speed $U = 30$ f.p.s.

Flight speed $= V_L$ (same as Condition I for wing)

Average $\bar{w} = UV_L m / 575$ where m is the slope of the lift curve for vertical surface. [The units of m must be C_L per radian corrected for aspect ratio.]

An aspect ratio of at least two shall be used. If m for the vertical surfaces is not available from wind tunnel tests the following approximate formula may be used:

$$\bar{w} = 0.226V_L \left(\frac{4}{3 + 6/\mathcal{R}} \right)$$

where $V_L = \text{m.p.h.}$

$\mathcal{R} = \text{aspect ratio (not less than 2)}$

The gust condition applies only to that portion of the vertical surface which has a well-defined leading edge.

The chord distribution shall be that for a symmetrical airfoil where data are available. The distribution in Fig. 2·12 may be used for the fin where desired.

(3) *Tabs on the rudder.* When the propeller axes are in the plane of symmetry the loads on the surfaces are such as to balance the load from a maximum tab deflection at speed V_L with no force applied by the pilot.

If the propeller axes are not in the plane of symmetry the loads are such as to balance the effect of a 200-lb. force applied by the pilot, plus the effect of maximum tab deflection, not at the speed V_L , but at a reduced speed V'_L , corresponding to the maximum speed in level flight with one engine inoperative. V'_L may be determined by the approximate formula $V'_L = 0.9V_L(1 - 1/n)^{1/2}$, where n is the number of engines.

Loads are distributed along the chord in the same manner as for the horizontal surfaces. See Figs. 2·12 and 2·13.

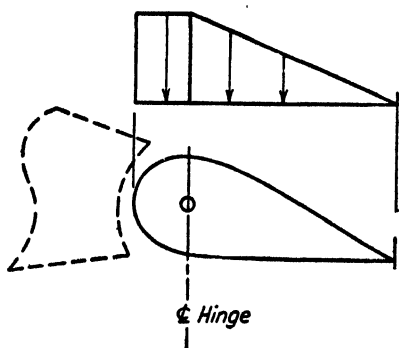


FIG. 2·14. Aileron load distribution.

(e) **Ailerons.** Ailerons are investigated for the following conditions:

(1) *Maneuvering.* If the propeller axes are in the plane of symmetry the ailerons are designed for a normal force coefficient, $C_N = 0.45$ at the pull-up speed V_p .

Then the *limit* average loading $\bar{w} = 0.45q_p$

The distribution is according to Fig. 2·14 which applies for all aileron loading conditions. If the *propeller axes are not in the plane of symmetry*,

the design speed shall not be less than the maximum speed in level flight with one engine inoperative.

The limit unit load in either direction need not exceed that corresponding to an 80-lb. force acting at the stick (or an 80-lb. force acting at the

rim of a control wheel) considered to be resisted by one aileron only, except that in no case shall it be lower than 12 lb. per sq. ft.

(2) *Tab effects.* Only those airplanes with propeller axes not in the plane of symmetry need be checked for the effect of tabs. When a tab is installed on one or both ailerons so that it can be used by the pilot to assist in moving the ailerons, the limit unit loading over both ailerons shall be of sufficient magnitude and in such a direction as to hold the ailerons in equilibrium with the tab or tabs deflected to their maximum throw. For this condition the loads on the tabs are computed at maximum level flight speed with one engine inoperative.

(3) *Flying conditions.* We must not lose sight of the fact that the ailerons are also part of the wing area. They must therefore be checked to insure that they meet all the requirements of the symmetrical load conditions for the wings. To check this condition reference is made to plots of chordwise distribution of pressure for the airfoil. The chordwise distribution varies with the angle of attack and is available in N.A.C.A. Reports as a plot of p/q against C_L .

Values of C_L and q are taken from the wing flight conditions. Having these values the pressure across the aileron is obtained. These values are *limit* values. As in all conditions described the design values are 1.5 times those obtained from the basic data.

(f) **Wing Flaps.** Flaps are designed for Conditions VII and VIII described in section 2-1. The minimum design speed V_f is $2V_{sf}$ (twice the stalling speed with flaps down).

The distribution of load over the flap is assumed uniform unless wind tunnel data are available to show the actual distribution. For aileron type flaps the normal force coefficients may be taken from reference 2-3. For split flaps for which the upper portion is a fixed part of the wing, the value of C_N may be obtained from the empirical relation

$$C_N = 0.273 + 0.021\gamma$$

where γ is the flap opening in degrees. Where no data on C_N are available it is assumed to be 1.60, which is a very conservative value.

(g) **Control-Surface Tabs.** The loads previously given for control-surface tabs are for the purpose of designing the surfaces to which they are attached. Actually the tabs themselves may carry higher loads when they are partially deflected at higher speeds. For design of the tabs only all usable combinations of speed and tab deflection up to the design speed V_g must be considered. The loads are considered to be uniformly distributed.

(h) **Effect of Horizontal Ground Gusts.** For large airplanes it has been found that the most severe loads on the tail surfaces may be

encountered when the airplane is parked on the ground or taxiing in a cross wind. For large airplanes, in addition to the Civil Aeronautics Authority requirements it is good practice to assume that the tail surfaces may have to withstand a ground gust up to 60-m.p.h. velocity applied in any direction up to 30 degrees from either side for the elevator, or up to 45 degrees from either side for the rudder. An approximate solution is as follows:

1. Assume that the trailing edge of the movable surface is the leading edge of a rectangular flat plate, that the surfaces are locked in neutral, and that the wind may come from the rear at any angle up to those noted in the preceding paragraph.

2. Take the normal force coefficient and center of pressure data from Fig. 11-12, p. 11:11 of reference 4.

3. Calculate the average normal force at the value of C_N for the maximum angle of attack (30 degrees for elevator, 45 degrees for rudder). Values of C_N are 0.895 at 30 degrees and 1.30 at 45 degrees.

It will be noted that the center of pressure lies between 34 and 35 per cent in the range from 30 to 45 degrees angle of attack. It is therefore assumed that the distribution is triangular over the entire tail surface with the maximum value at the trailing edge.

$$\text{Average } \bar{w} = C_N q, \text{ where } q = 0.002558 \times 60^2$$

$$\text{Maximum } w \text{ at trailing edge} = 2 \times \bar{w}$$

The values given above are *limit* loads. Design loads are 1.5 times the above values.

2-5. Landing Conditions

In addition to the flight loads it is necessary to consider the effects of landing loads on the airplane's structure. An infinite number of landing attitudes are possible; however, for purposes of analysis a limited number of attitudes, which are so designed as to give the most severe condition for the possible range of landing attitudes, are investigated. The main landing conditions, for a conventional tail-wheel gear, which must be considered are level landing, three-point landing, side-drift landing, one-wheel landing, and landing with brakes.

For a landing with zero angle of roll, two attitudes are investigated, namely, level landing in which the resultant of the ground reactions passes through the center of gravity with the thrust axis horizontal, and the three-point landing condition, i.e., the wheels and tail wheel strike the ground simultaneously. These conditions are assumed to cover the complete range for the following reasons:

1. If the resultant of the ground reaction lies aft of the center of gravity, the airplane will "nose over."

2. If the tail wheel strikes the ground first the ground reaction will produce a rotation causing the wheels to touch before the reaction on the tail wheel can fully develop.

The nosing-over condition is considered somewhat irregular and is consequently covered by special requirements which assume that damage to the airplane is unavoidable. However, the requirements provide for a structure of sufficient strength to prevent serious injury to the crew and passengers.

In the three-point landing attitude it is also necessary to consider the case in which the pilot lands with brakes on.

If the angle of roll is not zero, the limiting conditions are:

1. A three-point landing attitude with a side, rearward, and vertical reaction component acting on one wheel only. Each component being of the magnitude nW , where n is specified in CAR 04, and W is the gross weight. Assuming all forces to be acting on one wheel means that the airplane is in the three-point landing attitude with one wheel and tail wheel just off the ground.

2. An attitude in which the propeller axis is horizontal and all reaction forces act on one wheel. The vertical component is nW , the side component is zero, and the rearward component is such as to cause the resultant of the ground reaction to pass through the center of gravity. These two conditions cover the range in which the angle of roll is not zero.

Airplanes with a nose-wheel-type landing gear are investigated for the following landing conditions:

1. Three-wheel landing with vertical reactions
2. Three-wheel landing with inclined reactions
3. Two-wheel landing with vertical reactions—nose up
4. Two-wheel landing with inclined reactions—nose down
5. Two-wheel landing with brakes—nose down
6. Side-drift landing
7. Side-drift landing with brakes
8. One-wheel landing

These conditions represent for a nose-wheel-type gear the possible critical attitudes in which the airplane may be landed. A detailed discussion of these landing conditions is given in the Civil Aeronautics Authority bulletins CAR 04 and CAM 04.

The reaction forces are caused by upward accelerations, for, at the instant the airplane touches the ground it has a vertical and horizontal component of velocity. The vertical component in particular becomes

zero during a very short interval of time which indicates the existence of an upward acceleration and consequently a downward inertia force. The magnitude of the acceleration forces depends upon the weight of the airplane, the magnitude of the vertical component of velocity, and the efficiency of the shock absorbing unit in prolonging the period of upward acceleration. The lift forces on the wings and tail surfaces are small and are conservatively neglected.

2-6. Summary of Loads and Loading Conditions

In sections 2-1 to 2-5 we have discussed the loads and load factors for which the airplane's structure must be designed. The next step in the design procedure is to calculate the shears, bending moments, and torsional moments acting on the wings, tail surfaces and the fuselage. Since the distributed external loads are in general not uniform, a semi-graphical method of integration gives the most convenient method of calculation. Calculating the shears and bending moments on the tail surfaces and fuselage offers no difficulty for the external loads are either concentrated or distributed loads in pounds per unit area. The wing calculations are discussed below.

(a) **Wing—Shears and Moments.** The normal shears and bending moments acting on the wing structure can be considered as due to two sources, namely, the aerodynamic forces and the dead weight items. The latter include the structural weight of the wings and the weights of such items as are either attached to or housed in the wing structure. Because the load factors for the air forces are not the same as those for the dead weight items it is necessary to calculate the design shears and moments due to each source separately.

Consider a wing plan form as indicated in Fig. 2-15a with a corresponding C_N distribution as shown in Fig. 2-15b. Dividing the span into a convenient number of elements, we can represent the total lifting force acting on one span by an equation of the form

$$L = q \sum_{i=1}^{i=n} \bar{C}_{N_i} \bar{c}_i \Delta b_i \quad [2-8]$$

where the summation extends over one-half span and

\bar{C}_{N_i} = mean value of C_N over the increment of span Δb_i ,
 \bar{c}_i = mean chord length over the increment of span Δb_i .

Now the air-load shear, S_{k+1} , at any station b_{k+1} is equal to the total

lifting force acting on the wing outboard of this station, and is given by the equation

$$S_{k+1} = q \sum_{i=1}^{i=k} \bar{C}_{N_i} \bar{c}_i \Delta b_i \quad [2.9]$$

It is convenient first to calculate the air-load shears and moments for a unit load factor, generally referred to as the *basic* air-load shears and

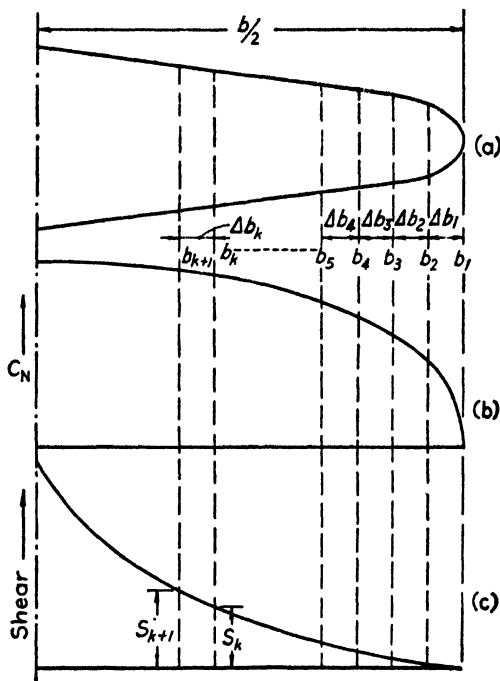


FIG. 2-15. Determination of air-load shear curve.

moments. The air-load shears and moments for any one of the flight conditions can then be obtained by merely multiplying the basic air loads by the appropriate load factor. The given C_N curve will be for an arbitrary value of q , which is not necessarily the value which satisfies the condition that for a unit load factor the total lifting force equals the weight of the airplane. Since the C_N distribution is assumed to be the same for all values of q , the value of q' which satisfies the above condition can be obtained by equation 2.8, namely:

$$q' = \frac{L}{\sum_{i=1}^{i=n} \bar{C}_{N_i} \bar{c}_i \Delta b_i} = \frac{W/2}{\sum_{i=1}^{i=n} \bar{C}_{N_i} \bar{c}_i \Delta b_i} \quad [2.10]$$

Substituting the value of q' for q in equation 2.9 the basic air-load shear at any station can be calculated.

The normal bending moment, M_{k+1} , at any station b_{k+1} is equal to the area under the shear curve to the right of this station and can be expressed as

$$M_{k+1} = \sum_{i=1}^{i=k} \left(\frac{S_{i+1} + S_i}{2} \right) \Delta b_i \quad [2.11]$$

This equation gives the basic air-load bending moment at any station. The design shear or bending moment due to the air loads can be obtained from the calculated basic shear and bending moment values by multiply-

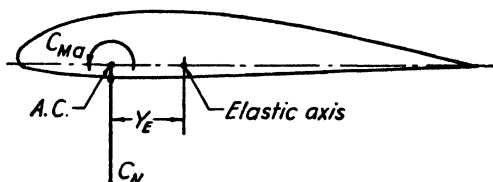


FIG. 2.16. Forces and moments causing wing torsion.

ing by the appropriate load factor for the particular condition which is being investigated.

The shears and moments due to the dead weight items are also calculated for a unit load factor. The design values are obtained by multiplying by the appropriate *net* load factor. The actual design shears and bending moments will be the algebraic sum of the air load and the dead weight design shears and bending moments. Since the inertia forces of the dead weight items oppose the aerodynamic forces the signs of the dead weight shears and bending moments will be opposite to those due to the aerodynamic forces.

The above methods of calculation would be exact if the variation of the chord width, the C_N distribution and the shear were linear between two consecutive stations. This will in general not be true for C_N , the shear, and for the chord near the wing tips. The deviation from a linear variation will in general be small, and if the stations are taken reasonably close together the results will be sufficiently accurate for practical purposes.

The torsional moments can also be considered as being due to aerodynamic forces and dead weight items. The aerodynamic forces acting on the wing are as shown in Fig. 2.16, where C_{M_a} is the moment coefficient about the aerodynamic center. Let us first consider the torsional moments, due to these forces, in a plane parallel to the longitudinal

axis of the airplane and about an axis which coincides with the locus of the aerodynamic centers.

Consider an element of area ΔS_i a distance x_i from station b_k , as shown in Fig. 2-17. The torsional moment at this station due to the air forces acting on ΔS_i is

$$\Delta M_{T_k} = C_{M_a} q \Delta S_i \bar{c}_i - C_N q \Delta S_i y_i \quad [2.12]$$

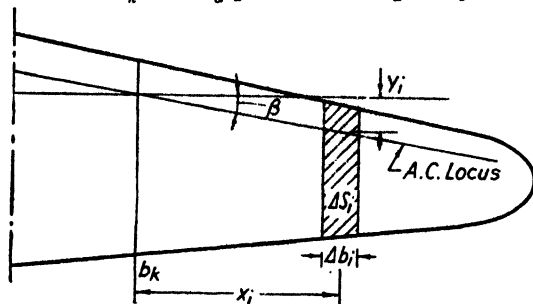


FIG. 2-17.

If the angle between the locus of the aerodynamic centers and the perpendicular to the longitudinal axis of the airplane is assumed constant and equal to β then,

$$y_i = x_i \tan \beta$$

Substituting this value of y_i in equation 2.12 gives

$$\Delta M_{T_k} = C_{M_a} q \Delta S_i \bar{c}_i - C_N q \Delta S_i x_i \tan \beta$$

and the torsional moment at station b_k due to the air forces on the surface to the right of this station is

$$M_{T_k} = C_{M_a} q \sum_{i=1}^{i=k} \Delta S_i \bar{c}_i - q \tan \beta \sum_{i=1}^{i=k} \bar{C}_{N_i} \Delta S_i x_i \quad [2.13]$$

Now the expression

$$q \sum_{i=1}^{i=k} \bar{C}_{N_i} \Delta S_i x_i$$

is just equal to the air-load bending M_k at the station b_k , hence we can write

$$M_{T_k} = C_{M_a} q \sum_{i=1}^{i=k} \Delta S_i \bar{c}_i - M_k \tan \beta \quad [2.14]$$

where M_{T_k} will be the design torsional moment due to the air forces if q and M_k are design values.

Since the weight and positions of all dead weight items will be known and also the design net load factors, the design torsional moments due to these items can be readily calculated. The actual design torsional moments will be the algebraic sum of the air load and dead weight torsional moments.

In the analysis of the shear stresses due to torsion it is necessary to calculate the torsional moments about the elastic axis of the wing, i.e., the locus of the shear centers of the wing cross sections. However, the elastic axis will not be known until the wing structure is designed and, furthermore, its position changes with a change in wing structure. It is, therefore, desirable first to calculate the torsional moments about a fixed axis, which is not dependent on the wing structure. The torsional moments can then later be transferred to the elastic axis. For example, if at the station b_k the elastic axis is a distance y_E (Fig. 2-16) aft of the aerodynamic center, the actual design torsional moment about the elastic axis will be

$$M_T = M_{T_k} + S_k y_E \quad [2-15]$$

where M_{T_k} and S_k are the actual design values due to the aerodynamic forces and the dead weight items.

(b) Margins of Safety. In the strength calculations of the airplane's structure it is necessary to have some standard method by which it will be possible to express quantitatively the relation between the load which will be imposed upon a given structural element and the amount it is capable of carrying safely. In airplane design it is customary to express the relation by means of a margin of safety which is defined as

$$\text{M.S.} = \frac{\text{Allowable load}}{\text{Actual load}} - 1$$

or

$$\text{M.S.} = \frac{\text{Allowable stress}}{\text{Actual stress}} - 1$$

In determining margins of safety it is necessary to have a clear understanding of what is meant by allowable load or stress. It simply means that it is the ultimate load to which the particular element can be subjected, as, for example:

1. If buckling is the design criteria, then the buckling load is the ultimate load, i.e., the allowable load on a column is the load which causes buckling.

2. If the load is pure tension, the allowable load is the ultimate tensile load or the load corresponding to the yield point stress, depending on the design condition.

3. If the load is pure shear the same conditions as in 2 apply.

4. For cases of combined loading, i.e., shear plus compression, or shear plus tension, the ultimate load is either the buckling load, if buckling is the design criteria, or the ultimate load which the material can carry under the combined loading conditions.

The Civil Aeronautics Authority in "Strength of Aircraft Elements," ANC-5, specifies that at the *limit load* factor the stress shall not exceed the yield point of the material. Hence, for a material in which the yield point stress is less than two-thirds of the ultimate stress the allowable stress would be the yield point stress and the actual stress would be that corresponding to the *limit load* factor. If the yield point stress is greater than two-thirds of the ultimate stress the margin of safety would be based on the ultimate stress and design load factor. In addition to the above requirement, certain minimum margins of safety are specified. All castings must show a 100 per cent margin; all fittings, 20 per cent; all parts subjected to shock loads, 100 per cent; and for aluminum alloys and steel parts in bearing subjected to reversed stresses, a 50 per cent margin. The Army and Navy have their own requirements for minimum margins.

REFERENCES FOR CHAPTER 2

- 2-1. *Civil Air Regulations*, Part 04.
- 2-2. *Civil Aeronautics Manual* 04.
- 2-3. E. N. JACOBS and R. M. PINKERTON, "Pressure Distribution over a Symmetrical Airfoil Section with Trailing Edge Flap," *N.A.C.A. Tech. Rep.* 360.
- 2-4. K. D. WOOD, *Technical Aerodynamics*, McGraw-Hill, 1935.

PART II
METHODS OF STRUCTURAL ANALYSIS

CHAPTER 3

STRESS-STRAIN RELATIONSHIPS FOR STABLE STRUCTURES

3-1. Fundamental Considerations

The first problem confronting an engineer who is designing a load-carrying structure is the determination of the actual loads acting on the various component parts of that structure. The second problem is that of determining the loads which these component parts can carry without exceeding certain limiting criteria. These criteria may be (a) the amount of load causing failure or complete collapse of the part; (b) the amount of load which will cause the part to deform permanently; (c) the amount of load possible before the part will deflect a certain limiting amount. The first problem, that of determining the loads on an airplane structure, has been discussed in Part I; the second problem will form the basis for Part II.

(a) Stress. It is obvious that load alone is not a good criterion for determining the strength of a structural element for, if the part is large in cross section, physical reasoning tells us that it will carry a greater load than a similar, but smaller, member. The strength properties are then in some way connected with the applied load and the cross-sectional area of the member. The simplest form of this relationship can be seen in the case of a vertical, hanging member carrying a weight, P . (See Fig. 3-1a.) If we make a cut through the member perpendicular to the direction of the applied load P , such as section $A-A$, and assume that the cross-sectional area of the member at this section is A , then we can define a value σ such that

$$\sigma = \frac{P}{A} \qquad [3.1]$$

The value σ is known as the *normal stress* in the rod due to the load P . The term normal stress arises from the fact that the two portions of the

member could be held together by tension links which act perpendicular to the cut surface (see Fig. 3·1b).

It is frequently the naive assumption of engineers that the above equation giving the value of the normal stress in a tension member indicates the only stress which might cause failure. A little study will show that through any given point in a loaded body there are an infinite number of possible stresses and that it is possible to define completely only the stress at a point relative to a given plane of reference. In mathematical language this means that a stress is a tensor quantity which, to be completely defined, must have given the magnitude, direction, and a plane of reference as compared to a vector quantity which is completely determined if the magnitude and direction are specified.

To illustrate this point further, let us consider a cross section $B-B$ through the tension member. Now if, as in Fig. 3·1c, tension links are

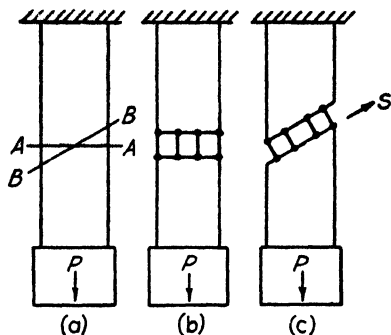


FIG. 3·1.

placed perpendicular to the cut surface, it is immediately apparent that

the relative position of the upper and lower portions will change unless an additional force, S , is brought into play. Thus, we have in addition to the normal forces acting perpendicular to the surface $B-B$, a force acting parallel to this surface. This is known as a *shear force* and, again it is referred to the area over which it acts giving rise to a *shearing stress*.

$$\tau = \frac{S}{A} \quad [3\cdot2]$$

where A in this case is the cross-sectional area of a section through the member parallel to the plane $B-B$.

The normal stress in the example above is known as a *tensile stress* since the forces necessary to keep the cross sections together are tension forces. If the picture were inverted, in other words, if the member were supporting a dead weight P acting on top of it, then the normal stress would be known as a *compressive stress*, and the direction of the shear force S for any cross section would be reversed.

Certain relationships between the various stresses can be determined by the conditions of equilibrium of an element of a loaded member. Consider a unit element with the coordinate system indicated in Fig.

3.2a. Now consider the stresses acting parallel to the XY -plane (Fig. 3.2b). We see that there are two normal stresses σ_x and σ_y and two shearing stresses τ_{xy} and τ_{yx} . From the condition that the element must be in equilibrium we can say that

$$\tau_{xy} = \tau_{yx} \quad [3.3]$$

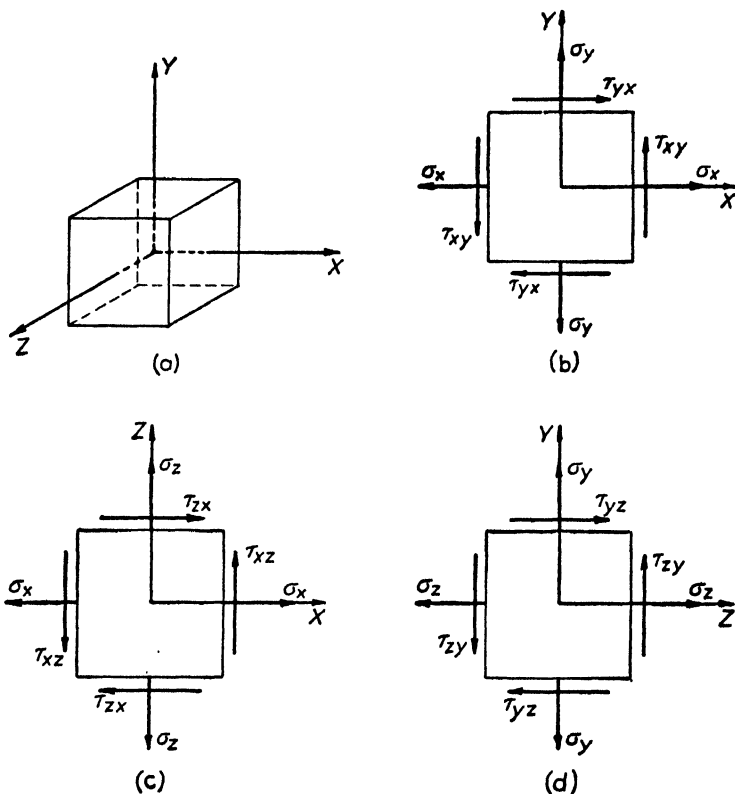


FIG. 3.2. Coordinate axes for stresses.

Similarly (Fig. 3.2c and Fig. 3.2d),

$$\tau_{xz} = \tau_{zx} \quad [3.4]$$

$$\tau_{yz} = \tau_{zy} \quad [3.5]$$

So that, for the complete three-dimensional case we see that there are a total of six possible stresses which can act in any element. These are:

σ_x = normal stress acting parallel to the X -axis.

σ_y = normal stress acting parallel to the Y -axis.

σ_z = normal stress acting parallel to the Z -axis.

τ_{xy} = shearing stress acting on the face of the element which is perpendicular to the X -axis; the direction of this stress being parallel to the Y -axis. It also refers to an equal stress acting on the face of the element which is perpendicular to the Y -axis, the stress acting parallel to the X -axis.

τ_{yz} = shearing stress referred to the YZ -plane and defined similarly to that above.

τ_{zx} = shearing stress referred to the XZ -plane.

If now we have such a system of stresses referred to a given set of orthogonal axes, the question arises as to what the stresses will be if

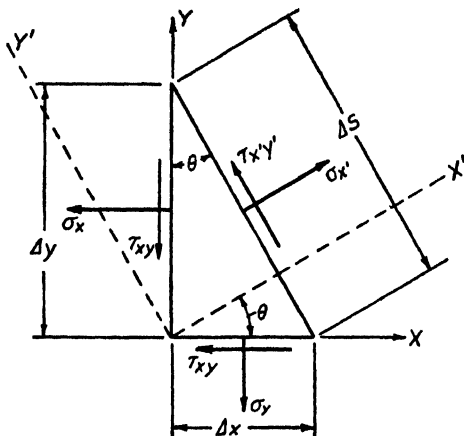


FIG. 3-3. Transfer of stress axes.

referred to a plane at an angle θ to one of the axes. Consider a cross section parallel to the XY -plane with stresses σ_x , σ_y , and τ_{xy} , and assume it is desired to determine the stresses acting on a surface which makes an angle θ with the Y -axis. See Fig. 3-3. Consider the element to be of unit thickness and let the dimensions of the cross section be as indicated. Then, since a force is equal to the stress times the cross-sectional area over which it acts, we can write the equilibrium conditions of the element as follows:

$$\sigma_{x'} \Delta s = \sigma_x \Delta y \cos \theta + \sigma_y \Delta x \sin \theta + \tau_{xy} \Delta y \sin \theta + \tau_{xy} \Delta x \cos \theta \quad [3.6]$$

$$\tau_{x'y'} \Delta s = -\sigma_x \Delta y \sin \theta + \sigma_y \Delta x \cos \theta + \tau_{xy} \Delta y \cos \theta - \tau_{xy} \Delta x \sin \theta \quad [3.7]$$

since

$$\Delta y / \Delta s = \cos \theta \quad \text{and} \quad \Delta x / \Delta s = \sin \theta$$

$$\sigma_{x'} = \sigma_x \cos^2 \theta + \sigma_y \sin^2 \theta + 2\tau_{xy} \sin \theta \cos \theta$$

$$\tau_{x'y'} = (-\sigma_x + \sigma_y) \sin \theta \cos \theta + \tau_{xy} (\cos^2 \theta - \sin^2 \theta)$$

By considering a section perpendicular to the Y' -axis it can also be shown that

$$\sigma_{y'} = \sigma_x \sin^2 \theta + \sigma_y \cos^2 \theta + 2\tau_{xy} \sin \theta \cos \theta$$

These equations may be written in the form

$$\sigma_{x'} = \frac{\sigma_x + \sigma_y}{2} + \frac{\sigma_x - \sigma_y}{2} \cos 2\theta + \tau_{xy} \sin 2\theta \quad [3.8]$$

$$\sigma_{y'} = \frac{\sigma_x + \sigma_y}{2} + \frac{\sigma_y - \sigma_x}{2} \cos 2\theta + \tau_{xy} \sin 2\theta \quad [3.9]$$

$$\tau_{x'y'} = -\frac{\sigma_x - \sigma_y}{2} \sin 2\theta + \tau_{xy} \cos 2\theta \quad [3.10]$$

The angle θ at which the shear stress $\tau_{x'y'}$ is zero is given by the equation

$$\tan 2\theta = \frac{2\tau_{xy}}{\sigma_x - \sigma_y} \quad [3.11]$$

Now, since $\tan 2\theta = \tan 2(\theta + 90^\circ)$, we see that two perpendicular directions can be found for which the shearing stress is zero. These directions are called *principal directions* and the corresponding normal stresses, *principal stresses*. If we designate the principal stresses by σ_1 and σ_2 and substitute

$$\sigma_1 = \sigma_{x'} \quad \sigma_2 = \sigma_{y'} \quad \tau_{x'y'} = 0$$

into equations 3.8 to 3.10 inclusive using the relationship of equation 3.11, we obtain

$$\sigma_1 = \frac{\sigma_x + \sigma_y}{2} + \sqrt{\frac{(\sigma_x - \sigma_y)^2}{4} + \tau_{xy}^2} \quad [3.12]$$

$$\sigma_2 = \frac{\sigma_x + \sigma_y}{2} - \sqrt{\frac{(\sigma_x - \sigma_y)^2}{4} + \tau_{xy}^2} \quad [3.13]$$

If, in equation 3.10 we set $\sigma_x = \sigma_1$, $\sigma_y = \sigma_2$, and $\tau_{xy} = 0$, it is easily seen that the absolute value of the maximum shear is equal to

$$|\tau_{\max}| = \frac{|\sigma_1 - \sigma_2|}{2} \quad [3.14]$$

The above relationships can be shown graphically by what is known as *Mohr's circle*. See Fig. 3.4. Let us assume that on a given cross

section of a stressed element there are acting the stresses σ_x , σ_y , and τ_{xy} . On a set of orthogonal axes representing normal and shearing stresses lay off σ_x and τ_{xy} , locating point A . Similarly locate point B by laying off σ_y and τ_{xy} . Then pass a circle having its origin on the σ -axis through points A and B . Any diameter of this circle now represents the complete stress picture of a given plane in the stressed member. For example, at an angle θ from the original plane, we find the position where the shearing stress is zero, and the only stresses acting are the principal stresses. Likewise, 45 degrees from this position we find the position where the value of the shearing force is a maximum, and has the value

$$\tau_{\max} = \frac{\sigma_1 - \sigma_2}{2}$$

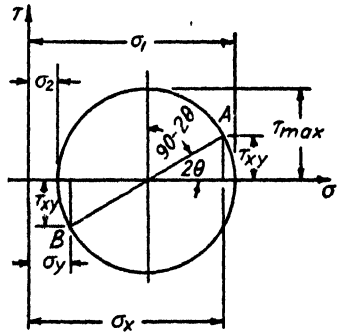


FIG. 3-4. Mohr's stress circle.

Example. Consider an element of a stressed member which, analysis shows, is subjected to the stresses shown in Fig. 3-5a. A rectangular set of axes representing σ and τ are drawn (the same scale must be used for both axes) and points A and B

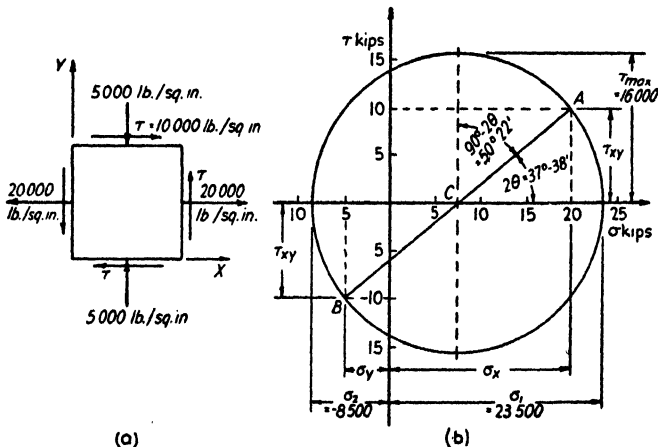


FIG. 3-5. Mohr's circle analysis.

are located from the known values of σ_x , σ_y , and τ_{xy} . (See Fig. 3-5b.) The value of σ_y is laid off as a negative value since it is a compression stress. A line is drawn between A and B , intersecting the axis at C . Using C as a center and CA as a radius, a circle is drawn which is the Mohr's circle for the given stress state. From this can be seen that at an angle $\theta = 18^\circ 49'$ from the original element axes there are

principal stresses of 23,500 lb. per sq. in. and -8500 lb. per sq. in., respectively. At 45 degrees to the direction of the principal stresses there will be found the maximum shear stress, in this case equal to 16,000 lb. per sq. in.

The above discussion has been based on the assumption that the stress field was uniform throughout the part under consideration. In most structural and machine design members this is not true and the stress varies from point to point in the member. We will now study the effect of this variation in the equilibrium conditions of an element and will discuss only the two-dimensional case since the equations for

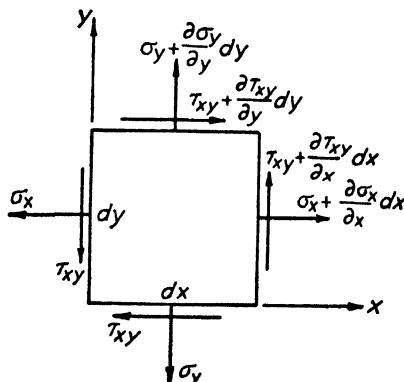


FIG. 3-6. Equilibrium diagram.

the three-dimensional problem can be derived by analogy. Consider the element shown in Fig. 3-6 in which the stresses vary as one progresses from one side of the element to the other. Writing the equilibrium equation for the forces in the X -direction we get

$$\left(\sigma_x + \frac{\partial \sigma_x}{\partial x} dx \right) dy - \sigma_x dy + \left(\tau_{xy} + \frac{\partial \tau_{xy}}{\partial y} dy \right) dx - \tau_{xy} dx = 0$$

which reduces to

$$\frac{\partial \sigma_x}{\partial x} + \frac{\partial \tau_{xy}}{\partial y} = 0 \quad [3 \cdot 15]$$

Similarly, for the forces in the Y -direction

$$\frac{\partial \tau_{xy}}{\partial x} + \frac{\partial \sigma_y}{\partial y} = 0 \quad [3 \cdot 16]$$

Equations 3-15 and 3-16 are known as the *equations of equilibrium* in two dimensions.

For the general three-dimensional case, it can be shown that the equations of equilibrium are

$$\begin{aligned}\frac{\partial \sigma_x}{\partial x} + \frac{\partial \tau_{xy}}{\partial y} + \frac{\partial \tau_{xz}}{\partial z} &= 0 \\ \frac{\partial \tau_{xy}}{\partial x} + \frac{\partial \sigma_y}{\partial y} + \frac{\partial \tau_{yz}}{\partial z} &= 0 \\ \frac{\partial \tau_{xz}}{\partial x} + \frac{\partial \tau_{yz}}{\partial y} + \frac{\partial \sigma_z}{\partial z} &= 0\end{aligned}\quad [3 \cdot 17]$$

Any stress state in an elastic body must satisfy these equilibrium equations but, as will be shown later, satisfying the equilibrium equations is not always sufficient because, as yet, no deformation considerations have entered the analysis.

(b) Strain. If a material such as rubber is subjected to a tensile or a compressive load, it is immediately obvious that it deflects in the direction of the applied load. The same is true of all materials although for those materials used in construction, the deformations are so small they can only be measured with very sensitive instruments.

For a member of length L , subjected to a load P , the deformation is, up to a certain limit, directly proportional to the load. The *unit strain*, that is, the deformation per unit length is then given by

$$\epsilon = \frac{e}{L} = K \frac{P}{A} = K\sigma \quad [3 \cdot 18]$$

where ϵ = unit strain in inches per inch in the direction of the applied load

e = total deformation in the length L

K = a constant which is a function of the material

The constant K is usually written in the form $1/E$ where E is known as the *Young's modulus* or *modulus of elasticity* of the material, and equation 3.18 becomes

$$\epsilon = \frac{\sigma}{E} = \frac{P}{AE} \quad [3 \cdot 19]$$

Similarly, to a shearing stress there is related a shearing strain which is given by an angle, since the shearing stress will tend to distort the sides of any rectangular element as in Fig. 3.7. Again, up to a certain limiting

value, the shearing strain is proportional to the shearing stress and the equation is of the form

$$\gamma = \frac{\tau}{G} = \frac{S}{AG} \quad [3 \cdot 20]$$

where γ = unit shearing strain

S = shearing force

τ = shearing stress

G = shearing modulus which is a constant for any material below a certain stress limit

Let us return to the consideration of rubber. Since its deformations under load are large enough to be visible, if a block of rubber is com-

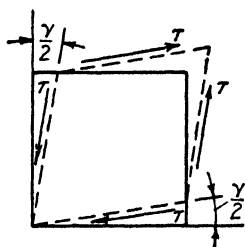


FIG. 3-7. Shear strain.

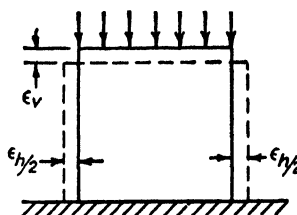


FIG. 3-8. Normal strain.

pressed by a vertical load, it will not only shorten in the direction of the applied load but it will also tend to expand in the horizontal direction. (See Fig. 3-8.) The ratio of the two unit deformations is known as *Poisson's ratio* or

$$\frac{\epsilon_h}{\epsilon_v} = \mu \quad [3 \cdot 21]$$

where ϵ_h = total horizontal deformation divided by the width of the specimen

ϵ_v = total vertical deformation divided by the length of the specimen

Considering now the completely general case of the unit cube acted upon by the six possible stresses $\sigma_x, \sigma_y, \sigma_z, \tau_{xy}, \tau_{yz}, \tau_{zx}$, the general stress-strain relationships can be shown to be of the form

$$\begin{aligned} \epsilon_x &= \frac{1}{E} [\sigma_x - \mu(\sigma_y + \sigma_z)] \\ \epsilon_y &= \frac{1}{E} [\sigma_y - \mu(\sigma_x + \sigma_z)] \end{aligned} \quad [3 \cdot 22]$$

$$\epsilon_z = \frac{1}{E} [\sigma_z - \mu(\sigma_y + \sigma_x)]$$

$$\gamma_{xy} = \frac{\tau_{xy}}{G}, \quad \gamma_{yz} = \frac{\tau_{yz}}{G}, \quad \gamma_{zx} = \frac{\tau_{zx}}{G} \quad [3.23]$$

In the above, the stresses are taken as positive when in the direction shown in Fig. 3.2.

Equations 3.22 and 3.23 are only true when the material is isotropic and homogeneous; however, most engineering structural materials, al-

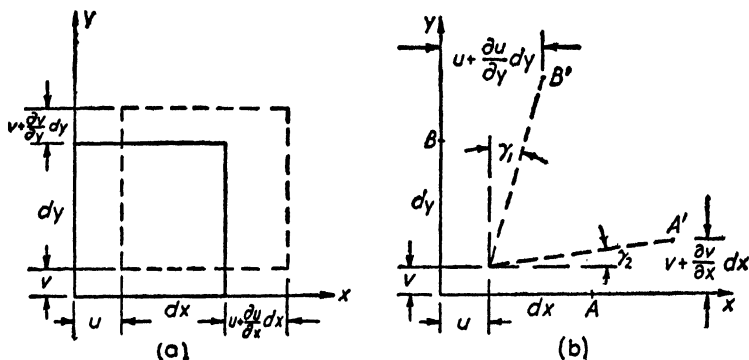


FIG. 3-9. Strain notation.

though made up of a mixture of crystalline elements satisfy these conditions sufficiently so that the equations may be used with negligible errors.

It would appear from equations 3.22 and 3.23 that there are three constants necessary to determine the stress-strain relationships of any given material, the Young's modulus, E ; the shear modulus, G ; and the Poisson's ratio, μ . It can be shown, however, that these are not mutually independent for any one can be expressed as a function of the other two by the equation,

$$G = \frac{E}{2(1 + \mu)} \quad [3.24]$$

With the use of equations 3.22 and 3.23 and the differential relationship between deformation and unit strain it is possible to determine another set of equations which must be satisfied by any stress system in an elastic body. Since these equations essentially determine the fact that the deformations in any one element are compatible with the deformations in all adjacent elements, they are known as the *compatibility equations*.

Consider deformations u , v , w parallel to the X -, Y -, and Z -axes, respectively, then, if a two-dimensional element is subjected to σ_x and σ_y stresses it will deform as shown in Fig. 3.9a. The total change in length in the X -direction is

$$u + \frac{\partial u}{\partial x} dx - u = \frac{\partial u}{\partial x} dx$$

and the unit deformation ϵ_x is equal to the total deformation divided by the original length of the specimen; and similarly for ϵ_y and ϵ_z giving rise to the equations

$$\begin{aligned}\epsilon_x &= \frac{\partial u}{\partial x} \frac{dx}{dx} = \frac{\partial u}{\partial x} \\ \epsilon_y &= \frac{\partial v}{\partial y} \\ \epsilon_z &= \frac{\partial w}{\partial z}\end{aligned}\tag{3.25}$$

Now, if the element is considered to be acted upon by shear stresses in addition to the normal stresses shearing deformations as in Fig. 3.9b occur. Since all deformations are assumed small compared to the size of the element, we can write, neglecting second order terms

$$\gamma_1 = \frac{\partial u}{\partial y} \frac{dy}{dy} = \frac{\partial u}{\partial y}$$

and

$$\gamma_2 = \frac{\partial v}{\partial x} \frac{dx}{dx} = \frac{\partial v}{\partial x}$$

The total shearing strain in the XY -plane, γ_{xy} , is equal to $\gamma_1 + \gamma_2$ and using a similar analysis for the YZ - and the ZX -planes we can write

$$\begin{aligned}\gamma_{xy} &= \frac{\partial u}{\partial y} + \frac{\partial v}{\partial x} \\ \gamma_{yz} &= \frac{\partial v}{\partial z} + \frac{\partial w}{\partial y} \\ \gamma_{zx} &= \frac{\partial w}{\partial x} + \frac{\partial u}{\partial z}\end{aligned}\tag{3.26}$$

By performing suitable differentiations and combining, the six equations shown above may be reduced to three, namely,

$$\begin{aligned}\frac{\partial^2 \gamma_{xy}}{\partial x \partial y} &= \frac{\partial^2 \epsilon_x}{\partial y^2} + \frac{\partial^2 \epsilon_y}{\partial x^2} \\ \frac{\partial^2 \gamma_{yz}}{\partial y \partial z} &= \frac{\partial^2 \epsilon_y}{\partial z^2} + \frac{\partial^2 \epsilon_z}{\partial y^2} \\ \frac{\partial^2 \gamma_{zx}}{\partial z \partial x} &= \frac{\partial^2 \epsilon_z}{\partial x^2} + \frac{\partial^2 \epsilon_x}{\partial z^2}\end{aligned}\quad [3 \cdot 27]$$

By separately combining the stress-strain equations 3.22 with the equilibrium equations 3.17 and the compatibility equations 3.27, two sets of three equations may be obtained. One of these sets gives the relationships which must be satisfied by the stress and the other those which must be satisfied by the strains in order that any assumed stress or strain pattern fulfils all the requirements for validity in an elastic body.

For any problem in an actual structure there is one additional set of requirements that must be fulfilled. This consists of the stress and deformation conditions at the boundary of the body which must conform to the applied loads and external restraints of the specific problem. These conditions are known as the *boundary conditions* of the problem.

(c) **Stress-Strain Curves.** To determine the usefulness of any material for structural purposes, it is necessary to know the elastic properties of that material. These properties are determined by applying known loads to a sample of the material and measuring its elongation by means of suitable testing and measuring equipment. The simplest test is a tension test of the material in which a pure tensile load is applied to a specimen and the elongation of a given original length of the specimen is measured. If this elongation is divided by the length over which it has been measured, the unit elongation is obtained which can be plotted against the stress, or the load divided by the cross section of the specimen. We will now examine a few typical examples of such curves.

(1) *Soft iron.* The stress-strain curve for soft iron is similar to that shown in Fig. 3.10. It will be noticed that for low stresses, the unit

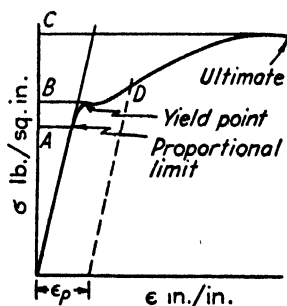


FIG. 3-10. Stress-strain curve for soft iron.

elongation is directly proportional to the stress. This region is known as the *Hooke's law regime* and corresponds to the straight line portion of the stress-strain curve shown. The slope of this part of the curve gives the modulus of elasticity, E , of the material since, from equation 3-19

$$E = \frac{\sigma}{\epsilon}$$

At some stress value, shown as point A on the diagram, the curve deviates from the straight line, indicating that the strain is no longer proportional to the stress. This is then appropriately called the *proportional limit* of the material.

If loading is continued, a point will be found at which the strain will increase with no increase in stress, i.e., the stress-strain curve has a horizontal tangent. This stress, shown at point B , is known as the *yield point* of the material.

Continued increase of the load on the member produces an ever-increasing rate of elongation and finally the specimen ruptures. This stress value, point C on the curve, is the *ultimate stress* which the material is able to stand under loading conditions similar to those applied during the tests.

It is well to mention here that nearly all the simple equations of stress and strain developed in applied mechanics, elementary structures, and machine design assume a linear relationship between the applied stress and the unit elongation. They are therefore strictly speaking valid only up to the proportional limit stress of any material. Small deviations between calculated and actual values would be expected for stresses up to the yield point, and, after the yield point stress has been exceeded, a number of the simple stress and deflection equations become very inaccurate.

If, at any stress below the proportional limit, the load is removed from the specimen, the deformation will return to zero. However, if the specimen is loaded to stress greater than the proportional limit and the load is then removed, the deformation will not return to zero, but the specimen will have a permanent set or will be permanently deformed. For example, consider that a stress corresponding to point D in the curve has been reached and the load is removed. Instead of the material going back to its original state, the stress-strain curve from point D to zero stress will be approximately parallel to the original straight line region all the way to zero stress, giving rise to a permanent elongation in the specimen equal to the permanent unit strain, ϵ_p , times the length of the member.

(2) *Steels and aluminum alloys.* It is a characteristic of the stress-strain curves of a number of common structural materials that they have no true yield point, that is, no point on the curve has a horizontal tangent. This is true of all the aluminum alloys and the alloy steels. In order to establish a design value corresponding to the yield point, a point on the curve corresponding to a given permanent set is arbitrarily defined as the yield point. In aircraft design the yield point of

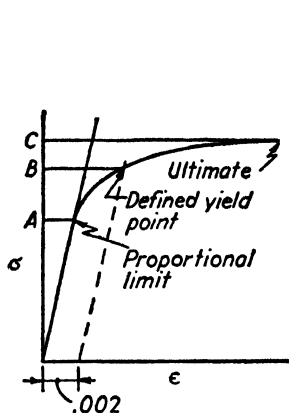


FIG. 3-11. Stress-strain curve for aluminum alloys and common steels.

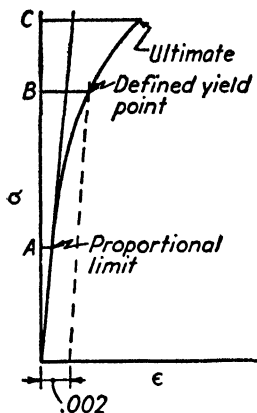


FIG. 3-12. Stress-strain curve for high strength steels.

any material is defined as that point corresponding to a unit permanent set of 0.2 per cent or, in other words,

$$\epsilon = 0.002$$

Typical curves for aluminum alloys and high strength steels are shown in Figs. 3-11 and 3-12 and the important points on these curves are indicated.

Design values for the material properties of aircraft structural materials can be found in various handbooks. Among these are ANC-5 (Reference 3-1), *Army Handbook for Airplane Designers*, and a number of other handbooks (References 3-2 to 3-4).

The conceptions of stress and strain are simple; however, it is very common for a designer to forget that, for a given material, increasing the stress also increases the deformation. This may not be important in short machine members, but in parts such as wing beams in an airplane with a span of 100 ft., the total deformation due to stressing the material may be considerable. As an example consider an aluminum alloy (Young's modulus 10.3×10^6 lb. per sq. in.) having a yield point

of 40,000 lb. per sq. in. which is used to fabricate a member 50 ft. long. If the stress in the member is made equal to the yield point, the total deformation will be

$$e = \frac{\sigma L}{E} = \frac{40,000 \times 50 \times 12}{10.3 \times 10^6} = 2.33 \text{ in.}$$

which deformation may cause alignment difficulties, interferences, or other troubles unless the designer is careful.

If the above material is improved in strength by cold working or by any other means so that it can be stressed to 60,000 lb. per sq. in. before reaching the yield point, it must be realized that not only will the structure made now of this stronger material be able to carry more load, but it will also deflect 50 per cent more. In other words, the price the designer has to pay in order to utilize high strength materials is that of providing for the large deflections which come from high stresses. The only material property which will affect a change in the relationship between unit stress and unit strain is Young's modulus, and the only way this can be changed is by going to a different material. Unfortunately a limit is soon reached in this direction because the various steels have the highest modulus (approximately 30.0×10^6 lb. per sq. in.) of any material which is available in sufficient quantities to be used as a structural material. This modulus is about three times as high as that for the aluminum alloys; however, steel is approximately three times as heavy as the aluminum alloys so little actual gain can be made in reducing the deformations by using the high modulus steels as construction materials.

In summary, the designer is again reminded that high stresses mean high unit deformations, so whenever analysis shows that a part is subject to high stresses, it is well to check whether or not the attendant deformations may cause trouble. This is particularly true of long members where the deformations may be a matter of inches (or even feet as for wing beams under bending, as is not uncommon) and may therefore introduce clearance and interference problems of major importance.

3-2. Load, Shear, and Moment Relationships in Beams

A beam is, by definition, a member that is long compared to its cross-sectional dimensions and that can not only withstand axial loads but also has a resistance against bending. The general case, therefore, consists of a structural member loaded with forces and moments which may either come from other structural members attached to the beam in question or from directly applied loads and moments.

The basic assumption that is made in beam analysis is that the complete system of forces and moments is in equilibrium. This not only applies to the beam as a whole but to every individual element of the beam. In order to set up a basis for discussion, certain sign conventions will be established which will be used consistently throughout the analysis which follows. It is well to remember that there are no restric-

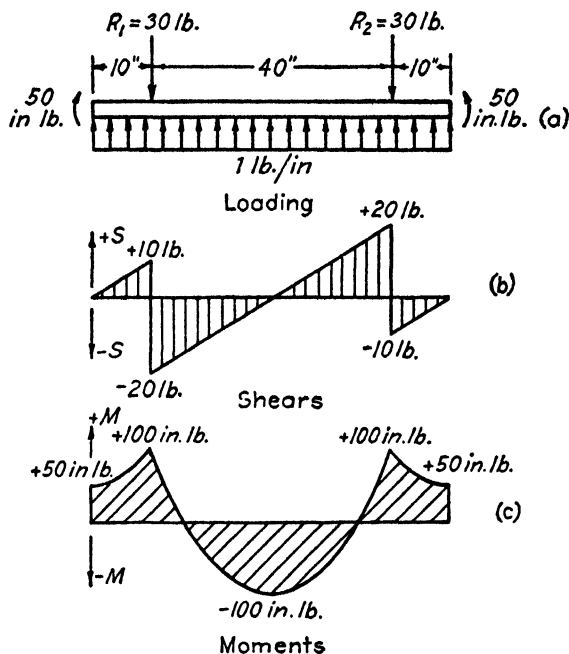


FIG. 3-13.

tions on sign conventions; it is only necessary to be consistent once a particular convention has been established. Consider the beam loaded as shown in Fig. 3-13a which leads to the shear and moment diagrams of Fig. 3-13b and c.

From this figure it will be seen that the established sign convention is as follows:

a. Loads. Loads and reactions are considered positive when acting upward. This is in contradiction to the usual civil engineering conception, but nearly all loads on an aircraft structure in normal operation act upward, hence the decision as to sign.

b. Shears. The shear on any section will be considered positive if the summation of the loads on all portions of the beam to the left of that section acts upward.

c. *Moments.* The moment on any section will be considered positive if it is such as to cause compressive stresses in the upper fibers of the beam at that section. Let us now consider an infinitesimal length of a beam, as shown in Fig. 3·14, and write the equilibrium equations of the

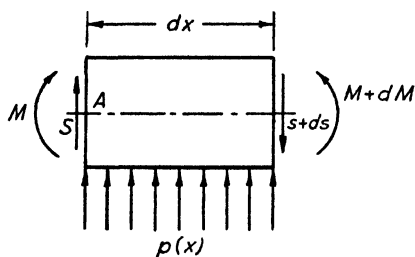


FIG. 3·14.

moments and forces. From the fact that the summation of vertical forces must equal zero we have

$$S + p(x) dx - (S + dS) = 0$$

which gives

$$\frac{dS}{dx} = p(x) \quad [3\cdot28]$$

or, that the rate of change of shear along any beam is equal to the load

increment over that portion. Taking the summation of moments around A, we obtain

$$M + dM - (S + dS)dx + p(x) dx \cdot \frac{dx}{2} - M = 0$$

which gives

$$\frac{dM}{dx} = S \quad [3\cdot29]$$

since $dSdx$ and $p(x) (dx)^2/2$ are of second order and may be neglected. This indicates that the rate of change of the bending moment is equal to the shear. Differentiation of equation 3·29 leads to

$$\frac{d^2M}{dx^2} = \frac{dS}{dx} = p(x) \quad [3\cdot30]$$

From these last two equations it can be immediately inferred that (a) when the shearing force is zero, the bending moment is a minimum or maximum, and (b) when the distributed loading $p(x)$ is zero, the bending moment curve is linear.

3-3. Bending Stresses and Bending Deflections.

Let us now consider a beam initially straight and of uniform cross section, Fig. 3·15a, subjected to pure bending in the XY -plane. For our problem we assume:

a. That the *centroidal axis* of the beam, i.e., the line connecting the centers of gravity of the cross sections, coincides with the X -axis.

b. That transverse planes (YZ) remain plane.

c. That Hooke's law holds, i.e., $\sigma = E\epsilon$ where σ = unit stress, ϵ = the unit strain and E is Young's modulus.

Let Fig. 3·15b represent a unit length of the beam after it has been subjected to the bending moments M and let

R = radius of curvature,

ϵ_0 = extension in a unit length along the centroidal axis, i.e.,

$\epsilon_{x(y)}$ = extension in a unit length parallel to the beam axis for arbitrary y .

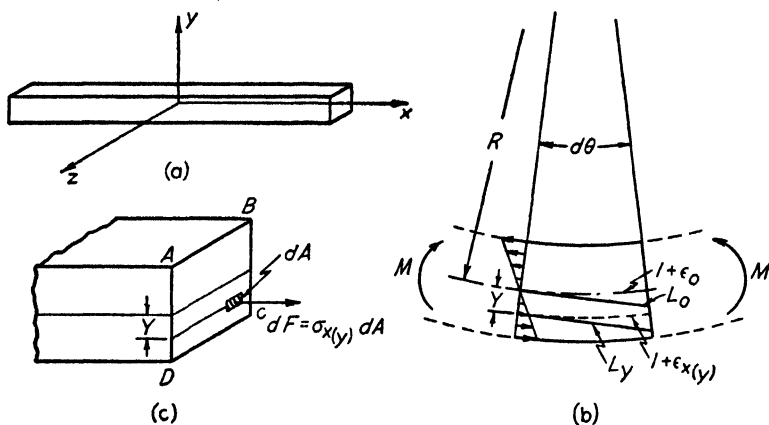


FIG. 3·15. Beam analysis notation.

From simple geometrical relations we have

$$\frac{L_y}{L_0} = \frac{R - y}{R} = \frac{1 + \epsilon_{x(y)}}{1 + \epsilon_0}$$

This gives

$$1 + \epsilon_{x(y)} = (1 + \epsilon_0) \left(1 - \frac{y}{R} \right) = 1 + \epsilon_0 - \frac{y}{R} - \frac{\epsilon_0 y}{R}$$

Now $\epsilon_0 \ll 1$ and $y \ll R$

Hence, $\frac{\epsilon_0 y}{R}$ is of second order and may be neglected, and the above equation can be written as

$$\epsilon_{x(y)} = \epsilon_0 - \frac{y}{R} \quad [3\cdot31]$$

From the stress-strain relationships, equation 3·22,

$$\epsilon_x = \frac{1}{E} [\sigma_x - \mu(\sigma_y + \sigma_z)]$$

However, since there are no external forces acting in the Y - or Z -direction we have

$$\sigma_y = \sigma_z = 0$$

Hence

$$\epsilon_x = \frac{\sigma_x}{E} \quad [3.32]$$

Substituting equation 3.32 in equation 3.31 gives

$$\sigma_x = \epsilon_{x(y)}E = E\epsilon_0 - \frac{E}{R}y \quad [3.33]$$

Now consider the section $ABCD$, Fig. 3.15c. The resultant of the stresses σ_x must be equal to the resultant of the axial loads, and the resultant moment of the stresses σ_x must be in equilibrium with the bending moment M and, since for pure bending there is no axial load,

$$\int_A \sigma_x dA = 0 \quad [3.34]$$

$$- \int_A \sigma_x y dA = M \quad [3.35]$$

Using equation 3.33 we have

$$\int_A \sigma_x dA = E\epsilon_0 \int_A dA - \frac{E}{R} \int_A y dA = 0$$

By the definition of the center of gravity of an area, $\int_A y dA = 0$, and consequently, since $E \int_A dA$ is not equal to zero

$$\epsilon_0 = 0$$

This means that all fiber elements lying on a straight line through the center of gravity of the cross section and normal to the plane of bending remain unstrained. This line is called the *neutral axis*.

The moment of the stresses about the neutral axis is, from equations 3.33 and 3.35

$$- \int_A \sigma_x y dA = \frac{E}{R} \int_A y^2 dA = M$$

The expression $\int_A y^2 dA$ is known as the moment of inertia I , hence

$$M = \frac{EI}{R} \quad \text{or} \quad \frac{1}{R} = \frac{M}{EI} \quad [3.36]$$

Also from equation 3.33, since $\epsilon_0 = 0$,

$$\sigma_x = \frac{-Ey}{R} \quad \text{or} \quad \frac{1}{R} = -\frac{\sigma_x}{Ey}$$

substituting this value of $1/R$ in equation 3.36 we obtain for the bending stress the following relation:

$$\sigma_x = -\frac{My}{I} \quad [3.37]$$

Equation 3.36 can be used directly to determine the relation between the deflection y in the direction of the Y -axis and the applied bending moment M . The curvature $1/R$, of a line $y = y(x)$ is given by the equation

$$\frac{1}{R} = \frac{\frac{d^2y}{dx^2}}{\left[1 + \left(\frac{dy}{dx}\right)^2\right]^{3/2}} \quad [3.38]$$

where y is measured positive upward and $\frac{1}{R}$ is positive if the deflection curve is concave if seen from above. Substituting the value for $\frac{1}{R}$ from equation 3.36 in equation 3.38 the differential equation for the deflection curve becomes:

$$\frac{d^2y}{dx^2} = \frac{M}{EI} \left[1 + \left(\frac{dy}{dx}\right)^2\right]^{3/2} \quad [3.39]$$

If we confine ourselves to small deflections, the second order term $\left(\frac{dy}{dx}\right)^2$ may be neglected and the differential equation becomes

$$EI \frac{d^2y}{dx^2} = M \quad [3.40]$$

From the relations of equations 3.29, 3.30, and 3.40 we can immediately write the following relations between the distributed load $p(x)$, the shear force S , and the deflection y .

$$\frac{d}{dx} \left[EI \frac{d^2y}{dx^2} \right] = \frac{dM}{dx} = S \quad [3.41]$$

$$\frac{d^2}{dx^2} \left[EI \frac{d^2y}{dx^2} \right] = \frac{d^2M}{dx^2} = \frac{dS}{dx} = p(x) \quad [3.42]$$

The above three equations are of fundamental importance in the calculation of beam deflections for they enable us to calculate the deflection of a beam if either the moment, M , the shear force, S , or the load, $p(x)$, is given.

Since all the equations relating to the problems of bending of beams have been derived on the basis of certain specific assumptions it might be well to consider the limitations of these equations. The first of these assumptions is that the deformations are small compared with the physical dimensions of the beam. Too great deviations from this assumption will tend to destroy the validity of equations 3.31 and 3.40. The assumption of a linear stress-strain relation breaks down if bending

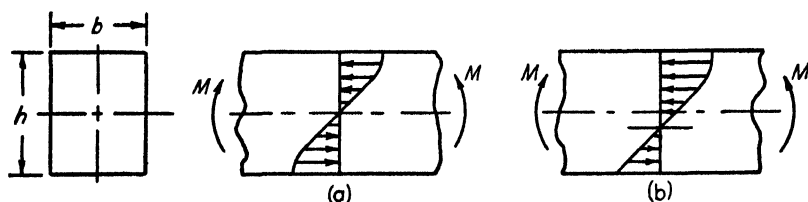


FIG. 3.16.

is continued beyond the proportional limit of the material. The longitudinal fiber stress will no longer be proportional to the longitudinal strains, and the distributions of stress will not be in accordance with equation 3.37. If the stress-strain curve is the same in compression as in tension, the stress distribution beyond the proportional limit will be as indicated in Fig. 3.16a. Since the stress-strain diagram is the same in compression and tension, the neutral axis will continue to pass through the center of gravity of the cross section. If the proportional limit is much lower, say, in compression than in tension, the stress distribution, after exceeding the compressive yield stress, will be as shown in Fig. 3.16b. It is seen that not only is the stress non-linear, but the neutral axis shifts toward the tension side. This shift of the neutral axis is a direct consequence of the condition that the resultant moment of the stresses must be in equilibrium with the bending moment M . A simple rectangular beam has been chosen as an illustration; however, the above discussion applies in general to a beam of any uniform cross section. Equation 3.36, which defines the curvature of the beam, is also based on a linear stress relation and any deviation from this relationship will cause inaccuracies in the curvature calculation and consequently in the bending deflection calculations.

The bending equations as derived are valid if the beam has one or more planes of symmetry. If a beam has only one plane of symmetry, it is

necessary that the bending couple lie in this plane. In this case the neutral axis will be perpendicular to the plane of symmetry and will pass through the center of gravity of the cross-sectional area. The effect of bending couples in planes other than the plane of symmetry will be discussed later.

So far, we have considered the distribution of longitudinal stresses and the deflections due to bending loads. We will now consider a few

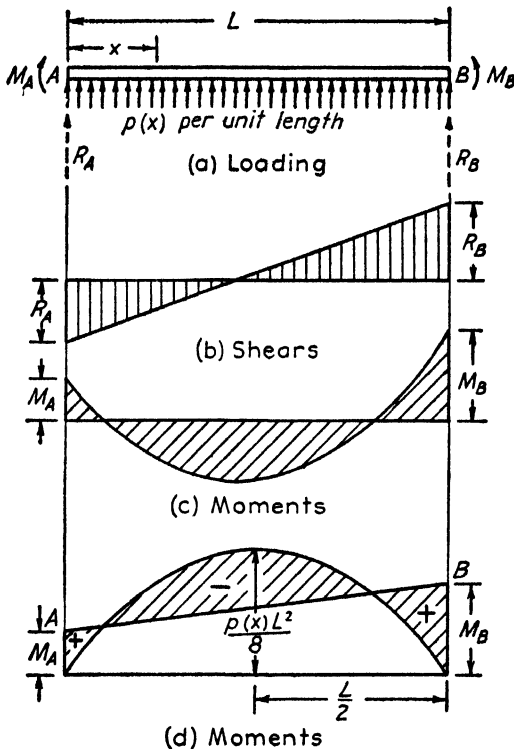


FIG. 3-17.

of the elementary methods of calculating the bending moments, reactions, and shearing forces on a beam when certain external loads are given. Consider a beam, Fig. 3-17a, subjected to a system of external loads as shown. The unknown reactions R_A and R_B are assumed to act in the positive direction, the results of the calculations showing whether or not that assumption is correct.

Taking moments about A,

$$-M_A + \frac{p(x) L^2}{2} + M_B + R_B L = 0$$

and

$$R_B = -\frac{p(x)L}{2} - \frac{M_B - M_A}{L} \quad [3.43]$$

Taking moments about B ,

$$-M_A - \frac{p(x)L^2}{2} + M_B - R_A L = 0$$

and

$$R_A = -\frac{p(x)L}{2} - \frac{M_A - M_B}{L} \quad [3.44]$$

If $M_A = M_B = 0$, this indicates that the assumed direction of the reactions was wrong, and that they act in the negative direction or downward. It should be noted that the total vertical force on the beam

$$\Sigma F_v = p(x)L + R_A + R_B = 0$$

The expression for the reactions, R_A and R_B , indicate that each consists of two parts, one due to the distributed loading $p(x)$ and the other due to the concentrated moments M_A and M_B . Hence for any system of lateral loading the reactions can be written in the form

$$\begin{aligned} R_A &= R'_A + \frac{M_B - M_A}{L} \\ R_B &= R'_B + \frac{M_A - M_B}{L} \end{aligned} \quad [3.45]$$

Where R'_A and R'_B are the reactions due to the lateral loading alone. The shear load diagram is Fig. 3.17b. The bending moment at a distance x from A is given by

$$M_x = p(x) \frac{x^2}{2} + M_A + R_A x$$

Substituting the value of R_A from equation 3.44 we have

$$M_x = -\frac{p(x)Lx}{2} + p(x) \frac{x^2}{2} + M_A - \frac{(M_A - M_B)x}{L} \quad [3.46]$$

The above expression is shown graphically in Fig. 3.17c. The second two terms on the right-hand side of equation 3.46 represent the effects of the end moments alone. If we plot these two expressions, we obtain the straight line AB in Fig. 3.17d. The first two terms on the right-hand side of equation 3.46 give the parabola due to the uniform loading.

If, therefore, we plot the parabola with its sign reversed, then the difference of the two curves will be equal to the bending moment. By this device, changes in the end moments can be investigated without completely redrawing the diagram. If, as is sometimes done, the line AB is considered as a new zero axis, the moments as read from this axis will have the opposite sign. This is indicated in Fig. 3-17d. The bending moment on a beam due to the lateral loading alone, assuming the beam pin-jointed at each support, is sometimes referred to as the *free bending moment*.

In most of the practical problems which occur in airplane design, the distributed load $p(x)$ is not a uniform load, neither can it be readily

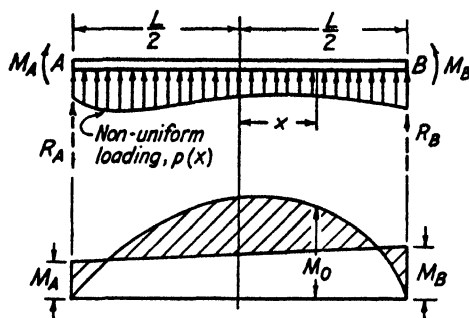


FIG. 3-18.

expressed analytically. For this reason then we shall consider the general case in which the distributed load is irregular. Many cases also arise in which the reaction points are not co-linear, i.e., all reactions do not lie in the same plane. An example of this is an elevator spar; for under load the stabilizer undergoes a certain deflection and, since the hinge brackets of the elevator are attached to the stabilizer spar, it is necessary to analyze the elevator spar, assuming the hinge reaction to lie in the plane of the deflected stabilizer spar.

The general case of continuous beams can be most readily treated by the method of end slopes and deflections, hence we shall first consider the equations involving end slopes and end deflections. Consider, for example, a simply supported beam as shown in Fig. 3-18, with any irregular lateral loading which, with no end moments, produces a moment M_0 at a distance x from the center, M_0 being the free bending moment. For convenience, the origin has been placed at the center of the span. If we now apply end moments M_A and M_B we have, from equation 3-40

$$EI \frac{d^2y}{dx^2} = \frac{M_A + M_B}{2} + \frac{M_B - M_A}{L} x - M_0 \quad [3-47]$$

Integrating over the span from $-L/2$ to $L/2$ we obtain

$$EI \left[\left(\frac{dy}{dx} \right)_B - \left(\frac{dy}{dx} \right)_A \right] = \frac{M_A + M_B}{2} L - \int_{-L/2}^{L/2} M_0 dx \quad [3.48]$$

If we now let

$$i_A = \left(\frac{dy}{dx} \right)_A = \text{slope of the deflection curve at } A, \text{ and}$$

$$i_B = \left(\frac{dy}{dx} \right)_B = \text{slope of the deflection curve at } B$$

the equation becomes

$$EI (i_B - i_A) = \frac{M_A + M_B}{2} L - \int_{-L/2}^{L/2} M_0 dx = (M_A + M_B) L/2 - \bar{A} \quad [3.49]$$

where \bar{A} is the area of the bending moment diagram for M_0 alone from A to B . The above equation gives us directly the difference in slopes between A and B . The area under the free bending moment curve can be determined either analytically or graphically.

If the reaction points A and B lie distances y_A and y_B , respectively, from the beam reference axis, the effect can be determined as follows. It is easily seen that

$$x \frac{d^2 y}{dx^2} = \frac{d}{dx} \left(x \frac{dy}{dx} - y \right)$$

Hence, multiplying equation 3.47 by x and integrating between $-L/2$ and $L/2$ we have

$$EI \left[\frac{L}{2} \left(\frac{dy}{dx} \right)_B - y_B + \frac{L}{2} \left(\frac{dy}{dx} \right)_A + y_A \right] = \frac{M_B - M_A}{12} L^2 - \int_{-L/2}^{L/2} M_0 x dx$$

which gives

$$EI \left[\frac{L}{2} (i_A + i_B) - \bar{y} \right] = \frac{M_B - M_A}{12} L^2 - \bar{A} \bar{x} \quad [3.50]$$

where

$$\bar{y} = y_B - y_A$$

$$\int_{-L/2}^{L/2} M_0 x dx = \bar{A} \bar{x}$$

Adding $EI (i_B - i_A) L/2$ to each side of equation 3.50 and applying equation 3.49 we obtain the following expression for the slope at B :

$$EI (i_B L - \bar{y}) = \frac{(M_A + 2M_B) L^2}{6} - \bar{A} \bar{x} - \frac{\bar{A} L}{2}$$

or

$$E I i_B = \frac{M_A + 2M_B}{6} L - \frac{\bar{A}}{2} \left(\frac{2\bar{x}}{L} + 1 \right) + \frac{E I \bar{y}}{L} \quad [3.51]$$

In a similar manner it can be shown that

$$E I i_A = -\frac{2M_A + M_B}{6} L - \frac{\bar{A}}{2} \left(\frac{2\bar{x}}{L} - 1 \right) + \frac{E I \bar{y}}{L} \quad [3.52]$$

\bar{A} and \bar{x} may be obtained analytically or graphically. It is necessary that appropriate signs be given to \bar{A} and \bar{x} . With a distributed up

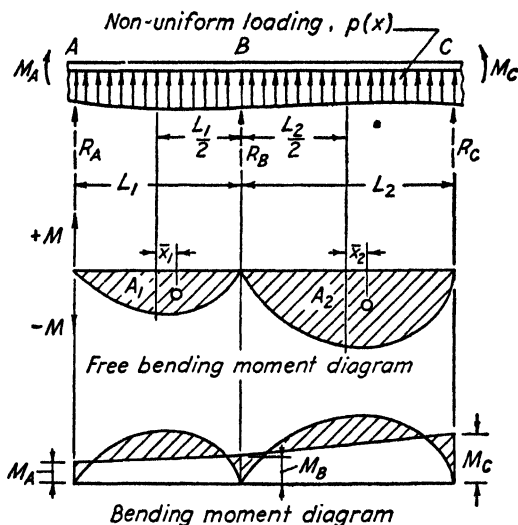


FIG. 3-19.

load $p(x)$, M_0 is positive everywhere and consequently \bar{A} is positive; \bar{x} is positive when the centroid of the bending moment (M_0) area lies to the right of the center of the beam. For a uniform load $p(x)$, $\bar{x} = 0$ and

$$\bar{A} = \frac{p(x) L^3}{12}$$

In order to determine the equations for a *continuous beam* let us consider a beam, Fig. 3-19, supported at the three points A , B , and C , and subjected to a given distributed load $p(x)$. It is evident that the reactions at the supports cannot be determined, and the question arises as to whether or not the bending moment diagram for the beam can be determined from pure statics. We can calculate from pure statics the

moments at A and C due to the external loading, but for the moments between A and C we have to consider the elastic behavior of the beam. If we consider the moment at B as the unknown, we can write a relation between the slope at B , the lateral loading on AB , and the moments at A and B , from equation 3.51.

$$i_B = \frac{1}{EI_1} \left[\frac{M_A + 2M_B}{6} L_1 - \frac{\bar{A}_1}{2} \left(\frac{2\bar{x}_1}{L_1} + 1 \right) + \frac{EI_1 \bar{y}_1}{L_1} \right] \quad [3.53]$$

and, considering the bay BC , from equation 3.52 we have

$$i_B = \frac{1}{EI_2} \left[-\frac{2M_B + M_C}{6} L_2 - \frac{\bar{A}_2}{2} \left(\frac{2\bar{x}_2}{L_2} - 1 \right) + \frac{EI_2 \bar{y}_2}{L_2} \right] \quad [3.54]$$

Since the slopes are equal we can equate the above two equations which gives

$$\begin{aligned} \frac{M_A L_1}{I_1} + 2M_B \left(\frac{L_1}{I_1} + \frac{L_2}{I_2} \right) + \frac{M_C L_2}{I_2} &= \frac{3\bar{A}_1}{I_1} \left(\frac{2\bar{x}_1}{L_1} + 1 \right) \\ &\quad - \frac{3\bar{A}_2}{I_2} \left(\frac{2\bar{x}_2}{L_2} - 1 \right) - 6E \left(\frac{\bar{y}_1}{L_1} - \frac{\bar{y}_2}{L_2} \right) \end{aligned} \quad [3.55]$$

where \bar{y}_1 is the height of B above A and \bar{y}_2 is the height of C above B . The quantities \bar{A}_1 , \bar{A}_2 , \bar{x}_1 , and \bar{x}_2 are as shown in Fig. 3.19. If the reactions are at the same level, the last term on the right-hand side of equation 3.55 vanishes. If the beam extends over more than three supports the intermediate moments can be obtained by a repeated application of the above equation. When the moment at B is determined the reactions can be obtained from pure statics, i.e., the section AB of the beam can be regarded as a single bay beam with the moment M_B applied at B . The reaction at A can then be obtained and in a similar manner, the reaction at C can be obtained. The reaction at B can then be determined from the equilibrium equation $\Sigma F_v = 0$.

3-4. Shearing Stresses and Shearing Deflections

In equation 3.30 was shown the relation between the shearing force S , the bending moment M , and the distributed load $p(x)$; and the distribution of the bending stress has just been discussed. The distribution of the shearing stresses, which are produced by the shearing force S , are of considerable importance in airplane design. Their dis-

tribution will now be considered in detail. We shall begin our investigation by considering the simple case of a beam of rectangular cross section. Let Fig. 3·20a represent a section of a rectangular beam of width b and depth h . The coordinate system is so placed that the X -axis coincides with the centroidal axis of the beam and the Y -axis is parallel to the direction of the shearing force S . The plane of the applied bending moment is parallel to the XY -plane. For our problem we shall assume first, that the shearing stress τ_{xy} is parallel to the shearing force S and secondly, that the distribution of τ_{xy} is uniform across the width, b , of the beam. If the height of the beam, h , is large com-

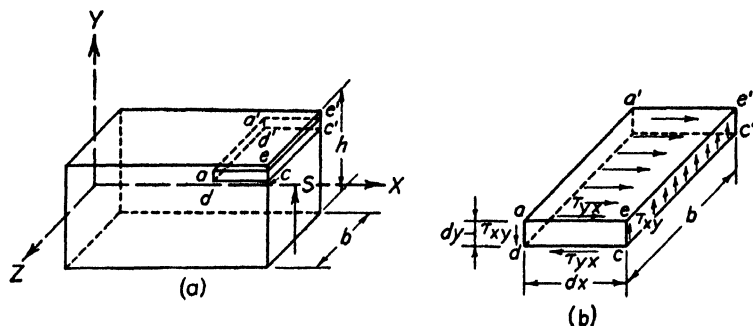


FIG. 3·20. Shear stresses in beams.

pared to the width, b , use of the equilibrium conditions yields a distribution of the shearing stresses which, although not absolutely correct, contains errors which are negligible in nearly all practical engineering problems.

Although the calculation below refers to the distribution of the horizontal shearing stresses, it is well to remember that there are equal vertical shearing stresses acting in the beam and vice versa. Thus, if the shearing force S in Fig. 3·20a gives rise to vertical shearing stresses τ_{xy} , there will be equal horizontal shearing stresses, τ_{yx} , acting in each element. This was shown in equation 3·3 and can further be proven by writing the equilibrium equation for the beam element shown in Fig. 3·20b. The distribution of the horizontal shearing stress τ_{yx} can easily be calculated from the conditions of equilibrium of the element $mm'pp'$, Fig. 3·21, cut from the beam by the two cross-section planes mn and $m'n'$ a distance dx apart. Fig. 3·21c represents the element $mm'pp'$ as a free body with the horizontal forces shown. (Vertical forces are omitted in the figure.) Upon the left face the moment is M and the variable unit compressive stress is $\sigma_x = -\frac{My}{I}$. The force upon the

differential area $b dy$ is $-\frac{My}{I} b dy$ and the total horizontal force on the face mp is

$$-\frac{M}{I} \int_{y_0}^{h/2} y b dy = -\frac{M}{I} \int_{y_0}^{h/2} y dA$$

where the minus sign indicates a compression force on the surface in question.

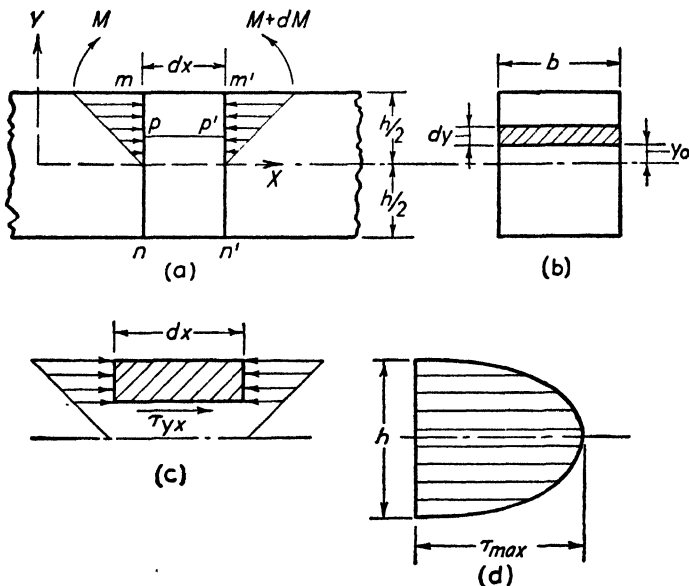


FIG. 3-21. Beam shears.

Similarly, the total force acting to the left upon the face $m'p'$ is given by

$$-\frac{M + dM}{I} \int_{y_0}^{h/2} y dA$$

The shearing force on the surface pp' is $\tau_{yx} b dx$. Since the free body is in equilibrium, the summation of the horizontal forces is equal to zero, that is

$$-\frac{M + dM}{I} \int_{y_0}^{h/2} y dA + \frac{M}{I} \int_{y_0}^{h/2} y dA + \tau_{yx} b dx = 0$$

from which

$$\tau_{yx} = \frac{1}{bI} \frac{dM}{dx} \int_{y_0}^{h/2} y dA$$

Since

$$\frac{dM}{dx} = S$$

from equation 3.29 we have

$$\tau_{yx} = \tau_{xy} = \frac{S}{bI} \int_{y_0}^{h/2} y b dy \quad [3.56]$$

Hence

$$\tau_{xy} = \frac{S}{2I} \left[\frac{h^2}{4} - y_0^2 \right] \quad [3.57]$$

and it is seen that the shearing stresses τ_{xy} are not uniformly distributed, but have a parabolic distribution over the depth of the beam. The shearing stress is zero when $y_0 = h/2$ and reaches a maximum when $y_0 = 0$, i.e., at the neutral axis, and is then equal to

$$\tau_{xy\max} = \frac{Sh^2}{8I} = \frac{3S}{2bh} \quad [3.58]$$

Since the quantity S/bh is the average unit shearing stress, the maximum shearing stress is 1.5 times greater than the average. The distribution of the shearing stress is shown in Fig. 3.21d.

A beam of rectangular cross section was chosen to begin the investigation of the distribution of the shearing stress because of the simple manner in which these calculations can be carried out. Let us now consider the distribution of the shearing stresses in an I beam as shown in Fig. 3.22. For the distribution of the shearing stresses over the web cross section the same assumptions are made as for the beam of rectangular cross section. These assumptions were that the shearing stresses τ_{xy} are parallel to the shearing force S and are uniformly distributed over the web thickness b_1 .

In order then to calculate the distribution of the shearing stresses τ_{xy} over the web we can use equation 3.56. The moment of the shaded area with respect to the neutral axis is

$$\int_{y_0}^{h/2} y dA = \frac{b}{8} (h^2 - h_1^2) + \frac{b_1}{2} \left(\frac{h_1^2}{4} - y_0^2 \right) \quad [3.59]$$

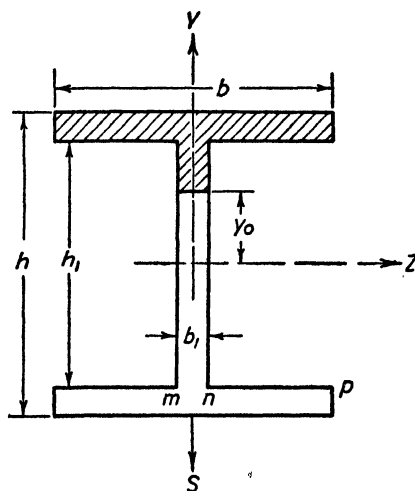


FIG. 3.22.

Substituting the above expression in equation 3.56 we obtain for the distribution of the shearing stress the following equation.

$$\tau_{xy} = \frac{S}{2b_1I} \left[\frac{b}{4} (h^2 - h_1^2) + b_1 \left(\frac{h_1^2}{4} - y_0^2 \right) \right] \quad [3.60]$$

Again as in the case of the beam of rectangular cross section, the distribution of the shearing stress is parabolic over the web cross section. The maximum value of τ_{xy} occurs when $y_0 = 0$ and the minimum value when $y_0 = h_1/2$; the values are given by the equations

$$\tau_{xy\max} = \frac{S}{8b_1I} [b(h^2 - h_1^2) + b_1h_1^2] \quad [3.60a]$$

$$\tau_{xy\min} = \frac{Sb}{8b_1I} (h^2 - h_1^2) \quad [3.60b]$$

In calculating the distribution of the shearing stresses over the flanges we can no longer assume that τ_{xy} is uniformly distributed across the width b of the flanges. For example, along the free surface np the horizontal shearing stress τ_{yx} is zero, and since $\tau_{xy} = \tau_{yx}$ it means that the vertical shearing stress is zero at the surface np . However, across the section mn the shearing stress is not zero but is equal to $\tau_{xy\min}$ as

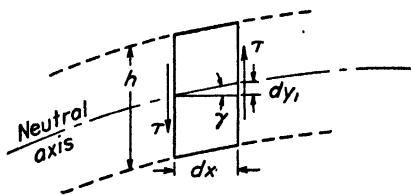


FIG. 3.23.

calculated above. Hence, the assumption of uniform stress in the Z -direction is no longer valid and the distribution of the shearing stress at the junction of the web and flange cannot be calculated by our elementary theory. As regards the magnitude of the vertical shear-

ing stresses τ_{xy} across the flange cross section we can conclude that, since τ_{xy} is zero at both the upper and lower free surface of the flange, $\tau_{xy\max}$ will be small as h_1 approaches h . When the web thickness, b_1 , is very small compared to the flange width, b , there is no great difference between $\tau_{xy\max}$ and $\tau_{xy\min}$, and the distribution of the shearing stress in the web is practically uniform.

In the discussion on beam deflections, only the displacement of the beam axis due to bending moment was considered. An additional deflection will be produced by the shearing force since any shearing force must be accompanied by a shearing deformation. Considering the rectangular beam of Fig. 3.20, the shearing stress at the neutral axis is equal to $3S/2bh$ from equation 3.58 and the shearing strain is then

$$\gamma = \frac{\tau_{y=0}}{G} = \frac{dy_1}{dx} = \frac{3S}{2bhG} \quad [3.61]$$

where dy_1 is the displacement of the neutral axis in a distance dx , due to the shearing stress τ . (See Fig. 3·23.) Differentiating with respect to x gives the curvature of the neutral axis due to shear, or

$$\frac{d^2y_1}{dx^2} = \frac{3}{2bhG} \frac{dS}{dx} = \frac{3}{2bhG} p(x) = \frac{3}{2AG} p(x) \quad [3\cdot62]$$

This must be added to the curvature due to bending, equation 3·40, which gives

$$\frac{d^2y}{dx^2} = \frac{M}{EI} + \frac{3}{2AG} p(x) = \frac{1}{EI} \left[M + \frac{3}{2} \frac{EI}{AG} p(x) \right] \quad [3\cdot63]$$

This equation can then be integrated to determine the total deformation of the neutral axis due to both bending and shear. In general, the influence of the shear in the total deflection is small in most normal beams. However, if the beam becomes short and heavily loaded, the shearing deflections may predominate.

For beams with sections other than rectangular, the general form of equation 3·56

$$\tau_{xy} = \frac{S}{Ib} \int_{y_0}^{h/2} y b dy \quad [3\cdot56a]$$

must be used in the derivation of equation 3·63. For simple cross sections, such as circles and ellipses, the result will be to change merely the constant in the last term of equation 3·63 to a different value. For example, for beams of circular cross section, equation 3·63 becomes

$$\frac{d^2y}{dx^2} = \frac{1}{EI} \left[M + \frac{4}{3} \frac{EI}{AG} p(x) \right] \quad [3\cdot63a]$$

3-5. Beams with One Axis of Symmetry

In the previous discussion we have dealt with beams in which the bending moment was applied in one of the two principal planes of bending. As for bending by transverse loads, we have only discussed the case in which they are in a plane of symmetry of the beam. From this symmetry, it can be concluded that the plane of the deflection curve coincides with the plane of the loads. We must now consider the more general case in which the beam has only one axis of symmetry and the loads are applied in a plane perpendicular to the plane of symmetry of the beam. Examples of beams having such cross sections are shown in Fig. 3·24. Let us consider now the position of the vertical plane in which the shear load S must be applied to produce simple bending.

By simple bending we mean that bending takes place with no rotation of the cross section.

In order to calculate the position of the plane in which S must be applied to satisfy the condition of no rotation of the cross section, it is

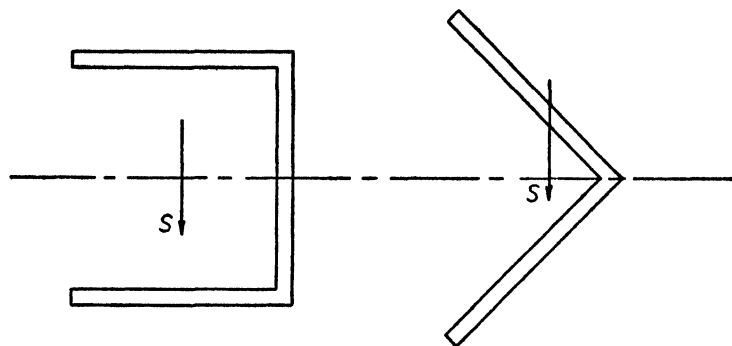


FIG. 3-24.

necessary to consider the shear distribution over the cross section. For our calculations, consider the section as shown in Fig. 3-25 with a coordinate system as indicated. The X -axis lies in the neutral plane of the section. As previously mentioned, if the flanges are thin, the vertical shearing stress τ_{xy} will be small over the cross-sectional area of

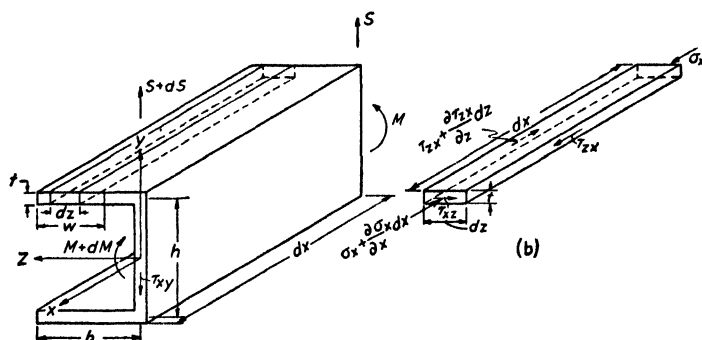


FIG. 3-25. Channel section shear analysis.

the flange. For our purpose we shall assume that it is sufficiently small so that it can be considered to be zero, i.e., the web carries the entire vertical shear. However, the horizontal shearing stresses $\tau_{xz} = \tau_{zx}$ cannot be considered as zero. To calculate the distribution of these stresses consider a section as shown in Fig. 3-25b cut from the flange by two adjacent cross sections a distance dx apart and cut by two vertical planes parallel to the web, a distance dz apart. The force acting on the rear

face of the element is equal to $\sigma_x t dz$ and, since $\sigma_x = -\frac{My}{I_z}$, $\sigma_x t dz = -\frac{Myt}{I_z} dz$. Similarly, the force on the front face of the element is

$$\left(\sigma_x + \frac{\partial \sigma_x}{\partial x} dx\right) t dz = -\left(M + \frac{\partial M}{\partial x} dx\right) \frac{yt}{I_z} dz$$

These forces must be in equilibrium with the shearing forces or

$$\frac{Myt}{I_z} dz + \tau_{xz} t dx - \left(M + \frac{\partial M}{\partial x} dx\right) \frac{yt}{I_z} dz - \left(\tau_{xz} + \frac{\partial \tau_{xz}}{\partial z} dz\right) t dx = 0$$

which gives

$$\frac{\partial \tau_{xz}}{\partial z} = -\frac{y}{I_z} \frac{\partial M}{\partial x}$$

or

$$\tau_{xz} = -\frac{1}{I_z} \int y \frac{\partial M}{\partial x} dz = -\frac{S}{I_z} \int y dz \quad [3.64]$$

since $\frac{\partial M}{\partial x} = S$ is independent of z . Also, since in this example y is a constant, we can see that the shear stress τ_{xz} is proportional to the distance w from the edge of the flange and is therefore not uniformly distributed over the flange width. At the junction of the flange and web the distribution of the shearing stress is complicated, and in our approximate calculation we assume that equation 3.64 holds to the center line of the web. We further assume that equation 3.56 holds to the center line of the flange.

Let us now calculate the position of the plane in which it is necessary to apply the shear force S in order to comply with the condition that there shall be no rotation of the cross section. Consider a beam in which the cross section is a simple channel, as shown in Fig. 3-26, subjected to a vertical shearing force S . If the vertical shearing force on the section acts downward, then in accordance with our sign convention, the shearing stress from m to n is given by

$$\tau_{xz} = \frac{-S}{I_z} \int \frac{h}{2} dz = \frac{-Sh}{2I_z} z + C$$

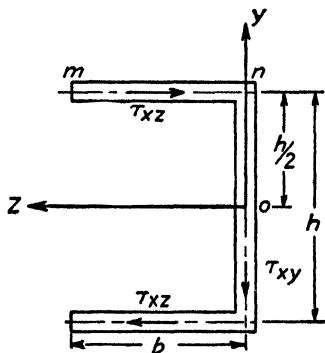


FIG. 3-26.

The boundary condition at $z = b$, i.e., at m , is

$$\tau_{xz} = 0$$

Hence

$$C = \frac{Shb}{2I_z}$$

and the shearing stress along the flange is given by

$$\tau_{xz} = \frac{Sh}{2I_z} (b - z)$$

From n to 0 the shearing stress is given by the equation (see equation 3.56)

$$\tau_{xy} = -\frac{S}{I_z} \int y dy = -\frac{S}{I_z} \frac{y^2}{2} + C$$

Now, when $y = h/2$, τ_{xy} is equal to the value of τ_{xz} at $z = 0$ since the shear flux, given by the product of the shearing stress times the thickness, must be a constant value at the corner. Therefore, at $y = h/2$,

$$\tau_{xy} = \frac{Sh}{2I_z} b$$

Hence

$$C = \frac{Sh}{2I_z} b + \frac{Sh^2}{8I_z} = \frac{S}{2I_z} \left(hb + \frac{h^2}{4} \right)$$

And the shearing stress along the web is

$$\tau_{xy} = \frac{S}{2I_z} \left(hb + \frac{h^2}{4} - y^2 \right)$$

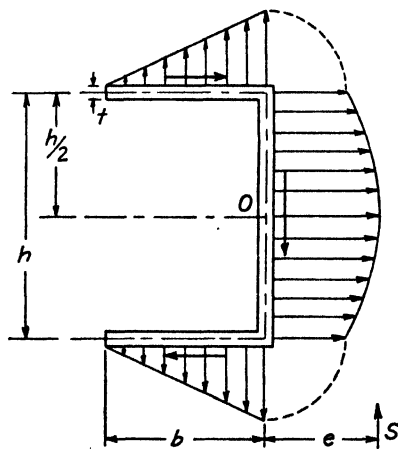


FIG. 3-27. Shear distribution in a channel section.

Since the Z -axis is an axis of symmetry, the shear distribution over the lower half will be similar to that over the upper half. The distribution of the shear intensity over the cross section is shown in Fig. 3-27. We can show that the resultant of the vertical forces is equal to S , that is,

$$R_v = \frac{S}{2I_z} \int_{-h/2}^{h/2} \left(hb + \frac{h^2}{4} - y^2 \right) t dy = \frac{St}{I_z} \left[\frac{h^2 b}{2} + \frac{h^3}{12} \right]$$

Now I for the channel section is

$$I = \left[\frac{h^2b}{2} + \frac{h^3}{12} \right] t$$

Hence $R_y = S$.

The moment of the horizontal forces about the point O , Fig. 3·27, is

$$M = \frac{Sh}{I_z} \int_0^b (b - z) \frac{ht}{2} dz = \frac{Sh^2b^2t}{4I_z}$$

Substituting the value of I_z in the above equation gives

$$M = \frac{Sh^2b^2t}{4 \left(\frac{h^2b}{2} + \frac{h^3}{12} \right) t} = \frac{Sb}{2 \left(1 + \frac{h}{6b} \right)}$$

Now assume the vertical plane in which the shearing force must be applied, to conform with the requirement that there shall be no rotation of the cross section, is at a distance e from the point O , then

$$Se = \frac{Sb}{2 \left(1 + \frac{h}{6b} \right)}$$

and

$$e = \frac{b}{2 \left(1 + \frac{h}{6b} \right)} \quad [3 \cdot 65]$$

From this equation we see that as the ratio of $h/b \rightarrow \infty$, $e \rightarrow 0$, and as $h/b \rightarrow 0$, $e \rightarrow b/2$. Hence the shear center (i.e., the point of intersection of the axis of symmetry with the vertical plane in which the shear force must be applied to cause simple bending) of any channel section lies between the values $e = 0$ and $e = b/2$. Our discussion so far has been limited to the case in which one of the principal axes is an axis of symmetry. The method as given above is also applicable to unsymmetrical sections. It is only necessary that the shear be applied alternately in the plane of the principal axes. In this manner two planes can be calculated in which the shear must be applied to cause simple bending. The intersection of these two planes gives the shear center of the section.

3-6. Torsion

In pure bending only the stress components at right angles to the cross section are different from zero, whereas in the case of pure torsion of a straight bar, the components of shear stress in the plane of the cross section are the important items.

(a) **Torsion of Bars with Solid Cross Section.** If, to a cylindrical bar of circular cross section, as shown in Fig. 3-28a, are applied couples acting in planes perpendicular to the cylinder axis, we have a case of pure torsion. It has been shown by experiment, that during twisting of the bar all circular sections remain circular and that their radii and

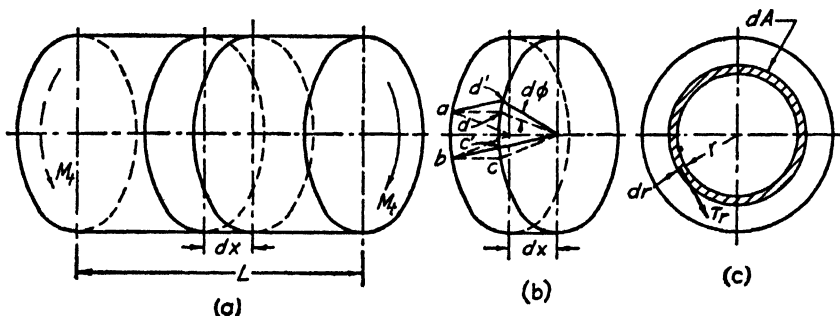


FIG. 3-28. Notation for the torsion problem.

the distances between them do not change, provided the angle of twist is small. In the analysis of circular bars it is further assumed that all plane sections perpendicular to the axis of the bar remain plane and each element on the cross section has the same angular rotation; that is all diameters remain straight. Therefore, the cross section of the bar will only rotate with respect to some arbitrary reference cross section.

The boundary conditions at the free surface require that the resultant shear stress at the outer boundary be tangent to the boundary. This means that the resultant shearing stress at any given point on the outer boundary will be perpendicular to the radius vector drawn from the axis of the bar to the given point.

Since all sections remain plane and circular sections remain circular, we can conclude that the stress conditions on any inner circular boundary will be the same as on the outer boundary. Hence, the lines of shearing stress are concentric circles. Lines of shearing stress are defined as the curves drawn on the cross section of a twisted bar, in such a manner, that the resultant shearing stress at any point on the curve is in the direction of the tangent to the curve at the same point.

The magnitude of the shearing stresses, τ , and the angle of twist, θ , per unit length, for a given torsional moment, M_t , can be obtained in the following manner. Consider an element of length dx cut from the shaft, Fig. 3-28*b*. The element will be in a state of pure shear and the shearing strain at the outer boundary is given by

$$\gamma = \frac{dd'}{ad} = R \frac{d\phi}{dx}$$

For a constant torque the angle of twist is proportional to the length; and $d\phi/dx$, the angle of twist per unit length, is a constant. Denoting the angle of twist per unit length by θ , we have

$$\gamma = R \theta$$

According to our assumptions, the shearing strain at any inner boundary will be proportional to the distance of the boundary from the center. Hence, at any distance r from the center the shearing strain is

$$\gamma_r = r \theta$$

Since the lines of shearing stress are circles, the resultant shear stress at any given point on the cross section will be perpendicular to the radius vector drawn from the axis of the bar to this point. Hence the shearing force $\tau_r dA$, Fig. 3-28*c*, produces a moment $\tau_r r dA$ about the axis of the bar and the total moment produced by the shearing stresses distributed over the cross section of the bar is

$$M_t = \int_0^R \tau_r r dA \quad [3.66]$$

This moment, which is produced by the shearing stress, must be in equilibrium with applied couple.

From equation 3-20, we have

$$\gamma_r = \frac{\tau_r}{G} = r \theta \quad [3.67]$$

Substituting for τ_r in equation 3-66 gives

$$M_t = G \theta \int_0^R r^2 dA = G \theta J$$

where J is the polar moment of inertia of the cross section. The angle of twist per unit length is given by

$$\theta = \frac{M_t}{GJ} \quad [3.68]$$

Substituting this value of θ in equation 3.67 gives

$$\tau = \frac{M_t r}{J} \quad [3.69]$$

The above equation indicates, that for a given bar of circular cross section and a given torsional moment, the shear stress is proportional only to the distance from the center of the cross section. Hence, the lines of constant shear are parallel to the lines of shearing stress.

The next simplest case is that of a bar of elliptical cross section as shown in Fig. 3.29a. Again on the outer boundary the resultant stress is tangent to the boundary. However, the lines of shearing stress are

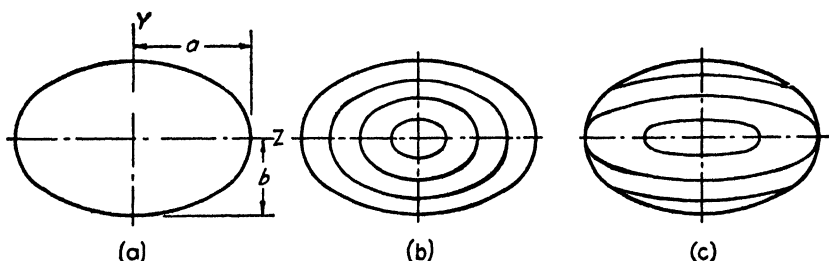


FIG. 3.29. Torsional stress in elliptical cross section.

not parallel to the outer boundary, but form ellipses, each having a different eccentricity, as shown in Fig. 3.29b.

A solution of this problem can be readily obtained; however, the theoretical treatment is beyond the scope of this text, and only the results will be given here. The stress components, τ_{xz} and τ_{xy} , are given by the following two equations,

$$\tau_{xz} = \frac{2M_t y}{\pi a b^3} \quad [3.70]$$

$$\tau_{xy} = \frac{2M_t z}{\pi a^3 b} \quad [3.71]$$

The twist per unit length is given by the equation,

$$\theta = \frac{M_t(a^2 + b^2)}{\pi a^3 b^3 G} \quad [3.72]$$

The maximum shearing stress is at the outer boundary, and it can easily be proved that this maximum occurs at the ends of the minor axis of the ellipse. Substituting $y = b$ in equation 3.70, we have for the absolute value of the maximum shear stress,

$$\tau = \frac{2M_t}{\pi a b^2} \quad [3.73]$$

The lines of constant shear, as shown in Fig. 29c, are also ellipses, each having a different length of axis but the same eccentricity.

In the above two cases we were able, due to the simplicity of the cross sections, to determine the lines of shearing stress and were consequently able to determine the shear stresses and the lines of constant shear. Consider now a bar of a rectangular cross section, Fig. 3-30a. The condition that the resultant shear stress at the boundary be tangent to the boundary still holds. However, due to the sharp discontinuities

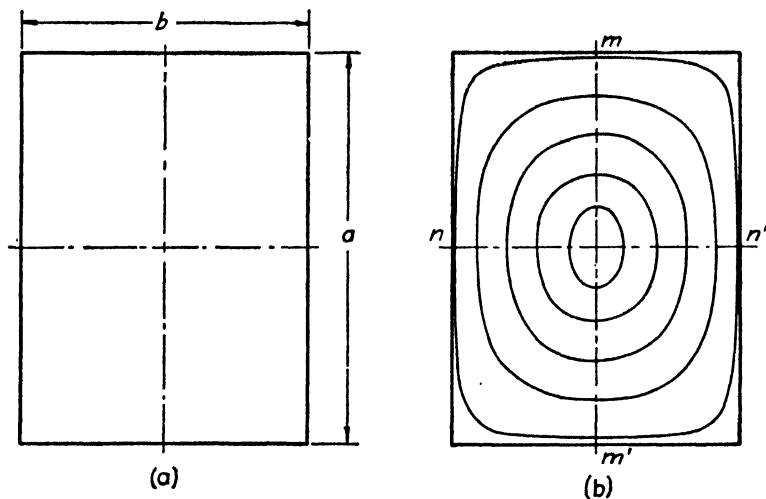


FIG. 3-30. Torsion in rectangular bars.

in the boundary, the lines of shearing stress will no longer be parallel to, or have the general shape of, the boundary.

In bars having cross sections in which the boundaries are discontinuous, or in bars of irregular cross section, it is possible to study the distribution of the shear stress over the cross section by means of the *membrane analogy*. It was first pointed out by L. Prandtl, that if a membrane with outlines similar to the cross section of the twisted bar, be stretched at the edges with a uniform tension q per unit length and subjected to a uniform pressure p per unit area, then for small deflections the equation of equilibrium of the membrane will be identical to that of the torsion problem, provided we put

$$\frac{p}{q} = 2G\theta$$

This analogy is of great importance in the solution of torsion problems, both analytically and experimentally. The important relations between

the deflected surface of the membrane and the twisted bar are as follows:

1. Contour lines of the deflected membrane surface correspond to lines of shearing stress of the twisted bar.
2. The tangent to a contour line at a given point on the membrane surface gives the direction of the resultant shear at the corresponding point on the cross section of the bar.
3. The maximum slope of the membrane at any point, with respect to the plane of its edges, is equal in magnitude to the shear stress at the corresponding point on the cross section of the twisted bar.
4. Twice the volume included between the deflected surface of the membrane and the plane of its edges is equal to the applied torsional moment acting on the twisted bar.

On the basis of the above relations we can now consider the twisted bar of rectangular cross section. The contour lines of the corresponding membrane surface will be as indicated in Fig. 3-30b. Near the center the lines of shearing stress are nearly circular, and as the boundary is approached they tend to take the shape of the boundary.

It can be readily seen that the slopes at the contours along the line nn' will be greater than the slopes on the corresponding contours along the line mm' . From this we can conclude that the shear stress at any point along the nn' will be greater than the shear stress at the corresponding points along mm' . The maximum slope, and hence the maximum shear stress, will occur at n and n' . Since the membrane slope is zero at the four corners and at the center of the cross section, the shear stress will be zero at these points.

Where an analytic expression can be obtained for the equation of equilibrium of the deflected membrane, it is possible to calculate the distribution of the shear stress over the cross section of the twisted bar. If the cross section of the bar is such that it does not lend itself to an analytic expression, the membrane slopes can be obtained experimentally. In the experimental methods it is customary to employ a soap film stretched over a hole, cut in a thin plate, having the same shape as the cross section of the bar. A uniform pressure is applied to one side of the membrane surface and the slopes measured, generally, by optical methods.

For a bar of rectangular cross section the shear stresses and the twist per unit length can be calculated analytically. The following equations are obtained for the maximum shear stress and the twist per unit length,

$$\tau_{\max} = \frac{M_t}{\alpha a b^2} \quad [3.74]$$

$$\theta = \frac{M_t}{\beta G a b^3} \quad [3.75]$$

where a is the longer side and α and β are functions of the ratio a/b . The values of α and β as a function of the ratio a/b are shown in Fig. 3-31. As the ratio of a/b becomes large, $\alpha \rightarrow \beta \rightarrow 0.333$, therefore, in thin-walled sections, the value $\alpha = \beta = 0.333$ is commonly used.

Although the above equations have been derived for a rectangular bar, they are equally applicable to the type of sections shown in Fig. 3-32. For the T -section and channel section the results are only approximate, for at the junction of the web and flanges there will be stress concentrations, the magnitude of

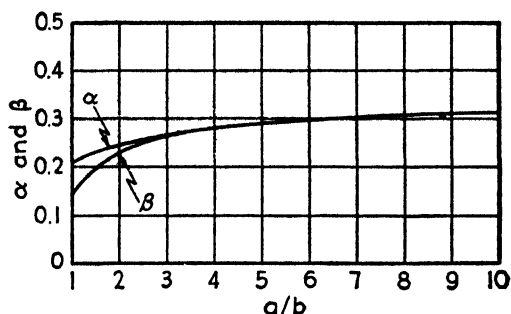


FIG. 3-31. α and β in equations 3-74 and 3-75.

which will depend upon the radius of the fillets. Approximate values of the shear stresses and angular twist per unit length are obtained by assuming that the section, which consists of a number of connected rectangular elements, can be replaced by the same number of separate

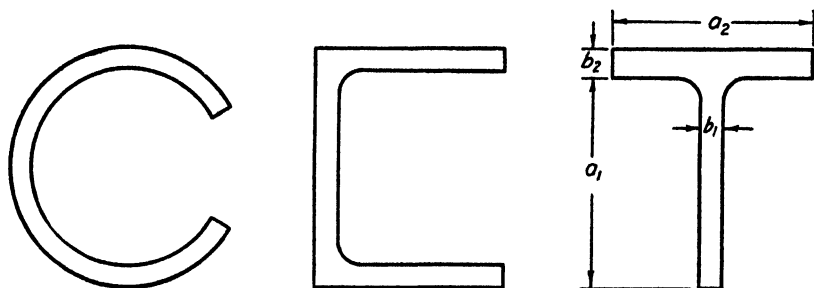


FIG. 3-32.

bars of narrow rectangular cross section. For example, based on the above assumptions the following equations can be derived for the T -section,

$$\theta = \frac{3 M_t}{(a_1 b_1^3 + a_2 b_2^3) G} \quad [3.76]$$

For the web the shear stress is

$$\tau = b_1 \theta G = \frac{3 M_t b_1}{(a_1 b_1^3 + a_2 b_2^3)} \quad [3.77]$$

If the maximum shear stress in the flange is desired, b_1 in the numerator is replaced by b_2 . If $b_1 = b_2 = b$, then

$$\tau = \frac{3M_t}{b^2(a_1 + a_2)}$$

$$\theta = \frac{3M_t}{b^3(a_1 + a_2)G}$$

and it is seen that the results are the same as for a rectangle whose sides are b and $a = a_1 + a_2$. The same method can be extended to the channel section or any other section whose cross section consists of a number of rectangular cross sections.

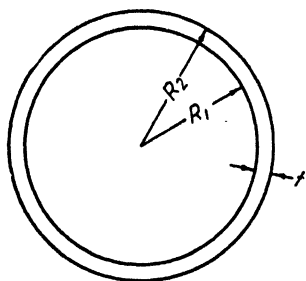


FIG. 3-33.

(b) Torsion of Hollow, Thin-Walled Sections. The conditions which were discussed for the solid circular section are also applicable to the case of a hollow circular cylinder. Consider the hollow circular cylinder shown in Fig. 3-33; the applied torque must now be resisted by the wall of a thickness $R_2 - R_1$ and we have

$$M_t = \int_{R_1}^{R_2} \tau_r r dA$$

In the case of thin-walled cylinders we can introduce instead of the quantities $R_1 - R_2$ and τ_r , a mean radius R , a thickness t , and a mean shear stress τ . Then the torsional moment is given by

$$M_t = 2\pi R^2 t \tau$$

or

$$\tau = \frac{M_t}{2\pi R^2 t} \quad [3.78]$$

and from equation 3-67

$$\theta = \frac{\tau}{GR} = \frac{M_t}{2\pi R^3 t G} \quad [3.79]$$

Since $2\pi R^3 t = J$, the polar moment of inertia of a thin annular ring of radius R and thickness t , the above equations are similar to those developed for the solid circular bar.

For a thin-walled section of arbitrary shape our problem is somewhat simplified, for we can say that the lines of shearing stress follow in

general the shape of the section, that is, we know that on the inner and outer boundaries the resultant shearing stress must be tangent to the boundaries; hence, we can assume that the resultant of the average shear stress across the wall thickness will be tangent to the median line. Based on the above assumptions, and using average shear stresses, we can in a very simple manner derive the equations defining the average shear stress across the wall thickness and the angular rotation of the cross section per unit length. Consider an arbitrary cross section of

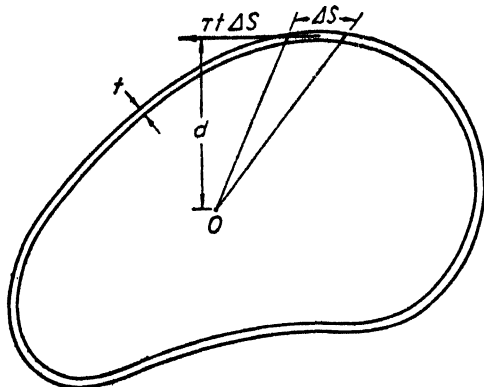


FIG. 3-34. Torsion in thin-walled sections.

uniform wall thickness as shown in Fig. 3-34. The moment produced about any arbitrary axis O by the shear force $\tau t \Delta s$ will be

$$\Delta M_0 = \tau t \Delta s d$$

where d is the perpendicular distance from the shear force to the axis. The total moment produced by the shear forces $\tau t \Delta s$ about this axis is the summation, taken around the curve C defined by the median line of the section, of the moments due to the individual elements. This summation can be expressed as

$$M_0 = \Sigma \tau t \Delta s d$$

Now, τt is a constant, and can be factored out of the summation. Also, $\Delta s d$ is twice the area of the triangle shown in Fig. 3-34. Hence,

$$M_0 = \tau t \Sigma \Delta s d = 2A\tau t$$

where A is the total area bounded by the curve C .

Since the axis was arbitrarily chosen, it is obvious that $2A\tau t$ expresses the moment about any axis due to the distribution of shear stress over

the cross section. This moment must be in equilibrium with the applied torsional moment; hence,

$$M_t = 2A\tau t$$

or

$$\tau = \frac{M_t}{2At} \quad [3 \cdot 80]$$

where A is the area bounded by the median line of the section.

If the thickness is variable, we can still determine the average shear stress τ from the above equation; however, τ will no longer be a constant around the boundary. From the equilibrium conditions of an element of the cross section it follows that

$$\tau_1 t_1 = \tau_2 t_2 = \text{constant} \quad [3 \cdot 81]$$

This equation resembles the equation of continuity in fluid mechanics, that is,

$$qS = \text{constant}$$

where q is the flow velocity and S the cross-sectional area. The product of τt is therefore commonly referred to as the shear flow, and we say that the shear flux across the wall thickness at any point on the periphery is a constant.

Assuming that plane sections remain plane, the relationship between the applied torque and the angle of twist per unit length can be obtained from the energy relationships which follow. (Strain energy is discussed in detail in Chapter 4.)

The strain energy per unit length $= U = \frac{1}{2}M_t \theta$.

The strain energy per unit volume $= U = \frac{1}{2}\tau^2/G$.

If p is the perimeter of the cross section, then equating the two energies gives

$$M_t \theta = \frac{\tau^2}{G} pt$$

Substituting from equation 3-80 for τ we have

$$\theta = \frac{M_t p}{4A^2 Gt} \quad [3 \cdot 82]$$

or

$$\theta = \frac{\tau p}{2AG} \quad [3 \cdot 83]$$

It should be noted that the above equations are only applicable to thin-walled sections, i.e., the thickness is small compared to the cross-sectional dimensions.

Let us now consider the case in which the cross section, of the member of arbitrary cross section, has more than two boundaries. If we take, for example, a cross section as shown in Fig. 3-35, we have from equation 3-80

$$M_t = 2A_1t_1\tau_1 + 2A_2t_2\tau_2 \quad [3-84]$$

and from equation 3-83

$$\tau_1p_1 + \tau_3p_3 = 2G\theta A_1 \quad [3-85]$$

$$\tau_2p_2 - \tau_3p_3 = 2G\theta A_2 \quad [3-86]$$

The shear flow across any junction is a constant, that is, going back to the hydrodynamic analogy, we can say that the volume of fluid flow-

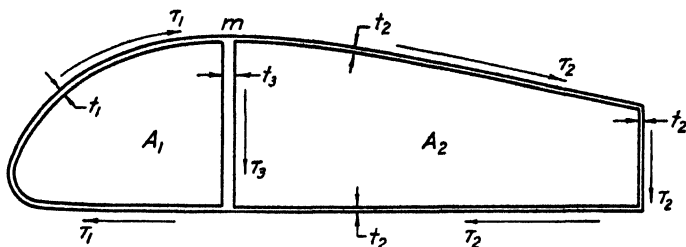


FIG. 3-35. Torsion in doubly connected cross sections.

ing into the junction per unit time must equal the volume of fluid flowing out per unit time. For example, at the junction m , we can write

$$t_1\tau_1 - t_3\tau_3 = t_2\tau_2$$

or in general we can write

$$\sum_{i=1}^{i=n} t_i\tau_i = 0 \quad [3-87]$$

It is readily seen that this equation satisfies the conditions of equilibrium at any junction.

These four equations, 3-84 to 3-87, are sufficient to determine the shear stresses, τ_1 , τ_2 , τ_3 , and the angle of twist per unit length. The same type of analysis can be extended to sections with any number of boundaries.

The particular problems of torsion discussed in this section are those which are most frequently encountered in airplane design.

REFERENCES FOR CHAPTER 3

- 3-1. S. TIMOSHENKO, *Strength of Materials*, Parts I and II, Van Nostrand, 1930.
- 3-2. S. TIMOSHENKO, *Theory of Elasticity*, McGraw-Hill, 1934.
- 3-3. R. V. SOUTHWELL, *Theory of Elasticity*, Oxford Press, 1936.

CHAPTER 4

TRUSS AND FRAME ANALYSIS

4-1. Truss Analysis

A truss consists of an arrangement of straight bars connected in such a manner as to divide the area enclosed by the perimeter of the truss, into a system of triangular spaces, Fig. 4-3a. Since the rigidity or stability of a truss is accomplished by triangulation of its members, it is generally assumed that all external loads and reactions applied at the joints are resisted by pure axial loads, which are commonly referred to as the primary loads. This would be true if the centroidal axes of all members, at a joint, intersected at a common point and if the members were freely pinned together at the joints. In practice, pin-connected trusses are very seldom encountered; the common types of joints are either welded or gusset joints. Since the rigidity of such joints is a function of the elastic properties of the material and the particular type of construction employed at the joints, they are called elastically constrained joints. If such a truss is loaded at the joints, the joints will offer a certain amount of bending resistance to strain deformation and these induced bending loads will introduce secondary tension and compression stresses in the members in addition to the primary stresses. However, the analyses of such trusses are generally made under the assumption that all joints are pin-connected, which means that secondary loads are neglected and the members of the truss are designed for the primary loads only. If external loads are introduced at points other than the joints, the loads must be resisted by bending and the effects of bending on the member must be taken into account. In the following discussion on truss analysis we shall consider pin-connected trusses only; however, in the discussion on frame analysis the bending stiffness of the members will be taken into account.

From an analysis point of view, trusses can conveniently be divided into two classes, those which are statically determinate and those which are statically indeterminate. Consider, for example, the simple truss structure shown in Fig. 4-1 in which the loads in each member can be determined from purely statical considerations. Now if a fourth member *CD* is introduced, Fig. 4-2, the loads in each member can no longer

be found from statical considerations alone. In this case it is necessary to consider the elastic properties of the members. The first truss is therefore statically determinate, while the second one is statically indeterminate.

In addition to the above classification, consideration should also be given to the geometrical configuration of the members. Here again trusses can be divided into two groups, namely, plane trusses and space trusses. In the former group the axes of all members lie in the same plane whereas in the latter group the axes may lie in different planes so

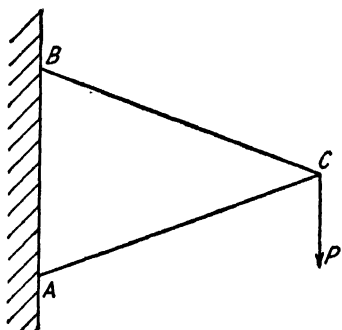


FIG. 4-1. Statically determinate truss.

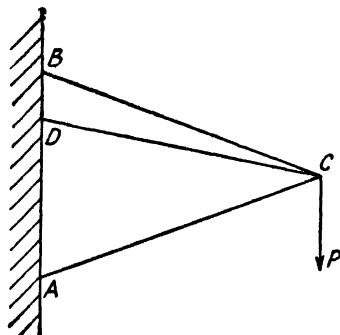


FIG. 4-2. Statically indeterminate truss.

that a three-dimensional figure is formed. In the majority of cases it will be possible to divide a space truss into a system of plane trusses, each of which is then calculated separately. Certain members may be common to two or more plane trusses and, if this is true, the loads obtained from the separate determinations should be added algebraically.

Since the determination of the loads in the members of a statically determinate truss, under the action of a given system of external loads, is covered in detail in elementary texts on applied mechanics, no detailed description of basic principles is intended in the following discussion, but merely a review of the more useful methods and their application. The following three methods are most commonly used; the particular one employed in any given problem will depend on the circumstances and the nature of the problem. These methods are as follows: (1) Calculation of the loads by resolution of forces at each junction or node. From the equilibrium equations $\Sigma F_v = 0$, $\Sigma F_h = 0$ the unknown forces in each member can be calculated. (2) The load in each member is determined graphically by means of a stress diagram. This method is quite useful in complicated truss systems inasmuch as it is self-checking. (3) Calculation of the loads in each member by taking sections of the

truss and calculating the loads in the "cut" members from the equilibrium equations $\Sigma M = 0$, $\Sigma F_v = 0$, $\Sigma F_h = 0$.

(a) Method of Resolution of Forces. Consider the simple truss shown in Fig. 4-3a subjected to the external forces W_1 and W_2 . To obtain the loads in members 1-2 and 1-5, resolve the forces in each member into their vertical and horizontal components and from the equilibrium equation $\Sigma F_v = 0$, solve for the vertical component of force in each member in terms of the known external force W_1 . In this particular case, member 1-2 has no vertical component, hence the vertical component of member 1-5 is equal to W_1 . In the same manner from the equilibrium equation $\Sigma F_h = 0$, solve for the horizontal component of force in each member in terms of the external force W_1 . Then, in general, from the two equations $\Sigma F_v = 0$ and $\Sigma F_h = 0$ the load in each member can be calculated. Since there are only two distinct equilibrium equations for each node, it is necessary that there be only two members of each node in which the loads are not known, or one member and one reaction, or two reactions. The above method is advantageous in the simpler cases.

(b) Method of Stress Diagram. In drawing stress diagrams a type of notation, known as "Bow's notation," is particularly useful. Considering again the truss shown in Fig. 4-3a, letters A, B, C, D, E, F, G , and H are placed in all the spaces of the frame, and in the spaces between external forces. Note that the reactions are treated as external forces. For each member or force separating two spaces in the truss diagram there corresponds a line joining two points in the stress diagram, Fig. 4-3b. The stress diagram must be started at a node where there are no more than two unknown forces. The reactions R_1 and R_2 are calculated from the equilibrium conditions of the frame as a whole. In Fig. 4-3a we could begin at node 1 or 3 but not at 2. Beginning at node 1, we draw ab downwards parallel to W_1 , and of a length representing W_1 to a suitable scale. Through a we draw a line parallel to 1-5 and through b a line parallel to 1-2. These lines intersect in g and abg is the stress diagram for point 1. The lengths ag and bg give the magnitude of the forces in 1-5 and 1-2. Proceed now to point 5 and draw a line parallel to 5-4 through a , and through g a line parallel to 5-2. These lines intersect in f . The magnitudes of af and gf give the loads in 5-4 and 5-2, respectively. We now go to point 2.

At b draw bc vertically downwards representing W_2 . Through f draw a line parallel to 2-4 and through c a line parallel to 2-3; these lines intersect in e . Going to point 3, draw a line parallel to R_1 through c in the direction of R_1 and equal to R_1 . Since 3-4 is normal to 2-3 and R_1 , the load in 3-4 is zero and d and e coincide. Now considering point 4,

through d draw a line parallel to R_1 in the direction of R_1 and equal in magnitude to R_1 . Since the two reactions are equal, c and h coincide. Furthermore, since R_2 is vertical and is equal to the external forces, h must be vertically below a . The stress diagram was really completed after the point 3 was considered, for all the reactions and forces in the members at point 4 were then known. However, a check of whether the stress diagram closes is obtained by considering all points.

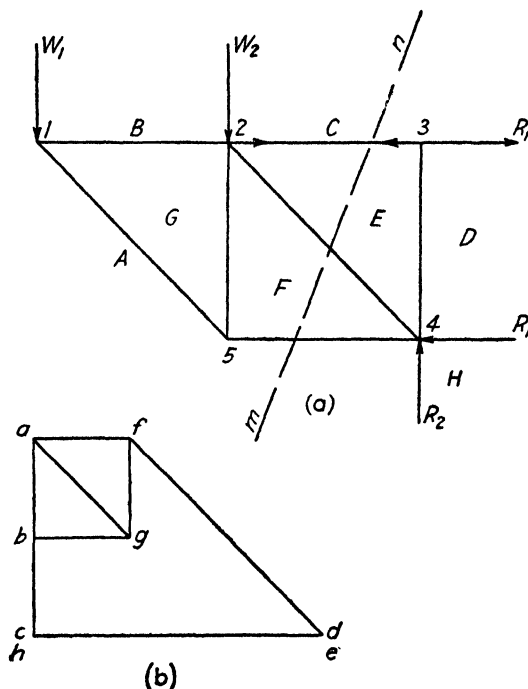


FIG. 4-3. Truss notation and force diagram.

If at any stage no node can be found having two or less unknown forces it is necessary to calculate the loads in some of the members by the method of sections in order that the diagram may be continued.

The direction of the forces in the members can be found by the following rule. If we pass round a node always in the clockwise direction, the direction of the lines in the stress diagram will give the direction of the forces. Thus passing clockwise from A to B around 1 the force W_1 is downwards and ab is drawn downward; passing on from B to G we see that bg is to the right, hence the force in 1-2 at 1 is to the right and is a tension force. In a similar manner the direction of the forces can be determined at any node. The above method is advantageous in the case of a complicated truss.

(c) Method of Sections. This method is particularly advantageous if it is only desired to determine the load in certain members. Assume, for example, that the loads in members 2-3, 2-4, and 4-5 are desired. Cutting the truss along the line mn , Fig. 4-3a, the loads in the cut members are found by considering the equilibrium of one part of the structure under the external loads on this part and the forces in the cut members. For instance if the load in member 5-4 is desired it is only necessary to take moments about point 2.

As previously pointed out, the equations of pure statics are not sufficient for determining the loads which occur in a statically indeterminate truss. It should in no way be construed that the equations of statics are no longer valid, but it merely means that there are more unknowns that can be solved for by the available number of equations of statics. It is evident from the analysis of statically determinate trusses, that the load distribution between the various members is not a function of the size of the members or their elastic properties, but merely a function of their geometrical configuration. This assumes, of course, that the members are sufficiently strong to carry the loads and any elongation of the members does not materially alter the geometry of the truss. In the truss, shown in Fig. 4-2, any one of the members may be removed and the truss will still be capable of carrying an external load P . This means, that essentially we have three trusses, namely, ABC , ADC , or BDC , each one being capable of carrying the load. Actually the load will be divided between the various members according to their relative stiffnesses and their geometrical configurations. Structures of this type are termed redundant and are of considerable importance in airplane design. It is not necessarily the arrangement of members only that gives rise to redundancies, for reactions and stiff joints may equally well cause a redundancy. A redundancy of members can easily be detected if an attempt is made to solve the structure by pure statics. The maximum number of statically determined reactions, for a plane body, is three, hence if more than three reactions are present in any plane body, the reactions will constitute a redundancy.

One of the properties common to all statically indeterminate structures is that a state of self-strain may be set up in the members without the application of an external load. For example, the shortening of member AC , Fig. 4-2, would produce a state of strain in the other members. As will be shown later in the analysis this particular property of statically indeterminate structures is of considerable importance in the solution of such problems. Statically determinate structures are incapable of self-strain; for instance the shortening of a member in a determinate

truss would merely alter the geometry of the structure and would produce no strain in the other members.

(d) Work and Strain Energy. Work is defined as the product of force and distance. If a constant force P moves through a distance δ then the work done will be $P\delta$, provided δ is the component of displacement in the direction of the force. If the force is not constant, the work done will be given by $\int P d\delta$. Consider, for example, a straight bar, Fig. 4-4a, gradually loaded at one end. During application of the load, the bar will stretch and, if the final load is P , and the corresponding deforma-

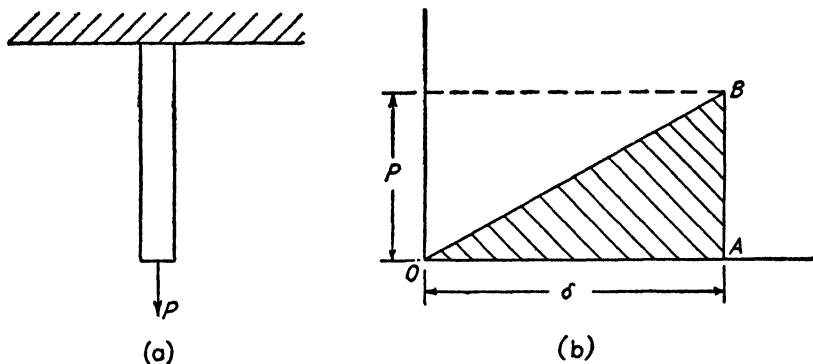


FIG. 4-4. Strain energy due to tension load.

tion is δ , the work, W , done by the external force will be equal to the area OAB , Fig. 4-4b, or

$$W = \frac{P\delta}{2} \quad [4.1]$$

If we consider a prismatical bar of length L and cross-section area A , the deflection will be

$$\delta = \frac{PL}{AE} \quad [4.2]$$

By substituting this relation in equation 4.1 we have

$$W = \frac{P^2 L}{2AE} \quad [4.3]$$

or

$$W = \frac{\delta^2 AE}{2L} \quad [4.4]$$

The first equation gives the work in terms of the external load P , and the second equation gives the work in terms of the deflection δ .

During the process of loading, the bar has been strained and has absorbed strain energy. If it is assumed that the deformation δ is purely elastic, then by the law of conservation of energy the *external work* done by the force in moving through the distance δ , must be equal to the internal work or the strain energy U absorbed by the bar. Hence we may write

$$\text{Strain energy} = U = W = \frac{P^2 L}{2AE} = \frac{\delta^2 AE}{2L} \quad [4.5]$$

Although the load application was restricted to a gradual one, the principle holds for sudden applications as well. A sudden application of load will produce kinetic energy in the form of vibrations. However, after these initial vibrations have been damped out, the state of strain will be the same as that resulting from a gradual application of the load. This assumes that all deformations are elastic, i.e., the bar obeys Hooke's law at all times.

It also follows from the law of conservation of energy, that for any elastic system, the work done by the external forces is equal to the total strain energy of the system. Hence, if to any truss system we apply a system of external loads, P_1, P_2, \dots, P_n which produce only axial loads in the truss members, the total strain energy in the system will be

$$U = \sum_{i=1}^{i=n} \frac{P_i^2 L_i}{2A_i E_i} = \frac{P_1 \delta_1}{2} + \frac{P_2 \delta_2}{2} + \dots + \frac{P_n \delta_n}{2} \quad [4.6]$$

where the summation extends over all the members of the truss, and

P_i = load in member i due to the external loads P ,

L_i = length of member i ,

A_i = cross-section area of member i ,

E_i = Young's modulus for member i ,

δ_n = displacement of P_n in the direction of P_n .

(e) Strain Energy of Bending. So far we have considered only the strain energy due to axial loads. In applying pure bending to an elastic body a certain amount of external work is done which must equal the strain energy absorbed by the body. Consider, for example, an element of length dx , Fig. 4.5a, cut from a bent beam. For a given bending moment M and the corresponding angular deflection $d\theta$, the increment of work done by the applied moment will be equal to the area OAB , Fig. 4.5b, or

$$dU = \frac{M d\theta}{2} \quad [4.7]$$

For small angles we can write

$$d\theta = \frac{dx}{R}$$

and from equation 3.36 $\frac{1}{R} = \frac{M}{EI}$

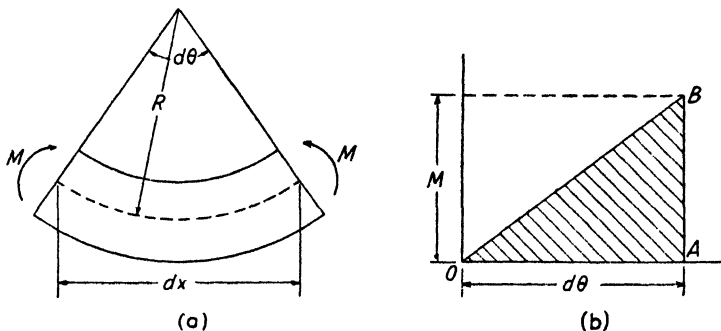


FIG. 4.5. Strain energy due to bending.

Substituting these relations in equation 4.7 we have

$$dU = \frac{M^2 dx}{2EI}$$

The total strain energy of bending for a beam of length L is then

$$U = \frac{1}{2} \int_0^L \frac{M^2}{EI} dx \quad [4.7a]$$

By substituting for M the relation given by equation 3.40, the total strain energy of bending can also be written as

$$U = \frac{1}{2} \int_0^L EI \left(\frac{d^2 y}{dx^2} \right)^2 dx \quad [4.8]$$

(f) Strain Energy of Shear and Torsion. Consider an element of length L subjected to the shearing loads P as indicated in Fig. 4.6a. For simplicity we assume the origin to be the reference point from which displacements are measured. Then, for a given shear force P and the corresponding shearing strain γ , the work done by the external force is equal to the area OAB , Fig. 4.6b, or

$$U = \frac{P\delta}{2}$$

Substituting the relations

$$\gamma = \frac{\delta}{L} = \frac{\tau}{G} = \frac{P}{AG}$$

in the above equation we have

$$U = \frac{P^2 L}{2AG} \quad [4.9]$$

or

$$U = \frac{AG \delta^2}{2L} \quad [4.10]$$

The strain energy of an elastic bar subjected to couples in planes perpendicular to its longitudinal axis can be derived in a similar manner. If

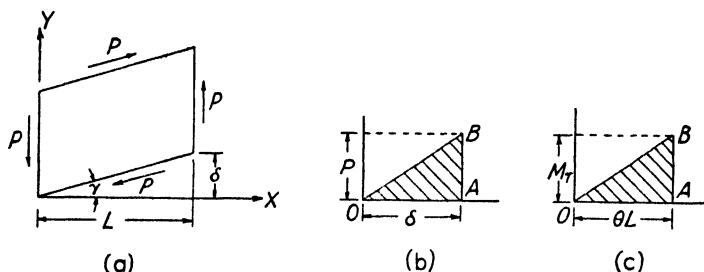


FIG. 4.6. Strain energy due to direct shear and torsion.

φ is the angular twist, θ the angular twist per unit length and C the torsional rigidity of the bar, then the relation between the applied torque M_t , the unit angular twist θ and the angular twist φ is, by definition,

$$\theta = \frac{M_t}{C} = \frac{d\varphi}{dx}$$

For a bar of length L subjected to a constant torque M_t , the total work done by the applied torque is equal to the area OAB , Fig. 4.6c, or

$$U = \frac{M_t L \theta}{2}$$

and from the above relations we have

$$U = \frac{M_t^2 L}{2C} \quad [4.11]$$

or

$$U = \frac{\theta^2 CL}{2} \quad [4.12]$$

If the applied torque is not constant over the length of the bar, the

difference in angular twist of two elements a distance dx apart will be $\frac{d\varphi}{dx} dx$ and we can write:

$$\frac{d\varphi}{dx} dx = \frac{M_t}{C} dx$$

The strain energy of the differential length dx will be

$$du = \frac{M_t}{2} \frac{d\varphi}{dx} dx = \frac{C}{2} \left(\frac{d\varphi}{dx} \right)^2 dx$$

Hence, the total strain energy is

$$U = \frac{C}{2} \int_0^L \left(\frac{d\varphi}{dx} \right)^2 dx \quad [4.13]$$

For example, for a bar of circular cross section the torsional rigidity is JG , see equation 9.3, hence the total energy for a constant torque is

$$U = \frac{M_t^2 L}{2JG}$$

or

$$U = \frac{\theta^2 JGL}{2} \quad [4.12a]$$

(g) Principle of Superposition. Before considering in detail the methods for calculating redundant structures it will be necessary to give some consideration to the derivation of certain general theorems relating to the strain energy of elastic bodies. However, the validity of these theorems is based on the applicability of the principle of superposition. Therefore, it is desirable that the student have a clear understanding of what is meant by the principle of superposition before we consider the general energy theorems.

If the bar shown in Fig. 4.4a is subjected to a tension load $P_1 + P_2$, the strain deformation, Fig. 4.7a, will be

$$\delta = \frac{(P_1 + P_2)L}{AE} = \frac{P_1 L}{AE} + \frac{P_2 L}{AE} = \delta_1 + \delta_2 \quad [4.14]$$

where δ_1 and δ_2 are the strain deformations due to the loads P_1 and P_2 acting separately. This relation, that the strain deformation due to the load $P_1 + P_2$ is equal to the sum of the deformations of P_1 and P_2 acting separately, is called the *principle of superposition*. The above relation only holds if the deformations are elastic, for if the strain is not a linear

function of the load, i.e., if Hooke's law does not hold, the strain deformation due to $P_1 + P_2$ will no longer be equal to the sum of the strain deformations due to P_1 and P_2 acting separately. For example, if the deformation increases at a greater rate than the load, Fig. 4-7b, then δ will be greater than $\delta_1 + \delta_2$.

The principle of superposition is of fundamental importance in the strain energy theory. It means, that for any structure in which all the members obey Hooke's law, and the deflections are linear functions of the applied loads, we can calculate the total deflection at any point, due

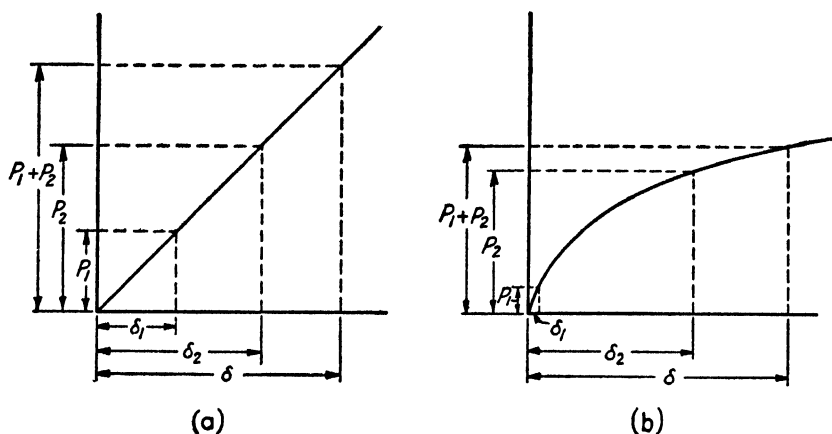


FIG. 4-7. Effect of Hooke's law on principle of superposition.

to a system of loads, by adding algebraically the deflections due to each of the loads acting separately.

(h) Maxwell's Reciprocal Theorem. Before we can proceed with the derivation of a general method for calculating the load distribution in a statically indeterminate structure, it will be necessary to prove a general theorem, the proof of which was first given by Maxwell. Consider the structure shown in Fig. 4-8, subjected to a load P_a at A in the direction θ_a and a load P_b at B in the direction θ_b . The structure is held in equilibrium by the reactions R_1 , R_2 , R_3 , and R_4 which are considered to be fixed, hence they do no work. We assume that all the members in the structure obey Hooke's law of deformation and that the work done by the external forces acting on the structure depends only on the end positions. As a consequence of the first assumption it follows that the displacement of any point in any given direction, produced by an applied load at any other point in any given direction, will be proportional to the applied load. If by the first subscript we designate the point at which the displacement occurs, and by the second subscript the cause of the

displacement. then the displacements due to the loads may be written as follows:

The displacement at A in a direction θ_a due to the load $P_a = \delta_{aa}$.

The displacement at A in a direction θ_a due to the load $P_b = \delta_{ab}$.

The displacement at B in a direction θ_b due to the load $P_a = \delta_{ba}$.

The displacement at B in a direction θ_b due to the load $P_b = \delta_{bb}$.

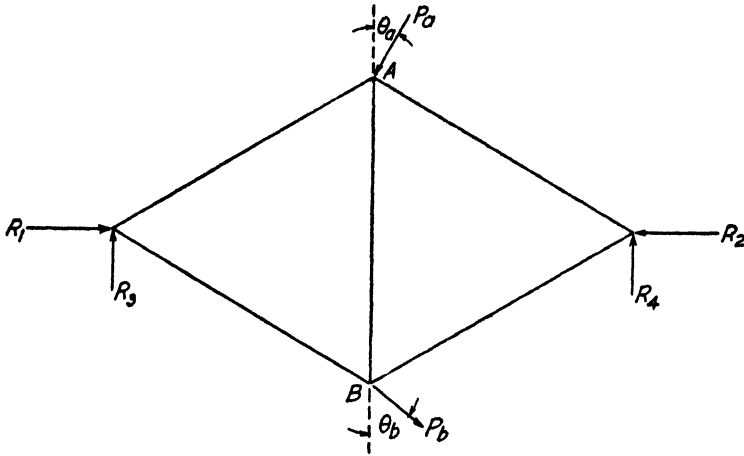


FIG. 4-8.

Assume that we apply the load P_a first, then the external work done by this force will be $P_a \delta_{aa}/2$. The load P_a causes the point B to deflect an amount δ_{ba} , but since there is no external load at this point no work is done. Let us now apply the load P_b , then the external work done at

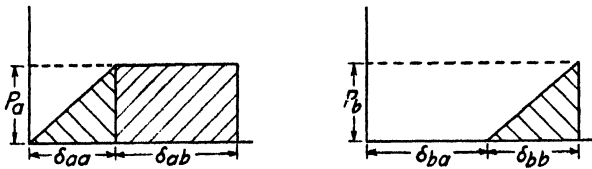


FIG. 4-9.

point B will be $P_b \delta_{bb}/2$. The load P_b produces a displacement δ_{ab} at the point A and since the load P_a already exists, the external work done at point A by P_a due to the application of P_b is $P_a \delta_{ab}$. The work done at each point by these forces is represented graphically by the shaded areas of Fig. 4-9. The total work done is, therefore,

$$U_1 = \frac{1}{2}P_a \delta_{aa} + \frac{1}{2}P_b \delta_{bb} + P_a \delta_{ab} \quad [4.15]$$

In a similar manner it can be shown that if we apply the load P_b first and then P_a that the external work done will be as illustrated graphically by the shaded areas of Fig. 4-10, and the total work done will be

$$U_2 = \frac{1}{2}P_b\delta_{bb} + \frac{1}{2}P_a\delta_{aa} + P_b\delta_{ba} \quad [4-16]$$

Since we postulated that the work done by the external forces is a function only of the final loads and displacements, it follows that the energy state given by U_1 is equal to that given by U_2 , for the final deflections will be the same for each, being independent of the order in which the loads are applied. By equating these two expressions for the work we have

$$P_a\delta_{ab} = P_b\delta_{ba} \quad [4-17]$$

The physical meaning of equation 4-17 is, that the force P_a acting through the displacement produced by the load P_b at A, in the direction θ_a ,

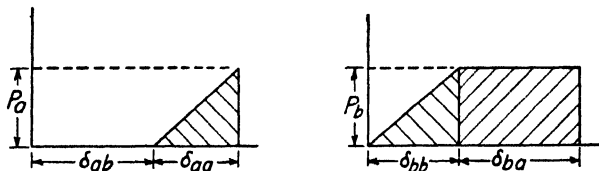


FIG. 4-10.

does the same amount of work as the force P_b acting through the displacement produced by P_a at B, in the direction θ_b . This particular relationship is known as Maxwell's reciprocal theorem. Maxwell's theorem is not restricted to loads only, but may be extended to include the following theorem for moments.

If M_a and M_b are moments applied to A and B, respectively, then the moment M_a acting through the angular displacement produced at A, by the moment M_b does the same amount of work as the moment M_b acting through the angular displacement produced, at B, by the moment M_a .

If $P_a = P_b$ it follows from equation 4-16 that

$$\delta_{ab} = \delta_{ba} \quad [4-18]$$

This means that the component of displacement at A, in the direction θ_a , due to an application of a load at B, in the direction θ_b , is equal in magnitude to the component of displacement at B, in the direction θ_b , due to the application of an equal load at A, in the direction θ_a . The relation expressed by equation 4-17 is particularly useful in calculating deflections.

(i) **Castigliano's Theorem.** It has been shown, equation 4-5, that the strain energy of an elastic body can be expressed as either a quadratic

function of the external load, or as a quadratic function of the displacement. From the energy expressions for a few of the loading conditions for which the deflections are known, it can readily be shown that the derivative of the strain energy with respect to the applied load gives the deflection of the point at which the load is applied, in the direction of the applied load. For example, in the case of a rod subjected to pure tension, equation 4.3,

$$\frac{dU}{dP} = \frac{d(P^2L/2AE)}{dP} = \frac{PL}{AE} = \delta_P \quad [4.19]$$

For a simple beam loaded at the center, we obtain from equation 4.7 for the strain energy due to bending

$$U = \frac{P^2L^3}{96EI}$$

From this the deflection at the center is

$$\frac{dU}{dP} = \frac{PL^3}{48EI} = \delta_P$$

Castigliano's theorem is a more general statement of these results and can be stated as follows:

The partial derivative of the strain energy, expressed in terms of the external loads, of any elastic system with respect to any one of the external loads, gives the displacement of the system, at this load, in the direction of the load.

Consider, for example, a structure subjected to a system of external loads, $P_1, P_2, \dots P_n$, then the elastic energy stored in the system will be

$$U = \frac{1}{2}[P_1\delta_1 + P_2\delta_2 + \dots + P_n\delta_n] \quad [4.20]$$

Now if to each external load is added an increment of load ΔP , the deflections at each load will increase by an amount $\Delta\delta$. Correspondingly the strain energy of the system will be increased by an amount ΔU , and the new energy in the system can be expressed as

$$U + \Delta U = \frac{1}{2}[(P_1 + \Delta P_1)(\delta_1 + \Delta\delta_1) + (P_2 + \Delta P_2)(\delta_2 + \Delta\delta_2) + \dots + (P_n + \Delta P_n)(\delta_n + \Delta\delta_n)] \quad [4.21]$$

Now subtracting equation 4.20 from equation 4.21 and neglecting second order terms gives

$$\Delta U = \frac{1}{2}[P_1\Delta\delta_1 + P_2\Delta\delta_2 + \dots + P_n\Delta\delta_n] + \frac{1}{2}[\Delta P_1\delta_1 + \Delta P_2\delta_2 + \dots + \Delta P_n\delta_n] \quad [4.22]$$

From the reciprocal theorem, equation 4.17, it follows that, $P_1\Delta\delta_1 = \Delta P_1\delta_1$ or, in general, $P_n\Delta\delta_n = \Delta P_n\delta_n$, hence

$$\Delta U = \Delta P_1\delta_1 + \Delta P_2\delta_2 + \cdots + \Delta P_n\delta_n \quad [4.23]$$

If an increment of load ΔP_i is added to the load P_i only, that is, all other loads in the system remain constant, then all the terms in equation 4.23 vanish except the term $\Delta P_i\delta_i$ and it follows that

$$\frac{\Delta U}{\Delta P_i} = \frac{\partial U}{\partial P_i} = \delta_i \quad [4.24]$$

If this theorem is applied to the general expression for the strain energy

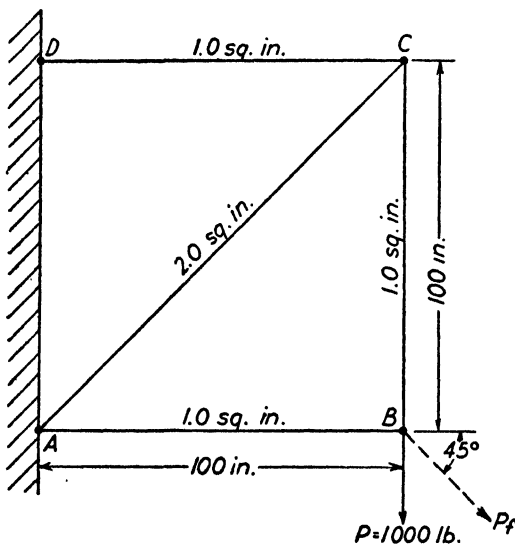


FIG. 4.11. Example of statically determinate truss.

in a truss structure, equation 4.6, we obtain the following expression for the component of deflection of the load P_k in the direction of P_k

$$\delta_k = \frac{\partial U}{\partial P_k} = \sum_{i=1}^{i=n} \frac{P_i L_i}{A_i E_i} \frac{\partial P_i}{\partial P_k} \quad [4.25]$$

The derivative $\partial P_i / \partial P_k$ is the rate of change of the load in member i due to the application of the load P_k . Numerically this derivative is equal to the change produced in the load carried by member i due to an application of a unit load at K in the direction of P_k . This fact is particularly useful in calculating deflections in general. Assume, for instance, that it is desired to calculate the component of displacement of B , Fig. 4.11, due to the load P , in any direction. In order to apply Castigli-

ano's theorem it is only necessary to introduce a fictitious load P_f in the direction in which the component of displacement is desired and to evaluate the derivative $\partial U/\partial P_f$. Since, actually the load P_f is non-existent, it is set equal to zero in the expression for the derivative $\partial U/\partial P_f$, i.e.,

$$\delta_f = \left(\frac{\partial U}{\partial P_f} \right)_{P_f=0} = \sum_{i=1}^{i=n} \frac{P_i L_i}{A_i E_i} \frac{\partial P_i}{\partial P_f} \quad [4.26]$$

The loads P_i are those due to P only since $P_f = 0$ and the derivative $\partial P_i/\partial P_f$ is evaluated by applying a unit load in the direction of P_f and calculating the loads in each member due to this unit load.

Example. Consider the truss system shown in Fig. 4.11. The cross-section areas and the lengths of the members are as indicated in the figure. Young's modulus $E = 30 \times 10^6$ lb. per sq. in. is the same for all members. It is desired to calculate at the point B , the vertical displacement and the component of displacement at an angle of 45 degrees to the horizontal. Equations 4.25 and 4.26 can be conveniently evaluated in a tabular form as shown below. Column 5 is obtained by applying a unit load at point B in the direction of P and column 8 by applying a unit load at an angle of 45 degrees to the horizontal. In each case, when the unit load is applied, all other external loads are zero.

1	2	3	4	5	6	7	8	9
i	L_i	$E_i A_i$	P_i	$\frac{\partial P_i}{\partial P_k}$	$\frac{P_i L_i}{A_i E_i}$	$\frac{P_i L_i}{A_i E_i} \left(\frac{\partial P_i}{\partial P_k} \right)$	$\frac{\partial P_i}{\partial P_f}$	$\frac{P_i L_i}{A_i E_i} \left(\frac{\partial P_i}{\partial P_f} \right)$
AB	100	30×10^6	0	0	0	0	0.707	0
BC	100	30×10^6	1000	1	0.333×10^{-2}	0.333×10^{-2}	0.707	0.236×10^{-2}
CD	100	30×10^6	1000	1	0.333×10^{-2}	0.333×10^{-2}	0.707	0.236×10^{-2}
CA	141.4	60×10^6	-1414	-1.414	0.333×10^{-2}	0.472×10^{-2}	-1.0	0.333×10^{-2}

$$\delta_p = \sum_{i=1}^{i=n} \frac{P_i L_i}{A_i E_i} \frac{\partial P_i}{\partial P_k} = 1.138 \times 10^{-2} \text{ in.}$$

$$\delta_f = \sum_{i=1}^{i=n} \frac{P_i L_i}{A_i E_i} \frac{\partial P_i}{\partial P_f} = 0.805 \times 10^{-2} \text{ in.}$$

So far we have applied Castigliano's theorem only to statically determinate trusses. It is apparent from equation 4.24 that in order to calculate the deflection or its components at any point it is necessary that the loads in all members be calculable in terms of the external loads. Therefore, in a statically indeterminate truss it would be impossible to calculate the deflections by means of equation 4.25 or equation 4.26. If, on the other hand, at any joint the deflection is known, the magnitude of the external load can be calculated. In particular, redundant reactions

can be calculated when the reactions are either fixed so that their displacements are zero, or if their motion is restricted to a finite known magnitude. In such cases, the strain energy is expressed in terms of known external loads and the unknown reactions, which can be considered as external loads. The magnitudes of the unknown reactions can then be calculated by means of equation 4.25.

(j) **Castigliano's Second Theorem.** In redundant members we can apply Castigliano's general theorem to obtain a theorem which is known as Castigliano's second theorem. Consider for example the member

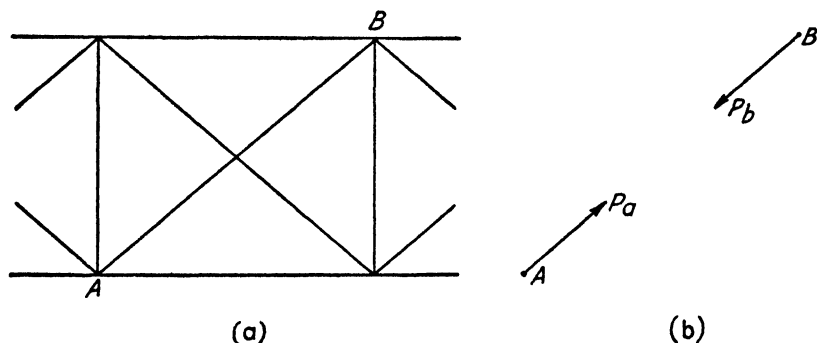


FIG. 4.12.

AB , Fig. 4.12a, in any truss system which is subjected to external loads $P_1, P_2, P_3, \dots, P_n$. Now let us replace the member AB by two external forces P_a and P_b , Fig. 4.12b, equal in magnitude to the force in the member AB . If by U' we designate the work done by the external loads including P_a and P_b , then U' will be equal to the strain energy of the system excluding member AB . The total strain energy of the system in terms of the external loads will be given by

$$U' = \sum_{i=1}^{i=n} \frac{(\alpha_i P_a + \beta_i P_b + \gamma_i P_1 + \dots + \nu_i P_n)^2}{2A_i E_i} L_i \quad [4.27]$$

Where $\alpha, \beta, \gamma, \dots, \nu$ are constants depending only upon the geometrical configuration of the system.

By Castigliano's theorem

$$\frac{\partial U'}{\partial P_a} = \text{component of displacement of } A \text{ in the direction of } P_a$$

$$\frac{\partial U'}{\partial P_b} = \text{component of displacement of } B \text{ in the direction of } P_b$$

If the original unstrained distance between A and B be denoted by L , and the final distance between A and B be denoted by L' , then

$$L' = L - \left(\frac{\partial U'}{\partial P_a} + \frac{\partial U'}{\partial P_b} \right) \quad [4.28]$$

From equation 4.27

$$\frac{\partial U'}{\partial P_a} + \frac{\partial U'}{\partial P_b} = \sum_{i=1}^{i=n} \frac{(\alpha_i + \beta_i) [\alpha_i P_a + \beta_i P_b + \gamma_i P_1 + \cdots + \nu_i P_n] L_i}{A_i E_i} \quad [4.29]$$

Now let $P_a = P_b = P_{ab}$, where P_{ab} is the tension load in member AB , then

$$\frac{\partial U'}{\partial P_{ab}} = \sum_{i=1}^{i=n} \frac{(\alpha_i + \beta_i) [\alpha_i P_{ab} + \beta_i P_{ab} + \gamma_i P_1 + \cdots + \nu_i P_n] L_i}{A_i E_i} \quad [4.30]$$

Since $P_a = P_b = P_{ab}$, the right-hand side of equations 4.29 and 4.30, are identical we can write

$$\frac{\partial U'}{\partial P_{ab}} = \frac{\partial U'}{\partial P_a} + \frac{\partial U'}{\partial P_b} \quad [4.31]$$

Substituting this relation in equation 4.28 gives

$$L' = L - \frac{\partial U'}{\partial P_{ab}}$$

If the original unstrained length of the member AB was $L - \lambda$, i.e., the member was too short by an amount λ , then the final length of AB due to the load P_{ab} will be

$$L_1 = (L - \lambda) \left(1 + \frac{P_{ab}}{AE} \right)$$

But the final length of member AB must equal the final distance between A and B , hence $L_1 = L'$ and

$$L - \frac{\partial U'}{\partial P_{ab}} = (L - \lambda) \left(1 + \frac{P_{ab}}{AE} \right) \quad [4.32]$$

Expanding the right-hand side of equation 4.32, we have

$$\frac{\partial U'}{\partial P_{ab}} + \frac{P_{ab}}{AE} (L - \lambda) = \lambda$$

But

$$\frac{P_{ab}}{AE} (L - \lambda) = \frac{\partial u}{\partial P_{ab}}$$

where u is the strain energy of the member AB , hence,

$$\frac{\partial(U' + u)}{\partial P_{ab}} = \lambda$$

Since $(U' + u)$ is the total strain energy of the system including member AB , we have

$$\frac{\partial U}{\partial P_{ab}} = \lambda \quad [4.33]$$

This equation states, that the partial derivative of the total strain energy with respect to the load in a redundant member is equal to the original lack of fit, λ , of this member.

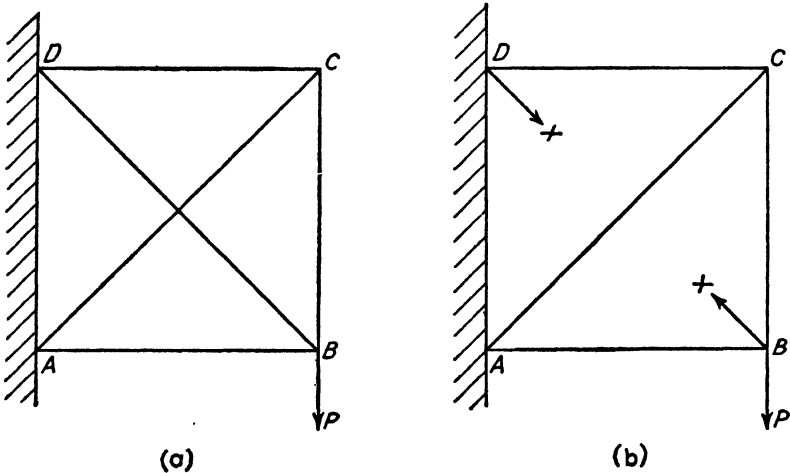


FIG. 4.13.

For a perfect fit $\lambda = 0$ and we obtain the equation

$$\frac{\partial U}{\partial P_{ab}} = 0 \quad [4.34]$$

This equation is generally referred to as the principle of least work, since it is the condition that the force, P_{ab} , in the bar be such as to make the strain energy of the system a minimum.

In a truss system having only a few members the above equations can be applied directly. However in a complicated truss system a direct application of these equations becomes very laborious since it necessitates carrying through the calculations for the load in each member in terms of the unknown load in the redundant member and the known external loads.

By an application of the above principle a system of equations can be derived which simplifies to some extent the calculations of statically indeterminate truss systems. Consider for example the redundant truss, Fig. 4·13*a*, in which member *BD* is the redundant member. Let us replace this member by a force *X*, equal to that in the bar, at each node point as shown in Fig. 4·13*b*. If for *X* we substitute a known force, say, a unit force which we designate by *x*, then the load in each member may be considered as being produced by two sources, namely, the external load *P* and the unit force *x* each acting separately. If by *P_{Ei}* we designate the force produced in member *i*, while *P* alone is acting and by *x_i* the force produced while *x* alone is acting, then when *P* and *X* are both acting the force *P_i* in member *i* will be

$$P_i = P_{Ei} + x_i X \quad [4 \cdot 35]$$

The total strain energy of the system including the redundant member *BD* is

$$U = \sum_{i=1}^{i=n} \frac{(P_{Ei} + x_i X)^2 L_i}{2A_i E_i} \quad [4 \cdot 36]$$

where the summation extends over all the members including the redundant member

and
$$\frac{\partial U}{\partial X} = \sum_{i=1}^{i=n} \frac{(P_{Ei} + x_i X) x_i L_i}{A_i E_i} \quad [4 \cdot 37]$$

But for a perfect fit, equation 4·34

$$\frac{\partial U}{\partial X} = 0$$

Hence

$$\sum_{i=1}^{i=n} \frac{(P_{Ei} + x_i X) x_i L_i}{A_i E_i} = 0$$

Writing $Q_i = \frac{L_i}{A_i E_i}$ and solving for *X* from the above equation we have

$$X = - \frac{\sum_{i=1}^{i=n} P_{Ei} x_i Q_i}{\sum_{i=1}^{i=n} x_i^2 Q_i} \quad [4 \cdot 38]$$

The same method is applicable to a system with any number of redundancies, for example in the case of two redundancies with the corresponding forces *X* and *Y*, the load in any member *i* can be expressed by

$$P_i = P_{Ei} + x_i X + y_i Y$$

Then the total strain energy is

$$U = \sum_{i=1}^{i=n} \frac{(P_{Ei} + x_i X + y_i Y)^2 L_i}{2A_i E_i}$$

and by equation 4.34

$$\frac{\partial U}{\partial X} = \sum_{i=1}^{i=n} \frac{(P_{Ei} + x_i X + y_i Y) x_i L_i}{A_i E_i} = 0 \quad [4.39]$$

$$\frac{\partial U}{\partial Y} = \sum_{i=1}^{i=n} \frac{(P_{Ei} + x_i X + y_i Y) y_i L_i}{A_i E_i} = 0$$

In the general case a system of equations linear in the unknown forces X , $Y \dots$ is obtained, and since the number of equations will equal the number of unknowns, the unknown forces can be calculated.

From equation 4.39 we can obtain for X and Y the following expressions

$$X = \frac{\left(\sum_{i=1}^{i=n} P_{Ei} x_i Q_i \right) \left(\sum_{i=1}^{i=n} y_i^2 Q_i \right) - \left(\sum_{i=1}^{i=n} x_i y_i Q_i \right) \left(\sum_{i=1}^{i=n} P_{Ei} y_i Q_i \right)}{\left(\sum_{i=1}^{i=n} x_i y_i Q_i \right)^2 - \left(\sum_{i=1}^{i=n} x_i^2 Q_i \right) \left(\sum_{i=1}^{i=n} y_i^2 Q_i \right)} \quad [4.40]$$

$$Y = \frac{\left(\sum_{i=1}^{i=n} P_{Ei} y_i Q_i \right) \left(\sum_{i=1}^{i=n} x_i^2 Q_i \right) - \left(\sum_{i=1}^{i=n} x_i y_i Q_i \right) \left(\sum_{i=1}^{i=n} P_{Ei} x_i Q_i \right)}{\left(\sum_{i=1}^{i=n} x_i y_i Q_i \right)^2 - \left(\sum_{i=1}^{i=n} x_i^2 Q_i \right) \left(\sum_{i=1}^{i=n} y_i^2 Q_i \right)} \quad [4.41]$$

Examples. 4.1. Given the truss shown in Fig. 4.14 with dimensions as indicated Required to compute the load in each member.

Assuming BD to be the redundant member, equation 4.38 can be readily evaluated in a tabular form as shown below.

1	2	3	4	5	6	7	8
i	L_i	$Q_i = \frac{L_i}{A_i E_i}$	P_{Ei}	x_i	$P_{Ei} x_i Q_i$	$x_i^2 Q_i$	P_i
$A-B$	30	0.5×10^{-6}	-1000	-0.577	0.288×10^{-3}	0.167×10^{-6}	-1122
$B-C$	30	1.0×10^{-6}	1000	-0.577	-0.577×10^{-3}	0.333×10^{-6}	878
$B-D$	25.98	0.866×10^{-6}	0	1.	0	0.866×10^{-6}	212
				$\Sigma =$	-0.289×10^{-3}	1.366×10^{-6}	

$$X = \text{force in } BD = - \frac{\Sigma P_{Ei} x_i Q_i}{\Sigma x_i^2 Q_i} = \frac{0.289 \times 10^{-3}}{1.366 \times 10^{-6}} = 212 \text{ lb.}$$

The positive sign obtained for X means that the assumed sign of x was correct.

1	2	3	4	5	6	7	8	9	10	11	12	13	14
i	P_i	Q_i	P_{Ei}	x_i	y_i	$P_{Eix}Q_i$	$P_{Eiy}Q_i$	$x_{Di}Q_i$	$x_i^2Q_i$	$y_i^2Q_i$	x_iX	y_iY	P_i
$A-B$	30.0	0.5×10^{-6}	-1000	-0.3954	0.7426	0.1977×10^{-3}	-0.3713×10^{-3}	-0.147×10^{-6}	0.078×10^{-6}	0.2755×10^{-6}	-156	85	-1071
$B-C$	30.0	1.0×10^{-6}	1000	-0.7426	0.3954	-0.7426×10^{-3}	0.3954×10^{-3}	-0.294×10^{-6}	0.551×10^{-6}	0.1562×10^{-6}	-293	45	752
$D-B$	26.4	0.882×10^{-6}	0	1	0	0	0	0	0.882×10^{-6}	0	394	0	394
$B-B$	26.4	0.882×10^{-6}	0	0	-1	0	0	0	0	0.882×10^{-6}	0	-114	-114
					$\Sigma =$	-0.5449×10^{-3}	0.0241×10^{-3}	-0.441×10^{-6}	1.511×10^{-6}	1.314×10^{-6}			

Substituting the numerical values of the summations in equations 4.40 and 4.41 gives

$$X = 394 \text{ lb.}, \quad Y = 114 \text{ lb.}$$

The load in any member will be given by

$$P_i = P_{Ei} + Xx_i + Yy_i$$

It should be noted that although the addition of redundant members redistributes the loads in the structure, it does not necessarily decrease the loads in the original members. Thus without members *BD* and *BE* the load in member *AB* is 1000 lb.; however, when these members are added, the load in *AB* increases to 1071 lb.

If more than two redundancies occur in a truss system the calculations become quite laborious. In present-day metal aircraft construction only the engine mounts are statically indeterminate trusses which have, in general, only one or two redundant members.

Castigliano's second theorem is useful in calculating induced strains in the members of a statically indeterminate structure due to either a misfit of a certain member or variable temperatures. Since a redundant structure has the property of self-strain, it is apparent that the stresses in the members of a loaded truss may be varied by intentional misfits in certain members. This idea is sometimes employed to obtain a better distribution of stresses.

4-2. Frames

Before proceeding with the analysis of frames it might be well to consider the difference between a truss and a frame. As previously pointed out, the stability of a truss is accomplished by triangulation of its members, which are assumed to carry only axial loads. In a frame structure the bending stiffness of the joints as well as the bending stiffness of members may be relied upon to provide the necessary requirements for stability. The members of a frame may be subjected to axial, shear, and bending loads. It is not to be implied that any structure in which the members are triangulated is necessarily a truss; in general, if any one member is bending resistant the structure is considered to be a frame. The difference lies essentially in the assumption as to the manner in which the external loads are resisted rather than the geometrical configuration of the members.

In the analysis of frame structures we can apply Castigliano's theorem as well as the so-called least-work principle. So far we have been dealing only with axial or concentrated forces and linear displacements. In the following discussion we shall consider forces and displacements to have their generalized meaning, that is, they are to include couples and angu-

lar displacements respectively. Consider for example a section of a beam, Fig. 4-16, subjected to an external couple M . Now any couple may be replaced by two equal and opposite forces so that $M = Ph$, and

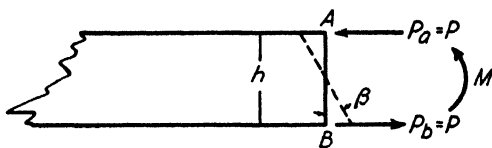


FIG. 4-16. Beam under bending.

if we indicate by the subscripts a and b their points of application, we have from equation 4-31

$$\frac{\partial U}{\partial P_a} + \frac{\partial U}{\partial P_b} = \frac{\partial U}{\partial P} = \delta_a + \delta_b$$

and

$$\frac{1}{h} \frac{\partial U}{\partial P} = \frac{\delta_a + \delta_b}{h}$$

but

$$\frac{1}{h} \frac{\partial U}{\partial P} = \frac{\partial U}{\partial (Ph)} = \frac{\partial U}{\partial M} = \frac{\delta_a + \delta_b}{h}$$

Since in the theory of the bending of beams we assume that all cross sections remain plane, we have

$$\frac{\partial U}{\partial M} = \frac{\delta_a + \delta_b}{h} = \beta \quad [4.42]$$

where β is the angular displacement of the end cross section related to a plane perpendicular to the longitudinal axis of the beam. Hence, if an external couple M is applied to one end of a horizontal beam, then equation 4-42 will yield the slope of the deflection curve at that end.

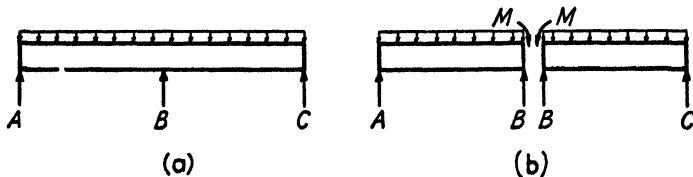


FIG. 4-17. Statically indeterminate beam.

The foregoing relation can be used to investigate redundant internal couples. Consider a loaded beam resting on three supports (Fig. 4-17a). The moment at B is redundant. Let us cut the beam at B (Fig. 4-17b), and replace the internal moment at B by an equal external couple, M .

We can now consider the system as two separate beams subjected to end couples as shown. Now if U_1 = strain energy of beam AB , and U_2 = strain energy of beam BC , we can apply equation 4.42 and obtain

$$\theta_1 = \frac{\partial U_1}{\partial M}, \quad \theta_2 = \frac{\partial U_2}{\partial M}$$

where θ_1 and θ_2 represent the slope at B . But inasmuch as the beam, and hence the deflection curve, is continuous

$$\theta_1 = -\theta_2$$

and

$$\frac{\partial U_1}{\partial M} + \frac{\partial U_2}{\partial M} = 0$$

or

$$\frac{\partial(U_1 + U_2)}{\partial M} = 0$$

But $U_1 + U_2 = U$ where U is total strain energy of the beam. Hence,

$$\frac{\partial U}{\partial M} = 0$$

where M is a redundant internal couple. The application of the energy equation to frame structure will be illustrated in the following examples:

Example 4.3. Consider the beam of Fig. 4-18. It is subjected to a uniformly distributed upward load, w , and is fixed at A , so that either the moment at A or the tension in BC is statically indeterminate. If we replace the member BC by the tension load T acting as shown, we can then write, for the moment at any point X on the beam

$$M = \frac{wx^2}{2} - Tx \cos 60^\circ = \frac{wx^2}{2} - \frac{Tx}{2}$$

Let A_1 be the cross-sectional area of the beam, A_2 the cross-sectional area of the tension member BC , E_1 the modulus of elasticity of the beam, and E_2 the modulus of elasticity of BC .

We can now write for the strain energy in bending from B to A

$$\begin{aligned} U_1 &= \frac{1}{2E_1I} \int_0^L (M_x)^2 dx = \frac{1}{2E_1I} \int_0^L \left(\frac{wx^2}{2} - \frac{Tx}{2} \right)^2 dx \\ &= \frac{1}{8E_1I} \left(\frac{w^2 L^5}{5} - \frac{2wTL^4}{4} + \frac{T^2 L^3}{3} \right) \end{aligned}$$

and for the strain energy in compression in AB

$$U_2 = \frac{P^2 L}{2AE} = \frac{(T \cos 30^\circ)^2 L}{2A_1 E_1} = \frac{3T^2 L}{8A_1 E_1}$$

Hence, the total strain energy in the beam will be

$$U = U_1 + U_2 = \frac{1}{8E_1I} \left(\frac{w^2L^5}{5} - \frac{2wTL^4}{4} + \frac{T^2L^3}{3} \right) + \frac{3T^2L}{8A_1E_1}$$

From Castigliano's first theorem, the component of the deflection of B in the direction of T will be

$$\delta_1 = \frac{\partial U}{\partial T} = \frac{TL^3}{12E_1I} - \frac{wL^4}{16E_1I} + \frac{6TL}{8A_1E_1}$$

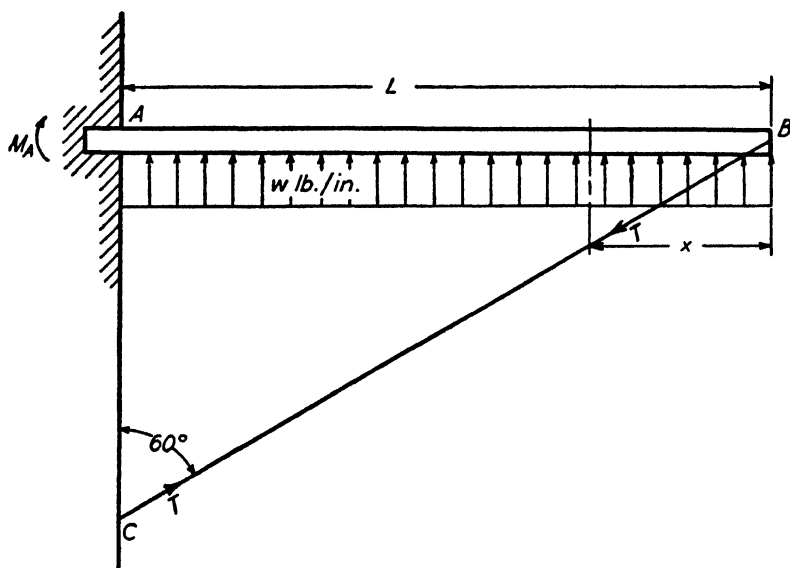


FIG. 4-18. Example of a statically indeterminate system.

From a consideration of the deformation in BC due to the axial load T , we can also write

$$\delta_2 = \frac{PL}{AE} = \frac{TL \csc 60^\circ}{A_2E_2} = \frac{2TL}{\sqrt{3}A_2E_2}$$

and, since δ_2 is equal and opposite to δ_1 ,

$$\delta_1 = -\delta_2$$

or

$$\frac{TL^3}{12E_1I} - \frac{wL^4}{16E_1I} + \frac{6TL}{8A_1E_1} = \frac{-2TL}{\sqrt{3}A_2E_2}$$

from which

$$T = \frac{\frac{wL^3}{16E_1I}}{\frac{L^2}{12E_1I} + \frac{3}{4A_1E_1} + \frac{2}{\sqrt{3}A_2E_2}}$$

This result can also be obtained by considering the total energy of the system and

applying the principle of least work. The strain energy of the beam has already been obtained. The strain energy of the tension member BC is

$$U_3 = \frac{T^2 L \csc 60^\circ}{2A_2 E_2} = \frac{T^2 L}{\sqrt{3} A_2 E_2}$$

Hence the total strain energy of the system can be written

$$U = U_1 + U_2 + U_3$$

or

$$U = \frac{1}{8E_1 I} \left(\frac{w^2 L^5}{5} - \frac{2wTL^4}{4} + \frac{T^2 L^3}{3} \right) + \frac{3T^2 L}{8A_1 E_1} + \frac{T^2 L}{\sqrt{3} A_2 E_2}$$

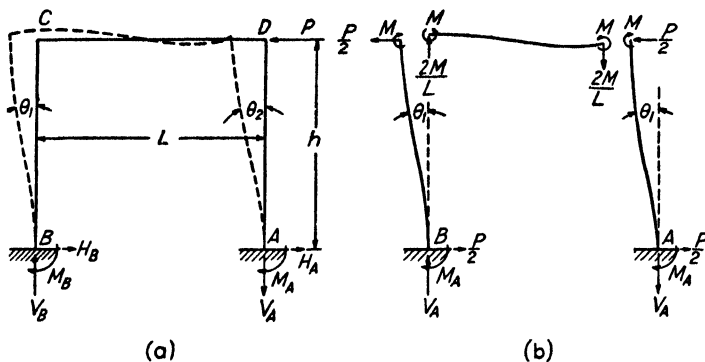


FIG. 4-19. Rectangular frame.

If we consider the member BC to be redundant, then by the principle of least work

$$\frac{\partial U}{\partial T} = 0$$

Hence

$$-\frac{wL^4}{16E_1 I} + \frac{TL^3}{12E_1 I} + \frac{3TL}{4A_1 E_1} + \frac{2TL}{\sqrt{3} A_2 E_2} = 0$$

from which

$$T = \frac{\frac{wL^3}{16E_1 I}}{\frac{L^2}{12E_1 I} + \frac{3}{4A_1 E_1} + \frac{2}{\sqrt{3} A_2 E_2}}$$

which is identical to the result previously obtained.

The problem could have been solved equally well by considering M_A as the redundancy, solving for the total energy of the system in terms of M_A and writing

$$\frac{\partial U}{\partial M_A} = 0$$

This, then, would yield the expression for M_A .

Example 4-4. Given the frame shown in Fig. 4-19a. Assume E and I constant for all members. From the symmetry of the frame we can assume that the deflections θ_1 and θ_2 due to the horizontal load P will be equal. This means that in the free-body dia-

gram (Fig. 41·19b), the horizontal loads at C and D must be the same and hence equal to $P/2$. This determines the horizontal reactions at A and B and we have $H_A = H_B = P/2$. Inasmuch as members AD and BC are subjected to the same loading conditions, we can also write: $M_A = M_B$. Similarly, $M_C = M_D = M$. The foregoing assumes identical end conditions at A and B .

The strain energy for member AD can be written

$$U_1 = \frac{1}{2EI} \int_0^h \left(M - \frac{P}{2} y \right)^2 dy$$

This also gives the strain energy in member BC .

For CD , we can write

$$U_2 = \frac{1}{2EI} \int_0^L \left(M - \frac{2M}{L} x \right)^2 dx$$

The total strain energy will be

$$U = 2U_1 + U_2 = \frac{1}{EI} \int_0^h \left(M - \frac{P}{2} y \right)^2 dy + \frac{1}{2EI} \int_0^L \left(M - \frac{2M}{L} x \right)^2 dx$$

From the principle of least work

$$\frac{\partial U}{\partial M} = 0$$

Hence

$$\frac{2}{EI} \left(Mh - \frac{Ph^2}{4} \right) + \frac{1}{EI} \left(ML - 2ML + \frac{4}{3} ML \right) = 0$$

and

$$M = \frac{Ph}{4 \left(1 + \frac{L}{6h} \right)} \quad (1)$$

Taking moments about A (Fig. 4·19a)

$$M - \frac{Ph}{2} + M_A = 0$$

Substituting (1) for M

$$M_A = \frac{Ph}{2} \left(1 - \frac{1}{2 \left(1 + \frac{L}{6h} \right)} \right)$$

It is also evident from Fig. 4·19b, that the vertical reactions will be

$$V_A = V_B = \frac{2M}{L} \quad (\text{directions as indicated})$$

Hence

$$V_A = \frac{Ph}{2L \left(1 + \frac{L}{6h} \right)}$$

Example 4·5. Given a circular frame, Fig. 4·20a, subjected to a tangential-running shear load of magnitude $w \sin \varphi$ lb. per in., where φ is measured as indicated. It is assumed that the tangential shear acts at the centroid of the frame and that EI is a constant. Required to compute the bending moment at any point.

From the free-body diagram, Fig. 4-20b, the moment at any point on the ring at an angle θ is

$$\begin{aligned} M_\theta &= M + PR(1 - \cos \theta) - \int_0^\theta wR \sin \varphi [1 - \cos (\theta - \varphi)] R d\varphi \\ &= M + PR(1 - \cos \theta) - wR^2 \left(1 - \cos \theta - \frac{\theta}{2} \sin \theta \right) \end{aligned}$$

The bending energy from C to B is

$$U = \int_0^{\pi/2} \frac{M_\theta^2 R d\theta}{2EI}$$

And from the principle of least work we have

$$\frac{\partial U}{\partial M} = \frac{1}{EI} \int_0^{\pi/2} M_\theta R \left(\frac{\partial M_\theta}{\partial M} \right) d\theta = 0; \quad \frac{\partial U}{\partial P} = \frac{1}{EI} \int_0^{\pi/2} M_\theta R \left(\frac{\partial M_\theta}{\partial P} \right) d\theta = 0$$

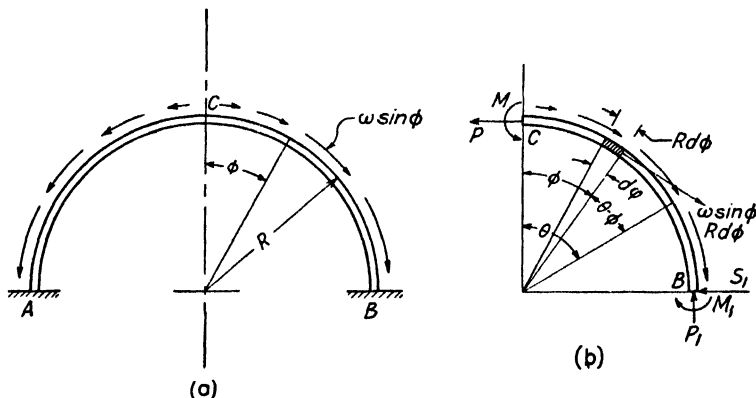


FIG. 4-20. Circular frame notation.

Substituting the expression for the moment M_θ in the above two expressions we have, respectively,

$$1.5708M + 0.5708PR - 0.0708wR^2 = 0$$

$$0.5708M + 0.3562PR - 0.0520wR^2 = 0$$

Solving these two equations simultaneously we obtain

$$M = -0.019wR^2, \quad P = 0.1762wR$$

Substituting these values of M and P in the equation for M_θ , the moment at any point can be calculated in terms of w and R , which will be known quantities in a given structure.

REFERENCES FOR CHAPTER 4

- 4-1. S. TIMOSHENKO, *Strength of Materials*, Part I, Van Nostrand, 1930.
- 4-2. R. V. SOUTHWELL, *Theory of Elasticity*, Oxford Press, 1936.
- 4-3. A. J. S. PIPPARD and J. L. PRITCHARD, *Aeroplane Structures*, Longmans, Green and Co., 1935.

CHAPTER 5

THE PROBLEM OF INSTABILITY

5-1. Columns with Stable Cross Sections

Short, heavy sections under compression loads obey the laws discussed in Chapter 3, and such sections will suffer permanent set when the normal compressive stress passes the compressive yield point of the material; failure of the section will occur when the compressive stress has reached the ultimate compressive stress of the material. If, on the other hand, we consider a very long, slender rod subjected to a compression load along its axis, experience tells us that it will suffer a lateral, bending deformation and cease to carry additional load at a stress which is much below the yield point or ultimate stress of the material. Such a structural element is known as a long column and the failure is

one of instability in a direction perpendicular to the direction of applied load.

In one way or another, structural elements whose failure is of the column type make up a large percentage of the stress-carrying portions of an airplane. It is therefore desirable to review the various forms of column failure and the theoretical and empirical methods which are used to calculate the allowable loads for such structural elements. Consideration will first be given to columns having cross sections which are not subject to local instability or torsional failure and, in a later section, the effects of these phenomena will be investigated.

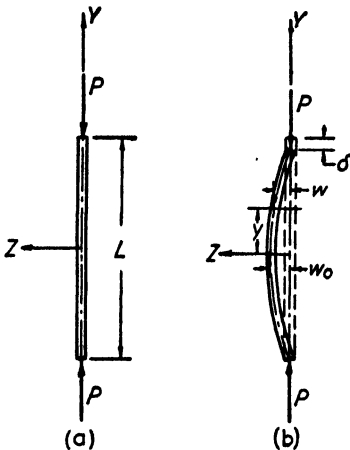


FIG. 5-1. Column notation.

Stated in words, long column failure can be expressed as follows: When the elastic energy of a rod under a compressive load is greater when the rod is bent in a direction perpendicular to its axis (Fig. 5-1b) than it is when the rod is straight (Fig. 5-1a) then the rod will remain straight. When the energy in the bent condition is less than it is in the straight condition, the rod will stay in the bent condition and will be

said to have suffered column failure. When the two energies are equal, we have a condition of neutral equilibrium and the compressive load giving rise to this condition is known as the critical column load for the section. An energy method of determining the critical column load may be used but, in this case, the use of the differential equation relating the curvature to the bending moment, equation 3.40, is simpler.

(a) The Euler Column Formula. Considering the column shown in Fig. 5.1b, the moment at any cross section is given by

$$M_y = -Pw$$

This is substituted into equation 3.40, giving

$$EI \frac{d^2 w}{dy^2} = -Pw \quad [5.1]$$

which equation has a solution of the form

$$w = A \cos \sqrt{\frac{P}{EI}} y + B \sin \sqrt{\frac{P}{EI}} y \quad [5.2]$$

The constants A and B must be so adjusted that they satisfy the boundary conditions of the problem. At

$$y = 0, \quad \left(\frac{dw}{dy} \right)_{y=0} = 0$$

which yields $B = 0$, leaving

$$w = A \cos \sqrt{\frac{P}{EI}} y \quad [5.3]$$

At the ends of the column $y = \pm \frac{L}{2}$, $w = 0$ and this is satisfied if

$$A = 0$$

which indicates that the straight column is stable or has the lowest energy state. Equation 5.3 is also satisfied when

$$\cos \sqrt{\frac{P}{EI}} \frac{L}{2} = 0$$

or when

$$\sqrt{\frac{P}{EI}} \frac{L}{2} = \frac{\pi}{2}$$

which can be reduced to

$$P = \frac{\pi^2 EI}{L^2} = P_E \quad [5.4]$$

where P_E is known as the critical column load for a long column. If the ends are not free to rotate, this equation times a constant can be shown to apply, the general equation being

$$P_E = \frac{C\pi^2 EI}{L^2} \quad [5.5]$$

where C is the *end fixity coefficient* and depends upon the end restraint. For pin-ended columns $C = 1.0$, and for columns having the ends completely restrained from rotation, $C = 4.0$, other restraints giving coefficients between these two values. The critical column stress is obtained by dividing the load by the cross-sectional area or

$$\sigma_E = \frac{P_E}{A} = \frac{C\pi^2 EI}{L^2 A} = \frac{C\pi^2 E}{(L/\rho)^2} \quad [5.6]$$

where ρ = the radius of gyration of the cross section which is equal to $\sqrt{I/A}$.

Considering an example in which $C = 1.0$, $E = 10^7$ lb. per sq. in., the curve of σ_E versus L/ρ is as shown in curve (a) of Fig. 5.2. Equation 5.6 is valid only as long as the material is in the Hooke's law range, that is, as long as there is a linear relationship between σ_E and the strain. As soon as any portion of the cross section is subjected to a stress beyond the proportional limit of the material, one should expect to find deviations from the Euler curve.

(b) Reduced Modulus Curve. When the Euler buckling stress becomes greater than the proportional limit of the material, any tendency of the column to buckle will cause the outer fibers on the concave side to have an increased compressive stress due to bending, and these fibers will be acting at an increased distance away from the proportional limit. On the other hand, fibers on the convex side will be acting under a reduced compressive stress which will tend to bring their stress level nearer to the Hooke's law regime. Therefore, in order to use equation 5.6 for stresses above the proportional limit, it is necessary to determine some effective value of E . Kármán (reference 5.1, p. 156) suggests the use of a reduced modulus given by the equation

$$E_r = \frac{4EE_s}{(\sqrt{E} + \sqrt{E_s})^2} \quad [5.7]$$

where E_s is the tangent modulus of elasticity at the stress and E is the modulus of elasticity in the Hooke's law range. This reduced modulus

equation is derived on the assumption that the cross section is rectangular; however, it is sufficiently exact for engineering purposes for most stable cross-sectional shapes. Considering a typical material with the stress-strain curve shown in Fig. 5·3, the reduced modulus is calculated

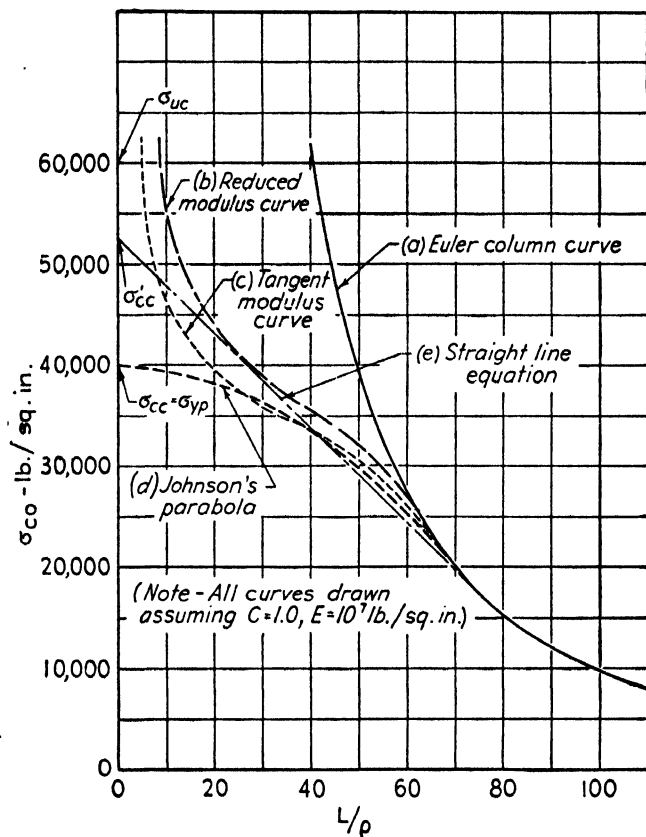


FIG. 5-2. Comparison of different column curves.

in Table 5·1. In this table the L/ρ corresponding to σ_{sc} is calculated from the equation

$$\left(\frac{L}{\rho}\right)_{E_r} = \pi \sqrt{\frac{E_r}{\sigma_{sc}}} \quad [5.8]$$

in which σ_{sc} is the critical stress in the short column range. The maximum value of σ_{sc} will be the ultimate compressive strength, σ_{uc} of the material and curve (b), which corresponds to Table 5·1, will be terminated by a horizontal line through this stress value.

TABLE 5.1

σ_{sc}	E_{σ}	E_r	$(L/\rho)E_r$	$(L/\rho)E_{\sigma}$
20,000	10.0×10^6	10.0×10^6	69.9	69.9
25,000	9.8×10^6	9.9×10^6	62.6	62.2
30,000	8.5×10^6	9.2×10^6	55.0	52.6
35,000	4.0×10^6	6.0×10^6	41.0	33.6
40,000	1.5×10^6	3.1×10^6	27.8	19.3
45,000	0.6×10^6	1.5×10^6	18.4	11.4
50,000	0.3×10^6	0.9×10^6	13.1	7.7
60,000	0.15×10^6	0.5×10^6	8.8	5.0

(c) **Tangent Modulus Curve.** For specimens in which extreme care in manufacturing and testing is used, it is possible to check experimen-

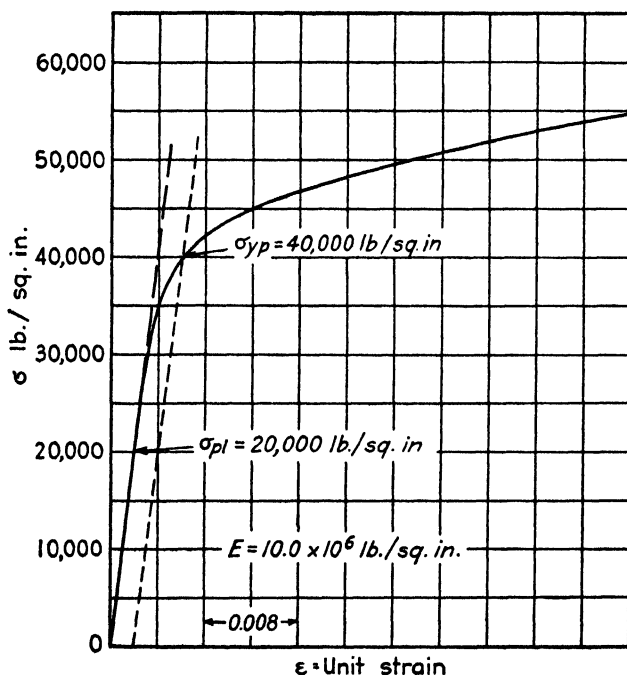


FIG. 5.3. Typical stress-strain curve of dural.

tally the reduced modulus curve very closely. However, for columns in which ordinary workmanship and care in testing are used, the experimental points in the short column regime will generally fall somewhat below the reduced modulus curve. For this reason, it is quite often

found that the use of the tangent modulus directly in equation 5.6 gives somewhat better agreement with the experimental points. If this is done, curve (c) in Fig. 5.2 is obtained, the values of $(L/\rho)_{E_\sigma}$ in Table 5.1 being obtained from the equation

$$(L/\rho)_{E_\sigma} = \pi \sqrt{\frac{E_\sigma}{\sigma_{sc}}} \quad [5.9]$$

As can be seen, this curve is somewhat more conservative than the reduced modulus curve, this conservatism usually being sufficient to take care of small inaccuracies in the specimen and the methods of loading. Representative values of the tangent modulus for 17ST, 17SRT, 24ST, and 24SRT aluminum alloys can be found in a paper by Howland (reference 5.2). Reference 5.3 gives a very complete discussion of the tangent modulus curve as compared with experimental test data from a number of aluminum-alloy sections.

(d) Johnson Parabolic Formula. The Johnson column equation approximates the tangent modulus curve in the intermediate region between the very short and the Euler long columns. Graphically it is represented by a parabola which is tangent to the Euler curve at the proportional limit and has its vertex (at $L/\rho = 0$) at a point corresponding to a stress equal to twice the proportional limit. If this end point is defined as the crushing strength of the section, σ_{cc} , the Johnson equation gives for the critical short column stress

$$\sigma_{co} = \sigma_{sc} = \sigma_{cc} - \frac{\sigma_{cc}^2 (L/\rho)^2}{4C \pi^2 E} \quad [5.10]$$

Using the stress-strain curve of Fig. 5.3 in which the proportional limit is 20,000 lb. per sq. in., corresponding to $\sigma_{cc} = 40,000$ lb. per sq. in., equation 5.10 is plotted as curve (d) in Fig. 5.2. The curve indicates that the Johnson parabola gives a good approximation to the tangent modulus curve, and a somewhat conservative approximation to the reduced modulus curve, in the range of $L/\rho > 20$. In general, the maximum value of the crushing strength is taken as the yield point of the material, although experimental evidence may at times indicate that a somewhat higher value is justified.

For sections in which local buckling or torsional failures take place before the yield point of the material is reached, the crushing strength is defined as the end point of the curve, projected to $L/\rho = 0$, drawn through data obtained from tests on columns of the section in question, and having L/ρ values between 20 and 50. Since there are two basic unknown quantities in equation 5.10, the crushing strength, σ_{cc} , and the end fixity coefficient, C , the complete parabola can be drawn for the

short column range, if σ_{sc} can be accurately determined for two L/ρ values. As can be seen from Fig. 5-2, it is necessary to use care not to take L/ρ values which are too small for this determination, since there is the danger of obtaining points on the high left-hand portion of the modified modulus curve. Too small L/ρ test values will lead to a parabola which is non-conservative in the intermediate range.

(e) Straight Line Equation. Another method of approximating the column curves in the short column range is by the use of a straight line. The straight line is, in general, drawn tangent to the Euler curve and has an equation of the form

$$\sigma_{co} = \sigma_{sc} = \sigma'_{cc} \left(1 - \frac{kL/\rho}{\sqrt{C}} \right) \quad [5-11]$$

in which σ'_{cc} and k are chosen so as to give the best agreement with the experimental evidence. The value of C is determined by finding the Euler curve to which the straight line is tangent. To determine experimentally the constants in equation 5-11 it is necessary to have accurate test values of σ_{sc} for two values of L/ρ , since the independent unknowns in equation 5-11 are σ'_{cc} and k/\sqrt{C} . Since it is known that, at the point of tangency of the straight line equation and the Euler curve, the value of σ_{co} is the same for both curves and the slope of the two curves is identical, one can derive an equation for C of the form.

$$C = \frac{4\sigma'_{cc}}{27\pi^2 E (k/\sqrt{c})^2}$$

thus completely determining all the factors in equation 5-11.

For columns with inherently stable cross sections, the straight line may be used over nearly the entire range from $L/\rho = 0$ to the point where it becomes tangent to the Euler curve. For sections which may be subject to local buckling, the straight line is usually terminated by a horizontal line through a value of $\sigma_{sc} = \sigma_{cc}$ as previously defined. The maximum value of σ_{cc} for such sections is generally taken as the yield point of the material and, if local buckling of the section occurs before the yield point is reached, the critical buckling value is taken as the crushing strength. A typical straight line curve is drawn as curve (e) in Fig. 5-2. Reference 5-3 also gives a valuable discussion of the straight line equation as compared to column test data.

The straight line equation will give a better approximation than the Johnson parabola for stable sections such as round or rectangular bars or sheet sections with relatively heavy walls. Sections of this type will tend to follow the tangent or reduced modulus curves nearly up to the

ultimate compressive strength of the material, and a straight line equation can generally be made to closely approximate the test points for the smaller L/ρ values.

(f) **Other Short Column Curves.** It is readily apparent that for any given set of experimental data a curve could be drawn which might possibly give a better approximation than any of those discussed above. However, the percentage increase in accuracy obtained usually does not justify such a procedure and the lack of generality in such a method makes correlation with other data very difficult. For purposes of uniformity it is therefore suggested that a designer use one of these four curves (Euler long column, tangent modulus, Johnson parabolic, or straight line) in reducing column test data and, if possible, to choose that one which can be defined by a minimum number of test points. For certain stable sections, it is felt that more attention should be given to the tangent modulus curve, since it can be determined analytically and only needs a few experimental points to indicate its accuracy.

Columns having cross sections falling into the stable classification, (not subject to local instability) can be analyzed by means of the general Euler equation

$$\sigma_E = \frac{C \pi^2 \bar{E}}{(L/\rho)^2} \quad [5.12]$$

in which \bar{E} is the effective modulus of elasticity of the material at the stress σ_E . Complete discussions of equation 5.12 are available in a number of references (reference 5.1, 5.3, and others) and will not be presented here. The chief question confronting the designer is the choice of the proper value of E to use in the development of the column curve in the short column regime.

Experimental evidence seems to indicate that, for most cross sections, the use of the tangent modulus for the material (tested in compression) in equation 5.12 gives good agreement with the experimentally determined short column failing stresses. Reference 5.3 gives the results of tests on two aluminum-alloy *H*-section columns and Figs. 5.4 and 5.5 show the agreement of the test data with the calculated curve in which E was taken as the tangent modulus of the material as determined by compression tests.

Figure 5.6 shows the result of applying this method to heavy-walled, barrel- and rectangular-shaped tubes tested by the Boeing Aircraft Company. For the determination of the tangent modulus curve in this figure, an average tension stress-strain curve had to be used inasmuch as a compression stress-strain curve of the material was not available. In view of this fact, the agreement of the test points with the

calculated curve is quite satisfactory. Similar agreement is found in tests on round tubes acting as columns.

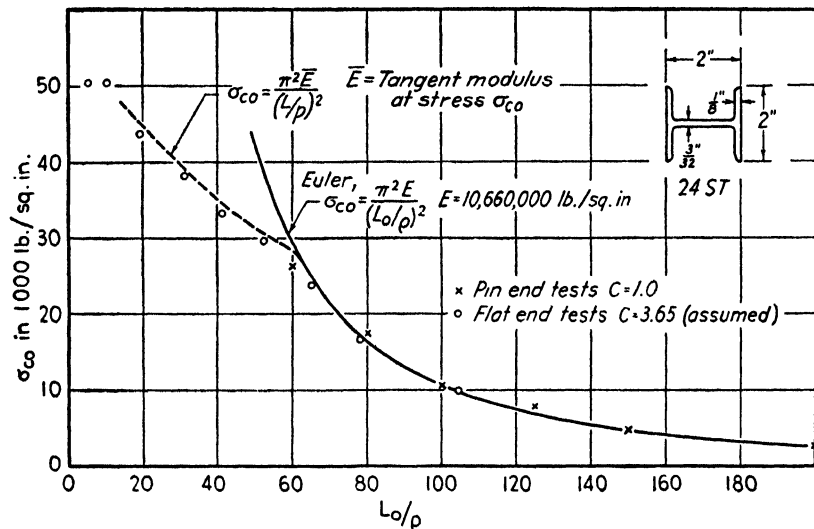


FIG. 5-4. Test points and calculated curves for H-section.

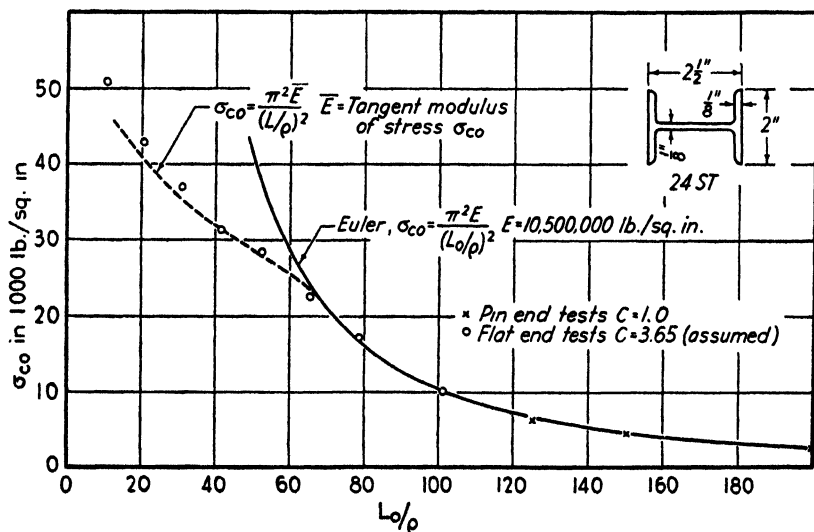


FIG. 5-5. Test points and calculated curves for H-section.

In the light of considerable experimental evidence, it is, therefore, suggested that the tangent modulus curve be used in the short column range for sections which are not subject to local instability. Section

5.3 will discuss the column properties of sections subject to local instability and will treat the torsional failure of columns.

If a number of tests are made on a series of similar columns in which there is a variation in the material yield point, the test data can be made

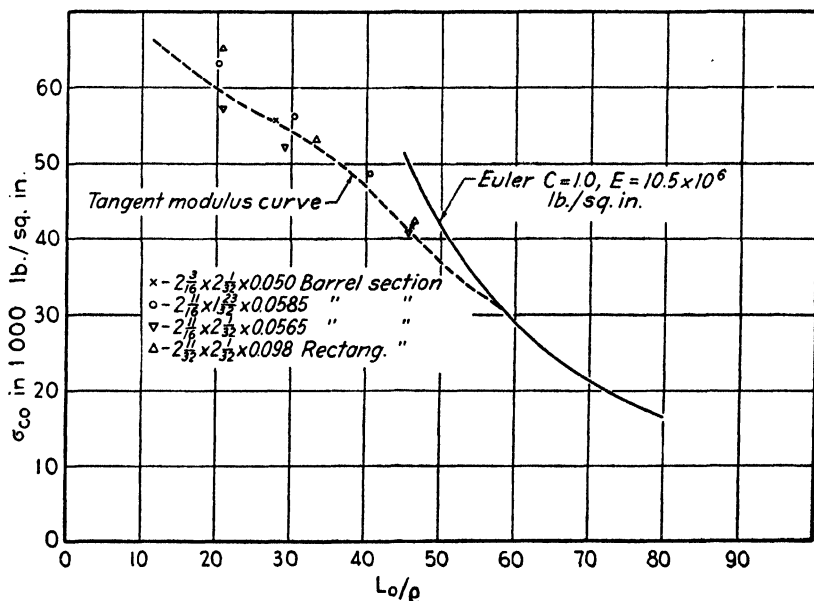


FIG. 5-6. Column curve for barrel and rectangular sections.

to lie on one curve if the results are plotted using the non-dimensional parameters

$$\delta = \frac{\sigma_{ce}}{\sigma_{cyp}} \quad \text{vs.} \quad \lambda_o = \frac{1}{\pi} \frac{L_o}{\rho} \sqrt{\frac{\sigma_{cyp}}{E}}$$

where σ_{cyp} = compressive yield point of the material

L_o = effective free length = L/\sqrt{C}

In all the above it has been assumed that the column has been concentrically loaded, that is, that the line of application of the load has been through the neutral axis of the cross section. If this is not true, the problem is essentially no longer a stability problem but becomes one which should be more accurately considered as a beam problem, in which the beam is subjected to end load and applied end moments. It will, however, be briefly discussed at this point.

Let us consider a column supporting a load which is applied a distance, e , from the neutral axis of the cross section. It can be shown that the

maximum bending moment is at the center of the column and has a magnitude

$$M_{\max} = Pe \sec \left(\frac{L}{2} \sqrt{\frac{P}{EI}} \right) \quad [5 \cdot 13]$$

and that the maximum compressive stress at that point is

$$\sigma_{c \max} = \frac{P}{A} \left[1 + \frac{ec}{\rho^2} \sec \left(\frac{L}{2} \sqrt{\frac{P}{EI}} \right) \right] \quad [5 \cdot 14]$$

where c = distance of outermost fiber on the compression side from the neutral axis

ρ = minimum radius of gyration

It is readily apparent that the solution of the above equation involves either the use of a trial and error or a graphical method since the value P occurs in the secant term.

For relatively short struts, the secant term can be written as

$$\sec \left(\frac{L}{2\rho} \sqrt{\frac{P}{AE}} \right)$$

and, when L/ρ approaches 0, the value of the secant approaches 1.0. Thus, for struts with a small value of L/ρ , the maximum stress becomes

$$\sigma_{c \max} = \frac{P}{A} \left(1 + \frac{ec}{\rho^2} \right) \quad [5 \cdot 15]$$

where the limit of $\sigma_{c \max}$ is usually taken as the yield point of the material.

5-2. Instability of Flat Sheet Subjected to Loads in the Plane of the Sheet

A monocoque or semi-monocoque structure consists primarily of a thin shell which may be reinforced by a network of stiffener members. This reinforced shell is then subjected to a variety of loads, some of which may produce compressive or shearing stresses acting in the plane of the sheet.

The aeronautical engineer, in the design of such structures carrying compression or shear, or both, must, in general, choose between one of two design criteria. Under certain circumstances it may be desirable that he proportion the sheet so that it will not wrinkle or buckle before a given load is being carried by the structure. In other instances, his most important problem is the prevention of collapse or total failure of the structure until the maximum design load has been reached. In semi-

monocoque structure he must not only proportion flat, curved, or corrugated sheets to carry the loads desired, but he must also provide stiffening members and other reinforcements to furnish the required local strength or stiffness, or to distribute loads locally concentrated.

At times the designer may be seriously interested in the stresses causing local buckling or wrinkling of the sheet covering of the wing, tail surfaces, and fuselage. He may wish to know whether or not the buckling or wrinkling deformations of portions of such structures under normal flying loads will be sufficient to affect adversely the aerodynamic efficiency, the handling characteristics, the covering attachment and adjacent structure, or the appearance. In the interior of the structure, such sheet wrinkling may cause a redistribution of stress which may be important from the standpoint of accurate design analysis. For example, to provide for the effects of shear lag between wing spar and wing covering, or to determine when the web of a spar ceases to be shear resistant and starts to act as a tension field, the stress analyst must know the intensity of stress at which buckles form. The material in this section will deal with the stresses which produce wrinkles in smooth, flat sheet.

It has been found that if a plane sheet is supported along the edges by stiffeners or other adjacent structure, it will continue to carry additional load beyond that causing buckling. From the standpoint of the ultimate design strength, therefore, the stress analyst is interested in the ultimate load which such a sheet panel can support. In addition, it may be important to know when some portion of the buckled sheet has reached a stress corresponding to the yield point of the material so as to be able to determine where the first permanent deformation of the structure will occur. These and related problems will be discussed in detail in other chapters.

The stresses causing buckling of a flat sheet depend upon the type of loading to which the sheet is subjected, the panel dimensions, the material, and the method of support of the edges of the sheet. A simply supported edge is one that is constrained to remain straight throughout its length, but is free to rotate about the median line of the edge as an axis. Various experimental methods of providing an approximation to this type of edge support have been used. Holding the edges in *U*- or *V*-shaped grooves, between round rods, or in a slotted tube, all seem to give reasonably good simulations of a simply supported edge condition. A clamped edge is not only constrained to remain straight throughout its length but is also restrained against any rotation. A sheet clamped between heavy flat plates simulates this condition. A free edge, as the name implies, is not restrained in any way.

Consider a sheet panel as shown in Fig. 5-7, loaded with a compressive load of P lb. acting parallel to the sheet elements in the middle plane of

the sheet ($z = 0$), and uniformly distributed across the edges $y = 0$ and $y = a$. This load, P , will then give rise to a uniformly distributed stress σ lb. per sq. in., acting along the edges $y = 0, a$. There are no external loads applied to the edges $x = 0, b$.

Without going into the mathematical derivation of the problem, which can be found in detail in references 5.1, 5.4, and others, it will be suffi-

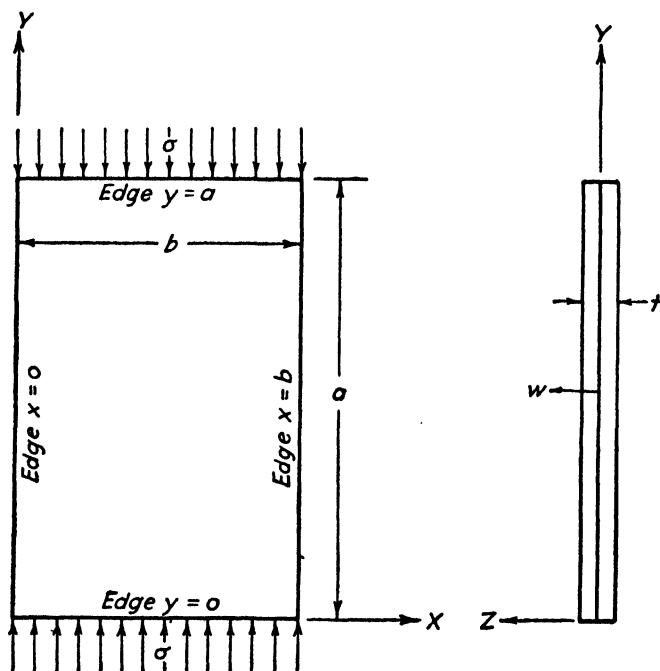


FIG. 5.7. Notation for flat sheet under compression.

cient to say that the differential equation of such a loaded plate can be expressed by the equation

$$\frac{Et^2}{12(1 - \mu^2)} \left(\frac{\partial^4 w}{\partial x^4} + 2 \frac{\partial^4 w}{\partial x^2 \partial y^2} + \frac{\partial^4 w}{\partial y^4} \right) = -\sigma \frac{\partial^2 w}{\partial y^2} \quad [5.16]$$

This equation is based upon the equilibrium conditions in a plate under external loads. The general equation, which is given in Reference 5.1, page 305, considers both normal pressures and all edge stresses, while equation 5.16 considers only one edge stress, i.e.,

$$\sigma_y = -\sigma; \quad \sigma_x = 0; \quad \tau_{xy} = 0; \quad p = 0$$

It can be shown (see references above), if the four edges of the panel are simply supported, that a deflection pattern of the sheet of the form

$$w = w_0 \sin \frac{n\pi x}{b} \sin \frac{m\pi y}{a} \quad [5.17]$$

not only will satisfy the boundary conditions of the problem, i.e., that

$$\begin{aligned} \text{at } x = 0, b; \quad w = 0 \quad \text{and} \quad \frac{\partial^2 w}{\partial x^2} + \mu \frac{\partial^2 w}{\partial y^2} = 0 \\ y = 0, a; \quad w = 0 \quad \text{and} \quad \frac{\partial^2 w}{\partial y^2} + \mu \frac{\partial^2 w}{\partial x^2} = 0 \end{aligned}$$

but also corresponds to the deflection pattern having the smallest internal energy. Incidentally, it also agrees with the experimentally determined deflection shape of such a plate under a compression load as indicated.

Substituting equation 5.17 into equation 5.16 yields the following equation for σ which corresponds to the critical buckling stress of the flat plate:

$$\sigma_{cr} = \left(\frac{a}{mb} + \frac{mb}{a} \right)^2 \frac{\pi^2 E}{12(1 - \mu^2)} \left(\frac{t}{b} \right)^2 \quad [5.18]$$

in which m is the number of half waves in the length direction (the analysis showing that $n = 1$ gives the smallest value of the buckling stress). Putting this equation into the form

$$\sigma_{cr} = K \frac{\pi^2 E}{12(1 - \mu^2)} \left(\frac{t}{b} \right)^2 \quad [5.19]$$

in which

$$K = \left(\frac{a}{mb} + \frac{mb}{a} \right)^2$$

we can plot a curve of K as a function of the a/b ratio of the sheet as shown by the central curve of Fig. 5.8 (edges $y = 0, a; x = 0, b$ simply supported).

Any change in the end fixity of such a flat plate merely changes the value of K in equation 5.19, the form of the equation remaining the same. Figure 5.8 gives the values of the coefficient K as a function of the edge support and the a/b ratio. These are the theoretical curves, and the experimental data that have been collected are in reasonable accord with the theoretical values. (Note: Some of these curves have been plotted from data given in reference 5.1 in which a value of $\mu = 0.25$ was used. Using this value for the Poisson's ratio instead of $\mu = 0.30$ introduces an error of approximately 2 per cent, which is, in general, within the desired accuracy of engineering calculations.)

When the edges of the sheet are attached to other structural members of the airplane, the support given to the sheet is, in general, different

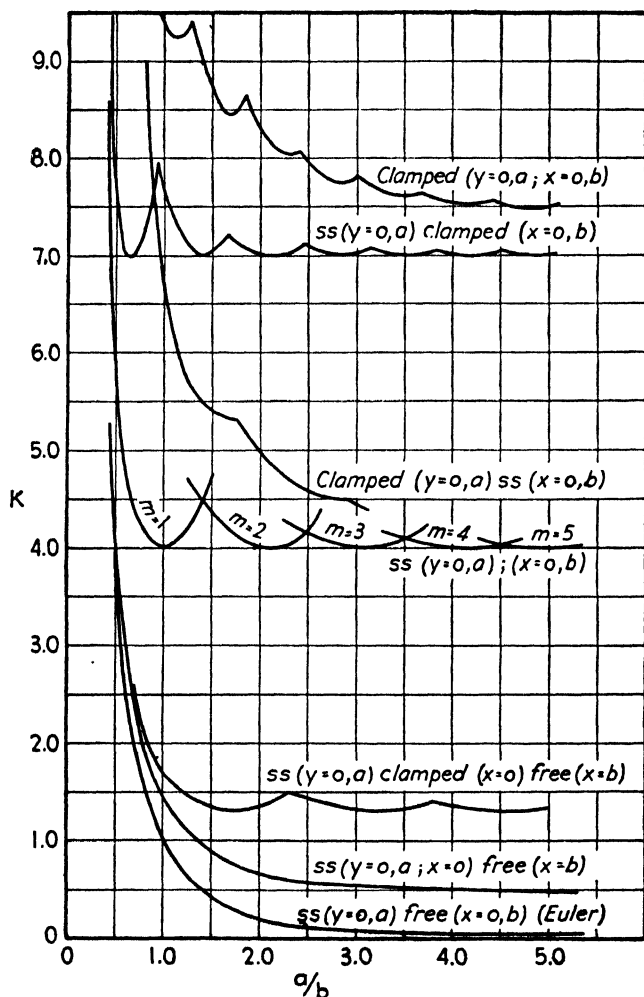


FIG. 5-8. Values of K versus a/b for various edge conditions.

from that given by the theoretical edge conditions mentioned above. Two of these cases will be briefly discussed.

(a) Edges $x = 0, b$ completely restrained from bending deformation but elastically restrained in rotation. Edges $y = 0, a$ simply supported. In this case, the two edges of the sheet parallel to the load are held straight but are allowed to rotate against an elastic restraint. This corresponds to a stiffener edge support in which the stiffener has an

infinite bending rigidity, but a finite torsional rigidity. Zero torsional rigidity would correspond to the case of the plate with four sides simply supported and infinite torsional rigidity would correspond to the case of the plate with the two loaded edges simply supported and the other two edges clamped. Intermediate values of the rotational restraint would lead to cases between these two limits. The equations are similar to those previously discussed, namely,

$$\sigma_{cr} = K \frac{\pi^2 E}{12(1 - \mu^2)} \left(\frac{t}{b}\right)^2 \quad [5.20]$$

in which

$$K = \text{fnc } (a/b, C) \quad [5.21]$$

where C = torsional edge restraint corresponding to

$$M_t = C \frac{\partial^2 w}{\partial x \partial y} \quad [5.22]$$

in which M_t = twisting moment in support due to edge rotation.

The general problem in which the bending rigidity as well as the torsional rigidity of the edge support is considered has been investigated in detail by Chwalla (reference 5.5). The problem has also been treated by Dunn (reference 5.6), assuming infinite bending rigidity and finite torsional rigidity of the edge support. For this condition curves, giving K as a function of the a/b ratio and the rotational edge restraint, are shown in Fig. 5.9.

The curves shown in Fig. 5.9 are for a plate elastically supported along the two edges parallel to the applied load. If a continuous sheet and stiffener panel are considered, the sheet on each side of the stiffener will transmit bending moments to the stiffener. It can be shown that, for symmetrical buckling, these moments will have the same sense. From these considerations it is evident that, for a continuous sheet, the effective torsional rigidity will be one-half of that obtained for an isolated panel in the evaluation of α . The torsional rigidity C of the longitudinal stiffening elements can be determined either by the methods given in Chapter 3 or experimentally by the relation:

$$C = \frac{M_t}{\theta}$$

in which M_t is the applied torsional moment and θ is the unit angular deflection.

(b) Edges, $x = 0, b$, completely free in rotation but elastically restrained in deformation. Edges, $y = 0, a$, simply supported.

This case corresponds to a plate having the loaded edges simply supported, and the edges parallel to the load attached to beams having a

finite bending rigidity but zero torsional rigidity. This problem has been treated by a number of investigators, and the results have been summarized by Timoshenko (reference 5.1, p. 347). The curves plotted in Fig.

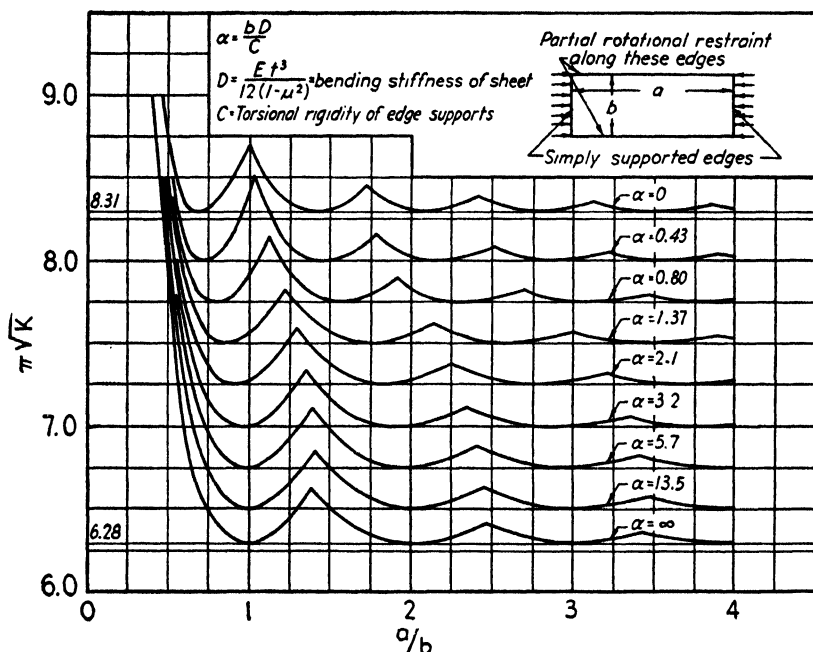


FIG. 5.9. Effect of stiffener torsional rigidity on sheet buckling.

5.10 will aid in the solution of problems of this type. The variables involved are

$$\varphi = \frac{m\pi}{a/b} \quad [5.23]$$

$$\psi = b \sqrt{\frac{t\sigma_{cr}}{D}} \quad [5.24]$$

$$\theta = \frac{EI}{bD} - \frac{A\psi^2}{bt\varphi^2} \quad [5.25]$$

in which $D = \frac{Et^3}{12(1-\mu^2)}$

EI = bending rigidity of the edge supports,

A = area of the edge supports, and the other terms are the same as previously defined.

It can be seen from the above equations that a trial and error method of solution will be necessary for any specific solution.

In general, any given sheet-stiffener structure will combine the above two conditions. A method of treating this combined problem is given

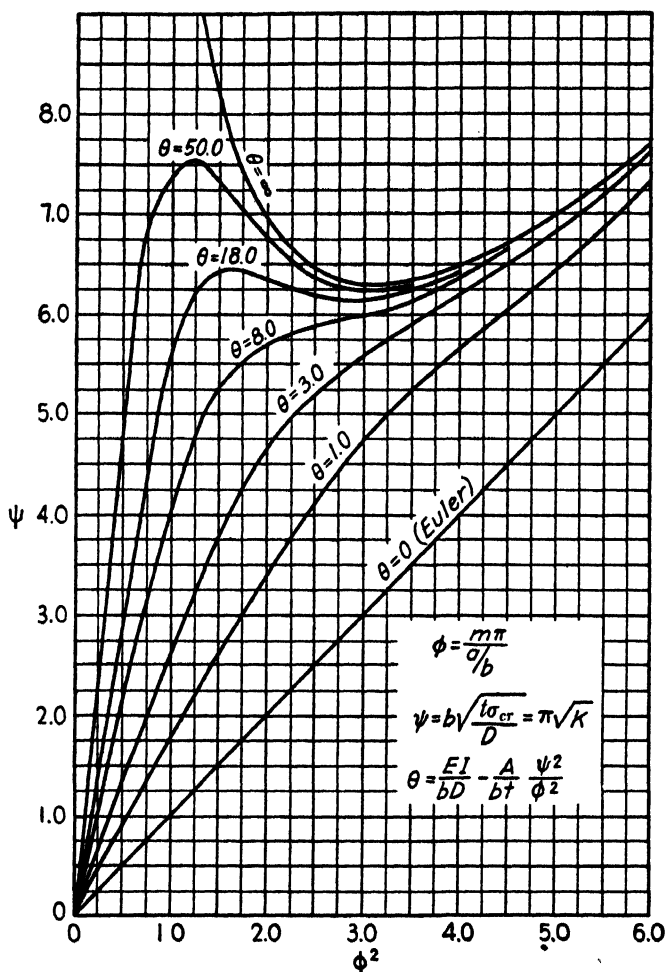


FIG. 5-10. Effect of elastic restraint of unloaded edges on sheet buckling.

by Chwalla (reference 5-5); however, a reasonably close approximation to the critical buckling stress can usually be obtained by judiciously taking into account the effects of the two restraints discussed in *a* and *b* above. In this manner it may be possible to avoid the cumbersome mathematics involved in the exact solution of the problem.

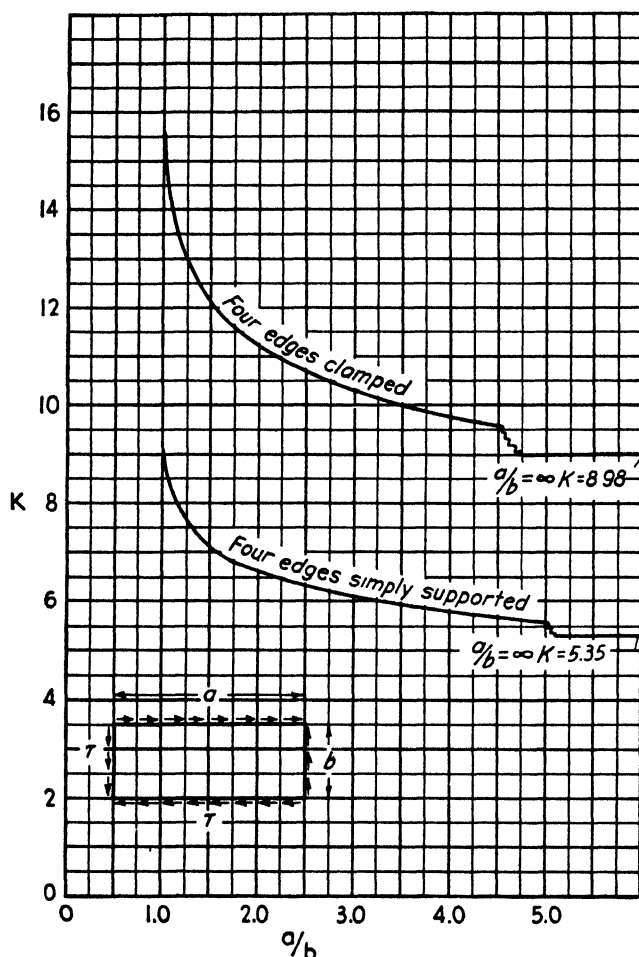


FIG. 5-11. Value of K for sheets under shear loads.

The general expression for the shearing stress at the onset of buckling has the same form as equation 5-19, namely,

$$\tau_{cr} = K \frac{\pi^2 E}{12(1 - \mu^2)} \left(\frac{t}{b} \right)^2 \quad [5-26]$$

in which τ_{cr} = intensity of uniformly distributed shearing stress at start of buckling in pounds per square inch,

b = short dimension of the rectangular sheet in inches,

a = long dimension of the rectangular sheet in inches,

and the other terms have been previously defined. Figure 5-11 gives the values of K as a function of the a/b ratio for the two cases which are

of the most general interest, i.e., four sides simply supported and four sides clamped. A number of investigators have indicated that the experimental values for the critical shearing stress are considerably lower than those given by the theoretical curve. Cox (reference 5-7) finds reasonably good agreement between theory and experiment for plates which are nearly square, but finds serious discrepancies for plates with large a/b ratios. The observations seem to indicate that initial buckles or wrinkles in the plate are more detrimental to the buckling load in shear than they are to the buckling load of plates subjected to compression.

5-3. Columns with Thin Walls

Stiffeners, or other members used to carry compression loads, are frequently made by forming sheet into channels, hat-sections, U -, J -, or

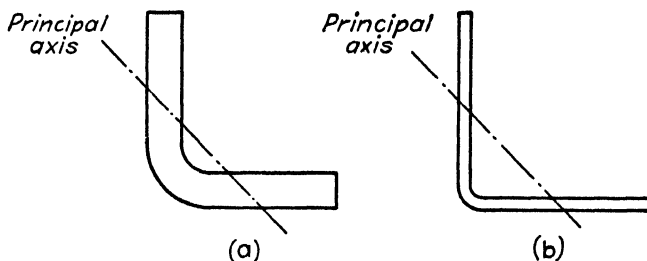


FIG. 5-12. Two types of angle cross sections.

Z -sections, and the design of these members is essentially a problem of their strength as columns. Such sections are subject to three major types of failure. First, if the material is sufficiently thick, they may fall into the class of columns having a stable cross section and, as such, can be analyzed by the methods discussed in section 5-1. Second, if the material is relatively thin, portions of the cross section may be subject to local buckling, and the crushing strength of the column will largely depend upon the stability properties of the various parts of the cross section. Third, open sections are subject to a torsional type of failure in which induced shearing stresses tend to cause the column to fail by twisting.

(a) Bent-Up Sheet Angle Sections. We will consider first of all the simplest of bent-up sections, namely, an equal-legged angle. If the cross section of the angle is as shown in Fig. 5-12a, with very heavy walls and short outstanding legs, it will tend to fail as an Euler column if long and, in the short column range, will follow one of the short column curves discussed in section 5-1. On the other hand, if the section is made up of long thin legs, as in Fig. 5-12b, it is possible that

at some value of L/ρ the allowable stress given by one of the column curves will be higher than the stress which will cause the legs to buckle and go into the wave state. Experiments show that for such sections, if one calculates the stress causing failure by column action and the stress which would cause buckling of the legs (assuming three sides simply supported and the fourth free), that value which is the lower will be in

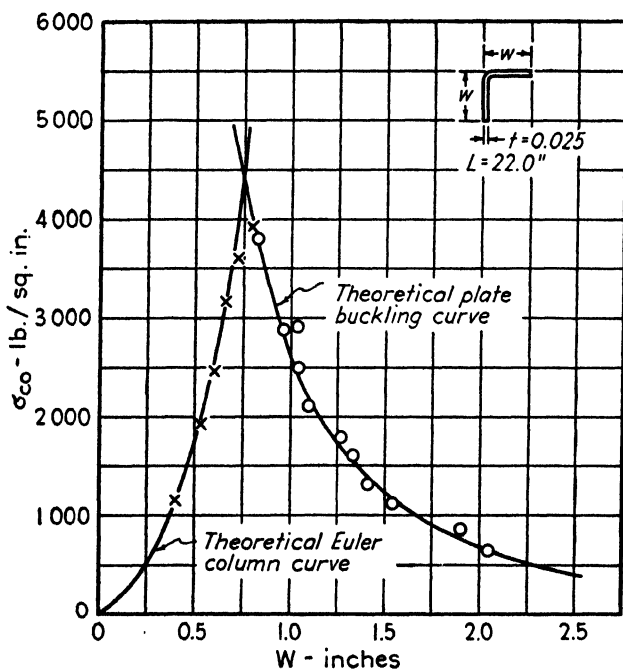


FIG. 5-13. Experimental agreement with calculated column stresses for equal-legged angle.

close agreement with the experimentally determined failing stress. Figure 5-13 shows a plot of such results (see reference 5-8), and it can be seen that the agreement of the experimental results with the two theoretical curves is excellent.

(b) Channel and Equal-Legged Z-sections. The next most complex sections are those of the formed sheet channel or equal-legged Z-section (Fig. 5-14). These sections are subject to four possible types of failure depending upon their cross-sectional dimensions and their length. They are: (1) column failure about the axis $Y-Y$, (2) column failure about the axis $X-X$, (3) plate buckling (local failure), (4) torsional failure.

Again, the first two forms of failure are covered in section 5-1, and the fourth will be discussed later. The plate buckling of this type of

section has been treated theoretically by Parr and Beakley (reference 5·9), and in a somewhat more general manner by Lundquist (reference 5·10). The theoretically predicted loads agree reasonably well with

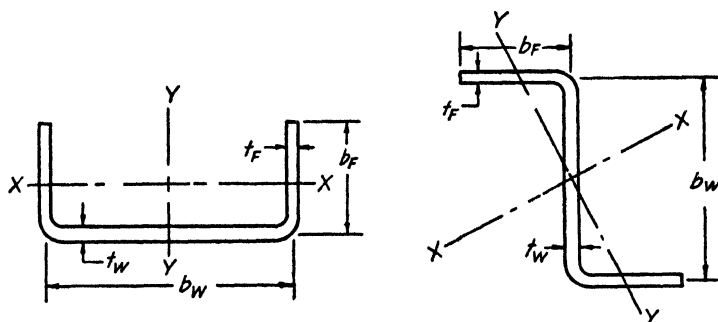


FIG. 5·14. Notation for channel and Z-section.

those obtained in experimental tests. The theoretical results are given in the form of the usual plate stability equation:

$$\sigma_{cr} = K_F E \left(\frac{t_F}{b_F} \right)^2 \quad [5 \cdot 27]$$

in which K_F = a function of b_W/b_F and t_W/t_F ,

E = Young's modulus of the material in pounds per square inch,

t_F = thickness of the flange in inches,

t_W = thickness of the web, or back, in inches,

b_F = width of flange in inches,

b_W = width of web in inches.

A plot of K_F versus b_W/b_F is shown in Fig. 5·15. This figure applies to the Z-section as well as to the channel. The dotted curves in Fig. 5·15 are those derived by Lundquist and the solid curve is that suggested by Parr and Beakley and it is seen that, over the useful range of b_W/b_F , the values of K_F as given in references 5·9 and 5·10 are essentially the same.

Equation 5·27 is valid only so long as σ_{cr} is below the proportional limit of the material. When σ_{cr} exceeds the proportional limit, a factor must be introduced which takes into account the reduction in E for stresses above σ_{pL} . The general equation is, therefore,

$$\sigma_{cr} = \eta K_F E \left(\frac{t_F}{b_F} \right)^2 \quad [5 \cdot 28]$$

or

$$\sigma_{cr}/\eta = K_F E \left(\frac{t_F}{b_F} \right)^2 \quad [5 \cdot 28a]$$

where $\eta = 1.0$ for stresses below the proportional limit. Lundquist in reference 5-11 summarizes the methods of determining η for cross sections which are subject to local buckling. On the basis of assumed parabolic short column curves with values of σ_{cc} equal to the yield point, curves of σ_{cr} versus σ_{cr}/η for materials with various yield points have been plotted in Figs. 5-16 and 5-17.

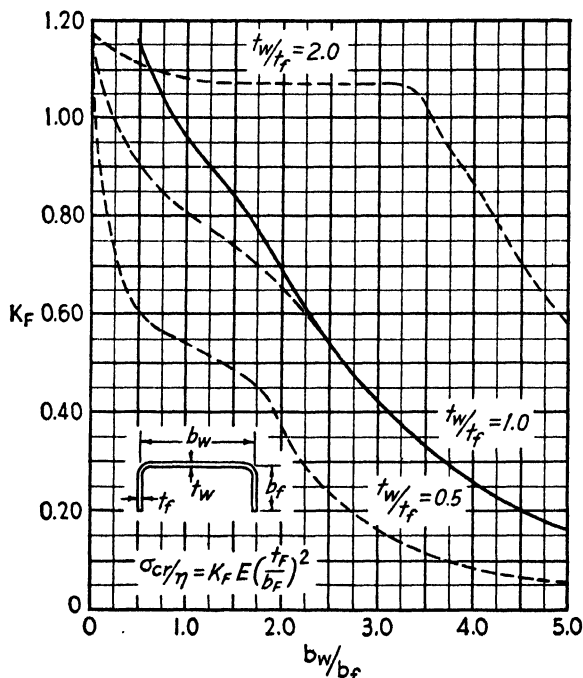


FIG. 5-15. Value of K_F versus b_w/b_f for channel or Z-section.

Few data for checking this method are available, but Table 5-2 shows the results of checking tests from various sources with the method outlined above. Unfortunately, the columns tested by Parr and Beakley, although they showed plate buckling, were of such a length that the effect of torsional instability was apparent in the test results. Additional tests are now in progress which will add more values to Table 5-2; however, this table indicates that, with one exception, the predicted values are conservative. The degree of conservatism in the last group of specimens is somewhat doubtful since the values of σ_{yp} and E had to be estimated. The test values in all cases have been taken as the end point ($L/\rho = 0$) of the curve faired through the plotted points of σ_{cc} versus L/ρ and are, therefore, the values to be used for the crushing strength, σ_{cc} in the Johnson formula.

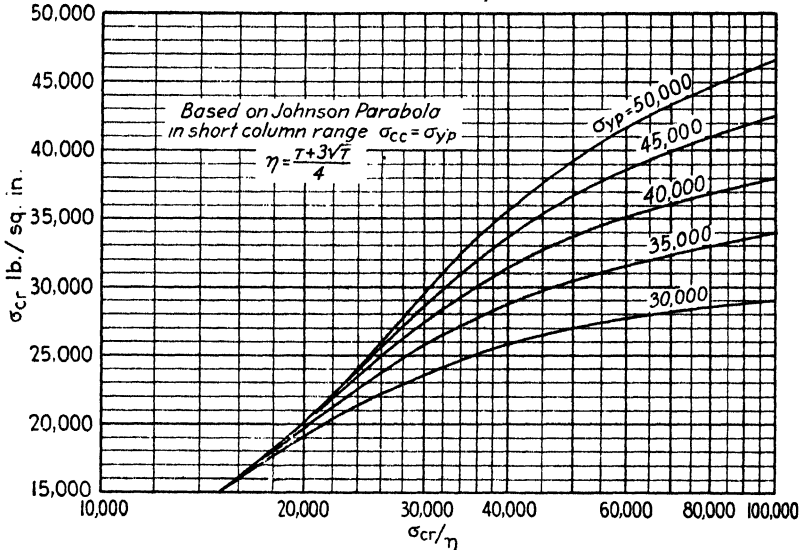


FIG. 5-16. Values of σ_{cr} versus σ_{cr}/η for various yield points.

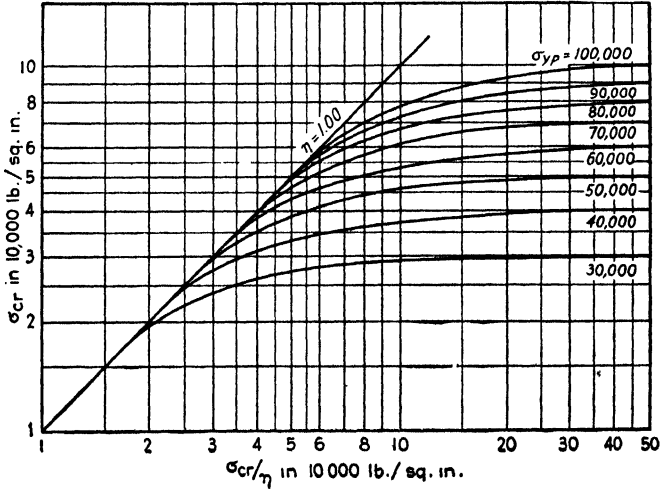


FIG. 5-17. Values of σ_{cr} versus σ_{cr}/η for various yield points.

TABLE

b_F (in.)	b_W (in.)	t (in.)	b_F/b_W	K_F	t/b_F	$E \times 10^{-6}$ (lb./sq. in.)	σ_{yp} (lb./sq. in.)	σ_{cr}/η (lb./sq. in.)	σ_{cr} (lb./sq. in.)	Test σ_{cr} (lb./sq. in.)	Ref.
0.483	0.715	0.032	0.676	0.840	0.0662	10.35	39,500	38,100	30,600	28,000	MIT
1.250	2.500	0.050	0.500	0.692	0.0400	9.73	37,000	10,750	10,750	12,500	5.12
0.920	1.750	0.052	0.526	0.722	0.0565	9.73	37,000	22,420	21,900	23,800	5.12
0.720	1.250	0.052	0.576	0.771	0.0722	9.73	37,000	38,000	29,500	30,000	5.12
1.000	2.625	0.035	0.378	0.510	0.0350	10.30	40,000	6,440	6,440	8,000	5.13
1.000	2.625	0.049	0.378	0.510	0.0490	10.30	40,000	12,630	12,630	16,000	5.13
1.000	2.625	0.065	0.378	0.510	0.0650	10.30	40,000	22,200	22,100	25,000	5.13
1.000	2.625	0.083	0.378	0.510	0.0830	10.30	40,000	35,110	29,700	35,000	5.13
1.000	2.625	0.095	0.378	0.510	0.0950	10.30	40,000	47,410	33,200	42,000	5.13
1.375	2.625	0.083	0.524	0.720	0.0604	10.30	40,000	27,050	25,500	29,000	5.13
1.375	2.625	0.095	0.524	0.720	0.0691	10.30	40,000	35,400	29,800	35,000	5.13
1.375	2.625	0.125	0.524	0.720	0.0909	10.30	40,000	61,250	35,500	39,500	5.13

The above theoretical treatment holds for channels and Z's whose length is two to three times the width of the largest cross-sectional dimension. For shorter lengths, the effect of the rapidly rising portion of the stability buckling curve (Fig. 5·8) for small a/b ratios becomes apparent. This is shown in Fig. 5·18 in which are plotted the results of tests made at Massachusetts Institute of Technology on a $\frac{3}{4}$ by $\frac{1}{2}$ by 0.032 channel section. At values of L/ρ less than 15, the effect of small a/b ratios on the value of the buckling coefficient K becomes apparent,

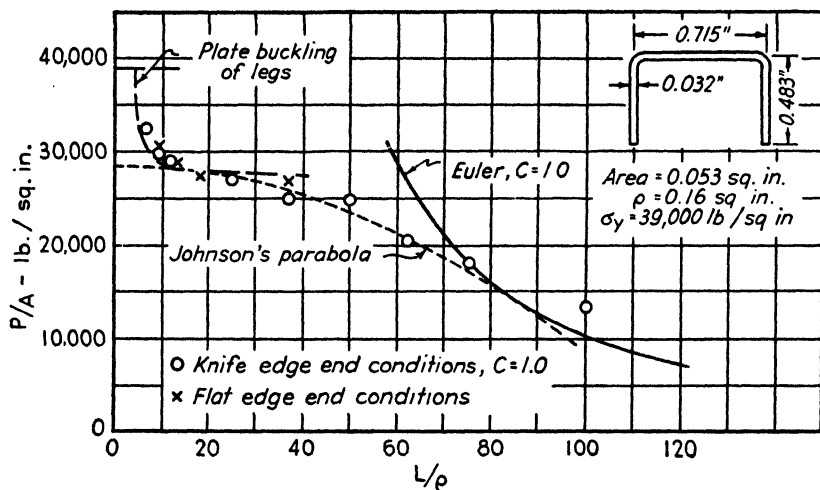


FIG. 5-18. Experimental and calculated column curve for channel section.

as is shown by the calculated buckling stress for the outstanding legs. The back of this particular section at no time goes into the wave state. It must also be mentioned that part of the rise in buckling stress for small L/ρ values is due to the shape of the reduced modulus curve as a function of the critical stress. The above curve indicates that it is possible to build up a complete column curve in the short column range, which is in good agreement with the test results, by using the plate buckling value for the crushing strength, and then using a Johnson parabola up to the Euler regime.

(c) **Square and Rectangular Tubes with Thin Walls.** Lundquist (reference 5·11) has developed a solution for the buckling of thin rectangular tubes under edge compression. The method considers the interaction of the two walls of the tube on each other during buckling and the results are given in the usual buckling equation notation:

$$\sigma_{cr} = K \frac{\pi^2 E}{12(1 - \mu^2)} \left(\frac{t_h}{h} \right)^2 \quad [5 \cdot 29]$$

where the dimensions of the tube are as shown in Fig. 5·19 below. Curves of K versus b/h for three values of t_b/t_h are shown in Fig. 5·20.

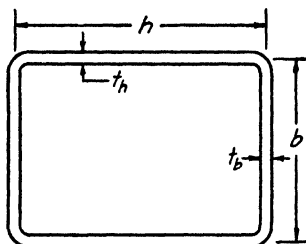


FIG. 5·19. Rectangular section notation.

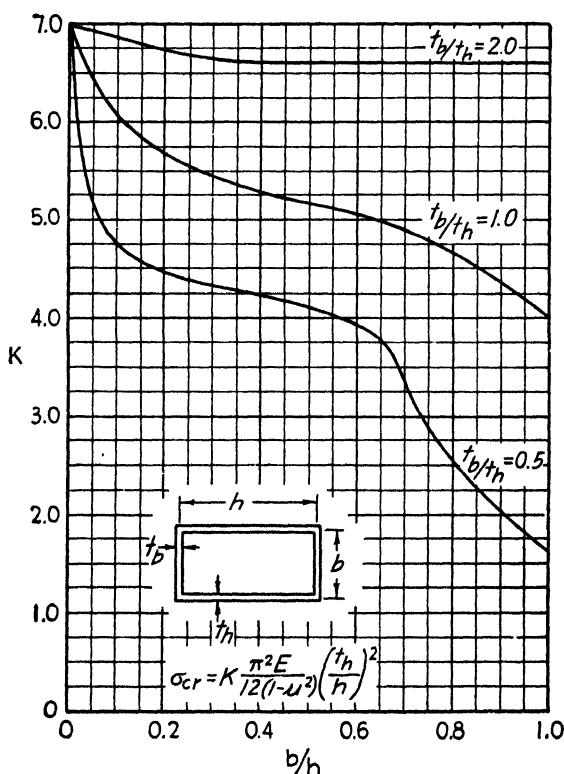


FIG. 5·20. Values of K for rectangular sections.

As discussed previously for the channel sections for stresses above the proportional limit, the general equation is

$$\frac{\sigma_{cr}}{\eta} = K \frac{\pi^2 E}{12(1 - \mu^2)} \left(\frac{t_h}{h} \right)^2 \quad [5 \cdot 29a]$$

and Figs. 5·16 or 5·17 must be used to determine σ_{cr} . Data obtained from one manufacturer on square 17ST tubes having $E = 10^7$ lb. per sq. in. and $\sigma_{yp} = 46,000$ lb. per sq. in. are shown in Table 5·3.

TABLE 5·3

No.	$t_b = t_h$ (in.)	$b = h$ (in.)	K	σ_{cr}/η	σ_{cr} (lb./sq. in.)	Test Fail- ing Stress (lb./sq. in.)
1	0.040	4.0	4.0	3,620	3,620	12,500
2	0.040	3.0	4.0	6,430	6,430	16,140
3	0.041	2.0	4.0	15,200	15,200	23,170
4	0.040	1.0	4.0	52,700	38,000	45,600

As can be seen in the last two columns of Table 5·3, the stress at which buckling occurs is not the stress at which the tube loses its load-carrying ability. In open sections such as channels or angles, buckling of the plate sections destroys the section properties of the column, and failure will follow almost immediately unless column end fixities provide

TABLE 5·4

No.	Buckling Stress (lb./sq. in.)	$\sigma_{se}/\sigma_{cr} =$ σ_{yp}/σ_{cr}	w_c/b *	w_c (in.)	Effec- tive Area (sq. in.)	P_{calc} (lb.)	σ_{ave} (lb./sq. in.)	σ_{test} (lb./sq. in.)
1	3,620	13.25	0.107	0.428	0.1370	6,300	9,840	12,500
2	6,430	7.46	0.135	0.405	0.1296	5,960	12,410	16,140
3	15,200	3.16	0.210	0.420	0.1376	6,330	19,300	23,170
4	38,000	1.26	0.450†	0.450	0.1440	6,620	41,400	45,600

* w_c/b values taken from Fig. 6·2.

† From upper curve in Fig. 6·2 since the edge stress is only a small amount greater than the buckling stress.

additional restraints. For a section such as a square or rectangular tube, the corners remain essentially straight and are stabilized by the fact that the section is closed. In this case, the corners will probably carry a stress near the yield point of the material, and the problem becomes one of effective width of sheet acting with the corners. (Note: The whole problem of the effective width is discussed in detail in Chapter 6.) If it is assumed then that the corners carry a stress equal to the yield point, results as shown in Table 5·4 are obtained for the same tubes.

Table 5-4 indicates much better agreement between experimental and predicted failing stresses, even though the predicted stresses are still quite conservative. However, this is explainable by the fact that the corners of the tube were formed to a rather sharp radius and, because of this cold working, probably had a yield point considerably in excess of the 46,000 lb. per sq. in. found for the average material in the tube. In general, the conclusion that can be drawn from the above and other similar data is that equation 5-29a probably gives reasonable agreement with the test buckling stresses in thin-walled rectangular tubes, but, because the section is closed and self-stabilizing, the crushing strength of the column should be calculated on the basis of two effective widths at each corner carrying the yield point of the material. Similar results are shown in tests made at Massachusetts Institute of Technology, data for which are given in Table 5-5.

TABLE 5-5 *

$t_b = t_h$ (in.)	$h = b$ (in.)	K •	σ_{cr}/η	σ_{cr} (lb./sq. in.)	Calc. Failing Stress (lb./sq. in.)	Test Failing Stress (lb./sq. in.)
0.031	0.9375	4.0	39,600	33,000	38,700†	42,250
0.016	0.8125	4.0	14,040	14,040	18,950	22,200
0.016	0.6875	4.0	19,600	19,600	23,300	24,000
0.016	0.5625	4.0	29,210	27,800	35,600†	32,200

* $E = 10^7$ lb. per sq. in.; $\sigma_{yp} = 44,000$ lb. per sq. in.

† Using upper curve in Fig. 6-2.

For tubes with relatively large radius corners, the following assumptions seem to check the experimental values within reasonable limits: (1) Assume that the corners will carry the yield point stress of the material, or the buckling stress of a circular tube with the same R/t ratio, whichever is the lower. (2) Assume that the flat plate regions are acting as buckled flat plates with an edge stress equal to the stress in the circular corners. The width of the flat plate to be used in the buckling equation is to be taken from the points of tangency of the corner arcs.

Although the experimental agreement for such sections is not perfect, a check of a large number of specimens indicates that the method will give at least a first approximation to the crushing strength of such sections and can be used for determining the short column curve for struts

having cross sections of this type. It is advisable, however, to supplement these calculations with a limited number of actual tests inasmuch as the range of dimensions over which this method is accurate is not well established.

(d) General Thin-Walled Shapes. No theoretical treatment is available for determining the crushing strength of general sections made up of circular arcs and straight segments, or even of sections made up of a series of straight line segments of different lengths (Fig. 5-21). The

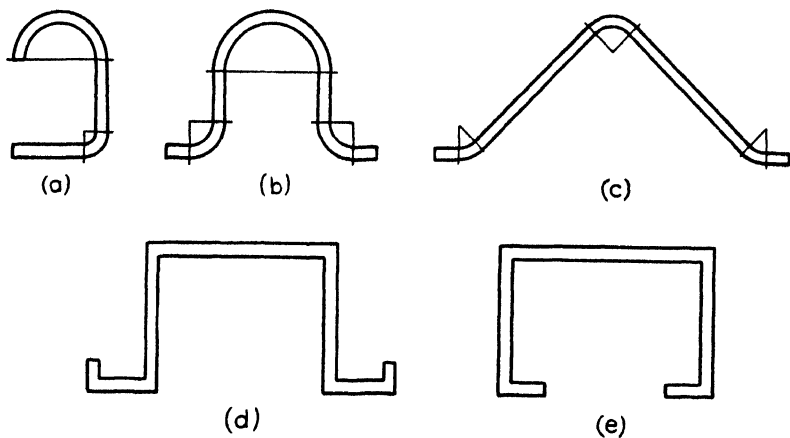


FIG. 5-21. Miscellaneous stiffener sections.

most accurate method of determining the column curve for such sections is by actually testing sufficient lengths of each section in compression and then fairing the column curve through the test points. For most sections a Johnson parabola will fit the test points very well in the range between $L/\rho = 20$ and the Euler curve and is, therefore, satisfactory for design use. Since this is true, it is only necessary to determine carefully the short column strength for two L/ρ values, and from these results, the unknown quantities, σ_{ec} and C in the Johnson equation can be determined. The effectiveness of this method is shown in Fig. 5-22, data for which were taken from reference 5-14. The test values for the two L/ρ 's considered were

	L/ρ	σ_{sc}	L/ρ	σ_{sc}
	29.50	32,000	43.24	27,470
	31.48	29,960	44.50	27,750
	32.55	29,000	45.85	27,050
	<hr/>		<hr/>	
Average	31.24	30,320	44.53	27,420

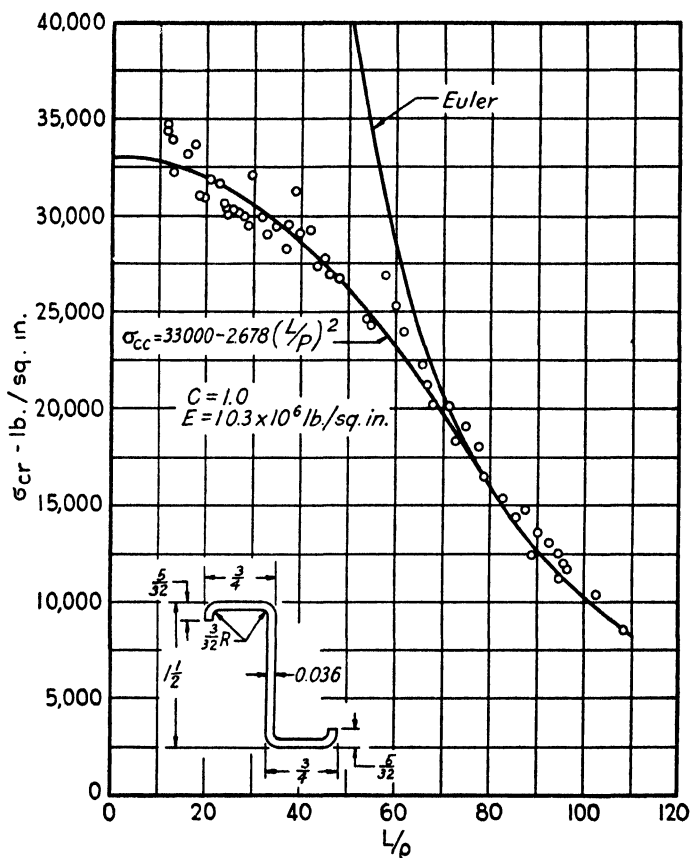


FIG. 5-22. Column curve for Z-section.

These data yield the two Johnson equations:

$$30,320 = \sigma_{cc} - \frac{\sigma_{cc}^2}{C 4\pi^2 \times 10.3 \times 10^6} (31.24)^2$$

$$27,420 = \sigma_{cc} - \frac{\sigma_{cc}^2}{C 4\pi^2 \times 10.3 \times 10^6} (44.53)^2$$

which gives

$$\sigma_{cc} = 33,150 \text{ lb. per sq. in.}$$

$$C = 0.932$$

The parabola shown in Fig. 5-22 was calculated on the basis of $\sigma_{cc} = 33,000$ lb. per sq. in. and $C = 1.0$ and shows excellent agreement with the remainder of the test values. The agreement is particularly good

when one considers the possible variations in materials and section properties of such bent-up sheet sections. A similar method has been used to determine the column curves for the sections shown in Fig. 5-23, which were tested by the Glenn L. Martin Company. The test points for L/ρ values of approximately 40 and 65 were used to determine the values of σ_{cc} and C in the Johnson parabolas which have been drawn on the figure. The other test points were spotted on the chart and show good

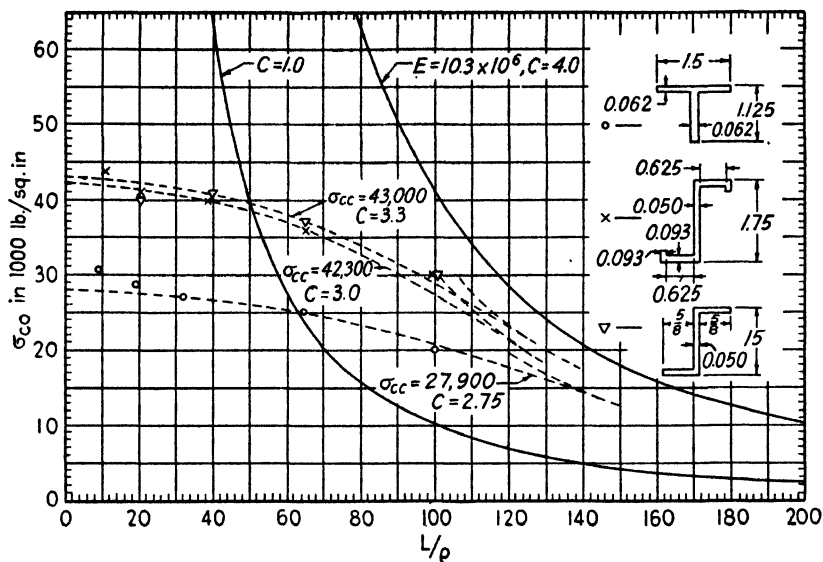


Fig. 5-23. Test column curves for various sections.

agreement except for L/ρ values of 10. This method immediately gives the short column curve for the section and the effective end fixity of the test. Corrections to other end fixities are easily made since the crushing stress remains constant and is not a function of end fixity.

The other correction which may be necessary for the short column curves is that of reducing the allowable stresses to take into account the difference between the strength of the material actually tested and the minimum allowable strengths for the given alloy. It is suggested that the crushing strength be reduced in the manner described in section 6-2(c).

In summary, the suggested procedure for test and analysis would be as follows:

(1) Test specimens of at least two lengths, giving failing strengths for L/ρ values lying between $L/\rho = 20$ and the appropriate Euler column curve. If the test is carried out on pin-ended specimens, test L/ρ values

should be approximately 20-25 and 40-45; and if on flat-ended specimens, they should be approximately 25-35 and 65-75 (for aluminum alloy).

(2) Solve for σ_{cc} and C in the Johnson parabolic equation, using the known values of σ_{sc} and L/ρ . These values are then $\sigma_{cc \text{ test}}$ and C_{test} .

(3) Reduce $\sigma_{cc \text{ test}}$ by the methods of section 6-2(c) to take account of the minimum specified yield point of the material. This will give $\sigma_{cc \text{ design}}$.

(4) Substitute the allowable end fixity value, C_{design} and $\sigma_{cc \text{ design}}$, in the Johnson equation, giving the final design formula:

$$\sigma_{sc \text{ design}} = \sigma_{cc \text{ design}} - \frac{\sigma_{cc \text{ design}}^2 (L/\rho)^2}{4\pi^2 EC_{\text{design}}} \quad [5.30]$$

A number of empirical methods of determining the crushing strength of bent-up sheet sections have been proposed. Most of these have little or no theoretical background but seem to work satisfactorily over at least a limited range of section types. It must, however, be kept in mind that these methods, until they have been checked theoretically, or by a very large number of systematically selected test specimens, should only be used as a first approximation to the actual crushing strength of a particular cross section. For the final answer, it will usually be necessary to make at least a few column tests in the short column regime.

(1) *Sections made up of flat elements.* For sections made up of flat elements, one method of predicting the crushing strength of the cross section is to calculate the buckling loads for each element of the cross section, add these loads, and set the total equal to the crushing strength of the section. Take, for example, a general cross section such as shown in Fig. 5-24. Element (1) is considered as a plate simply supported on three sides with the fourth free and the appropriate value of K is used in the buckling equation.

From Fig. 5-8, $K_1 = 0.50$ (assuming $L = 5b_1$) and the buckling load is given by

$$P_1 = A_1 \left[\frac{0.50 \pi^2 E}{12(1 - \mu^2)} \left(\frac{t_1}{b_1} \right)^2 \right] = 0.452E \frac{t_1^3}{b_1}$$

Elements (2) and (3) are considered as flat plates simply supported on

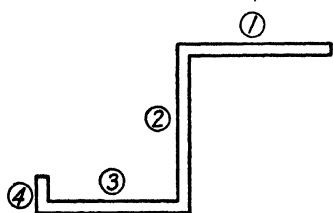


FIG. 5-24.

four sides and the coefficient for this case will be $K_2=4.0$. The buckling load for (2) is, therefore,

$$P_2 = A_2 \left[\frac{4\pi^2 E}{12(1 - \mu^2)} \left(\frac{t_2}{b_2} \right)^2 \right] = 3.617E \frac{t_2^3}{b_2}$$

similarly for element (3)

$$P_3 = A_3 \left[\frac{4\pi^2 E}{12(1 - \mu^2)} \left(\frac{t_3}{b_3} \right)^2 \right] = 3.617E \frac{t_3^3}{b_3}$$

If the buckling stresses for any section, which are given by the bracketed quantities above, are greater than the yield point of the material, the yield point stress should be used to determine the load carried by that section. However, some discretion must be used in this matter as can be shown by considering element (4). If it is short, as indicated, the buckling stress will be very high, and one might expect it to carry a load equal to $P_4 = b_4 t_4 \sigma_{yp}$. However, unless some other part of the section remains active up to the yield point stress, it is obvious that element (4) will fail at a stress equal to that in element (3), and its critical load will be

$$P_4 = b_4 t_4 \sigma_3$$

The crushing load for the section is then given by

$$P_{cc} = P_1 + P_2 + P_3 + P_4$$

and the crushing stress is equal to

$$\sigma_{cc} = P_{cc}/A_{total}$$

It can be seen that this method is exact for the case of the equal-legged angle because it was essentially by this method that the plate-buckling curve of Fig. 5-13 was calculated. The method is also exact for channel sections when the buckling stress of the back and the legs is the same, that is, when $b_w/b_f = \sqrt{8} = 2.83$. For a number of other sections, the errors seem sufficiently small so that the method can be used in preliminary design calculations.

Example 1. Consider the channel section shown in Fig. 5-18.

$$\sigma_w = 3.617 \times 10.3 \times 10^6 \times (0.032/0.715)^2 = 74,600 \text{ lb. per sq. in. which is greater than 39,000 lb. per sq. in.}$$

$$P_w = 0.715 \times 0.032 \times 39,000 = 892 \text{ lb.}$$

$$\sigma_f = 0.452 \times 10.3 \times 10^6 \times (0.032/0.483)^2 = 20,420 \text{ lb. per sq. in.}$$

$$P_f = 2 \times 0.483 \times 0.032 \times 20,420 = 632 \text{ lb.}$$

$$P_T = 892 + 632 = 1524 \text{ lb.} = P_{cc}$$

$$\sigma_{cc} = 1524/(0.715 + 2 \times 0.483)0.032 = 28,320 \text{ lb. per sq. in.}$$

$$\text{Test value} = 28,500 \text{ lb. per sq. in.}$$

Example 2. Let us consider the bent-up Z-section, Fig. 5-25, the test results for which are shown in Fig. 5-22. For this analysis, center-line dimensions will be used throughout.

$$\sigma_1 = \sigma_5 = 40,000 \text{ lb. per sq. in.}$$

$$\sigma_2 = 3.617 \times 10.3 \times 10^6 \times (0.036/0.714)^2 > 40,000 \text{ lb. per sq. in., therefore use}$$

$$\sigma_2 = \sigma_4 = 40,000 \text{ lb. per sq. in.}$$

$$\sigma_3 = 3.617 \times 10.3 \times 10^6 \times (0.036/1.464)^2 = 22,500 \text{ lb. per sq. in.}$$

$$P_1 = P_5 = 0.138 \times 0.036 \times 40,000 = 199 \text{ lb.}$$

$$P_2 = P_4 = 0.714 \times 0.036 \times 40,000 = 1029 \text{ lb.}$$

$$P_3 = 1.464 \times 0.036 \times 22,500 = 1186 \text{ lb.}$$

$$P_{cc} = 3642 \text{ lb.}$$

$$\sigma_{cc} = 3642/0.1139 = 32,000 \text{ lb. per sq. in.}$$

as compared to a test value of 33,000 lb. per sq. in.

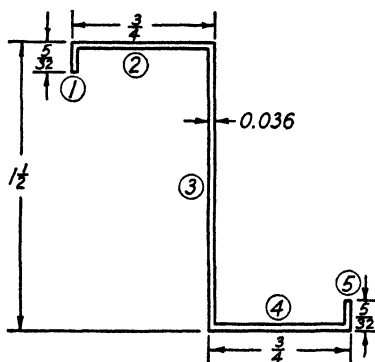


FIG. 5-25.

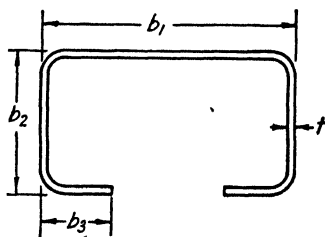


FIG. 5-26.

Table 5-6 gives the predicted and test results for a series of lipped channels, Fig. 5-26, tested by the General Aviation Corporation. The

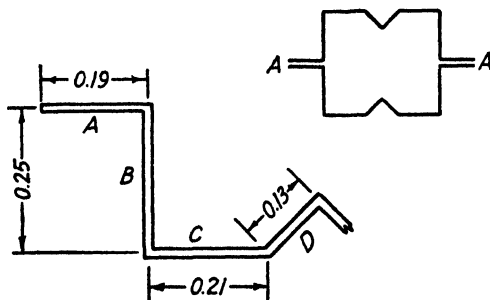


FIG. 5-27. Stainless steel section.

agreement between predicted and test results is, with few exceptions, satisfactory. Since the tests were made on columns with a finite L/ρ value, and the predicted crushing strength is to be used at $L/\rho = 0$, the method is somewhat more conservative than is indicated in Table 5-6.

The same method has been used to check the test results of the Budd stainless steel stiffeners shown in Table 5·7. This was a symmetrical section formed in two halves and welded along the flange *A* (Fig. 5·27). Since the bonding between the two flanges was very good, in calculating the crushing strength of the section it has been assumed that the allowable stress in the outstanding flanges was twice that which could be supported by a single flange. Inasmuch as variations in material thickness were sometimes as high as 10 per cent, the agreement between predicted and calculated crushing strengths is reasonably satisfactory. The method of calculation is as follows:

$$E = 26.0 \times 10^6 \text{ lb. per sq. in.}$$

$$\sigma_{yp} = 140,000 \text{ lb. per sq. in.}$$

$$\sigma_{crA} = 2 \times 0.452E(t_A/b_A)^2 = 2.350(t/b_A)^2 \times 10^7$$

The factor 2 is assumed to account for the stiffening effect of the welding at section *A*.

$$\sigma_{crB} = 3.617E(t/b_B)^2 = 9.405(t/b_B)^2 \times 10^7$$

and similarly for σ_{crC} and σ_{crD} , whenever these stresses are less than σ_{yp} .

The plot of column stresses versus L/ρ for the section shown in Fig. 5·27 agreed very well with a Johnson parabolic short column curve. However, with certain types of sections made from very thin material, plate buckling may occur for a considerable portion of the cross section even before the various elements of that portion would buckle individually. In these cases, the experimental points would not be expected to agree with any of the short column curves discussed at the beginning of this section. This occurs in the section shown in Fig. 5·28. The region between points *A* and *B* buckled as a stiffened plate at a very low load, but the remainder of the section was sufficiently strong to keep the column from collapsing. In this case the short column curve drawn through the test points could be analyzed as consisting of two parts as indicated in the figure. Curve *A* shows the load-carrying ability of the stiffened plate *A-B*, while curve *B* gives the short column curve for the remainder of the section. The sum of these two values yields a short column curve of the same shape as that given by the experimental points. It is felt that the short column curves for such sections will have to be determined by experimental methods as no approximate methods of analysis are available. It is interesting to note, however, that the crushing strength of this section, calculated by the method outlined above, lies on the experimental curve faired through $L/\rho = 0$.

TABLE 5-6

No.	b_1 (in.)	b_2 (in.)	b_3 (in.)	t (in.)	L (in.)	σ_{yp} (lb./sq. in.)	P_1 (lb.)	P_2 (lb.)	P_3 (lb.)	P_{total} (lb.)	Crushing Stress	
											Predicted* (lb./sq. in.)	Test† (lb./sq. in.)
1	3.23	1.5	0.75	0.0795	6	38,600	5800	4600†	2300†	19,600	31,900	37,200
2	3.23	1.5	0.75	0.050	4	37,000	1440	2775†	780	8,550	22,100	26,000
3	2.69	1.5	0.75	0.050	8	53,000	1730	3105	780	9,500	26,400	29,200
4	2.69	1.5	0.75	0.050	8	39,500	1730	2960†	780	9,210	25,600	25,500
5	2.69	1.5	0.75	0.050	8	39,500	1730	2960†	780	9,210	25,600	25,000
6	2.69	1.5	0.75	0.050	8	11,700	1575†	880†	440†	4,215	11,700	12,600
7	2.69	1.5	0.75	0.050	8	14,900	1730	1115†	560†	5,080	14,150	11,700
8	2.69	1.5	0.75	0.081	4	38,600	7260	4690	2430†	21,420	36,800	35,000
9	2.69	1.5	0.75	0.041	4	42,500	955	1715	430	5,245	17,800	21,800
10	2.375	1.5	0.75	0.049	3	46,000	1630	2920	730	8,930	25,350	23,900
11	2.375	1.25	0.406	0.0513	6	36,000	2120	2310†	750†	8,240	28,200	26,400
12	2.375	1.25	0.430	0.02108	5	38,500	141	268	98	875	7,350	10,870
13	2.375	1.25	0.438	0.0529	6	37,400	2320	2470†	865†	8,990	29,600	29,800
14	2.375	1.313	0.375	0.0613	5	31,700	3615	2550†	850†	10,415	28,900	29,800
15	1.53	1.47	0.375	0.0625	5	37,000	3535†	3400†	865†	12,065	37,000	37,400
16	1.375	1.00	0.313	0.039	6	36,500	1610	1425†	455†	5,370	34,400	32,000
17	1.375	1.00	0.188	0.025	6	40,000	423	582	188†	1,965	21,000	19,600
18	1.00	1.00	0.188	0.0208	8	36,000	335	335	141†	1,285	18,300	15,600
19	1.00	1.00	0.188	0.0251	4	36,000	522	522	163†	1,890	23,200	21,500
20	1.00	1.00	0.188	0.0153	6	36,000	134	134	103	610	11,800	14,600

* Area used to determine this stress = $(b_1 + 2b_2 + 2b_3)t = A_{calc}$ † This stress determined by taking P_{test}/A_{actual} ‡ Indicates $P_n = A_w \sigma_{yp}$ since σ (buckling) $> \sigma_{yp}$

TABLE 5.7

Section	L	$t = 0.0057$		$t = 0.00946$		$t = 0.01045$		$t = 0.01307$	
		σ_{cr}	$\sigma_{cr} \cdot L$	σ_{cr}	$\sigma_{cr} \cdot L$	σ_{cr}	$\sigma_{cr} \cdot L$	σ_{cr}	$\sigma_{cr} \cdot L$
A	0.19	21,150	4,020	58,200	11,050	70,700	13,420	111,200	21,100
B	0.25	48,900	12,230	134,600	33,500	140,000	35,000	140,000	35,000
C	0.21	69,300	14,550	140,000	29,400	140,000	29,400	140,000	29,400
D	0.13	140,000	18,200	140,000	18,200	140,000	18,200	140,000	18,200
	0.78		49,000		92,150		96,020		103,700
		$\sigma_{ave} = 49,000/0.78$ $= 62,800 \text{ lb./sq. in.}$		$\sigma_{ave} = 92,150/0.78$ $= 118,000 \text{ lb./sq. in.}$		$\sigma_{ave} = 96,020/0.78$ $= 123,100 \text{ lb./sq. in.}$		$\sigma_{ave} = 103,700/0.78$ $= 133,000 \text{ lb./sq. in.}$	
Test values $L/\rho = 0$		75,000		105,000		124,000		132,000	

(2) *Combined curved and flat-element sections.* Comparatively few data are available on the crushing strength of columns whose cross sections are combinations of curved and flat-sheet elements. Tests on curved sheet panels under compression indicate that the failure of such sections

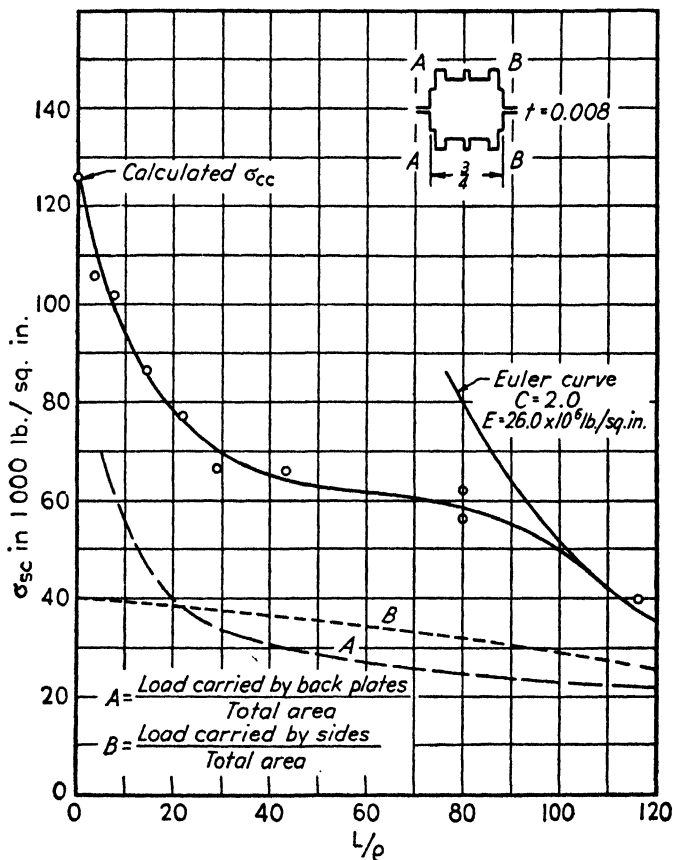


FIG. 5-28. Column curve breakdown for stainless steel section.

is very rapid when the critical stress is reached. If the edges of the curved panel are supported, there seems to be some evidence that, unlike the flat-sheet panel, the edge stress cannot be carried much beyond the stress causing buckling of the center part of the curved panel. On the basis of this evidence, it is suggested that the estimation of the crushing strength of such sections be obtained in the following manner: First, if no flat area of the panel goes into the wave state before the weakest curved element becomes unstable, the crushing stress will be equal to the stress causing buckling of the weakest curved section.

Second, if certain flat elements buckle before the weakest curved section becomes unstable, then the total load carried by the section will be the sum of the buckling loads of the flat portions which have buckled, plus the critical buckling stress of the weakest curved portion times the remaining unbuckled area of the cross section. For example, consider the section shown in Fig. 5-29. Section (1) is calculated on the basis of a plate simply supported on three sides with the fourth free. Critical buckling stress is σ_{cr_1} . Section (2) (to point of tangency of curved portion) is calculated on the basis of four simply supported edges. Critical buckling stress is σ_{cr_2} . Section (3) is calculated from equation 8-2 or, the critical stress is determined from Fig. 8-2. Critical buckling stress is σ_{cr_3} . Then, if $\sigma_{cr_3} < \sigma_{cr_1}$ and $\sigma_{cr_3} < \sigma_{cr_2}$, the crushing stress will be equal to

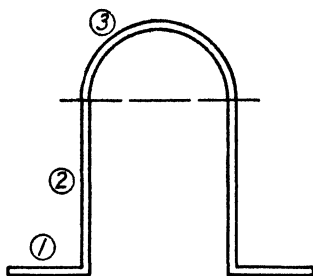


Fig. 5-29.

$$\sigma_{cc} = \frac{\sigma_{cr_3}(2A_1 + 2A_2 + A_3)}{(2A_1 + 2A_2 + A_3)} = \sigma_{cr_3}$$

If $\sigma_{cr_1} < \sigma_{cr_3}$ and $\sigma_{cr_2} > \sigma_{cr_3}$, the crushing stress will be equal to

$$\sigma_{cc} = \frac{2\sigma_{cr_1}A_1 + \sigma_{cr_3}(2A_2 + A_3)}{(2A_1 + 2A_2 + A_3)}$$

If $\sigma_{cr_1} < \sigma_{cr_3}$ and $\sigma_{cr_2} < \sigma_{cr_3}$, the crushing stress will be equal to

$$\sigma_{cc} = \frac{2\sigma_{cr_1}A_1 + 2\sigma_{cr_2}A_2 + \sigma_{cr_3}A_3}{(2A_1 + 2A_2 + A_3)}$$

The limiting value of any of the above stresses is to be taken as the yield point of the material.

Numerous other methods have been proposed for estimating the crushing strength of bent-up sheet sections; however, it is felt that the above methods will, in general, give as good approximation as any. It must again be pointed out, nevertheless, that the methods are only approximations, and the values obtained should not be used for final design purposes unless checked by experimental tests on the sections. In order to obtain a first approximation to the short column curve of the section, the crushing strength as determined above is substituted in the Johnson column equation with the proper end fixity coefficient.

(e) Extruded Shapes. For simple sections such as plain angles and channels without bulbs, an estimation of the crushing strength can be

made in the manner described in (a) and (b) above. In general, extrusions have relatively large fillets in the corners and these will tend to increase the effective side fixity of the plate elements and thus raise the buckling load of these elements. Therefore, if the method described previously for sheet sections is used for analysis, the resulting predicted crushing strength may be considerably lower than that which the sections actually develop.

For sections having bulbs (see Fig. 5-30) no rational methods of analysis are available, and recourse must be had to testing enough lengths of the sections to determine the coefficients in the short column equation.

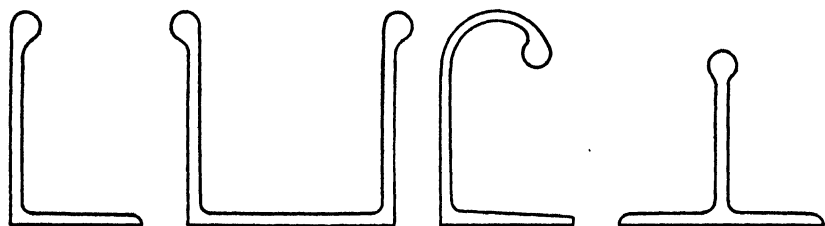


FIG. 5-30. Typical extruded bulb section stiffeners.

Methods have been suggested in which it was assumed that the bulb supplied simple support to the edge of the sheet to which it was attached, and the section was analyzed as a series of flat or curved elements in a manner similar to that described for bent-up sheet sections. However, unless justified by experimental evidence, such methods should be used with a great deal of caution.

A number of companies have developed methods of determining the crushing strengths of extruded and formed sheet sections. These methods appear to be satisfactory for the particular sections considered, but are not sufficiently general in character to be offered as general design methods. It may be possible at some later date to obtain and correlate sufficient data so that crushing strengths may be calculated for such sections, but at present new sections should be checked by experimental tests in order to eliminate the possibility of unknown factors influencing the column strength values.

If sections such as these are to be used as stiffening members on sheet construction, the column curve which is important is that obtained when the stiffener section is restricted to fail in the same manner as it does when attached to the sheet. For this reason column curves of asymmetrical sections tested alone are, in general, of little use for predicting their behavior when attached to sheet structures.

5-4. The Torsional Instability of Columns

In all the above it has been assumed that failure of the column was due to a bending instability, that is, that the deflected column axis lay in a plane through the neutral axis of the section. There is, however, a type of failure which may occur in certain sections in which failure occurs by a twisting of the central portion of the column relative to the two ends. This is called torsional instability since it occurs only in those sections which have a low torsional rigidity.

Wagner (references 5·15 and 5·16) presented the first discussion of this type of failure, and the analysis was expanded by Kappus (reference 5·17). Lundquist and Fligg (reference 5·18) discuss this problem and give detailed calculations for certain special types of sections. The general equation for the failing stress of a concentrically loaded column subject to twisting failure is (using the notation of Lundquist and Fligg)

$$\sigma_{BT} = \frac{1}{I_p} \left(GJ + \frac{\pi^2}{L_0^2} E C_{BT} \right) \quad [5\cdot31]$$

where σ_{BT} = the critical torsional failing stress of the concentrically loaded column,

I_p = the polar moment of inertia of the cross section about the axis of rotation,

GJ = torsional rigidity of the section,

E = the Young's modulus of the material,

L_0 = the effective length of the column,

C_{BT} = the torsion-bending constant, which is dependent upon the location of the axis of rotation and the dimensions of the cross section.

A complete discussion of the derivation of equation 5·31 is omitted owing to space limitation, and the designer is referred to the papers indicated above for the underlying assumptions and methods of derivation.

For columns tested alone, i.e., not attached to sheet, twisting failure will occur by a rotation of the sections of the column about the shear center of the cross section. A method of determining the shear center of thin, flat-sheet cross sections is given in Chapter 3 and for other sections in references 5·19 and 5·20 in addition to the references given above. For column sections attached to plates as stiffening elements, the center of rotation may no longer be at the shear center of the section due to restraints introduced by the sheet. As a first approximation, it may be assumed that the section rotates about some point in the plane of the sheet. The method would then be to calculate the critical tors-

ional buckling stress for a number of assumed locations for the center of rotation and to take that location giving the lowest critical stress.

The value of the torsion-bending constant, C_{BT} , may be calculated either analytically or graphically. Considering a general section such as that shown in Fig. 5-31a, the value of C_{BT} is given by the expression

$$C_{BT} = \int_A w^2 dA - \frac{1}{A} \left[\int_A w dA \right]^2 \quad [5.32]$$

where w is the circumferential warping and is given by the equation

$$w = \int_0^u r_t du \quad [5.32a]$$

In the above expression the cross-sectional warping $r_n \cdot n$ has been neglected. Since n , at the most, is equal to $t/2$, the warping $r_n \cdot n$ will,

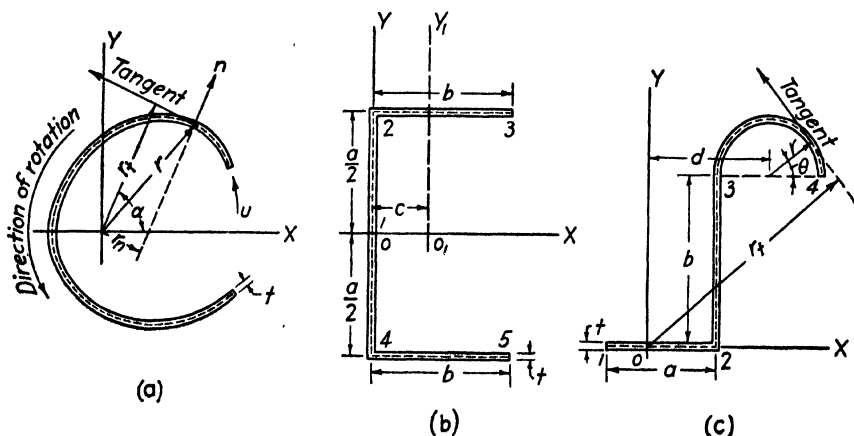


FIG. 5-31. Notation for torsion column failure.

in general, be small compared to the circumferential warping and may be neglected.

In evaluating the warping, w , the following sign conventions have been adopted. We arbitrarily choose a direction of rotation, then the circumferential coordinate u is taken positive in the direction of rotation. Also the positive sense of rotation indicates the positive direction of the tangent to the circumferential coordinate u . When looking in the positive tangential direction, the positive normal n points to the right and a line drawn from O in the positive n direction indicates the positive r_t direction. The angle α is measured in the positive sense of rotation, i.e., from

+X to +Y. As an illustration consider the channel section shown in Fig. 5·31b, and let us first calculate C_{BT} about the point O .

Choose the origin of u at O then,

from 1 to 2, $r_t = 0$

from 2 to 3, $r_t = +a/2$, du is negative and $w = -au/2$

from 1 to 4, $r_t = 0$

from 4 to 5, $r_t = +a/2$, du is positive and $w = au/2$

from which

$$\int_A w dA = -\frac{at}{2} \int_0^b u du + \frac{at}{2} \int_0^b u du = 0$$

hence

$$C_{BT} = \frac{a^2 t}{4} \int_0^b u^2 du + \frac{a^2 t}{4} \int_0^b u^2 du = \frac{a^2 b^3 t}{6}$$

Now let us calculate C_{BT} about the point O_1 . Again taking the origin of u at O we have,

from 1 to 2, $r_t = +c$, du is negative, and $w = -cu$

from 2 to 3, $r_t = +a/2$, du is negative, and $w = -au/2 - ac/2$

from 1 to 4, $r_t = +c$, du is positive, and $w = cu$

from 4 to 5, $r_t = +a/2$, du is positive, and $w = au/2 + ac/2$

from which

$$\int_A w dA = 0$$

and

$$\begin{aligned} C_{BT} &= 2 \left\{ c^2 t \int_0^{a/2} u^2 du + \frac{a^2 t}{4} \int_0^b (u + c)^2 du \right\} \\ &= \frac{a^2 t}{12} \left\{ c^2 (a + 6b) + 2b^2 (b + 3c) \right\} \end{aligned}$$

The integral $\int_A w dA$ will not be zero if, for example, the origin of u is taken at point 2. However, the algebraic sum of the two integrals of equation 5·32 will always be constant for a given axis of rotation, i.e., the expression for C_{BT} is invariant with respect to the origin of the circumferential coordinate u . The origin of the rectangular coordinates XY must of course be taken at the axis of rotation. Assume, for example,

that the center of rotation of the section shown in Fig. 5-31c is at the point O then C_{BT} is evaluated as follows:

Taking the origin of u at point 4, then from 4 to 3

$$r_t = r + d \cos \theta + b \sin \theta$$

and

$$\begin{aligned} w_{4-3} &= \int_0^u r_t du = r \int_0^\theta (r + d \cos \theta + b \sin \theta) d\theta \\ &= r[r\theta + d \sin \theta - b \cos \theta + b] \end{aligned}$$

From 3 to 2

$$r_t = r - d$$

and

$$w_{3-2} = w_{4-3} \big|_{\theta=\pi} + \int_0^u (r - d) du = r^2\pi + 2rb + (r - d)u$$

From 2 to 1

$$r_t = 0$$

and

$$w_{2-1} = w_{3-2} \big|_{u=b} = r^2\pi + b(3r - d)$$

Hence

$$\begin{aligned} C_{BT} &= \int_A w^2 dA - \frac{1}{A} \left[\int_A w dA \right]^2 \\ &= tr^3 \int_0^\pi [r\theta + d \sin \theta - b \cos \theta + b]^2 d\theta \\ &\quad + t \int_0^b [r^2\pi + 2rb + (r - d)u]^2 du \\ &\quad + t \int_0^a [r^2\pi + b(3r - d)]^2 du \\ &\quad - \frac{1}{A} \left\{ r^2t \int_0^\pi [r\theta + d \sin \theta - b \cos \theta + b] d\theta \right. \\ &\quad + t \int_0^b [r^2\pi + 2rb + (r - d)u] du \\ &\quad \left. + t \int_0^a [r^2\pi + b(3r - d)] du \right\}^2 \end{aligned}$$

where A is the total cross-section area of the section. It can be seen, for example, that if the origin of the circumferential coordinate u is taken at

point 1 the resulting expression for C_{BT} would be considerably simplified, since the warping from 1 to 2 would be zero.

Since nearly all extruded angle sections, when used as sheet stiffeners, are subject to torsional failure, this problem is very important from the standpoint of the designer. Unfortunately, however, very little specific information is available on the subject and few experimental checks on predicted critical column loads for torsional failure of these sections are available. Some work has been carried out by Dunn at GALCIT on this subject (reference 5-6) and more research is now in progress. Until more exact methods of analysis are available, however, designers should be cognizant of the fact that nearly all open-section stiffeners may be subject to torsional instability under end load and they should check each section by the method indicated above or by experimental tests to determine the allowable critical stresses and the mode of failure of the section.

As the stress on any column approaches its ultimate strength, the cross section undergoes distortions which may be local or may extend over the length of the member. Such distortion of the section causes a shift of the axis of resistance of the member from the axis of loading, thus creating moments due to the eccentricity of the axial load. These moments cause the member to deflect with the result that a shear is developed on the affected sections whose magnitude is $P(\sin i)$ where i represents the slope of the deflected section and P the axial load on the column. Such shear stresses produce forces on the elements of an open section which may cause it to rotate as a whole or which may aggravate the bending of the deflected elements. Where a stiffener is fastened to a sheet, these forces are normally insufficient to cause the combination of sheet and stiffener to rotate about the center of twist of the stiffener, but they may suffice to bend the elements of the stiffener itself and cause it to fail in a combination of bending and twisting.

Figure 5-32 shows representative shapes of stiffeners and the direction of the shear forces acting on their elements when the load is applied eccentrically. A study of this figure shows why sections such as channels sometimes fail by the legs bowing inward or outward if they do not fail by twisting as a whole. When bending subjects one leg to compression and the other to tension, the section tends to twist as a whole as shown at (a). When the eccentricity is along the other axis, the tendency is to fail by bending the outstanding portions inward or outward owing to the shear forces, as shown in (b) to (f), the direction depending upon whether the point of loading is on one side or the other of the centroid and on whether such flanges as may be used bend inward or outward. Sketches (e) and (f) do not present an entirely true picture of the shear forces acting

since they are unsymmetrical sections. They would tend to deflect about both of the axes shown owing to a moment in the plane of either, the axes not being principal axes for these sections.

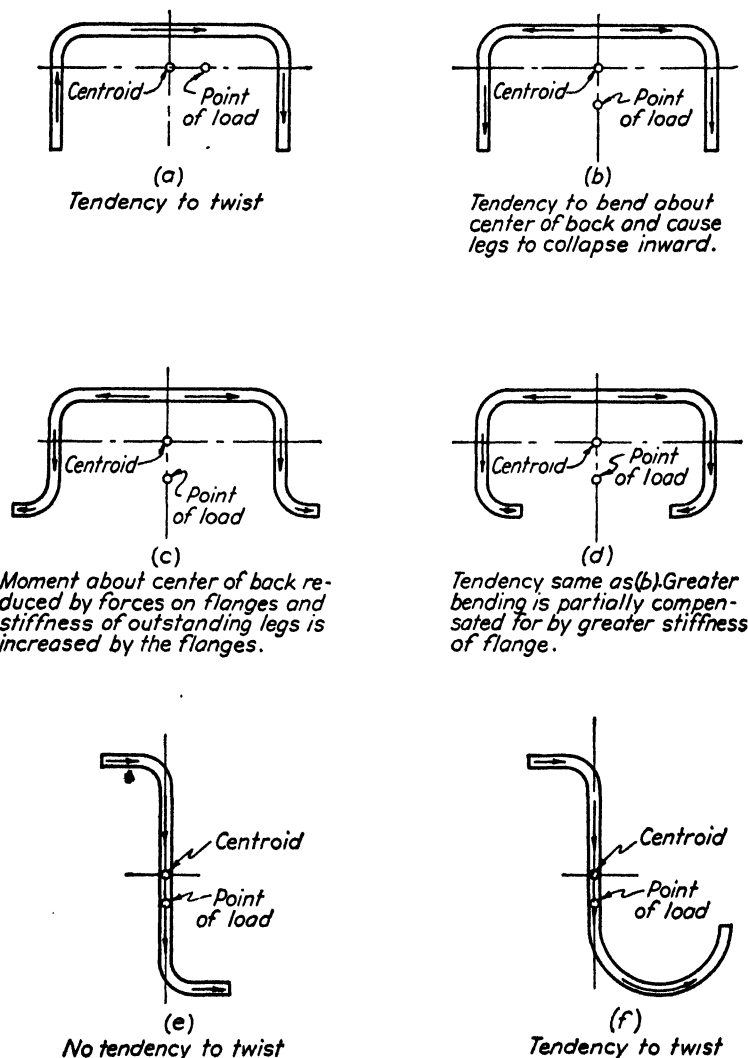


FIG. 5-32. Induced stresses in stiffener sections.

From the above, it is seen that open-section stiffeners may fail because of secondary moments and shears induced in them by eccentricity of the loading or by bending of the stiffener and the material to which it is attached. Since in some stiffeners the principal axes are not parallel and perpendicular to the sheet to which they are attached, these sections will

tend to buckle about an axis which is not parallel to the sheet. The skin reduces this tendency so the effective L/ρ is greater than the minimum, but the exact effect is difficult to evaluate. It should also be noted that tests of certain sheet-stiffener combinations made on flat panels will not indicate the true strength of such combinations in a wing or fuselage where bending of the structure produces a curvature in the panel which, with unsymmetrical sections, causes them to rotate and produce secondary bending and torsional effects, thereby inducing failure at stresses which may be materially below those obtained on the flat panel. In developing stiffener types this feature should be considered since it is not always possible to predict the magnitudes of the secondary shears and moments developed by such accidental but unavoidable eccentricities. Hence, it is impossible to determine the stresses produced in the stiffener by them. Effort should therefore be made to avoid unstable shapes wherever possible.

The use of curved elements instead of all flat ones appears to stabilize some shapes of stiffeners and cause them to develop high crushing stresses. It is probable that they restrict the buckling of the flat sheet to one direction, that is, it must buckle so that its tendency is to reduce the radius of the contiguous curved sheet but not to increase it, thereby causing it to develop higher stress intensities before failure.

Closed stiffener sections offer distinct advantages over open sections because of their increased stability at high loads or when they are bent owing to the distortion of the sheet or structure to which they are attached. It is appreciated that such sections are subject to corrosion difficulties but, from the standpoint of strength, they are superior to the open section which, when once deflected, develops internal shear or compressive forces tending to twist it or to deflect it still further.

Designers should consider all the above effects in determining the allowable stresses to be used with such sections, since tests made on the stiffener alone or on isolated stiffened panels may give appreciably lower strength properties due to the instability of the elements of the section than will be developed when the stiffener is attached to the structure; assuming, of course, that the method of attachment tends to stabilize the critical elements. On the other hand, stiffener sections which are unsymmetrical may be expected to fail at lower stresses in an actual structure than in a test. As normally used they are constrained, by the material to which they are attached, to a plane which does not contain one of the principal axes of the section, so they are forced to bend in a direction normal to that plane as well. Such stiffeners roll over readily and may not develop as high loads when part of a structure subject to secondary deformations as when tested on a panel under a direct compressive load.

REFERENCES FOR CHAPTER 5

- 5-1. S. TIMOSHENKO, *Theory of Elastic Stability*, McGraw-Hill, 1936.
- 5-2. W. LAVERN HOWLAND, "Variation of the Modulus of Elasticity of Duralumin," *J. Aero. Sci.*, October, 1937.
- 5-3. "Column Strength of Various Aluminum Alloys," *Aluminum Res. Lab., Tech. Paper 1*, Aluminum Company of America, 1938.
- 5-4. R. V. SOUTHWELL, *Theory of Elasticity*, Oxford Press, 1936.
- 5-5. E. CHWALLA, "Das allgemeine Stabilitätsproblem der gedruckten, durch Randwinkel verstärkten Platte," *Ingenieur—Archiv.*, Vol. V, p. 54 (1934).
- 5-6. L. G. DUNN, "An Investigation of Sheet-Stiffener Panels Subjected to Compression Loads with Particular Reference to Torsionally Weak Stiffeners," *N.A.C.A. Tech. Note 752*.
- 5-7. H. L. COX, "Summary of the Present State of Knowledge Regarding Sheet Metal Construction," *R. & M. No. 1553, British A.R.C.*, 1933.
- 5-8. F. J. BRIDGET, C. C. JEROME, and A. B. VOSSELLER, "Some New Experiments on Buckling of Thin-Wall Construction," *A.S.M.E. Trans.*, APM 56-6, August, 1934, p. 569.
- 5-9. W. S. PARR and W. M. BEAKLEY, "An Investigation of Duralumin Channel Section Struts in Compression," *J. Aero. Sci.*, Vol. 3, September, 1935, p. 21.
- 5-10. E. E. LUNDQUIST, "Local Instability of Centrally Loaded Columns of Channel Section and Z-Section," *N.A.C.A. Tech. Note 722*.
- 5-11. E. E. LUNDQUIST, "Local Instability of Symmetrical Rectangular Tubes Under Axial Compression," *N.A.C.A. Tech. Note 686*.
- 5-12. R. A. MILLER, "Compressive Strength of Duralumin Channels, *A.C.I.C.* No. 598.
- 5-13. *Ford Motor Co. Rep. on C-4A Transport*, "Strength of Structural Shapes," 1930.
- 5-14. CROSHIRE and DUNN, "An Investigation of the Crippling Stress of Thin Sheet Columns," M.I.T. Thesis, 1939.
- 5-15. H. WAGNER and W. PRETSCHNER, "Torsion and Buckling of Open Sections," *N.A.C.A. Tech. Memo. 784*.
- 5-16. H. WAGNER, "Torsion and Buckling of Open Sections," *N.A.C.A. Tech. Memo. 807*.
- 5-17. R. KAPPUS, "Twisting Failure of Centrally Loaded Open-Section Columns in the Elastic Range," *N.A.C.A. Tech. Memo. 851*.
- 5-18. E. E. LUNDQUIST and C. M. FLIGG, "A Theory for Primary Failure of Straight Centrally Loaded Columns," *N.A.C.A. Tech. Rep. 582*.
- 5-19. F. B. SEELY, *Advanced Mechanics of Materials*, Wiley, 1932, p. 81 ff.
- 5-20. S. TIMOSHENKO, *Strength of Materials*, Vol. I, Van Nostrand, 1930, p. 191 ff.

CHAPTER 6

THE ULTIMATE STRENGTH OF STIFFENED FLAT SHEET

6-1. The Ultimate Load for Rectangular Isotropic Flat Plates in Compression

Inasmuch as the sheets used as aircraft structural elements are generally quite thin, the buckling stresses of these sheet elements are necessarily low. The designer is therefore confronted with the problem of using sheet metal in the buckled or wave state, and of determining the stress distribution and allowable stresses in such buckled plates. Up to the critical buckling load, the direct compressive stress on the loaded edges of a plate is uniformly distributed. After buckling occurs, the central portion of the plate, due to its curvature, can carry little or no additional load; however, the edges of the plate, being constrained to remain straight owing to their being supported, can and do carry an increasing amount of stress. A stress-distribution pattern, which is in reasonable agreement with the experimental data, is given by the equation

$$\sigma_c = \frac{1}{2} \left[(\sigma_{se} + \sigma_{cr}) - (\sigma_{se} - \sigma_{cr}) \cos \frac{2\pi x}{b} \right] \quad [6.1]$$

in which σ_{se} = stress at the supported edges of the sheet,

σ_{cr} = critical buckling stress of the plate as determined by equation 5.19. (Sec Fig. 6.1.)

The total load which the plate carries can be obtained by integrating the above compression stress over the entire width of the panel, or

$$P_{sh} = t \int_{-b/2}^{b/2} \sigma_c dx = \frac{bt}{2} (\sigma_{se} + \sigma_{cr}) = \frac{bt\sigma_{se}}{2} \left(1 + \frac{\sigma_{cr}}{\sigma_{se}} \right) \quad [6.2]$$

In order to simplify the calculations, especially when dealing with plate-stiffener analyses, the conception of an "effective width" of sheet was introduced by Kármán. In this method, it is assumed that there is a uniform compressive stress equal to σ_{se} acting on a width of plate equal to w_e , directly adjacent to the supported edges. The value of w_e is adjusted so that $2\sigma_{se}w_e t$ is equal to the total load carried by the plate.

Thus, for a sheet having the distribution given by equation 6.1, the effective width can be determined from equation 6.2, since

$$P_{sh} = \frac{bt\sigma_{se}}{2} \left(1 + \frac{\sigma_{cr}}{\sigma_{se}} \right) = 2\sigma_{se}w_e t$$

or

$$w_e = \frac{b}{4} \left(1 + \frac{\sigma_{cr}}{\sigma_{se}} \right) \quad [6.3]$$

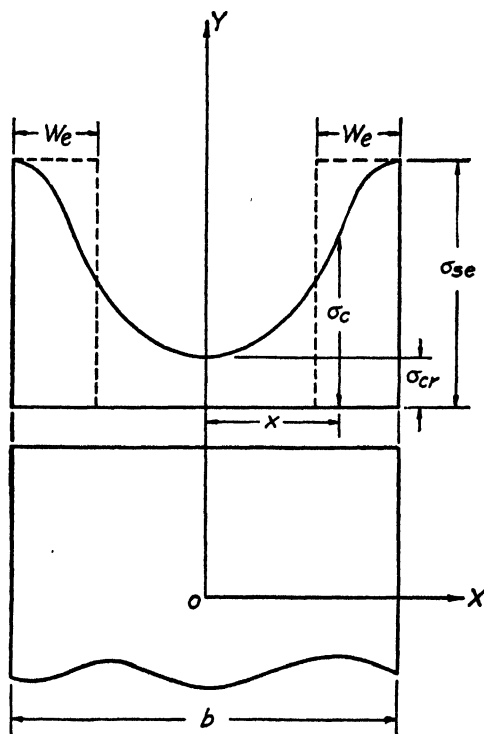


FIG. 6.1. Compressive stress distribution in a buckled flat plate.

This is usually put in the form of the ratio

$$\frac{w_e}{b} = 0.25 \left(1 + \frac{\sigma_{cr}}{\sigma_{se}} \right) \quad [6.4]$$

This ratio has been plotted as a function of σ_{se}/σ_{cr} in Fig. 6.2 and is shown as the upper curve in that figure.

At some value of the edge stress σ_{se} , certain portions of the sheet have combined stresses exceeding the yield point of the material. If the edge stress is increased beyond this point, it seems reasonable to assume that

the stress distribution given by equation 6.1 will no longer hold and that the effective width will deviate from the value given by equation 6.4. These assumptions are borne out by experimental evidence. Thus, for any given panel, subjected to a compression load in its plane, the following order of events would occur with regard to the w_e/b ratio. (1) Before buckling, the effective active sheet would equal the entire panel width, or $w_e/b = \text{constant} = 0.5$. (2) After buckling occurs, and until

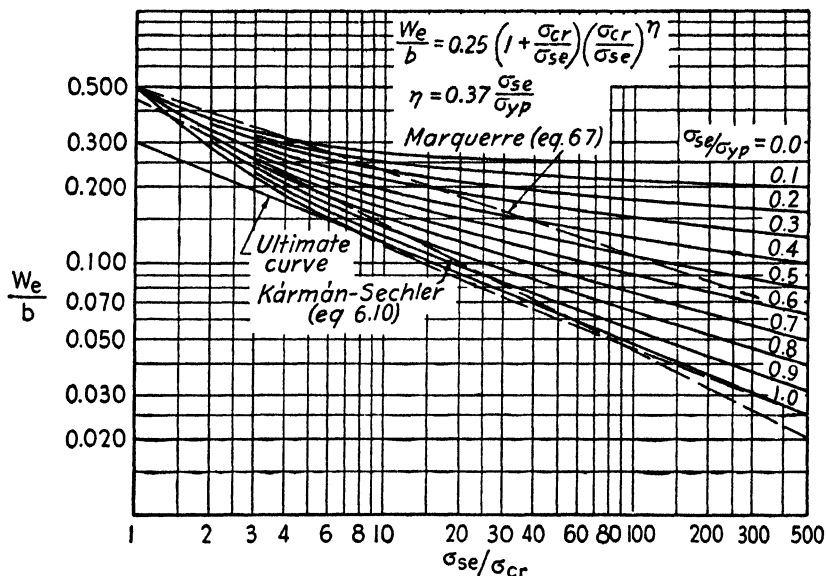


FIG. 6-2. Curve for determining the effective width.

some point in the sheet has reached the yield point, the w_e/b ratio will follow the curve given by equation 6.4. (3) At some value of σ_{se}/σ_{cr} , the stress distribution on the loaded edges will depart from that given by equation 6.1 and the effective width will deviate from the value given by equation 6.4. The deviation will increase as more and more of the sheet goes into the plastic regime. (4) As the value of σ_{se}/σ_{cr} continues to increase, sufficient material in the plate will eventually be stressed beyond the yield point that the plate can carry no additional load. This will correspond to the ultimate load-carrying ability of the buckled sheet.

The curves shown in Fig. 6-2 for regimes 1 and 2 have been justified by a large number of compression tests on panels. The ultimate load value (item 4, above) has also been determined experimentally and an empirical curve has been suggested by Sechler on the basis of a large number of tests made at GALCIT, Massachusetts Institute of Tech-

nology and elsewhere. The empirical curve giving the end points of the various w_e/b curves is shown as the lower curve in Fig. 6.2 marked ultimate curve.

Regime 3, inasmuch as the plate has a relatively high deformation, making necessary a large deflection theory analysis, coupled with the fact that portions of the sheet are in the plastic regime, has not as yet been amenable to theoretical treatment. For this reason a family of empirical curves is suggested, these curves being based on a conservative empirical analysis of all of the available experimental information. The suggested empirical equation for the w_e/b ratio is

$$\frac{w_e}{b} = 0.25 \left(1 + \frac{\sigma_{cr}}{\sigma_{se}} \right) \left(\frac{\sigma_{cr}}{\sigma_{se}} \right)^n \quad [6.5]$$

where

$$n = 0.37 \frac{\sigma_{se}}{\sigma_{yp}} \quad [6.6]$$

The family of curves given by this equation is plotted in Fig. 6.2 for various values of the σ_{se}/σ_{yp} ratio. An indication of the agreement with experimental data is shown in Fig. 6.3 for t/b ratios of 0.005, 0.0064, and 0.008, respectively. These curves indicate that the values of w_e/b given by equation 6.5 are in reasonably good agreement with the experimental data and are conservative.

It must again be mentioned that these curves are purely empirical in nature and are subject to change as more theoretical and experimental data are obtained on the transition regime. Care must be exercised in the use of Fig. 6.2 for very small values of σ_{se}/σ_{cr} . The empirical curves become increasingly conservative as the value of the σ_{se}/σ_{cr} approaches 1.0, since, for very small values of this ratio, the value of w_e/b obviously follows the upper curve for some distance before dropping down to the appropriate σ_{se}/σ_{cr} value. Additional experimental data are necessary before a more accurate determination of the w_e/b ratio in this region is possible.

A number of theoretical investigations have been made on the stress distribution in a flat plate after buckling. Two theoretical treatments are contained in references 6.1 and 6.2.

As a comparison, the curve given by the equation for the effective width suggested by Marguerre (reference 6.1).

$$\frac{w_e}{b} = \frac{1}{2} \sqrt[3]{\frac{\sigma_{cr}}{\sigma_{se}}} \quad [6.7]$$

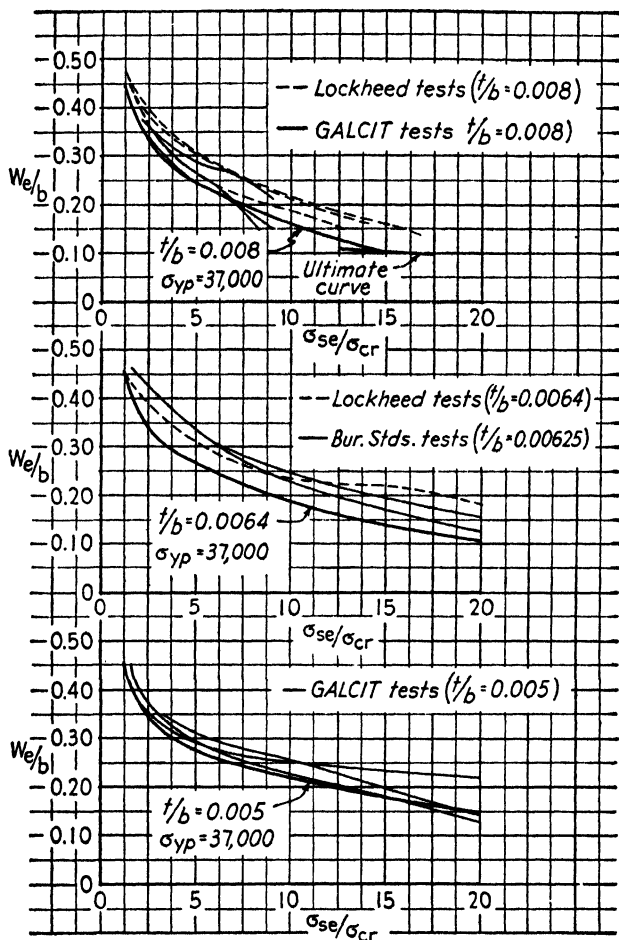


FIG. 6.3. Experimental effective width curves.

is shown in Fig. 6.2. The equation suggested by Kármán and Sechler (reference 6.2) and given as a design equation in ANC-5,

$$P_{sh} = 1.7 \sqrt{E \sigma_{se}} t^2 \quad [6.8]$$

$$w_e = \frac{1.7}{2} \sqrt{\frac{E}{\sigma_{se}}} t \quad [6.9]$$

$$\frac{w_e}{b} = 0.447 \sqrt{\frac{\sigma_{cr}}{\sigma_{se}}} \quad [6.10]$$

is also plotted in this figure.

6-2. Stiffened Flat Panels Under Compression Loads

In order to support more load than can be carried by a flat sheet alone, it is common practice to attach to the sheet, stiffening members which run parallel to the direction of the compressive stress. If the stiffeners have a comparatively low bending rigidity, their chief function will be to delay the buckling of the flat sheet beyond the point where it would have wrinkled with no stiffening present. This case has been treated by Timoshenko (reference 6-3, p. 371) and is handled as a stability prob-

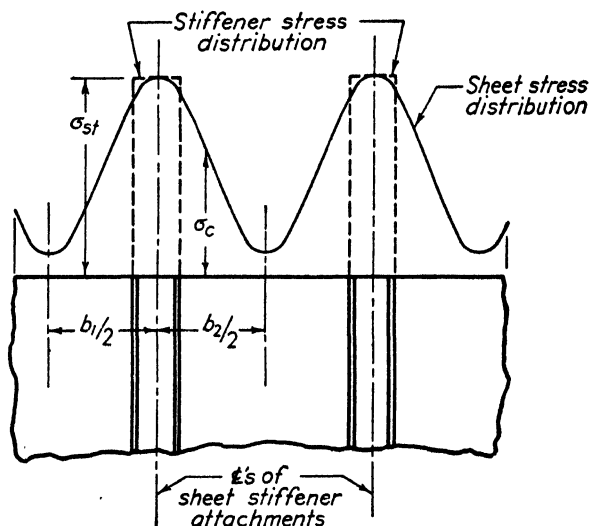


FIG. 6-4. Stress distribution in a stiffened flat plate.

lem. The equation for the critical buckling stress has the same form as that for the flat plate alone, namely,

$$\sigma_{cr} = K \frac{\pi^2 E}{12(1 - \mu^2)} \left(\frac{t}{b} \right)^2 \quad [6.11]$$

However, in this case, the factor K is not only a function of the dimensions of the plate but is also dependent upon the number and the bending rigidities of the stiffeners.

Such a type of construction may be used where it is desirable to delay the buckling of relatively large unsupported panels from aerodynamic considerations rather than from the standpoint of strength. This would be the case where minimum gages over large areas give sufficient structural strength but are subject to buckling deformations at loads within the normal flying regime. The reference given above contains sufficient

information so that it may be used by designers in the solution of problems of this type.

Normally, stiffened sheet structural elements, which are part of the main structure of an airplane, are so proportioned that the stiffeners remain essentially straight even though the sheet between them has buckled. Under these circumstances the stress distribution over the loaded edges of the stiffened panel will be as shown in Fig. 6-4. The stiffeners are subjected to a uniform compressive stress over their area, but the compressive stress in the sheet is a maximum at the point of

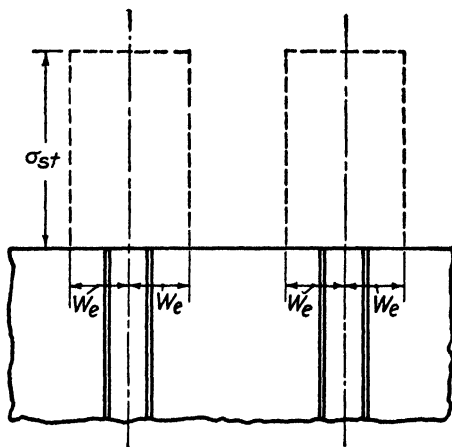


FIG. 6-5. Stiffened sheet reduced to effective columns.

attachment of sheet and stiffener and falls off towards the center of the sheet owing to the relief in stress caused by buckling. The total load carried by such a stiffened panel will then be

$$P_{\text{total}} = \sum^n \sigma_{st} A_{st} + \sum^m t \int_{-b/2}^{b/2} \sigma_c dx \quad [6.12]$$

where P_{total} = total load carried by the stiffened panel in pounds,
 n = number of stiffeners in the panel,
 m = number of sheets in the panel,
 A_{st} = area of each stiffener in square inches,
 σ_{st} = stress in the stiffeners in pounds per square inch,
 σ_c = direct compressive stress in the sheet at any point
 "x" in pounds per square inch,

$$\sum^n \sigma_{st} A_{st} = \text{total load carried by the } n \text{ stiffeners in pounds,}$$

$$\sum^m t \int_{-b/2}^{b/2} \sigma_c dx = \text{total load carried by the } m \text{ sheets in pounds.}$$

For a continuous panel with uniform stiffener size, and spacing, and with one line of attachment between sheet and stiffener, the use of the

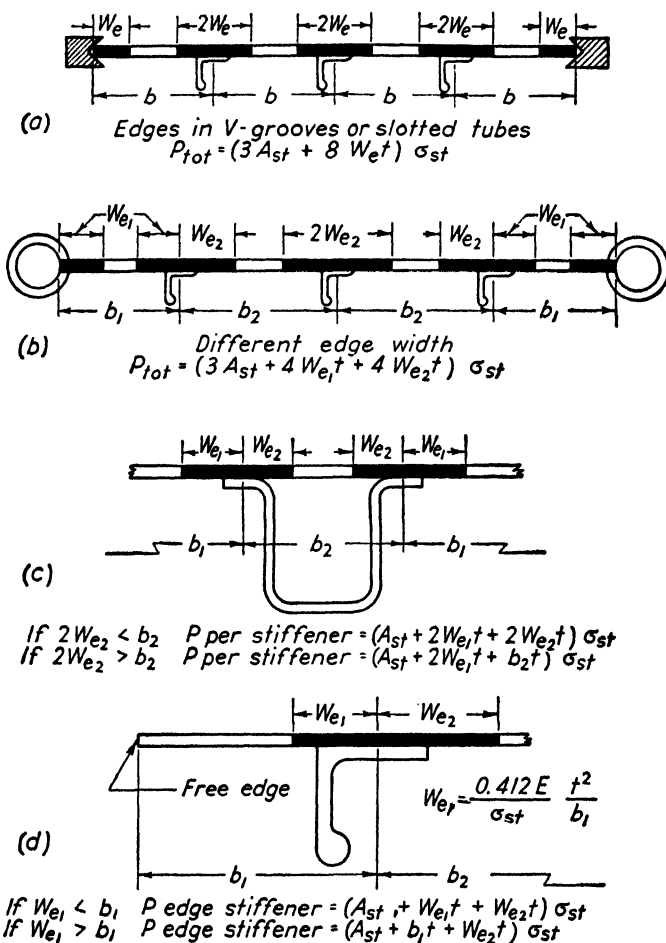


FIG. 6.6. Effective columns for various sheet-stiffener combinations.

effective width conception allows a simplification of equation 6.12 into the form

$$P_{total} = n \sigma_{st} (A_{st} + 2w_e t) \quad [6.13]$$

where $2w_e$ is the effective width of sheet acting with each stiffener. The effective load distribution will be as shown in Fig. 6.5. A number of possible combinations of sheet and stiffener are shown in Fig. 6.6 and the appropriate equations for determining the total load carried are indicated. The values of w_e may be obtained from Fig. 6.2 in which

$\sigma_{se} = \sigma_{st}$ unless buckling takes place between the sheet-stiffener attachment points as discussed below.

In all the above it has been implicitly assumed that there is a continuous line of connection between sheet and stiffener and, except for structures in which seam welding is used, this assumption is not true. Generally, the connection between the stiffeners and sheet is made a finite distance apart by spot welds or rivets. If this spacing becomes large compared to the sheet thickness, Euler or short column failure of the sheet may take place between fastening points, and the stress in the edge of the sheet will no longer be equal to the stress in the stiffeners. This problem will be treated in detail at the end of this section.

(a) Prediction of the Load-Carrying Ability of a Stiffened Panel from Stiffener-Column Curves. If the axis of the least radius of gyration of the stiffener section is parallel to the sheet to which the stiffener is attached, it is possible to predict the load-carrying ability of a stiffened flat panel directly from the stiffener column curves. This is true because the stiffener tested alone tends to fail in the same direction as when it is attached to the flat sheet, and it is only necessary to modify the column curve of the stiffener to take into account the effect of the attached sheet. In order to use this method it is necessary to know (1) the crushing strength of the stiffener section, (2) the type of short column curve which the stiffener will follow when restrained to buckle in a plane perpendicular to the sheet to which it will be attached, (3) the Euler column curve (primarily the effective end fixity) of the stiffened panel, and (4) the effect of attached sheet on the column properties of the stiffener. (*Note:* For the present it will be assumed that the stiffener is not subject to torsional instability. This problem will be treated later.)

This method which is essentially that suggested by Lundquist (reference 6.4) can best be illustrated by an example. The test values quoted were taken from reference 6.5. Consider the panel shown below stiffened with the channel section indicated (Fig. 6.7) where

$$\begin{aligned} A_0 &= 0.0566 \text{ sq. in.} \\ \rho_0 &= 0.160 \text{ in.} \\ \sigma_{vp} &= 36,000 \text{ lb. per sq. in.} \end{aligned}$$

The crushing strength of the channel section can be found from Fig. 5.15 and 5.16. From Fig. 5.15

$$bw/b_F = 0.715/0.4825 = 1.482$$

$$K_F = 0.747$$

$$\sigma_{cr}/\eta = 0.747 \times 10.3 \times 10^6 \left(\frac{0.035}{0.4825} \right)^2 = 40,500 \text{ lb. per sq. in.}$$

and from Fig. 5-16, with

$$\sigma_{yp} = 36,000 \text{ lb. per sq. in.}$$

$$\sigma_{cr} = 29,400 \text{ lb. per sq. in.} = \sigma_{cc} = \text{crushing strength at } L/\rho = 0.$$

It will be assumed that the effective end fixity of the panels (they were tested flat ended) was equal to 2.0. A more careful analysis of the test

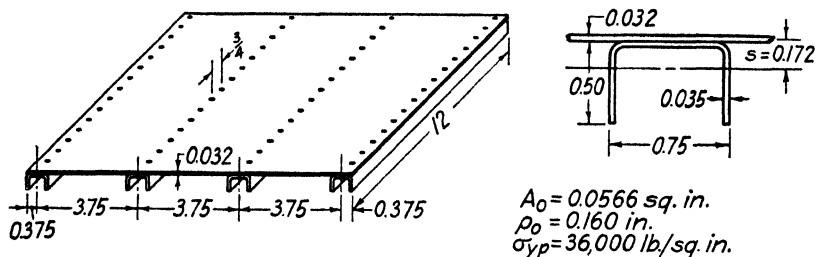


FIG. 6-7. Experimental test panel.

results indicates that there was an apparent change in end fixity of the specimens ranging from approximately 1.8 for those with 0.020-in. to

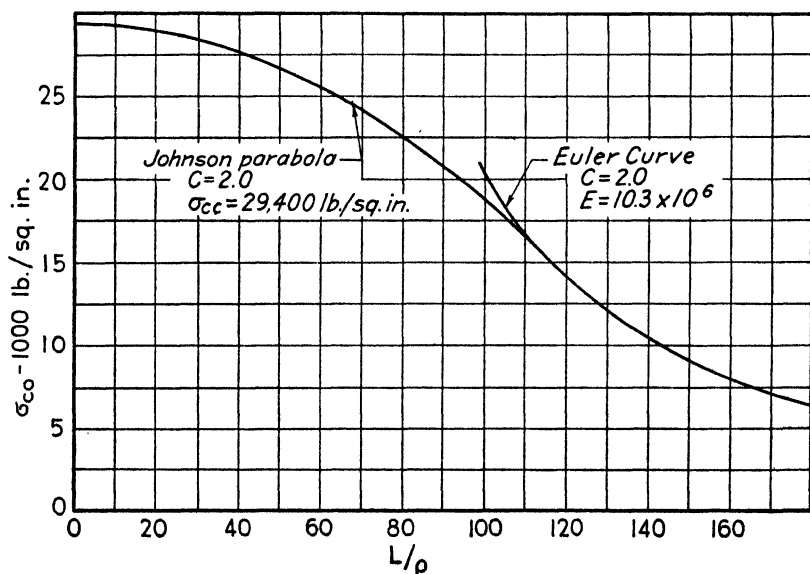


FIG. 6-8. Column curve for stiffener alone.

approximately 2.2 for those with 0.051-in. sheet. An average of 2.0 will suffice to indicate the method.

Considering a crushing strength of 29,400 lb. per sq. in., an end fixity of 2.0, and a Johnson parabola between the crushing strength and the

Euler column curve, the column curve for the section is as shown in Fig. 6·8. For the channel without sheet, 12 in. long, $L/\rho_0 = 12/0.16 = 75.0$ and $\sigma_{sc} = 23,300$ lb. per sq. in.

Column tests on 12-in. lengths of this channel showed an average failing stress of 23,000 lb. per sq. in.

To determine the effective width of sheet acting with the stiffener, assume as a first approximation that 23,300 lb. per sq. in. is the stress on the edge of the sheet. Then, from Fig. 6·2, with

$$\sigma_{cr} = 3.617E \left(\frac{t}{b} \right)^2 = 3.617 \times 10.3 \times 10^6 \left(\frac{0.032}{3.75} \right)^2 = 2710 \text{ lb. per sq. in.}$$

$$\sigma_{se}/\sigma_{cr} = 8.6 \quad \sigma_{se}/\sigma_{yp} = 0.65 \quad w_e/b = 0.167$$

and

$$w_e = 0.167 \times 3.75 = 0.626 \text{ in.}$$

For the center stiffeners the new effective column is as shown in Fig. 6·9. The radius of gyration of this new section can be found from Fig. 6·10 in which

$$S/\rho_0 = 0.172/0.160 = 1.08$$

$$t/A_0 = 0.032/0.0566 = 0.57$$

$$b_e = 1.252$$

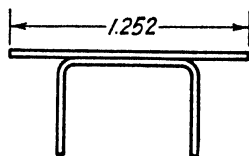


FIG. 6·9. Effective column for center stiffeners.

This gives

$$(\rho_1/\rho_0)^2 = 0.89$$

$$\rho_1 = 0.151 \text{ and the new } L/\rho_1 = 79.5$$

From the column curve in Fig. 6·8, the new critical column stress is

$$\sigma_{co1} = 22,650 \text{ lb. per sq. in.}$$

Repeating the process using 22,650 lb. per sq. in. as the new value of σ_{se} , we obtain from Fig. 6·2

$$\sigma_{se}/\sigma_{cr} = 8.3 \quad w_e/b = 0.170$$

$$\sigma_{se}/\sigma_{yp} = 0.63 \quad w_{e2} = 0.637 \text{ in.}$$

and from Fig. 6·10

$$b_e = 1.274 \quad (\rho_2/\rho_0)^2 = 0.88$$

$$\rho_2 = 0.150 \quad L/\rho_2 = 80.0$$

from which

$$\sigma_{co2} = 22,500 \text{ lb. per sq. in.}$$

Further repetition is unnecessary, and the effective column will be one having 1.274 in. of sheet acting with the channel and capable of supporting a stress equal to 22,500 lb. per sq. in.

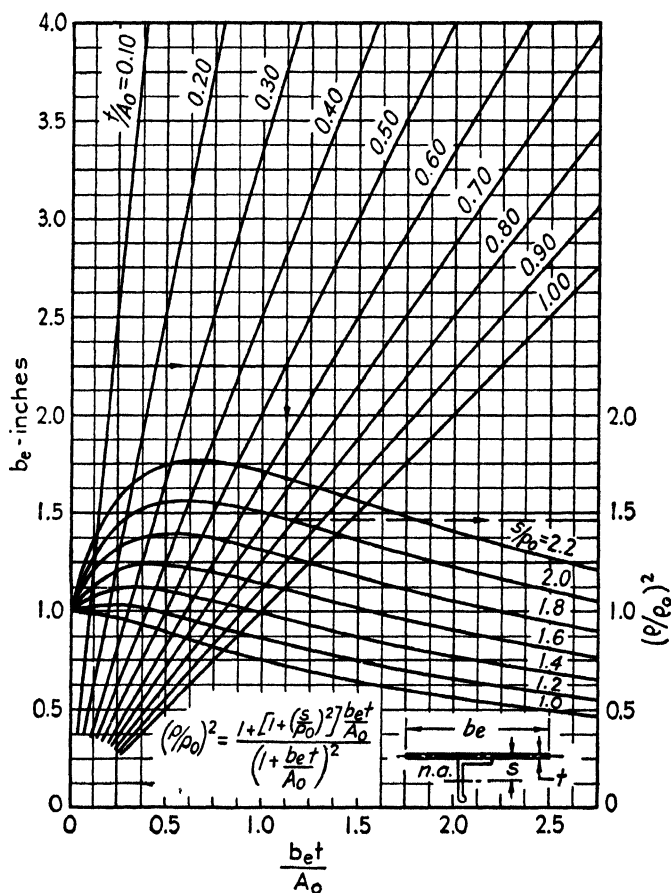


FIG. 6-10. Chart for determining $(\rho/\rho_0)^2$.

For the edge stiffeners there is one effective width acting on the panel side, while there is a 0.375-in. length extending beyond the rivet line on the outside. (Figure 6-11.) The buckling stress of this free edge is given by

$$\sigma_{cr} = 0.452E \left(\frac{t}{b} \right)^2 = 0.452 \times 10.3 \times 10^6 \left(\frac{0.032}{0.375} \right)^2 = 33,900 \text{ lb. per sq. in.}$$

This stress is higher than the allowable column stress for the combined section, therefore the whole 0.375-in. length of sheet will be included in

the effective area. The effective column is then as shown. From Fig. 6-10, since b_e for the edge stiffeners is less than b_e for the center stiffeners, it would be concluded that the edge stiffeners could carry a somewhat higher stress than the central columns. Conditions of the test, however, were such that the panel was loaded with uniform strain; therefore, up to the time of failure of the center stiffeners, all straight stiffener sections would carry the same stress. Upon failure of the central stiffeners, the sudden reduction in their load-carrying ability would tend to overload the edge stiffeners and probably collapse the panel. It is therefore conservative to assume that the entire effective panel fails at 22,500 lb. per sq. in.

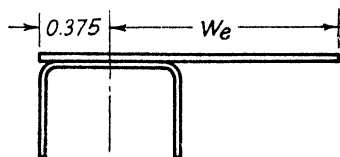


Fig. 6-11. Effective column for end stiffeners.

The effective panel area is then

$$\text{From stiffeners} \quad A_1 = 4 \times 0.0566 = 0.2264 \text{ sq. in.}$$

$$\text{From free edges on sides} \quad A_2 = 2 \times 0.375 \times 0.032 = 0.0224 \text{ sq. in.}$$

$$\text{From effective widths} \quad A_3 = 6 \times 0.637 \times 0.032 = 0.1222 \text{ sq. in.}$$

$$A_0 = 0.3710 \text{ sq. in.}$$

And the total load-carrying ability of the panel should be

$$P_{\text{total}} = 0.3710 \times 22,500 = 8350 \text{ lb.}$$

The test loads carried by two panels of this type were 8450 lb. and 7570 lb., respectively, averaging 8010 lb.

Additional panels in this series have been checked with the results shown in Table 6-1. For the panels with 0.020 sheet, the edge beyond

TABLE 6-1

Length (L in.)	Sheet Thickness (t in.)	No. Stiffeners (n)	Effec. Width (w_e in.)	Effec. L/ρ	Column Stress (σ_{co} lb./sq. in.)	Effec. Area (A_e sq. in.)	Predicted Load (P_P lb.)	Test Loads (P_T lb.)	
12	0.020	4	0.469	76.2	23,200	0.2913	6,760	6,390	6,470
12	0.032	4	0.637	80.0	22,500	0.3710	3,350	8,450	7,570
12	0.051	4	0.990	92.3	20,250	0.5677	11,490	12,500	13,200
18	0.020	3	0.861	120.0	14,100	0.2528	3,560	3,280	3,270
18	0.032	3	1.181	133.0	11,450	0.3484	3,990	4,300	3,830
18	0.051	3	1.855	164.5	7,500	0.5463	4,400	4,650	4,890

the rivet line buckles at 13,250 lb. per sq. in., and the effective material acting at the given column-failing stress was determined from the equation

$$w'_e = 0.375 \frac{13,250}{\sigma_{co}}$$

Table 6.1 shows good agreement between predicted and test loads, particularly if one considers the fact that the following assumptions were necessary in making the calculations: (1) end fixity assumed constant = 2.0; (2) average value of $\sigma_{yp} = 36,000$ lb. per sq. in. assumed for all material; (3) nominal thicknesses were assumed for all sheet stock.

The above method works equally well for stainless steel as can be seen from Table 6.2. The test results were taken at random from reference 6.6. For these specimens, the crushing strength of 120,000 lb. per sq. in. was taken from tests on a series of columns consisting of the stiffener plus the sheet across the open legs as shown in type *D* in Fig. 6.12. This was considered as the basic stiffener, and effective widths were taken as acting on either side of this section for central stiffeners and on one side for edge stiffeners. The value of end fixity used in the calculation, $C = 1.3$, was determined from flat end tests of the basic stiffener tested alone.

For the specimens of Table 6.2 the end stiffeners with the smallest amount of effective sheet had the lowest critical column stress. In calculating the predicted failing load, it has therefore been assumed that the inside stiffeners failed at the same stress as that causing column failure of the edge stiffeners. This is a conservative assumption and may explain the fact that the predicted values are, with one exception, lower than the test values. This procedure is recommended in design, however, since the degree of conservatism is, in general, not excessive.

TABLE 6-2

Type Spec.	Length (L in.)	Eff. Width (w_e in.)	Col. Stress (σ_{sc} lb./sq. in.)	Eff. Area (A_e sq. in.)	Predict. Load (P_P lb.)	Test Load (P_T lb.)	$(P_P - P_T)/P_T$ (%)
<i>A</i>	9.24	0.448	106,310	0.317	33,710	33,010	+2.1
<i>A</i>	13.83	0.556	89,300	0.325	29,010	30,480	-4.5
<i>A</i>	18.48	0.716	65,800	0.337	22,180	23,020	-3.6
<i>B</i>	9.22	0.352	106,320	0.310	32,970	36,230	-9.0
<i>B</i>	13.86	0.422	89,200	0.315	28,100	28,240	-0.5
<i>B</i>	18.48	0.536	65,750	0.324	21,300	21,650	-1.6
<i>C</i>	9.24	0.283	106,250	0.411	43,700	47,680	-8.4
<i>C</i>	13.86	0.328	89,000	0.415	36,950	39,930	-7.5
<i>C</i>	18.46	0.398	65,350	0.423	27,630	29,760	-7.2

This method has also been used to analyze a series of stiffened panels tested at GALCIT (reference 6.7). These panels were stiffened by the bulb-angle stiffeners *A* and *B*, Fig. 6.13, the stiffener spacing being 5 in. in every case. As shown in the figure, there was a $2\frac{1}{2}$ -in. width of sheet

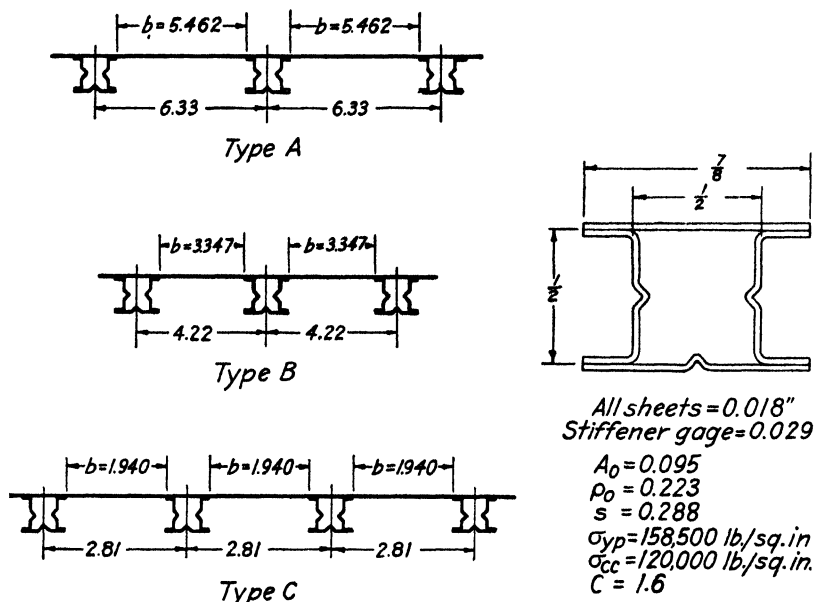


FIG. 6.12. Stainless steel test panels.

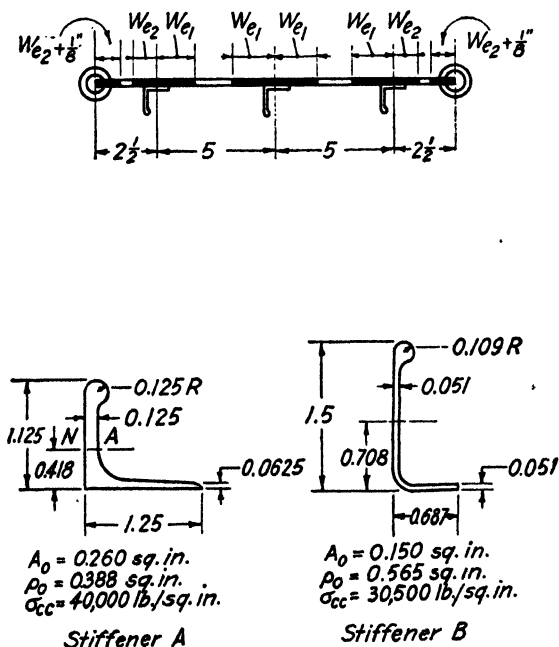


FIG. 6.13. Aluminum-alloy test panels.

beyond the first and last stiffeners, and the free edge of this sheet was supported in slotted tubes. Table 6-3 shows the agreement between the calculated and test values of the ultimate load-carrying ability of the panels. In calculating the results shown in Table 6-3, the crushing strengths of the sections were taken from short column test results, and a Johnson curve with a fixity equal to 3.0 was taken for the short column range.

The first group of specimens indicates that the method gives somewhat conservative results for all lengths tested. The specimens stiffened with bulb angle *B* show good agreement for the shorter lengths of panel and increasingly poor agreement as the panels become longer. This difference in action between stiffeners *A* and *B* is probably due to the difference in torsional rigidities of the two sections. Section *A* has a torsional rigidity 3.2 times as great as section *B* although the areas differ by a factor of only 1.75. Section *A* is so torsionally rigid that the buckling of the 0.040 sheet caused very little rotation of the stiffener and thus had a negligible effect on the column strength of the effective section. On the other hand, the sheet buckling tended to rotate stiffener *B* sufficiently to cause a combined flat plate and torsional failure of the effective column. The rotation would be small for very short panels where end effects have a stabilizing action on the stiffener, and would tend to reach a nearly constant value as the length of the column increased.

The above phenomenon frequently occurs for extruded bulb angles and other extruded open sections. As yet there are no theoretical or empirical methods available for predicting the magnitude of this effect of sheet buckling on the column strength of the stiffeners. Qualitatively, one can say that whenever light, open sections are used to stiffen relatively heavy sheets, the buckling of the flat sheet will tend to reduce the allowable column stress of the effective stiffener. With closed sections and heavy extrusions on thin sheet, the change in column strength of the stiffener due to sheet buckling is negligible.

Considerable research is being carried out on this subject, and correction factors, taking into account the torsional strength of the stiffener and the bending stiffness of the sheet, may be available in the near future; however, at present it is advisable to check any stiffened panel design incorporating torsionally weak sections by a few tests to determine the magnitude of this effect. A preliminary treatment of this problem is given in reference 6-7. The torsional strength of the stiffener will also have an influence on the critical buckling load of the sheet, thus changing the calculated effective width. The effect of this change in effective width on the total strength of the panel is relatively small and can, in general, be neglected. The change in the buckling load of flat panels,

TABLE 6-3

Stiffener Type	No. Stiffeners (n)	Length (L in.)	Sheet Thickness (t in.)	Effective Widths		Effective L/ρ	Column Stress (σ_{co} lb./sq. in.)	Effective Area (A_e sq. in.)	Predicted Load (P_P lb.)	Test Load (P_T lb.)	$\frac{P_P - P_T}{P_T}$ (%)
				w_{c1} (in.)	w_{c2} (in.)						
A	3	12	0.040	0.500	0.451	30.8	38,760	0.9422	36,500	39,360	- 7.3
A	3	16	0.040	0.500	0.475	41.0	37,800	0.9460	35,750	38,740	- 7.7
A	3	21	0.040	0.505	0.487	53.6	36,200	0.9587	34,700	38,180	- 9.1
A	3	27	0.040	0.575	0.534	69.2	33,730	0.9674	32,620	35,550	- 8.2
B	2	12	0.040	0.660	0.594	20.9	30,170	0.4578	13,800	13,540	+ 1.9
B	3	12	0.040	0.660	0.594	20.9	30,170	0.6606	19,920	19,410	+ 2.6
B	4	12	0.040	0.660	0.594	20.9	30,170	0.8634	26,020	24,490	+ 6.2
B	2	16	0.040	0.670	0.594	27.5	29,920	0.4585	13,710	12,650	+ 8.4
B	3	16	0.040	0.670	0.594	27.5	29,920	0.6621	19,800	17,940	+10.4
B	4	16	0.040	0.670	0.594	27.5	29,920	0.8657	25,890	24,730	+ 4.7
B	2	21	0.040	0.680	0.606	36.0	29,460	0.4614	13,590	12,280	+10.7
B	3	21	0.040	0.680	0.606	36.0	29,460	0.6658	19,600	17,100	+14.6
B	4	21	0.040	0.680	0.606	36.0	29,460	0.8702	25,620	23,450	+ 9.3
B	2	27	0.040	0.695	0.615	46.3	28,850	0.4640	13,370	12,240	+ 9.2
B	3	27	0.040	0.695	0.615	46.3	28,850	0.6695	19,300	16,950	+13.9
B	4	27	0.040	0.695	0.615	46.3	28,850	0.8750	25,220	22,550	+11.8

elastically supported in torsion along two edges, can be determined from Fig. 5-9.

(b) Allowable Design Values from Stiffened Panel Tests. The proper analysis of test data, from a series of panels tested under compression, is essentially a reversal of the above outlined procedure. At the conclusion of the test program, the data available usually include the variation of the total load carried by the panel as a function of the panel length. Considering the first set of panels in Table 6-3, the designer would have, in addition to the dimensions of the panel, the information given in columns 1 and 2 of Table 6-4, which data were obtained in compression tests of the panel shown in Fig. 6-18.

The simplest analysis would be to determine merely the average stress carried by the test specimen. If this is done, the total load is divided by the total area giving the values in column 3, Table 6-4. Unfortunately, these values cannot be used for design purposes for several reasons. First, the effect of the supported sheet edges is included in the test load and unless the width of the side panels is equal to the stiffener spacing, the stress distribution over the test panel is not the same as that over a continuous panel.

Second, the end fixity of the test specimens will not, in general, be the same as that given to a similar panel in an actual structure. To make a correction for end fixity, it is necessary to put the results in the form of stress versus L/ρ and, in this case, the effective ρ is unknown. As will be discussed later, carefully machined panels, tested flat ended, usually have an end fixity coefficient close to 3.0, and if this is assumed to hold, it might be possible to solve the Johnson column equation

$$\sigma_{sc} = \sigma_{cc} - \frac{\sigma_{cc}^2 (L/\rho)^2}{4C \pi^2 E}$$

for two values of L and obtain σ_{cc} and an effective value of ρ . If this is done, however, no check is possible on the correctness of the assumption that $C = 3.0$ and, for some sections, this assumption may be considerably in error.

The third item which will be difficult to take into account will be the correction for the difference between the material properties of the test specimen and the specified minimum properties of the material. Unless the crushing strength of the effective column, or at least the crushing strength of the stiffener section, is known, it is impossible to determine whether or not the failure is a function of yield point or is only dependent upon the modulus of elasticity of the material. It is therefore difficult to determine what correction will be necessary to account for variation in material properties.

The next simplest, and a considerably more exact, method would be to assume that some reasonable amount of sheet was acting with each stiffener, and then calculate the failing stress of the effective columns. The assumption that an effective width of sheet equal to $15t$ acts on each side of the rivet line seems to give a good average value suitable for a number of design purposes.

Figure 6-14 shows the effective material which leads to an effective area of $A_e = (2 \times 0.725 + 3 \times 1.20)0.040 + 3 \times 0.260 = 0.982$ sq. in. The ρ of the stiffener plus the effective sheet is obtained from Fig. 6-10

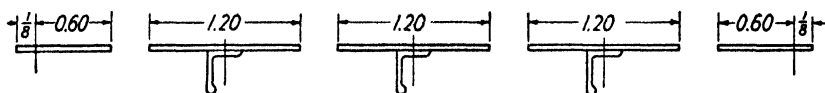


FIG. 6-14.

and is equal to 0.390 in. This gives L/ρ values as shown in column 5, Table 6-4.

The column failing stresses as a function of L/ρ are plotted in Fig. 6-15, and it is found that the test points can be matched by a Johnson parabola in which

$$\sigma_{cc} = 41,150 \text{ lb. per sq. in.}$$

$$C = 3.75$$

A short column curve is now available which can be corrected for design purposes without difficulty.

Let us assume that the material in the test panel had an experimentally obtained compressive yield point of 44,000 lb. per sq. in. and an E of 10.3×10^6 lb. per sq. in., and that the minimum specified values for this material were 42,000 lb. per sq. in. and 10.3×10^6 lb. per sq. in., respectively. The material correction factors on the crushing strength are then, from Fig. 6-20 and 6-21 (see (c) of this section for detailed discussion of material correction factors),

$$K_1 = 1.00 \quad K_2 = 0.966$$

and the design crushing strength is then

$$\sigma_{cc \text{ design}} = 1.00 \times 0.966 \times 41,150 = 39,750 \text{ lb. per sq. in.}$$

The coefficient of end fixity for design is usually specified as 1.5 and, with these two values, it is possible to obtain the design short column using a Johnson parabola with $\sigma_{cc} = 39,750$ lb. per sq. in. and $C = 1.5$. This is shown as the dotted curve in Fig. 6-15, and the design values for the various lengths are shown in column 6, Table 6-4. Column 7

shows the total load carried by the effective column as a function of its length.

The third method of analysis is one in which the effective width is not assumed but is calculated from Fig. 6-2. Inasmuch as the effective width is a function of the column stress, and the allowable column stress is dependent upon the amount of sheet acting with the stiffener, this method is essentially one of trial and error. A column stress is assumed,

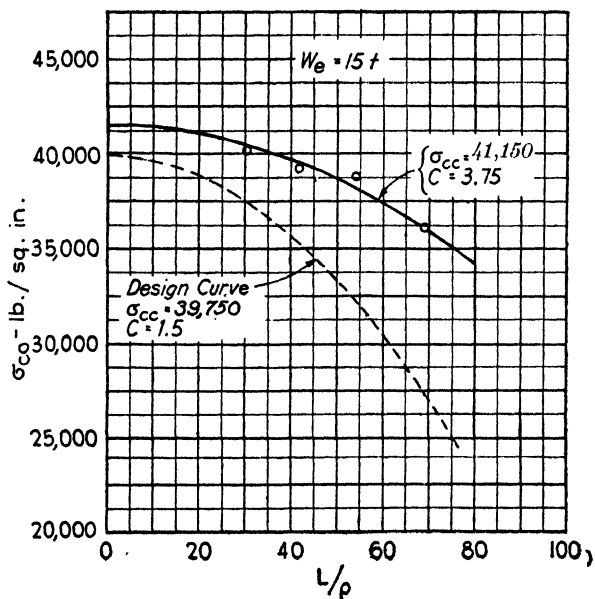


FIG. 6-15. Correction of test points to design column curve.

the effective area is calculated, and the total load in the panel is found by the product of these two values. If this load is equal to that carried by the panel, the correct column stress has been chosen. Knowing the effective width, the new ρ for the column can be found from Fig. 6-10. This gives sufficient data (see columns 8 to 12 inclusive, Table 6-4) to plot σ_{cc} versus L/ρ which has been done for this example in Fig. 6-16. The experimental points are matched by a Johnson parabola having $\sigma_{cc} = 43,700$ lb. per sq. in. and $C = 3.3$.

This column curve cannot be corrected directly as was done in Fig. 6-15 since a reduction in stress value changes the effective width acting with the stiffener and consequently the radius of gyration of the combined section. A trial and error method of solution is used in which the allowable stresses as a function of the column length are determined.

The first step is to correct the crushing strength, and this is done by the equation

$$\sigma_{cc \text{ design}} = 43,700 \times 0.966 = 42,200 \text{ lb. per sq. in.}$$

The design value of end fixity is again taken as 1.5, and the short column range will be assumed to follow the Johnson equation

$$\sigma_{co} = 42,200 - \frac{42,200^2 (L/\rho)^2}{4 \times 1.5 \times \pi^2 \times 10.3 \times 10^6} = 42,200 - 2.881(L/\rho)^2$$

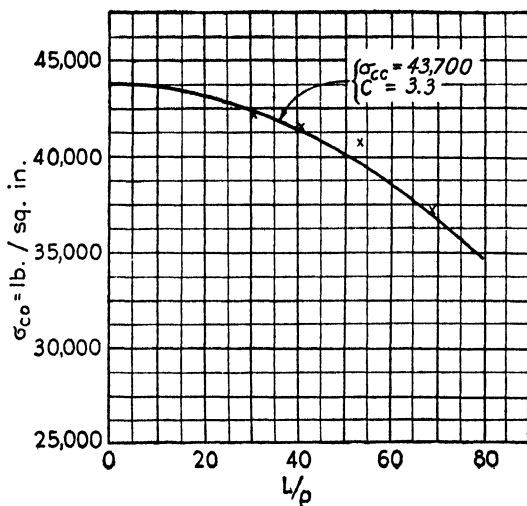


FIG. 6-16. Test column curve.

As an example consider a 25-in.-long column. The stiffener properties are, from Fig. 6-13

$$A_0 = 0.260 \quad \rho_0 = 0.388 \quad S/\rho_0 = 1.13 \quad t/A_0 = 0.154$$

Assume a new value of ρ , say $\rho = 0.390$ in., then

$$L/\rho = 64.1 \quad \sigma_{sc1} = 42,200 - 11,830 = 30,370 \text{ lb. per sq. in.} = \sigma_{se}$$

$$\sigma_{se}/\sigma_{cr} = 12.75 \quad \sigma_{se}/\sigma_{yp} = 0.723 \text{ from Fig. 6-2}$$

$$w_e/b = 0.137 \quad w_e = 0.685 \quad b_e = 2w_e = 1.370 \text{ in.}$$

Since design values are being sought, the specified yield point is used in the ratio σ_{se}/σ_{yp} . From Fig. 6-10, or the corresponding equation,

$$(\rho/\rho_0)^2 = 1.010 \quad \rho = 0.390 \text{ in.} \quad L/\rho = 64.1$$

and further approximations are unnecessary.

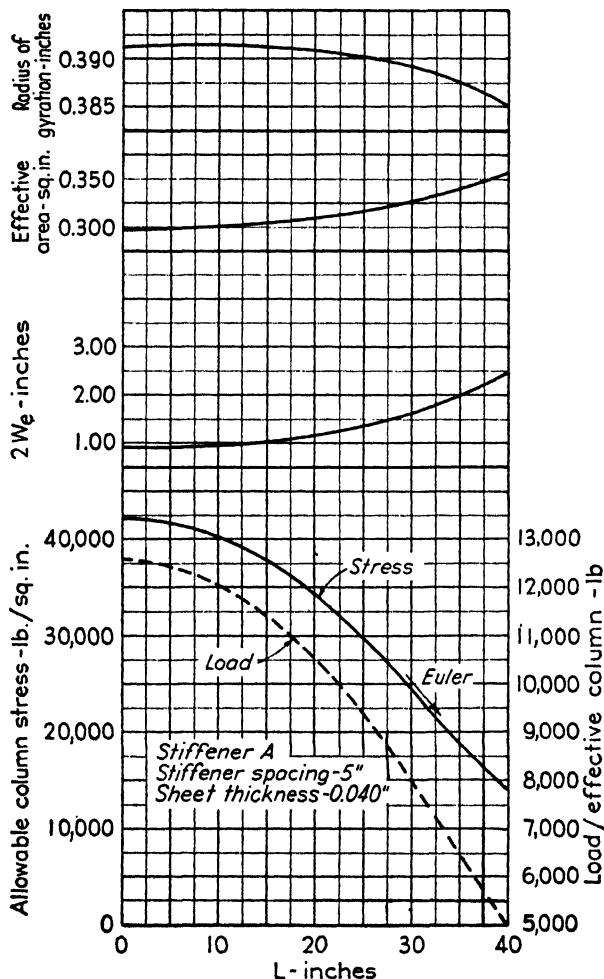


FIG. 6-17. Design values for effective column.

Therefore, for a column 25 in. long:

Critical failing stress = 30,370 lb. per sq. in.

Effective sheet = $2w_e = 1.370$ in.

Effective radius of gyration = 0.390 in.

Effective area = 0.315 in.

Total load carried by one stiffener and its effective sheet = 9,570 lb.

This has been carried out for a series of lengths and the results plotted in Fig. 6-17. For the lengths considered previously, the pertinent results have been entered in Table 6-4, columns 12 to 15 inclusive.

As can be seen from columns 6, 7, 14, and 15, the last two methods give results which are in reasonable agreement. In this example the method using $2w_e = 30t$ would be conservative if used for design, since the allowable stresses and the effective column load are both

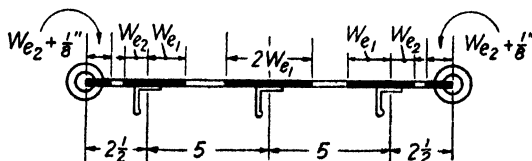


FIG. 6-18.

smaller than the corresponding values found by the exact method. The good agreement between the two methods in the above example is largely due to the fact that the actual effective widths of sheet acting with the stiffener is close to $30t$, ranging from $24.8t$ for the 12-in. length to $36.2t$ for the 27-in. length. This, however, is not always the case.

For low values of allowable column stress due to a low crushing strength of the stiffener section or to a very long column length, the effective width of sheet acting with the stiffener will, in general, be con-

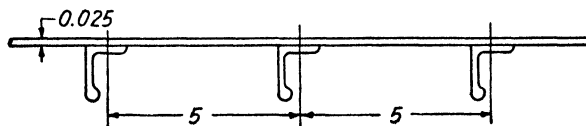


FIG. 6-19.

siderably over $30t$. To illustrate this fact, consider the stiffener sheet combination shown in Fig. 6-19,

where stiffener $A_0 = 0.057$ sq. in.,

$\rho_0 = 0.269$ in.,

$\sigma_{cc} = 25,000$ lb. per sq. in.

Assuming a column length of 20 in., the exact calculation yields the following values:

Allowable column stress = 18,780 lb. per sq. in.

Effective sheet = $2w_e = 1.590$ in. = $63.6t$

Effective column area = 0.0968 sq. in.

Load per column = 1820 lb.

On the basis of $30t$ the effective column area is only 0.0757 sq. in. which is 21.8 per cent lower than the probable actual effective area. This would be important in a structure under bending in which the area of the various elements would be used to calculate the moment of inertia

TABLE 6.4

Panel Length Load (P_T lb.)		Average Stress (σ_{ave} lb./sq.in.)	$u_{e1} = u_{e2} = 15t = 0.600$ in.					Exact Method						
							Test Values		Cont. Panel Design Values					
			Stress (σ_{e0} lb./sq.in.)	L'/ρ	Design Allow. Stress (σ_d lb./sq.in.)	Load/Eff. Column (P_e lb.)	Effective Widths		L'/ρ (σ_{e0} lb./sq.in.)	Col. Stress (σ_{e0} lb./sq.in.)	Eff. Sheet Area ($2u_{e1}$ in.)	Eff. Area (A_e sq.in.)	Allow. Stress (σ_d lb./sq.in.)	Load/Eff. Column (P_e lb.)
u_{e1} (in.)	u_{e2} (in.)													
12	39,360	28,520	40,100	30.8	37,290	11,480	0.475	0.450	30.7	42,000	0.99	0.299	39,500	11,810
16	38,740	28,090	39,480	41.8	35,200	10,840	0.480	0.452	41.0	41,300	1.06	0.302	37,500	11,300
21	38,180	27,650	38,890	53.8	32,250	9,940	0.485	0.455	53.8	40,600	1.19	0.308	34,000	10,450
27	35,550	25,760	36,200	69.2	27,350	8,420	0.570	0.502	69.2	37,000	1.45	0.318	28,100	8,950

and the position of the neutral axis of the cross section. Furthermore, assuming the same load-carrying ability of the effective stiffener, the allowable stress on the basis of $30t$ would be $1820/0.0757 = 24,050$ lb. per sq. in., a value which is very near the crushing strength of the section. Although this value is purely a fictitious allowable stress which is correct if the design calculations are based on $30t$ effective width (correct only from an allowable stress standpoint, not from the standpoint of moment of inertia and neutral axis position) the fact that it is almost as high as the crushing strength of the section may lead to erroneous conclusions in the analysis of test data on such panels.

(c) Correction to Standard Material Properties. Owing to the fact that there is a rather wide scatter in the mechanical properties of different lots of the same material, it is necessary to reduce all test data so that the results will apply to a material having the minimum specified properties. The failure of stiffened panels is a complex phenomenon in which parts of the composite structure may collapse owing to buckling, and other portions may fail because they are subjected to stresses beyond the yield point of the material.

Considering that failure in a stiffened panel takes place as some form of column failure of an effective column section, several stress regimes are of importance. If the failing stress of the effective column is very low, indicating that the column lies within the Euler or long column regime, failing stress is almost entirely dependent upon the value of the Young's modulus of the material and is independent of the other mechanical properties such as yield point and ultimate strength. Thus, any correction made to the test results should be in the form of a factor taking into account the difference between the Young's modulus of the test material and that specified for design. In most cases this variation is negligible for any one material specification. It is believed that the most satisfactory correction is one in which the test results are corrected in the direct ratio of the two moduli for all stresses up to the proportional limit, and this correction being linearly reduced to zero as the yield point of the material is approached. The equation will be

$$\sigma_{\text{design}} = K_1 \sigma_{\text{test}}$$

where K_1 is inversely proportional to $E_{\text{test}}/E_{\text{specified}}$ up to the proportional limit with a linear variation between the proportional limit and the yield point becoming equal to 1.0 at the latter stress value. This is shown in Fig. 6-20. It has been assumed that the proportional limit of any material is equal to one-half the yield point stress which is in reasonable agreement with most of the materials now being used for aircraft structural design.

Above the material proportional limit, the effect of the material yield point on failure becomes more and more pronounced. If the failing stress on a test specimen is equal to the yield point of the material in the test specimen, it is logical to assume that for any material having a different yield point, the test stresses would be changed by a factor which is a function of the two yield points. This problem has been

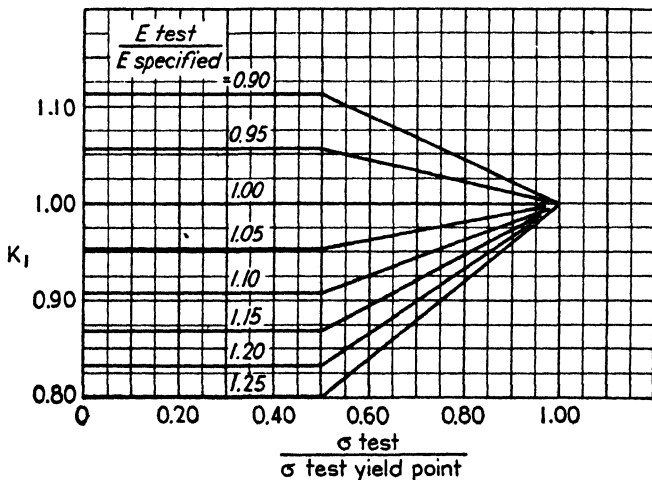


FIG. 6-20. Chart for Young's modulus correction.

treated in detail by Epstein (see reference 6-8), and a correction factor curve has been given. The equation is

$$\sigma_{\text{design}} = K_2 \sigma_{\text{test}}$$

where K_2 is given in Fig. 6-21. This correction factor has been derived in reference 6-8 on the basis of a straight line short column equation. Analysis shows, however, that it is conservative to use this correction factor for the Johnson parabolic and the tangent modulus short column curves.

Therefore, any stress values obtained in tests should be corrected in the following manner:

$$\sigma_{\text{design}} = K_1 K_2 \sigma_{\text{test}}$$

where K_1 takes into account the variation of the Young's modulus and K_2 corrects for the value of the material yield point.

In all the above, the values of yield point and Young's modulus should be taken from compression tests on the material. However, such compression material properties are not available in many cases. Reference 6-8 gives approximate relationships between the tensile properties and

the compressive properties of the more important aluminum alloys. The use of these relationships makes possible the correction of experimental tests for changes in material properties from the properties of the material obtained in a tension test. However, errors of unknown magnitude are introduced by the use of such tension values; therefore, every effort should be made to obtain the compressive mechanical properties of the material.

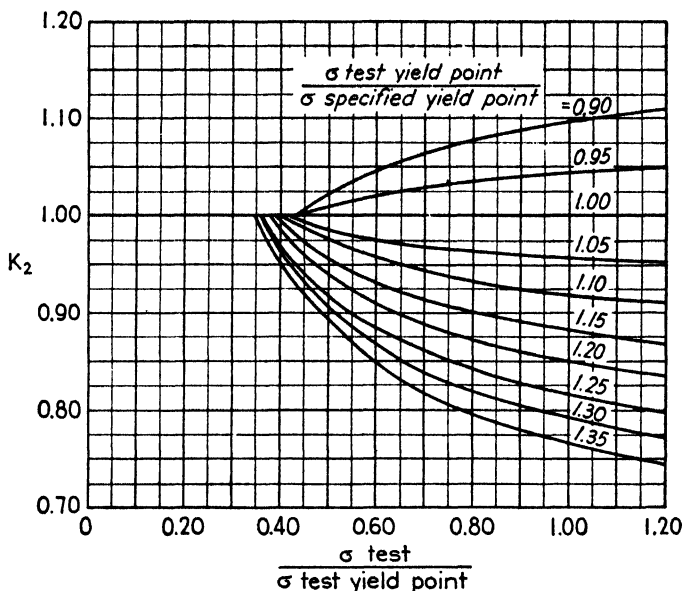


FIG. 6-21. Chart for yield point correction.

(d) **Effective End Fixity of Experimental Panel Tests.** The best method of determining the end fixity of any series of experimental panel tests would be to test sufficient specimen lengths so that the complete column curve for the section could be drawn. For preliminary design work this procedure is seldom justified and knowledge of an approximate end fixity for analysis purposes would be of considerable value.

Experience has shown that the short column curves of a large percentage of stiffened sheet panels can be approximated by the Johnson parabola

$$\sigma_{sc} = \sigma_{cc} - \frac{\sigma_{cc}^2 (L/\rho)^2}{4C \pi^2 E}$$

If this is rewritten in the form

$$\frac{\sigma_{sc}}{\sigma_{cc}} = 1 - \frac{\sigma_{cc} (L/\rho)^2}{4C \pi^2 E}$$

and σ_{sc}/σ_{cc} is plotted against $\sigma_{cc}(L/\rho)^2$ for any given material, the result is a straight line whose slope is dependent upon the fixity coefficient C . This has been done in Fig. 6-22, and a number of experimental test results have been spotted on the curve. All these tests were made flat ended, with the ends of the specimens carefully milled flat and parallel. Although there is considerable scatter, as would be expected since a variety of stiffener shapes and sheet thicknesses have been included,

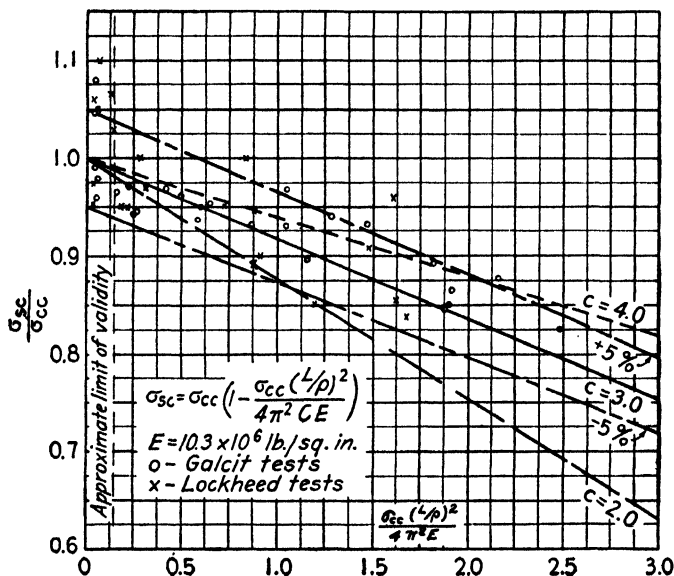


Fig. 6-22. Effective end fixity of panels tested flat ended.

Fig. 6-22 shows that 75 per cent of the test points lie within ± 5 per cent of the curve for $C = 3.0$. It is therefore suggested that for a rough analysis of a stiffened panel tested flat ended that $C = 3.0$ be used as a good average value of the panel end fixity.

For more precise results at least two panels in the short column range should be tested, and with known values of σ_{sc} and L/ρ the values of σ_{cc} and C can be calculated from the Johnson equation. As mentioned previously in Chapter 5, care should be exercised not to test specimens which are too short. If this is done, the stresses given for small L/ρ values cannot be approximated by the parabolic column curve.

(e) Effect of Rivet Spacing on the Strength of Stiffened Panels. In all of the above discussion of stiffened panels it has been assumed that the stiffener and the sheet have been continuously connected. As will be shown, this assumption is only valid for seam welding or for riveted and

spot-welded connections when the rivets or spot welds are placed very close together. For large rivet or spot-weld spacings, it will be necessary to introduce a correction into the effective width calculation in order to take into account the effect of sheet buckling between connection points.

The work of Howland (reference 6·9) indicates that it is satisfactory to assume that the sheet between rivets acts as a column with fixed ends, the column lengths being taken as the rivet spacing. Since, up to the time the sheet buckled between rivets, the sheet and stiffener will carry the same stress (if they are of materials having the same value of E), the stiffener stress at which buckling will occur between rivets is given by the Euler equation for sheet buckling (two sides fixed, two sides free)

$$\sigma_{\text{stiff}} = \frac{4\pi^2 E}{(1 - \mu^2)(RS/\rho)^2} \quad [6 \cdot 14]$$

where RS = rivet spacing in inches

ρ = radius of gyration of the sheet

Substituting the value of ρ in equation 6·14, we obtain

$$\sigma_{\text{stiff}} = \frac{\pi^2 E t^2}{3(1 - \mu^2)(RS)^2} \quad [6 \cdot 15]$$

where t is the sheet thickness. For aluminum alloys, assuming $E = 10.3 \times 10^6$ lb. per sq. in. and $\mu = 0.3$, the equation reduces to

$$\sigma_{\text{stiff}} = 37.28 \times 10^6 \left(\frac{t}{RS} \right)^2 \quad [6 \cdot 16]$$

This is plotted in Fig. 6·23 for any given rivet spacing, RS , and sheet thickness t . The critical value of the stiffener stress at which buckling will occur between rivets can be obtained from this figure.

Equation 6·15 above is valid only so long as the value of σ_{stiff} is less than, or equal to, the proportional limit of the material. Above that stress value, E no longer is constant and must be taken as the value of E for the stress in question. In order to correct for the change in E above the proportional limit, Newell (reference 6·10) suggests the use of the Johnson parabolic curve for the short column range. If this is done, the limiting value of σ_{stiff} will be the yield point of the material, and the value of E will be modified above a stress value equal to one-half of the yield point. Since there is very little evidence to justify any other method, and also because this method would appear to give conservative results, it should be used for design purposes. Curves for several values of yield point have been included in Fig. 6·23.

Up to the point where the sheet buckles between rivets, the effective width of sheet acting with the stiffener can be determined from Fig. 6-2 in which

$$\sigma_{se} = \sigma_{stiff}$$

After the sheet buckles, it is reasonable and conservative to assume that the sheet will carry the load it was carrying just before buckling

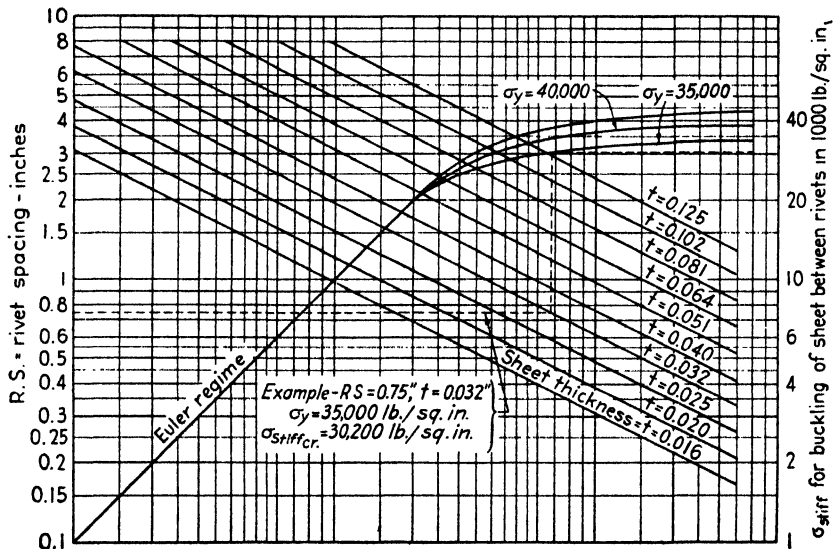


FIG. 6-23. Chart for determining sheet buckling between rivets.

but will not be able to carry additional load. The load which the sheet can carry is given by the equation

$$P_{sh} = 2w_e \sigma_{se} t \quad [6-17]$$

Therefore

$$2w_{e1} \sigma_{stiff1} t = 2w_{e2} \sigma_{stiff2} t \quad [6-18]$$

$$w_{e2} = w_{e1} \frac{\sigma_{stiff1}}{\sigma_{stiff2}} \quad [6-19]$$

where w_{e1} = effective width of sheet at time of buckling between rivets,
 σ_{stiff1} = stiffener stress at time of sheet buckling between rivets,
 w_{e2} = effective width of sheet at any higher stress, σ_{stiff2} .

The buckling of the sheet between rivets may have a detrimental effect on the panel strength other than that caused by a reduction of the effective width. If the sheet buckles at a relatively low stress, it no longer offers support to the part of the stiffener to which it is attached but actually introduces loads into the stiffener at the rivet or attach-

ment points. These loads are tensile loads in the rivets and when carried into the stiffener may precipitate early local failure of the stiffener section. For this reason early sheet buckling between rivets should be avoided particularly when the part of the stiffener attached to the sheet may be subject to local failure.

It may be of interest to know at what stiffener stress permanent set will take place in the sheet which has buckled between stiffeners. This

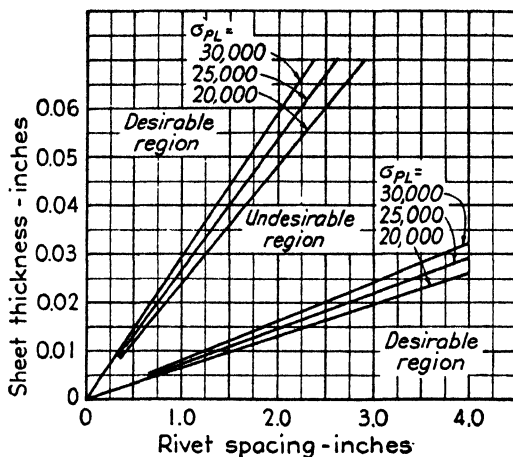


FIG. 6-24. Desirable and undesirable rivet spacings.

has also been investigated by Howland in reference 6-9 and an equation of the form given below has been derived.

$$\sigma_{\text{stiff}} = \frac{E}{RS^2} \left[\left(\frac{\sigma_{sh} RS^2}{2\pi E t} - \frac{\pi t}{6} \right)^2 + \frac{\pi^2 t^2}{3} \right] \quad [6-20]$$

where σ_{stiff} = the stiffener stress

σ_{sh} = total stress in the sheet due to bending and direct compression

Permanent set in the sheet would be expected to occur, whenever σ_{sh} became greater than the proportional limit of the material. If we assume that the sheet and stiffener will have the same elastic properties, permanent set in both would occur when $\sigma_{\text{stiff}} = \sigma_{sh} = \sigma_{pL}$. Putting these values into equation 6-20, we get

$$\begin{aligned} (t/RS)^2 &= \frac{\sigma_{pL}}{E} \frac{42 \pm 36}{26\pi^2} \\ &= 0.304 \frac{\sigma_{pL}}{E} \quad \text{or} \quad 0.023 \frac{\sigma_{pL}}{E} \end{aligned} \quad [6-21]$$

This equation yields curves as shown in Fig. 6-24 for various values of σ_{pL} . The region between the two sets of curves indicates that the stiffener stress would be less than the sheet stress in order to cause permanent set to occur in the sheet, whereas the region outside of the curves indicates that a stiffener stress higher than the sheet stress would be necessary. This is better illustrated in Fig. 6-25 in which the stiff-

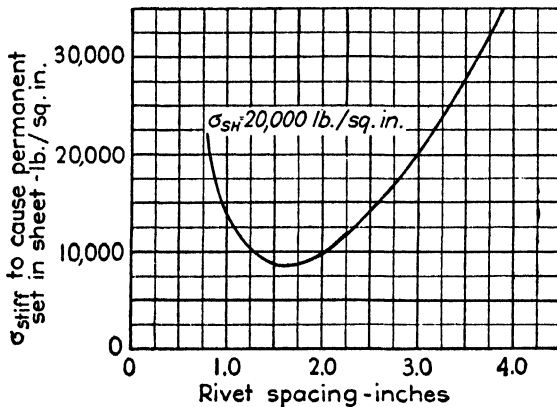


FIG. 6-25. Rivet spacing to cause permanent set in sheet.

ener stress to cause permanent set in the buckled sheet is plotted against rivet spacing.

6-3. The Ultimate Strength of Flat Panels Under Shear

In the analysis of the wing beams of airplanes, the designer is faced with several problems which, in general, are not present in civil engineering structural design. The civil engineer endeavors to make the web sheet of all beams thick enough so that the web will not buckle before the design load is reached on the structure. Buckling in this case is therefore considered as failure and the shearing stress causing buckling determines the allowable maximum shear that can be applied. For the solution of problems of this type, the discussion given in section 5-2 applies, in which the critical shearing stress is given by

$$\tau_{cr} = K \frac{\pi^2 E}{12(1 - \mu^2)} \left(\frac{t}{b} \right)^2 \quad [6 \cdot 22]$$

where b = the narrow dimension of the shear panel,

K = a function of the type of support given to the sheet edges

The value of K can be obtained from Fig. 5-11.

For very thin sheets, the buckling stress given by equation 6.22 is extremely low and, in the interest of making efficient use of all available material, the aircraft engineer raises the question of how much additional shear can be carried by such a buckled plate before (a) some portion of the sheet has a total stress equal to the yield point of the material, thus giving rise to permanent deformations; or (b) the ultimate strength of the structure is reached.

The aircraft designer would further like to know the effect of this web buckling and the additional load above buckling in the loads, in the beam flanges, and in any web-stiffening members which may be used.

This problem has been the subject of considerable research (see references 6.11 to 6.16 inclusive). No attempt will be made to discuss each reference in detail but a short indication of the development of the various theoretical ideas and their agreement with practice will be given.

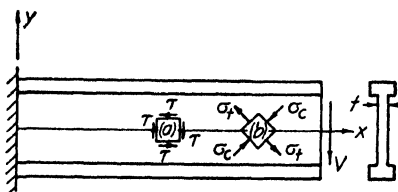


FIG. 6-26. Stress distribution in a thick-webbed beam.

Consider a beam having a relatively thick web under the action of shear and bending. See Fig. 6-26. For such a section, the usual bending moment and shear equations of applied mechanics are valid, namely,

$$\sigma_x = \frac{M_x y}{I} \quad \text{and} \quad \tau = \frac{VQ}{Ib}$$

where M_x = bending moment at any value x ,

y = distance from neutral axis to the fiber under the normal stress σ_x ,

I = moment of inertia of the cross section,

V = applied shearing force,

Q = static moment of the section above the plane for which τ is determined, about the neutral axis,

b = thickness of the section at which τ is determined; for the web, $b = t$.

These equations have been discussed in Chapter 3. Considering an element of the web on the neutral axis, so that bending stresses are absent, we see that if an element is considered whose sides are parallel and perpendicular to the shear force, the stress pattern is given by uniform shearing stresses on the four faces of the element—element (a) Fig. 6-26. However, the same result and system can be represented by an

element at 45 degrees to the direction of applied shear by pure normal stresses σ_c and σ_t of equal magnitude in which

$$\sigma_c = \sigma_t = \tau$$

See element (b) Fig. 6-26. For web plates which are thick, this stress distribution (plus the bending stresses) will hold up to stress values approaching the yield point of the material, at which time plastic flow will enter the picture.

If now, we assume that the web plate in the beam is very thin, the above discussion of the principal stress patterns takes on new significance. Considering the normal stresses, we see that one of them is a

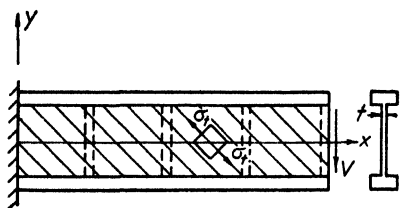


FIG. 6-27. Stress distribution in thin-webbed beams.

compressive stress against which thin plates have a very low resistance. The tendency will then be for the plate to buckle in a direction perpendicular to the compressive stress at a value of the applied shear which becomes less and less as the web becomes thinner and thinner, the limiting case being for a sheet of zero thickness. (See Fig. 6-27.) In this

case, the sheet buckles upon the application of any shear load and can only resist shear by means of the tensile stresses at 45 degrees. With such a stress pattern, it is obvious that the tensile stresses will tend to pull the two beam flanges together, thus necessitating vertical members to counteract this tendency (shown dotted in Fig. 6-27).

The limiting case of a web having no compressive strength has been treated in detail by Wagner (reference 6-13) and beams approximating this are known as Wagner beams.

Wagner assumes that the web buckles immediately upon the application of the shear load and that the only stresses resisting the shear forces are the tensile stresses which act at approximately 45 degrees. Considering infinitely rigid parallel span flanges and vertical stiffeners (Fig. 6-28), the following equations for this limiting case can be shown to apply.

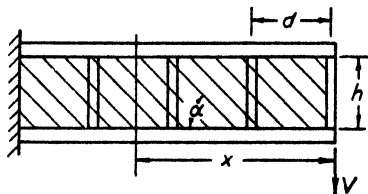


FIG. 6-28. Notation for vertical web stiffeners.

Diagonal tension stress developed in the web

$$\sigma_t = \frac{2V}{ht} \frac{1}{\sin 2\alpha} \quad [6-23]$$

Axial force in the tension flange

$$F_t = \frac{Vx}{h} - \frac{V}{2} \cot \alpha \quad [6.24]$$

Axial force in the compression flange

$$F_c = -\frac{Vx}{h} - \frac{V}{2} \cot \alpha \quad [6.25]$$

Axial force in the vertical stiffeners

$$F_v = -V \frac{d}{h} \tan \alpha \quad [6.26]$$

where V = applied shear load,
 h = effective web height,
 t = web thickness,
 d = vertical stiffener spacing,
 α = angle of web buckles, theoretically 45 degrees for this case, but practically usually somewhat less.

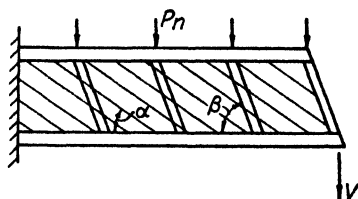


FIG. 6.29. Notation for oblique web stiffeners.

For the case of non-vertical struts and external loads acting at the strut points (Fig. 6.29) the equations are:

$$\sigma_t = \frac{2V}{ht} \frac{1}{\sin 2\alpha(1 - \tan \alpha \cot \beta)} \quad [6.27]$$

if the struts have infinite bending stiffness in the plane of the web, and

$$\sigma_{tT,c} = \frac{V_L + V_R}{ht} \frac{1}{\sin 2\alpha(1 - \tan \alpha \cot \beta)} \mp \frac{1}{2} \frac{P_n}{dt \sin^2 \alpha} \quad [6.28]$$

for struts with zero bending rigidity in the plane of the web.

$$F_T = \frac{M}{h} - \frac{V}{2} (\cot \alpha - \cot \beta) \quad [6.29]$$

$$F_C = -\frac{M}{h} - \frac{V}{2} (\cot \alpha - \cot \beta) \quad [6.30]$$

$$F_{VT,c} = -\frac{V_L + V_R}{2} \frac{d \tan \alpha}{h \tan \beta} \frac{1}{(1 - \tan \alpha \cot \beta)} \mp \frac{P_n}{\sin \beta} \quad [6.31]$$

where V = total shear on the section considered,

M = total moment on the section considered,

V_L = shear in bay to left of strut considered,

V_R = shear in bay to right of strut considered,

P_n = external load applied at the strut,

β = angle between web and stiffener,

Subscripts T and C , such as for σ_{tT} , σ_{tC} indicate the stresses or loads at the end of the strut on the tension flange or compression flange of the beam respectively.

In all the above it has been assumed that the flanges are infinitely stiff in bending. If, however, they can deform in the web direction, there will be a tendency to unload the sheet between verticals owing to this deflection. This effect can be taken into account by a correction factor which is a function of the flange moments of inertia and the beam dimensions. The correction factor is given by

$$\frac{1}{R} = \frac{\sigma_{t_{\max}}}{\sigma_{t_{\text{ave}}}} = \frac{wd \sinh wd + \sin wd}{2 \cosh wd - \cos wd} \quad [6.32]$$

where

$$wd = 1.25d \sqrt[4]{\frac{t}{(I_C + I_T)h}} \sin \alpha \quad [6.33]$$

and $\sigma_{t_{\text{ave}}}$ = average sheet tensile stress given by equations 6.23, 6.27 and 6.28,

$\sigma_{t_{\max}}$ = maximum tensile stress developed in the sheet,

I_C = moment of inertia of compression flange about its own neutral axis,

I_T = moment of inertia of tension flange about its own neutral axis.

The correction factor R can be found either from equations 6.32 and 6.33 or from Figs. 6.30 and 6.31. It is only applied to the sheet tensile stress and to that portion of the flange load arising from the sheet tension. The end load in the verticals, since it is independent of the tensile stress distribution between panels, is not affected.

To summarize the pure tension field case, it has been assumed: (a) The sheet carries the entire shear load, i.e., no shear load is carried by the flanges. (b) The flanges are pinned to the verticals and are pin-connected at the fixed end of the beam (in the case of the cantilever beam). This leads to the assumption that (c) There is no gusset or Vierendeel truss action at the connection of the verticals to the flanges. (d) The sheet immediately goes into the wave state and supports the applied shear entirely by means of the diagonal tension field.

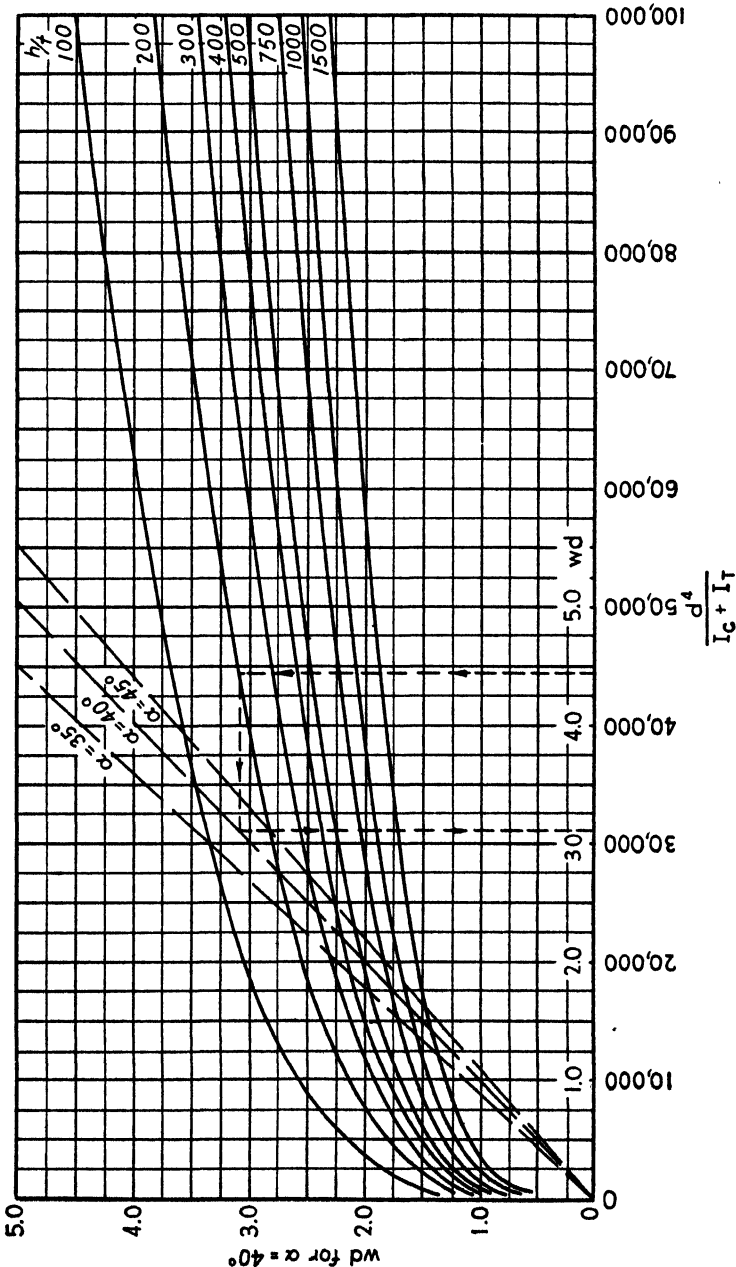


Fig. 6-30. Chart for determining $w\delta$.

On the basis of these assumptions, equations 6.23 to 6.31 have been derived and would be expected to give reasonable predicted stresses for deep beams with very thin webs. In actual practice, the equation found to be the most in error is that giving the compression load in the web stiffeners which gives values which may be two to five times too high.

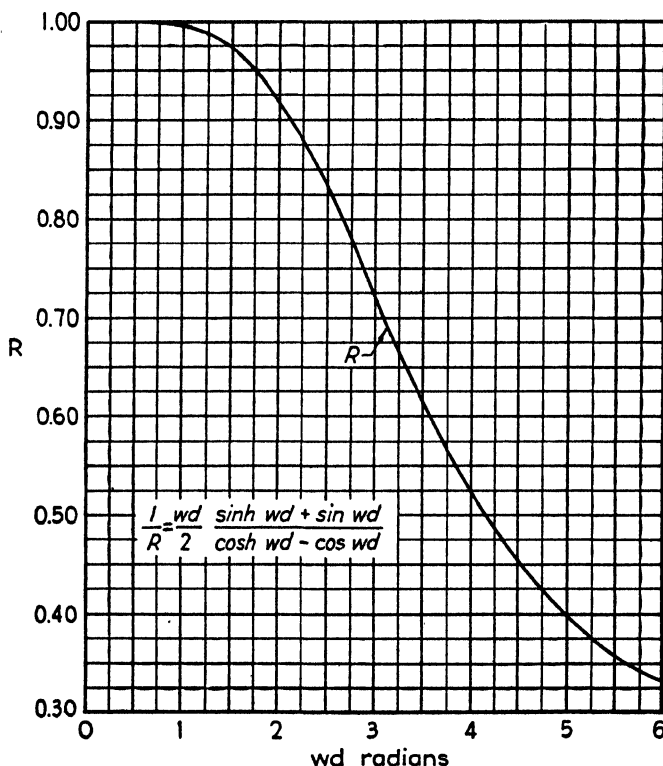


FIG. 6-31. Chart for determining R .

The other equations give reasonable first approximations for web thicknesses up to 0.030 in. Every result will again be conservative, the degree of conservatism increasing rapidly with increasing web thickness and increasing flange stiffness. The degree of conservatism can be seen in the more accurate analysis which follows.

Since the Wagner equations always lead to designs which are ultra-conservative and hence too heavy, a more accurate investigation of the true stress condition in such beams is called for. A number of investigators have worked on this subject and all have arrived at essentially the same conclusions; however, very little published work is available. References 6.16, 6.17 and 6.18 contain a limited discussion of the

incomplete tension field problem and reference 6·16 contains some experimental data.

The method discussed below summarizes the theoretical work that has been done and is checked by a number of tests made by various aircraft companies (see references 6·19–6·23 incl.). In this method, the total shear carried by the beam is considered to be made up of these items: (a) The shear carried by the flanges due to their small but finite shear stiffness. (b) The shear carried by the web as a shear-resistant member, i.e., before it buckles. (c) The shear carried by the web in the buckled state, due to the diagonal tension field.

To account for the shear carried by the flanges, a method suggested by Green (reference 6·21) is used, in which it is assumed that the shear flow is uniform between the flanges and that this shear flow is equal to the value conventionally calculated for such a beam at the flange rivet line by the equation

$$q = \frac{VQ}{I} \quad [6\cdot34]$$

where q = shear flow in web in pounds per inch,

V = total shear in pounds,

Q = static moment of the flange about the neutral axis of the beam,

I = moment of inertia of the entire beam cross section when V is not greater than the buckling strength; and equals the moment of inertia of the flange material only when V is the shear resisted by a diagonal tension field.

The shear resisted by the web plate only, would then be given by

$$V_w = \frac{V}{I/Qh} \quad [6\cdot35]$$

where h = effective depth of the web, taken as the distance between the centroids of the flange rivets.

At the buckling stress of the web, the shear carried by the web is equal to

$$V_{cr} = \tau_{cr} h t \quad [6\cdot36]$$

and the stress distribution on a unit element of the end vertical (point of shear application) is as shown in Fig. 6·32, in which

$$\sigma_{c1} = \sigma_{t1} = \tau_{cr}$$

The value of τ_{cr} is given by equation 6·22 where K is obtained from Fig. 5·11. It is conservatively assumed that the shear panels in such beams correspond to panels simply supported on all four edges.

Above the critical buckling stress, it is assumed that the compressive stress remains constant at the value τ_{cr} and that any additional shear is carried by an increase in the value of σ_t only. The stress pattern for this case is as shown in Fig. 6-33 and the shear carried by the tension field only is

$$V_t = \sigma_{t_2} h t \sin \alpha \cos \alpha \quad [6-37]$$

where α = angle of tensional diagonal or the angle of plate buckling. The total average tensile stress is then

$$\sigma_{t_{ave}} = \sigma_{t_2} + \sigma_{t_1} = \sigma_{t_2} + \tau_{cr} \quad [6-38]$$

Because of the deformation of the flanges under the action of the tension field, the correction term given by equation 6-32 must be applied to σ_{t_2} . Also, since some material is removed by the flange and vertical attaching rivets, a rivet correction factor must be applied to $\sigma_{t_{ave}}$ to obtain the maximum value. This rivet factor is given by

$$C_r = \frac{\text{rivet spacing} - \text{rivet diameter}}{\text{rivet spacing}} \quad [6-39]$$

The maximum value of the tensile stress is then

$$\sigma_{t_{max}} = \left(\frac{\sigma_{t_2}}{R} + \tau_{cr} \right) \frac{1}{C_r} \quad [6-40]$$

from which

$$\sigma_{t_2} = \left(\sigma_{t_{max}} - \frac{\tau_{cr}}{C_r} \right) C_r R \quad [6-41]$$

and

$$V_t = \left(\sigma_{t_{max}} - \frac{\tau_{cr}}{C_r} \right) C_r R h t \sin \alpha \cos \alpha \quad [6-42]$$

When the maximum tensile stress equals the tensile yield point of the material, σ_{ty} , the value of the web shear above buckling is given by

$$V_{ty} = \left(\sigma_{ty} - \frac{\tau_{cr}}{C_r} \right) C_r R h t \sin \alpha \cos \alpha \quad [6-43]$$

and when it is equal to the ultimate tensile strength, σ_{uts} , the corresponding shear is

$$V_{tu} = \left(\sigma_{uts} - \frac{\tau_{cr}}{C_r} \right) C_r R h t \sin \alpha \cos \alpha \quad [6-44]$$

The total shear carried by the beam for $\sigma_{t_{max}} = \sigma_{ty}$ and $\sigma_{t_{max}} = \sigma_{uts}$, respectively, is then

$$V_y = (V_{cr} + V_{ty}) \frac{I}{Qh} \quad [6-45]$$

and

$$V_u = (V_{cr} + V_{tu}) \frac{I}{Qh} \quad [6.46]$$

The above equations are all based on vertical web-stiffening members. In the event the stiffeners are not at 90 degrees to the flanges, equations

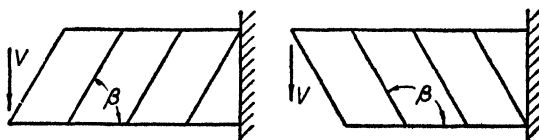


FIG. 6-34. Definition of β for oblique web stiffeners.

6.43 and 6.44 should be multiplied by a correction factor equal to $(1 - \tan \alpha \cot \beta)$ where β is the upright angle, measured as shown in Fig. 6-34. Also, for oblique stiffeners it is found that the diagonal tension-

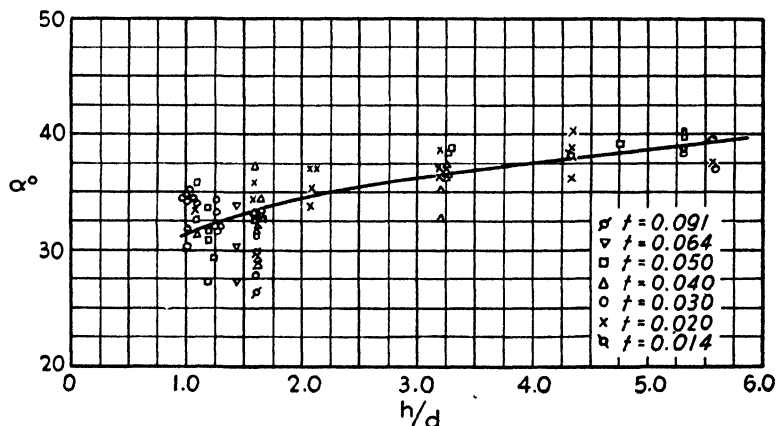


FIG. 6-35. Experimental values of α versus h/d .

field angle, α , is always equal to $\beta/2$, and it can be assumed that $R = 1.0$; so only for these cases, the equations become

$$V_{tu} = \frac{1}{2} \left(\sigma_{tvp} - \frac{\tau_{cr}}{C_r} \right) C_r h t \frac{1 - \cos \beta}{\sin \beta} \quad [6.47]$$

$$V_{tu} = \frac{1}{2} \left(\sigma_{uts} - \frac{\tau_{cr}}{C_r} \right) C_r h t \frac{1 - \cos \beta}{\sin \beta} \quad [6.48]$$

The one unknown in equations 6.43 and 6.44 which is troublesome is the diagonal tension-field angle α . As yet, the dependence of this angle upon the various physical parameters of the beam assembly is unknown. Figure 6-35 shows test values of α for the beams tested by the Consolidated Aircraft Corporation, plotted against h/d . Consider-

able scatter is evidenced, but the use of the curve should give a reasonable approximation since changes in α only make secondary changes in the value of V_{ty} and V_{tu} .

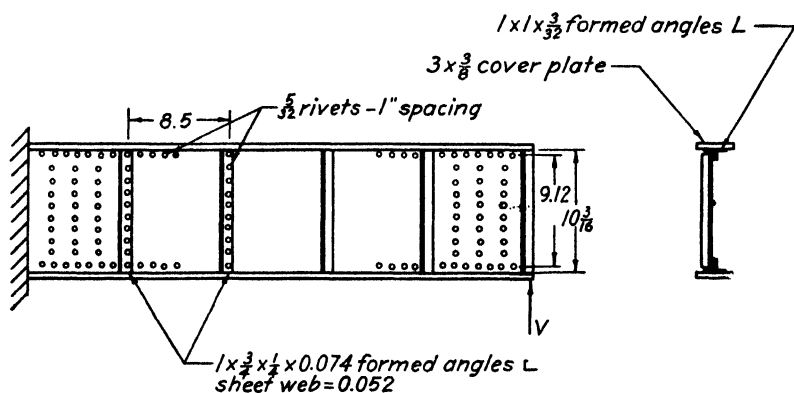


FIG. 6-36. Typical test beam.

To illustrate the method, beam No. 242, reference 6-21, will be calculated in detail. This beam is shown in Fig. 6-36 and the pertinent data are:

Effective web height	$= h = 9.12$ in.
Web thickness	$= t = 0.052$ in.
Web-stiffener spacing	$= d = 8.5$ in.
Rivet factor	$= C_r = 0.841$
Height/depth ratio	$= h/d = 1.07$
Tension-field angle	$= 31.8^\circ$ from Fig. 6-35 (actual test showed $\alpha = 35.8^\circ$)
Stress distribution factor	$= R = 0.876$ from equations 6-32 and 6-33 or Figs. 6-30, 6-31
Tensile yield of material	$= \sigma_{typ} = 43,650$ lb. per sq. in.
Tensile ultimate of material	$= \sigma_{uts} = 62,100$ lb. per sq. in.
Flange static moment	$= Q = 7.675$ in. ³
Flange moment of inertia about beam n.a.	$= I = 79.46$ in. ⁴
Correction for flange shear	$= I/Qh = 1.135$

From the above data, the following items can be calculated:

From Fig. 5-11, the buckling constant

$$K = 8.41$$

which gives

$$\tau_{cr} = 8.41 \frac{\pi^2 \times 10.3 \times 10^6}{12(1 - 0.3^2)} \left(\frac{0.052}{8.5} \right)^2 = 2930 \text{ lb. per sq. in.}$$

and

$$V_{cr} = 2930 \times 9.12 \times 0.052 = 1390 \text{ lb.}$$

from equation 6-43

$$V_{ty} = \left(43,650 - \frac{2930}{0.841} \right) 0.841 \times 0.876 \times 9.12 \times 0.052 \times 0.5270 \times 0.8499 = 6270 \text{ lb.}$$

and from equation 6-44

$$V_{tu} = \left(62,100 - \frac{2930}{0.841} \right) 0.841 \times 0.876 \times 9.12 \times 0.052 \times 0.5270 \times 0.8499 = 9160 \text{ lb.}$$

The total shear carried by the beam at the yield point stress, is then from equation 6-45

$$V_y = (1390 + 6270)1.135 = 8690 \text{ lb.}$$

and the ultimate shear load that can be supported is, from equation 6-46,

$$V_u = (1390 + 9160)1.135 = 11,970 \text{ lb.}$$

The test values were 7000 lb. (by visual inspection) and 12,100 lb., respectively, with the failure occurring as web tension.

The beam considered is somewhat of a limiting case, being shallow and having a relatively thick web, but it was chosen to illustrate the magnitude of the factors which were neglected in the earlier Wagner tension field equations. In the example above it can be seen that the total shear carried by the beam is made up of

- (a) 1420 lb. or 11.9%, carried by the flanges
- (b) 1390 lb. or 11.6%, carried by the web in pure shear before buckling.
- (c) 9160 lb. or 76.5%, carried by the diagonal tension field set up after the web buckles

The pure tension field analysis ignores all but item (c) thus leading to a web which is too conservative by the amounts indicated in items (a) and (b).

The result of using this method in seven beams tested by the Consolidated Aircraft Corporation is shown in Table 6-5. All these beams actually failed in web tension. The agreement between predicted and test ultimate shear loads is very good and indicates that the method is able to predict tensile failure in the web of such beams within very close limits. The agreement between predicted and test loads at yield point is not so good; however, the test loads were obtained merely from visual observation and would therefore not be expected to be too accurate.

A check on a beam tested by the Douglas Aircraft Company (Reference 6-22) and on one tested by the Vultee Aircraft, Incorporated (reference 6-23) also shows good agreement between predicted and test ultimate loads. Because complete data is lacking in these reports, certain items had to be estimated; however, the estimates could be made with a reasonable degree of accuracy. The results of the analyses follow.

	<i>Douglas Beam</i>	<i>Vultee Beam No. 26</i>
h	= 27.5 in. (estimated)	= 11.50 in.
d	= 4.5 in.	= 4.75 in.
t	= 0.091 in. (nominal)	= 0.040 in. (nominal)
σ_{uts}	= 63,300 lb. per sq. in.	= 62,500 lb. per sq. in. (estimated)
h/d	= 6.11	= 2.42
α	= 39.5	= 35.6 from Fig. 6-35
K	= 5.51	= 6.35 from Fig. 5-11
C_r	= 0.555	= 0.750
R	= 0.98 (estimated)	= 1.00 (estimated)
I/Qh	= 1.06 (estimated)	= 1.10 (estimated)
τ_{cr}	= 21,000 lb. per sq. in.	= 4,200 lb. per sq. in.
V_{cr}	= 52,600 lb. per sq. in.	= 1,930 lb.
V_{tu}	= 17,000 lb.	= 9,280 lb.
V_u	= 73,800 lb.	= 12,330 lb.
$V_{u_{test}}$	= 81,200 lb.	= 13,100 lb.
M.S.	= + 10.0%	= 6.5%

Checks on several other beams tested by Vultee Aircraft, Incorporated indicate that the method gives agreement between predicted and test-failure loads that is reasonable and conservative.

In view of the above experimental checks, it is felt that the method is satisfactory for the determination of the load at which web failure can be expected in a thin-web beam. Additional complete test data is, of course, desired in order to determine the possible experimental scatter limits which are to be expected with the use of this design method. A limited amount of test data indicates that the method is very conservative for stiffener spacings which are greater than the spar depth. This is, however, practically never true in present designs.

TABLE

Beam No.	t (in.)	h (in.)	d (in.)	α (deg.)	β (deg.)	C_r	R	σ_{tys}		V_{ty} (lb.)	V_{tu} (lb.)	V_{σ} (lb.)	Predicted		Test	
								σ_{typ}	σ_{uts}				V_y (lb.)	V_u (lb.)	V_y (lb.)	V_u (lb.)
								(lb./sq. in.)								
186	0.025	28.69	6.0	52.5*	105	0.846	1.000	44,500	65,000	17,190	25,280	650	18,790	27,320	12,800	26,800
209	0.025	28.69	9.0	37.0	90	0.841	0.978	48,500	66,750	13,540	18,710	310	14,500	19,910	10,900	18,400
224	0.0255	28.62	6.0	37.5*	75	0.841	1.000	46,600	64,700	10,710	14,970	690	12,050	16,560	10,900	17,700
234	0.026	38.62	9.0	38.3	90	0.841	0.982	47,500	66,400	17,030	24,640	450	18,130	26,010	17,100	27,100
236	0.0495	13.12	4.0	37.2	90	0.804	1.000	44,400	64,800	8,500	13,620	5,540	16,910	23,090	15,500	22,500
242	0.052	9.12	8.5	31.8	90	0.841	0.876	43,650	62,100	6,270	9,160	1,390	8,690	11,970	7,000	12,100
243	0.039	9.25	6.0	33.5	90	0.834	0.999	46,600	63,600	5,980	8,330	1,000	10,550	14,110	8,750	13,750

* Here α equals $\beta/2$.

The next problem is the determination of the loads on the flange rivets. These are easily calculated from the equations developed above. The rivet load per inch at web buckling is equal to

$$V'_{cr} = \frac{V_{cr}}{h} \frac{I_F}{I_T} \quad [6.49]$$

where V'_{cr} = rivet load in pounds per inch at web-buckling load,
 I_F = moment of inertia of flanges about the beam neutral axis,
 I_T = total moment of inertia of the beam cross section,
 Other terms are as previously defined.

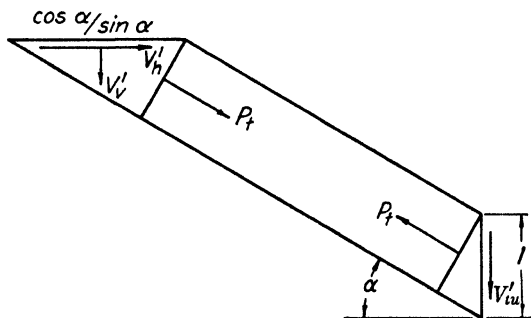


FIG. 6.37.

For the shear load carried above buckling by the tension field, the rivet load is made up of horizontal and vertical components. These are (see Fig. 6.37)

$$P_t \sin \alpha = V'_{tu}, \quad P_t = \frac{V'_{tu}}{\sin \alpha} \quad [6.50]$$

where

$$V'_{tu} = \frac{V_{tu}}{h} \quad [6.51]$$

and

$$V'_h = \frac{P_t \cos \alpha}{\cos \alpha / \sin \alpha} = P_t \sin \alpha = V'_{tu} = \frac{V_{tu}}{h} \quad [6.52]$$

$$V'_v = \frac{P_t \sin \alpha}{\cos \alpha / \sin \alpha} = P_t \frac{\sin^2 \alpha}{\cos \alpha} = V'_{tu} \tan \alpha = \frac{V_{tu}}{h} \tan \alpha \quad [6.53]$$

The total rivet load per inch is then given by

$$\begin{aligned} P_R &= [(V'_{cr} + V'_h)^2 + V'^2_v]^{1/2} \\ &= \left[\left(\frac{V_{cr}}{h} \frac{I_F}{I_T} + \frac{V_{tu}}{h} \right)^2 + \left(\frac{V_{tu}}{h} \tan \alpha \right)^2 \right]^{1/2} \end{aligned} \quad [6.54]$$

A check of this method is shown in Table 6-6. Several beams which failed owing to causes other than rivet failure are included to show that equation 6-54 can be used to predict whether or not rivet failure is likely to occur. Detailed calculations for these beams are not given; however, they follow the procedure outlined previously in this section. Table 6-6 indicates that the method will definitely show whether or not flange rivet failures are to be expected in any beam assembly. As can be readily seen, it can also be used to determine the shear load at which rivet failure will occur. Beam No. 200 in Table 6-6 is a limiting case in which rivet failure and vertical stiffener failure should occur at approximately the same shear load. In the test panel, the stiffener failed first.

Timoshenko (reference 6-3, p. 382) discusses the problem of buckling under shearing stresses of plates stiffened by ribs, where the plates and ribs buckle simultaneously. The designer is referred to this work for the design parameters involved. Generally, however, the web stiffeners are sufficiently stiff so that the web sheet will buckle between stiffeners without immediately causing them to fail. This is the case which will be considered here.

If the uprights between the spar flanges were not attached to the web, it would be possible, from a study of equations 6-26 or 6-31, to determine the stresses in these uprights and, from the column properties of the section, to determine the allowable stresses. The shear stress up to the point of web buckling would introduce no load in these members and their load would only consist of the vertical component of the tension field load on the flanges, correctly proportioned between the verticals present.

Riveting these members to the beam web makes such simple considerations impossible. Here a certain part of the sheet must be considered to be working with the vertical in resisting the tendency for the beam flanges to come together. The amount of sheet to be considered is unknown and it probably varies between the flange and the center of the sheet. In addition to the axial load applied to the stiffener by the tension field, there is also a load which arises from the fact that the stiffener, where riveted to the web, tends to break up the web buckles which, otherwise, would form a continuous pattern across the beam web. These sheet waves tend to deform the stiffener torsionally and in bending and to precipitate early failure due to localized stress conditions.

In view of the complexity of the problem, no satisfactory theoretical analysis for determining the design or allowable stresses in the web-stiffening members of tension-field beams has as yet been developed. A series of over fifty parallel flange beams with formed sheet stiffeners on one side of the web, which failed due to stiffener failure, have been

TABLE 6-6

Beam No.	t (in.)	h (in.)	d (in.)	α (deg.)	I_F (in. ⁴)	I_T (in. ⁴)	V_{cr} (lb.)	V_{tu} (lb.)	P_R (lb./in.)	P_R^* (lb./in.)	Rivet Failure Expected	Actual Type of Failure	Actual Rivet Load at Failure
192	0.050	18.50	16.0	32.1	502	554	670	17,960	1,174	1,107	Yes	Rivets	938
196	0.040	28.75	9.0	37.0	880	968	1,270	27,010	1,210	1,044	Yes	Rivets	991
198	0.050	18.50	3.5	39.0	645	677	9,720	22,180	1,959	1,382	Yes	Rivets	1,404
199	0.051	18.50	3.5	39.0	645	678	10,410	22,710	2,029	1,643	Yes	Rivets	1,622
200	0.0515	18.50	3.5	39.0	645	678	10,700	23,410	2,084	1,536	Yes	Stiffeners	1,520
203	0.0565	16.62	3.5	38.6	525	552	12,880	20,700	2,170	1,262	Yes	Rivets	1,187
209	0.025	28.69	9.0	37.0	944	999	310	18,710	826	2,436	No	Web	779
228	0.049	18.50	3.5	39.0	637	668	9,240	21,710	1,904	2,172	No	Stiffener	1,391
234	0.026	38.62	9.0	38.3	1,684	1,820	450	24,640	822	1,625	No	Web	881
235	0.052	13.00	4.0	37.1	259	269	6,380	15,040	1,832	2,172	No	Web	1,318

* Based on standard rivet strength calculations.

studied and an empirical equation has been developed for such cases. The equation is

$$V_{twv} = 0.023E \sqrt[3]{J_e(th^2/d)} \quad [6.55]$$

in which V_{twv} = the total web shear above V_{cr} which can be carried before stiffener failure occurs.

J_e = the effective torsional moment of inertia of the stiffener which, for formed sheet stiffeners is taken as

$$J_e = \frac{1}{3} (\text{developed width}) t_{stiff}^3 = \frac{1}{3} A t_{stiff}^2 \quad [6.56]$$

For other stiffener sections this factor must be determined by test.

Equation 6.55 is only for beams having parallel flanges and web stiffeners which are perpendicular to these flanges. Methods of taking into account non-parallel flanges and oblique web stiffeners will be discussed later.

The torsional moment of inertia has been taken as the influencing factor rather than the bending moment of inertia since a study of the failures of such beams indicates that nearly always the stiffener has not failed as an Euler or short column, but has twisted. This twisting is due to the high local stresses set up by the sheet-wave pattern. As indicated above, the effective torsional moment of inertia of formed sheet stiffeners is taken as equal to that for the equivalent flat sheet rectangle. Insufficient data are available at the present time to check this value for bulb angles and other extruded sections and for closed sections but, in lieu of other information, it is suggested that this value be obtained from a torsion test on the particular stiffener. The accuracy of this equation for such sections is unknown and it therefore must be used with caution.

The agreement of the values of V_{tu} as predicted by this equation with those obtained from tests on beams which failed owing to stiffener collapse is shown in Table 6.7. Considerable scatter is noticed and it is possible that additional theoretical study and experimentation will indicate modifications of equation 6.55 which will make it more accurate. However, the equation does give, for the first time, some means of determining the shear load at which failure in the web stiffeners may be expected and, in general, it will be found that the predicted loads will be within ± 10 per cent of those which a test panel will develop.

As mentioned previously, all the beams in Table 6.7 had eccentric vertical stiffeners, i.e., stiffeners on only one side of the web plate. Six specimens were tested which had stiffeners on both sides of the web plate, arranged as indicated in Fig. 6.38. By calculating the shear load for stiffener failure as before, results are obtained as shown in Table 6.8. Here the effective torsional moment of inertia of the pair of stiffeners was

TABLE 6-7

Beam No.	t (in.)	h (in.)	d (in.)	J_e (in. ⁴ × 10 ⁶)	V_{ult} (lb.)	$K = I/Qh$	V_{ult}/K (lb.)	V_{cr} (lb.)	Test V_{tu} (lb.)	Predic. V_{tu} (lb.)
43	0.030	12.00	12.0	2.32	5,600	1.119	5,010	190	4,820	4,810
45	0.030	12.00	12.0	10.41	7,300	1.119	6,530	190	6,340	7,940
47	0.030	12.00	12.0	2.40	6,400	1.119	5,720	190	5,530	4,860
48	0.014	34.62	8.0	2.40	10,200	1.055	9,670	80	9,590	8,750
49	0.030	18.66	15.0	2.32	5,850	1.098	5,330	160	5,170	5,990
51	0.030	18.66	15.0	3.80	7,950	1.098	7,240	160	7,080	7,070
52	0.0395	28.81	18.0	2.40	9,000	1.061	8,480	360	8,120	8,350
53	0.0305	18.84	15.0	7.28	8,600	1.098	7,840	170	7,670	8,550
54	0.040	28.75	18.0	3.26	9,750	1.061	9,190	370	8,820	9,280
55	0.030	18.80	15.0	5.93	8,950	1.098	8,160	160	8,000	8,230
56	0.024	10.80	10.0	2.67	6,570	1.118	5,880	120	5,760	4,640
57	0.025	18.76	9.0	2.66	8,250	1.067	7,730	220	7,510	7,020
58	0.024	28.62	9.0	6.12	14,250	1.048	13,600	270	13,330	12,150
59	0.030	38.75	7.0	6.08	21,000	1.031	20,360	1,100	19,260	17,350
60	0.050	18.80	16.0	2.58	9,800	1.080	9,070	680	8,390	7,250
71	0.040	28.75	9.0	3.02	15,375	1.061	14,490	1,270	13,220	11,400
72	0.040	28.75	9.0	11.30	21,000	1.061	19,790	1,270	18,520	17,700
85	0.0395	28.75	9.0	16.42	25,800	1.061	24,310	1,220	23,090	19,950
86	0.0395	28.75	18.0	18.51	15,700	1.061	14,790	360	14,430	16,480
87	0.041	9.25	8.5	2.55	7,150	1.119	6,490	680	5,710	5,190
89	0.050	9.12	8.5	5.60	9,650	1.119	8,630	1,240	7,370	7,140
93	0.030	38.75	7.0	19.72	26,000	1.031	25,200	1,100	24,100	25,690
94	0.027	28.62	9.0	10.09	17,400	1.048	16,600	390	16,210	14,900
96	0.049	18.62	16.0	9.64	15,150	1.080	14,030	550	13,480	11,100
100	0.064	18.62	18.0	2.59	13,830	1.080	12,800	1,950	10,850	8,380
101	0.064	18.62	13.0	6.76	16,050	1.080	14,860	1,950	12,910	11,550
102	0.030	18.81	13.0	12.03	10,830	1.098	9,860	160	9,710	10,430
103	0.030	18.81	15.0	6.42	9,420	1.098	8,580	160	8,420	8,480
109	0.050	18.62	15.0	26.91	17,500	1.080	16,200	680	15,520	15,720
110	0.025	18.69	16.0	4.42	9,800	1.071	9,150	220	8,930	8,300
111	0.025	38.81	9.0	3.39	17,650	1.032	17,100	640	16,460	13,420
112	0.024	38.81	7.0	19.15	22,000	1.032	21,310	350	20,960	21,720
113	0.025	28.62	9.0	10.78	11,750	1.045	11,240	90	11,150	11,780
114	0.025	28.62	18.0	15.64	12,950	1.045	12,380	90	12,290	13,340
115	0.049	28.75	18.0	2.59	8,100	1.040	7,790	680	7,110	9,190
116	0.049	28.62	18.0	9.54	14,600	1.045	13,960	680	13,280	14,160
126	0.050	9.12	8.5	9.81	11,080	1.119	9,910	1,240	8,670	8,620
127	0.039	28.75	9.0	18.84	24,600	1.061	23,190	1,180	22,010	20,800
129	0.025	18.62	9.0	8.58	11,150	1.075	10,370	220	10,150	10,320
130	0.049	28.62	18.0	13.63	16,850	1.045	16,100	680	15,420	15,950
132	0.0395	28.75	18.0	21.53	17,500	1.061	16,490	360	16,130	17,320
147	0.050	18.80	16.0	13.07	15,720	1.080	14,550	680	13,870	12,460
148	0.0295	12.06	12.0	12.49	9,100	1.111	8,200	180	8,020	8,420
157	0.0245	38.75	9.0	5.46	14,100	1.033	13,650	370	13,280	14,390
170	0.092	28.62	18.0	3.27	17,650	1.057	16,690	4,480	12,210	12,230
171	0.091	28.62	18.0	17.20	26,750	1.057	25,300	4,345	20,820	21,170
173	0.063	18.75	13.0	27.60	23,420	1.080	21,680	1,890	19,790	18,460
174	0.025	18.69	9.0	10.12	11,700	1.072	10,910	220	10,690	10,920
175	0.050	28.62	18.0	22.74	26,160	1.067	24,510	720	23,790	19,020
176	0.040	28.75	18.0	28.20	19,850	1.051	18,870	370	18,500	19,050
177	0.040	28.75	9.0	23.50	26,400	1.051	25,100	1,270	23,830	22,590

taken as twice the value obtained for one stiffener using equation 6.56. These few tests indicate that the method is conservative when pairs of stiffeners are used and may, at times, become very conservative. For specimens 44 and 99 the agreement is satisfactory, whereas for specimen

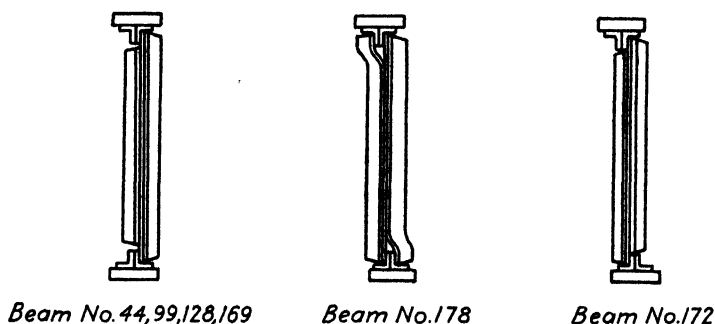


Fig. 6.38. Stiffener arrangements on test beams.

128 the predicted load is 45 per cent too low. These are insufficient data to draw any general conclusions and Table 6.8 is given merely to indicate possible trends.

TABLE 6.8

Beam No.	t (in.)	h (in.)	d (in.)	J_e (in. ⁴ $\times 10^5$)	V_{ult} (lb.)	$K =$ I/Qh	V_{ult}/K (lb.)	V_{cr} (lb.)	Test V_{tu} (lb.)	Predic. V_{tu} (lb.)
44	0.030	12.00	12	4.65	7,500	1.119	6,710	190	6,520	6,060
99	0.0395	28.81	18	6.10	12,550	1.061	11,820	360	11,460	11,400
128	0.041	28.75	9	8.27	26,300	1.061	24,790	1,370	23,420	16,080
169	0.0395	28.81	18	6.46	16,000	1.061	15,070	360	14,710	11,640
172	0.030	11.87	12	4.94	8,400	1.108	7,580	190	7,390	6,140
178	0.030	11.87	12	4.94	9,250	1.108	8,350	190	8,160	6,140

If the web stiffeners are not perpendicular to the flange but inclined at an angle β , equation 6.55 should be multiplied by a correction factor which is a function of the stiffener angle. A limited number of tests indicate that reasonable results are obtained by an equation of the form

$$V_{tu\gamma} = 0.023E \sqrt[3]{J_e(th^2/d)} \sqrt[3]{(\beta/90)^2} \quad [6.57]$$

when β is measured in degrees. Table 6.9 indicates the agreement between predicted and test loads for stiffener angles of 60 to 120 degrees. There are too few specimens to determine an exact correlation factor but it is felt that equation 6.57 will give results for design purposes which are conservative.

TABLE 6-9

Beam No.	β (deg.)	h (in.)	d (in.)	t (in.)	J_e (in. ⁴ $\times 10^8$)	V_{ult} (lb.)	I/Qh	$\frac{V_{ult}}{I/Qh}$ (lb.)	V_{σ} (lb.)	Test V_{tu} (lb.)	Pred. V_{tu} (lb.)
230	60	28.62	6	0.025	2.549	10,500	1.057	9,930	650	9,280	8,020
231	60	28.50	6	0.024	5.120	11,500	1.061	10,840	580	10,260	9,940
223	75	28.62	6	0.025	2.522	11,400	1.057	10,780	650	10,130	9,280
222	75	28.62	6	0.025	6.610	16,700	1.057	15,800	650	15,150	12,800
219	90	28.75	6	0.025	2.449	13,200	1.044	12,640	660	11,980	10,400
220	90	28.75	6	0.0245	5.670	16,750	1.044	16,050	620	15,430	13,680
221	90	28.75	6	0.0245	9.070	21,300	1.044	20,400	620	19,780	16,000
62	105	28.75	6	0.025	6.020	20,800	1.051	19,790	660	19,130	15,660
95	105	28.75	6	0.026	9.500	22,000	1.051	20,920	740	20,180	18,350
232	120	28.50	6	0.025	5.920	21,600	1.061	20,330	650	19,680	16,890
233	120	28.50	6	0.025	19.220	26,400	1.061	24,860	650	24,210	24,880

It is very likely that there are certain classes of stiffeners in which the stiffener failure is more dependent upon the bending stiffness (EI_e) than the torsional stiffness (GJ_e). For the tests discussed above, correlation with the moments of inertia of the vertical stiffeners gave less satisfactory agreement and more experimental scatter than that obtained from equation 6-55. Several authors give discussions of the vertical stiffeners treated as columns, but no very satisfactory method is suggested for obtaining the shear load producing stiffener failure. To determine this properly a series of tests should probably be run on specimens which have vertical stiffeners which are torsionally strong but weak in bending.

To determine the size of rivets to use for attaching the verticals to the flanges, one must know the loads in the verticals at their point of attachment to the flanges. No one as yet has made an exact study of this problem and experimental data are meager and confusing. As a first approximation one can use the results of Wagner and Lahde (reference 6-16) which were obtained in brass specimens. They develop, from test data, an equation of the form

$$\frac{A_v}{dt} = fnc \left[\frac{\sigma_v}{\tau_w}, \frac{\tau_w}{E} \left(\frac{h}{t} \right)^2 \text{ or } \frac{\tau_w}{E} \left(\frac{d}{t} \right)^2 \right] \quad [6-58]$$

where A_v = area of the vertical stiffeners to give a compression stress in the stiffener equal to σ_v

and the other terms are as previously defined.

The results led to a set of curves representing equation 6-58 which have been replotted in Fig. 6-39. Actually the stress in the stiffener will vary as one goes from the spar flange to the center of the sheet owing to gusset interaction in the corner between the vertical and the flange and to effective width phenomena on both members. A limited amount of test data indicates that the compressive stress in the stiffener at the web center line will be from 50 to 60 per cent higher than it is at the flange rivet line as given by Fig. 6-39.

The stresses in the beam flanges can be considered to be made up of three major items. These are: (a) the primary beam bending stresses, (b) compression and tension stresses due to the components of the diagonal tension field acting parallel to the flanges, and (c) secondary bending stresses in the flanges due to the components of the diagonal tension field acting perpendicular to the flanges.

The primary beam bending stresses can be determined by the usual beam equation

$$\sigma_{t,c} = \pm \frac{My}{I_F} \quad [6-59]$$

Actually, up to the point of web buckling, the total moment of inertia including that of the web should be used in the above equation; however, it is generally not too conservative to neglect the contribution of the web to the bending resistance and to assume that tension and compression loads in the flanges resist the entire bending moment. If h_1 is the distance between the centers of gravity of the two flanges, it is

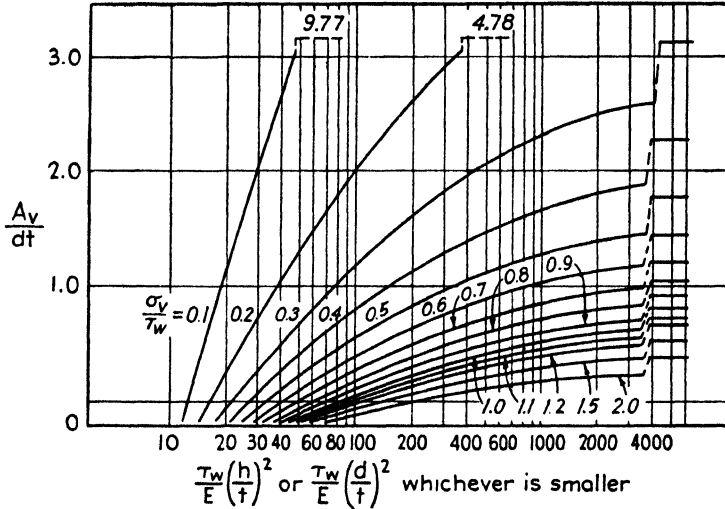


FIG. 6-39. Chart for determining web stiffener areas.

easily seen that the end loads in the tension and compression flanges, respectively, are

$$(P_{t,c})_1 = \pm \frac{M}{h_1} \quad [6-60]$$

For the end load in the flanges due to the diagonal tension field, consider the stress distribution on the end vertical. It can readily be seen that the only stress contributing to the flange end load is σ_t , since the horizontal components of σ_t and σ_c cancel each other. The horizontal force per unit height is equal to

$$P'_h = \frac{V_t}{h \tan \alpha} \quad [6-61]$$

where V_t = shear carried by the web in diagonal tension and the total horizontal force on the end vertical is

$$P'_h \cdot h = V_t \cot \alpha \quad [6-62]$$

which is to be divided between the upper and lower flanges, giving

$$(P_{t,c})_2 = -\frac{1}{2} V_t \cot \alpha \quad [6-63]$$

Thus, the total end load in the tension and compression flanges is given by the sum of equations 6.60 and 6.63, namely,

$$P_{t,c} = \pm \frac{M}{h_1} - \frac{1}{2} V_t \cot \alpha \quad [6.64]$$

The secondary bending stresses in the beam are due to the vertical component of the diagonal tension field. The unit distributed load on the flanges tending to bring them together is given by equation 6.53,

$$V'_v = \frac{V_t}{h} \tan \alpha \quad \text{pounds per inch} \quad [6.65]$$

If this running load is placed on the flange and the flange bending moments are calculated as though the flange acted as a continuous beam supported on the verticals, the secondary bending moments are given by

$$M_{vb} = \frac{1}{12} V'_v d^2 \quad \text{at the verticals} \quad [6.66]$$

and

$$M_{vb} = \frac{1}{24} V'_v d^2 \quad \text{midway between the verticals} \quad [6.67]$$

Tests show that the actual secondary bending moment is nearly constant between uprights and can conservatively be given by

$$M_{vb} = 0.10C V'_v d^2 = 0.10C \frac{V_t}{h} d^2 \tan \alpha \quad [6.68]$$

where C is a factor depending upon the flexibility of the flanges and is given by the curve in Fig. 6.31. This equation is checked by a few tests and, until a more detailed analysis is available, is suggested for design purposes.

If the flanges are not parallel, equation 6.64 gives only the horizontal components of the flange loads. Taking into consideration the vertical components of the flange forces we have, for the total web shear

$$V_{w1} = V_w - (P_t \tan \delta_t + P_c \tan \delta_c) \quad [6.69]$$

where V_{w1} = web shear for non-parallel flanges,

V_w = web shear for parallel flanges.

(See Fig. 6.40.) This equation is only approximate and should not be used for highly tapered flanges or where the end vertical is very rigidly attached to the flanges. No test data are available to check the accuracy of this equation and it is suggested that tests be run to determine the importance of this factor in the design of such beams.

The shear deflections of incomplete tension field beams are usually sufficiently great that they cannot be neglected. In order to determine

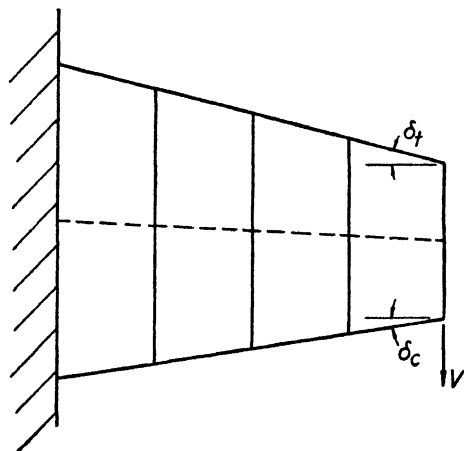


FIG. 6-40. Beam with tapering spar caps.

these deflections, it is necessary to have some means of determining an effective shear modulus for the assembly. The analysis of Wagner and

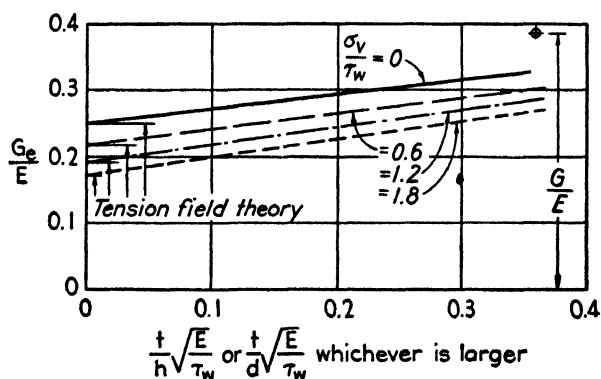


FIG. 6-41. Effective shear modulus chart.

Lahde leads to an equation for the effective shear modulus which has the form

$$\frac{G_e}{E} = fnc \left(\frac{\sigma_v}{\tau_w}, \frac{t}{h} \sqrt{\frac{E}{\tau_w}} \text{ or } \frac{t}{d} \sqrt{\frac{E}{\tau_w}} \right) \quad [6.70]$$

where G_e = effective shear modulus. The suggested value of G_e/E to use for design is shown in Fig. 6-41 which is taken from reference 6-16

6-4. The Use of Corrugated Sheet

When stiffening members are connected to flat plates in order to raise the allowable compressive load, certain design conditions may call for so small a stiffener spacing that consideration must be given to the use of some form of continuous stiffening member. This logically leads to the use of corrugated sheet attached to the flat sheet, forming a structural element which is very resistant to compressive loads applied parallel to the corrugation axis. Consideration will first be given to the crushing strength and column properties of corrugated sheet alone (without being attached to smooth sheet), and then the allowable strength of various combinations of corrugated and flat sheet will be studied.

There are obviously a very large number of different types of corrugations; however, a few of these have become more or less standardized and these will be discussed in some detail. The strength properties of the corrugations alone will first be treated and then consideration will be given to the effect of attaching such corrugated sheets to flat sheet.

(a) **ANC Circular Arc Corrugations.** The oldest standardized type of corrugation is that made up of a series of circular arcs of equal radii. See Fig. 6-42a. This has been very widely used and considerable information is available on its strength properties. One pitch/depth ratio has been established as standard; however, others have been used. The standard ratio is equal to $3\frac{1}{3}$, which gives rise to the following properties of the corrugation:

$$P/D = \text{pitch/depth ratio} = 3\frac{1}{3}$$

$$I = \text{moment of inertia per unit width} = 0.158tD^2 \text{ in.}^4 \text{ per in.}$$

$$\rho = \text{radius of gyration of cross section} = 0.359D \text{ in.}$$

$$K_w = \text{developed width/corrugated width} = 1.228$$

$$R = \text{radius of the circular elements} = 0.282P \text{ in.}$$

The geometrical properties for other pitch/depth ratios have been calculated and are given in graphical form in Fig. 6-43.

Research on the failure of cylindrical shells under axial compression indicates that a first approximation to the failure stress of such cylinders can be obtained from an equation of the form (see section 8-1)

$$\sigma_{cr} = KE \frac{t}{R} \quad [6-71]$$

Since this type of corrugation is made up of a series of cylindrical elements, it seems reasonable to assume that the crushing stress of the section (failure stress of a specimen that is so short that column action is

negligible) could be given by an equation similar to equation 6.71. The theoretical treatment of the problem is as yet incomplete so the value of the constant K will be determined by a correlation of the available experimental information.

The test data contained in references 6.24 to 6.27 inclusive have been studied, corrected to standard material properties by means of the

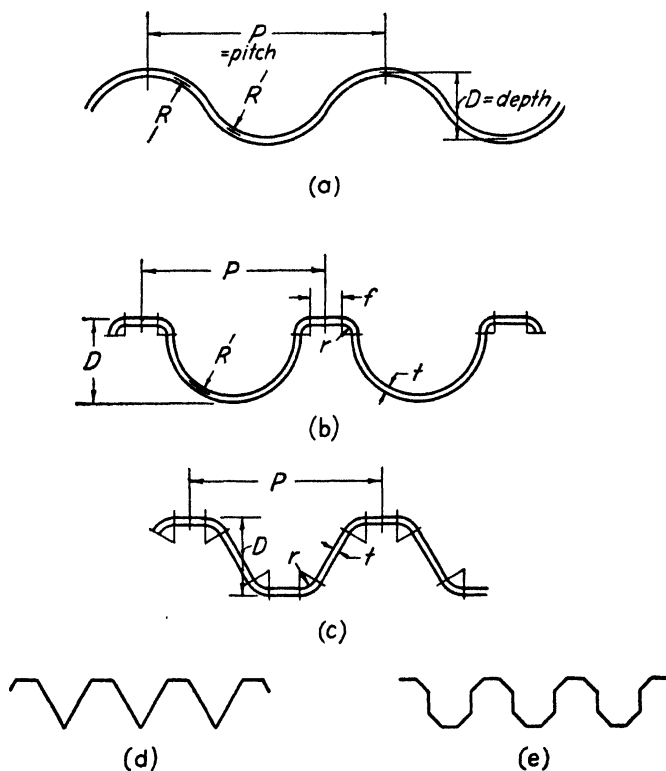


FIG. 6.42. Typical corrugation sections.

methods suggested in reference 6.8, and are plotted in Fig. 6.44. Inasmuch as it is very difficult to obtain uniform stress distribution on corrugated panels during static testing, it was felt that a conservative design curve would be a mean curve through the test points rather than a curve through the lowest of the test values. These faired mean curves have been replotted in Fig. 6.45, giving the allowable crushing strengths of the standard circular arc corrugation as a function of the R/t ratio and the material. Sometimes values shown in Fig. 6.45 are higher than those given in ANC-5, and until the values shown in this figure are accepted, the design values shown in ANC-5 must be used, at least for commercial airplanes.

Since the subject of specified allowables has come up with regard to allowable design stresses on corrugations, it might be well to digress for a moment and clarify the whole problem of usable design allowables. The curves given in this text are those obtained by a very careful correlation of all of the test data that could be gathered by the authors. It is realized that considerable data has been missed in this survey; however, it is felt that the test points presented give a representative picture

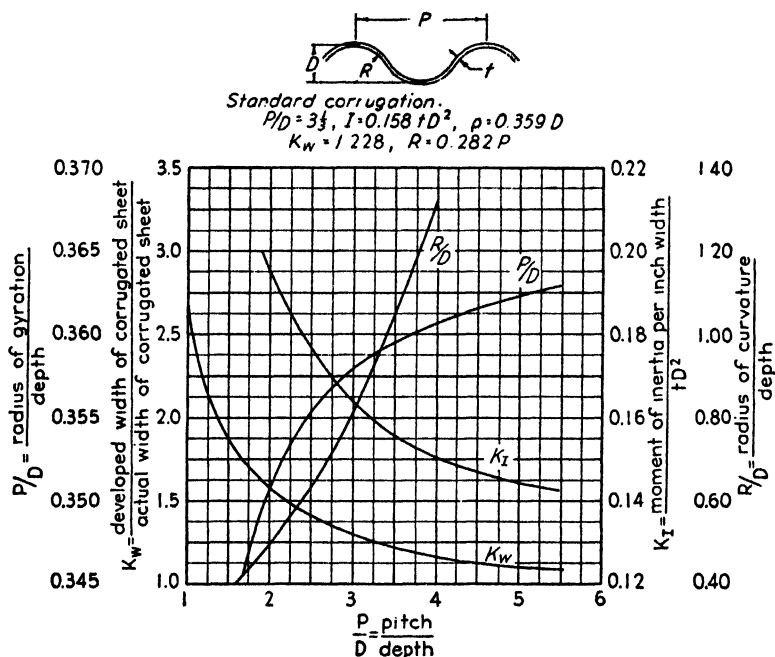


FIG. 6-43. Properties of standard circular arc corrugations.

of the latest test values available. On the other hand, certain governmental organizations have, in the interest of standardization, set up design rules and allowable design stresses for a number of the more important structural elements of an airplane. The design values specified by the various purchasing or inspection agencies must, of course, be used in structural analyses unless it is desired to ask for waivers on the basis of new theoretical or experimental information. It should be remembered that to change specification handbooks such as ANC-5 and the *Army Designer's Handbook* requires considerable time and effort, and they therefore contain values which may be in error in the light of newer information. The purpose of the curves and the design values given in this text is not to contradict the design allowables set up by the ANC committees, but to attempt to present a correlation and study of

what may be newer material than that considered when ANC-5 was written.

The crushing strength values given in Fig. 6-44 have all been determined by taking the end point ($L/\rho = 0$) of a Johnson parabola repre-

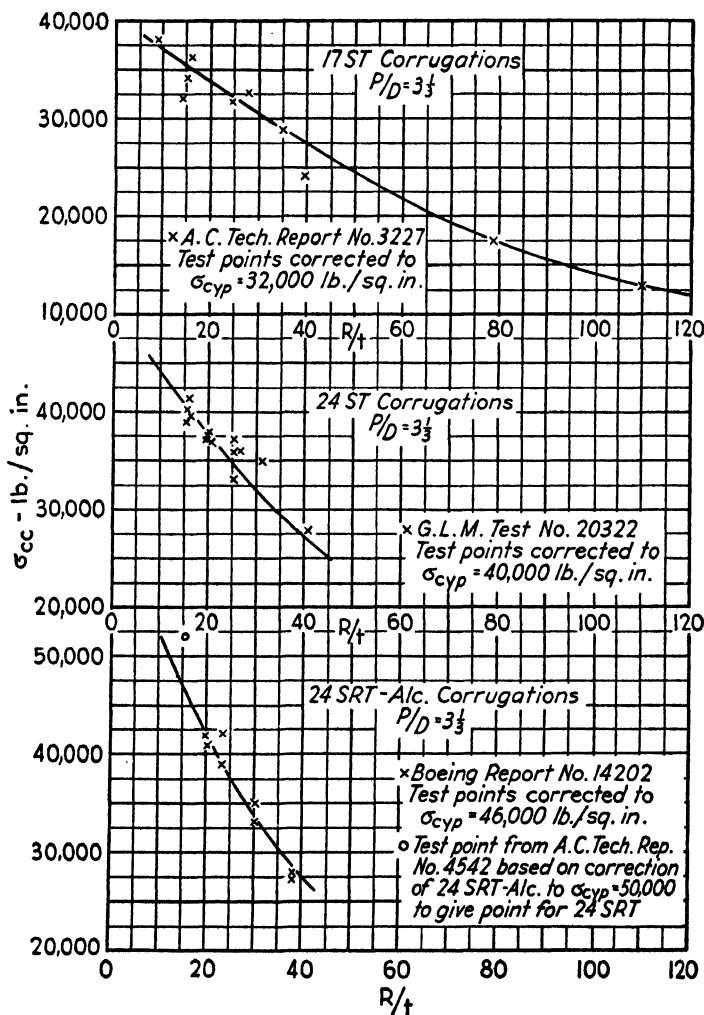


FIG. 6-44. Test values of σ_{cc} for dural circular arc corrugations.

senting the closest approximation to the experimental failing stresses plotted against L/ρ . In all cases investigated it was found that the use of a parabolic short column curve gave as good agreement between the Euler curve and an L/ρ value of approximately 20 as any other type of short column curve and was therefore used throughout the study. The

short column curve for any circular arc corrugation with a P/D ratio equal to $3\frac{1}{3}$ would then be determined by a Johnson parabola having a value of the crushing strength σ_{cc} taken from Fig. 6-45 and an end fixity value determined by the particular structural design or by some specified maximum value.

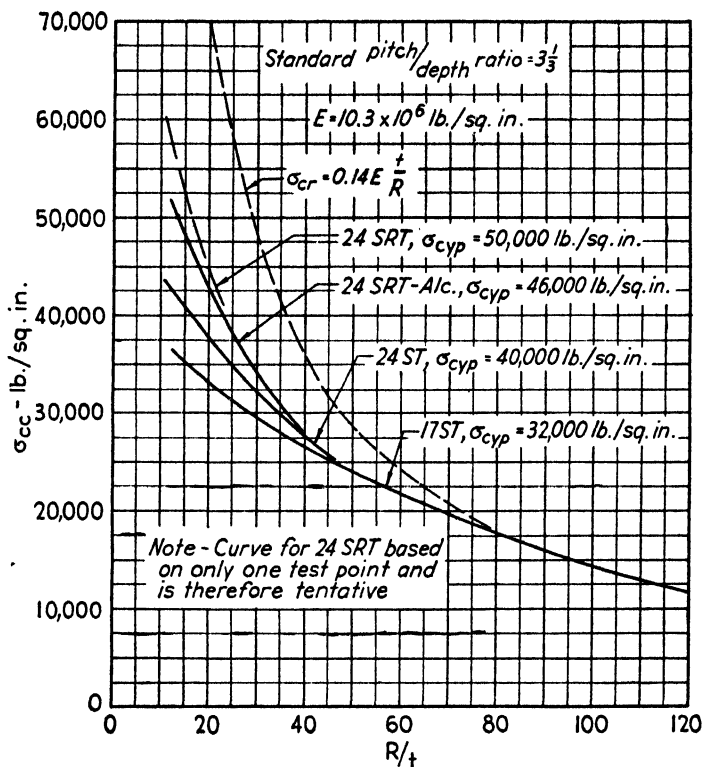


FIG. 6-45. Design curves for σ_{cc} .

For comparison purposes only, the curve given by the equation

$$\sigma_{cr} = 0.14E \frac{t}{R}$$

is also plotted in Fig. 6-45. The value of the constant equal to 0.14 was picked so that the curve would go through the lower points of the 17ST curve. Considering this curve, the form of the others seems reasonable since a deviation from any curve having the equation of the form of equation 6-71 would be expected at stress values above the proportional limit of the material, because the value of E is no longer constant. More deviation would be expected for materials having lower

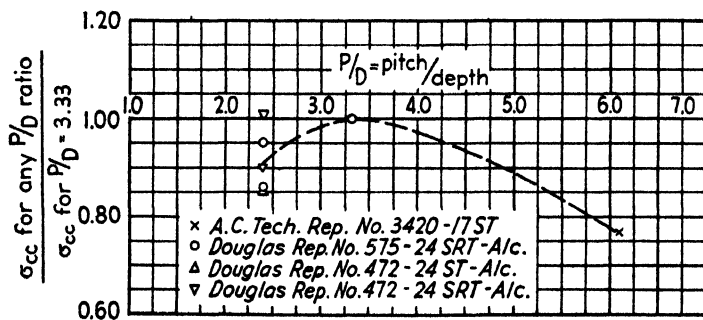
yield point values, and this is borne out by the experimental curves shown.

It is to be expected that the crushing strength values obtained by the use of Fig. 6-45 would not be correct for pitch/depth ratios other than $3\frac{1}{3}$. Unfortunately, however, there are very few data which would give the variation of the crushing strength as the P/D ratio changes. References 6-28 and 6-29 contain a limited number of tests on corrugations with P/D ratios differing from the standard and Table 6-10 shows the comparative crushing strength values.

TABLE 6-10

Material	P/D	R/T	σ_{cc} (lb./sq. in.)	σ_{cc} $P/D = 3\frac{1}{3}$ (lb./sq. in.)	Ratio	Reference
17ST	6.11	49.6	19,200	24,500	0.78	6.28
24SRT-Alc	2.40	12.1	48,400	51,000	0.95	6.29 (575)
24SRT-Alc	2.40	15.2	40,900	47,400	0.86	6.29 (575)
24ST-Alc	2.40	12.1	34,300	40,300	0.85	6.29 (472)
24SRT-Alc	2.40	15.2	42,700	47,400	0.90	6.29 (472)
24SRT-Alc	2.40	12.1	51,300	51,000	1.01	6.29 (472)

These points have been plotted in Fig. 6-46. The curve given is tentative and is given merely as a possible trend of this variation. That the curve is not universally true for all circular arc corrugations is

FIG. 6-46. Effect of P/D on σ_{cc} (dural).

demonstrated by tests on stainless steel (which will be discussed later) showing a considerably different tendency.

Data on circular arc stainless steel corrugations are meager and somewhat inconclusive. The experimental test results of reference 6-6 have been plotted as column curves in Fig. 6-47, each curve corresponding to a constant value of R/t and P/D . The end points ($L/\rho = 0$) of

these curves have been replotted in Fig. 6-48, giving the variation of the crushing strength of such stainless steel corrugations as a function of the radius/thickness and the pitch/depth ratios. These data indicate that

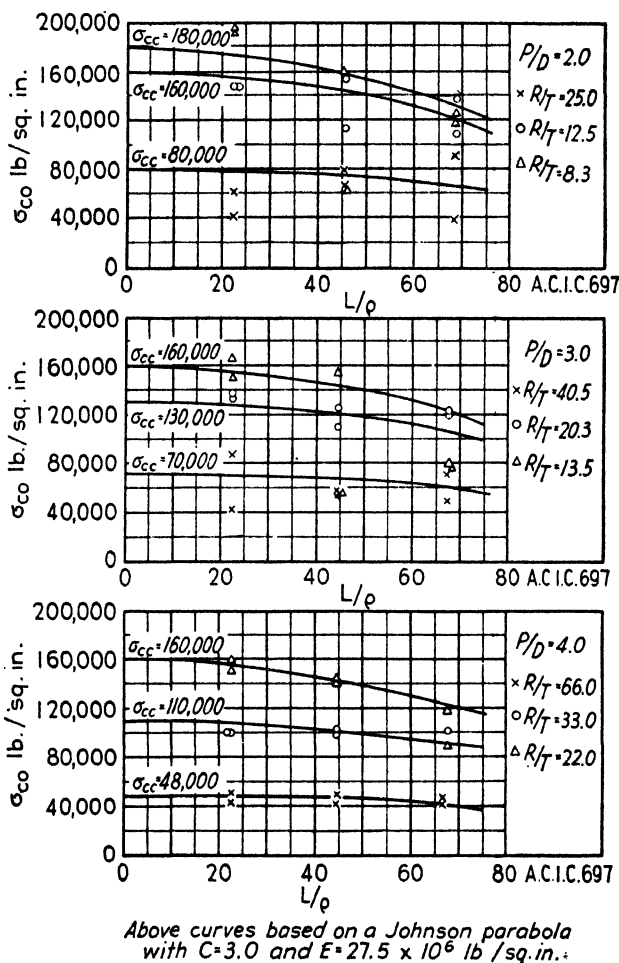


FIG. 6-47. Column curves for stainless corrugations.

there is a tendency for the crushing strength to increase as the pitch/depth ratio increases. That this is not a conclusive statement is indicated by the one point for a P/D ratio equal to 6.29 from reference 6-28. Even though the material used for this test had a much lower ultimate strength than that used for the tests of reference 6-6, the difference in ultimate strength could hardly account for the great reduction indicated in the crushing strength.

The design curve of the Edw. G. Budd Manufacturing Company, Aircraft Division (reference 6·30, discussed in detail later), using the proper value of the ultimate tensile strength is shown dotted in Fig. 6·48, and, at least for this series of tests, indicates that it may give very non-conservative predicted crushing strengths. Since, as will be shown later, the Budd curve gives predicted crushing strengths which are in good agreement with test values for other corrugation shapes, the discrepancy

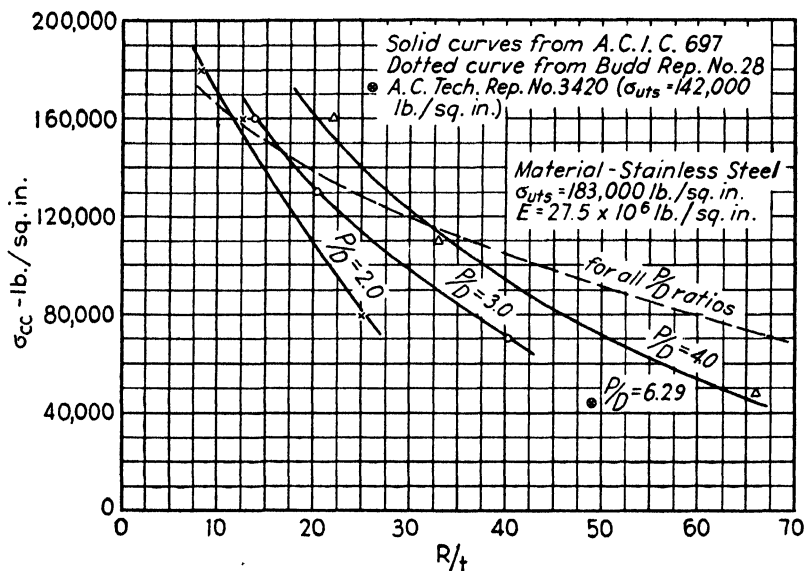


FIG. 6·48. Effect of P/D on σ_{cc} (stainless steel).

shown in Fig. 6·48 may be due to reasons other than an inherent fault in the design curve. These may be (1) because the flat region at the point of tangency of the circular arcs has been ignored, or (2) the possibility of poor alignment of the loaded edges of the specimens or of non-parallel motion of the testing machine heads during loading.

The main conclusion that can be drawn from the above study of the existing data on the crushing strength of circular arc corrugations is that although considerable test data are available, the data are incomplete and at times contradictory. It is felt that using Fig. 6·45, for the crushing strength of standard corrugations with $P/D = 3\frac{1}{2}$, is satisfactory, and that if this value is used in the Johnson parabolic equation with the proper end fixity coefficient, short column allowable stresses will be obtained which are suitable for design. Much additional data are needed to determine completely the effect of all the variables on the strength of such corrugations.

(b) **Flat-Topped or Omega Corrugations.** When circular arc corrugations are formed, there is nearly always a short length of straight section near the point of tangency of the two arcs. This is due to the natural springback of the material after the forming operation. This

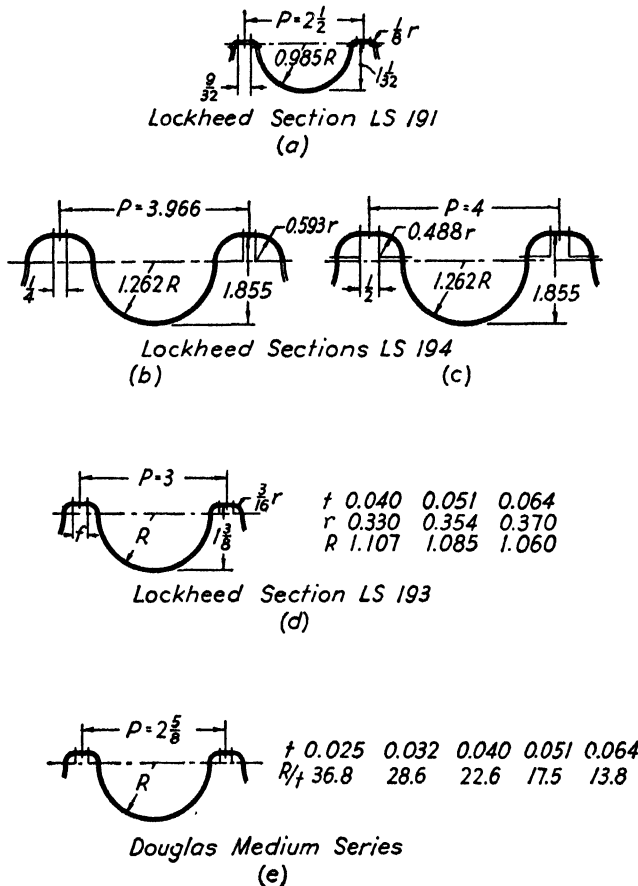


FIG. 6-49. Typical omega corrugations.

flat section has a lower buckling stress than the circular arc portion and failure usually starts in this region and proceeds into the curved parts of the corrugation. In order to eliminate this feature, and also to attempt to use more efficiently the material in the corrugation, corrugations having the forms shown in Fig. 6-49 have recently been the subject of considerable research. This type of corrugation primarily consists of a large semicircular portion connected by a flat region which is just long enough to give room for riveting the corrugation to sheet or structure.

Since the ends of the semicircular section are immediately adjacent to a region which has undergone severe forming, these ends are well supported, and the corrugation should develop the full strength of the curved section.

Figure 6-50 shows the results of tests on a number of corrugations of this type, giving the crushing strength as a function of the R/t ratio.

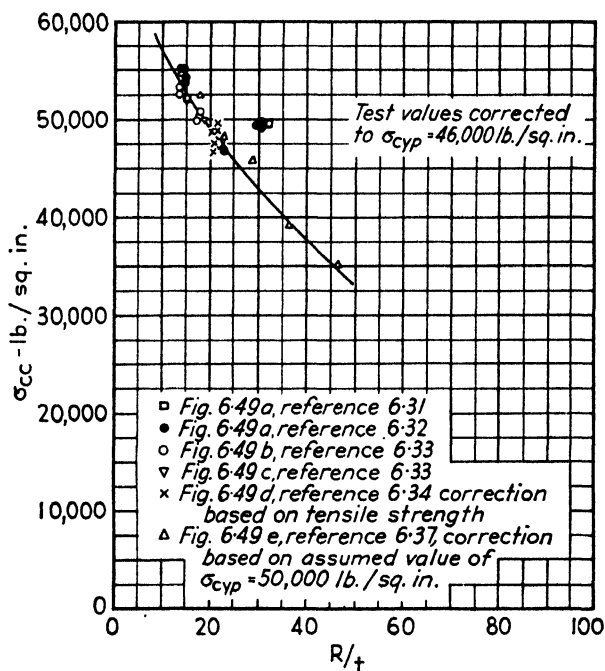


Fig. 6-50. Design values for omega corrugations.

All tests shown were made on 24SRT Alclad material, and the test points have been corrected for the minimum material properties using the method of reference 6-8. No difference in crushing strengths could be distinguished between the various types of cross sections shown on Fig. 6-49. The complete test reports can be found in references 6-31 to 6-34, inclusive, and reference 6-37. The value of σ_{cc} plotted was always taken as the end point of the Johnson parabola which gave the closest approximation to the test points.

(c) **Corrugations of Flat or Composite Sections.** A number of corrugation shapes consisting of flat elements have been tried as flat sheet reinforcement. A typical shape of such a corrugation in dural is shown in Fig. 6-51 along with its appropriate column curve as determined by test (reference 6-35). This curve is for the material as tested and has

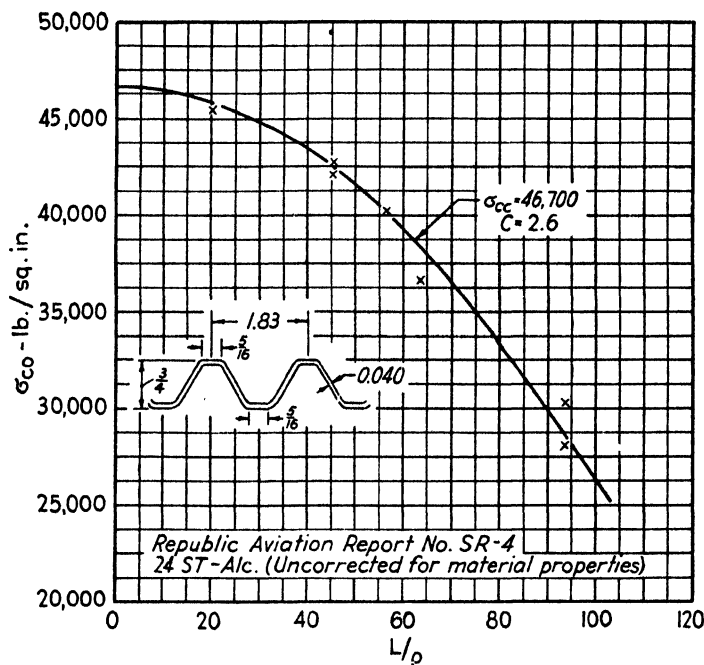


Fig. 6-51. Column curve for a flat corrugation.

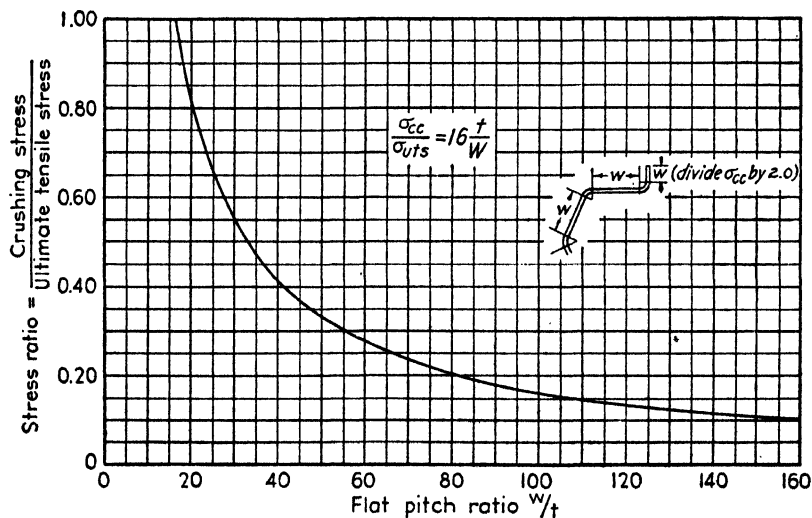


Fig. 6-52. Design curve for flat elements in stainless steel corrugations.

not been reduced for minimum material properties. Although such a section alone shows a relatively high crushing strength, when attached to sheet, the sheet buckling (particularly sheet buckling between rivets)

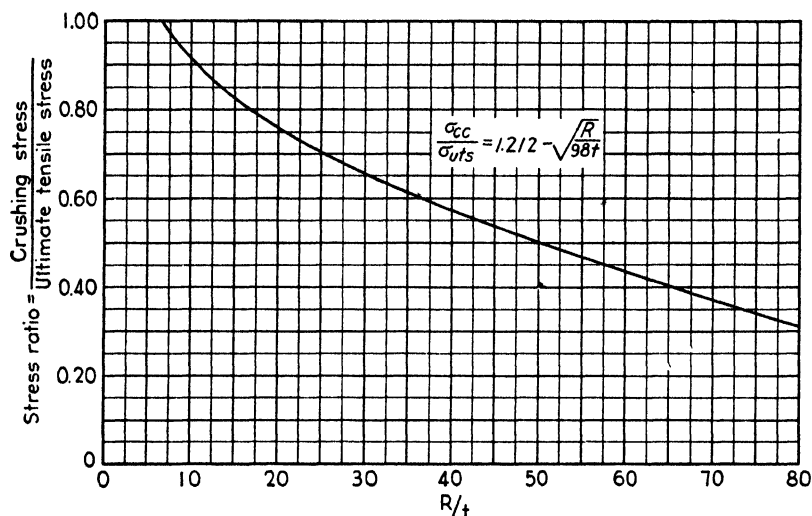


Fig. 6-53. Design curve for circular elements in stainless steel corrugations.

has a tendency to precipitate failure in the flat sides of the corrugation. This will be shown in the discussion of corrugation plus sheet assemblies.

Stainless steel lends itself very well to corrugation design. The Edw. G. Budd Manufacturing Company, Aircraft Division (reference 6-30), has developed design curves for stainless steel shapes from which the crippling stress of any formed shape of stainless steel may be determined. These curves are shown in Figs. 6-52 and 6-53. The method of using these curves will be illustrated by an example. Consider

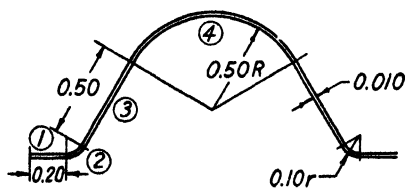


Fig. 6-54.

the stiffener shape shown in Fig. 6-54 made of stainless steel with an ultimate tensile strength of 185,000 lb. per sq. in. Then for

- (1) $w/t = 0.20/0.010 = 20$
 $\sigma_{cc_1} = 74,000$ lb. per sq. in.
 $\sigma_{cc}/\sigma_{uts} = 0.40$ (Fig. 6-52)
- (2) $R/t = 0.10/0.010 = 10$
 $\sigma_{cc_2} = 166,500$ lb. per sq. in.
 $\sigma_{cc}/\sigma_{uts} = 0.90$ (Fig. 6-53)

$$(3) \quad w/t = 0.50/0.010 = 50$$

$$\sigma_{cc_3} = 59,750 \text{ lb. per sq. in.}$$

$$\sigma_{cc}/\sigma_{uts} = 0.322$$

$$(4) \quad R/t = 0.50/0.010 = 50$$

$$\sigma_{cc_4} = 94,000 \text{ lb. per sq. in.}$$

$$\sigma_{cc}/\sigma_{uts} = 0.508$$

In the use of these curves, it is assumed that each section will carry a load given by the crushing strength shown in Figs. 6·52 or 6·53 times the area of the section, except that the section will fail when the weakest curved portion exceeds its crushing strength. On this basis the crushing load of the section shown would be equal to the sum of the loads shown below.

$$(1) \quad P_{cc_1} = 74,000 A_1$$

$$(2) \quad P_{cc_2} = 94,000 A_2 \text{ since the weakest curved section, (4), has a crushing strength of this value.}$$

$$(3) \quad P_{cc_3} = 59,570 A_3$$

$$(4) \quad P_{cc_4} = 94,000 A_4$$

and

$$P_{cc} = P_{cc_1} + P_{cc_2} + P_{cc_3} + P_{cc_4}$$

$$\sigma_{cc} = P_{cc}/A_{\text{total}}$$

A check of this method against a number of experimental tests on various shapes of stainless steel corrugations indicates good agreement between the predicted and test values. The method has frankly no theoretical basis, but as it seems to agree with actual test values, it is suitable for design purposes unless very unusual shapes are used for the corrugations.

(d) Corrugations Attached to Flat Sheet—General Analysis Method. Combinations of corrugation plus flat sheet will be analyzed by the same method as that used for flat sheet plus stiffeners, i.e., by the determination of the amount of sheet acting with the corrugation as an effective column. The pitch of the corrugation corresponds to the width of unsupported sheet which in turn will determine the buckling stress of the sheet. The appropriate column stress for the corrugation alone will, in general, give the value of σ_{se} , the sheet edge stress. With proper consideration of the effect of rivet spacing, material properties, etc., an effective width of sheet can be calculated and the combined cross section treated as a column. The examples which follow will illustrate the method.

(e) **Flat Sheet with Circular Arc Corrugations.** Reference 6-26 gives data on a number of tests using the standard circular arc corrugation attached to flat sheet. Consider a test panel with the following specifications (specimen 26, Table 6-11):

Panel 11.38 in. wide and 8 in. long tested in flat end compression.

Corrugation—pitch = 2.69 in., depth = 0.75 in., radius = 0.79 in., thickness = 0.0255 in., $R/t = 31.0$, material = 24SRT Alc., area = 0.3483 sq. in.

Sheet—thickness = 0.0235 in., material = 24SRT Alc.

Crushing strength of the corrugation from Fig. 6-45— $\sigma_{cc} = 33,400$ lb. per sq. in.

It is assumed that the short column failing stress for a length of 8 in. is equal to the crushing strength of the section. It is also to be noted here that a change in the corrugation thickness or in the amount of effective sheet acting with it has so little effect on the radius of gyration of the cross section that it can be neglected.

Critical buckling stress of the sheet is

$$\sigma_{cr} = 3.62 \times 10.3 \times 10^6 \times (0.0235/2.69)^2 = 2850 \text{ lb. per sq. in.}$$

Since exact values of the material yield point are not given it will be assumed that $\sigma_{cyp} = 46,000$ lb. per sq. in. Then

$$\sigma_{se}/\sigma_{cr} = \sigma_{cc}/\sigma_{cr} = 11.7 \quad \sigma_{sc}/\sigma_{cyp} = 0.73$$

and from Fig. 6-2

$$w_e/b = 0.128 \quad \text{and} \quad w_e = 0.345 \text{ in.}$$

There are four corrugations in the panel, therefore the sheet area is

$$A_{sh} = 8 \times 0.345 \times 0.0235 = 0.0648 \text{ sq. in.}$$

and the total area is

$$A_{\text{total}} = A_{sh} + A_{cor} = 0.0648 + 0.3483 = 0.4131 \text{ sq. in.}$$

This is acting under the stress of 33,400 lb. per sq. in. giving a predicted load that the panel should carry of

$$P_{\text{pred}} = 0.4131 \times 33,400 = 13,800 \text{ lb.}$$

as compared to the experimentally determined failing load of

$$P_{\text{exp}} = 14,575 \text{ lb.}$$

Table 6-11 shows the comparison for the other panels tested in this series. It will be noted that except for those panels which failed due to rivet failure, the method generally gives conservative estimates of the load that can be carried. The degree of conservatism is rather large, but it is felt that this is probably due to variations in actual material

TABLE 6.11

Spec. No.	t_c (in.)	t_s (in.)	R/t_c	$J_{ce} = \frac{\sigma_{co}}{\sigma_{es}}$ (lb./sq. in.)	σ_{cr} (lb./sq. in.)	w_c/b	w_c (in.)	$2w_c/t_s$	A_{eh} (sq. in.)	A_{cor} (sq. in.)	A_{total} (sq. in.)	P_{pred} (lb.)	P_{test} (lb.)
1	0.016	0.016	49.4	24,700	1,320	0.129	0.347	43.3	0.0444	0.2185	0.262	6,490	5,060†
2	0.016	0.015	49.4	24,700	1,160	0.122	0.328	43.7	0.0394	0.2185	0.2579	6,360	5,455†
3	0.016	0.021	49.4	24,700	2,270	0.170	0.457	43.5	0.0768	0.2185	0.2953	7,300	5,825
4	0.016	0.021	49.4	24,700	2,270	0.170	0.457	43.5	0.0768	0.2185	0.2953	7,300	6,075
5	0.020	0.016	39.5	28,500	1,320	0.110	0.296	37.0	0.0376	0.2731	0.3107	8,860	9,475
6	0.020	0.016	39.5	28,500	1,320	0.110	0.296	37.0	0.0376	0.2731	0.3107	8,860	9,475
7	0.020	0.0205	39.5	28,500	2,160	0.149	0.401	38.7	0.0658	0.2731	0.3389	9,660	8,500†
8	0.020	0.0205	39.5	28,500	2,160	0.149	0.401	38.7	0.0658	0.2731	0.3389	9,660	9,155
9	0.020	0.0235	39.5	28,500	2,850	0.160	0.430	36.6	0.0809	0.2731	0.3540	10,090	12,120
10	0.020	0.0235	39.5	28,500	2,850	0.160	0.430	36.6	0.0809	0.2731	0.3540	10,090	11,330
11	0.025	0.021	31.0	33,000	2,270	0.130	0.350	33.3	0.0588	0.3415	0.4003	13,290	15,810
12	0.0255	0.021	31.0	33,000	2,270	0.130	0.350	33.3	0.0588	0.3483	0.4071	13,600	15,395
13	0.025	0.0325	31.6	33,000	5,440	0.178	0.479	29.5	0.1245	0.3415	0.4660	15,360	17,335
14	0.0255	0.033	31.0	33,400	5,610	0.130	0.350	21.2	0.0923	0.3483	0.4406	14,710	16,610
15	0.033	0.0235	23.9	38,700	2,850	0.119	0.320	27.2	0.0602	0.4510	0.5112	19,780	23,225
16	0.033	0.0235	23.9	38,700	2,850	0.119	0.320	27.2	0.0602	0.4510	0.5112	19,780	23,225
17	0.033	0.033	23.9	38,700	5,610	0.155	0.417	25.3	0.1101	0.4510	0.5611	21,710	25,005
18	0.033	0.033	23.9	38,700	5,610	0.155	0.417	25.3	0.1101	0.4510	0.5611	21,710	25,060
19	0.033	0.040	23.9	38,700	8,250	0.186	0.500	25.0	0.1602	0.4510	0.6112	23,650	26,260
20	0.033	0.040	23.9	38,700	8,250	0.186	0.500	25.0	0.1602	0.4510	0.6112	23,650	26,260
21	0.039	0.033	20.3	41,700	5,610	0.142	0.382	23.1	0.1009	0.5330	0.6339	26,400	29,825
22*	0.039	0.032	20.3	41,700	5,280	0.139	0.374	23.4	0.0718	0.5330	0.6339	26,400	29,825
23	0.039	0.039	20.3	41,700	7,850	0.166	0.447	22.9	0.1394	0.5330	0.6724	28,020	23,290
24*	0.039	0.039	20.3	41,700	7,850	0.166	0.447	22.9	0.1394	0.5330	0.6724	28,020	27,020†
25	C.025	0.0235	31.6	33,000	2,850	0.129	0.347	29.5	0.1045	0.3415	0.5195	21,650	21,875†
26	0.0255	0.0235	31.0	33,400	2,850	0.128	0.345	29.3	0.0648	0.3483	0.4131	13,800	15,825
													14,585

* Three corrugations wide, all others four.

† Rivet failure precipitated panel failure; 0.016 Material 24ST Alc., all other, 24SRT Alc.

TABLE 6.12

Spec. No.	L/ρ	$\sigma_{co} = \sigma_{ec}$ (lb./sq. in.)	t_s (in.)	σ_{cr} (lb./sq. in.)	w_e/b	w_e (in.)	$2w_e/t_s$	A_{st} (sq. in.)	A_{cr} (sq. in.)	A_{total} (sq. in.)	P_{pred} (lb.)	P_{test} (lb.)
28a	21.4	151,400	0.005	2,490	0.071	0.071	28.4	0.0067	0.2458	0.2525	38,200	40,570
28b	21.4	151,400	0.005	2,490	0.071	0.071	28.4	0.0067	0.2561	0.2628	39,800	43,680
29a	43.0	141,400	0.005	2,490	0.080	0.080	32.0	0.0064	0.2490	0.2554	36,100	36,200
29b	43.0	141,400	0.005	2,490	0.080	0.080	32.0	0.0064	0.2474	0.2538	35,900	40,500
30a	69.8	119,000	0.005	2,490	0.101	0.101	40.4	0.0081	0.2576	0.2657	31,600	43,075
30b	69.8	119,000	0.005	2,490	0.101	0.101	40.4	0.0081	0.2514	0.2595	30,800	32,050
31a	21.0	151,500	0.010	9,950	0.116	0.116	23.2	0.0186	0.2423	0.2609	39,500	43,210
31b	21.0	151,500	0.010	9,950	0.116	0.116	23.2	0.0186	0.2478	0.2664	40,400	46,930
32a	42.1	141,800	0.010	9,950	0.125	0.125	25.0	0.0200	0.2385	0.2585	36,700	42,330
32b	42.1	141,800	0.010	9,950	0.125	0.125	25.0	0.0200	0.2432	0.2632	37,300	43,190
33a	63.1	125,500	0.010	9,950	0.141	0.141	28.2	0.0226	0.2517	0.2743	34,400	33,990
33b	63.1	125,500	0.010	9,950	0.141	0.141	28.2	0.0226	0.2440	0.2666	33,500	34,410
34a	21.2	151,400	0.0145	20,900	0.155	0.155	21.4	0.0360	0.2450	0.2810	42,500	46,990
34b	21.2	151,400	0.0145	20,900	0.155	0.155	21.4	0.0360	0.2418	0.2778	42,200	44,560
35a	42.5	141,600	0.0145	20,900	0.165	0.165	22.8	0.0383	0.2439	0.2822	40,000	42,610
35b	42.5	141,600	0.0145	20,900	0.165	0.165	22.8	0.0383	0.2395	0.2778	39,300	43,180
36a	63.6	125,000	0.0145	20,900	0.185	0.185	25.5	0.0429	0.2471	0.2900	36,200	34,590
36b	63.6	125,000	0.0145	20,900	0.185	0.185	25.5	0.0429	0.2538	0.2967	37,100	36,560
37a	21.4	151,400	0.020	39,800	0.208	0.208	20.8	0.0666	0.2415	0.3081	46,600	43,400
37b	21.4	151,400	0.020	39,800	0.208	0.208	20.8	0.0666	0.2300	0.2966	43,900	43,900
38a	42.7	141,500	0.020	39,800	0.220	0.220	22.0	0.0704	0.2432	0.3136	44,300	46,980
38b	42.7	141,500	0.020	39,800	0.220	0.220	22.0	0.0704	0.2300	0.3004	42,500	40,200
39a	64.0	124,700	0.020	39,800	0.245	0.245	24.5	0.0784	0.2506	0.3290	41,000	32,920
39b	64.0	124,700	0.020	39,800	0.245	0.245	24.5	0.0784	0.2491	0.3275	40,800	38,480
40a	21.8	151,300	0.029	83,700	0.318	0.318	21.9	0.1475	0.2533	0.4008	60,600	59,230
40b	21.8	151,300	0.029	83,700	0.318	0.318	21.9	0.1475	0.2470	0.3945	59,700	59,450
41a	43.7	140,800	0.029	83,700	0.345	0.345	23.8	0.1600	0.2473	0.4073	57,790	57,790
41b	43.7	140,800	0.029	83,700	0.345	0.345	23.8	0.1600	0.2355	0.3955	55,700	56,250
42a	65.6	123,000	0.029	83,700	0.385	0.385	26.6	0.1785	0.2423	0.4208	51,800	43,200
42b	65.6	123,000	0.029	83,700	0.385	0.385	26.6	0.1785	0.2363	0.4148	51,000	44,050

Corrugations: stainless steel—1-in. pitch, $\frac{1}{2}$ -in. depth, 0.019-in. thickness, $P/D = 2.00$, $R/t = 12.5$, $\sigma_{ec} = 155,000$, from Fig. 6-48. For determination of σ_{co} , a parabolic short column curve was assumed with $C = 3.0$, $E = 27.5 \times 10^6$ lb. per sq. in. Material yield point = 183,000 lb. per sq. in.

properties of the specimens tested. For example, the range of yield points of the material was from 46,670 to 52,830 lb. per sq. in. (specific values for each panel were not taken) which would account for a considerable increase in load which could be carried by some of the test panels.

The same analysis method is used for a series of stainless steel specimens made up of circular arc corrugations spot-welded to flat stainless sheet. Data for these specimens are given in reference 6-28, and the comparison between calculated and test values of the yield point and modulus were used throughout the calculations.

(f) **Flat Sheet Reinforced with Flat Top Corrugations.** Table 6-13 shows the agreement between calculated and experimental values of the effective width, column stress, and ultimate load for a series of panels

TABLE 6-13

Spec. No.	L (in.)	t_c (in.)	t_s (in.)	Predicted Values			Test Values		
				w_e (in.)	σ_{co} (lb./sq. in.)	P_{co} (lb.)	w_e (in.)	σ_{co} (lb./sq. in.)	P_{co} (lb.)
2201A	12	0.032	0.040	0.420	41,300	28,050	0.350	43,350	28,500
2201B	12	0.032	0.040	0.420	41,300	28,050	0.303	45,700	29,300
2202A	12	0.032	0.051	0.570	41,300	32,900	0.595	41,900	33,750
2202B	12	0.032	0.051	0.570	41,300	32,900	0.538	44,350	34,650
2204B	12	0.064	0.051	0.477	49,330	63,200	0.263	48,300	57,600
2212A	18	0.032	0.040	0.440	39,360	26,250	0.460	37,320	25,100
2212B	18	0.032	0.040	0.440	39,360	26,250	0.363	43,300	27,800
2217A	24	0.032	0.040	0.475	36,500	24,750	0.478	40,300	27,350
2221B	24	0.032	0.040	0.475	36,500	24,750	0.445	40,700	27,200
2218A	24	0.032	0.051	0.645	36,500	29,200	0.690	31,700	38,800
2218B	24	0.032	0.051	0.645	36,500	29,200	0.665	38,600	31,150
2224A	24	0.064	0.051	0.555	42,370	55,000	0.441	41,350	52,300
2224B	24	0.064	0.051	0.555	42,370	55,000	0.500	41,350	53,350
2225A	12	0.064	0.051	0.477	49,330	63,200	0.255	50,600	55,100
2225B	12	0.064	0.051	0.477	49,330	63,200	0.735	48,100	66,600

Both predicted and test values corrected to $\sigma_{cyp} = 46,000$ lb. per sq. in.

t_c = corrugation thickness.

t_s = sheet thickness.

σ_{co} = critical column stress of corrugation plus the effective width of sheet.

P_{co} = critical column load corresponding to σ_{co} .

consisting of flat-top corrugations (Fig. 6-49a) attached to flat sheet. Data for this table were taken from reference 6-31. For this series of tests actual stresses in the corrugations were measured, making it possible to determine the load carried by the sheet and from this, the

experimental value of the effective width. Stress-strain curves were also taken for all specimens making possible a correction for material properties. The calculation for specimen 2201A will be carried out in detail to show the method.

Corrugation—pitch = $2\frac{1}{2}$ in., $t = 0.032$ in., $R/t = 31.3$, material = 24SRT Alc., area = 0.545 sq. in., $\sigma_{cc} = 43,000$ lb. per sq. in. from Fig. 6-50.

Specimen is 12 in. long corresponding to an $L/\rho = 33.5$ and, using an end fixity coefficient of 3.0 and σ_{cc} as given above in the parabolic column equation, we get $\sigma_{co} = 41,300$ lb. per sq. in.

The cover sheet is 0.040 in. thick, 24ST Alc. The buckling stress for $b = P = 2\frac{1}{2}$ in. is $\sigma_{cr} = 9540$ lb. per sq. in.

The rivet spacing on these specimens was 1.0 in. and, from Fig. 6-23, the sheet would buckle between rivets at a stress of

$$\sigma_{rb} = 31,500 \text{ lb. per sq. in. (for } \sigma_{yp} = 37,000 \text{ lb. per sq. in.)}$$

The effective width ratio at this stress is obtained from Fig. 6-2, in which

$$\sigma_{se}/\sigma_{cr} = \sigma_{rb}/\sigma_{cr} = 3.30 \quad \sigma_{rb}/\sigma_{yp} = 0.85 \quad (w_e/b)\sigma_{rb} = 0.22$$

The effective width ratio at the critical column stress, σ_{co} , is

$$(w_e/b)\sigma_{co} = 0.222 \times 31,500/41,300 = 0.168$$

giving an effective width of

$$w_e = 0.168 \times 2.5 = 0.420 \text{ in.}$$

This gives an effective sheet area (4 corrugations = 8 effective widths) of

$$A_{sh} = 8 \times 0.420 \times 0.040 = 0.134 \text{ sq. in.}$$

making a total area of

$$A_{total} = A_{cor} + A_{sh} = 0.545 + 0.134 = 0.679 \text{ sq. in.}$$

which should support a load of

$$P_{pred} = \sigma_{co} \times A_{total} = 41,300 \times 0.679 = 28,050 \text{ lb.}$$

The panel actually tested carried a load of 30,600 lb. with a stress in the corrugation at that load of 48,300 lb. per sq. in. The material in the corrugation has a compressive yield point of 52,600 lb. per sq. in. with a minimum specified of 46,000 lb. per sq. in. Using Fig. 6-21

$$\sigma_{test}/\sigma_{cyp} = 0.92 \quad \sigma_{cyp}/46,000 = 1.14 \quad K = 0.898$$

giving a corrected value of the allowable corrugation stress of

$$\sigma_{co_{test}} = 48,300 \times 0.898 = 43,350 \text{ lb. per sq. in.}$$

The measured effective width

$$w_{e_{test}} = (P_{cc} - \sigma_{co} A_{cor}) / 2\sigma_{co} t \quad (\text{these values from test data}) = 0.350 \text{ in.}$$

It is felt that the agreement shown in Table 6-13 is satisfactory, the variation between the predicted and test values being of the same order as the variation between identical specimens and that the method is satisfactory for use with flat-top or omega corrugations.

A number of other corrugation-sheet combinations from references 6-31 to 6-34 inclusive have been checked by this method and show agreement as good as or better than that shown in Table 6-13. It is therefore felt that this method is suitable for predicting the allowable loads on such stiffened sheets. In general it will be found that the calculated effective widths at low corrugation stresses will be smaller than those measured in tests. This is probably due to the not inconsiderable support given to the skin by the rivets and the flat attachment area of these corrugations. However, at failure the calculated and measured effective widths are in reasonably good agreement, and the method is therefore satisfactory for design purposes.

(g) Flat and Composite Section Corrugations Plus Sheet. Data from reference 6-35, for the corrugation shown in Fig. 6-51 attached to flat sheet, have been checked by the effective width method given above. The results are indicated in Table 6-14. Here, for the first time, we see non-conservative predicted loads for the combination, but it is felt that this is not a fault of the method but of the corrugation. Such sections seem to be very sensitive to the buckling of the sheet to which they are attached, and particularly to the buckling of the sheet between rivets. If the sheet is very light, it will have little effect on the corrugation; but if it is heavy (thickness equal to or greater than that of the corrugation), the formation of waves in the flat sheet will tend to distort the flat sides of the corrugation and precipitate failure at loads below those predicted by the effective column curves. That this is borne out by the tests is indicated by the fact that for the 0.032 sheet attached to these 0.040 corrugations, the test load averaged 7.6 per cent lower than the predicted loads; for the 0.025 sheet it was 2.4 per cent lower; and for the 0.020 sheet it was only 0.9 per cent lower than the test loads. This indicates that the heavier sheet tended to reduce the predicted column load of the section, probably by deforming the flat sides of the section and causing them to buckle at loads below their normal critical buckling loads. Where sheet buckling between rivets was delayed by smaller rivet spac-

TABLE 6.14

Spec. No.	L (in.)	L/ρ	σ_{eo} (lb./sq. in.)	l_s (in.)	σ_{cr} (lb./sq. in.)	σ_{rb} (lb./sq. in.)	w_c (in.)	A_{sh} (sq. in.)	A_{cor} (sq. in.)	A_{total} (sq. in.)	P_{pred} (lb.)	P_{test} (lb.)
1	6	20.0	45,800	0.032	11,400	28,000	0.303	0.222	0.819	1.041	47,700	43,100
2	6	20.0	45,800	0.025	6,950	22,200	0.222	0.145	0.819	0.964	44,100	42,100
3	6	20.0	45,800	0.020	4,450	14,800	0.160	0.099	0.819	0.918	42,100	41,350
4	14	46.7	42,200	0.032	11,400	28,000	0.330	0.338	1.326	1.664	70,200	60,700
5	14	46.7	42,200	0.032	11,400	28,000	0.330	0.233	0.819	1.052	44,400	41,800
6	14	46.7	42,200	0.025	6,950	22,200	0.241	0.211	1.326	1.537	64,900	59,600
7	14	46.7	42,200	0.025	6,950	22,200	0.241	0.151	0.819	0.970	40,900	39,100
8	14	46.7	42,200	0.020	4,450	14,800	0.173	0.141	1.326	1.467	61,900	59,100
9	14	46.7	42,200	0.020	4,450	14,800	0.173	0.103	0.819	0.922	38,900	38,250
10	17	56.6	40,300	0.032	11,400	28,000	0.347	0.241	0.819	1.060	42,700	38,850
11	17	56.6	40,300	0.025	6,950	22,200	0.252	0.155	0.819	0.974	39,200	37,250
12	17	56.6	40,300	0.020	4,450	14,800	0.182	0.105	0.819	0.924	37,400	35,850
13	19	63.3	38,700	0.032	11,400	28,000	0.359	0.247	0.819	1.066	41,200	38,000
14*	19	63.3	38,700	0.032	11,400	22,200	0.362	0.248	0.819	1.067	41,300	41,600
15	19	63.3	38,700	0.025	6,950	22,200	0.260	0.158	0.819	0.977	37,800	35,750
16	19	63.3	38,700	0.020	4,450	14,800	0.188	0.138	0.819	0.957	37,000	34,250
17	28	93.4	27,400	0.032	11,400	28,000	0.503	0.473	1.326	1.799	49,300	48,800
18	28	93.4	27,400	0.032	11,400	28,000	0.503	0.311	0.819	1.130	30,500	33,700
19	28	93.4	27,400	0.025	6,950	22,200	0.367	0.287	1.326	1.613	44,200	44,700
20	28	93.4	27,400	0.025	6,950	22,200	0.367	0.195	0.819	1.014	27,900	31,500
21	28	93.4	27,400	0.020	4,450	14,800	0.267	0.182	1.326	1.508	41,300	42,300
22	28	93.4	27,400	0.020	4,450	14,800	0.267	0.129	0.819	0.948	25,900	29,500

* Rivet spacing $\frac{1}{2}$ in.; all others, 1 in. Panels 4, 6, 8, 17, 19, 21—12 corrugations wide; all others, 7.

ing, as in specimen 14, the predicted and test loads were almost exactly alike. Although this one specimen does not give conclusive evidence that smaller rivet spacing would solve the problem, it is entirely possible that it would aid in bringing up the allowable strength of such corrugation-sheet combinations.

In stainless steel, consider the corrugation-sheet combination shown in Fig. 6-55, taken from reference 6-36. It can be shown that the con-

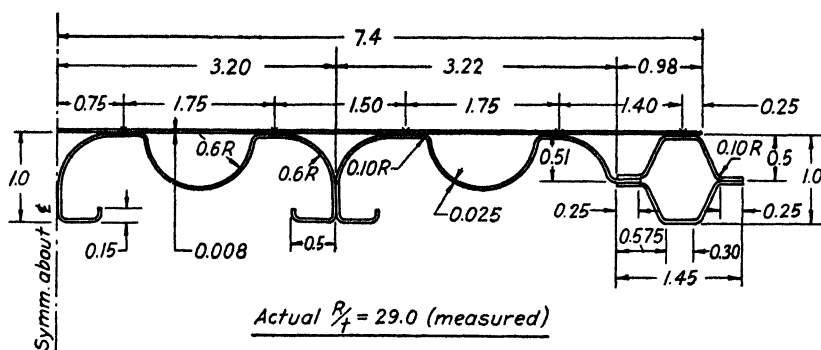


FIG. 6-55. Test panel of stainless steel.

trolling section for the corrugation is the curved portion having a measured R/t ratio of 29.0. For this section

$$\frac{\sigma_{cc}}{\sigma_{uts}} = 0.671$$

and

$$\sigma_{cc} = 185,000 \times 0.671 = 124,100 \text{ lb. per sq. in.}$$

The area of the corrugation is 0.7849 sq. in., which gives a crushing load for the corrugation of

$$P_{cc} = 124,100 \times 0.7849 = 97,400 \text{ lb.}$$

For the sheet, the following breakdown will hold:

No. Elements	w	w/t	σ_{cc}/σ_{uts}	σ_{cc}	P
2	0.25	31.25	0.512	94,600/2	190
2	1.40	175.0	0.0914	16,900	380
4	1.75	218.8	0.0732	13,500	755
3	1.50	187.5	0.0854	15,800	565

Crushing strength of sheet 1890 lb.

Total crushing strength of the section is then

$$P_{cc} = 97,400 + 1890 = 99,290 \text{ lb.}$$

with an average crushing stress of

$$\sigma_{cc} = \frac{99,290}{0.7849 + 0.1184} = 99,290/0.9033 = 108,800 \text{ lb. per sq. in.}$$

The section tested had an $L/\sqrt{C\rho}$ value of 20 (assuming $C = 2.0$). The column stress for this $L/\sqrt{C\rho}$ value, obtained from a parabolic short column equation, is

$$\begin{aligned}\sigma_{co} &= 108,800 - \frac{108,800^2 20^2}{4\pi^2 \times 2.6 \times 10^7} \\ &= 104,190 \text{ lb. per sq. in.}\end{aligned}$$

leading to a predicted load for a panel of this length of

$$P_{co} = 104,190 \times 0.9033 = 94,200 \text{ lb.}$$

The test panel carried a load of 93,100 lb., indicating an error of 1.1 per cent. Other tests of the same character gave similar results.

Tests have been made by the Edw. G. Budd Manufacturing Company, Aircraft Division, on a number of different stiffener and corrugation shapes formed from stainless steel. Flat section, curved section, and composite corrugations have been tested and, in nearly all cases, the failing loads predicted through the use of Figs. 6-52 and 6-53 have agreed reasonably well with the test-failing loads. For such sections, the use of nominal sheet thickness and other dimensions of the corrugation is not advised, but rather an attempt should be made to obtain these values by direct measurement of the cross section. This is due to the fact that the spring-back after forming may lead to cross-section radii which are considerably different from those specified in the drawing, which, in turn, lead to incorrect values of σ_{cc}/σ_{uts} for these elements.

REFERENCES FOR CHAPTER 6

- 6-1. K. MARGUERRE, "The Apparent Width of the Plate in Compression," *N.A.C.A. Tech. Memo.* 833.
- 6-2. T. VON KÁRMÁN, E. E. SECHLER, and L. H. DONNELL, "The Strength of Thin Plates in Compression," *A.S.M.E. Trans.*, APM-54-5, Vol. 54, No. 2, Jan. 30, 1932.
- 6-3. S. TIMOSHENKO, *Theory of Elastic Stability*. McGraw-Hill, 1936.
- 6-4. E. E. LUNDQUIST, "Comparison of Three Methods for Calculating the Compressive Strength of Flat and Slightly Curved Sheet and Stiffener Combinations," *N.A.C.A. Tech. Note* 455.

- 6-5. M.I.T. *Report on Aircraft Materials Testing for 1931-32.*
- 6-6. E. H. SCHWARTZ and C. G. BROWN, "An Investigation of the Compressive Strength Properties of Stainless Steel Sheet-Stringer Combinations," *A.C.I.C.* 697.
- 6-7. L. G. DUNN, "An Investigation of Sheet-Stiffener Panels Subjected to Compression Loads with Particular Reference to Torsionally Weak Stiffeners," *N.A.C.A. Tech. Note* 752.
- 6-8. A. EPSTEIN, "Correction of Compression Test Results of Aluminum Alloys for Material Properties," *Air Corps Tech. Rep.* 4519, 1940.
- 6-9. L. HOWLAND, "Effect of Rivet Spacing on Stiffened Thin Sheet in Compression," *J. Aero. Sci.*, Vol. 3, No. 12, October, 1936.
- 6-10. J. S. NEWELL, "Letter to the Editor," *J. Aero. Sci.*, Vol. 4, No. 6, April, 1937.
- 6-11. H. WAGNER, "Structures of Thin Sheet Metal, Their Design and Construction," *N.A.C.A. Tech. Memo.* 490.
- 6-12. J. MATHAR, "Metal Covering of Airplanes," *N.A.C.A. Tech. Memo.* 592.
- 6-13. H. WAGNER, "Flat Sheet Metal Girders with Very Thin Metal Web."
Part I, *N.A.C.A. Tech. Memo.* 604.
Part II, *N.A.C.A. Tech. Memo.* 605.
Part III, *N.A.C.A. Tech. Memo.* 606.
- 6-14. P. KUHN, "A Summary of Design Formulas for Beams Having Thin Webs in Diagonal Tension," *N.A.C.A. Tech. Note* 469.
- 6-15. O. S. HECK and H. EBNER, "Methods and Formulas for Calculating the Strength of Plate and Shell Constructions as Used in Airplane Design," *N.A.C.A. Tech. Memo.* 785.
- 6-16. R. LAHDE and H. WAGNER, "Tests for the Determination of the Stress Condition in Tension Fields," *N.A.C.A. Tech. Memo.* 809.
- 6-17. E. SCHAPITZ, "Contributions to the Theory of the Incomplete Tension Bay," *N.A.C.A. Tech. Memo.* 831.
- 6-18. A. KRONIN and K. MARGUERRE, "Behavior of a Plate Strip Under Shear and Compressive Stresses Beyond the Buckling Limit," *N.A.C.A. Tech. Memo.* 870.
- 6-19. "Static Tests of the Vertical Stiffeners on Plate Girder Beams," *Consolidated Aircraft Corp., Rep.* SG-516.
- 6-20. "The Design of Web Stiffeners for Plate Girder Beams," *Consolidated Aircraft Corp., Rep.* SG-644.
- 6-21. "The Design of the Web System of Plate Girder Beams," *Consolidated Aircraft Corp., Rep.* SG-646.
- 6-22. "Shear Web Tests, Model DC-4," *Douglas Aircraft Co., Rep.* 1831.
- 6-23. "Preliminary Report on Shear Web Test Results," *Vultee Aircraft, Inc., Rep.* 1808.
- 6-24. C. F. GREENE and C. G. BROWN, "The Column Properties of Corrugated Aluminum Alloy Sheet," *Air Corps Tech. Rep.* 3227.
- 6-25. A. EPSTEIN, "The Effect of Artificial Aging on the Tensile and Compressive Properties of Alclad 24SRT Corrugations," *Air Corps Tech. Rep.* 4542.
- 6-26. "Compression Tests of Plain Corrugations and Corrugations with Attached Skin," *Boeing Aircraft Co. Test* 14202.
- 6-27. "Wing Top Corrugations," *Glenn L. Martin Co. Test* 20322.
- 6-28. P. H. KEMMER and S. R. CARPENTER, "Comparative Column Tests of Some Corrugated Stainless Steel Sheets and Corrugated Aluminum Alloy Sheets," *Air Corps Tech. Rep.* 3420.
- 6-29. "Miscellaneous Tests, Model DC-2," *Douglas Aircraft Co., Rep.* 472 and 575.

- 6-30. "The Crippling of Stainless Steel," *Edw. G. Budd Mfg. Co., Aircraft Div., Rep.* 28 and 55.
- 6-31. "Corrugation Panel Tests," *Lockheed Aircraft Corp., Rep.* 1176-1.
- 6-32. "Panel Tests of LS 191 24SRT Alclad Corrugation," *Lockheed Aircraft Corp., Rep.* 1411, 1511, and 1745.
- 6-33. "LS 194 Corrugation Panel Tests," *Lockheed Aircraft Corp., Rep.* 1784.
- 6-34. "LS 193 Corrugation Stresses," *Lockheed Aircraft Corp., Rep.* 1268.
- 6-35. "Compressive Strength of Reinforced Flat Sheets," *Republic Aircraft Corp., Rep.* SR-4.
- 6-36. "Skin Stringer Test," *Edw. G. Budd Mfg. Co., Aircraft Div., Rep.* X-6190.
- 6-37. "Column Properties—Flat Bottom Corrugations—Medium Series," *Douglas Aircraft Co., Rep.* 1812.

CHAPTER 7

PLATES UNDER NORMAL PRESSURE

7-1. Unstiffened Flat Panels

The problem of determining the deflections and stresses of plates subjected to pressures normal to the plane of the plate has concerned structural designers for a number of years. In general it has been possible to classify the plate into one of two limiting classes. The first class is that of thick plates, in which the loads are almost entirely resisted by bending moments induced in the elements of the plate and in which the deflections are small compared to the thickness of the plate. The second classification is that of the very thin plate in which it can be assumed that the plate elements have no bending stiffness and in which the deflection is generally large compared to the plate thickness. Since the analysis of this second class is based on what is known as a membrane theory, such plates will be called membranes in the discussion which follows.

The plates which are used in aircraft structures usually fall in a range which is between the two limits mentioned above, that is, the deflections and stresses cannot be calculated entirely by a consideration of either the thick plate bending theory or the membrane theory alone, but both must be considered together. This regime will be called the thin plate regime. The theoretical treatment of these three regimes will be discussed as parts (a), (b), and (c), respectively, of this section. Unfortunately very few experimental data are available to check the theoretical results; however, wherever possible, an attempt will be made to give the approximate accuracy which can be expected from each of the theoretical treatments.

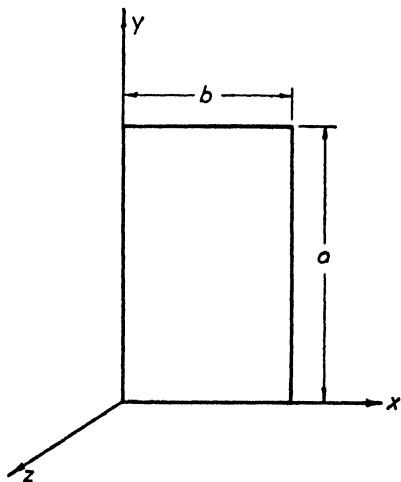


FIG. 7-1. Axis notation.

(a) **Thick Plate Analysis.** A very complete discussion of the theoretical treatment of thick plates under various loading conditions and with different forms of support for the plate edges is given in reference 7.1. In every case, the analysis has resulted in equations similar to those given below for the deflections, moments, and shearing forces of uniformly loaded plates as a function of the applied loading. The assumed reference axes are as shown in Fig. 7.1. For a thick plate loaded with a uniformly distributed lateral pressure the maximum deflection is given by

$$w_{\max} = \alpha \frac{pb^4}{Et^3} \quad [7.1]$$

$$x = \frac{b}{2}, \quad y = \frac{a}{2}$$

The maximum moments in planes parallel to XZ - and YZ -axes, respectively, are

$$M_{x_{\max}} = \beta pb^2 \quad [7.2]$$

$$x = \frac{b}{2}, \quad y = \frac{a}{2}$$

$$M_{y_{\max}} = \beta_1 pb^2 \quad [7.3]$$

$$x = \frac{b}{2}, \quad y = \frac{a}{2}$$

and the maximum shearing forces are

$$Q_{x_{\max}} = \gamma pb \quad [7.4]$$

$$x = \frac{b}{2}, \quad y = \frac{a}{2}$$

$$Q_{y_{\max}} = \gamma_1 pb \quad [7.5]$$

$$x = \frac{b}{2}, \quad y = a$$

The maximum vertical reactive forces along the sides $x = 0, b$ and the sides $y = 0, a$, respectively, are

$$V_{x_{\max}} = \delta pb \quad [7.6]$$

$$x = \frac{b}{2}, \quad y = \frac{a}{2}$$

$$V_{y_{\max}} = \delta_1 pb \quad [7.7]$$

$$x = \frac{a}{2}, \quad y = a$$

and the value of the vertical reaction at the corner of the plate is

$$R = \eta pb^2 \quad [7.8]$$

where p = the uniformly distributed load on the plate in pounds per square inch,

a = the plate length in the Y -direction in inches,

b = the plate width in the X -direction in inches,

E = Young's modulus in pounds per square inch,

which values, when placed in equations 7.1 to 7.8 inclusive, yield deflections in inches, bending moments in inch pounds per inch,

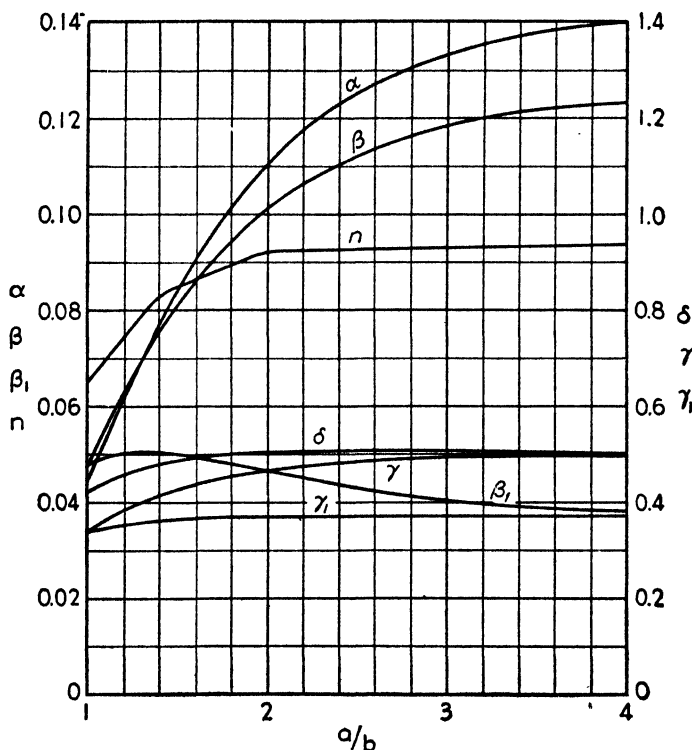


FIG. 7-2. Coefficients for uniformly loaded simply supported plate.

shears in pounds per inch, and corner reactions in pounds. Figure 7.2 gives the values for the coefficients as functions of the a/b ratio of the plate for all four edges simply supported. Figure 7.3 gives the coefficients for the deflections and moments for a uniformly loaded plate having all four edges built in (the data for this figure were taken from reference 7.2). Figure 7.4 contains similar information for a plate with four built-in edges and loaded with a concentrated load at the

center. Reference 7·1 contains numerous other similar data for plates having various edge conditions and types of load distributions.

From the bending moment equations, equations 7·2, 7·3, and the other equations on Figs. 7·3 and 7·4, it is possible to determine the

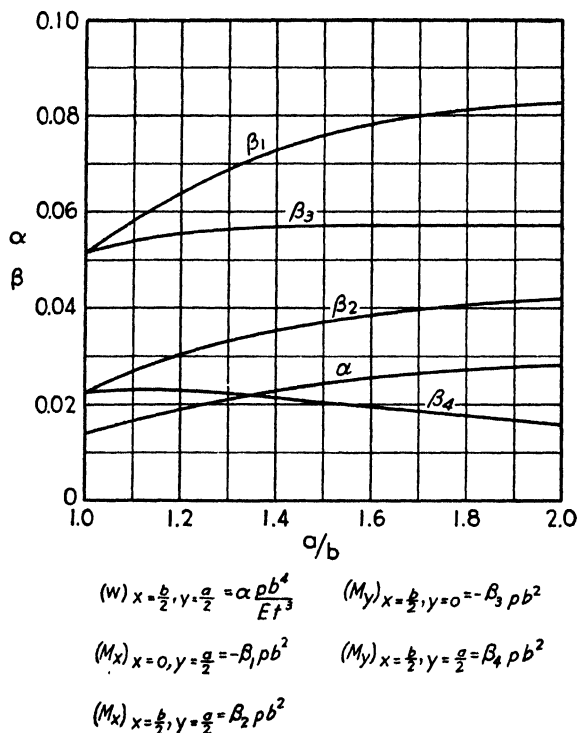


FIG. 7·3. Coefficients for plate having built-in edges and uniformly loaded.

bending stresses from the usual beam equation, $\sigma = Mc/I$. If a unit strip is considered parallel to the X-axis, the moment of inertia is given by

$$I_{yy} = \frac{t^3}{12}$$

and

$$c = \frac{t}{2}$$

thus

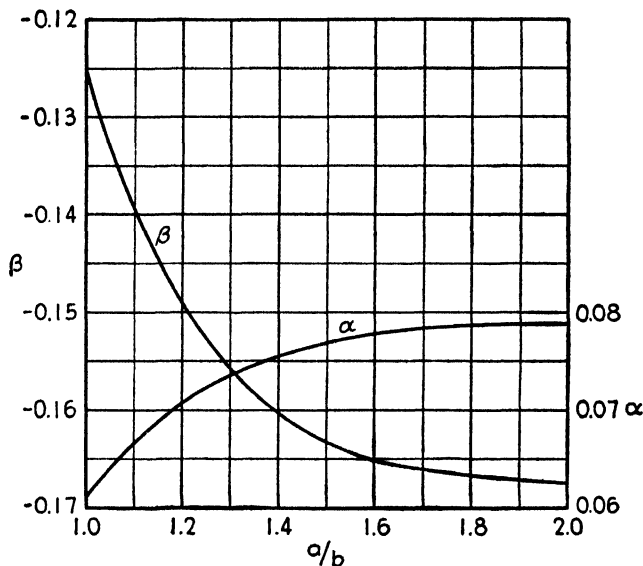
$$\sigma_x = \frac{M_x c}{I_{yy}} = \frac{6M_x}{t^2} \quad [7·9]$$

and similarly

$$\sigma_y = \frac{6M_y}{t^2} \quad [7·10]$$

The value of the shearing stresses can likewise be determined from the equations of shearing force, equations 7.4 and 7.5.

In the derivation of the above equations, it has been assumed that the center plane of the plate is not stressed and that the energy of the external forces is entirely balanced by the bending energies of the deflected plate. In order to meet the assumptions made in this anal-



$$w = \alpha \frac{Pb^2}{Et^3} \quad M = \beta P$$

FIG. 7.4. Coefficients for plate having built-in edges and a concentrated load at the center.

ysis, it is necessary that the deflections of the plate be small compared to the thickness. One author (see reference 7.3) has set the allowable limit of the deflections for validity of the thick plate equations as one-twentieth of the plate thickness although for most engineering problems, the calculated deflections, moments, and stresses are probably sufficiently accurate even though the deflections may reach considerably more than the above figure. The controlling element is whether or not the deflected middle surface is a developable surface or not. If developable, it is only necessary that the deflections be small compared to the width or length of the plate; if not developable, the deflection should be small compared to the thickness.

Limited test data indicate that the thick plate equations as given by Timoshenko (reference 7.1) give reasonable values for the heavier

plates used in aircraft. The item which is chiefly in error is that of the deflection at low loads, since it is very difficult to obtain initially flat plates as structural elements. Therefore, low loads have a tendency to straighten out any initial waviness in the plate causing considerable error in the measured deflections. Measured stresses appear to be in reasonably good agreement with those calculated, at least up to the proportional limit of the materials, and the equations would not be expected to hold beyond that stress value.

(b) Membrane Analysis. For plates which are so thin that they can be considered to have no bending rigidity, the problem is one of determining the deflection and stresses in a flexible membrane under pressure forces. The forces resisting the pressures will be forces in the plane of the membrane and uniformly distributed across its thickness.

The problem of the stresses and deflections in membranes has been treated by Hencky and Föppl (references 7·4 and 7·5) and is summarized by Heubert and Sommer in reference 7·6. There is also a discussion of their work in reference 7·1. Since the equations of Föppl seem to give better agreement with the limited test values over a wider range of pressure and also, since they give larger and therefore more conservative values, it is suggested that they be used for design of such membranes until more accurate test data are available. The equations as derived by Föppl for a rectangular membrane under a uniformly distributed pressure, p , are as follows:

For the deflection in the center of the panel

$$w = n_1 a \sqrt[3]{\frac{pa}{Et}} \quad [7 \cdot 11]$$

$$x = \frac{a}{2}, \quad y = \frac{b}{2}$$

and for the stress in the center of the panel

$$\sigma_x = n_2 \sqrt[3]{p^2 E \frac{a^2}{t^2}} \quad [7 \cdot 12]$$

$$x = \frac{b}{2}, \quad y = \frac{a}{2}$$

$$\sigma_y = n_3 \sqrt[3]{p^2 E \frac{a^2}{t^2}} \quad [7 \cdot 13]$$

$$x = \frac{b}{2}, \quad y = \frac{a}{2}$$

For the stresses in the center of the short sides of the rectangle, the following equations hold:

$$\sigma_x = n_4 \sqrt[3]{p^2 E \frac{a^2}{t^2}} \quad [7.14]$$

$$x = \frac{b}{2}, \quad y = 0, a$$

$$\sigma_y = n_5 \sqrt[3]{p^2 E \frac{a^2}{t^2}} \quad [7.15]$$

$$x = \frac{b}{2}, \quad y = 0, a$$

and for those in the center of the long sides,

$$\sigma_x = n_6 \sqrt[3]{p^2 E \frac{a^2}{t^2}} \quad [7.16]$$

$$x = 0, b; \quad y = \frac{a}{2}$$

$$\sigma_y = n_7 \sqrt[3]{p^2 E \frac{a^2}{t^2}} \quad [7.17]$$

$$x = 0, b; \quad y = \frac{a}{2}$$

where the values of $n_1, n_2 \dots n_7$ are coefficients which are functions of the a/b ratio as given in Fig. 7.5 and the other terms are as previously defined.

The only available experimental information is that plotted in Fig. 7.6, which was taken from reference 7.6. The test specimen used was an aluminum-alloy plate 23.6 by 23.6 in. by 0.055 in. thick. The Young's modulus of the material was 10.5×10^6 lb. per sq. in. and the edges of the plate were clamped. The plate was subjected to a uniform pressure by hydraulic means. The experimental value for the deflection as a function of the pressure is shown in Fig. 7.6 as compared with the theoretical curves of Föppl and Hencky. This figure indicates that, up to a pressure of approximately 30 lb. per sq. in. the deflection given by equation 7.11 is conservative, being very conservative at very low pressures. This effect would be expected, however, since the plate had all four edges clamped and a certain resistance to deflection is introduced by the small but finite bending rigidity of the plate. It is further inter-

esting to note that the theoretical curve of Föppl does not become non-conservative until a pressure which gives a stress of approximately 31,000 lb. per sq. in. in the sheet, which is above the proportional limit of the material. This is also shown by the curve in Fig. 7.6 giving the permanent strain as a function of the pressure.

It is obvious from the results of the one test shown above that for reasonable pressures such as those which are being considered for

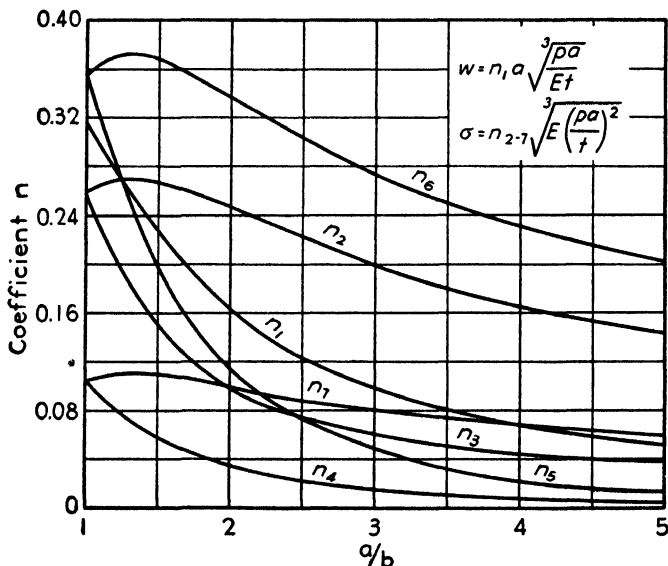


FIG. 7.5. Coefficients for uniformly loaded membrane.

pressurized cabins (5 to 15 lb. per sq. in.) more data are needed as differences of 100 per cent in deflections may be expected between the theoretical and the experimental values. There is also a complete lack of information regarding the effect of plate-stiffening members for either the thick plate or the membrane analysis.

(c) Thin Plate Analysis. When discussing the problems of the thin plate it is first necessary to determine the region covered by this classification. For purposes of analysis it will be assumed that the thick plate equations (equations 7.1 to 7.8, etc.) hold for plate deflections equal to one-fifth of the plate thickness. This is four times the value assumed by Moness (references 7.3 and 7.7); however, limited tests indicate that the thick plate equations will probably hold satisfactorily up to deflections of this order of magnitude. The membrane equations, 7.11 to 7.17 inclusive, will be assumed to be valid when the maximum deflection is equal to or greater than ten times the thick-

ness of the plate. Putting these limiting values into the appropriate equations yields the curves shown in Fig. 7-7. For b/t ratios and pressures, p , which give points below the thick plate curves, the thick plate

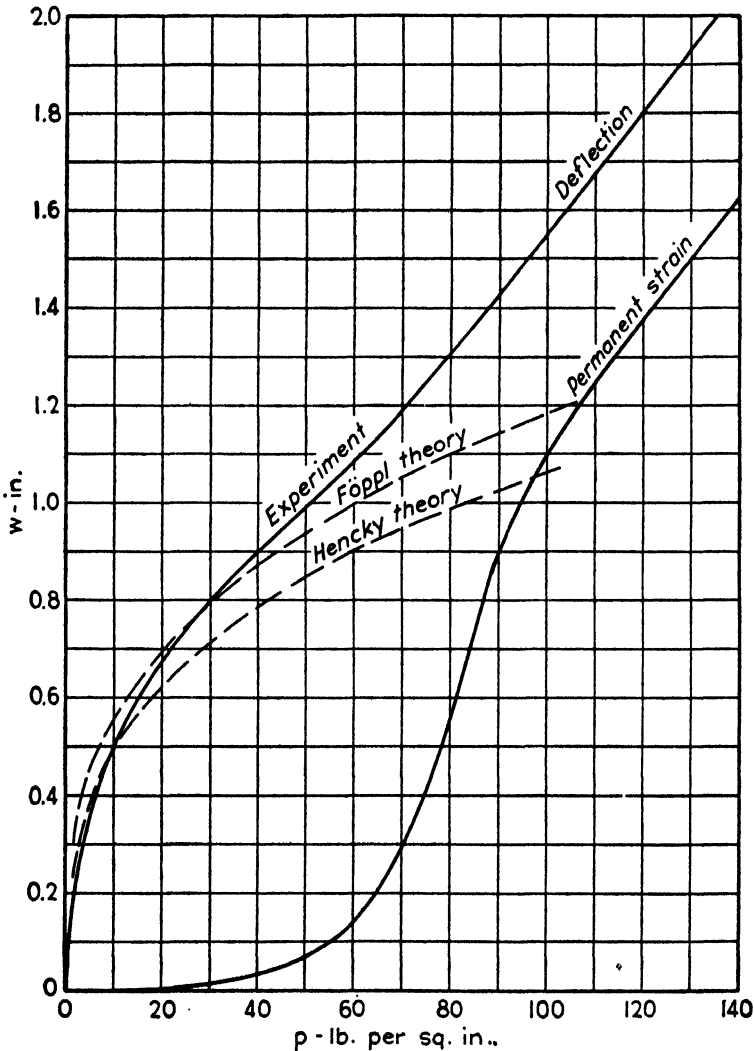


FIG. 7-6. Comparison of membrane theory with experiment.

equations will apply. For plate dimensions and pressures giving points above the appropriate membrane curve, the membrane equations will apply. Between these two regimes is the regime of the thin plates, which unfortunately includes most of the plate dimensions and pressures encountered in aircraft design.

Moness has suggested deflection and maximum stress curves for the region between the thick plate and membrane regime. These curves,

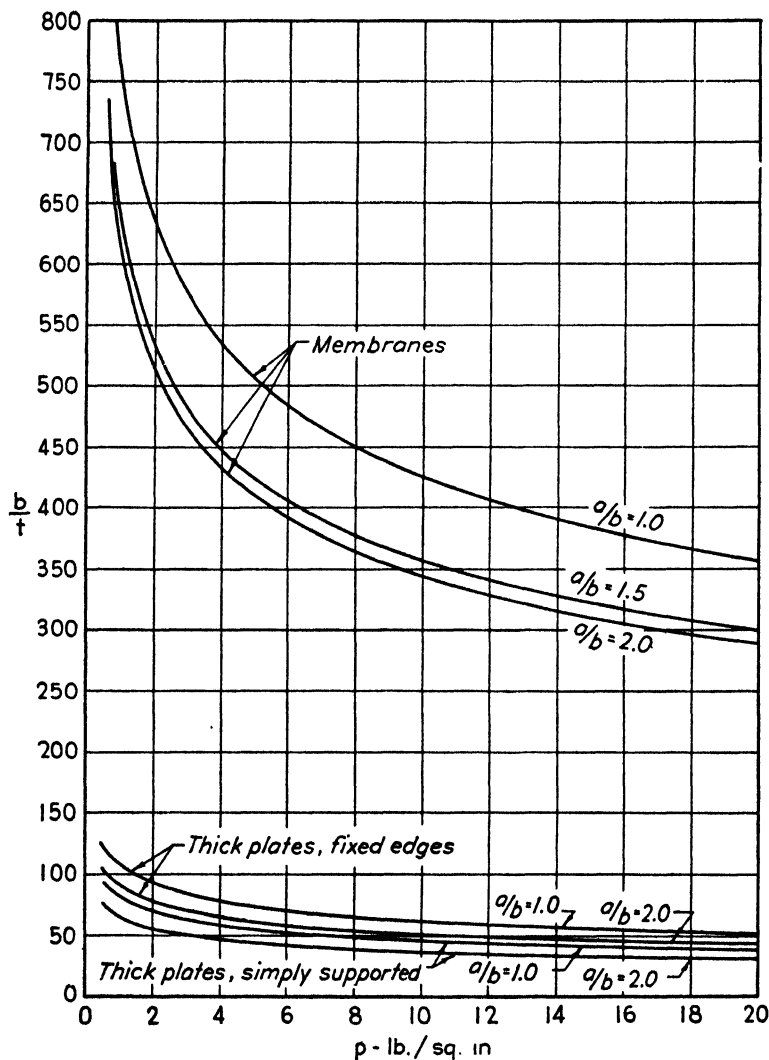


FIG. 7-7. Limiting regions for membrane and thick plate theories.

which are shown in Figs. 7-8 to 7-10 inclusive, are to be used merely to determine trends since they have not been checked experimentally. It is suggested that for any particular structural problem a limited number of tests be made on panels under pressure to determine the stress and deflection level and that the curves be used to determine

the effect of variations in the parameters of the problem. The edge condition coefficient, which has been assumed in the derivation of

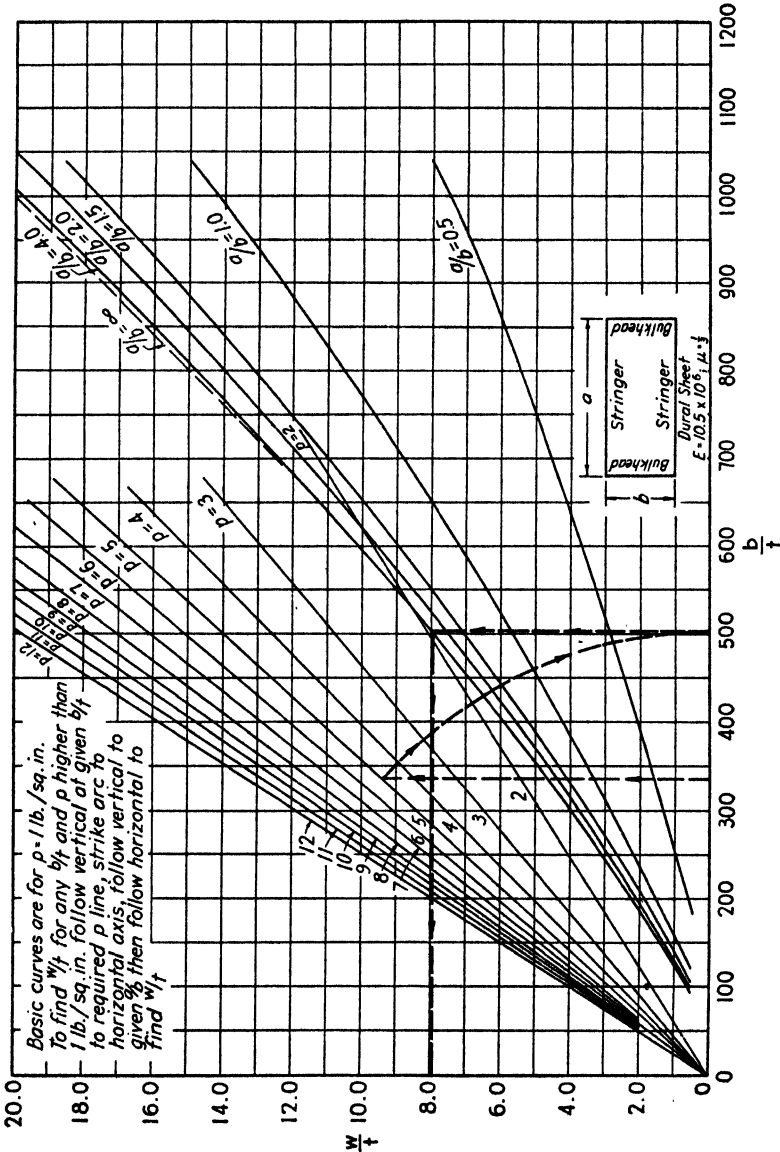


FIG. 7-8. Deflection of thin plates as a function of a/b and b/t .

Figs. 7-8 to 7-10, is an average between that for a simply supported plate and that for a plate with clamped edges.

Figure 7-8 gives the deflection of thin plates as a function of the a/b and the b/t ratios of the plate and the applied pressure. To determine

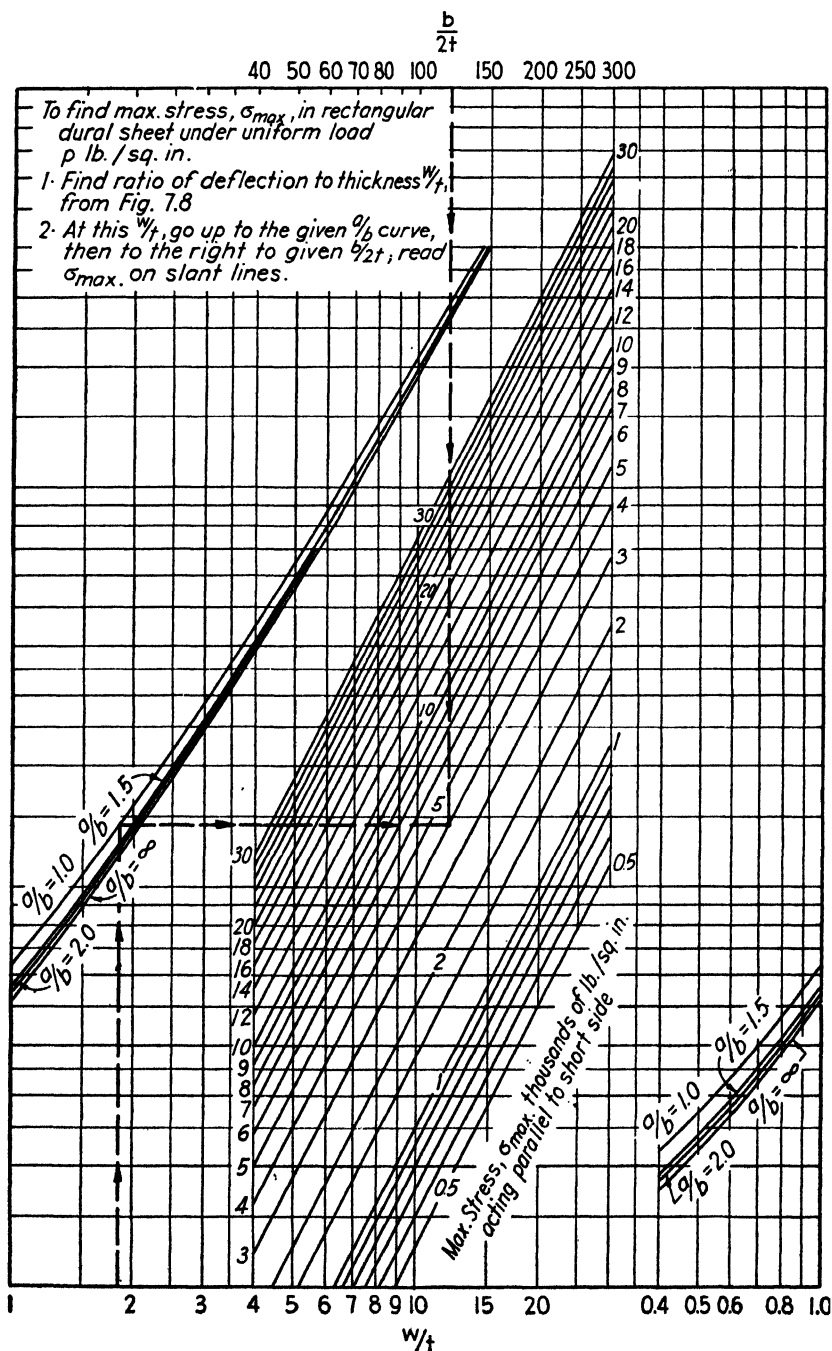


FIG. 7-9. Chart for determining maximum stress parallel to short sides.

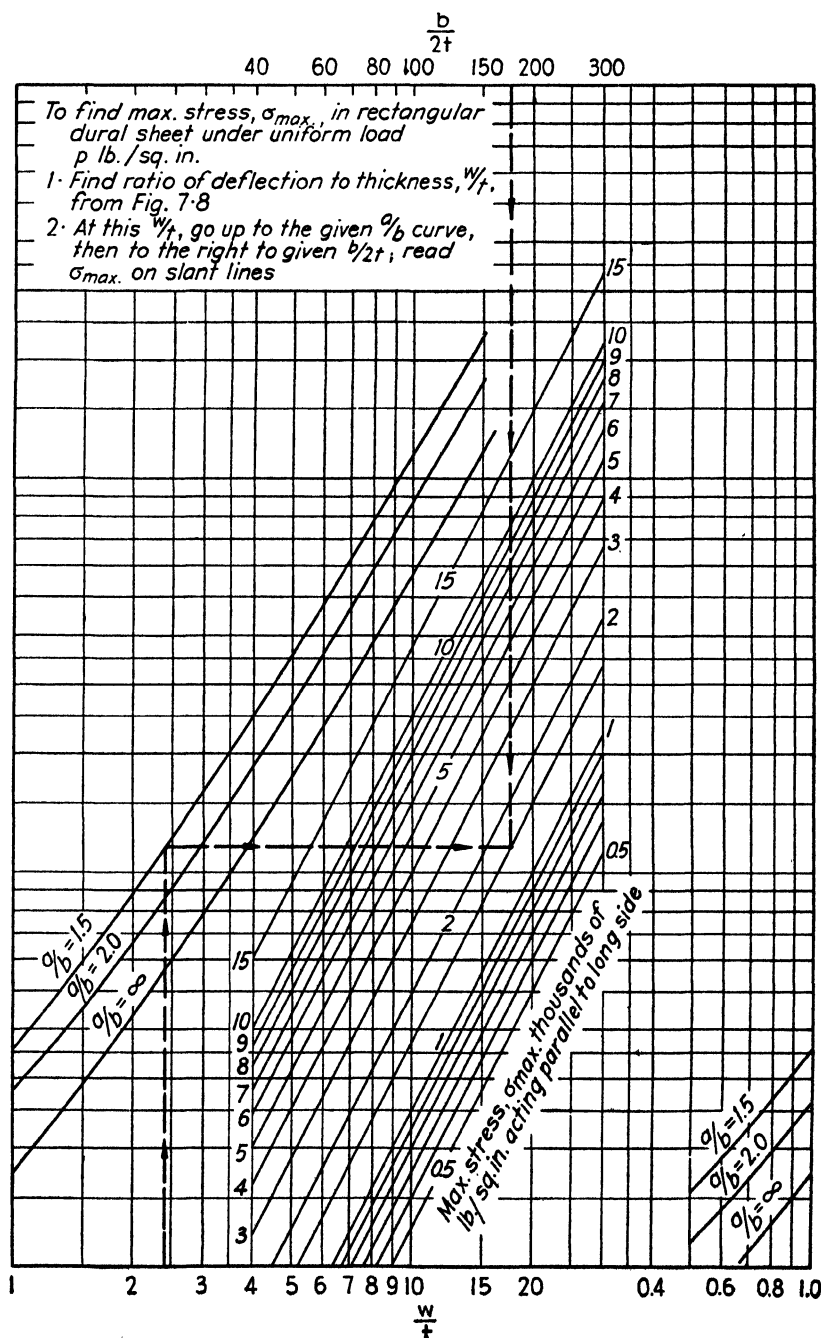


Fig. 7-10. Chart for determining maximum stress parallel to long sides.

the stresses one must first find the w/t ratio from Fig. 7·8 and then enter either Fig. 7·9 or 7·10 depending upon whether it is desired to find the maximum stress parallel to the short sides, or that parallel to the long sides of the plate. In either, the maximum stress occurs in the center of the plate and is a tensile stress made up of a combination of the membrane tensile stress and that due to bending. The transverse stress (that parallel to the short side) is always higher than the longitudinal stress; however, the longitudinal stresses may become important if they are added to stresses arising from loading conditions other than normal pressure.

The designer is again reminded that these curves are as yet not checked by experimental evidence and therefore should be used to indicate trends rather than to give exact deflection and stress values. It must also be realized that the equations developed in this section apply only for plate-edge supports which are infinitely rigid in a direction perpendicular to the plane of the plate. The effect of elastically supported plate edges will be discussed in the next section.

7-2. Stiffened Flat Plates Subjected to Normal Pressure

For large flat areas subjected to normal pressures, it is obvious that some steps must be taken to reduce the deflections of and the stresses in

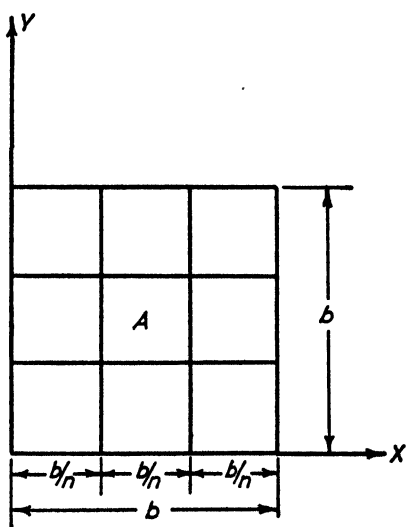


Fig. 7-11. Notation for stiffened square panels.

such surfaces. Increasing the plate thickness may lead to prohibitive weights, therefore the designer would like to know the effect of adding stiffening members to the surface. We shall first consider a square panel, Fig. 7·11, which is divided up into square panels by stringers equally spaced in the two directions. It will be assumed that both pairs of stringers are the same size and are continuous. This last assumption makes it necessary either to put the two sets of stringers on opposite sides of the sheet or to provide adequate clips to carry the stringer stresses across any joints which may be necessary.

It is assumed in the following discussion (which is due to Moness, reference 7·7) that the outer boundaries, $x = 0$, b , and $y = 0$, b , are infinitely rigid as compared to the

stringers and plate. It can be shown that the deflection of the stringers within one span is small compared with the maximum stringer deflection referred to the boundaries and for purposes of analyzing the sheet one can therefore analyze each panel individually as though the stringer in that span were rigid. Thus, for example, the total deflection of the center of panel *A* in Fig. 7·11 would be equal to the sheet deflection calculated as though the boundaries of that panel were rigid, plus the deflection of the stringers forming the panel boundaries.

The load on each stringer is then the vertical component, T_v , of the tension in the sheet, T , Fig. 7·12. Since, for membranes, and also approximately for thin plates, this tension is constant, the value of T_v

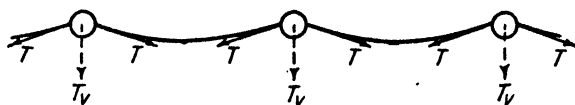


FIG. 7·12. Loads on stiffeners.

is a function of the slope of the sheet from point to point along the stiffener. Thus, it is a maximum at the center of each span and a minimum at the points between the two sets of stringers. Moness assumes a sine wave loading distribution for the stringers and the equations and curves which follow are based on his analysis.

By using the above assumptions, the maximum stringer deflection in a square plate broken up into square panels is given by the equation

$$w_{\max} = \frac{5}{768} \frac{pb^5}{NEI} \quad [7·18]$$

where N = the number of bays along each side,

p = the applied pressure, pounds per square inch,

I = moment of inertia of the stringers, inches.⁴

For aluminum alloys, this reduces to

$$I = 6.31 \times 10^{-10} \frac{p}{N} b^4 \left(\frac{b}{w_{\max}} \right) \quad [7·19]$$

which equation is plotted in Figs. 7·13 and 7·14.

Although equation 7·19 above allows one to choose a stringer that will permit any predetermined value of the maximum deflection, it does not say that the stringer will be strong enough to carry the load imposed upon it. The following equation gives the necessary section modulus for the stringer such that the stress will remain at a given value of σ_{allow} .

$$\frac{I'}{C} = \frac{1}{16} \frac{p}{N} \frac{b^3}{\sigma_{\text{allow}}} \quad [7·20]$$

This equation has been plotted in Figs. 7·15 and 7·16.

The above equations have been based on the assumption that the stringers were pin-ended at the boundaries. If they are completely fixed, the following values hold:

$$\text{For deflection} \quad I_{\text{fixed}} = \frac{1}{5} I_{\text{pinned}} \quad [7.21]$$

$$\text{For stress} \quad \left(\frac{I'}{C}\right)_{\text{fixed}} = \frac{2}{3} \left(\frac{I'}{C}\right)_{\text{pinned}} \quad [7.22]$$

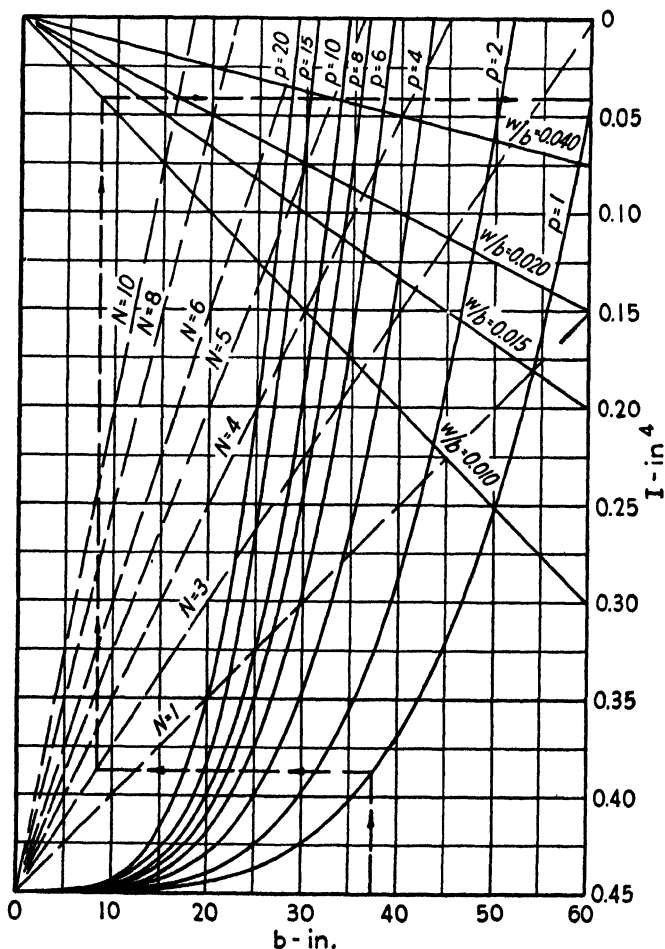


FIG. 7-13. Stiffener moment of inertia—square panels—stiffeners simply supported—deflection limiting.

In a practical design, some factor between these two values will probably be more accurate than either. The exact choice of the factor must lie with the designers' analysis of each specific structure. Actually,

the values of the moment of inertia used above should include any sheet which is rigidly attached to and which would act with any stringer subjected to bending loads.

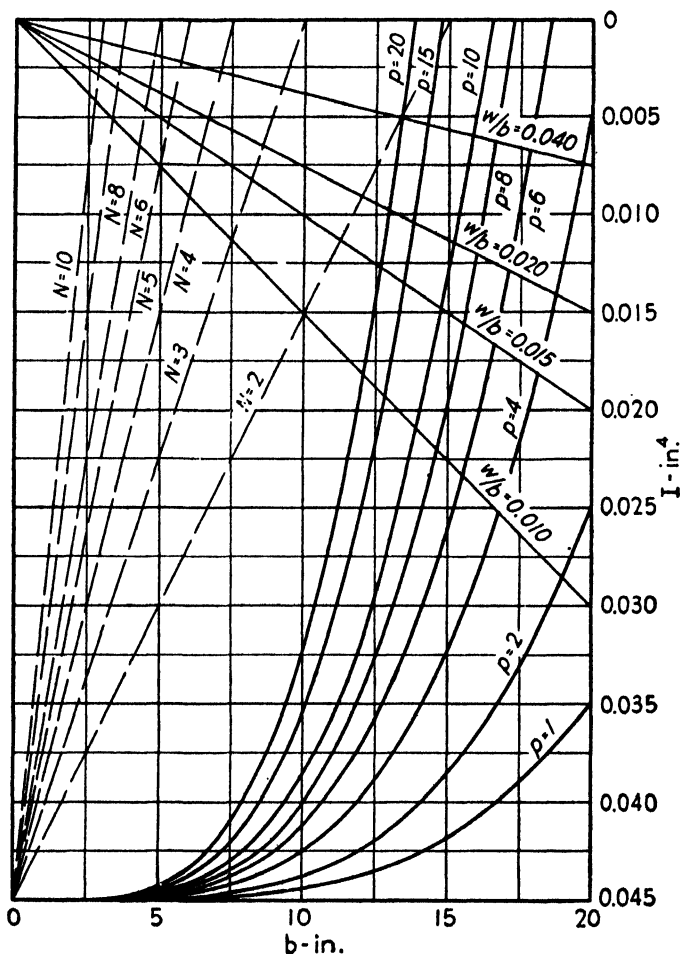


FIG. 7-14. Expanded scale for Fig. 7-13.

The next problem to be considered is that of reinforcing rectangular panels, Fig. 7-17. If it is assumed that the small panels have the same length to width ratio as the main panel, i.e., $a/b = L_a/L_b$, then, if no support is to be given the long stringers by the short ones, as was true for the square panels discussed above, the short stringers must be very much lighter than the long stringers. This becomes obvious when one remembers that the deflection of such a beam is proportional to the fourth

power of the beam length and also, that the loading on the short beam is smaller because the sheet slope is smaller on the short stringers than it is on the long stringers. For example, if $L_a/L_b = 2 = a/b$, then to

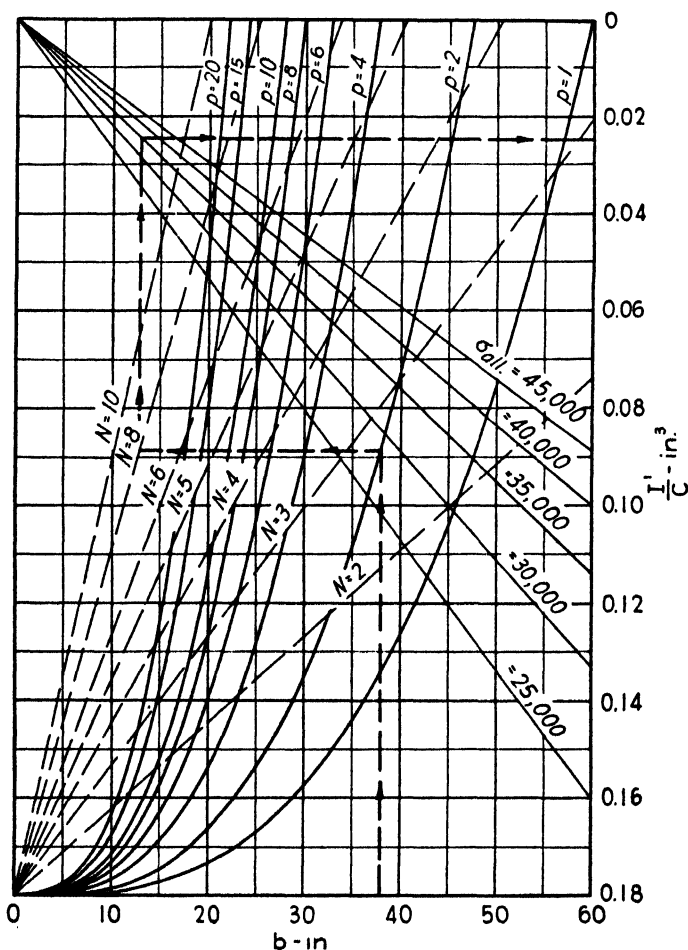


FIG. 7-15. Stiffener moment of inertia. Strength limiting.

have the short stringers deflect as far under load as the long stringers, it can be shown that I_b is of the order of 10 per cent of I_a .

where I_a = moment of inertia of long stringers, and
 I_b = moment of inertia of short stringers.

For the above reason, a different method of analysis is used for the rectangular panels. In this method, it is assumed that the short stringers are approximately the same size as the long stringers and can

therefore be considered to be infinitely rigid as compared with the long stringers. Under this assumption, the deflection of the panel will be only that coming from the deflection of the long stringers between the

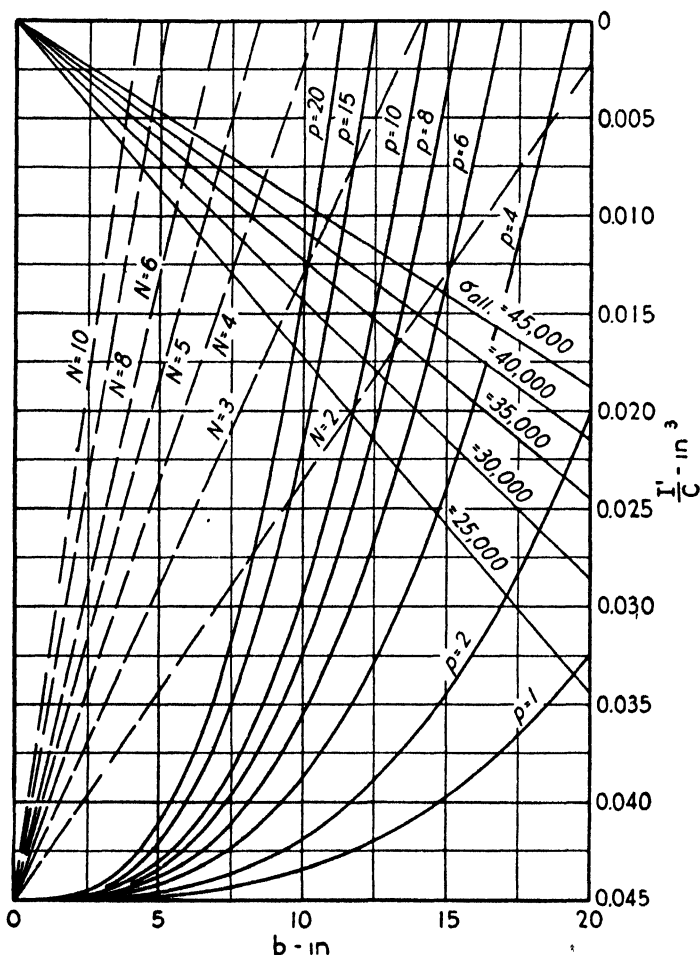


FIG. 7-16. Expanded scale for Fig. 7-15.

short stringers plus the sheet deflection in each bay. If, then, we have the original large panel divided into a number of equal-sized bays, it is necessary only to analyze one bay since all others will be like it, except those bays having one edge on the outer boundary, which bays will have less total deflection and, in general, less stress.

The same assumptions as to loading are made for the rectangular system as was done for the square system. Thus, a long stringer is

analyzed as though it were a beam on a number of supports (the supports being the short stringers) and loaded with a sinusoidal load coming from the vertical component of the sheet tension. Carrying through the analysis, Moness arrives at an equation for the moment

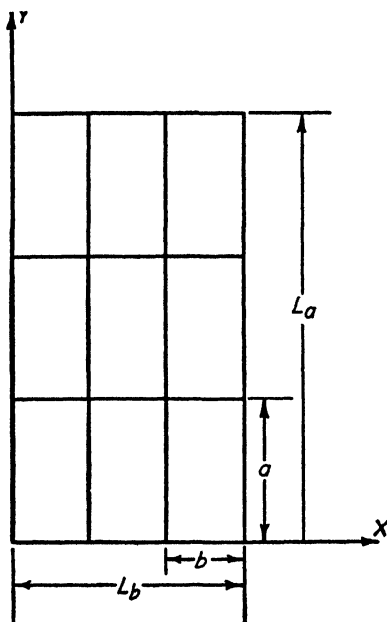


FIG. 7-17. Notation for rectangular panels.

of inertia of the long stringers, based on allowable deflections, of the following form

$$I_a = \frac{1}{2\pi^3 E} a^4 p \frac{a}{w_{st}} \frac{\left(\frac{a}{b} - 0.75\right) \left(\frac{w_{sh}}{w_{total}}\right)^3}{\left[1 + 4 \frac{a}{b} \left(\frac{a}{b} - 0.75\right) \left(\frac{w_{sh}}{w_{total}}\right)^3\right]} \quad [7.23]$$

where w_{st} = maximum deflection of the long stringer between the short stringer,

w_{sh} = sheet deflection measured from lowest point of long stringer,

$w_{total} = w_{sh} + w_{st}$ (see Fig. 7-18.)

To simplify calculations, equation 7.23 is rewritten as

$$I_a = I'_a K \quad [7.23a]$$

where

$$I'_a = \frac{1}{2\pi^3 E} a^4 p \quad [7 \cdot 24]$$

$$K = \frac{a}{w_{st}} \frac{\left(\frac{a}{b} - 0.75\right) \left(\frac{w_{sh}}{w_{total}}\right)^3}{\left[1 + 4 \frac{a}{b} \left(\frac{a}{b} - 0.75\right) \left(\frac{w_{sh}}{w_{total}}\right)^3\right]} \quad [7 \cdot 25]$$

Equations 7·24 and 7·25 are plotted in Figs. 7·19 and 7·20, respectively.

In the above calculation, the fact that the short stringers do have some slight deflection is taken into account by first calculating the long

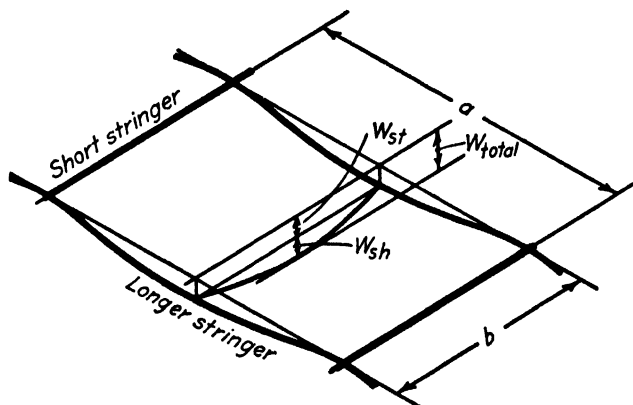


FIG. 7·18. Deflection notation.

stringer deflection on the basis of a pin-ended beam and then dividing the resultant moment of inertia by four. If the long stringer were truly fixed at the short stringer, the divisor would be five and the additional 20 per cent increase in I_a allows for the effect of short stringer deflection. Equation 7·23 above contains the proper factor, i.e., one-fourth.

The long stringers must, of course, be checked for stress. When the relationship between the section modulus, I'_a/c , and the stringer properties is established, the following equation results.

$$\frac{I'_a}{c} = I_a \frac{\pi^2 E w_{st}}{16 \sigma_{allow} a^2} = I'_a K_1 \quad [7 \cdot 26]$$

where $K_1 = 1/c$. Figure 7·21 gives the curves of K_1 as functions of w_{st}/a , a , and σ_{allow} .

For the short stringers, the loading conditions are somewhat different since they carry a sinusoidal load coming from the sheet, plus concentrated loads from the long stringers. If the deflection of the short

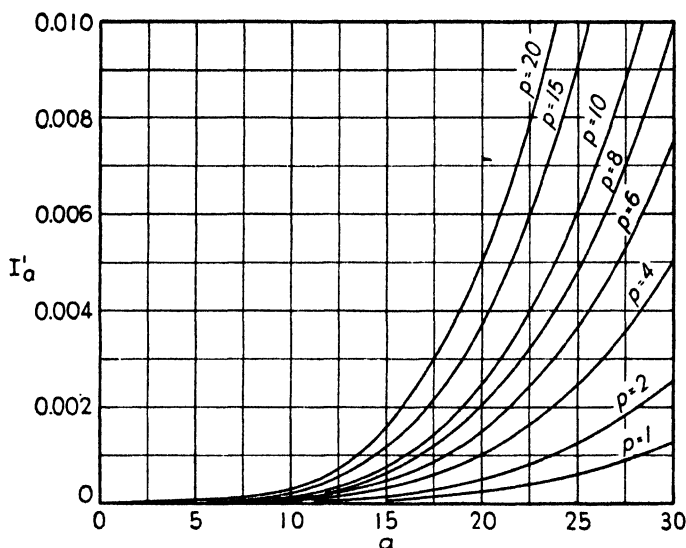


FIG. 7-19. Moment of inertia of long stringer—deflection limiting.

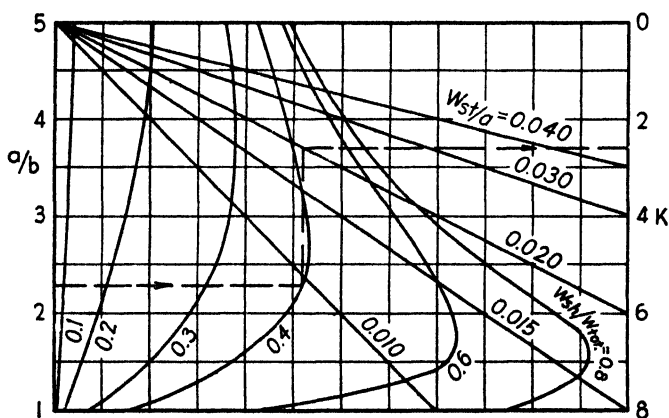


FIG. 7-20. Value of K in equation 7-25.

stringers is restricted to a value equal to w'_a , then the equation of the moment of inertia of the short stringer can be shown to be

$$I_b = \frac{5}{384} \frac{p L_b^5}{w'_a E} \eta \quad [7-27]$$

where η is a function of the a/b ratio and the number of bays into which the short side is divided. I_b is the total width of the short side of the panel. Values of η are plotted in Fig. 7-22. The above equation (equation 7-27) is for pin-ended stringers. If the short stringers are

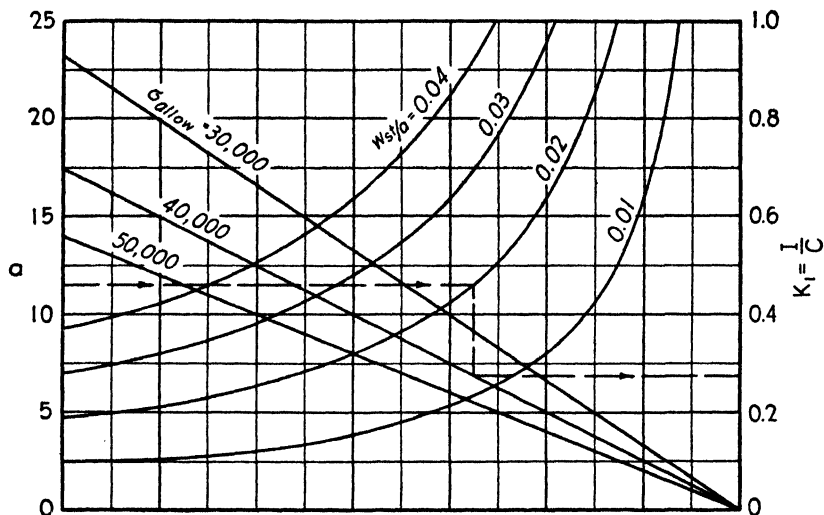


FIG. 7-21. Value of K_1 in equation 7-26.

fixed at the outer boundary, it is suggested that the following relationship be used

$$I_{b_{\text{pinned}}} = 4.5 I_{b_{\text{fixed}}} \quad [7-28]$$

To check the strength of the short stringer, the following equation for the moment of inertia holds

$$I'_b = \frac{48}{5} \frac{E w'_s}{\sigma_{\text{allow}} L_b^2} \mu \quad [7-29]$$

where values of μ are given in Fig. 7-23. Again, the above equation is for pin-ended stringers and, for those with fixed ends at the boundaries, the following equation will hold

$$I'_{b_{\text{fixed}}} = 0.6 I'_{b_{\text{pinned}}} \quad [7-30]$$

The designer is again cautioned that the equations presented in this section are theoretical and have not been entirely checked by experiment. However, they should give reasonable first approximations for the stiffener and sheet sizes, and will definitely give trends as the

parameters involved are changed. Thus, a limited amount of experimental testing plus the curves and equations given above should

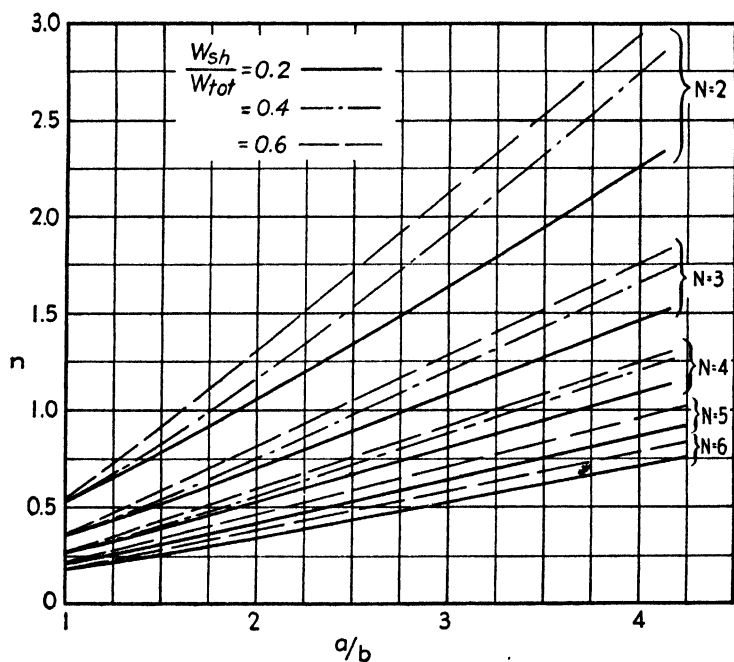


FIG. 7-22. Value of η in equation 7-27.

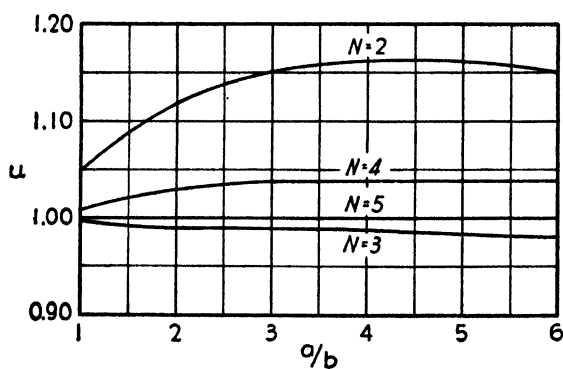


FIG. 7-23. Value of μ in equation 7-29.

provide a designer with fairly accurate information over a considerable range of panel and stiffener sizes.

7-3. Cylindrical Bodies Subjected to Internal Pressure

The problem of bodies subjected to a uniform internal pressure arises in airplanes having the fuselage pressurized for high altitude flying. In such ships, an attempt is made to keep the pressure inside the cabin at a comfortable level for the passengers, no matter how high the airplane may be flying. Thus, there is a pressure differential across the fuselage skin with an internal pressure higher than that outside.

To analyze the effect of this pressure on the structure, one uses the well-known equations for the longitudinal and hoop stress of a cylinder under internal pressure. The longitudinal stress is equal to

$$\sigma_L = \frac{\text{force}}{\text{area}} = \frac{p\pi R^2}{2\pi Rt} = \frac{pR}{2t} \quad [7.31]$$

and the hoop stress is

$$\sigma_h = \frac{2Rp}{2t} = \frac{pR}{t} \quad [7.32]$$

The above equations are those which would result if the fuselage were circular in cross section; however, it is a simple matter to put in the proper factors for other cross-sectional shapes. In fact, for fuselages which are pressurized, a definite attempt is made to keep the cross section circular because that is the shape which any flexible cylinder would take under pressure and, also, because the circular cross section leads to the lowest value of the hoop tension, σ_h .

The stresses given by equations 7.31 and 7.32 must, of course, be combined with any other stresses arising from the normal loading conditions of the fuselage. For example, the total longitudinal skin stress arising from a combination of the pressure stress and the bending stress would be given by the equation

$$\sigma_{LT} = \frac{pR}{2t} \pm \frac{M}{\pi R^2 t} \sin \theta \quad [7.33]$$

where M is the bending moment in the section and θ is the angle around the section measured from the vertical.

Section 7-1 gives equations that will enable the designer to estimate the deflections of the sheet panels of the fuselage since, in general, the radius of curvature of such fuselage sections is so large that individual panels can be assumed to be flat. Similarly section 7-2 gives equations for determining the probable loads that the internal pressures will apply to the stiffeners of the section.

One of the important considerations is the effect of the longitudinal and hoop tensions on sheet joints in the fuselage structure. The additional loads on such joints must be provided for by increasing the joint strength either with larger or more numerous rivets.

For pressurized fuselages having double curvature, the following relationship between the stress and the pressure holds.

$$\frac{\sigma_{Lt}}{R_1} + \frac{\sigma_{ht}}{R_2} = p \quad [7.34]$$

where R_1 = radius of curvature in the longitudinal direction,

R_2 = radius of curvature in the circumferential direction.

As in all stress conditions in which there are a number of stresses acting at one point, the maximum normal stresses and shears should be determined either graphically by the use of Mohr's circle or by the combined stress equations (see Chapter 3).

REFERENCES FOR CHAPTER 7

- 7-1. S. TIMOSHENKO, *Theory of Plates and Shells*, McGraw-Hill, 1940.
- 7-2. T. H. EVANS, "Tables of Moments and Deflections for a Rectangular Plate Fixed on All Edges and Carrying a Uniformly Distributed Load," *J. Ap. Mech.*, Vol. 6, No. 1, March, 1939.
- 7-3. E. MONESS, "Flat Plates Under Pressure," *J. of Aero. Sci.*, Vol. 5, No. 11, September, 1938.
- 7-4. H. HENCKY, "Die Berechnung dünner rechteckiger Platten mit verschwindender Biegungsteifigkeit," *Z. f.a. M.M.* Bd. 1, Heft 2, April 21, 1921.
- 7-5. A. and L. FÖPPL, "Drang und Zwang," Vol. 1, 1924.
- 7-6. M. HEUBERT and A. SOMMER, "Rectangular Shell Plating Under Uniformly Distributed Hydrostatic Pressure," *N.A.C.A. Tech. Memo.*, 965.
- 7-7. "Flat Plates Under Normal Loads," *Douglas Aircraft Co., Rep.*, 1862.
 - Part I, "Deflection of Flat Plates."
 - Part II, "Stresses in Flat Plates."
 - Part III, "Combined Stresses."
 - Part IV, "Reinforcement of Square Plates."
 - Part V, "Reinforcement of Rectangular Plates—Design of Longitudinal Stringers."
 - Part VI, "Reinforcement of Rectangular Plates—Design of Short Stringers."
 - Part VII, "Generalized Type of Reinforcement of Rectangular Plates."

CHAPTER 8

THE ANALYSIS OF CYLINDRICAL STRUCTURES

8-1. Compressive Strength of Thin-Walled, Unstiffened Circular Cylinders and Curved Plates

(a) **General.** A circular cylindrical structure tested under a compressive load acting parallel to its axis may fail in one of three ways. If the cylinder is short and has relatively thick walls, it may fail owing to the stresses passing the ultimate compressive strength of the material. This is a typical material failure and is only a function of the mechanical properties of the material.

If the cylinder is very long, and has a small diameter, failure may take place as a column, the laws of this failure corresponding to those governing one of the types of column failure discussed in Chapter 5. The ultimate strength of such a structure will thus be dependent primarily upon the L/ρ of the section and the Young's modulus of the material.

There is a third type of failure which will be found in structures having dimensions corresponding to those in modern semi-monocoque design. In this case, the cylinder will be comparatively short, of large diameter and thin-walled. For such a structure the failure is one of local instability of the thin section comprising the cylinder walls.

(b) **Buckling of Circular Cylinders.** A number of investigators (see references 8.1 to 8.3 and others) have made theoretical analyses of the problem and all have arrived at an equation for the critical buckling stress of the form

$$\sigma_{cr} = K E t/R \quad [8.1]$$

in which σ_{cr} = critical buckling stress,

t = cylinder wall thickness,

R = cylinder radius,

E = Young's modulus for the material.

The term K is a constant for any given analysis and varies between a value of 0.643 and 0.414 depending upon the buckled wave form chosen for the analytical solution. It is interesting to note that the lowest value, $K = 0.414$ (which shows the best agreement with experimental results), corresponds to a buckled wave form which is never found in

practice. The equation for the critical stress is seen to be independent of length, it being assumed by all of the investigators that the cylinder was long compared to the wave length of the buckles.

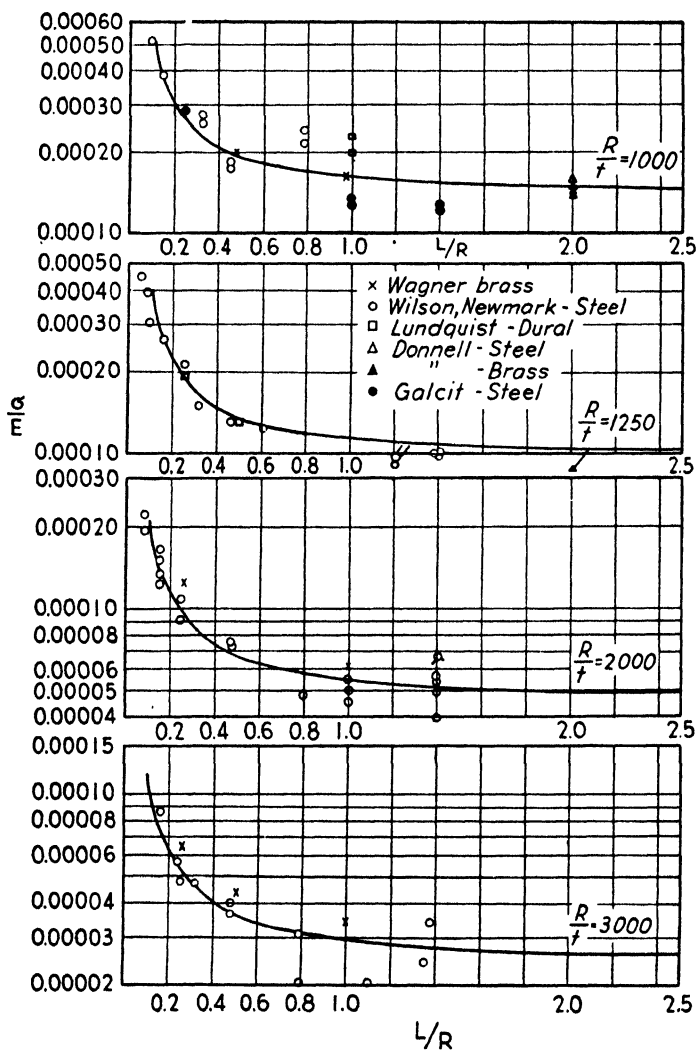


FIG. 8-1. Test results on unstiffened cylinders.

Numerous experiments have been carried out on circular cylinders under axial compression in order to determine empirically the value of K (see references 8-4 to 8-8). All the investigations have shown that K is a function of the R/t ratio of the cylinder, only approaching the theoretical value for very low values of the radius/thickness ratio and

decreasing to a small percentage (15 to 20 per cent) of the theoretical value for very high R/t ratios. Donnell (reference 8·6) attempted to explain the discrepancy between theory and experiment on the basis of the inaccuracies and initial deformations inherent in any experimental test specimen. Subsequent experimental and theoretical research indicates that only a small percentage of the difference between the two values of K can be explained in this manner. Some recent work on the buckling of spherical shells (reference 8·9) indicates that the wave form assumed by previous investigators was not correct, and that it is theoretically possible to obtain a much lower value for K than has been obtained in the past.

Kanemitsu and Nojima (reference 8·10) have experimentally determined the wave pattern at the start of buckling and have verified the conclusions reached above. They have also collected all the available experimental data on circular cylinders under axial compression, added to these data in order to cover not only a large range of R/t ratios but also a large range of L/R ratios, and have proposed an empirical equation for the critical buckling stress. The equation they suggest is

$$\frac{\sigma_{cr}}{E} = 9 \left(\frac{t}{R} \right)^{1.6} + 0.16 \left(\frac{t}{L} \right)^{1.3} \quad [8.2]$$

This equation appears to give satisfactory agreement with the experimentally determined values within the ranges of $500 \leq R/t \leq 3000$, and $0.10 \leq L/R \leq 2.5$, the value of σ_{cr}/E remaining essentially constant for values of L/R greater than 2.5 for a constant value of R/t . The equation has been checked by experiments carried out on brass, dural, and steel cylinders with greatly varying physical dimensions, and it is therefore felt satisfactory for design purposes. Examples of the agreement between equation 8·2 and experimental tests are shown in Fig. 8-1.

Figure 8·2 shows a graphical presentation of equation 8·2 in which σ_{cr}/E is plotted against L/R for constant values of the R/t ratio.

(c) Ultimate Load in Circular Cylinders. Since the theoretical calculations lead to an equation giving the stress at which buckling occurs in an axially loaded cylinder, the question naturally arises as to whether or not it is possible to exceed the buckling stress in such a structure. Experiments show that in all cases of complete cylinders, the load at buckling is also the ultimate load that can be carried by the specimen since the buckling of such specimens is catastrophic in nature, large axial deformations suddenly taking place. Equation 8·2 can therefore be taken as the ultimate stress which a circular cylinder subjected to axial compression can carry.

(d) **Curved Plates Under Axial Compression (Buckling).** Consider a portion of a circular cylinder with simply supported edges (Fig. 8-3) and subjected to a compression stress acting parallel to the elements of the cylindrical surface. This has been treated by Redshaw (reference

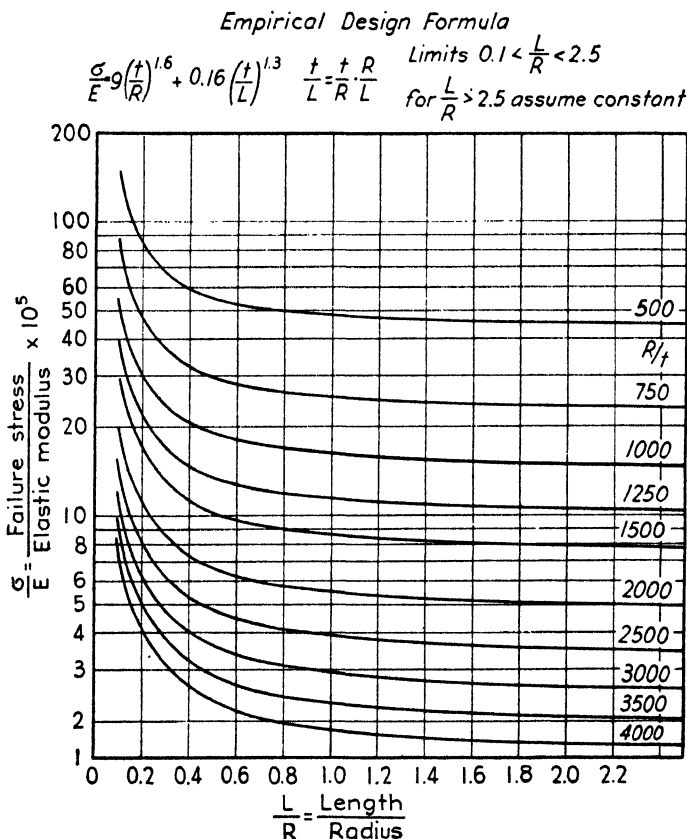


FIG. 8-2. Length effect on critical stress of circular cylinders.

8-11) who arrived at an equation for the critical buckling stress of the form

$$\sigma_{crp} = \frac{E}{6(1 - \mu^2)} \left(\sqrt{12(1 - \mu^2) \frac{t^2}{R^2} + \frac{\pi^4 t^4}{b^4}} + \frac{\pi^2 t^2}{b^2} \right) \quad [8-3]$$

It can be seen that if $(b/t)^2$ is large compared to R/t , the formula reduces to that for the complete cylinder, the form of which is indicated in equation 8-1; and if $(b/t)^2$ is small compared with R/t , the equation reduces to the equation for the buckling stress of the flat plate.

If the first term is multiplied into the bracket, the equation becomes

$$\frac{\sigma_{cr_p}}{E} = \sqrt{\frac{1}{3(1-\mu^2)} \left(\frac{t}{R}\right)^2 + \frac{\pi^4}{36(1-\mu^2)^2} \left(\frac{t}{b}\right)^4} + \frac{\pi^2}{6(1-\mu^2)} \left(\frac{t}{b}\right)^2$$

It can be seen that the first term under the radical is the square of the theoretical value of the σ_{cr}/E ratio for a complete cylinder; the second term is one-fourth of the square of the σ_{cr}/E ratio for a simply supported flat plate, and the last term outside the radical is one-half the σ_{cr}/E ratio for the simply supported flat plate. Thus, the equation can be written

$$\left(\frac{\sigma_{cr}}{E}\right)_p = \sqrt{\left(\frac{\sigma_{cr}}{E}\right)_c^2 + \frac{1}{4}\left(\frac{\sigma_{cr}}{E}\right)_f^2} + \frac{1}{2}\left(\frac{\sigma_{cr}}{E}\right)_f \quad [8.4]$$

where $\left(\frac{\sigma_{cr}}{E}\right)_p$ = buckling stress ratio of the simply supported curved plate,

$\left(\frac{\sigma_{cr}}{E}\right)_c$ = buckling stress ratio of a complete cylinder with an R/t ratio equal to that of the curved plate, and

$\left(\frac{\sigma_{cr}}{E}\right)_f$ = buckling stress ratio of a simply supported flat plate with the same t/b ratio as the curved plate.

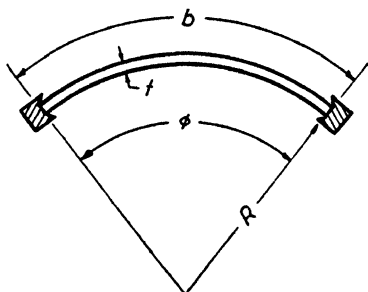


FIG. 8-3.

Inasmuch as the theoretical value of $(\sigma_{cr}/E)_c$ has been proven incorrect by experimental evidence, it is suggested that the value of $(\sigma_{cr}/E)_c$ as given by equation 8.2 be used in the above expression. The theoretical value of $(\sigma_{cr}/E)_f$ is shown by experiments to be correct; therefore this value will be taken from equation 5.19.

Considering a cylindrical panel with a length equal to 2.5 times its radius of curvature, equation 8.4 has been plotted in Fig. 8.4. Values of $(\sigma_{cr}/E)_c$ were taken from Fig. 8.2 for an L/R ratio of 2.5; however, Fig. 8.4 should be reasonably accurate down to L/R values of 1.5 and would under any circumstances be conservative for L/R values less than 2.5. This figure indicates that for t/b ratios greater than 0.02, the effect of curvature on the buckling stress of the panel is very small and can probably be neglected for R/t ratios greater than 750.

Wenzek (reference 8·12) suggests an equation for the critical buckling stress of an edge-supported curved sheet of the form

$$\left(\frac{\sigma_{cr}}{E}\right)_p = \left(\frac{\sigma_{cr}}{E}\right)_f + \left(\frac{\sigma_{cr}}{E}\right)_c \quad [8.5]$$

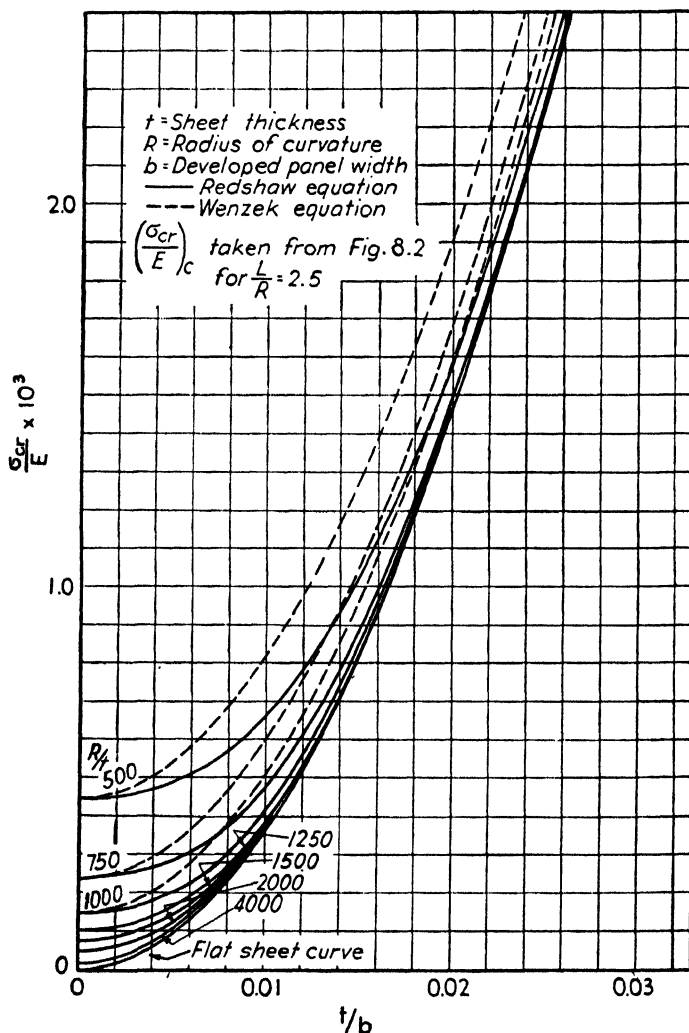


FIG. 8.4. Critical buckling stress for curved sheet panels.

where the notation is the same as that used above. It can readily be seen that this will give higher values of the critical buckling stress for the curved plate than the equation used by Redshaw. Equation 8.5 has been plotted in Fig. 8.4 (dotted curves) and shows a considerable in-

crease in predicted buckling stress, especially for large t/b and small R/t ratios.

Experimental evidence to prove or disprove either of the above equations is very meager. A limited number of test values are given by both Redshaw and Wenzek; however, the panels reported on by Redshaw were stiffened both longitudinally and radially, and those investigated by Wenzek were tested in caisson form in which three panels were tested simultaneously, being joined at their edges by a longitudinal connecting stiffener (see Fig. 8-5).

Since the length of the test specimens in reference 8-11 was not given, and since $(\sigma_{cr}/E)_e$ is dependent upon the L/R ratio, these specimens have not been checked as to agreement with either equation. Table 8-1 shows the dimensions of the specimens tested by Wenzek and the test buckling stresses as compared with the predicted buckling stresses given by equations 8-4 and 8-5. Owing to the type of plate edge support, it has been assumed (as was done by Wenzek) that

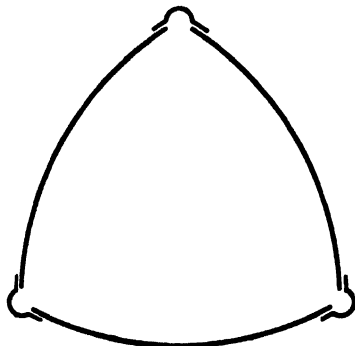


FIG. 8-5. Cross section of test specimen.

$$\left(\frac{\sigma_{cr}}{E}\right)_f = 5 \left(\frac{t}{b}\right)^2 \quad [8-6]$$

rather than to use a constant equal to 3.62 which would correspond to the simply supported case. The first two predicted values are found by considering the value of $(\sigma_{cr}/E)_e$ taken from Fig. 8-2 whereas the last column in the table shows the values predicted by Wenzek using the equation

$$\left(\frac{\sigma_{cr}}{E}\right)_e = 0.3 \frac{t}{R} \quad [8-7]$$

assuming no variation in the constant with either R/t or L/R .

Examination of Table 8-1 shows that both equations 8-4 and 8-5 give predicted values of the critical stress which are much lower than that found experimentally. Agreement is good for very small values of $\varphi = b/R$, but for values of φ greater than 10 degrees the predicted values are only approximately 50 per cent of the test values. On the other hand, the predicted values using the equation

$$\left(\frac{\sigma_{cr}}{E}\right)_e = 0.3 \frac{t}{R}$$

TABLE 8-1

No.	$\varphi^\circ = b/R$	R (in.)	L (in.)	b (in.)	t (in.)	L/b	R/t	b/t	L/R	$\left(\frac{\sigma_{cr}}{E}\right)_f \times 10^5$	$\left(\frac{\sigma_{cr}}{E}\right)_c \times 10^5$	Red- shaw $\left(\frac{\sigma_{cr}}{E}\right)^n \times 10^5$	Wenzek $\left(\frac{\sigma_{cr}}{E}\right)^p \times 10^5$	Test $\left(\frac{\sigma_{cr}}{E}\right)^p \times 10^5$	$K = 0.3 \left(\frac{\sigma_{cr}}{E}\right)_c \times 10^5$	$K = 0.3 \left(\frac{\sigma_{cr}}{E}\right)^p \times 10^5$
1	2.5	161.4	18.7	7.4	0.0400	2.53	4040	185	0.116	14.61	6.94	17.37	21.55	21.05	7.43	22.04
2	5.0	97.6	21.7	8.5	0.0315	2.55	3100	270	0.222	6.86	5.60	10.00	12.46	16.27	9.68	16.54
3	8.5	70.9	22.7	10.6	0.0244	2.14	2910	434	0.320	2.65	4.79	6.30	7.44	10.24	10.31	12.96
4	13.0	40.6	23.0	9.2	0.0319	2.50	1270	288	0.566	6.03	12.81	16.18	18.84	35.40	23.62	29.65
5	13.0	47.3	25.9	10.6	0.0165	2.44	2870	642	0.548	1.21	3.76	4.41	4.97	12.53	10.45	11.66
6	19.5	20.9	17.7	7.1	0.0283	2.49	740	251	0.847	7.94	26.80	31.06	34.74	53.59	40.54	48.48
7	30.0	21.3	27.6	11.0	0.0142	2.51	1500	775	1.296	0.83	8.30	8.73	9.13	18.18	20.00	20.83
8	30.0	22.4	27.6	11.8	0.0205	2.34	1090	576	1.232	1.51	13.80	14.58	15.31	30.62	27.52	29.03
9	65.0	11.4	32.3	13.0	0.0177	2.48	640	734	2.833	0.93	30.22	30.68	31.15	63.16	46.87	47.80
10	66.0	9.8	27.6	11.3	0.0197	2.44	500	574	2.816	1.52	44.73	45.52	46.25	78.47	60.00	61.52
11	113.0	7.0	33.8	13.8	0.0161	2.45	430	857	4.829	0.68	56.88	57.22	56.56	76.55	69.77	70.45

show reasonable agreement throughout the range of specimens tested. This may or may not be accidental since it has been definitely proven that for a complete cylinder a constant value of K is non-conservative for L/R values greater than about 0.4 for all values of R/t . The only real conclusions that can be drawn from this limited number of tests are:

1. Equations 8.4 and 8.5, using equation 8.2 for $(\sigma_{cr}/E)_c$, will give conservative estimates of the buckling stress of supported circular plates, equation 8.4 giving the most conservative values.

2. Considerably more test work must be carried out before any definite statement can be made as to the validity of any method of predicting the buckling stress for such cylindrical plates, and

3. It is felt that the equation $(\sigma_{cr}/E)_c = 0.3 t/R$ should be used with caution even though it shows good agreement with experiment in this particular use.

(e) Ultimate Compressive Strength of Curved Plates. Unlike the complete cylinder, it might be expected that a curved plate with supported edges would carry a considerable amount of load beyond that causing buckling. This conclusion would be drawn from considerations similar to those applying to edge-supported flat plates tested under compression in which the ultimate load they can carry is higher than the buckling load because the supported edges can be loaded to stresses above the buckling stress. In other words, the primary question is whether or not the effective width method of analysis will apply to curved sheets as well as to flat plates.

From physical reasoning it would be expected that for curved plates in which there was little curvature, i.e., R large, the results would approach those for flat plates; and for curved plates in which b/R approached 2π , the complete cylinder, the results would approach those for complete cylinders under compression. As will be shown later, tests confirm these conclusions.

The method shown below for calculating the ultimate load-carrying ability of simply supported curved plates under axial compression is essentially based on the above considerations and upon physical analogy. It checks reasonably well with the few tests which are available; however, it is felt that much more experimental and theoretical work is necessary before the question of the ultimate strength of such structural elements can be considered solved. The basic assumptions made are:

1. That the edges carry a stress equal to the yield-point stress distributed over an effective width found from the lower, or failure, curve of Fig. 6.2. This essentially assumes that the edges act as the supported edges of a flat plate under its ultimate load. In using Fig. 6.2 $\sigma_{ee} = \sigma_{yp}$

and σ_{cr} = the buckling stress of a flat panel of the same developed width as the curved panel, or

$$\sigma_{cr} = 3.62E \left(\frac{t}{b} \right)^2$$

2. That the center of the panel, of width equal to $(b - 2w_e)$ carries the critical buckling stress of a circular cylinder having the same thickness and radius as the panel. This stress is found from equation 8·2 and Fig. 8·2. The equation of the total load is then of the form

$$P_{\text{total}} = 2w_e t \sigma_{yp} + (b - 2w_e) t \sigma_{cr_c} \quad [8\cdot8]$$

A number of tests made at Massachusetts Institute of Technology have been checked by equation 8·8 with the results shown in Table 8·2. The first specimen has been calculated in detail to show the method.

Example.

$$t = 0.020 \text{ in.} \quad b = 12 \text{ in.} \quad R = 30 \text{ in.} \quad L = 6 \text{ in.}$$

$$\sigma_{\sigma_f} = 3.62E(t/b)^2 = 3.62 \times 10^7 \times (0.020/12)^2 = 100 \text{ lb. per sq. in.}$$

$$\sigma_{sc}/\sigma_{\sigma_f} = \sigma_{yp}/\sigma_{\sigma_f} = 36,000/100 = 360$$

$$w_e/b = 0.026 \text{ from Fig. 6.2}$$

$$w_e = 0.026 \times 12 = 0.312 \text{ in.}$$

Load carried by the edges

$$P_e = 2 \times 0.312 \times 36,000 \times 0.020 = 450 \text{ lb.}$$

$$R/t = 30/0.020 = 1500 \quad L/R = 6/30 = 0.20$$

$$\sigma_{cr_c} = 17.0 \times 10^{-5} \times E = 1700 \text{ lb. per sq. in. from Fig. 8.2}$$

$$b - 2w_e = 12 - 0.624 = 11.376 \text{ in.}$$

Load carried by the center

$$P_c = 11.376 \times 1700 \times 0.020 = 387 \text{ lb.}$$

Total load carried by the panel

$$P_{\text{total}} = 450 + 387 = 837 \text{ lb.}$$

as compared with a test load of 950 lb., a difference of 12 per cent. This method has been used on all the specimens in Table 8·2. The agreement between predicted and test values is good throughout; particularly so since the value of E and σ_{yp} were assumed constant equal to 10^7 lb. per sq. in. and 36,000 lb. per sq. in., respectively, and nominal thicknesses were used for the sheets.

Using equation 8.8, a graphical method of determining the ultimate load has been established resulting in the curves of Fig. 8.6. The failure curve of Fig. 6.2 has been approximated by the equation

$$\frac{w_e}{b} = 0.3 \left(\frac{\sigma_{yp}}{\sigma_{crf}} \right)^{-0.4}$$

which holds very well throughout the useful design range. To calculate the curves in Fig. 8.6, values of $\sigma_{yp} = 36,000$ lb. per sq. in. and $E =$

$$E = 10^7 \text{ lb./sq. in.}$$

$$\sigma_{yp} = 36,000 \text{ lb./sq. in.}$$

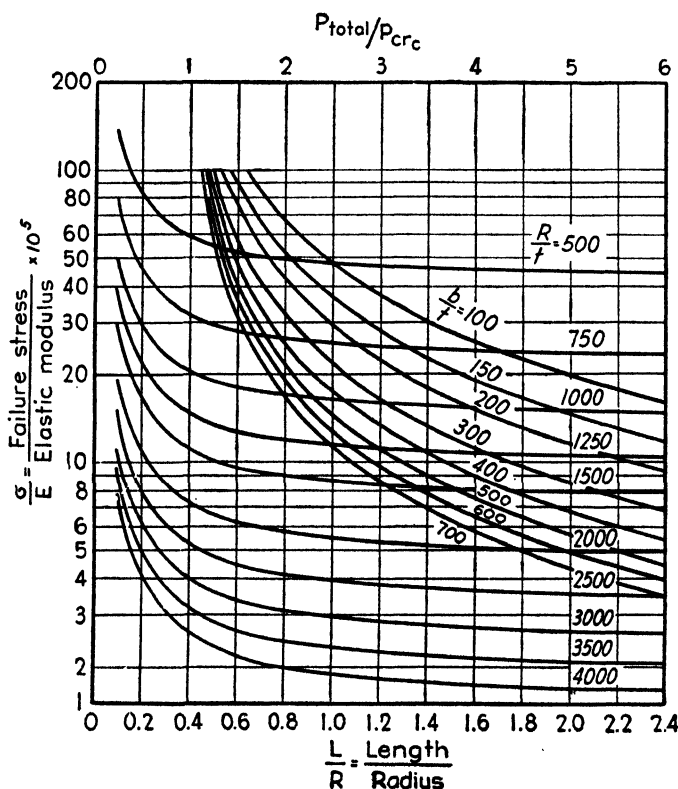


FIG. 8.6. Ultimate load of a simply supported curved sheet panel.

10.4×10^6 lb. per sq. in. have been used. The final equation is of the form

$$\frac{P_{total}}{P_{cr_e}} = 1.0 + \left(\frac{t}{b} \right)^{0.8} \left(\frac{\sigma_{yp}}{E} \right)^{0.6} \left(\frac{E}{\sigma_{cr_e}} - \frac{E}{\sigma_{yp}} \right) \quad [8.9]$$

TABLE 8.2

t (in.)	b (in.)	R (in.)	L (in.)	R/t	t/b	L/R	σ_{rc} (lb./sq. in.)	σ_{cr} (in.)	$\frac{\sigma_{yp}}{\sigma_{cr}}$	w_e (in.)	$b - 2w_e$ (in.)	P_e (lb.)	P_c (lb.)	P_{total} (lb.)	P_{test} (lb.)
0.020	12	30	6	1,500	0.00167	0.20	1,700	100	360.0	0.312	11.376	450	387	837	950
0.020	12	30	12	1,500	0.00167	0.40	1,130	100	360.0	0.312	11.376	450	257	707	701
0.020	12	30	18	1,500	0.00167	0.60	970	100	360.0	0.312	11.376	450	221	671	620
0.020	12	30	6	1,000	0.00167	0.30	2,370	100	360.0	0.312	11.376	450	539	989	1,145
0.020	12	20	12	1,000	0.00167	0.60	1,820	100	360.0	0.312	11.376	450	414	864	1,000
0.020	12	20	18	1,000	0.00167	0.90	1,600	100	360.0	0.312	11.376	450	378	828	735
0.020	12	20	6	500	0.00167	0.60	5,220	100	360.0	0.312	11.376	450	1,186	1,636	1,910
0.020	12	10	12	500	0.00167	1.20	4,700	100	360.0	0.312	11.376	450	1,070	1,520	1,850
0.020	12	10	18	500	0.00167	1.80	4,520	100	360.0	0.312	11.376	450	1,027	1,477	1,485
0.020	3	30	6	1,500	0.00667	0.20	1,700	1,610	22.3	0.264	2.472	380	84	464	540
0.020	3	30	12	1,500	0.00667	0.40	1,130	1,610	22.3	0.264	2.472	380	56	436	490
0.020	3	30	18	1,500	0.00667	0.60	970	1,610	22.3	0.264	2.472	380	48	428	420
0.020	3	20	6	1,000	0.00667	0.30	2,370	1,610	22.3	0.264	2.472	380	117	497	570
0.020	3	20	12	1,000	0.00667	0.60	1,820	1,610	22.3	0.264	2.472	380	90	477	540
0.020	3	20	18	1,000	0.00667	0.90	1,660	1,610	22.3	0.264	2.472	380	82	462	440
0.020	3	10	6	500	0.00667	0.60	5,220	1,610	22.3	0.264	2.472	380	288	638	795
0.020	3	10	12	500	0.00667	1.20	4,700	1,610	22.3	0.264	2.472	380	232	612	650
0.020	3	10	18	500	0.00667	1.80	4,520	1,610	22.3	0.264	2.472	380	224	604	525
0.033	12	30	6	910	0.00275	0.20	3,500	274	131.4	0.504	10.992	1,200	1,269	2,469	2,590
0.033	12	30	12	910	0.00275	0.40	3,410	274	131.4	0.504	10.992	1,200	875	2,075	2,100
0.033	12	30	18	910	0.00275	0.60	2,100	274	131.4	0.504	10.992	1,200	762	1,962	1,980
0.033	12	20	6	606	0.00275	0.30	5,020	274	131.4	0.504	10.992	1,200	1,820	3,020	3,635
0.033	12	20	12	606	0.00275	0.60	3,920	274	131.4	0.504	10.992	1,200	1,420	2,600	3,370
0.033	12	20	18	606	0.00275	0.90	3,620	274	131.4	0.504	10.992	1,200	1,314	2,514	2,760
0.033	12	10	6	303	0.00275	0.60	11,490	274	131.4	0.504	10.992	1,200	4,165	5,365	6,580
0.033	12	10	12	303	0.00275	1.20	10,400	274	131.4	0.504	10.992	1,200	3,770	4,970	6,085
0.033	12	10	18	303	0.00275	1.80	10,090	274	131.4	0.504	10.992	1,200	3,660	4,860	5,324

0.033	3	30	6	910	0.0110	0.20	3,500	4,380	8.22	0.393	2.606	935	301	1,236	1,210
0.033	3	30	12	910	0.0110	0.40	2,410	4,380	8.22	0.393	2.606	935	207	1,142	1,110
0.033	3	30	18	910	0.0110	0.60	2,100	4,380	8.22	0.393	2.606	935	181	1,116	1,040
0.033	3	20	6	606	0.0110	0.30	5,020	4,380	8.22	0.393	2.606	935	432	1,367	1,420
0.033	3	20	12	606	0.0110	0.60	3,920	4,380	8.22	0.393	2.606	935	337	1,272	1,300
0.033	3	20	18	606	0.0110	0.90	3,620	4,380	8.22	0.393	2.606	935	312	1,247	1,180
0.033	3	10	6	303	0.0110	0.60	11,490	4,380	8.22	0.393	2.606	935	988	1,923	1,905
0.033	3	10	12	303	0.0110	1.20	10,400	4,380	8.22	0.393	2.606	935	894	1,829	1,725
0.033	3	10	18	303	0.0110	1.80	10,090	4,380	8.22	0.393	2.606	935	868	1,803	1,355
0.051	12	30	6	588	0.00425	0.20	6,590	654	55.1	0.744	10.512	2,730	3,535	6,265	6,750
0.051	12	30	12	588	0.00425	0.40	4,660	654	55.1	0.744	10.512	2,730	2,500	5,230	5,925
0.051	12	30	18	588	0.00425	0.60	4,120	654	55.1	0.744	10.512	2,730	2,210	4,940	5,045
0.051	12	20	6	392	0.00425	0.30	9,620	654	55.1	0.744	10.512	2,730	5,165	7,895	9,060
0.051	12	20	12	392	0.00425	0.60	7,700	654	55.1	0.744	10.512	2,730	4,130	6,860	8,000
0.051	12	20	18	392	0.00425	0.90	7,160	654	55.1	0.744	10.512	2,730	3,840	6,570	6,815
0.051	12	10	6	196	0.00425	0.60	22,530	654	55.1	0.744	10.512	2,730	12,090	14,820	14,900
0.051	12	10	12	196	0.00425	1.20	20,600	654	55.1	0.744	10.512	2,730	11,050	13,780	12,310
0.051	12	10	18	196	0.00425	1.80	20,060	654	55.1	0.744	10.512	2,730	10,760	13,490	13,265
0.051	3	30	6	588	0.0170	0.20	6,590	10,450	3.45	0.552	1.896	2,030	637	2,667	2,550
0.051	3	30	12	588	0.0170	0.40	4,660	10,450	3.45	0.552	1.896	2,030	451	2,481	2,160
0.051	3	30	18	588	0.0170	0.60	4,120	10,450	3.45	0.552	1.896	2,030	398	2,428	2,050
0.051	3	20	6	392	0.0170	0.30	9,620	10,450	3.45	0.552	1.896	2,030	931	2,961	3,135
0.051	3	20	12	392	0.0170	0.60	7,700	10,450	3.45	0.552	1.896	2,030	745	2,775	2,765
0.051	3	20	18	392	0.0170	0.90	7,160	10,450	3.45	0.552	1.896	2,030	692	2,722	2,255
0.051	3	10	6	196	0.0170	0.60	22,530	10,450	3.45	0.552	1.896	2,030	2,180	4,210	5,000
0.051	3	10	12	196	0.0170	1.20	20,600	10,450	3.45	0.552	1.896	2,030	1,990	4,020	3,820
0.051	3	10	18	196	0.0170	1.80	20,060	10,450	3.45	0.552	1.896	2,030	1,935	3,965	2,900

Note: σ_{pp} = 36,000 lb. per sq. in.; E = 10×10^6 lb. per sq. in. (assumed for all calculations).

where P_{total} = total axial compression load that can be carried by a simply supported curved panel;

P_{cr_c} = load carried by a curved panel at buckling, assuming that the curved panel will buckle at the same load as a complete cylinder of the same wall thickness and radius. Found from equation 8-2 and Fig. 8-2.

The other terms have been previously defined. Thus, Fig. 8-6 gives immediately the value of $P_{\text{total}}/P_{cr_c}$ from the known dimensions of the panel. This curve may be modified as additional test data are made available; however, on the basis of the agreement shown in Table 8-2, it would seem to give reasonable and conservative results for dural specimens within the limits covered. It will be noticed that $P_{\text{total}}/P_{cr_c}$ approaches 1.0 for large b/t and small L/R ratios, corresponding to large b and small R values, which would indicate an approach towards a complete cylinder.

Wenzek (reference 8-12) gives another equation for calculating the ultimate load for curved plates. His equation, however, gives predicted values of the ultimate load which are not even of the same order of magnitude as those found in the Massachusetts Institute of Technology tests and has therefore not been discussed here.

8-2. Stiffened Cylinders under Compression

There are very few data on complete stiffened cylinders tested under axial compression loads. Most of the experimentation has been carried out on cylinders under bending and this problem will be discussed in section 8-3. A few systematic series of axial compression tests on complete cylinders with axial and circumferential stiffeners would be of great value in correlating the stiffened panel data which will be discussed in the remainder of this section.

For stiffened curved plates under compression we will consider such a curved plate having stiffeners parallel to its axis and subjected to a compression load acting parallel to the stiffeners. The problem will be to determine the compression load which will cause complete failure of the plate and its stiffeners. To do this, a method will be used which is essentially the same as that used in section 8-1 for determining the ultimate compressive strength of unstiffened curved plates, that is, an effective width of sheet, $2w_e$, based on the critical column stress of the stiffener will be calculated from the flat panel effective width curve, Fig. 6-2. The allowable column stress, σ_{co} , for the stiffener plus its effective width of sheet will then be calculated with the use of Fig. 6-15

and the effective column area (stiffener plus sheet) will be assumed to carry this stress. The center of the sheet, of width $(b - 2w_e)$, will be assumed to carry the critical buckling stress of a curved plate, σ_{cr_c} , which can be found from Fig. 8.2 knowing the R/t and L/R ratios of

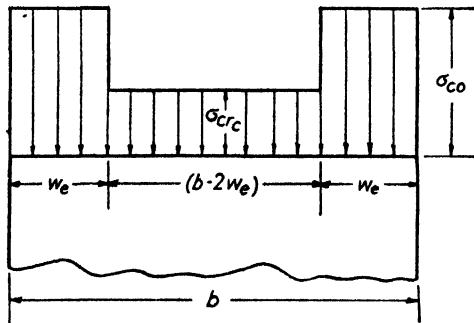


FIG. 8.7. Stress distribution $\sigma_{cr_c} > \sigma_{co}$.

the panel. However, if σ_{cr_c} is higher than σ_{co} , it will be assumed that σ_{co} will apply across the entire panel. See Figs. 8.7 and 8.8.

A number of curved, stiffened panels have been tested at Massachusetts Institute of Technology (reference 8.13) and the test loads have

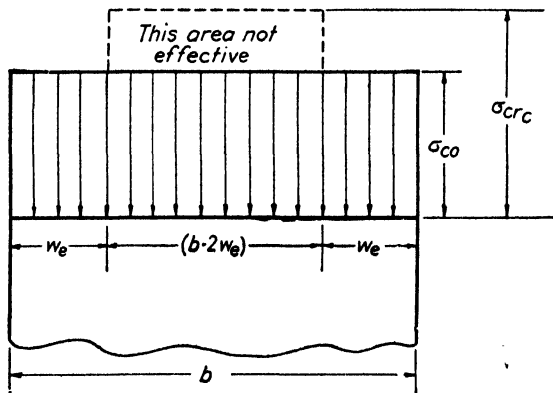


FIG. 8.8. Stress distribution $\sigma_{cr_c} < \sigma_{co}$.

been checked against the loads predicted by the method indicated above. Typical results are shown in Table 8.3 and, to illustrate the method, one panel will be calculated in detail. Consider the panel shown in Fig. 8.9, stiffened with channel section stiffeners having the column properties shown in Fig. 6.8. To determine the effective width of sheet acting with the stiffener, the flat panel effective width curve, Fig. 6.2,

is used. The critical buckling stress of a flat panel 5.625 in. wide and 0.019 in. thick is

$$\begin{aligned}\sigma_{crf} &= 3.617 \times 10.3 \times 10^6 \left(\frac{0.019}{5.625} \right)^2 \\ &= 425 \text{ lb. per sq. in.}\end{aligned}$$

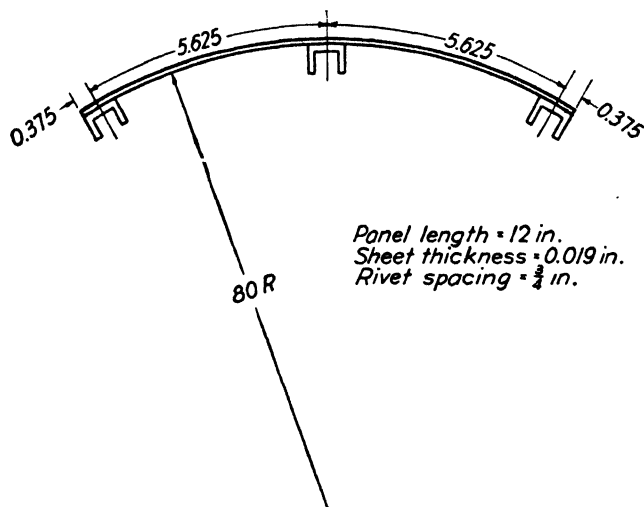


FIG. 8-9. Test panel.

The column failing stress for the 12-in. long stiffener alone is, from Fig. 6-8,

$$\begin{aligned}\frac{L}{\rho} &= \frac{12}{0.160} = 75.0 \\ \sigma_{co} &= 23,420 \text{ lb. per sq. in.}\end{aligned}$$

The stress at which buckling occurs between rivets is given by Fig. 6-23 as

$$\sigma_{rb} = 22,000 \text{ lb. per sq. in.}$$

Thus

$$\frac{\sigma_{rb}}{\sigma_{cr}} = \frac{22,000}{425} = 51.8$$

$$\frac{\sigma_{rb}}{\sigma_{yp}} = \frac{22,000}{36,000} = 0.61$$

and, from Fig. 6-2

$$\left(\frac{w_e}{b} \right)_{\sigma_{rb}} = 0.104$$

At the column stress, σ_{co} , this will be reduced to

$$\left(\frac{w_e}{b}\right)_{\sigma_{rb}} = 0.104 \frac{22,000}{23,420} = 0.0976$$

giving an effective width of

$$w_e = 0.0976 \times 5.625 = 0.549 \text{ in.}$$

Then, from Fig. 6-10 with

$$\frac{S}{\rho_0} = \frac{0.1655}{0.160} = 1.04 \quad \frac{t}{A_0} = \frac{0.019}{0.0566} = 0.336$$

$$b_e = 2w_e = 1.098$$

we get

$$\left(\frac{\rho_1}{\rho_0}\right)^2 = 0.944 \quad \text{and} \quad \rho_1 = 0.1554$$

This gives

$$\frac{L}{\rho_1} = 77.2$$

leading to a new column stress of

$$\sigma_{co_1} = 23,070 \text{ lb. per sq. in.}$$

A repetition of the method modifies these values slightly to give, for the final effective column values

$$w_e = 0.558 \text{ in.} \quad \sigma_{co} = 23,060 \text{ lb. per sq. in.}$$

Thus, for the center stiffener, we have an effective column as shown in Fig. 8-10 with a critical column stress of $\sigma_{co} = 23,060 \text{ lb. per sq. in.}$

For the end stiffeners, the buckling stress of the sheet beyond the rivet line is given by

$$\begin{aligned} \sigma_{cr} &= 0.452 \times 10.3 \times 10^6 \times \left(\frac{0.019}{0.375}\right)^2 \\ &= 11,950 \text{ lb. per sq. in.} \end{aligned}$$

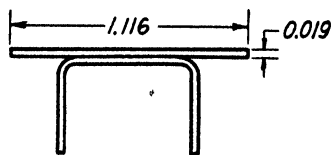


FIG. 8-10. Effective column for center stiffeners.

Which gives an effective width for a column stress of 23,060 lb. per sq. in of

$$w_{e_1} = 0.375 \frac{11,950}{23,060} = 0.194 \text{ in.}$$

So the end columns have an effective cross section as shown in Fig. 8-11. The column failing stress as given by Fig. 6-8 will be slightly higher than that for the center stiffener but it will be assumed that failure of the center stiffener will precipitate failure of the complete panel.

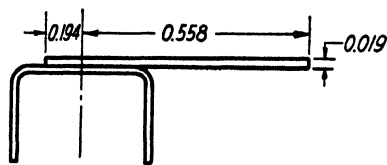


FIG. 8-11. Effective column for end stiffeners.

The effective material acting at the stress of 23,060 lb. per sq. in. is then

$$A_{co} = 3 \times 0.0566 + (2 \times 0.194 + 4 \times 0.558) 0.019 = 0.1698 + 0.0498 = 0.2196 \text{ sq. in.}$$

which will carry a total load of

$$P_{co} = 0.2196 \times 23,060 = 5060 \text{ lb.}$$

For the center of the panels, of width

$$(b - 2w_e) = (5.625 - 1.116) = 4.409 \text{ in.}$$

the critical stress of the curved panel is given by Fig. 8-2, we have

$$\frac{R}{t} = \frac{80}{0.019} = 4210, \quad \frac{L}{R} = \frac{12}{80} = 0.150$$

from which

$$\sigma_{cr_c} = 525 \text{ lb. per sq. in.}$$

Thus, the two center sheet portions will carry a load of

$$P_c = 2 \times 4.409 \times 0.019 \times 525 = 90 \text{ lb.}$$

and the total panel failing load would be predicted as

$$P_{\text{total}} = P_{co} + P_c = 5150 \text{ lb.}$$

This panel in test actually carried 4340 lb.

Table 8-3 gives the comparison between predicted and test failing loads of 32 panels having lengths of from 12 to 18 in., radii from 80 to 10 in. and sheet thicknesses of 0.019, 0.033, and 0.052 in. The agreement, although not perfect, is good when one considers the type of panel tested. The channel stiffeners used are noted for being a very inefficient section, being subject to early local buckling as well as being very weak in torsion. It will be noted that the three stiffener panels show poorer correlation than those having four stiffeners and this is felt to be caused by the tendency for plate buckling to distort the edge stiff-

TABLE 8-3

No.	No. Stiff. (n)	Sheet Thick. (t in.)	Radius (R in.)	Length (L in.)	R/t	L/R	σ_{cre} lb./sq. in.	Effec. L/p	σ_{co} (lb./sq. in.)	Effec. Col. Load (P_1 lb.)	Center Sheet Load (P_2 lb.)	P_{total} (lb.)	P_{rest} (lb.)
1	3	0.019	80	12	4.210	0.150	525	77.3	23,060	5,060	90	5,150	4,340
2	3	0.019	80	12	4.210	0.150	525	76.5	23,190	6,620	85	6,705	6,190
3	3	0.019	30	12	1.580	0.40	1,085	77.3	23,060	5,060	180	5,240	5,190
4	4	0.019	30	12	1.580	0.40	1,085	76.5	23,190	6,620	175	6,795	6,860
5	4	0.019	10	12	5.26	1.20	4,575	77.3	23,060	5,060	770	5,830	5,720
6	4	0.019	10	12	5.26	1.20	4,575	76.5	23,190	6,620	740	7,360	7,720
7	3	0.019	80	18	4.210	0.225	370	119.4	14,250	3,500	55	3,555	3,050
8	3	0.019	80	18	4.210	0.225	370	117.0	14,800	4,625	50	4,675	4,210
9	3	0.019	30	18	1.580	0.60	930	119.4	14,250	3,500	140	3,640	3,760
10	4	0.019	30	18	1.580	0.60	930	117.0	14,800	4,625	130	4,755	4,870
11	3	0.019	10	18	5.26	1.80	4,325	119.4	14,250	3,500	650	4,150	4,240
12	4	0.019	10	18	5.26	1.80	4,325	117.0	14,800	4,625	600	5,225	5,200
13	3	0.033	80	12	2.425	0.150	1,130	83.4	22,000	6,540	305	6,845	5,100
14	4	0.033	80	12	2.425	0.150	1,130	81.2	22,400	8,530	270	8,800	7,840
15	3	0.033	30	12	9.10	0.40	2,490	83.4	22,000	6,540	670	7,210	5,700
16	4	0.033	30	12	9.10	0.40	2,490	81.2	22,400	8,530	600	9,130	8,800
17	3	0.033	10	12	3.03	1.20	10,750	83.4	22,000	6,540	2,890	9,430	7,400
18	4	0.033	10	12	3.03	1.20	10,750	81.2	22,400	8,530	2,590	11,120	11,100
19	3	0.033	80	18	2.425	0.225	815	134.0	11,100	3,945	170	4,115	4,100
20	4	0.033	80	18	2.425	0.225	815	129.0	12,180	5,350	150	5,500	5,890
21	3	0.033	30	18	9.10	0.60	2,170	134.0	11,100	3,945	450	4,395	4,950
22	4	0.033	30	18	9.10	0.60	2,170	129.0	12,180	5,350	395	5,745	8,000
23	3	0.033	10	18	3.03	1.80	10,440*	134.0	11,100	3,945	2,195	6,140	5,450
24	4	0.033	10	18	3.03	1.80	10,440*	129.0	12,180	5,350	1,905	7,255	8,450
25	3	0.052	80	12	1.540	0.150	2,120	95.5	19,710	8,705	750	9,455	8,900
26	4	0.052	80	12	1.540	0.150	2,120	93.0	20,650	11,730	575	12,305	12,630
27	3	0.052	30	12	5.77	0.40	4,930	95.5	19,710	8,705	1,735	10,440	10,150
28	4	0.052	30	12	5.77	0.40	4,930	93.0	20,650	11,730	1,330	13,060	14,010
29	3	0.052	80	18	1.540	0.225	1,560	167.3	7,270	4,370	300	4,670	4,420
30	4	0.052	80	18	1.540	0.225	1,560	163.9	7,550	6,240	40	6,280	6,370
31	3	0.052	30	18	5.77	0.60	4,370	167.3	7,270	4,370	845	5,215	5,520
32	4	0.052	30	18	5.77	0.60	4,370	163.9	7,550	6,240	100	6,340	8,350

* This value higher than σ_{co} , therefore σ_{co} was used as failing stress for entire section.

eners. Two stiffener panels, which were also tested, showed very poor agreement between predicted and test loads. In the four stiffener panels, the effect of the end stiffeners is reduced to a minimum. Also, nominal gages and average values of material properties have been used throughout the calculations which should lead to some scatter in the results. In view of the above, it is felt that the method is useful for design purposes; however, more test data is needed to check its absolute accuracy. This is particularly true for sections having small

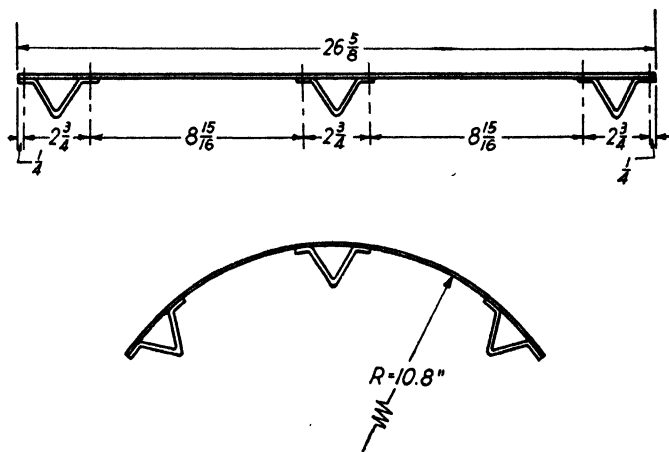


FIG. 8-12. Test panel.

curvature (large values of R) since for this series of tests, the experimental values indicated that such sections were weaker than the corresponding flat panels. Whether this is generally true, or whether it was caused by experimental conditions of the particular test, should be checked by additional experimentation.

The only other test data available are six panels tested by Consolidated, (reference 8-14) three of the panels being flat and the other three curved to a 10.8-in. radius. The panels were stiffened with hat-shaped stiffeners and had the major dimensions shown in Fig. 8-12. The R/t value of these panels was $10.8/0.040 = 270$ which is considerably out of the proven range of equation 8-2. However, the use of this equation gives reasonable agreement with the test loads carried by the panel. The same procedure as that outlined above was used to calculate the predicted loads on these specimens with the results shown in Table 8-4. The agreement shown in this table is good if it is considered that nominal gages and material properties were used and that equation 8-2 has been probably used beyond its range of exact validity.

The main conclusion that can be drawn from the study of the data on stiffened curved shells is that much more experimentation is necessary in this subject. Systematic series of tests should be made, particularly

TABLE 8.4

No.	L (in.)	σ_{cr_c} (lb./sq. in.)	(1) P_{flat} (lb.)	(2) P_c (lb.)	Curved Panel Loads (3)	
					Predicted (lb.)	Test (lb.)
1	11	13,060	22,865	10,000	32,865	29,530
2	18	12,580	21,575	9,420	30,995	29,070
3	22	12,410	22,240	9,400	31,640	29,480

(1) P_{flat} from tests on flat panels.

(2) P_c is total load carried by the sheet not included in the effective widths subjected to the stress σ_{cr_c} .

(3) $P_{predicted} = P_{flat} + P_c$.

on large radius sections, with sufficient variation in stiffener size, stiffener spacing, and sheet thicknesses so that the obvious gaps in this important problem may be filled.

8-3. The Failure of Stiffened Cylindrical Structures under Pure Bending

Stiffened shells as used in metal aircraft construction consist primarily of the following elements: (a) the sheet-metal covering, (b) the longitudinal stiffening elements, and (c) the transverse stiffening elements, generally referred to as ribs, bulkheads, or frames.

The functions of the sheet-metal covering are, first, to provide an aerodynamic surface upon which the air force acts (wings and control surfaces) and second, a covering for the contents of the airplane. In addition to the above functions the sheet covering is so designed that it is a load-resisting element and as such can be considered as part of the primary structure. In general, part of the load acting on an airplane structure will be compressive in nature. Since thin sheet is weak in compression it is necessary to provide stiffening elements which must fulfil one or both of two requirements, namely, (a) add additional strength in resisting compressive loads, (b) maintain the aerodynamic shape of the airplane.

In a fuselage, for example, the first is accomplished by attaching stiffening members to the sheet parallel to the axis of the cylinder; and

the second, by placing members of the proper shape perpendicular to the cylinder axis. These latter members also act as supports for the longitudinal members. In the following discussion the terms longitudinal and frame will be used to denote the above two classes of members respectively.

If a cylindrical structure of this type is subjected to, say, compressive loads parallel to its axis, it may fail in one of four distinct ways. The types of failure may be conveniently classified as material failure, local instability, panel instability, and general instability.

In general, the bending stress distribution is, for purposes of analysis, assumed to be in accord with the elementary beam theory. Where buckling of the sheet occurs, appropriate modifications are made in calculating section properties to allow for the reduction in the load-carrying ability of the buckled sheet. Hence, the first type of failure offers no difficulty to the designer, as it is only necessary that the ultimate strength of the material be known in order to determine the strength of the structure as a whole.

Local instability generally occurs in sections having wide and thin flanges, and it is characterized by an instability failure of some small portion of either a frame or longitudinal. This collapse of part of the stiffening member will precipitate its failure as a column and may also cause premature failure of the whole surrounding structure. The length of the portion of the member involved in local buckling is of the same order of magnitude as its cross-sectional dimensions, and the local buckling stress is not, in general, a function of the total length of the member. The buckling stress of such sections can be calculated by the methods given in section 5-3.

A panel instability failure is defined as one which will occur over a length of structure equal to one frame spacing and which is not caused by local instability spreading to adjacent members. This type of failure will occur in a structure having relatively heavy frames and light longitudinals, the structure tending to act as a number of isolated, axially stiffened cylinders, each of which is one frame spacing in length. Failure will occur by some form of instability of the longitudinals, the magnitude of the failure load being dependent upon the column or torsional strength of the longitudinals, modified by the effect of the attached buckled sheet. The only function of the frames in this case will be to determine the end fixity coefficient of the longitudinals. In the past, the designs of stiffened shell structures have been based almost entirely on failures of the panel type. Although an accurate theoretical treatment of the strength properties of curved stiffened panels is not yet available, it has been possible by experimental methods (see section

6-2) to design structures in which failures tended to fall in the panel instability classification.

The general instability type of failure will occur in a structure which has frames and longitudinals of such a size that both will fail simultaneously under the critical load. In other words, collapse takes place in such a manner as to destroy the load-carrying properties of all three structural elements: sheet, frames, and longitudinals.

The first three types of failure may occur regardless of the size of the airplane. In smaller airplanes (gross weight of 25,000 lb. or less) the frame sizes are determined by local loading conditions and practical manufacturing considerations, rather than from a standpoint of stability. These considerations lead to frames which are sufficiently rigid to preclude the possibility of general instability failures. As airplane sizes increase, the above considerations do not require a proportionate increase in frame sizes; consequently, the relative dimensions of the three structural elements may be very small compared to the external dimensions of the structure. Since general instability is a function of the stiffness of the structure as a whole, its occurrence in large airplanes is quite likely and should be investigated.

A complete and exact theoretical treatment of the general instability of stiffened cylinders is probably unattainable. However, a number of simplified treatments have been given. Since the validity of the results obtained from a theoretical treatment of the problem will depend on how closely the basic assumptions resemble the actual physical conditions, it might be desirable to consider the basic assumptions underlying these treatments.

Of the two possible types of failure which fall into the class of general instability, one occurs under bending loads and is characterized by a general flattening of the cylinders. This type of failure has been discussed for unstiffened and stiffened cylinders in references 8-19 and 8-17, respectively. Both theory and experiment indicate that for general flattening to occur, the length diameter ratio of the cylinder must be so large that it is completely out of the range of aircraft structures.

The second class of failure, for which two theoretical treatments are available, is that in which the wave form of the buckle is multi-lobed in nature and has, in general, a wave length less than the total length of the cylinder. This buckling form corresponds to the usual "diamond-shaped" wave pattern which is observed in the failure of unstiffened cylinders under compressive loads.

One method of investigation distributes the stiffnesses of the longitudinals and frames over the entire cylinder, forming an unstiffened

orthotropic cylinder, which is then treated as a simple unstiffened cylindrical shell. The thickness and stiffness of this shell in the longitudinal direction differ from that in the circumferential direction by amounts depending upon the areas and stiffness of the longitudinals and the frames respectively.

A second method that can be used is to consider the sheet, the longitudinals, and frames as components of a statically indeterminate truss system. The longitudinals and frames, each with its proper effective width of sheet, form the normal load-resisting members, whereas a suitable amount of sheet in each panel acts as a tension diagonal to transmit the shear forces.

A theoretical treatment of the problem has been given by Taylor (reference 8-15), Dschou (reference 8-16), and Hoff (reference 8-17). The first two authors have used the method of distributing the stiffnesses to form an orthotropic cylinder, whereas Hoff distributes only the longitudinals and does not distribute the stiffness of the frames, but considers the frames as local elastic supports for the longitudinal elements of the shell.

The results of these simplified treatments have been checked experimentally, and it was found that they do not give values sufficiently accurate for design purposes.

The result of an experimental investigation, reference 8-20, on this problem, which was carried out at the California Institute of Technology under the sponsorship of the Civil Aeronautics Authority, will be discussed in the remaining part of this section.

For a systematic experimental investigation it is necessary first to consider the variables involved in the problem of general instability. These variables may be divided into two classes—those dealing with the geometry of the structure, and those which involve the sectional properties of the stiffening elements as well as the sheet covering. The geometrical variables are as follows: the longitudinal spacing b , the frame spacing d , the diameter and length of the cylinder. The second group of variables includes the section properties of the longitudinals and frames, and the thickness of the sheet covering.

By a systematic variation of these variables it is possible to determine experimentally a suitable parameter for predicting the loads at which a stiffened cylindrical shell will fail by general instability. Investigating first the geometrical variables, b and d , it was found that the reciprocal of the maximum unit compressive strain at failure varied as \sqrt{bd} . The next question is, in what manner do the radius R and the section parameters ρ_x and ρ_y influence the design parameter sought for. By analogy with the buckling of unstiffened cylinders it can be expected that for

identical values of b , d , ρ_x and ρ_y the reciprocal of the critical values of the unit strain varies linearly with R . This surmise was checked experimentally and found to be correct. Hence it was concluded that the design parameter has the form

$$\frac{\sqrt[4]{bd}}{f(\rho_x, \rho_y)} R$$

From dimensional reasoning it follows that the function $f(\rho_x, \rho_y)$ must have the dimensions of the $\frac{3}{2}$ power of the length. The simplest assumption for the function which determines the influence of the section parameters, ρ_x and ρ_y , is that it depends only on the geometrical mean value $\sqrt{\rho_x \rho_y}$. Thus the design parameter appears in the form

$$\frac{\sqrt[4]{bd}}{(\rho_x \rho_y)^{3/4}} R \quad \text{or} \quad \frac{R}{\sqrt{\rho_x \rho_y}} \sqrt[4]{\frac{bd}{\rho_x \rho_y}}$$

Hence, the maximum unit strain at failure is given by an equation of the form

$$\frac{\sigma}{E'} = \frac{K \sqrt{\rho_x \rho_y}}{R} \sqrt[4]{\frac{\rho_x \rho_y}{bd}} \quad [8 \cdot 10]$$

where σ = maximum compressive stress at failure in pounds per square inch,

E' = effective modulus of elasticity in pounds per square inch,

ρ_x = radius of gyration of a longitudinal together with a portion of sheet covering in inches⁴,

ρ_y = same quantity for the circumferential frames in inches⁴,

R = radius in inches,

b = longitudinal spacing in inches,

d = frame spacing in inches.

Concerning the width of sheet to be used with the longitudinals and frames, it has been pointed out, reference 8-18, that the effective width associated with buckling phenomena is not necessarily that based on the load-carrying ability of the sheet, but is proportional to the rate of increase of the apparent stress to the rate of increase of the actual stress. Assuming that for our purpose the effective width as given by equation 6-7 is sufficiently accurate, then the apparent stress σ_a is

$$\sigma_a = \frac{2w_e \sigma_{st}}{b} = \sigma_{st} \sqrt[3]{\frac{\sigma_c}{\sigma_{st}}}$$

The effective width, w_e^* , for stability is then,

$$\frac{2w_e^*}{b} = \frac{d\sigma_a}{d\sigma_{st}} = \frac{2}{3} \sqrt[3]{\frac{\sigma_c}{\sigma_{st}}} \quad [8 \cdot 11]$$

This gives an effective width which is two-thirds of that based on the load-carrying ability of the sheet. However, the influence on the numerical value of ρ_x is quite small. For the specimens tested it was found that the difference was of the order of 3 per cent. Although an effective width as given by equation 8.11 was used in the experimental work it is felt that either value is sufficiently accurate for all practical purposes.

The amount of sheet acting with the frames is difficult to evaluate by analytical methods; trial calculations indicated that the best results were obtained if the total width of sheet between frames was used. For this reason then it is recommended that the entire width of sheet be used in calculating ρ_y .

The results of the experiments are shown in Fig. 8.13 where σ/E' is plotted as a function of $1/R \sqrt{\rho_x \rho_y} \sqrt[4]{\rho_x \rho_y / bd}$. In the majority of tests the frames had a solid rectangular cross section, Fig. 8.13, and were therefore not subject to local instability. Where frames, such as the channel section, are subject to local instability the failing load may be as much as 60 per cent lower than that given by the solid curve of Fig. 8.13 since the channel does not develop the strength corresponding to the calculated value of ρ_y . This can be illustrated by considering the behavior of an open-section column subjected to an axial load. Since the initial failure of the frame occurs over a relatively short length, the discussion will be confined to short columns. For columns having stable cross sections, i.e., columns which are not subject to local instability, the critical buckling stress is given with reasonable accuracy by the Johnson parabola, namely,

$$\sigma_B = \sigma_y \left[1 - \frac{\sigma_y L^2}{4\pi^2 C E \rho^2} \right] \quad [8.12]$$

In section 5-3, it was shown that for columns which fail by local instability, the buckling stress can be calculated by the equation

$$\sigma_c = \sigma_{cc} \left[1 - \frac{\sigma_{cc} L^2}{4\pi^2 C E \rho^2} \right] \quad [8.13]$$

If the crushing stress is lower than the yield-point stress the column will not develop the stress given by equation 8.12, but will fail at some lower stress given by equation 8.13. For columns which fail by local instability a reduced effective radius of gyration, ρ_{eff} , can be calculated in such a manner that if ρ_{eff} is substituted in equation 8.12 the resulting stresses would correspond to the values given by equation 8.13. This requires that for any column length the value of ρ_{eff} be such that,

$$\sigma_c = \sigma_B$$

from which it follows that

$$\rho_{eff} = \left[\left(\frac{\sigma_y^2 L^2}{4\pi^2 CE} \right) / \left(\sigma_y - \sigma_{cc} + \frac{\sigma_{cc}^2 L^2}{4\pi^2 CE \rho^2} \right) \right]^{1/2} \quad [8.14]$$

It is reasonable to assume that the frame behaves in a similar manner and that a reduced effective radius of gyration can be calculated. In

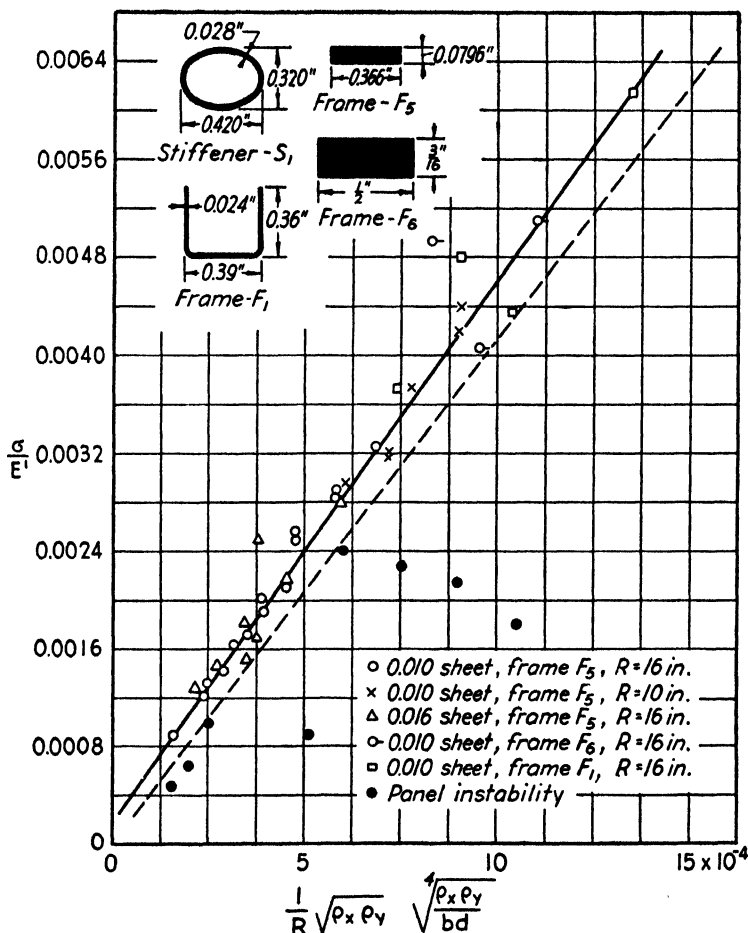


FIG. 8.13. Design curve for general instability of stiffened cylinders.

applying the above method to three specimens, in which general instability failure was precipitated by local instability of the frames, the resulting values of ρ_{eff} were such as to bring the experimental values in good agreement with the curve of Fig. 8.13. The length L was taken as the distance between longitudinals.

The experimentally derived parameter, $R/\sqrt{\rho_x\rho_y}\sqrt[4]{bd/\rho_x\rho_y}$, is the ratio between the radius and a quantity having the dimensions of a length defined by $\sqrt{\rho_x\rho_y}\sqrt[4]{\rho_x\rho_y/bd}$.

By analogy with the buckling of unstiffened cylinders, it appears that this length is proportional to some extent to an "equivalent" thickness of the reinforced cylindrical structure.

The failing stress of an unstiffened cylindrical shell of radius R is given by

$$\frac{\sigma}{E'} = \frac{Kt}{R} \quad [8.15]$$

Replacing the thickness t by the radius of gyration ρ of a strip of the shell of unit width, equation 8.15 can be written in the form

$$\frac{\sigma}{E'} = \frac{K\sqrt{12}\rho}{R} \quad [8.16]$$

For purposes of comparison the failing stress of the stiffened cylinders can be written in the form

$$\frac{\sigma}{E'} = K'\sqrt{12}\frac{\sqrt{\rho_x\rho_y}}{R}\sqrt[4]{\frac{\rho_x\rho_y}{bd}} \quad [8.17]$$

where K' is a numerical constant.

By introducing the geometrical mean value $\sqrt{\rho_x\rho_y}$, it can be assumed that the influence of the anisotropy of the structure is approximately taken into account. Then by comparison of equations 8.16 and 8.17 an effective radius of gyration can be defined as

$$\rho_e = \frac{K'}{K}\sqrt[4]{\frac{\rho_x\rho_y}{bd}}\sqrt{\rho_x\rho_y} = \varphi\sqrt{\rho_x\rho_y} \quad [8.18]$$

where $\varphi = \frac{K'}{K}\sqrt[4]{\frac{\rho_x\rho_y}{bd}}$ can be considered as a correction factor to the ratio $\frac{\sqrt{\rho_x\rho_y}}{R}$. Now d/ρ_x is the slenderness ratio of the longitudinal

considered as a column between two frames and similarly b/ρ_y is the slenderness ratio of the frame considered as a column between two longitudinals. If we define the geometrical mean value of these two slenderness ratios by λ , that is,

$$\lambda = \sqrt{\frac{bd}{\rho_x\rho_y}} \quad [8.19]$$

then the correction factor can be expressed as

$$\varphi = \frac{K'}{K} \frac{1}{\sqrt{\lambda}} \quad [8 \cdot 20]$$

It is evident that if the stiffened shell were to be considered as an equivalent shell in which all the materials are uniformly distributed, then the appropriate parameter to be used is $\frac{\sqrt{\rho_x \rho_y}}{R}$. The appropriate parameters, which enter into the problem of buckling of a truss, are the slenderness ratios which appear in the quantity $\lambda = \sqrt{\frac{bd}{\rho_x \rho_y}}$.

Since the experimentally derived relation involves both parameters, $\frac{\sqrt{\rho_x \rho_y}}{R}$ and λ , it indicates that a stiffened cylinder cannot be treated either as an equivalent cylinder of uniform thickness or as a cylindrical truss.

If we assume a value of $K = 0.3$, which is a reasonable average value for unstiffened cylinders in the range of $\frac{\sigma}{E}$ involved, and use for K' the values obtained from the experiments, then the numerical values of φ can be calculated. The average slenderness ratio λ varies from 280 to 26 and the values of φ corresponding to these limiting cases are $\varphi = 0.259$ and $\varphi = 0.865$. The lower limit is for a specimen with 10.12-in. longitudinal and 16-in. frame spacing, whereas the upper limit corresponds to a specimen with 2.53-in. longitudinal and 2.0-in. frame spacing. These results indicate that for structures in which the stiffening elements are widely spaced it is necessary that a multiplying factor much smaller than unity be applied to the quantity $\sqrt{\rho_x \rho_y}$, whereas in close spacings the factor is of the order of one.

If a reinforced cylinder fails by panel instability, the buckling stress should always be lower than the stress necessary to cause a general instability failure. This is obvious, for in order that panel instability may occur, it is necessary that the frame be sufficiently rigid to maintain closely the shape of the structure at the frame. If the frame is not sufficiently rigid, the frame will fail before the panel instability stress is reached, resulting in a general instability type of failure. The test results shown in Fig. 8-13 confirm the above statement.

For any given stiffened cylindrical structure it is necessary to determine the type of failure which gives the lowest failing stress. This stress is then the allowable design stress. Since the designer will have the necessary data to compute the numerical value of the parameter,

the general instability stress can be immediately obtained from the curve of Fig. 8·13.

In view of the fact that general instability causes a complete collapse of the structure it is recommended that allowance be made for ample margins, and the allowable stress should never exceed the boundary line indicated in Fig. 8·13.

8-4. Buckling of Thin-Walled Cylinders under Torsion

The buckling of thin-walled circular cylinders subjected to couples in planes perpendicular to the axis of the cylinder have been investigated both theoretically and experimentally by Donnell, reference 8·21, and experimentally by Lundquist, reference 8·22. The theoretical treatment, reference 8·21, considers two-edge support conditions, one in which the edges of the cylinder, at the ends, are clamped and one in which the edges are simply supported. The torsional shear stress at which buckling occurs is obtained from a solution of the differential equations of equilibrium of an element of the cylinder wall. This critical shear stress is very nearly expressed by the following two equations:

$$\tau_c = \frac{Et^2}{(1-\mu^2)l^2} \left[4.6 + \sqrt{7.8 + 1.67 \left(\sqrt{1-\mu^2} \frac{l^2}{td} \right)^{3/2}} \right] \quad (\text{Clamped edges})$$

$$\tau_c = \frac{Et^2}{(1-\mu^2)l^2} \left[2.8 + \sqrt{2.6 + 1.40 \left(\sqrt{1-\mu^2} \frac{l^2}{td} \right)^{3/2}} \right] \quad (\text{Simply supported edges}) \quad [8\cdot21]$$

where τ_c = buckling shear stress in pounds per square inch,

t = wall thickness in inches,

l = cylinder length in inches,

d = diameter in inches.

Comparing the experimental results with the theoretical curves, Fig. 8·14, it is seen that the average of the experimental values is about 75 per cent of the theoretical, with a minimum of 60 per cent for the metal cylinders. Since the observed wave form after buckling checks closely with that predicted by theory, the discrepancies between the theoretical and experimental values of the critical shearing stresses are attributed to initial imperfections of the test specimens. Some of the discrepancy may also be due to the fact that clamped edge conditions are quite difficult to attain experimentally. However, most of it is probably due to initial imperfections, that is, departure from a true cylindrical form.

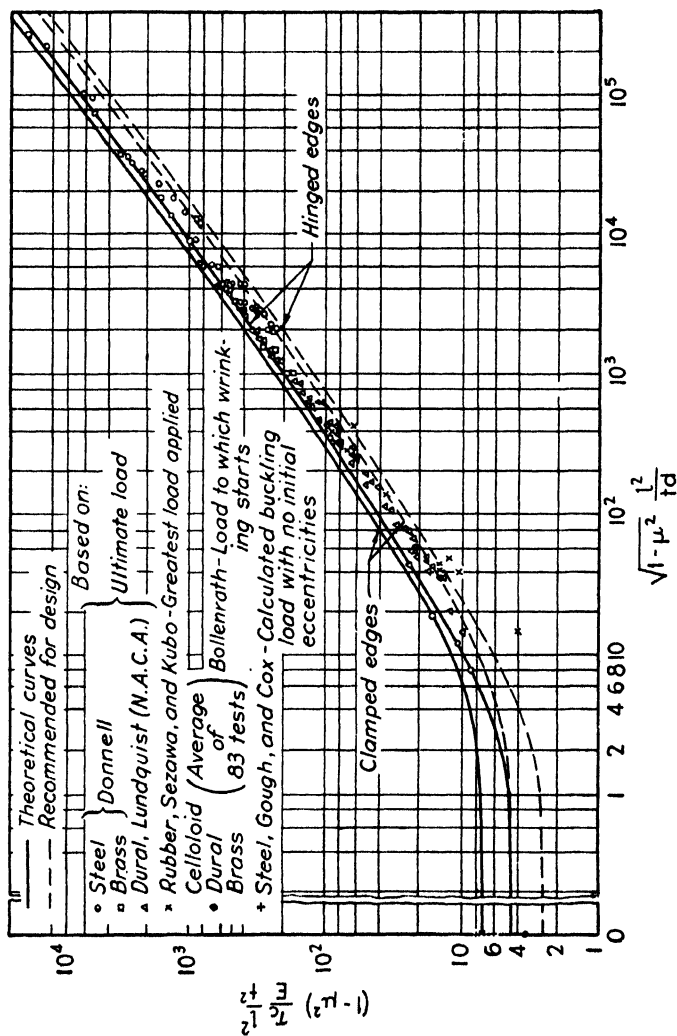


Fig. 8-14. Failure of unstiffened cylinders under torsion.

If the right-hand side of equations 8.21 is multiplied by 0.60 we obtain the minimum buckling shear stress which may be expected for an actual cylinder. Taking $\mu = 0.3$ we have,

$$\tau_c = E \left(\frac{t}{l} \right)^2 \left[3.0 + \sqrt{3.5 + 0.68 \left(\frac{l^2}{td} \right)^{3/2}} \right] \quad (\text{Clamped edges})$$

$$\tau_c = E \left(\frac{t}{l} \right)^2 \left[1.8 + \sqrt{1.2 + 0.57 \left(\frac{l^2}{td} \right)^{3/2}} \right] \quad (\text{Simply supported edges})$$
[8-22]

These equations are represented graphically by the broken lines, Fig. 8.14, and are recommended for design purposes. Since they are based on the minimum results from all available tests on metal cylinders they should give values which are always on the conservative side.

REFERENCES FOR CHAPTER 8

- 8-1. S. TIMOSHENKO, *Theory of Elastic Stability*. McGraw-Hill, 1936.
- 8-2. R. V. SOUTHWELL, "On the General Theory of Elastic Stability," *Phil. Trans. Roy. Soc. (London)*, Vol. 213, Series A, 1914.
- 8-3. W. R. DEAN, "On the Theory of Elastic Stability," *Proc. Roy. Soc. (London)*, Vol. 107, Series A, p. 734.
- 8-4. A. ROBERTSON, "The Strength of Tubular Struts," *R. & M.* 1185.
- 8-5. W. WILSON and N. NEWMARK, "The Strength of Thin Cylindrical Shells as Columns," *Bull. 225. Eng. Exp. Sta., Univ. Ill.*, 1933.
- 8-6. L. DONNELL, "A New Theory for the Buckling of Thin Cylinders Under Axial Compression and Bending," *Trans. A.S.M.E., Aero. Eng.*, November, 1934.
- 8-7. E. LUNDQUIST, "Strength of Thin-Walled Duralumin Cylinders in Compression," *N.A.C.A. Tech. Rep.* 473.
- 8-8. W. BALLERSTEDT and H. WAGNER, "Versuch über die Festigkeit Dunner unversteifter Zylinder," *Luftfahrtforschung*, Bd. 13, Heft 9, p. 309, 1936.
- 8-9. "General Instability Criteria for Stiffened Cylinders," Second Quarterly Report to the C.A.A., Part III, "Theoretical Investigations into the Principles Underlying the Failure of Thin Shells." Guggenheim Aero. Lab. of the Calif. Inst. of Tech., 1939.
- 8-10. S. KANEMITSU and H. NOJIMA, "Axial Compression Tests of Thin Circular Cylinders," M.S. Thesis. Guggenheim Aero. Lab. of the Calif. Inst. of Tech., 1939.
- 8-11. S. C. REDSHAW, "The Elastic Instability of a Thin Curved Panel Subjected to an Axial Thrust, Its Axial and Circumferential Edges Being Simply Supported," *R. & M.* 1565.
- 8-12. W. A. WENZEL, "Die mitttragende Breite nach dem Ausknicken bei krummen Blechen," *Luftfahrtforschung*, Vol. 15, p. 340, 1938.
- 8-13. Massachusetts Inst. of Tech., "Report on Aircraft Materials Testing for 1931-32."
- 8-14. "Compressive Tests of Aluminum Alloy Sheet Stiffener Combinations," *Consolidated Aircraft Corp. Rep.* 26 Z116.

- 8-15. J. L. TAYLOR, "Stability of a Monocoque in Compression," *R. & M.* 1679 (1935).
- 8-16. D. D. DSCHOU, "Die Druckfestigkeit verstiefter Zylinderischer Schalen," *Luftfahrtforschung*, Vol. 11, pp. 223-346 (1938).
- 8-17. N. J. HOFF, "Instability of Monocoque Structure in Pure Bending," *J. Roy. Aero. Soc.*, Vol. 42, pp. 291-346 (1938).
- 8-18. H. L. COX, "Stress Analysis of Thin Metal Construction," *J. Roy. Aero. Soc.*, Vol. 7, pp. 231-282 (1940).
- 8-19. L. G. BRAZIER, "On the Flexure of Thin Cylindrical Shells and Other Thin Sections," *R. & M.* 1081 (1926).
- 8-20. "General Instability Criteria for Stiffened Cylinders," Fifth Quarterly Report to the C.A.A. Guggenheim Aero. Lab. of the Calif. Inst. of Tech., 1940.
- 8-21. L. H. DONNELL, "Stability of Thin Walled Tubes under Torsion," *N.A.C.A. Tech. Rep.* 479.
- 8-22. E. E. LUNDQUIST, "Strength Tests on Thin-Walled Duralumin Cylinders in Torsion," *N.A.C.A. Tech. Note* 427.

PART III
APPLIED STRESS ANALYSIS

CHAPTER 9

WINGS AND CONTROL SURFACES

The preliminary design considerations and the calculations of the external loads acting on the airplane's structure were discussed in Part I. Part II was concerned with some of the fundamental problems of strength of materials and in particular with buckling phenomena. In Part III we will consider the distribution of the external loads to the various structural components, methods of stress calculation, and the application of the material discussed in Parts I and II. The student should realize that no two designs are alike and that in every design a number of special problems arise which are peculiar to this particular design. It is not the intention to treat such detailed problems here, but rather to limit the discussion to the more generalized methods of analysis.

9-1. Wings

Inasmuch as the material of Part II was primarily concerned with the behavior of thin-wall metal structures, only metal semi-monocoque structures will be treated in this chapter. An extensive treatment of other types of structures is given in reference 9-1.

In the design of a wing structure it is necessary to consider first the location of such items as control systems, cooling ducts, electrical installations, fuel and oil tanks. If due consideration is not given to the location of these items, it will invariably be necessary to cut large and numerous holes through some of the important stress-carrying elements of the wing. Since all cutouts must be reinforced, it has been found that the additional weight due to the reinforcements will frequently cause an otherwise light structure to become so heavy as to fall in the classification of a structurally inefficient design. It has been found in

practice that the most efficient wing structure can be realized if the above items are laid out first and the wing designed around them. This allows for the proper location of all items with the least amount of interference.

The structural members of a wing must be capable of resisting shear, bending and torsional loads. From a design standpoint the members resisting each of these loads can be considered separately.

(a) Shear-Carrying Members. The air loads act directly on the sheet covering which transmits the loads to the ribs. The ribs transmit the loads in shear to the spar webs and distribute the load between them in proportion to the web stiffnesses.

In the past it has been customary to design wings with three or more spars. The use of several spars permits a reduction in rib stresses and also provides a better support for the spanwise bending material. However, the available space in the wing will be greatly reduced if more than two beams are used. The housing of fuel tanks and landing gears (when retracted) inside the wing requires a large amount of space. This space requirement is the main reason for the growing tendency toward a two-spar wing construction. A two-spar wing construction usually consists of a main spar, located near the center of pressure, and a secondary spar which is so located that the control surface and flap hinge brackets can be attached to it. It also serves as the closing member of the torsion-resistant shell.

Spars can be divided into two general types, namely, (1) incomplete tension field beams, (2) truss-type beams. The two primary conditions which determine the over-all efficiency of a spar are its construction cost and its efficiency as a load-carrying member.

Construction cost should include both the cost of construction of the spar and also the assembly cost. By assembly is meant the attachment of the sheet covering and spanwise stiffening elements to the spars. The incomplete tension field beam is particularly adaptable to mass production because of the simplicity of its component parts. For example, the web requires a simple cutting operation in which several webs can be cut simultaneously by merely stacking the sheet. For the spar caps and vertical stiffeners extrusions or bent-up sections are used. The necessary tooling for production is relatively simple and inexpensive. Construction of a truss-type spar requires considerably more time because of the larger number of individual parts and because more elaborate tooling is necessary.

Since shear web beams divide the internal volume of a wing into a number of closed cells care must be taken to avoid difficulty with inaccessible rivets when the outer covering is applied. This problem is not too serious and can generally be worked out satisfactorily. The ease

with which ribs may be attached to the webs will offset the difficulty of applying the outer skin.

The load-carrying ability of a spar should not be judged purely on a strength-weight ratio basis, but due consideration should be given to rigidity and the ability to carry load after sustaining a certain amount of damage. Because of the high degree of redundancy present in an incomplete tension field beam it will carry load even when severely damaged. On the other hand a truss-type spar has no or a small degree of redundancy; which means, that if any one member in the spar fails, its load-carrying ability will be destroyed. Static tests have shown that incomplete tension field beams have a better strength-weight ratio and are

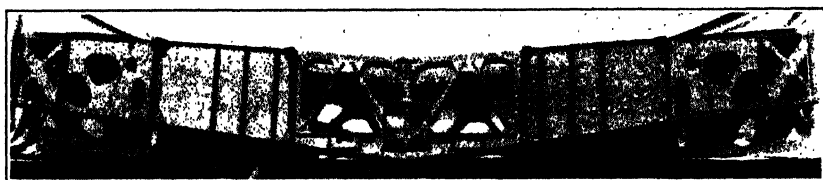


Fig. 9-1. Center section spar showing various types of construction.

much stiffer than the truss-type beams. Shear stiffness of the spars is important, because large deflections will cause deep shear wrinkles which may become permanent, in the leading edge of the wing. An extensive comparison between incomplete tension field beams and truss-type beams is given in reference 9-2. A center section spar showing the various types of spar construction is shown in Fig. 9-1.

It is generally considered that the classical bending theory when applied to thin-wall structures gives results which are sufficiently accurate for design purposes. However, the direct application is only valid when all elements of the structure are subjected to loads which are below the stability limit. It has already been indicated in Part II, that in the design of thin-wall structures, we make use of the fact that such structures are capable of carrying an increased load after certain elements of the structure are subjected to loads beyond their stability limit. In such cases it is necessary to make certain modifications in the calculations. In the following discussions on load distribution in thin-wall structures it will be indicated when such modifications are necessary.

In calculating the distribution of the shear load between the spars it is necessary to consider the shear in the leading edge section and in the bending material between the spars. In other words, it is necessary to calculate the shear flow over the entire cross section. The general equa-

tions for calculating the shear flow over a thin-wall structure can be derived from the following considerations. Consider a thin-wall cylinder of uniform cross section as shown in Fig. 9-2 in which X and Y are the principal axes; the calculation of principal axes is discussed in section 9-2(b). The Z -axis coincides with the line connecting the centers of gravity of the cross sections. The shear loads S_x and S_y are parallel to the principal axes and pass through the shear center of the section. In the wall of this section there will be longitudinal shear stresses which we will denote by τ . To find the magnitude of these stresses and the corre-

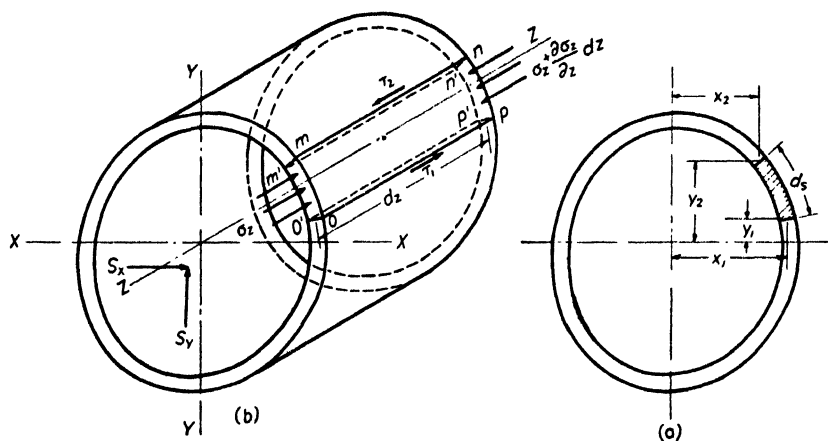


FIG. 9-2. Notation for cylinder analysis.

sponding shear flows let us consider an element of length dz , Fig. 9-2b, lying between two planes, $mnm'n'$ and $opo'p'$, normal to the surface of the section and a distance ds apart.

If τ is the average shear stress across the wall thickness, then the force on the face $opo'p'$ is $t_1\tau_1dz$ and on the face $mnm'n'$ the force is $t_2\tau_2dz$. The normal stresses produce the forces $\int_A \sigma_z dA$ and $\int_A \left(\sigma_z + \frac{\partial \sigma_z}{\partial z} dz \right) dA$ on the faces $mom'o'$ and $nnp'n'$, respectively.

For equilibrium, the sum of the forces on the element must equal zero, hence

$$(t_1\tau_1 - t_2\tau_2)dz - \int_A \left(\sigma_z + \frac{\partial \sigma_z}{\partial z} dz \right) dA + \int_A \sigma_z dA = 0$$

or

$$t_1\tau_1 - t_2\tau_2 - \int_A \frac{\partial \sigma_z}{\partial z} dA = 0 \quad [9.1]$$

According to the bending theory the normal stresses are distributed linearly across the cross section, namely,

$$\sigma_z = \frac{M_x y}{I_x} + \frac{M_y x}{I_y} \quad [9.2]$$

where M_x = bending moment about the X -axis in inch-pounds,

M_y = bending moment about the Y -axis in inch-pounds,

I_x = moment of inertia about the X -axis in inches⁴,

I_y = moment of inertia about the Y -axis in inches⁴.

From equation 9.2 we have

$$\frac{\partial \sigma_z}{\partial z} = \frac{y}{I_x} \frac{\partial M_x}{\partial z} + \frac{x}{I_y} \frac{\partial M_y}{\partial z}$$

but from equation 3.29.

$$\frac{\partial M_x}{\partial z} = S_y \quad \text{and} \quad \frac{\partial M_y}{\partial z} = S_x$$

hence

$$\frac{\partial \sigma_z}{\partial z} = \frac{S_y}{I_x} y + \frac{S_x}{I_y} x$$

Substituting these values in equation 9.1 gives

$$t_1 \tau_1 - t_2 \tau_2 - \frac{S_y}{I_x} \int_A y dA - \frac{S_x}{I_y} \int_A x dA = 0$$

The first integral is the static moment of the shaded area, Fig. 9.2a, with respect to the X -axis and the second integral is the static moment of the same area with respect to the Y -axis. Denoting these static moments by Q_x and Q_y respectively, the above equation can be written as

$$t_1 \tau_1 - t_2 \tau_2 - \left(\frac{Q_x}{I_x} S_y + \frac{Q_y}{I_y} S_x \right) = 0 \quad [9.3]$$

If the wall thickness t is uniform between y_1 and y_2 we can write for the static moments

$$Q_x = t \int_{y_1}^{y_2} y ds \quad \text{and} \quad Q_y = t \int_{x_1}^{x_2} x ds$$

then the shear flow at y_2 is given by

$$t \tau_2 = t \tau_1 - \frac{S_y}{I_x} t \int_{y_1}^{y_2} y ds - \frac{S_x}{I_y} t \int_{x_1}^{x_2} x ds \quad [9.4]$$

and the shear stress at y_2 by

$$\tau_2 = \tau_1 - \frac{S_y}{I_x} \int_{y_1}^{y_2} y ds - \frac{S_x}{I_y} \int_{x_1}^{x_2} x ds \quad [9.4a]$$

At the junction of two or more walls we have the equilibrium condition that,

$$\sum_{i=1}^{i=n} t_i \tau_i = 0 \quad [9.5]$$

where $t_i \tau_i$ is the shear flow at the junction in the i th wall and must be given its assumed sign. It should also be noted that the shear stress or shear flows in the direction of the longitudinal axis are equal to the shear stresses or shear flows in a plane perpendicular to the longitudinal axis, see section 3-1.

Equations 9.3, 9.4, and 9.5 guarantee only the equilibrium but do not define the absolute magnitude of the shear flow, since to the shear flow around the cell may be added a constant shear flow and the resultant shear flow will be likewise in accordance with equations 9.3, 9.4, and 9.5. Therefore, there are still as many unknowns as there are cells. Hence, for any cross section which has more than two boundaries the above equations are not sufficient to determine the shear flow over the cross section. By using equation 3.83 in conjunction with equations 9.3 or 9.4 and 9.5 all unknowns can be determined. As an illustrative example consider the section shown in Fig. 9.3 subjected to a vertical shear load S only. For our present calculations we are interested only in torsion-free bending. Torsion will be discussed later. To realize a condition of torsion-free bending it is necessary that the shear load be applied through the shear center. It is therefore assumed that the shear load passes through the shear center. The section is symmetrical about the X -axis, hence X and Y are principal axes.

The shear stresses at the neutral axis are denoted by τ_1 , τ_2 , and τ_3 for the leading edge, the front spar and the rear spar, respectively. The assumed direction of the shear flow is indicated in Fig. 9.3; if the actual shear flow is in a direction opposite from the assumed shear flow it will be indicated by a minus sign in the final expressions for the shear stresses.

From equation 9.4 the shearing stress in the circular section from E to A is

$$\begin{aligned} \tau_0 &= \tau_1 - \frac{S}{I} \int y \, ds \\ y &= R \sin \beta, \quad ds = R \, d\beta \\ \tau_0 &= \tau_1 - \frac{S}{I} \int_0^\beta R^2 \sin \beta \, d\beta = \tau_1 + \frac{SR^2}{I} (\cos \beta - 1) \\ \tau_{0A} &= \tau_1 - \frac{SR^2}{I} \end{aligned} \quad [9.6]$$

The shear stress in the front spar from the neutral axis to A is

$$\begin{aligned}\tau_F &= \tau_2 - \frac{S}{I} \int_0^y y dy = \tau_2 - \frac{Sy^2}{2I} \\ \tau_{FA} &= \tau_2 - \frac{SR^2}{2I}\end{aligned}\quad [9.7]$$

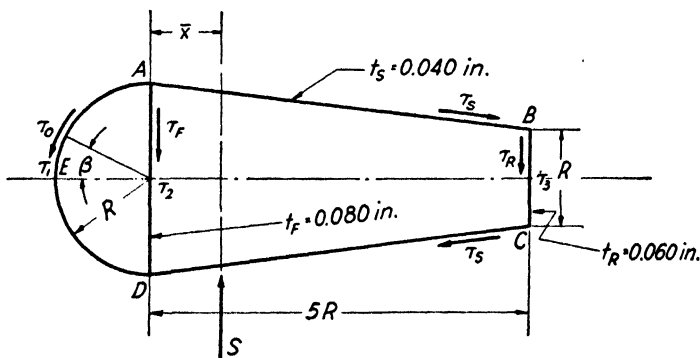


FIG. 9-3. Shear analysis for wing.

The shear stress in the rear spar from the neutral axis to B is

$$\begin{aligned}\tau_R &= \tau_3 - \frac{S}{I} \int_0^y y dy = \tau_3 - \frac{Sy^2}{2I} \\ \tau_{RB} &= \tau_3 - \frac{SR^2}{8I}\end{aligned}\quad [9.8]$$

The shear stress from B to A is

$$\begin{aligned}\tau_s &= \tau_{sB} - \frac{S}{I} \int_{s_0}^{s_1} y ds \\ s &= \frac{\sqrt{25.25}}{R/2} R(y - R/2) = 10.04(y - R/2), \quad ds = 10.04 dy \\ \tau_s &= \tau_{sB} - \frac{10.04}{I} S \int_{R/2}^y y dy = \tau_{sB} - 5.02 \frac{S}{I} \left(y^2 - \frac{R^2}{4} \right)\end{aligned}$$

From equation 9.5, we have at the junction B ,

$$t_s \tau_{sB} = t_R \tau_{RB}$$

Hence

$$\begin{aligned}\tau_s &= 1.5\tau_3 - 0.188 \frac{SR^2}{I} - 5.02 \frac{S}{I} \left(y^2 - \frac{R^2}{4} \right) \\ \tau_{sA} &= 1.5\tau_3 - 3.95 \frac{SR^2}{I}\end{aligned}\quad [9.9]$$

At A we have

$$t_0 \tau_{0A} + t_F \tau_{FA} + t_s \tau_{sA} = 0 \quad [9.10]$$

Substituting for the shear stress the values given by equations 9.6, 9.7, and 9.9 and the corresponding sheet thicknesses, gives

$$\tau_1 + 2\tau_2 + 1.5\tau_3 - 5.95 \frac{SR^2}{I} = 0 \quad [9.11]$$

In section 3-6, equation 3.83, it was shown that for a hollow circular section

$$\tau p = 2AG\theta$$

If τ is not constant around the perimeter p then τp must be replaced by the equivalent line integral around the perimeter, namely,

$$\oint \tau ds = 2GA\theta \quad \text{or} \quad \int \frac{(t\tau)ds}{t} = 2GA\theta \quad [9.12]$$

In torsion-free bending the angular twist per unit length θ is zero and we can write,

$$\oint \tau ds = 0 \quad [9.13]$$

In taking the line integral around any cell the sign of both τ and ds should agree with the convention adopted in setting up the corresponding shear expressions. Observing this rule we have for the front cell

$$\begin{aligned} \oint \tau ds &= + \int_{\pi/2}^{-\pi/2} \left[\tau_1 + \frac{SR^2}{I} (\cos \beta - 1) \right] R d\beta + \int_{-R}^R \left(\tau_2 - \frac{Sy^2}{2I} \right) dy = 0 \\ &= 1.57\tau_1 - \tau_2 - 0.403 \frac{SR^2}{I} = 0 \end{aligned} \quad [9.14]$$

around the rear cell

$$\oint \tau ds = \int_R^{-R} \tau_F dy + \int_D^C \tau_S ds + \int_{-R/2}^{R/2} \tau_R dy + \int_B^A \tau_S ds = 0$$

Substituting for the shear stresses and noting that $ds = 10.04dy$ gives

$$\begin{aligned} \oint \tau ds &= 2 \int_0^{-R} \left(\tau_2 - \frac{Sy^2}{2I} \right) dy \\ &\quad + 2 \int_{R/2}^R \left[1.5\tau_3 - 0.188 \frac{SR^2}{I} - 5.02 \frac{S}{I} \left(y^2 - \frac{R^2}{4} \right) \right] 10.04 dy \\ &\quad + 2 \int_0^{R/2} \left(\tau_3 - \frac{S}{2I} y^2 \right) dy = 0 \\ &= \tau_2 - 8.04\tau_3 + 9.23 \frac{SR^2}{I} = 0 \end{aligned} \quad [9.15]$$

It follows from equations 9·11, 9·14, and 9·15

$$\tau_1 = 1.16 \frac{SR^2}{I}, \quad \tau_2 = 1.42 \frac{SR^2}{I}, \quad \tau_3 = 1.33 \frac{SR^2}{I}$$

From equations 9·6 to 9·9 we have

$$\tau_{0A} = 0.16 \frac{SR^2}{I}, \quad \tau_{FA} = 0.92 \frac{SR^2}{I}, \quad \tau_{RB} = 1.20 \frac{SR^2}{I}, \quad \tau_{sA} = -1.96 \frac{SR^2}{I}$$

Substituting the above values in the equations for τ_0 , τ_F , τ_R , and τ_s the distribution of the shear stress over the cross section can be calculated, and it is shown in Fig. 9·4.

In all the above calculations it has been assumed that the shear rigidity is the same for all members. This is not always true, for if any one of the members buckle its shear rigidity decreases. If the rigidities are different, equation 9·13 should be replaced by,

$$\oint \frac{t\tau}{Gt} ds = 0 \quad [9\cdot16]$$

The appropriate value for G can then be used for each member of a cell.

Having calculated the shear distribution, the horizontal position of the shear center can be calculated. By definition, the shear center lies at the intersection of the X -axis and the vertical plane in which the shear load S must be applied to produce torsion-free bending.

Taking moments about the center of the front shear web, we have

$$\begin{aligned} M &= 2 \int_0^{\pi/2} t_0 \tau_0 R^2 d\beta - 2 \int_B^A 0.9996R t_s \tau_s ds - 10R \int_0^{R/2} t_r \tau_R dy \\ &= \frac{2SR^4 t_0}{I} \int_0^{\pi/2} (0.16 + \cos \beta) d\beta - 20.0 \frac{t_s RS}{I} \int_{R/2}^R (3.06R^2 - 5.02y^2) dy \\ &\quad - 10t_R \frac{RS}{I} \int_0^{R/2} (1.33R^2 - \frac{1}{2}y^2) dy \\ &= -0.338 \frac{SR^4}{I} \end{aligned}$$

The moment of inertia of the section about the x -axis is $0.355R^3$ and if \bar{x} is the distance from the front spar to the shear center (see Fig. 9·2) then,

$$\begin{aligned} S\bar{x} &= \frac{0.338SR}{0.355} \\ \bar{x} &= 0.953R \end{aligned}$$

The variation of the shear flow $t\tau$ along the walls depends on the amount of bending stress carried by the wall and the shear flows coming into the walls at junctions with other walls. Therefore, the influence of the spanwise stiffening elements cannot be neglected; however, the exact calculations of wing sections with stiffening elements are rather tedious and involved. It has been pointed out in reference 9.3 that the calculated position of the shear center for simple wing sections, such as the above example, do not check the experimentally observed position by approximately plus or minus 5 per cent of the chord length.

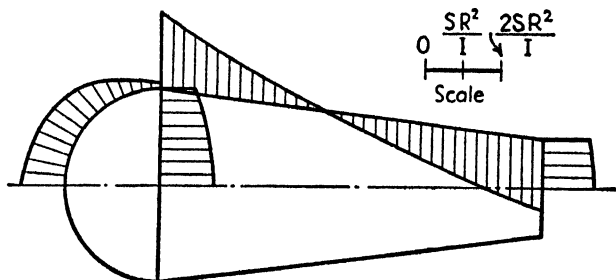


FIG. 9.4. Shear distribution in a wing.

Due consideration should also be given to the decrease in the shear rigidity due to buckling. The theoretical shear stiffness of a diagonal tension field (reference 9.4) is

$$G_e = 0.625G$$

The conditions of a pure tension field are not realized in the majority of structures and G_e may be much less for combined compression and shear. Therefore, the above value can only be used as a first approximation. Figure 6.41 gives a somewhat more accurate approximation for the value of G_e which is based essentially on the ratio of τ/τ_{cr} . It is sometimes more convenient to work with an effective thickness rather than a reduced shear modulus. For example, if the spar web is in a buckled state its thickness can be replaced by a thickness t_e given by the equation

$$t_e = t \frac{G_e}{G}$$

When corrugations are riveted to sheet the shear flow in the corrugation-sheet combination must be considered. For such a combination an effective sheet thickness can be obtained from the following considerations. One wave of the corrugated panel together with the sheet riveted to it forms a cell to which the general equations may be applied. The

shear flow in the equivalent sheet of thickness t_e must be the same as that in the corrugation and sheet together, that is,

$$t_e \tau_e = t_s \tau_s + t_c \tau_c$$

where the subscript s refers to the sheet covering and c to the corrugation. The shear deformation in the equivalent sheet must be the same as in the sheet covering, or

$$\frac{\tau_e}{G} = \frac{\tau_s}{G_s}$$

For the cell between the sheet and corrugation we can write from equation 9.16

$$\frac{\tau_s p_s}{G_s} - \frac{\tau_c p_c}{G_c} = 0$$

From these three equations it follows that

$$t_e = \frac{G_s}{G} t_s + \frac{G_c}{G} \frac{p_s}{p_c} t_c \quad [9.17]$$

where G_s , p_s and G_c , p_c are the effective shear moduli and perimeters of the sheet and corrugation, respectively.

In general, the corrugations will not be in a buckled state and G_c will be equal to G , whereas the sheet will be buckled and a reduced shear modulus must be used.

If both stringers and corrugations are riveted to the outer sheet, as shown in Fig. 9.5b, equation 9.3 together with equations 9.5 and 9.16 should be used for determining the shear flow. Exactly the same procedure is followed as in the given example, except that the shear flow $t\tau$ is used in the calculations rather than the shear stress τ . In so far as the sheet-stringer combination is concerned, the stringer, plus the effective width of sheet acting with the stringer, is considered to be concentrated at the stringer and to carry only axial loads whereas the intermediate sheet panels serve to take up shear stresses only. This means that, in calculating the static moments, only the area of the stringer plus the effective width of sheet is taken into account. It is also obvious that the integrals are replaced by summations. The sheet-corrugation combination is treated as an equivalent sheet according to equation 9.17.

It should be realized that the standard formulas for bending and shear stresses in a beam do not hold near an abrupt discontinuity in the beam cross section or near discontinuous loads. However, the errors due to the use of the elementary theories become negligible at some distance away from the discontinuity if this distance is of the same order of magnitude as the cross-sectional dimensions of the beam. The above methods of calculation are therefore only valid at some distance away

from any discontinuity in the structure or loading. Cutouts are the most troublesome; they are frequently quite large and it is difficult to estimate how far they influence the behavior of the structure.

It is recommended, reference 9·5, that when large discontinuities of the spanwise material exist, the direct load be determined for each

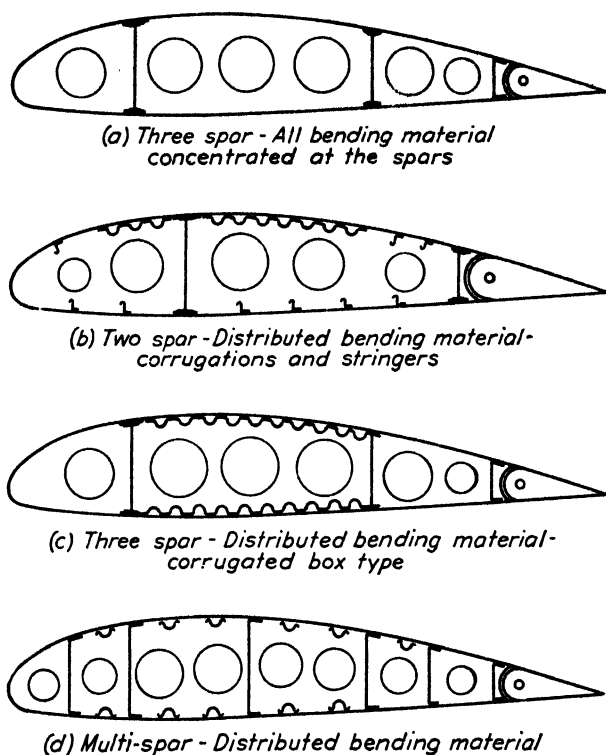


FIG. 9-5. Typical wing structures.

element of the wing (spar flanges, corrugations, etc.) at a certain wing station, using the formula

$$p_1 = \sigma_1 dA_1 = \frac{M_1 y_1 dA_1}{I_1}$$

Applying the same procedure to the same element at a station x inches from the previous one will produce the load

$$p_2 = \sigma_2 dA_2 = \frac{M_2 y_2 dA_2}{I_2}$$

where M_1 and M_2 , I_1 and I_2 , dA_1 and dA_2 are the total moments, the moments of inertia of the wing cross section and the areas of the ele-

ments respectively, at the respective stations. The calculations of normal stresses due to bending are discussed in section 9-1(b). The difference between p_1 and p_2 divided by the distance x gives the shear flow acting upon the element between the two stations. Obviously if p_1 is equal to p_2 the shear flow is zero, and when this is true for all longitudinal elements there will be no shear flow in the bending material and the shear load is entirely resisted by the shear webs.

The designer should not assume too sudden a transfer of shear to newly added material and should investigate the ability of the plating and of the rivets to transfer the load to the added material. Sudden discontinuities of the spanwise material may easily result in premature failure.

(b) Bending Material. In the consideration of bending material it is convenient to classify wing structures according to the disposition of the bending-load resistant material: (1) All bending material is concentrated in the spar caps. (2) The bending material is distributed around the periphery of the profile.

A typical wing cross section in which the bending material is concentrated in the spar caps is schematically illustrated in Fig. 9-5a. The number of spars may vary from one to any number—the practical limitations of a multi-spar construction has been discussed in the previous section.

Each of these types has certain distinct advantages over the other and a choice of the particular type to be employed in any design depends largely on the purpose for which the airplane is designed and on the available tools and materials. Some of the advantages that can be claimed for the first type are: simplicity of construction, hence requires less tooling and labor and lends itself to rapid mass production. Because of the concentration of materials, the spar caps can be so designed that buckling occurs near the ultimate stress of the material; this allows the use of higher allowable stresses. The analysis of such structures is also much simpler than that of the second type.

One of the principal disadvantages of the concentrated spar-cap type is that the sheet-metal covering will buckle at a very low load. The load-carrying ability of the covering in so far as bending is concerned, is therefore negligible, which means that we have a certain amount of material which is not being utilized. Furthermore, the airplane will be operating at all times with the sheet covering in a wave state having relatively large amplitudes. This results in a serious disturbance of the airflow over the wing profile and causes an increase in drag. It is also necessary to consider the possibility of fatigue failures due to the local bending stress in the buckled sheet.

In the second type, the distributed bending material consists of stiffening elements running in a spanwise direction. These elements may be either corrugations or stringers attached to the sheet or a combination of both. A few sketches are shown in Figs. 9·5*b* to 9·5*d* to illustrate the various combinations of stiffening members used in wing construction.

The wing-bending loads which cause compression at the upper surface of the wing are generally somewhat higher than those causing compression at the lower surface. This requires that the stiffening elements along the upper surface be more efficient and also more closely spaced than those on the bottom. Since corrugations meet both of these requirements it is common practice to use corrugations along the upper surface and some form of extruded or bent-up stringers along the lower surface. For highly loaded wings it may be desirable to use corrugations in both upper and lower surfaces. In the choice of stringers it should be kept in mind that the air loads acting on the covering tend to bend the stringers which are already subjected to high loads owing to the wing-bending loads. It is therefore advisable to use stringers with sufficiently high moments of inertia to resist the combined loads.

Static tests of completed wing structures have demonstrated that the elementary beam theory is sufficiently accurate for calculating the bending stress distribution, provided the following considerations are taken into account. On the compression side the metal sheet covering will buckle at relatively low loads which necessitates the use of effective widths (see section 6-1). For cutouts or discontinuities in the material, that is, a sudden change or redistribution in the bending material, the stress distribution near the discontinuity will not be according to the elementary beam theory. For example, if between two adjacent wing sections the corrugation gage is suddenly increased or a number of corrugations are added the stress distribution does not change suddenly to correspond to the new moment of inertia and neutral axis location. To understand fully the mechanism involved in the redistribution of normal stresses, it is necessary to consider two conditions. If the bending moment is constant, i.e., the shear is zero, then at the section where the additional material is added the spar will unload, through shear deformations of the sheet covering and corrugations, to the added material. This transfer of load from the spar to the added material by shear will continue until the stress in the whole assembly is again according to the bending theory. If the air-load shear is not zero, the air loads acting on the ribs are transmitted to the spar webs and are distributed between them in proportion to their stiffnesses. From the webs the shear must be transferred through the top or bottom sheet covering and corrugations to the point where the new bending material, capable of resisting

the bending loads imposed by the shear, is added. In tapered wings some of the shear is directly absorbed by the flange material and the above discussion applies only to the excess shear.

In each case the redistribution of stress involves shear stresses which in turn cause shear deflections. Therefore, the additional material will be, over a certain distance, not fully effective and will not develop the stress indicated by the bending theory. The distance required to cause a redistribution of the stresses to correspond to the bending theory will depend upon the sharpness of the discontinuity and upon the shear rigidity of the material through which the shear transfer of the normal

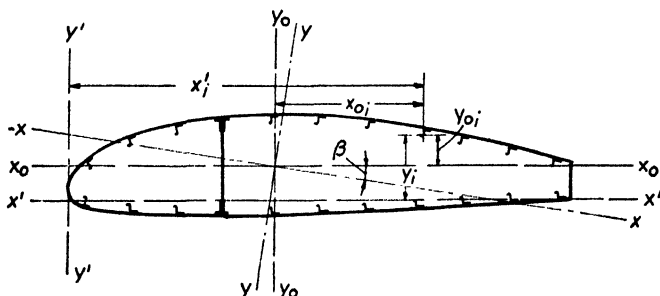


FIG. 9-6. Notation for wing analysis.

stresses takes place. The phenomena described above is commonly called "shear lag."

If a wing is uniformly tapered in plan form and the bending material is gradually added near the shear beams, the effect of "shear lag" will be negligible. A convenient method of allowing for the effects of shear lag is to assume a "reduced effective" area for the material, thereby reducing its effectiveness. It is obvious that the material farthest from the spars will be least effective.

Owing to the complexity of the shear lag problem only a few of the simpler cases have been treated analytically. References 9-6 to 9-10 include some of the theoretical and experimental work which has been done on this problem.

As an illustration of the method for calculating the bending stress distribution, consider a wing section as shown in Fig. 9-6. It should be kept in mind that the elementary bending equations are only applicable if the planes of the transverse shear loads (S_x and S_y) are parallel to the two principal planes of bending. Therefore if we calculate the distribution of the bending stress by means of equation 9-2, that is,

$$\sigma_z = \frac{M_x y}{I_x} + \frac{M_y x}{I_y} \quad [9-2]$$

it is necessary that x and y be principal axes.

The general equations for determining the principal axes and the moments of inertia about them are given in elementary texts on applied mechanics. The problem is somewhat more complex for a stiffened shell structure than for the cases commonly encountered in strength of materials and it will therefore be considered here in some detail. It is recommended that the outlined general procedure be followed.

1. Choose any convenient set of perpendicular axes. One will usually be the chord line.

2. Divide the section into numbered component parts, such as sections of skin, corrugations, stringers, spar caps.

3. Compute the area of each part.

4. Tabulate as follows (numbers in brackets refer to columns in table):

- (1) Number of part
- (2) Area of the i th part in square inches = A_i
- (3) y'_i the coordinate distance of A_i to the reference axis in inches
- (4) x'_i the coordinate distance of A_i to the reference axis in inches
- (5) $A_i y'_i$ moment of the area A_i about the x' -axis
- (6) $A_i x'_i$ moment of the area A_i about the y' -axis
- (7) $A_i y'^2_i$
- (8) $A_i x'^2_i$
- (9) $I_{x_{0i}}$ moment of inertia of A_i about an axis parallel to x' and passing through the centroid of A_i
- (10) $I_{y_{0i}}$ moment of inertia of A_i about an axis parallel to y_i and passing through the centroid of A_i .

Some parts will have negligible values for $I_{x'}$ and $I_{y'}$. The moments of inertia of the stringers about their own centroidal axes are usually negligible.

- (11) $A_i x'_i y'_i$
- (12) I_{pi} product of inertia of A_i about axes through its centroid and parallel to x' and y' .

5. Determine the moments and product of inertia of the section about the x' -, y' -axes.

$$I_{x'} = \sum_{i=1}^n A_i y'^2_i + \sum_{i=1}^n I_{x_{0i}}$$

$$I_{y'} = \sum_{i=1}^n A_i x'^2_i + \sum_{i=1}^n I_{y_{0i}}$$

$$I_{x'y'} = \sum_{i=1}^n A_i x'_i y'_i + \sum_{i=1}^n I_{pi}$$

6. Determine the position of the center of gravity of the section.

$$\bar{x} = \frac{\sum_{i=1}^{i=n} A_i x'_i}{\sum_{i=1}^{i=n} A_i} \quad \bar{y} = \frac{\sum_{i=1}^{i=n} A_i y'_i}{\sum_{i=1}^{i=n} A_i}$$

7. Choose a new set of axes x_0, y_0 , which are parallel to the x', y' -axes passing through the center of gravity of the section.

8. Calculate the moments and product of inertia about these new axes.

$$I_{x_0} = I_{x'} - A \bar{y}^2$$

$$I_{y_0} = I_{y'} - A \bar{x}^2$$

$$I_{x_0 y_0} = I_{x' y'} - A \bar{x} \bar{y}$$

where

$$A = \sum_{i=1}^n A_i$$

9. Determine the angle, β , between the principal axes x, y , and the x_0, y_0 -axes by the following equation

$$\tan 2\beta = \frac{2I_{x_0 y_0}}{I_{y_0} - I_{x_0}}$$

10. Determine the principal moment of inertia of the section by the equations,

$$I_x = I_{x_0} \cos^2 \beta - 2I_{x_0 y_0} \sin \beta \cos \beta + I_{y_0} \sin^2 \beta$$

$$I_y = I_{y_0} \cos^2 \beta + 2I_{x_0 y_0} \sin \beta \cos \beta + I_{x_0} \sin^2 \beta$$

Since most of the sheet in the compression zone will be in a buckled state, it is necessary to use an effective width of sheet to allow for the decrease in the load-carrying ability of the buckled sheet. On the tension side the sheet is fully effective. The effective width of sheet acting with each longitudinal stiffener depends on the magnitude of the normal stress σ . Consequently, the location of the principal axes and the moments of inertia about them are not directly calculable, but must be evaluated by a series of successive approximations. These approximations are carried out in the following manner.

1. Assume the sheet fully effective in the compression zone and calculate the position of the principal axes, the moments of inertia about them, and the corresponding stresses.

2. Ascertain with the formulas of section 6-2 which panels are in the buckled state and compute the effective width by one of the methods given in section 6-1 at each stringer or corrugation. The result is a new cross section with only part of the sheet effective in the compression zone. From the moments of inertia of this section, referred to a new set of principal axes corresponding to this new cross section, a new linear stress distribution is calculated. This distribution is now much closer to the actual distribution than the first one.

3. With the new stress distribution again calculate the effective widths, moments of inertia referred to a new set of principal axes corresponding to the new cross section and the stress distribution.

This latter stress distribution will, in general, be quite close to the actual distribution and will be sufficiently close for practical purposes. It should be noted that an appreciable amount of labor can be saved if the sheet elements in the compression zone are tabulated separately, for these are the only items which will vary in calculating the center of gravity of the cross section.

To eliminate the tedious second and third approximations the following approximate method has been suggested in reference 9-11. If σ_{i_0} is the stress at the i th stringer, assuming the sheet in the compression zone fully effective, and $(w_{eR} + w_{eL})_i$ is the total effective width corresponding to the stress σ_{i_0} at the stringer i , then the actual stress σ_i is

$$\sigma_i = \frac{A_{si} + \frac{1}{2}(b_R t_R + b_L t_L)_i}{A_{si} + (W_{eR} t_R + W_{eL} t_R)_i} \sigma_{i_0}$$

Where the subscripts R and L refer to the right and left of the stringer, A_s and b are the stringer area and spacings, respectively, and t is the sheet thickness. This approximation gives a non-linear stress distribution in the compression zone. An experimental check of the method indicated that for a stiffened cylinder in pure bending the maximum calculated stress was about 12 per cent higher than the measured value.

Having determined the distribution of the bending stress by one of the above methods the compression stress for each element will be known. These stresses can then be compared with the allowable stresses, which can be determined by the methods of section 6-2 or by simple static tests of representative panels of the structure, and the margins of safety can be determined.

(c) **Torsion Material.** The torsional moments are primarily resisted by the outer covering and the rear spar. The portion of the wing aft of the rear spar is usually, over the greater portion of the span, some form

of control surface and in such cases it does not resist any of the torsional loads. The contribution of the interior spar web or webs depends on the relative thickness of the spar webs and the enclosed areas of the cells. For example, if we have a section consisting of two identical cells, that is, $t_1 = t_2$, $p_1 = p_2$ and $A_1 = A_2$, Fig. 3-35, then the shear stress in the interior web is zero and the section behaves as if the interior web were not present.

Metal-covered wings are highly efficient torsion-resistant structures, provided there are no large cutouts. It should be realized that in the region where a cutout occurs over a cell its resistance to torsion is practically completely destroyed. In present-day construction cutouts are unavoidable; their detrimental effects can to some extent be minimized if they are properly reinforced so that the shear flow can be carried around the cutout and be redistributed over the periphery of the section. It is advisable to use heavy ribs or bulkheads adjacent to large cutouts; such members can then efficiently redistribute the torsional shear flow into the outer covering.

The torsional moments acting on a wing come from two sources:

1. Concentrated masses located at some distance from the shear center, such as nacelles, engines, landing gear, fuel and oil. The distributed wing weight might also contribute to the torsional moment if the chordwise position of the locus of the shear centers is not the same as that of the line connecting the centers of gravity of the wing.

2. When the shear center does not coincide with the center of pressure of the air forces, the air forces produce torsional moments about the shear center.

If the location of the shear center is known, the torsional moments can be readily calculated. If we assume the shear load in our previous example of Fig. 9-3 to be applied at a distance $1.953R$ aft of the front shear beam, then we can replace this shear force by a shear force at the shear center and a couple of magnitude

$$M_T = (1.953R - 0.953R)S = RS$$

For this the resultant shear distribution will be the algebraic sum of the shear due to the shear force S acting at the shear center and the shear due to the couple M_T . The shear stress or shear flow resulting from this couple can be calculated by means of equations 3-84, 9-12 and 3-87. From the data given in Fig. 9-3 we can write the following equations.

$$\frac{\pi R^2}{2} (tr)_1 + \frac{15}{2} R^2 (tr)_2 = RS$$

where $(t\tau)_1$ and $(t\tau)_2$ are the shear flows in the front and rear cells respectively,

$$\frac{\pi R}{0.040} (t\tau)_1 + \frac{2R}{0.080} (t\tau)_3 = \pi R^2 G\theta$$

$$\left(\frac{10.04R}{0.040} + \frac{R}{0.060} \right) (t\tau)_2 - \frac{2R}{0.080} (t\tau)_3 = \frac{15}{2} R^2 G\theta$$

and

$$(t\tau)_1 + (t\tau)_3 = (t\tau)_2$$

Solving these four equations for the four unknowns we have:

$$(t\tau)_1 = 0.104 \frac{S}{R} \quad (t\tau)_2 = 0.056 \frac{S}{R}$$

$$(t\tau)_3 = -0.048 \frac{S}{R} \quad \theta = 2.15 \frac{S}{R^2 G}$$

Where cutouts occur, the torsional moments will be resisted by the cells over which the cutouts do not extend and by the spars. If cutouts are adequately reinforced their effects occur only over local regions; in these regions assumptions and approximations are necessary for the analysis and generally static tests are resorted to for the determination of the exact allowable loads.

The theory upon which our torsion calculations have been based assumes that the cross section is free to warp. Therefore, near cross sections which are restrained from warping, the torsion equations are not applicable. This would be true, for example, near the plane of symmetry of a cantilever semi-monocoque wing or tail surface. At sections adjacent to the restrained section the torsional loads produce normal as well as shear stresses. These normal stresses may become very high and cause failure of the structure. The theoretical solutions of this problem are complex and accurate experimental conformation is still lacking. However, the designer should keep these conditions in mind when designing the torsion-resistant material. A discussion of the problem can be found in reference 9-4.

(d) Wing Ribs. The primary loads acting on a rib are the external air loads and the reaction forces at the spar webs. Once these forces are determined the rib can be treated as a beam. In so far as the analysis of the rib structure is concerned, the distribution of the reaction shears at the spar webs are not important; however, the magnitude is important. The component of the external air loads, normal to the wing chord line, acting on the ribs is usually of the type showing in Fig. 9-7. If the analysis of the wing is based on a shear distribution between the spar

webs as calculated by the methods of section 9-1(a), then the external air loads on the ribs should be resisted in the same manner. In this case the shear reactions are provided by the spar webs and the wing covering, provided the wing covering is attached to the rib. The vertical com-

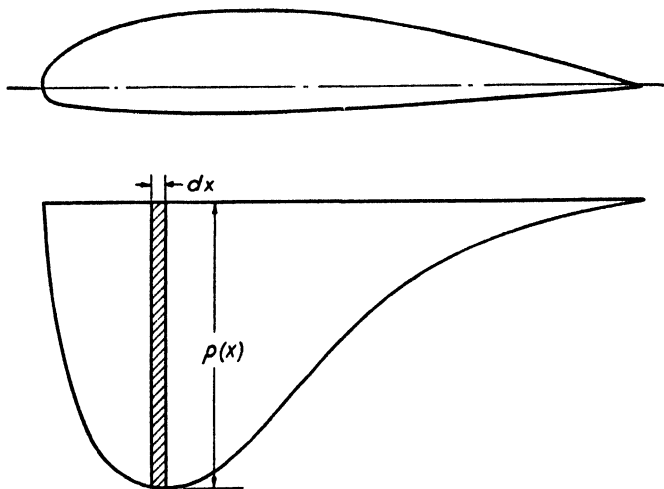


FIG. 9-7. Rib air load.

ponent of these reactions will be at the shear center and equal in magnitude to the vertical component of the air loads which here is given by

$$S_R = s \int_0^c p(x) dx$$

where $p(x)$ = air pressure in pounds per square inch,

s = rib spacing in inches.

If the ribs are not evenly spaced, s will be the mean of the spacing of two adjacent ribs. The magnitude of the shear reactions is obtained by resolving S_R into components parallel to the principal axis and substituting these components for S_x and S_y in the equations of section 9-1(a).

When the resultant of the reactions, which is equal to S_R , passes through the shear center the system will usually not be balanced in torsion. The torsional moment, which is equal to the product of S_R and the distance from the shear center to the center of pressure of the external loads $p(x)$, is resisted by the spar webs and the wing covering. The method of calculating the shear flow or shear due to a torsional moment was discussed in the previous section.

Since the rib transmits this shear to the covering and spar webs, the shear reactions on the rib will be the same as the shear in the covering

and spar webs. The magnitude of the shear flow due to the torque, together with that resulting from the shear load S_R passing through the shear center, determines the rivet spacing required to transfer the shear flow from the ribs to the covering and spar webs. The shear and bending moment at any section of the rib can be calculated from the external loads $p(x)$ and the shear reactions described above.

It has been shown, reference 9-12, that when a wing is subjected to bending loads, the bending of the wing as a whole tends to produce inward acting loads on the wing ribs. The inward acting loads which are in the direction of the radius of curvature arise from the fact that the normal stresses σ acting on an element of cross section area dA and a length ds give rise to two forces σdA inclined to each other at an angle ds/R . The radial component of these two forces is $\sigma dA \cdot ds/R$. If we substitute $1/R$ for its equivalent M/EI , then for a rib spacing s and an amount of bending material having a cross-sectional area A , the normal pressure exerted on the rib will have a magnitude

$$P = \frac{\sigma M s A}{EI} = \frac{M^2 s y A}{EI^2}$$

Since the inward acting loads P are oppositely directed on the tension and compression side they tend to compress the rib and their effects should be considered in addition to the loads previously discussed. It should also be kept in mind that when the sheet covering wrinkles in a diagonal tension field the ribs act as compression members.

The types of ribs employed in wing construction vary over such a wide range that a definite classification is rather difficult. A general classification includes, truss type, tension-field type similar to the incomplete tension-field beam, webs with lightening holes and stiffeners, and any combination of these. A number of these types are shown in Fig. 9-8. The two ribs at the nacelles and the end rib at the fuselage are of the tension-field type whereas the intermediate ribs are of the truss type. Not enough data are available on the structural efficiencies of the various types to allow a definite statement as to which type is the best. At times the type of rib employed is determined by conditions other than structural, for example, in integral fuel tanks the end ribs are part of the fuel tank and are of necessity of the tension-field type.

So far we have only considered the external loads and reaction forces acting on the ribs. The manner in which the rib structure resists these loads depends on the type of construction. In the truss-type ribs the distributed external loads and reaction forces are applied as concentrated loads at the joints and the structure is analyzed as a simple truss. The outer members on which the distributed loads act are relied upon

to transfer these loads, in shear, to the points where they can then be considered as concentrated loads. These outer members are therefore subjected to combined bending and compression or bending and tension. The effects of this combined loading must be taken into account in the design of the members. Tension-field type ribs can be treated in the same manner as the incomplete tension-field beams which were discussed



FIG. 9-8. Typical wing ribs.

in Chapter 6. This type of rib is usually provided either to distribute the concentrated loads, such as the nacelle and engine weights or landing-gear loads to the shear webs. A careful study should be made of the forces acting on the rib and of the reactions supporting these forces. When lightening holes are used in the webs of the ribs, they may be considered as being equivalent to a Vierendeel truss. A Vierendeel truss consists only of flanges and vertical members rigidly connected at the joints. It can be analyzed by assuming the structure to be pin-connected at the joints, then knowing the shears and bending moments acting on the truss, the loads in the members and the bending moments at the joints can be determined. A discussion of Vierendeel trusses is given in reference 9-13.

One of the important items in the wing analysis is the determination of the required rivet spacing at the various riveted connections. Connections which require analyses are the wing covering to the spar caps, the spar web to the spar caps, ribs to spar webs, the wing covering to the ribs or bulkheads, joints in the wing covering, and connections at the fuselage. The rivet spacing can in each be determined from the shear flow which has been calculated in the wing analysis. For example, the shear flow in pounds per inch at the connection of the spar caps and the wing covering will be known from the calculations of the shear distribution over the wing section. Based on the allowable bearing or shear load a rivet size and rivet spacing necessary to transfer this load from the wing covering to the spar cap can then be determined. The load on a rivet is the product of the shear flow and the rivet spacing. At the lap joints of the sheet covering the rivets should be checked for the normal loads, the tension loads usually determining the rivet size and spacing. Joints also occur in the stiffening elements and the necessary rivet spacing can be determined from the normal loads in the stiffening element. In addition to these general considerations numerous connections occur, such as landing-gear fittings to the spars, pulley brackets. In designing these connections it should be remembered that tension loads on rivets are not permissible.

It is customary to build wings in several sections, the usual number being five, namely, the center section, the two outer panels, and the two wing tips. Wings are built in several sections for two reasons, namely, maintenance and production. The maintenance and repair problems are simplified, for if any part of the wing is seriously damaged it can be readily replaced with a new section, whereas, if the wing was built as a single unit it would mean a complete new wing, or rebuilding of the damaged section, which is at best a difficult task and not always possible. Furthermore, if the damage occurs at some distance from a maintenance depot the problem of shipping the necessary parts and the assembly problems are greatly simplified. There are no facilities available for shipping the wing of a large airplane overland if it is built as a single unit. The building of wings in sections also lends itself better to mass production, for it requires less floor space for each unit, can be more easily handled and more men can work on the structure at the same time.

In designing a wing joint the first consideration is that of transmitting the loads from one section to the other. Connections at the tips are relatively simple because of the low loads and can usually be accomplished with some form of a riveted joint. At the center section the problem is more difficult for here we must consider the transfer of high

loads across the joint. Several methods can be employed; all the loads can be transmitted through the spar connections or the loads can be transferred directly by providing suitable connections between the distributed bending material as well as between the spars. If the first method is used, suitable provisions must be made to allow the loads in the distributed bending material to be transferred to the spars.

The direct transfer of loads can be accomplished by designing special fittings connecting the longitudinal stiffening elements and a doubler plate connecting the wing covering, or entirely by means of doubler plates. In the latter case, the loads are transferred from the stiffening elements to the plating and then back again. The method of direct transfer of loads is the most satisfactory from a weight standpoint for all the material is as effective near the joint as at some distance away from the joint.

The spars are connected at the joints by either shear bolts or tension bolts. Shear bolts require very close tolerances; for this reason the bolts are usually tapered, requiring reamed holes, and the assembly problem is particularly troublesome. Tension bolts do not require such close tolerances and are therefore much easier to assemble. However, the tension-bolt fittings are somewhat more difficult to design and also, the bolts should be thoroughly investigated for fatigue failure.

The effects of concentrated loads such as the loads coming from the engine mount or landing-gear loads resulting from the landing conditions must be checked for the effect of localized stresses. Suitable provisions must be made to carry these loads into the wing structure without causing high localized stress concentrations. This can be accomplished by designing the connecting fittings in such a manner that loads are gradually transferred to the wing structure; the addition of doubler plates may also be necessary. The individual members of the wing structure to which the above items are attached must also be checked for adequate strength. For the landing loads the wing structure as a whole, inboard of the landing gear, must be checked for bending, shear, and torsion.

9-2. Control Surfaces

The type of construction employed in the fixed-control surfaces, stabilizers and fins, is usually similar to the types of wing construction discussed in the first part of this chapter. The question, as to which type of construction is the most efficient for control-surface design, seems to be quite unsettled. Some designers favor the two-spar construction with all bending material concentrated in the spar caps, whereas others are inclined towards a multi-spar construction with the spars again

resisting all the bending loads. In the latter the individual spars are, of course, of lighter construction than in the two-spar design. A typical multi-spar construction is shown in Fig. 9-9. Control surfaces should not be designed purely on a strength basis, but due consideration should be given to rigidity which is an important item in the prevention of flutter. Large deflections of the fixed surface will impose severe loads on the movable surface attached to it and may also cause binding at the hinge brackets.

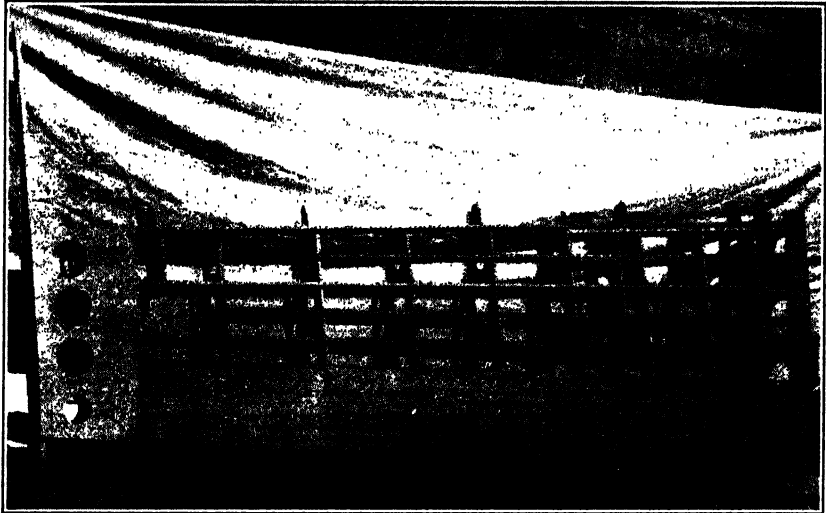


FIG. 9-9. Typical multi-spar construction.

It is felt that a design with distributed bending material would be more rigid than a two-spar, but not necessarily more than a multi-spar, construction. In general it is not possible to predict which type will be the lighter, since this depends on the size of the surface, the design loading, and mostly on the ability of the engineer to design a structure with good balance between weight, required rigidity, and strength.

Since these surfaces and the wings are similarly constructed, the analysis will also be similar, usually somewhat simpler, because of the absence of large cutouts. The only concentrated loads which must be taken into account are those at the hinges supporting the movable control surfaces. The structure may be either continuous through the fuselage or it may be built in sections and the spars attached to stiff fuselage bulkheads. The methods of attachment are similar to those used in the wing connections.

The torque loads on the elevators are relatively high and, in designing an elevator, one of the first requirements is that it be a good torsion-

resistant structure. There are essentially two types of construction, an all-metal construction and one in which the leading edge and the shear-resistant spar is metal with the section aft of the spar consisting of metal ribs with fabric covering. This latter type of construction has two advantages: it is a considerably lighter structure and has most of its weight concentrated near the hinge center line where it is needed for mass balancing. One of its disadvantages is that it has less torsional rigidity. The leading-edge section provides the torsion-resistant material and, since the hinge bracket is attached to the spar, cutouts through the leading edge are necessary. In order to carry the torsion loads around these cutouts heavy nose section ribs must be provided adjacent to the cutouts with proper reinforcement across them. The elevator spar is generally supported over three or more hinges, hence the equations for continuous beams, given in Chapter 3, are necessary for the analyses. Allowance should also be made for the fact that, as the stabilizer deflects the hinge supports deflect with it, giving rise to a condition of non-colinear supports. The leading edge and spar form a single cell which can be readily analyzed by the methods given in the previous sections. If the surface is an all-metal construction, the section will consist of two cells if the leading edge is properly reinforced around the cutouts; if not, it must be assumed that only the cell aft of the shear beam is effective. The construction and functions of the rudder are similar to that of the elevators.

Ailerons and flaps are analyzed for the external loads specified in section 2-3. The construction of the aileron will be either all metal or metal and fabric. The problems which arise in the analysis and construction are similar to those encountered in the elevator design. The flaps are usually of the stiffened shell construction which can be analyzed by the previously discussed methods. A number of flap types are used at the present time, such as the split flap and the Fowler flap. The essential difference lies in the aerodynamic forces produced and not in the general methods of construction.

Since these surfaces are attached to the wing structure, they assume the same deflection form as the wing. Frequently the loads imposed on these control surfaces because of the wing deflection will be the design criteria rather than the air loads acting on the surfaces. They should therefore also be investigated for these conditions.

The design problems and methods of analysis discussed in this chapter are of a general character. In the design of any airplane a large number of problems will be encountered which have not been discussed here; however, a thorough understanding of the fundamental methods of analysis will be of considerable aid in solving such problems. It should

also be realized that in all special problems a number of basic assumptions are necessary. How close these assumptions can be made to fit the physical facts is a matter of judgment and experience which can only be acquired with practical experience.

REFERENCES FOR CHAPTER 9

- 9-1. A. S. NILES and J. S. NEWELL, *Airplane Structures*, Vol. I, Wiley, 1938.
- 9-2. J. E. LIPP, "Shear Field Aircraft Spars," *J. Aero. Sci.*, Vol. 7, No. 1, pp. 1-5.
- 9-3. P. KUHN, "Remarks on the Elastic Axis of Shell Wings," *N.A.C.A. Tech. Note* 562.
- 9-4. P. KUHN, "Bending Stresses Due to Torsion in Cantilever Box Beams," *N.A.C.A. Tech. Note* 530.
- 9-5. W. A. KLIKOFF, "Notes on Thin Metal Aircraft Structures," Aeronautics Library, California Institute of Technology, 1937.
- 9-6. P. KUHN, "Stress Analysis of Beams with Shear Deformation of the Flanges," *N.A.C.A. Tech. Rep.* 608.
- 9-7. E. REISSNER, "The Influence of Taper on the Efficiency of Wide-Flanged Box-Beams," *J. Aero. Sci.*, Vol. 7, pp. 353-357 (1940).
- 9-8. E. REISSNER, "On the Problem of Stress Distribution in Wide-Flanged Box-Beams," *J. Aero. Sci.*, Vol. 5, pp. 295-299 (1938).
- 9-9. B. B. C. LOVETT and W. F. RODEE, "Transfer of Stress from Main Beams to Intermediate Stiffeners in Metal Sheet Covered Box Beams," *J. Aero. Sci.*, Vol. 3, No. 12, pp. 426-430 (October, 1936).
- 9-10. R. J. WHITE and H. M. ANTZ, "Tests on the Stress Distribution in Reinforced Panels," *J. Aero. Sci.*, Vol. 3, No. 6, pp. 209-212 (April, 1936).
- 9-11. H. EBNER, "The Strength of Shell Bodies—Theory and Practice," *N.A.C.A. Tech. Memo.* 838.
- 9-12. M. T. HUBER, "Bending of Beams of Thin Sections," *N.A.C.A. Tech. Memo.* 793.
- 9-13. DANA YOUNG, "Analysis of Vierendeel Trusses," *Trans. A.S.C.E.*, Vol. 102, pp. 869-938 (1937).
- 9-14. A. VAN DER NEUT, "Torsie en Afschuiving van Meervoudig Samenhangende Doosliggers," *Verslagen en Verhandeligen van den Rijks—Studiedienst voor de Luchtvaart*, Amsterdam, Deel VI, 1931, p. 67.
- 9-15. P. KUHN, "The Initial Torsional Stiffness of Shells with Interior Webs," *N.A.C.A. Tech. Note* 542.
- 9-16. H. EBNER and H. KOLLER, "Calculation of Load Distribution in Stiffened Cylindrical Shells," *N.A.C.A. Tech. Memo.* 866.
- 9-17. O. S. HECK and H. EBNER, "Methods and Formulas for Calculating the Strength of Plate and Shell Constructions as Used in Airplane Design," *N.A.C.A. Tech. Memo.* 785.
- 9-18. P. KUHN, "Approximate Stress Analysis of Multi-Stringer Beams with Shear Deformation of the Flanges," *N. A. C. A. Tech. Rep.* 636.
- 9-19. H. F. WINNY, "The Distribution of Stress in Monocoque Wings," *R. & M.* 1756.

CHAPTER 10

FUSELAGE ANALYSIS

The stiffened-shell type of fuselage construction is quite similar to the wing construction with distributed bending material. One of the essential differences is that in the wing shear webs are provided to carry the greater part of the vertical shear, whereas in the fuselage the walls of the structure are relied upon to resist the shear loads. The fuselage frames or bulkheads are equivalent to the ribs in the wing, for they transmit the shear loads to the covering and also maintain the shape of the structure. The bending loads are resisted by the sheet covering and the longitudinal stiffening elements. The stiffening elements are usually stringers such as bulb angles, bent-up open sections, and hat sections. The loads on the fuselage are usually not high enough to justify the use of corrugations, except in stainless steel construction where the material gage is very small and the required spacing of the longitudinals is close enough to warrant their use.

In calculating the bending stress it is again assumed that the elementary beam theory is sufficiently accurate resulting in a bending stress distribution given by the equation

$$\sigma_z = -\frac{M_x y}{I_x} + \frac{M_y x}{I_y} \quad [9 \cdot 2]$$

The shear force S_x , Fig. 10·1, is zero in practically all cases, except when maneuvering loads are applied to the rudder and fin. The principal axes and the moments of inertia about them are computed according to the method given in section 9-1(b). In general the fuselage cross section is symmetrical about the Y -axis, Fig. 10·1, hence the Y -axis is a principal axis if S_x is zero. When S_x is different from zero, the effective bending material will not be symmetrically distributed about the Y -axis because of the resulting bending stress. Also for sections near or at a cutout the bending material is not symmetrical about the Y -axis. The allowable compressive stresses are usually taken equal to the strength of the longitudinals, except in large fuselages where a general instability failure may occur. (See section 8-3.) In addition to the direct compression or tension stresses resulting from the bending loads, secondary stresses due

to the shear loads are imposed on the stringers. These secondary stresses will be discussed in the following paragraphs.

The shear loads are resisted by the sheet covering and the longitudinals, the resulting shear stresses can be computed by the formula

$$\tau = \frac{S_y Q_x}{I_x t} \quad [10.1]$$

if we assume S_x equal to zero. The static moment Q_x is calculated as follows: If the stress is to be calculated at B , Fig. 10.1, then Q_x is the static moment of the effective bending material from A to B , with respect

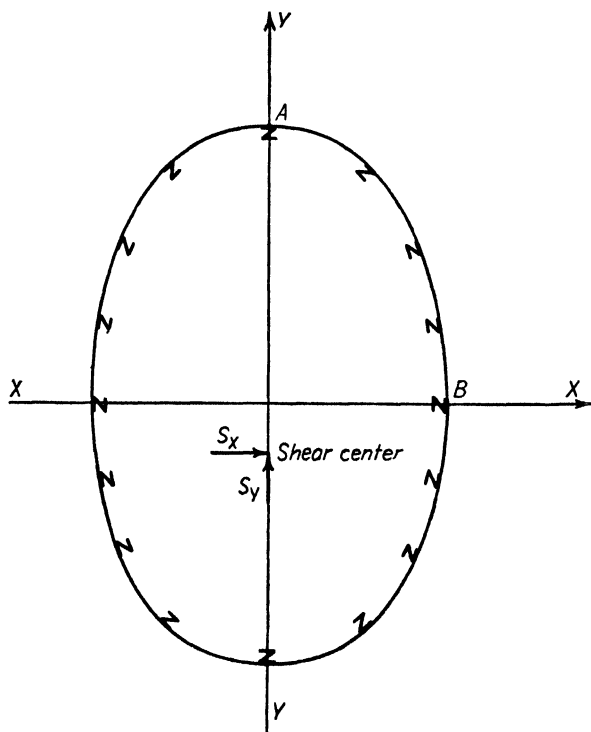


FIG. 10.1. Typical fuselage section.

to the neutral axis. The maximum shear flow, $t\tau$, occurs at the neutral axis and is zero at the top. It is advisable also to investigate some points other than at the neutral axis for the effects of combined shear and tension or shear and compression.

The sheet covering will buckle at relatively low shear stresses and any additional shear will then be carried by diagonal tension, see section 6-3.

The diagonal tension loads in the sheet covering should theoretically produce appreciable compressive loads in the longitudinals, if it is assumed that a complete tension field exists. Test results indicate that the compressive loads calculated on the basis of a complete tension field are not reached, and the incomplete tension field theory given in section 6-3 should give a closer agreement between calculations and experiment. If the curvature of the sheet covering is appreciable, secondary bending stresses of considerable magnitude may be produced in the longitudinals. The shear wrinkles tend to straighten the curved

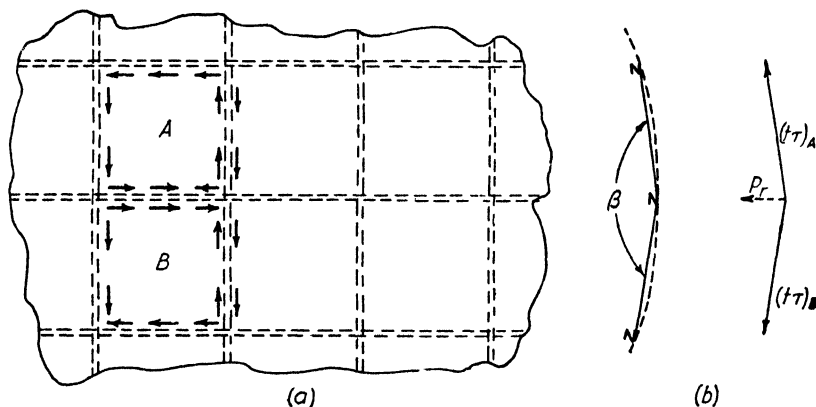


FIG. 10-2. Fuselage panels.

sheet between longitudinals thus producing a normal pressure on the longitudinal, which pressure is resisted in bending and shear by the longitudinal. The magnitude of the induced bending stresses can be estimated as follows:

Assume the shear stress to be uniform over a panel such as *A* or *B*, Fig. 10-2*a*, and calculate the shear flow, $(t\tau)_A$ and $(t\tau)_B$, at the center of the panel by equation 10-1. This shear flow acts in the plane of the sheet, which is assumed to be straight between longitudinals, Fig. 10-2*b*. It should be remembered that the conditions of equilibrium of a sheet element require that the shear stress along two perpendicular edges be equal in magnitude. If the angle between the chords to adjacent stiffeners is denoted by β then the load, in pounds per inch, tending to bend the longitudinal inward is

$$p_r = [(t\tau)_A + (t\tau)_B] \cos \beta/2 \quad [10-2]$$

If p_r is assumed constant between frames the stringer can be treated as a simple beam subjected to a uniform load. This method is only a rough approximation. A somewhat more accurate method is to consider only

the shear flow above the buckling value as the contributing value to the induced bending moments, that is, instead of equation 10·2, use

$$p_r = [t_A (\tau - \tau_c)_A + t_B (\tau - \tau_c)_B] \cos \beta/2 \quad [10\cdot3]$$

where τ_c is the buckling shear stress for the respective panels and τ is the shear stress corresponding to the shear load S_y . When τ is less than τ_c the equation has no meaning for the sheet is in the unbuckled state. Actually the sheet is not buckled at the frame and the load p_r is not constant between frames but drops off to zero at the frames. For a more accurate determination of the maximum stress the longitudinal should be analyzed as a beam column. By a beam column is meant a beam subjected to axial and transverse loads.

In addition to the shear and bending loads the fuselage structure will also be subjected to torsional loads. The torsional loads are a result of fin gust loads acting at right angles to the fin surface; side-load landing conditions in the case of a tricycle landing gear; and from the unbalanced loads in the unsymmetrical flight conditions. In the unsymmetrical flight conditions the wing reactions at the fuselage are not symmetrical, that is, the reactions on one side are larger than those on the other side. This unbalanced condition results in a torsional moment on the fuselage. The non-symmetry of the wing reactions are a result of the inertia forces in the fuselage due to the angular accelerations caused by the assumed difference in the lifting forces on each half span of the wing.

The torsional loads are transferred through the sheet covering to the members or parts of the airplane which are capable of resisting them. For example, the torsional load resulting from the side load on the fin is resisted by reactions at the connections between the fuselage and the wing. Similarly the torsional loads resulting from the unsymmetrical flight conditions are resisted by wing reactions. The shear flow and the angular twist per unit length θ , resulting from the torsional loads, can be calculated by equations 3·80 and 3·82 of section 3-6(b).

$$\tau t = \frac{M_t}{2A}$$

$$\theta = \frac{M_t p}{4A^2 G t}$$

As previously pointed out these equations are strictly valid only when warping of the cross section is not restrained, that is, when we have a condition of pure torsion. It should be noted, that for the condition of pure torsion the shell with longitudinal stringers has the same shear

flow as the unstiffened shell and the torsional stiffness is the same. If the walls of the fuselage consist of sheet plus corrugations, the combination of sheet and corrugations can be replaced by an equivalent sheet, the thickness of which can be calculated by the method given in section 9-1(a). If the torsional loads are sufficiently high, so that diagonal tension fields are formed between stiffeners, their effects will be to introduce secondary loads in the longitudinals and frames. These secondary loads are similar in character to those described for the vertical shear condition. Usually the torsional loads on the fuselage are not high enough to cause any appreciable secondary load.

The methods of analysis discussed so far do not take into account the effects of cutouts and discontinuities in the material and loads. A considerable number of large cutouts are necessary in the majority of fuselages, such as doors, windows, and emergency exits. Methods are not available for calculating the exact influence of such cutouts on the stress distribution. The usual procedure is to make an analysis based on the elementary beam theory with suitable allowances for the material at or near the cutouts, which is not fully effective. For example, in calculating moments of inertia and static moments, a stringer ending at a cutout is assumed ineffective from the cutout to the point where it crosses a frame. The discontinuity in the shear flow due to the cutouts is probably the most serious. Suitable provisions must be made to allow the shear loads to be carried around the cutouts. This can be accomplished by providing doubler plates and also some form of a stiffening frame work reinforcement around the cutout. If the cutouts are not properly reinforced with a stiffening framework, an excessive amount of warping will take place, this being especially true around doors. Sharp corners in cutouts should be avoided, since they cause high stress concentrations which may be either sufficiently high to cause direct failure of the material or, if lower, they may cause a fatigue failure of the material.

The floor and floor supports in passenger and cargo airplanes are part of the fuselage and as such should be considered in the fuselage analysis. The floor supports usually consist of beams which transfer the floor loads to the fuselage structure.

The ordinary beam theories are all that are necessary for the analysis of these supports. Occasionally they may be of a statically indeterminate nature and in such cases the methods given in Chapter 4 can be used. The concentrated loads coming from chairs, etc., are taken directly into the floor supports. The floor is designed for the maximum pressure, in pounds per square inch, to which it will be subjected. The actual magnitude of the pressure is determined by oper-

ating conditions. For example, it has been found that women's heels (especially of the French variety) cause very high local loads and map determine the floor design.

The transfer of loads from the floor supports into the fuselage structure must also be considered. The passenger loads are distributed over a large number of frames and the resulting load on each frame will be relatively small. In baggage compartments the loads may be sufficiently high to require an analysis of the frames which distribute the load. The transfer of loads by the frames into the fuselage structure is discussed in the following paragraphs.

In the design of fuselage frames two types of frames should be considered, namely, (a) intermediate frames and (b) main frames or bulkheads. The intermediate frames are provided to preserve the shape of the fuselage structure, to reduce the column length of the stringers and to prevent general instability failure. These frames are subjected to several types of loading such as radial loads due to the longitudinal curvature of the stringers, effects of diagonal tension fields in the sheet covering, or transfer of local shear loads to the sheet covering. Most of these loads are comparatively small and often tend to balance each other, therefore the design of intermediate frames is commonly based either on the experience of the designer or on some semi-empirical methods of analysis.

This applies only to localized shear loads which must be transferred to the fuselage structure. The frame sizes necessary for general instability criteria are determined by the methods of section 8-3. It must be realized that the experimental evidence on which the design criteria of section 8-3 are based was obtained from pure bending tests. Data on the influence of shear are not as yet available; it is therefore recommended that the pure bending data be used for the general instability calculations. Tests on stiffened cylinders which failed by panel instability, reference 10-2, indicated that the influence of shear was such as to give a higher maximum stringer stress before failure occurred. It is possible that in the general instability type of failure the same effects may occur.

The main frames are introduced primarily to distribute into the sheet covering such concentrated loads as the loads from the wings, tail surfaces, and landing gear. Main frames are usually statically indeterminate structures and their analysis is based on the methods discussed in Chapter 6. One of the first considerations in the analysis of frames is the distribution of the shear load over the frame. It should be remembered that the frame is somewhat analogous to a rib inasmuch as it is required to distribute the shear loads into the fuselage

structure. In order to agree with the bending theory, the distribution of shear over the frame should be according to equation 10·1 or the shear load in pounds per inch at any point on the frame should be

$$t\tau = \frac{S_y Q_x}{I_x} \quad [10\cdot4]$$

where Q_x is the same as in equation 10·1. This type of distribution gives a maximum value at the neutral axis, regardless of where the load is applied. Another way of considering the problem is that the fuselage covering will absorb the maximum amount of shear at the point of application of the concentrated load and that the shear resistance of the covering is reduced in proportion to its distance from the point of application of the concentrated load. This gives a linear shear distribution over the length of the frame. In addition to the distribution of the shear load, the magnitude of the concentrated load to be transmitted must be considered. The main frames which connect to the wing spars resist the spar shear reactions at the fuselage. The magnitude of the shear reaction at any spar is equal to the total shear load in the spar web. Similarly the frames at the tail surfaces resist the reaction loads coming from the stabilizer spars. In the tricycle type of landing gear the loads on the nose gear are transmitted to the fuselage structure; however, here the dissipation of load into the structure is usually more gradual, that is, several frames are used for transmitting the load. One method is to attach the gear to two spars extending over several frames, the loads are then transmitted from the gear into the spars, from the spars into the frames, and from the frames into sheet covering and distributed bending material. Since the surrounding structure, i.e., spars, frames, sheet covering, and distributed bending material, forms a statically indeterminate structure, the exact portion of the total load resisted by each frame is difficult to determine. By making some simplifying and overlapping assumptions an analysis giving results of a first order approximation can be obtained. For example, the spars may be considered as simple beams, the frames providing the necessary reactions.

The relative stiffness between the frame and the member which provides the reaction, and also the method of attachment to the member, will have an important bearing on the analysis. This is true, for example, for main-wing spars where the moment of inertia of the spar may be of the order of one thousand times that of the bulkhead, when it can be readily assumed that the frame is attached to a member of infinite rigidity. This assumption will to some extent simplify and shorten the work.

For the analysis of these frames we make use of Castigliano's second theorem, the theorem of least work. In order to clarify the general ideas involved in the solution, we shall first consider a very simple case and then treat the more general case. Consider a circular bulkhead of uniform cross section, Fig. 10·3*a*, attached to a spar at two points which lie on a diameter. It is assumed that the moment of inertia of the spar is very large compared to that of the bulkhead and the con-

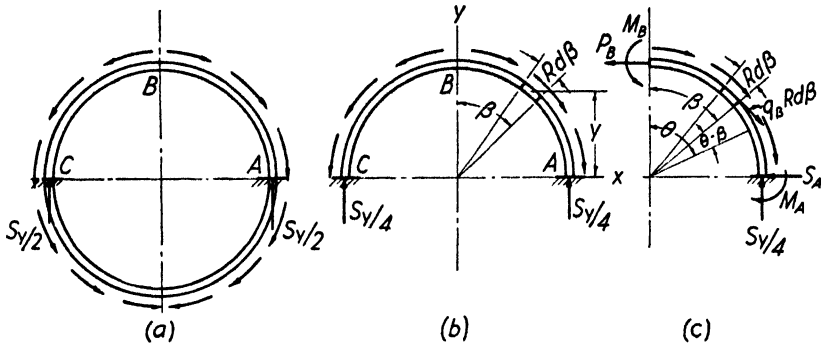


FIG. 10·3. Notation for frame analysis.

nection between spar and bulkhead is equivalent to a built-in end. The shear distribution is in agreement with the bending theory, that is,

$$t\tau = \frac{S_y Q_x}{I_x} \quad [10.4]$$

If we replace the distributed bending material by a sheet of uniform thickness t_0 around the frame, where t_0 is equal to the total area of the bending material divided by the perimeter of the cross section, the analysis is greatly simplified. From the symmetry of the system it is seen that the upper half of the frame will carry one-half the total shear reaction S_y distributed equally to the end of the half frame as shown in Fig. 10·3*b*. The axes of symmetry, X and Y , will also be the principal axes. The static moment of an element of length $R d\beta$, with respect to the neutral axis is

$$\Delta Q_x = y t_0 R d\beta$$

Substituting $R \cos \beta$ for y and denoting the shear flow by q gives for the shear flow for any value of β

$$q_\beta = \frac{S_y t_0 R^2}{I_x} \int_0^\beta \cos \beta d\beta = \frac{S_y t_0 R^2}{I_x} \sin \beta$$

Noting that for a thin-wall cylinder of wall thickness t_0 the moment of inertia about a diameter is $\pi t_0 R^3$ we have,

$$q_\beta = \frac{S_y \sin \beta}{\pi R} \quad [10.5]$$

This shear load in pounds per inch, acts along the outer surface of the frame and is at every point tangent to the surface of the frame. Since the bending axis of the frame is at its neutral axis the shear flow γ will introduce a secondary bending moment which is proportional to the distance from the neutral axis to the outer surface. If the frame depth is small compared to the frame diameter the effects of the secondary moments are also small and will be neglected in our present calculations.

Dividing the upper part of the frame into two halves, Fig. 10.3c, the unknown forces M_B and P_B must be applied at B to balance the external loads. Let us first calculate the moment M_{θ_q} , produced by the unit tangential shear loads q at θ . The shear load $q_\beta R d\beta$ acting over an element of length $R d\beta$ produces a moment at θ of magnitude

$$\Delta M_{\theta_q} = q_\beta R^2 [1 - \cos(\theta - \beta)] d\beta$$

or

$$M_{\theta_q} = \frac{S_y R}{\pi} \int_0^\theta [1 - \cos(\theta - \beta)] \sin \beta d\beta = \frac{S_y R}{\pi} \left(1 - \cos \theta - \frac{\theta}{2} \sin \theta \right)$$

We can now write the expression for the total moment at any point on the frame in the form

$$M_\theta = M_B + P_B R (1 - \cos \theta) - \frac{S_y R}{\pi} \left(1 - \cos \theta - \frac{\theta}{2} \sin \theta \right) \quad [10.6]$$

The unknown quantities M_B and P_B can be determined by Castigliano's second theorem, section 4-1, namely,

$$\begin{aligned} \frac{\partial U}{\partial M_B} &= \frac{1}{EI} \int_0^{\pi/2} M_\theta \frac{\partial M_\theta}{\partial M_B} R d\theta = 0 \\ \frac{\partial U}{\partial P_B} &= \frac{1}{EI} \int_0^{\pi/2} M_\theta \frac{\partial M_\theta}{\partial P_B} R d\theta = 0 \end{aligned}$$

By substituting the value of M_θ in these two equations and by performing the integration, we obtain two equations, linear in the two unknown quantities M_B and P_B , and from these two equations we can determine the magnitude of M_B and P_B in terms of the known quantities S_y and R . The moment at any point on the frame can now be calculated by equation 10.6. It has been assumed in the above energy expression that the expression for the bending strain energy of a beam is also applicable to curved members.

The shear force at right angles to the neutral axis, Fig. 10.4 can be calculated from the following relations.

$$S_\theta = \frac{dM}{dx} = \frac{1}{R} \frac{dM_\theta}{d\theta} \quad [10.7]$$

A general expression for the axial load in the frame can be obtained from the equation of equilibrium for a section of the frame, Fig. 10.4. Taking moments about the center of the frame gives

$$M_0 = M_B + P_B R + P_\theta R - M_\theta - \frac{S_y R}{\pi} \int_0^\theta \sin \phi \, d\phi = 0$$

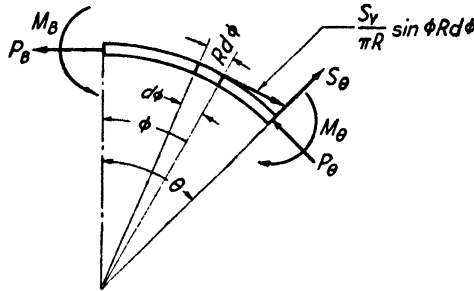


FIG. 10.4.

Substituting for M_θ the value given by equation 10.6 and integrating gives

$$P_\theta = \frac{S_y}{2\pi} \theta \sin \theta - P_B \cos \theta \quad [10.8]$$

With the bending moment and axial loads known the maximum compression or tension stresses are calculable.

Let us now consider the more general case (reference 10.4) in which the bending material is not uniformly distributed and the frame has a variable cross section. The cross section is again symmetrical with respect to the Y -axis and the total shear reactions are transmitted to the frame at points A and C , as shown in Fig. 10.5a. These shear reactions are also symmetrical with respect to the Y -axis. The axes X and Y are principal axes and their position is calculated by the method described in section 9-1(b). The shear distribution can be assumed either to be in agreement with the bending theory, that is,

$$q = \frac{S_y Q_x}{I_x}$$

or to vary linearly with the distance from the applied reaction as previously described. Because of the symmetry of the system the frame can be divided into two halves. The balancing loads at A and D are

indicated in Fig. 10-5b. For convenience we divide the frame into n sections of length ΔL , then the tangential shear load acting on the i th section is

$$\Delta S_i = q_i \Delta L_i$$

At any section J - J between $\theta = 0$ and $\theta = \theta_1$ the bending moment is equal to

$$M_j = M_B + P_B y_j - \sum_{i=1}^{i=j} \Delta S_i d_i \quad [10.9]$$

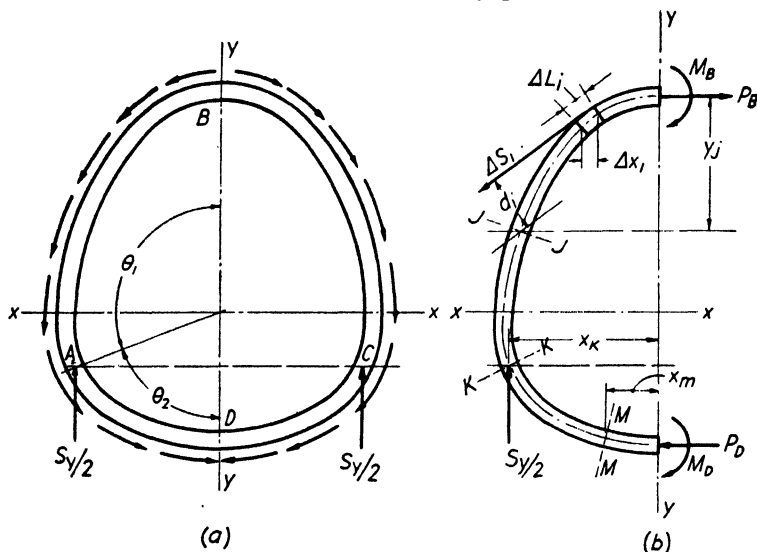


FIG. 10-5. Frame analysis.

and between $\theta = \theta_1$ and $\theta = \theta_2$ the bending moment at section M - M is

$$M_m = M_B + P_B y_m - \sum_{i=1}^{i=m} \Delta S_i d_i + \frac{S_y}{2} (x_k - x_m) \quad [10.10]$$

Replacing the integral expression for the bending strain energy by a summation, we can write for the total strain energy in one-half the frame,

$$U = \frac{1}{2} \sum_{j=1}^{j=k} \frac{\left[M_B + P_B y_j - \sum_{i=1}^{i=j} \Delta S_i d_i \right]^2}{E_j I_j} \Delta L_j$$

$$+ \frac{1}{2} \sum_{m=k}^{m=n} \frac{\left[M_B + P_B y_m - \sum_{i=1}^{i=m} \Delta S_i d_i + (S_y/2) (x_k - x_m) \right]^2}{E_m I_m} \Delta L_m$$

By Castigliano's second theorem

$$\begin{aligned} \frac{\partial U}{\partial P_B} &= \sum_{j=1}^{j=k} \frac{\left[M_B + P_B y_j - \sum_{i=1}^{i=j} \Delta S_i d_i \right]}{E_j I_j} y_j \Delta L_j \\ &+ \sum_{m=k}^{m=n} \frac{\left[M_B + P_B y_m - \sum_{i=1}^{i=m} \Delta S_i d_i + (S_y/2)(x_k - x_m) \right]}{E_m I_m} y_m \Delta L_m = 0 \\ \frac{\partial U}{\partial M_B} &= \sum_{j=1}^{j=k} \frac{\left[M_B + P_B y_j - \sum_{i=1}^{i=j} \Delta S_i d_i \right]}{E_j I_j} \Delta L_j \\ &+ \sum_{m=k}^{m=n} \frac{\left[M_B + P_B y_m - \sum_{i=1}^{i=m} \Delta S_i d_i + (S_y/2)(x_k - x_m) \right]}{E_m I_m} \Delta L_m = 0 \end{aligned}$$

For convenience we designate $\Delta L/EI$ by Z , then the latter two equations become

$$\begin{aligned} M_B \sum_{j=1}^{j=n} y_j Z_j + P_B \sum_{j=1}^{j=n} y_j^2 Z_j - \sum_{j=1}^{j=n} \left[y_j Z_j \sum_{i=1}^{i=j} \Delta S_i d_i \right] \\ + (S_y/2) \sum_{j=k}^{j=n} Z_j (x_k - x_j) y_j = 0 \quad [10.11] \end{aligned}$$

$$\begin{aligned} M_B \sum_{j=1}^{j=n} Z_j + P_B \sum_{j=1}^{j=n} y_j Z_j - \sum_{j=1}^{j=n} \left[Z_j \sum_{i=1}^{i=j} \Delta S_i d_i \right] \\ + (S_y/2) \sum_{j=k}^{j=n} Z_j (x_k - x_j) = 0 \quad [10.12] \end{aligned}$$

From these two equations the two unknown quantities P_B and M_B can be determined. All expressions can be readily evaluated except the expression $\sum_{i=1}^{i=j} \Delta S_i d_i$ which requires a considerable amount of work. It

should be noted that all values of d_i are different for each section ΔS . Since $\Delta L_i d_i$ is equal to twice the area of the triangle abc , Fig. 10.6a, it is

seen that the expression $\sum_{i=1}^{i=j} \Delta L_i d_i$ is just equal to twice the area $ebcda$.

Now the expression $\sum_{i=1}^{i=j} \Delta S_i d_i$ can be written as

$$\sum_{i=1}^{i=j} \Delta S_i d_i = \sum_{i=1}^{i=j} q_i \Delta L_i d_i = \bar{q} \sum_{i=1}^{i=j} \Delta L_i d_i \quad [10 \cdot 13]$$

if \bar{q} is the mean of the shear flow between the points e and d . Hence the expression can be best evaluated in the following manner:

1. Plot the distribution of q , Fig. 10·6b, as a function of the length of the frame, the length being measured along the outer surface from the point d , Fig. 10·6a.

2. Plot the value of twice the area, similar to the area $ebcda$, at each section as a function of the frame length. This gives $\sum \Delta L_i d_i$ as a function of the length as shown in Fig. 10·6a.

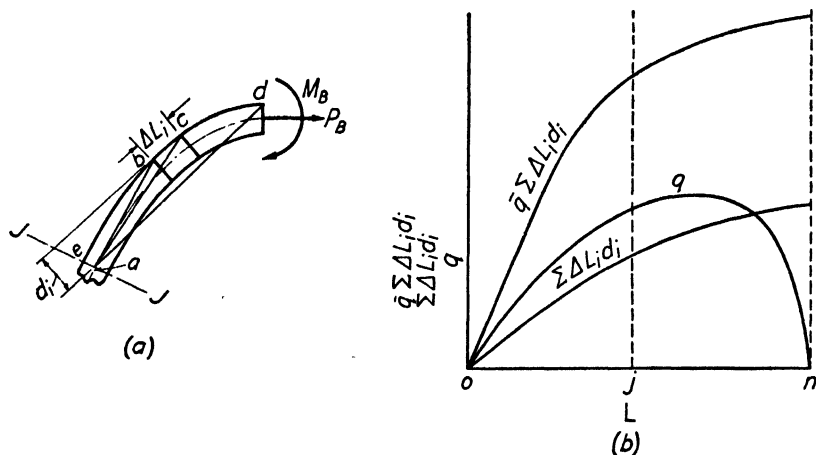


FIG. 10-6. Graphical solution of equation 10-13.

3. Plot the values of $\bar{q} \sum \Delta L_i d_i$ as a function of the frame length. The mean value of \bar{q} , for example, at section J - J is the area under the q curve up to j , divided by the length to j , Fig. 10·6b, and $\sum_{i=1}^{i=j} \Delta L_i d_i$ is the value given by the $\sum \Delta L_i d_i$ curve at j .

The summations of equations 10·11 and 10·12 can now be evaluated in a tabular form as shown in Table 10·1. Substituting the numerical values of the summations in equations 10·11 and 10·12, the quantities P_B and M_B are determined and their values substituted in equations

TABLE 10-1

Section	Z_i	y_i	$Z_i y_i$	$Z_i y_i^2$	$\sum_{i=1}^{t-j} \Delta S_i d_i^*$	$Z_i \sum_{i=1}^{t-j} \Delta S_i d_i$	$Z_i y_i \sum_{i=1}^{t-j} \Delta S_i d_i$	$x_k - x_j$	$Z_j(x_k - x_j)$	$Z_j y_j(x_k - x_j)$	M
1											
2											
n											
	$\sum_{j=1}^{t-j} Z_j$		$\sum_{j=1}^{t-j} Z_j y_j$	$\sum_{j=1}^{t-j} Z_j y_j^2$		$\sum_{j=1}^{t-j} \Delta S_j d_j$	$Z_j \sum_{j=1}^{t-j} \Delta S_j d_j$		$\sum_{j=1}^{t-j} Z_j(x_k - x_j)$	$\sum_{j=1}^{t-j} Z_j y_j(x_k - x_j)$	

* Note that $\sum_{i=1}^{t-j} \Delta S_i d_i = \bar{q} \sum_{i=1}^{t-j} \Delta L_i d_i$. For each section the corresponding value of $\bar{q} \sum_{i=1}^{t-j} \Delta L_i d_i$ is obtained from the upper curve of Fig. 10-6b.

10·9 and 10·10. The bending moment M can now be calculated at any frame section. To determine the axial load and the transverse shear at any section, construct a force polygon of all the forces starting with P_B and continuing along the frame with the ΔS_i forces. Then the component of all the forces, acting above section $J-J$, in a direction parallel to the tangent at section $J-J$, gives the axial load acting on the frame at this section. The component of these forces perpendicular to the tangent, at section $J-J$, gives the transverse shear force at the section. With all the loads known the combined stresses at any section can be calculated.

The above method of analysis is strictly only applicable to frames which are unsupported by the fuselage covering and the distributed bending material, that is, their deflections are not restricted by the surrounding fuselage structure. Actually the frame deflections may become quite pronounced in which case the outward deflections are resisted by the fuselage covering due to double curvature effects and by the support of adjacent frames through the longitudinal stiffening elements. This action of the surrounding structure is equivalent to an introduction of inward acting loads which resist bending of the frame and which thereby reduce the frame stresses to values smaller than that indicated by the above analysis. However, at present, methods are not available for determining the actual reduction in stresses due to these effects, and it is therefore recommended that the above method of analysis be used in the design of main frames.

So far we have considered only the stresses resulting from vertical shear reactions. As previously pointed out, for example, in the unsymmetrical flight conditions the shear reactions are not symmetrical about the Y -axis. The unsymmetrical reactions can be replaced by a system of symmetrical vertical reactions plus a torsional moment equal to the unbalanced couple produced by the unequal reactions. These two loading conditions, vertical shear and torsion, can then be treated separately by the previously given methods of analysis. The stresses resulting from the separate loadings are added algebraically to give the total stress.

Other cases which give rise to combined torsion and shear can be treated in a similar manner. The distribution of the shear flow due to torsion is constant around the frame and is given by the equation

$$q = \tau t = \frac{M_t}{2A}$$

Because of the uniform shear flow over the fuselage cross section the calculations of the frame stresses, due to torsion, are somewhat simpler;

for example, \bar{q} in equation 10.13 has the same value at every section. When a large cutout occurs adjacent to a main frame, its influence on the shear distribution should be taken into account. In addition to the frame stresses, the loads acting at the various connections between the frames and wing spars and between the frames and sheet coverings are obtained from the frame analysis.

The fuselage analysis covered in this chapter is of a general nature and no attempt has been made to cover detailed methods of analysis or to treat special problems. The references included at the end of the chapter treat many of these problems as well as giving a more detailed treatment of the methods of analysis.

REFERENCES FOR CHAPTER 10

- 10.1. H. EBNER and H. KOLLER, "Calculation of Load Distribution in Stiffened Cylindrical Shells," *N.A.C.A. Tech. Memo.* 866.
- 10.2. H. EBNER, "The Strength of Shell Bodies—Theory and Practice," *N.A.C.A. Tech. Memo.* 838.
- 10.3. O. S. HECK and H. EBNER, "Methods and Formulas for Calculating the Strength of Plate and Shell Constructions as Used in Airplane Design," *N.A.C.A. Tech. Memo.* 785.
- 10.4. W. A. KLINKOFF, "Notes on Thin Metal Aircraft Structures," Aeronautics Library, California Institute of Technology, 1937.
- 10.5. E. E. LUNDQUIST and W. F. BURKE, "General Equations for the Stress Analysis of Rings," *N.A.C.A. Tech. Rep.* 509.

CHAPTER 11

ENGINE MOUNTS, LANDING GEARS, AND FITTINGS

11-1. Engine Mounts

In the analysis of an engine mount the first problem to be considered is that of determining the magnitude of the external forces to be resisted by the structure. All forces and moments acting on the engine mount can be classified as either direct or induced. The former includes thrust, torque, and the air forces on the engine or cowling, whereas the latter is concerned with inertia forces. Although the induced forces are of the same fundamental character, they arise from such a variety of causes that it might be well to consider them in some detail together with the direct forces. A further classification according to the cause of the force can be made as follows (see reference 11·1):

a. The thrust and torque forces are produced by the propeller and their values depend on the engine and propeller characteristics as well as on the flight conditions. Their values can be calculated by standard methods given in courses on aerodynamics.

b. The lift and drag (or anti-drag) forces on the cowling of a radial engine may be of sufficient magnitude to warrant their inclusion in the engine mount analysis. The magnitude of these forces can be estimated from wind tunnel test data.

c. The linear acceleration forces arise from the acceleration of the airplane as a whole, caused by the resultant air forces, and are given by

$$F_a = \frac{W}{g} a$$

where W = the weight of the engine

a = the linear acceleration of the airplane in any direction.

d. The angular acceleration forces and moments arise from the angular acceleration of the airplane about its center of gravity. The force is given by

$$F_a = \frac{W}{g} l \alpha$$

and the moment by

$$M_{\alpha} = I\alpha$$

where l = the distance from the center of gravity of the airplane to the center of gravity of the engine-propeller combination,

I = the mass moment of inertia of the airplane about the axis of rotation, and

α = the angular acceleration.

e. The radial acceleration force arises from the angular velocity, ω , of the airplane about its center of gravity and is given by

$$F_{\omega} = \frac{W}{g} \omega^2 l$$

f. Gyroscopic couples arise from the rotation of the propeller and certain parts of the engine, both of which act in conjunction with an angular velocity of the airplane. The equations for calculating these couples are given in reference 11-1.

g. Vibration forces arise from unbalanced engine parts, propellers, etc. The nature of these forces is such that they are not included in the usual static stress calculations, but must be considered from a standpoint of fatigue of the structure. In addition to the above any special loading requirements as given by the Civil Aeronautics Authority or the Services must be met. For these, see CAR 04, CAAM 04 and the appropriate service manuals and handbooks.

The above loads apply to either air-cooled or liquid-cooled engines. The remainder of the discussion on engine mounts will be primarily concerned with the design of air-cooled radial engine mounts since this type of engine predominates in both service and commercial airplanes of this country.

After the loads have been determined the next problem is that of choosing a structure which will (1) carry the applied loads, and (2) allow easy access to the back of the engine since this region contains nearly all of the engine accessories and accessory drives. In the majority of the normal-sized airplanes built today, a welded steel tubular mount is used. (See Fig. 11-1.) The analysis of such mounts follows the usual methods of analysis for space frameworks given in Chapter 4 or in numerous other reference texts (see reference 11-2). It is almost

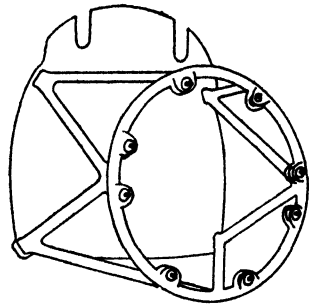


FIG. 11-1. Welded steel tubular engine mount.

mandatory that these trusses be redundant so that loss of one member due to fatigue failure or any other reason, will not cause complete loss of an engine. This redundancy may extend to all four sides of the mount. The only member of the mount which does not lend itself easily to types of analysis previously discussed is the engine mounting ring, to which is attached the engine. A method of analysis of this member is given in detail in reference 11-3 and will not be given here.

Every effort should be made to have the center lines of all members entering a joint intersect at one point. This will prevent fatigue failure arising from reversal of loads applied through eccentric points. A certain amount of gusseting at the joints is usually necessary and, to permit an accurate stress analysis, typical joints should be tested to determine the appropriate end restraint to use for the tubes.

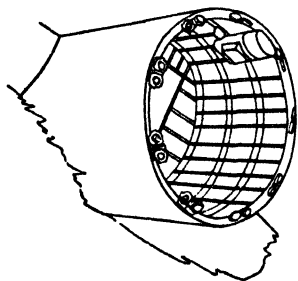


FIG. 11-2. Semi-monocoque engine mount.

There are two major disadvantages inherent in the welded tubular mount. The first of these is the need for highly skilled welders to manufacture the structure. The labor on this type of mount is therefore

expensive and the construction does not lend itself readily to mass production using relatively unskilled labor. The second disadvantage is that the mount must be covered with an inner cowl for aerodynamic reasons and, since the air forces and vibration forces in this cowl are relatively large the cowl is heavy but actually contributes nothing to the strength properties of the engine mount itself.

For the above reasons, considerable thought has been given to the use of a semi-monocoque engine mount. (See Fig. 11-2.) This structure takes the place of both the engine mount and inner cowl and thus one structure is made to serve two purposes. The major disadvantage of the semi-monocoque cowl is the difficulty of providing sufficient access holes in the mount without destroying the strength properties of the structure. In very large installations it is possible to reach the rear of the engine from inside the nacelle and in these cases there is no problem. However, the design for reasonably large radial engines looks promising and the access doors present no more of a problem than do cutouts in the wings and fuselage of the airplane. Methods of analysis for this type of mount are identical with those discussed previously for the wings and fuselages, although the loadings are in general more complex.

11-2. Landing Gears

There are two types of ground plane landing gears in common use at the present time. The first of these is the one that has been used for a number of years and consists of two main wheels forward of the center of gravity of the airplane and a smaller wheel located somewhere near the tail. This is commonly known as the *conventional* type of landing gear. A somewhat newer innovation which is rapidly gaining favor is the *tricycle* gear which consists of two main wheels aft of the center of gravity and a nose wheel as far forward in the nose of the fuselage as it can be placed. These two types are discussed in detail in Chapter XII of reference 11-4 and only the major advantages and disadvantages will be mentioned here. In general, it can be said that the tricycle gear is heavier, has a shorter wheel base, has more drag if unretracted than the conventional gear, and does not allow ground-looping in emergencies. To offset these disadvantages, the tricycle gear allows full use of the brakes in landing without danger of nosing over, has no tendency to ground-loop accidentally, is more suitable for blind landing, and usually allows shorter take-off runs. Structurally, the design of the nose wheel follows the same pattern as that for the main wheels except that it must have incorporated in it devices to permit swiveling, centering when retracting, and possibly steering when taxiing. The same statements are true concerning the tail wheel; however, the loads on the tail wheel are very much smaller than those on the nose wheel and it is consequently much smaller.

Considering main landing gears, they fall into two major classifications: those which retract while in flight and those which remain extended at all times. The obvious advantage to the retractable gear is the reduction in drag which must be paid for by an increase in weight, not only by the addition of the retraction mechanism but also because the retracted wheel makes large cutouts necessary in the wing or fuselage into which it goes thus causing structural inefficiency and an additional weight increase. However, the drag saving is sufficient to make retraction justifiable, if not mandatory, on all large, high-performance airplanes and the non-retractable type is therefore seen only on smaller or low-performance airplanes.

Structurally, there are again two classifications into which nearly all landing gears will fall. These are the truss-type gear (Fig. 11-3) and the cantilever (Fig. 11-4) or semi-cantilever (Fig. 11-5) types. The truss-type gear has the advantage that the oleo strut is in pure compression which leads to a smoother action particularly in taxiing. It has more drag and therefore is never used for a non-retracting gear,

however, the drag increase is not so serious and for some considerations may be an advantage for a retracted system. It does have the serious disadvantage that it gives more structural interference when retracted owing to the over-all dimensions of the truss. It has one other disad-

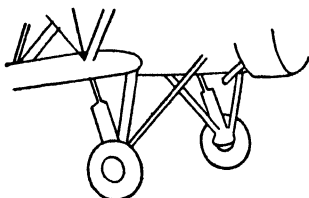


FIG. 11-3. Truss-type landing gear.

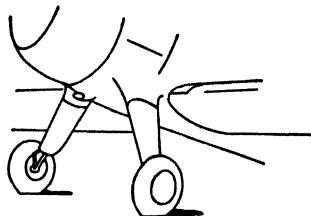


FIG. 11-4. Cantilever landing gear.

vantage since removal of a wheel is more complicated; however, this may be offset by the possibility of having brakes on both sides of the wheel and by being able to run direct pressure leads from the truss structure on both sides. The cantilever gear, with its low drag, is always used for non-retracting systems and because of the relatively

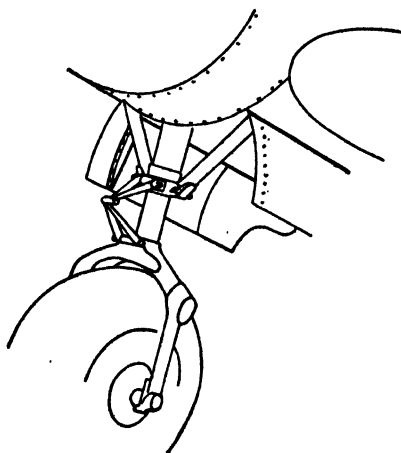


FIG. 11-5. Semi-cantilever landing gear.

small size of the structure is being used considerably in retracted systems. It has the disadvantage that the oleo strut is in bending and, if the design is not carefully handled, this fact may cause serious sticking and consequently poor shock absorber action. Owing to the necessity for attaching the retraction mechanism to the gear, it is frequently possible to use part of the retraction system to take some of the loads which may lead to a structure which is cantilever for side loads and trussed for fore and aft loads, or vice versa.

The loads in the landing-gear system have been briefly outlined in

Chapter 2 and are more specifically given for commercial airplanes in CAR 04 and CAAM 04. For the truss system, the method of analysis follows the methods given in Chapter 4. The cantilever or semi-cantilever gear analysis follows the principle of beam analysis, in which the beam is loaded with bending and shear in one or more planes and, in addition, may be subjected to torsion. The only part of the analysis which introduces new features is the analysis for the bend between

the oleo and the axle, and this part must be analyzed by the methods employed for curved beams under bending. A short description of this method will be given and more detailed derivations may be found in reference 11.5 and 11.6 and others.

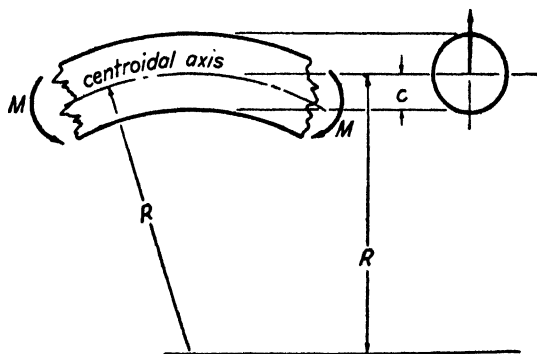


FIG. 11-6. Curved beam notation.

Consideration of the beam in Fig. 11.6, shows that the stress at any distance y from the centroidal axis of the section is given by the equation

$$\sigma = \frac{M}{AR} \left(1 + \frac{1}{Z} \frac{y}{R + y} \right) \quad [11.1]$$

where M = bending moment in inch-pound, considered positive when it tends to increase the curvature;

A = cross-sectional area of the beam in square inches;

R = radius of the beam measured to the centroidal axis of the section, in inches;

Z = a non-dimensional property of the cross section, somewhat similar to the moment of inertia in the straight beam formula;

y = distance to fiber in question from the centroidal axis, in inches—positive towards convex side of beam.

Values for Z for various beam cross sections are given in the above references. For circular and elliptical cross sections, the values may be calculated from the equation

$$Z = -1 + 2 \left(\frac{R}{c} \right)^2 - 2 \left(\frac{R}{c} \right) \sqrt{\left(\frac{R}{c} \right)^2 - 1} \quad [11.2]$$

where R is as defined above and c is the distance to the outer fiber measured from the centroidal axis. (Fig. 11.6).

In general, the stresses at this section of the oleo strut will determine the outside diameter of the oleo strut. Since the effect of the curved beam disappears in the straight portion of the strut and also, since the torsion links take out the torsion stresses, the upper part of the oleo strut need not be as strong and may be bored out to reduce weight.

The shock-absorbing mechanism is either purchased as a complete assembly or in large companies is designed by a special group, therefore it will not be discussed. One item, however, which must be kept in mind is that the oleo piston and cylinder must slide together under load and should therefore have the same load-deflection curve. In order that this may be true it is advisable that the oleo cylinder and strut have as nearly as possible the same moment of inertia.

The retraction mechanisms, although they may appear complex, are basically determinant truss systems and are so analyzed. No attempt will be made to show a typical system because they are different for nearly every airplane. The only design features that should be emphasized are (1) that the system be not adversely affected by deflections of adjacent structures such as the wings; (2) that manual retraction and lowering be provided if the power supply (usually hydraulic) fails; and (3) that positive locks be provided to assure rigidity of the landing gear when it is extended.

11-3. Fittings

In the interest of structural efficiency it is desirable to keep the number of fittings in an airplane to an absolute minimum. The ideal airplane would be one that contained no fittings. However, from the standpoint of production, assembly, and maintenance, it is necessary to break the structure into small units to facilitate handling. Each such unit which must be attached to the rest of the structure involves the use of fittings. Such fittings must be as strong as the members they join and they will weigh as much as the structure they replace plus any additional material necessary to pick up the loads in the structure plus the weight of bolts, nuts, rivets, or other means of attaching the fitting to the structure. In addition to the above, regulations specify an additional fitting margin of safety over and above the design loads. Meeting this margin of safety, which is 1.20 for commercial airplanes and 1.15 for military airplanes, adds additional weight to the structure.

There are additional factors which make fittings responsible for weight increases other than those mentioned above. Provisions for attaching bolts may make the adjacent structure larger and heavier because of stress concentrations around bolt holes. Fittings may change a column-

end fixity and may add secondary loads due to unavoidable eccentricities. And it must not be forgotten that such items take time to manufacture and therefore increase the cost of producing the airplane in addition to increasing its weight. In the light of the above, it is therefore obvious that a designer's efforts should be directed towards reducing fittings to a minimum and to making them as simple to analyze and to manufacture as is possible.

The fact that fittings must be manufactured with appropriate tolerances on all dimensions also adds to the weight problem. For example, a fitting with a $\frac{1}{8}$ -in. web may have a tolerance of $\frac{1}{64}$ which immediately makes it necessary to analyze on the minimum dimension of $\frac{7}{64}$ in. whereas a large portion or even all the fittings may come through with the maximum dimension of $\frac{9}{64}$ in., which immediately gives a weight penalty of 30 per cent in such fittings. In general, due to their small size, fitting tolerances will be proportionally greater than those in large structural members and thus the weight penalty will be more severe.

The designer should be completely familiar with the machine operations used in manufacturing fittings and for that purpose should read the appropriate parts of reference 11·7. The most common manufacturing methods are:

a. To cut the fittings from solid bar stock. This method is slow and is therefore generally used on experimental models or for fittings which are simple enough to be finished on an automatic screw machine or lathe equipment.

b. To form the fittings from sheet stock. This is a satisfactory method for small attachment clips and similar parts.

c. Casting the fitting in aluminum or magnesium-alloy or high-strength steel. One of the major disadvantages of this method lies in the very severe penalties which are imposed upon any castings used as structural members of an airplane. These restrictions make margins of safety of 100 per cent sometimes necessary and this imposes a very severe weight penalty on this type of fitting. A detailed discussion of this problem is given in reference 11·7.

d. Forging the fitting. For any production airplane, those fittings which are made by casting or cutting from solid stock on the experimental model are usually reworked so that they can be made into forgings. Forgings have very good strength properties, do not have weight penalties imposed upon them, and are suitable for large-scale production at a low cost.

In the light of the above discussion, it is easy to see why nearly all fittings in a production airplane fall into classes *b* and *d* and very few are found which are made by methods *a* and *c*.

Various means may be used to attach fittings to the main structure. Bolting, riveting, welding, and spot-welding have all been used satisfactorily in the appropriate places. One note of caution should be mentioned, however, regarding the use of a combination of bolts and rivets. Inasmuch as rivets are driven so as to fill the hole completely and bolts must have some tolerance for ease in installation, the rivets will carry the entire load until they deflect far enough to take up the

bolt tolerances. This usually means that the rivets have failed before the bolts begin to be loaded, an undesirable and overweight method of construction.

Methods of analysis of fittings follow the usual laws of applied mechanics and strength of materials. The most important point from the design standpoint is the determination of the loads acting in the fitting. The direct loads from the main structure are usually easily determined from the structural analysis; however, there may be secondary stresses introduced into the fittings, which in combination with the direct stresses may cause failure. These secondary stresses may be due to eccentricities of the fitting with regard to the load application point which may introduce bending stresses; vibration loads

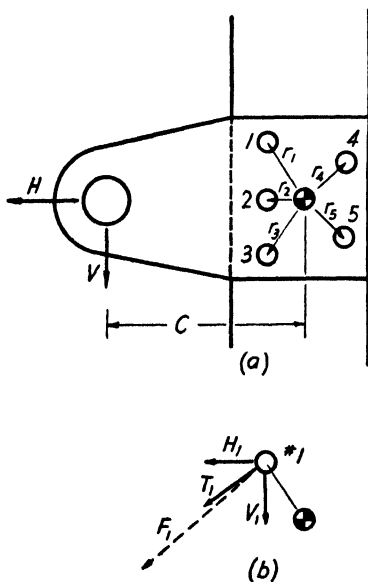


FIG. 11-7. Eccentric fitting.

coming into the fitting through control cables or rigging wires; shock loads that may arise due to worn bearings either in the fitting or in an adjacent structure; accidental handling loads; and numerous other loads which are not immediately apparent from a consideration of a strictly routine analysis. The designer must try to envision all possible loads on the fitting, and the damage to the airplane which might be caused by a fitting failure and govern his design accordingly. Obviously the failure of a fitting holding ash trays in the cabin need not be given as careful consideration (except from a weight standpoint) as one which attaches the wing to the fuselage. There are all degrees of importance between these two extremes.

A question that often arises is the method of rivet design to use for a fitting such as that shown in Fig. 11-7 where a group of rivets or bolts attaches a cantilever fitting to a main structural member. The method assumes the rivets are all of the same size. Referring to Fig. 11-7, it is

assumed that the horizontal and vertical forces H and V are uniformly distributed between the rivets so that

$$H_1 = H_2 = H_3 = H_4 = H_5 = \cdots = H_n = \frac{H}{n} \quad [11.2]$$

$$V_1 = V_2 = V_3 = V_4 = V_5 = \cdots = V_n = \frac{V}{n}$$

where $H_1 \cdots H_n$ are the horizontal forces on rivets $1 \cdots n$, respectively, and $V_1 \cdots V_n$ are the corresponding vertical forces.

The next step is to determine the center of gravity of the rivet system which gives the value of c shown in Fig. 11.7. The turning moment on the fitting is then equal to

$$M = Vc \quad [11.3]$$

which is resisted by forces on the rivets acting perpendicular to the radii. Assuming that the fitting rotates as a rigid body the tangential rivet forces, $T_1 \cdots T_n$, will have ratios as follows:

$$\frac{T_1}{T_2} = \frac{r_1}{r_2} \cdots \frac{T_1}{T_n} = \frac{r_1}{r_n} \quad [11.4]$$

or

$$T_2 = T_1 \frac{r_2}{r_1} \cdots T_n = T_1 \frac{r_n}{r_1} \quad [11.4a]$$

The torque developed by these forces acting around the rivet centroid is given by

$$M = Vc = T_1 r_1 + T_2 r_2 \cdots T_n r_n \quad [11.5]$$

or, substituting equation 11.4a into equation 11.5

$$\begin{aligned} Vc &= T_1 \left(r_1 + \frac{r_2^2}{r_1} + \frac{r_3^2}{r_1} + \cdots + \frac{r_n^2}{r_1} \right) \\ &= \frac{T_1}{r_1} (r_1^2 + r_2^2 + \cdots r_n^2) \end{aligned} \quad [11.6]$$

giving, for the tangential forces

$$\begin{aligned} T_1 &= \frac{M r_1}{r_1^2 + r_2^2 + \cdots r_n^2} \\ T_2 &= \frac{M r_2}{r_1^2 + r_2^2 + \cdots r_n^2} \\ T_n &= \frac{M r_n}{r_1^2 + r_2^2 + \cdots r_n^2} \end{aligned} \quad [11.7]$$

The total force system acting on one rivet, say rivet 1, is shown in Fig. 11-7b. These forces are added vectorially and from this vector sum the total load and hence the stress on the rivet can be obtained. This is repeated until all the rivet loads are determined. The rivet size is then chosen on the basis of the maximum rivet load, it not being advisable from a manufacturing standpoint to have a group of rivets of different sizes.

Simple fittings such as that discussed above are relatively easy to analyze. Some of the more complex fittings which may be complicated forgings with reinforcing flanges, etc., are very difficult to analyze since the stress distribution in the fitting for even simple loadings is unknown and hard to estimate. For such fittings large margins of safety must be used just to offset the designer's ignorance. Newer photoelastic methods, notably those which make possible a three-dimensional analysis, may make the designer's task easier when this technique of investigation has been clarified. Until that time recourse must be had to simpler analysis methods aided by static tests to destruction and generous margins of safety.

REFERENCES FOR CHAPTER 11

- 11-1. P. DONELY, "The Forces and Moments on Airplane Mounts," *N.A.C.A. Tech. Note*, 587 (1936).
- 11-2. A. S. NILES and J. S. NEWELL, *Airplane Structures*, Vol. II, John Wiley, 1938.
- 11-3. J. G. WILLIS, "Stress Analysis of Engine Mounting Rings," *J. Aero. Sci.*, Vol. 6, No. 7 (May, 1939).
- 11-4. F. K. TEICHMANN, *Airplane Design Manual*, Pitman, 1939.
- 11-5. A. P. POORMAN, *Strength of Materials*, McGraw-Hill, 1937.
- 11-6. S. TIMOSHENKO, *Strength of Materials*, Vol. II, Van Nostrand, 1930.
- 11-7. N. H. ANDERSON, *Aircraft Layout and Detail Design*, McGraw-Hill, 1941.

PROBLEMS

Problems for Chapter 3

3-1. A hard-drawn copper wire having a diameter of 0.128 in. is supported at one end and allowed to hang vertically; a load of 250 lb. is applied to the other end. The wire has an elastic limit of 28,000 lb./sq. in. and a Young's modulus of 16,000,000 lb./sq. in. Will the wire return to its original length upon removal of the load? What elongation will take place per foot of length when the load is applied?

3-2. A square plate of metal 4 ft. on a side and $\frac{1}{2}$ in. thick is subjected to a shearing stress which tends to twist the square surface into a rhombus. To apply this stress one edge is securely fixed, and a bar, fastened to the other edge, is pulled with a force of 180 tons. As a result the bar is observed to advance a distance of 0.069 in. in the direction of the pull. Find the shearing strain, the shearing stress, and the shear modulus of the plate.

3-3. A square steel rod 1 in. on a side is to be bent into the arc of a circle. What is the smallest radius to which it can be bent (cold), assuming that the maximum stress is limited to 35,000 lb./sq. in. and the modulus of elasticity is 30×10^6 lb./sq. in.?

3-4. A steel bar 2 in. wide, 1 in. thick, and 12 in. long, with $E = 30 \times 10^6$ lb./sq. in. is stressed by a tensile load of 60,000 lb. parallel to the 12-in. axis and a compression load of 576,000 lb. parallel to the 1 in. axis. Compute the new dimensions of the bar. (Poisson's ratio = 0.30.)

3-5. Find graphically the magnitudes of the maximum and the minimum principal stress and the direction of the plane on which each acts, also the magnitude of the maximum shearing stress and the direction of the planes on which it acts, for the combination of stresses as shown in the figure.

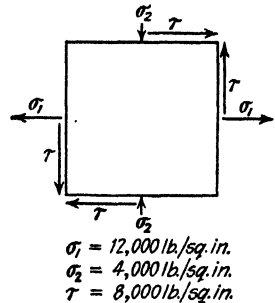


FIG. 3-5.

3-6. A structural steel bar $\frac{3}{4}$ in. in diameter and 10 in. long is subjected to an axial tensile load of 12,000 lb. (a) Calculate the tensile and shearing unit stresses on a plane making 60° with the direction of the load, and check the result by a graphical solution using Mohr's circle. (b) Find the maximum unit shearing stress.

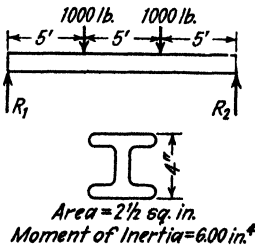


FIG. 3-8.

3-7. A steel bar 1.06 in. wide and 0.17 in. thick failed in diagonal shear on a plane at an angle of 42° with the cross section when subjected to a tensile load of 10,050 lb. What was the amount of the unit shearing stress on this plane? What was the value of the theoretical maximum unit shearing stress?

3-8. A 4-in. I-beam is loaded as shown. Determine the following:

- (a) Shear curve.
- (b) Moment curve.
- (c) Maximum bending stress.

3-9. A simple beam 20 ft. long carries a uniformly distributed load of 500 lb. per linear foot and a concentrated load of 8000 lb. at a point 8 ft. from the left end. Write

expressions for the moment between the left reaction and the concentrated load, and for the moment between the concentrated load and the right reaction. Draw the moment diagram. Compute position and amount of maximum moment if the beam is supported at the right end and at a point 8 ft. from the left end.

3-10. A cantilever beam 2 in. wide, 12 in. deep, and 5 ft. long carries a uniformly distributed load of 300 lb. per linear foot, including its own weight. If E is 1,200,000 lb./sq. in., compute the expression for the deflection at any point x and at the end.

3-11. Find the deflection at 25 in. from the right end of the beam of Fig. 3-11.

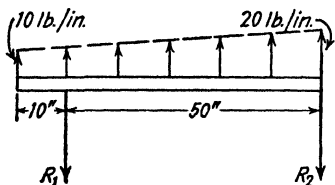


FIG. 3-11.

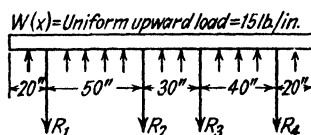


FIG. 3-12.

3-12. Draw the shear and bending moment diagrams for the beam of Fig. 3-12.

3-13. Calculate the following for the beam illustrated. (a) maximum bending moment, (b) maximum shear, (c) maximum bending stress, (d) maximum shear stress, (e) the deflection at $L/2$.

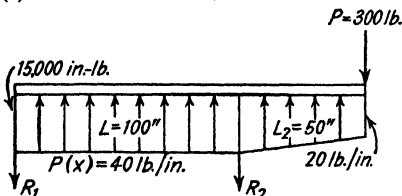


FIG. 3-13.

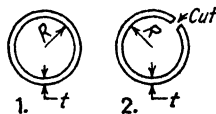


FIG. 3-14.

3-14. Given two sections of equal geometrical dimensions as illustrated. For equal applied torsional moment, find the ratio of angles of twist in terms of t and R . Solve when $t = 0.04$ in., $R = 2$ in., $M = 100$ in.-lb.

3-15. Given the bent-up section in the figure. Applied torque = 400 in.-lb. Assume $G = 3.85 \times 10^6$ lb./sq. in. Obtain: (a) shearing stress, (b) unit twist, (c) torsional rigidity of the section.

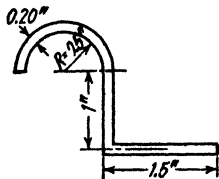


FIG. 3-15.

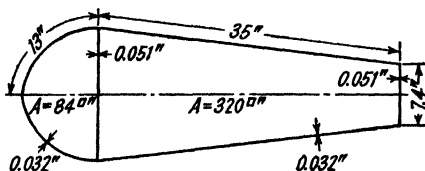


FIG. 3-16.

3-16. Given the stabilizer section shown in Fig. 3-16. The maximum torque at this section is 41,400 in.-lb. Calculate the resultant shear stresses in the nose sheet, front spar web, top and bottom skin aft of nose section, and rear spar web. Section is symmetrical about the chord line, and the depth at the front spar is 14 in.

Problems for Chapter 4

4-1. Determine the loads in each member of the truss $ABCD$ of Fig. 4-1. All joints are pin joints.

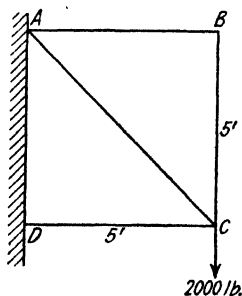


FIG. 4-1.

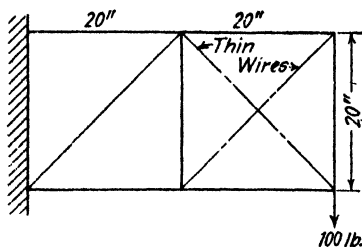


FIG. 4-2.

4-2. Given the pin-jointed truss with thin wire bracing in the outer bay as shown in Fig. 4-2. Obtain loads in all members. (Indicate direction.)

4-3. Given the truss shown, with dimensions as indicated. Compute the load in each member.

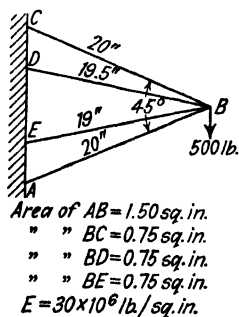


FIG. 4-3.

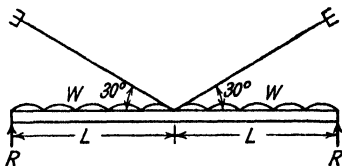


FIG. 4-4.

4-4. Determine the tension in the wire as shown, where

A = cross-sectional area of wire

E = Young's modulus of the wire

E' = modulus of elasticity of the beam

l = one-half length of beam

I = moment of inertia of beam (constant)

w = uniformly distributed downward load.

4-5. One-half of the wing structure of an aeroplane is illustrated. AB and CD are the rear spars; $A'B'$ and $C'D'$ are the front spars; BC and $B'C'$ are rear and front struts between the upper and lower wings. The other members operating are steel wires BD , $A'C'$, BC' . The external loads are as shown. In plan view each wing is as shown (a), the cross members being wooden struts and the diagonals steel wires. The cross section of each front spar is 3.59 sq. in. and of each rear spar 2.47 sq. in. ; $BD =$

0.0538 sq. in.; $A'C' = 0.0269$ sq. in.; all the other wires are 0.0158 sq. in. For steel $E = 30 \times 10^6$ lb./sq. in., for the wood $E = 1.4 \times 10^6$. Considering only the struc-

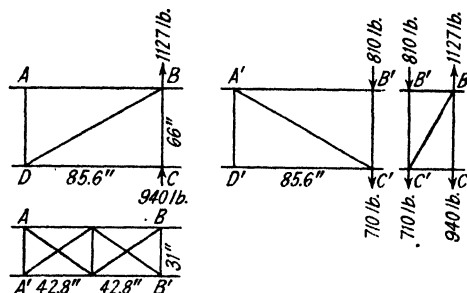


FIG. 4-5.

ture $ABB'C'D'A'$ and neglecting the strain energy of the struts, find the load in the wire BC' .

4-6. The frame work $ABCFED$ in the figure is loaded by the three forces W , P , Q . All the bars have the same cross section, are of the same material, and are pin-jointed

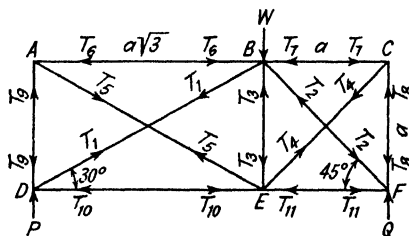


FIG. 4-6.

at their ends. Find the loads in all the members in terms of W . (A plane frame with 6 joints and 9 bars is necessary to prevent collapse; actually there are 11 bars. Regard BD and BF as the redundant bars.)

Problems for Chapter 5

5-1. Given the column with a cross section as shown. The stress-strain data for this material are as follows:

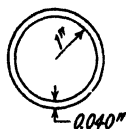


FIG. 5-1.

Stress (lb./sq. in.)	Strain (in./in.)
24,000	0.00242
28,000	0.00291
32,000	0.00355
36,000	0.00450
40,000	0.00626
44,000	0.00906

Assume section is stable and that column is pin-ended. Plot column curve, using the tangent modulus curve in the short column regime. (Proportional limit = 24,000 lb./sq. in. $\sigma_{ult} = 56,000$ lb./sq. in.)

5-2. Given the column with a cross section as shown. Assume column is pin-ended and that the stress-strain characteristics are the same as in Problem 5-1. Draw column curve, using Johnson parabola in short column regime.

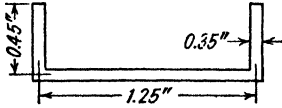


FIG. 5-2.

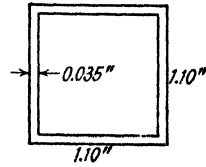


FIG. 5-3.

5-3. Given the column with the cross section illustrated. Assume column is pin-ended and of the same material as in Problem 5-1. Draw column curve, using Johnson parabola in short column regime.

5-4. Given the channel section column illustrated. Minimum moment of inertia = 0.00156 in.^4 ; area = 0.075 sq. in. ; $E = 10^7 \text{ lb./sq. in.}$; end fixity coefficient = 1.0; column length = 10 in.; $\sigma_{yp} = 39,000 \text{ lb./sq. in.}$ Calculate column buckling stress.

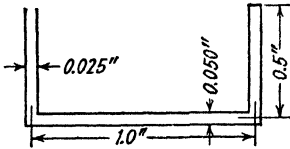


FIG. 5-4.

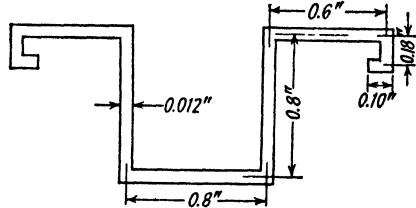


FIG. 5-5.

5-5. Given the column with the cross section shown. Calculate the approximate crushing stress in lb./sq. in. by considering the various elements as flat plates. ($a/b = 4$), $\sigma_{yp} = 39,000 \text{ lb./sq. in.}$

5-6. Given the stiffened panel in the sketch. Sheet thickness = 0.035 in. Use

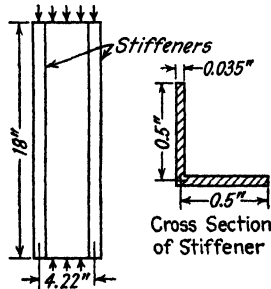


FIG. 5-6.

$E = 10^7 \text{ lb./sq. in.}$; $G = 3.85 \times 10^6$. Calculate the critical buckling stress for the sheet when

- the sheet is assumed simply supported along all four edges and
- the edges at the stiffeners are completely restrained from bending deformation but elastically restrained in rotation. The loaded edges are simply supported.

5-7. Consider the channel section shown in the figure. Determine σ_x

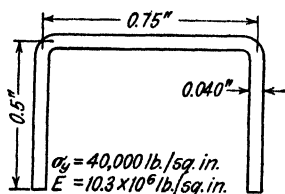


FIG. 5-7.

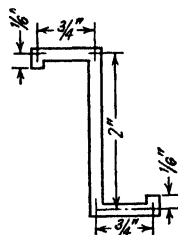


FIG. 5-8.

5-8. Consider the bent-up Z-section shown, with $E = 10.3 \times 10^6$ lb./sq. in. and $t = 0.050$ in. Determine σ_{xx} .

5-9. Consider the section which is illustrated. Determine σ_{xx} .

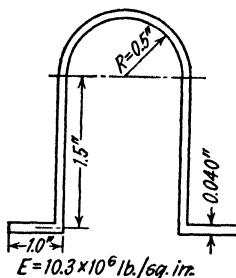


FIG. 5-9.

Problems for Chapter 6

6-1. Consider a simply supported flat plate loaded in compression on two edges. Discuss the important stress regimes in this plate as the compressive load is gradually increased. How would you calculate the effective width of sheet for each regime?

6-2. A 17ST dural sheet, 0.032 in. thick, 6 in. wide, and 12 in. long is simply supported, and the 6 in. sides are loaded by compression forces in the plane of the plate. Find the effective width and the total load carried by the plate for the following edge stresses: 1000 lb./sq. in.; 5000 lb./sq. in.; 10,000 lb./sq. in.; 20,000 lb./sq. in.

6-3. A panel made of 0.040 24ST sheet is 18 in. wide and 18 in. long. The panel is stiffened by 24ST extruded bulb angles placed on 6-in. centers. These angles have an area of 0.177 sq. in. and a moment of inertia about an axis parallel to the sheet of 0.0253 in.⁴. S is equal to 0.375 in. The rivet spacing on the stiffener is 1 in. Consider the plate to be simply supported on all edges. Determine:

- The curve of panel load vs. stiffener stress.
- The stiffener stress at which buckling between rivets will take place.
- The maximum allowable load on the panel.

If the panel length is changed, determine the allowable panel load as a function of the panel length. Assume the crushing stress of the stiffener section is equal to 32,000 lb./sq. in. and that the end fixity coefficient is equal to 1.5.

6-4. A series of 24ST panels with cross section as shown were tested in compression. The other panel data were:

- (a) Sheet thickness = 0.040 in.
- (b) Stiffener area = 0.1464 sq. in.
- (c) Stiffener moment of inertia = 0.0486 in.⁴.
- (d) Rivet spacing = 1.0 in.
- (e) $S = 0.60$ in.
- (f) The failing loads of the panel for these lengths tested were:

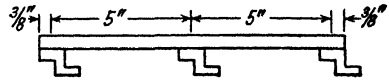


FIG. 6-4.

$L = 8$ in.	$P = 20,600$ lb.
$L = 16$ in.	$P = 19,800$ lb.
$L = 24$ in.	$P = 18,500$ lb.
$L = 32$ in.	$P = 17,500$ lb.

The material was tested and was found to have a yield stress of 44,000 lb./sq. in. and a Young's modulus of 10.3×10^6 lb./sq. in. Make all the necessary corrections and determine a design allowable curve for this panel, giving P allowable in terms of L .

Use a design end fixity coefficient of 1.5. Consider the plate to be simply supported on all edges.

6-5. Design an incomplete tension field beam with a total height of 18 in. that will support a shear load of 25,000 lb. In so far as it is possible, failure of web, rivets, and web stiffeners should be simultaneous. Assume that the upper and lower flanges are T -sections as shown. All material is 24ST.

6-6. Compare the allowable strength of a 6-in.-long panel of 24SRT-Alclad corrugations if the corrugations are (a) standard circular arc and (b) omega type corrugations.

6-7. A sheet panel is stiffened with omega corrugations. All material is 24SRT Alclad and the panel has the following dimensions:

- (a) Sheet covering thickness = 0.032 in.
- (b) Corrugation Lockheed LS-193 with $t = 0.040$ in.
- (c) Rivet spacing = 2 in.

Determine the allowable column stress vs. length curve for this panel.

6-8. Prove that the controlling section for the stainless steel corrugation shown in Fig. 6-55 (page 279) is the largest curved portion.

Problems for Chapter 7

7-1. Consider a thick flat plate 18 in. wide and 36 in. long with a uniformly distributed load on the plate of 40 lb./sq. in., and $E = 10.5 \times 10^6$ lb./sq. in. Determine:

- (a) Bending moment.
- (b) Shear.
- (c) Corner reactions for all four edges simply supported.

7-2. Consider the plate of Problem 7-1 with all four edges built in. Determine deflection and moment.

7-3. Determine bending stresses for the plates of Problems 7-1 and 7-2.

7-4. Consider an aluminum-alloy plate 25 in. by 25 in. by 0.045 in. thick, with a Young's modulus of 10^7 lb./sq. in., subjected to a uniform load of 25 lb./sq. in. Determine:

- (a) Deflection at center of plate.
- (b) Stress in the center of the plate.
- (c) Stress in the center of the sides of the plate.

7-5. Consider a 25 in. square plate of stiffened aluminum alloy which satisfies the assumptions as stated on pp. 296 and 297. Determine the moment of inertia of the stringers when $w_{\max} = 1$ in.; $p = 4$ lb./sq. in.; $N = 4$. (Work on the assumption that the stringers are pin-ended at the boundaries.)

7-6. Determine the necessary section modulus for the stringers of Problem 7-5, if the stringers are completely fixed and $\sigma_{\text{allow}} = 40,000$.

7-7. Calculate the moment of inertia of the long stringers when $w_{\text{total}} = 1$ in.; $w_{st} = 0.40$ in.; $w_{sh} = 0.60$ in.; $a = 20$ in.; $b = 5$ in.

Problems for Chapter 8

8-1. Determine the total load carried by the following panel. $t = 0.020$ in.; $b = 3$ in.; $R = 30$ in.; $L = 12$ in.; $\sigma_{yp} = 36,000$ lb./sq. in.; $E = 10^7$ lb./sq. in. Compare with the tested load as given in Table 8-2.

8-2. Carry out the necessary calculations for specimen number 10 of Table 8-3.

AUTHOR INDEX

A

ALUMINUM CO. OF AMERICA, 202
ANDERSON, N. H., 396
ANTZ, H. M., 369

B

BALLENRATH, 339
BALLERSTEDT, E., 340
BEAKLEY, W. M., 175, 202
BOEING AIRCRAFT COMPANY, 161, 262,
281
BRAZIER, L. G., 341
BRIDGET, F. J., 202
BROWN, C. G., 281
BUDD MANUFACTURING COMPANY, AIR-
CRAFT DIVISION, 189, 266, 270, 280,
282
BURKE, W. F., 385

C

CALIFORNIA INSTITUTE OF TECHNOLOGY,
369, 385
CHWALLA, E., 169, 171, 202
CIVIL AERONAUTICS AUTHORITY, 332,
341, 387
CONSOLIDATED AIRCRAFT CORPORATION,
243, 246, 281, 328, 340
COX, H. L., 173, 202, 339, 341
CROSHERE, 202

D

DEAN, W. R., 340
DONELY, P., 396
DONNELL, L. H., 280, 310, 311, 338, 339,
341
DOUGLAS AIRCRAFT COMPANY, 13, 246,
281, 282, 308
DSCHOU, D. D., 332, 341
DUNN, 202
DUNN, L. G., 169, 199, 281

E

EBNER, H., 281, 369, 385
EPSTEIN, A., 228, 281
EVANS, T. H., 308

F

FLIGG, C. M., 195, 202
FÖPPL, A. and L., 288, 289, 290, 308
FORD MOTOR CO., 202

G

GALCIT, 205, 207, 216, 310, 332, 340
341
GENERAL AVIATION CORPORATION, 188
GOUGH, 339
GREEN, 241, 281

H

HECK, O. S., 281
HEUBERT, M., 288, 308
HICKS, O. S., 369, 385
HOFF, N. J., 332, 341
HOWLAND, W. L., 159, 202, 231, 281
HUBER, M. T., 369

J

JACOBS, E. N., 77
JEROME, C. C., 202

K

KANEMITSU, S., 311, 340
KAPPUS, R., 195, 202
VON KÁRMÁN, T., 156, 203, 205, 207, 280
KLIKOFF, W. A., 369, 385
KOLLER, H., 369, 385
KRONIN, A., 281
KUBO, 339
KUHN, P., 281, 369

L

LAHDE, R., 255, 258, 281
 LIPP, J. E., 8, 12, 41, 369
 LOCKHEED AIRCRAFT CORPORATION, 2,
 207, 282
 LOVETT, B. B. C., 369
 LUNDQUIST, E. E., 175, 176, 179, 195,
 211, 280, 310, 338, 339, 340, 341, 385

M

MARGUERRE, K., 205, 206, 280, 281
 MARTIN, GLENN L., COMPANY, 185, 262,
 281
 MASSACHUSETTS INSTITUTE OF TECH-
 NOLOGY, 179, 182, 202, 205, 281, 318,
 322, 323, 340
 MATHAR, J., 281
 MILLER, R. A., 202
 MONESS, E., 290, 296, 308

N

NEWELL, H. S., 231, 281, 369, 396
 NEWMARK, N., 310, 340
 NILES, A. S., 369, 396
 NOJIMA, H., 311, 340

P

PARR, W. S., 175, 202
 PINKERTON, R. M., 77
 PIPPAED, A. J. S., 153
 POORMAN, A. P., 396
 PRANDTL, L., 117
 PRETSCHNER, W., 202
 PRITCHARD, J. L., 153

R

REDSHAW, S. C., 312, 314, 315, 340
 REISSNER, E., 369
 REPUBLIC AIRCRAFT CORPORATION, 282

ROBERTSON, A., 340
 RODEE, W. F., 369

S

SCHAPITZ, E., 281
 SCHWARTZ, E. H., 281
 SECHLER, E. E., 205, 207, 280
 SEELY, F. B., 202
 SEZAWA, 339
 SOMMER, A., 288, 308
 SOUTHWELL, R. O., 123, 153, 202, 340
 STEEL, 339

T

TAYLOR, J. L., 332, 341
 TEICHMANN, F. K., 41, 396
 TIMOSHENKO, S., 123, 153, 170, 202, 208,
 249, 280, 287, 308, 340, 396

U

U. S. BUREAU OF STANDARDS, 207

V

VAN DER NEUT, A., 369
 VOSSELLER, A. B., 202
 VULTEE AIRCRAFT, INCORPORATED, 246,
 281

W

WAGNER, H., 195, 202, 236, 255, 258
 281, 310, 340
 WENZKE, W. A., 314, 315, 322, 340
 WHITE, R. J., 369
 WILLIS, J. G., 396
 WILSON, W., 310, 340
 WINNY, H. F., 369
 WOOD, K. D., 77

Y

YOUNG, D., 369

SUBJECT INDEX

A

Acceleration and load factors, 47
 human tolerance of, 48
 related to maneuverability, 48
 Acceleration forces, 46
 Accelerations, angular, 59
 during landing, 72
 linear, 59
 Accelerometers, 48
 Accommodations, for cargo, 31.
 for crew, 30
 for passengers, 30
 Aerodynamic center, 50
 Aileron design, 368
 Aileron forces, flying conditions, 69
 maneuvering, 68
 tab effects on, 69
 Aileron load distribution, 68
 Aileron type flaps, loads on, 69
 Airfoil characteristics, 49
 corrected, 45
 Air load, on wing ribs, 362
 Air-load moments, wing, 73
 Air-load shear curve, wing, 73
 Air-load shears, wing, 73
 Alignment, effect of deformation on, 92
 Allowable loads, 76
 Allowable stresses, for circular arc corrugations, 263
 Altitude, effect on load factor, 48
 ANC-5, 207, 260, 261, 262
 Angle, for zero shear stress, 82
 of plate buckling in tension-field beams, 243
 of twist in torsion, in hollow, thin-walled sections, 122
 in solid circular cylinders, 115
 in solid elliptical cylinders, 116
 in solid rectangular cylinders, 119
 in *T*-section bars, 119

Angle sections, as columns, 173
 stress causing leg buckling in, 174
 Army Handbook for Airplane Designers, 91, 261
 Arrangement, 21, 32
 Aspect ratio, limits for vertical surfaces, 68
 Aspect ratio correction, 51
 Axial compression, of cylindrical shells, 259
 Axial loads, strain energy due to, 129
 Axes, principal, in wings, 357
 of column sections, 199-201

B

Baggage, loading of, 27
 passengers', weight of, 37
 Baggage compartment, location, 24
 Balance, effect, of fuselage moments on, 63
 of moving engines, wings, and other items, 40
 of nacelle moments on, 63
 of useful load on, 23
 of weight empty on, 22
 importance of proper, 41
 Balance table, 62
 Balancing elevator load, 64
 limits on, 64
 Balancing load on tail, 59, 60, 63
 distribution of, 64
 Balancing stabilizer loads, distribution of, 64
 Balancing the airplane, 59
 Ballast, use to locate center of gravity position, 33
 Bar, circular, strain energy in, due to torsion, 133
 rectangular, as columns, 160
 torsion in, 118

- Bar, round, as columns, 160
 Basic air-load shears and moments on wing, 73
 Beam, definition of, 92
 neutral axis of, 96
 on three supports, 148
 radius of curvature in, 95
 shear in, sign convention for, 93
 Beam analysis, 93
 assumptions in, 98
 curved, 391
 for distributed loads and external moments, 99
 graphical, 99-104
 non-uniform load, 101
 notation for, 95
 of continuous beams, 101
 pure bending, 94-99
 for beams with one axis of symmetry, 109-113
 shear deflections, 108
 shearing stresses, 104-109
 Beam bending moments, 94
 sign convention for, 94
 Beam flanges, secondary stresses in, 257
 stresses in, 255
 tapered, 258
 Beam reactions, 100
 Beams, 49
 centroidal axis of, 94
 continuous, 101
 curved, 391
 distributed load in, 94
 incomplete tension field, 241-258
 load, shear, and moment relationships in, 97
 load in, sign convention for, 93
 pure bending in, 94-99
 shear deflections in, 108
 shear web, 234-258
 statically indeterminate, 148
 strain energy in, 149
 stress distribution in thick-webbed, 235
 stressed beyond proportional limit, 98
 thin-webbed, 236
 Wagner, 236-240
 Beam shears, 94
 Beam slopes, 102-104, 148
 Beam theory, as applied to wing structures, 355
 Bearing margin of safety, 77
 Bending, of stiffened cylinders, 329-338
 strain energy of, 130
 wing, material resisting, 8
 Bending material, in wing structures, 354-359
 Bending moment, free, 101
 in beams, 94
 sign convention for, 94
 in eccentrically loaded column, 164
 Bending rigidity, of beam, effect of web stiffeners, 237
 of plate stiffeners, 208
 Bending stiffness, in frames, 147
 Bending stress, in fuselages, 370
 Bent-up sheet section columns, 173-201
 Boundary conditions, 89
 Bow's notation, in truss analysis, 126
 Braked landing conditions, 71
 Buckling, as a design criterion, 76
 local, in column cross sections, 159
 of circular cylinders, 309-312
 of curved plates, 312-317
 of thin plates under shear, 172, 234
 of thin plates and stiffeners, 208
 of thin plates with elastically restrained edges, 168-171
 Buckling failure of channel- and Z-sections, 174
 Bulb angles, as sheet stiffeners, 216
 Bulb section stiffeners, 194
 Buffet supplies, 27
 effect of trip length on, 38
 location as affecting the center of gravity, 38
 weight of, 38
 Bulkhead analysis, fuselage, 375-385
- ### C
- Cabin arrangements, 27
 laid out in the mock-up, 6
 Cargo, accommodations for, 31
 disposition for balance, 40
 effect on center of gravity location, 33, 38
 location with respect to propeller, 38
 maximum and minimum allowable, 39
 Castigliano's theorems, 136, 140
 Casting margin of safety, 77

Center of gravity, of airplane, 33, 45
 effect of seating arrangement on, 37
 limits of, 35
 referenced to chord, 35
 travel, 35
 limits of, 33
 while loading, 26
 of area, 96
 of wing sections, 358
 Center of gravity limits, 60
 how adjusted, 40
 Center of gravity location, affected by
 buffet supplies, 38
 effect of cargo on, 38
 on the ground, 41
 Center of gravity travel, affected by fuel
 and oil, 36
 Center of pressure, for tail group, 60
 position of, 50
 Center of rotation, of sheet stiffeners, 195
 Center stiffeners, effective columns of,
 213
 Centroidal axis of a beam, 94
 Channel section, beam shear analysis of,
 110
 shear distribution in, 112
 torsional failure of, 197
 Channel sections, as columns, 174
 Chord load, in tail surface, 61
 Chordwise pressure distribution effect on
 aileron, 69
 Circular arc corrugations, 259-266
 and flat sheet, 272
 design allowables for, 263
 effect of pitch/depth ratio on, 264
 effect of yield point on, 263
 in stainless steel, 265
 properties of, 259
 Civil Aeronautics Authority Manual
 (CAAM-04), 42, 46, 50, 71, 77,
 387, 390
 Civil Air Regulations (CAR-04), 1, 2, 4,
 8, 20, 22, 24, 36, 37, 38, 42, 46,
 48, 50, 58, 60, 70, 71, 77, 387, 390
 Clamped edge condition, 165
 Cockpit, arranged in the mock-up, 6
 Coefficient of end fixity, 156, 159
 Cold working, effect of, 92
 Column analysis, 154-164
 comparison of column curves, 157

Column analysis, effective free length,
 163
 empirical methods of, 186-194
 Euler column curve, 157
 for eccentric loading, 163-164
 Johnson's parabola, 157
 Johnson's parabolic equation, 159
 local buckling in, 159
 long, or Euler columns, 154-156
 notation in, 154
 reduced modulus curve, 156-157
 secant equation, 164
 short column curves, 161
 stainless steel sections, 188-193
 straight line equation, 157, 160
 tangent modulus curve, 157, 158
 where yield point varies, 163
 Column curves, for sheet stiffener com-
 binations, 211-220
 Column failure, above the proportional
 limit, 175
 of angle sections, 173
 of channel and Z-sections, 174
 of square and rectangular tubes, 179
 torsional, notation for, 196
 types of, 154-164
 Columns, energy in, 154-155
 procedure for testing and analyzing,
 185
 thin-walled, 173-201
 angle sections, 173
 channel and Z-section, 174
 extruded shapes for, 193
 general design considerations, 201
 general shapes for, 183
 made up of flat elements, 186
 made up of curved elements, 192
 square and rectangular tube, 179
 stainless steel sections for, 188-
 193
 torsional instability of, 195
 with torsional instability, 195
 Combined loading, 77
 Comfort, effect, of noise level on, 23
 of propeller location and clearance
 on, 23
 heating and ventilating, 25
 Compatibility equations, 87
 Composite section corrugations and flat
 sheet, 277

- Compression, axial, of cylindrical shells, 259
 - of stiffened cylinders, 322-329
 - Compression loads in bars, 154
 - Compression stress, 79
 - Compression tests, material, 228
 - Concentrated load on thick plate, 287
 - Conservation of energy, 130
 - Construction cost of wing spars, 343
 - Controls, engine, 29
 - flight, 28
 - laid out in the mock-up, 6
 - power plant, weight of, 3
 - surface, weight of, 4
 - Control surfaces, design of, 366-369
 - effect of speed on size of, 44
 - horizontal, loads on, 64
 - loads on, 63
 - size limits of, 48
 - tabs for, loads on, 69
 - vertical, loads on, 67
 - Corrected airfoil characteristics, 45
 - Correction for material properties, 220, 227-229
 - Corrugated sheet, use of, 259-280
 - Corrugations, and flat sheet, 271-280
 - ANC circular arc, 259
 - composite sections for, 270
 - flat element sections for, 268
 - omega or flat-topped, 267
 - plus flat sheet in shear, 351
 - typical sections for, 260
 - stainless steel, 265, 269, 270
 - Couples, internal, redundant, 148
 - on frame members, 148
 - Crew, accommodations for, 30
 - weight of, 38
 - Critical buckling stress, 167
 - of circular cylinders, 309-312
 - of stiffened plates, 208
 - Critical column load, 156
 - Critical structural loading, 46
 - Crushing strength, of a column cross section, 159
 - of thin-walled sections, 173-194
 - Curvature, 97
 - Cutouts in fuselages, effects of, 374
 - Cylinder, shear distribution in, 345
 - Cylinders, circular, ultimate load on, 311
 - under axial compression, 309-312
 - Cylinders, stiffened, general instability of, 331-338
 - under compression, 322-329
 - under pure bending, 329-338
 - thin-walled, shear distribution in, 345
 - torsion in, 120-123
 - under internal pressure, 307
 - under torsion, 338-340
 - Cylindrical shells under axial compression, 259
- D
- d'Alembert's principle, 47
 - Dead weight items in wing, 74
 - Dead weight factor, 58
 - Deflection, beam, pure bending, 97
 - in a truss, 138
 - of membranes, 288
 - of simply supported flat sheet, 167
 - of thick plates under normal pressure, 184
 - of thin plates, large, 206
 - under normal pressure, 293
 - Deformation, 85
 - rate of, 134
 - total, effect in design, 91
 - Deformation equations, 88
 - Deformations, in elastic bodies, 133
 - normal, 88
 - De-icer, weight of, 4, 21
 - Derivative of strain energy, 137
 - Design criteria, for flat sheet, 164
 - Design gliding speed, 43
 - Design level speed, 42
 - Design load factor, 47
 - Design maneuvering speed, 43
 - Design power loading, 45
 - Design shear and bending moments for wing, 74
 - Design weight, 44
 - Design wing loading, 44
 - Discontinuities in structures, effects of, 353
 - Displaced ailerons, effect on design load factors of, 55
 - Displacement, from derivative of strain energy, 137
 - of points in a truss, 134
 - of points in truss analysis, 134
 - Distribution, of shear in a wing, 351

Distribution, of shear load between wing spars, 344
 Down loads on wing, 54
 Drag, parasite, where applied, 61
 Drag coefficient, 49
 Drag force on wing, total, 49
 where applied, 61
 Drag truss, 49
 Drawing, three-view, 21, 22
 Dressing rooms, location of, 37
 Ducts, heating and ventilating, 25
 layout in mock-up, 6

E

Eccentricity in thin-walled columns, 200
 Eccentric loading in columns, 163-164
 Economics of design, 28
 Edge stiffeners, effective column for, 215
 Edge supports, definition of, 165
 Effective column, in stiffened cylinders, 325, 326
 Effective columns, in stiffened plates, 209-210
 in stiffened sheet, 210, 213, 215, 217
 Effective free length of a column, 163
 Effective shear modulus, 258
 Effective width, in rectangular tubes, 181
 in stiffened plates, 209
 in wing analysis, 359
 of flat plates, 203
 Effective width curve, limitations on, 206
 Effective width ratio, 204
 Effective wing area, 50
 Elastically restrained edges of plates, 168-171
 Elastic axis, wing, 76
 Elastic system, work in an, 129-133
 Electrical equipment, weight of, 21
 Electrical system, equipment in, 31
 Elevator design, 366
 Elevator load, balancing, 64
 limits on, 64
 maneuvering, 65
 Elevator loads, effects of tabs on, 65
 Elevator ribs, design criteria for, 66
 Elevator spar, loads due to stabilizer deflection on, 101
 Elliptical bars, torsion in, 115
 Emergency exits, 27

Emergency fuel, effect on center of gravity location, 36
 Emergency horsepower, 44
 End fixity, of flat plates, 167
 of sheet stiffeners, 211, 212, 216, 220, 221, 229
 End fixity coefficient, 156, 159
 End moments, effects of, 100
 Energy, conservation of, 130
 in columns, 154-155
 internal, of buckled plates, 167
 strain, of bending, 130
 of direct load, 129
 Engine controls, 29
 Engine mount design, 386-388
 Engine mounts, as redundant structures, 147
 forces on, 386
 types of, 387-388
 Engineer, equipment for, 29
 Engine ratings, 44
 Engines, accessories, weight of, 3
 weight of, 3
 Equation, three-moment, 104
 Equilibrium equations, for beam shears, 105
 for non-uniform stress, 84
 for uniform stresses, 79
 three-dimensional stresses, 85
 two-dimensional stresses, 84
 Equilibrium, force, 47
 momentary, 59
 neutral, 155
 Equilibrium condition for shear flow, 347
 Equipment, arranged in the mock-up, 6
 communicating, weight of, 4, 20
 electrical, 31
 weight of, 21
 engineer's, 29
 fixed, 28
 heating and ventilating, 32
 location, 4
 miscellaneous, 32
 navigator's, 30
 pilot's, 28
 radio operator's, 30
 power plant, 31
 Equivalent shear modulus for corrugated sheet, 352
 Euler column formula, 155

- Experimental panel tests, end fixity of, 229
- Extruded sections as columns, torsional failure of, 199
- Extruded shapes as columns, 193
- F
- Factor of safety, 47
- Failure in channel or Z-sections, types of, 174
- Fin design, 366
- Fitting analysis, 392
- Fitting margins of safety, 77
- Fittings, eccentric, 394
- manufacturing methods for, 393
- Fire extinguishers, 27
- Fixed edge condition, 165
- Fixed equipment, 28
- Fixity coefficient, 156, 159
- Flange forces in Wagner beams, 237
- Flange stiffness, correction factor in thin-webbed beams for, 238
- effect of, 238
- Flap design, 368
- Flaps, design flight conditions with, 57
- wing, 69
- Flap warning signals, 28
- Flat element corrugations, 269
- Flat plates, buckling of, under shearing stress, 172
- edge conditions of, 168
- stiffened, under compression, 208-234, 259-280
- under shear, 234-259
- thin, history after buckling, 205
- under normal pressure, 283-307
- Flat sheet and corrugations, 271-280
- Flat sheet buckling, effect of, 165
- Flat sheet loaded in the plane of the sheet, 164-173
- Flat-topped corrugations, 267
- and flat sheet, 275
- Flight condition, inverted, 57
- Flight controls, 29
- Flight design conditions, dive with flaps down, 57
- gliding, 57
- inverted flight, 57
- negative gust with flaps down, 57
- negative high angle of attack, 54
- Flight design conditions, negative low angle of attack, 56
- positive gust with flaps down, 57
- positive high angle of attack, 52
- positive high angle of attack (modified), 53
- positive low angle of attack (modified), 55
- Flight load, factors of, 46
- external, 46, 47
- Floors, fuselage, 374
- Force, shearing, 79
- Force coefficients, 49
- Forces, external, points of application of, 60
- on engine mounts, 386-387
- Frame, definition of, 147
- Frame analysis, 147-153
- circular, 152
- notation for, 153
- effect of symmetry on, 151
- fuselage, 375-385
- main, 375
- rectangular, 151
- Frames, loads on, 147
- bending stiffness in, 147
- Free body diagram, 151
- Free edge condition, 165
- Fuel, emergency, effect on center of gravity location of, 36
- order of filling the tanks, 33
- weight per gallon of, 37
- Fuel and oil, emergency reserve, 36
- ratio to be carried, 36
- residual weight of, 4
- Fuel and oil loads, effect on center of gravity location of, 36
- Fuel and oil tanks, order of filling and emptying, 36
- Fuel consumption, 37
- effect on center of gravity location, 35
- Fuel system, weight, 3, 17
- Fuel tanks, weight, 18
- Furnishings, weight, 4, 20
- Fuselage analysis, 370-385
- bending stress in, 370
- effects of cutouts on, 374
- floor analysis, 374
- frame analysis, 375-385
- landing gear loads, 376

Fuselage analysis, shear stresses in, 371-373

torsional loads in, 373

Fuselage moments, effect on balance of, 63

Fuselage panel design, 372

Fuselage weight, 3

as affected by wing position, 41

breakdown of, 13, 14

general trend in, 13

G

Gear, tricycle, weight of, 3

Gliding design condition, 57

Graphical analysis, of fuselage frames, 382

of trusses, 125

Ground gusts, 69

Gust load factors, 46, 50

Gust loads on vertical tail surfaces, 67

Gust reduction factor, 51

Gusts, horizontal, 69

Gust velocity, 51

H

Heating and ventilating, 25

equipment for, 32

Heating sources, 26

High strength materials limited by high stresses, 92

Hinge moments, 66, 67

Hooke's law, 90, 130, 134, 156

H-sections as columns, 161, 162

I

I-beam, shearing stress in, 107

Indicated air speed, 42

with flaps, 43

Induced shear in column sections, 199

Inertia forces, 59

in flight, 47

Initial buckles, effect of, 173

Inspection, 27

Instability, general, of stiffened cylinders, 331-338

design curves for, 335

local, in stiffened cylinders, 330

of flat sheet, 164-173

torsional, of columns, 195-201

Instruments, 28

weight of, 4, 18

J

Johnson parabolic equation, 159

Joints, truss, rigidity of, 124

L

Landing attitudes, 70

Landing conditions, level, 70

nosing-over, 71

one-wheel, 71

side-drift, 71

three-point, 71

two-wheeled, 71

Landing gear, design conditions for, conventional, 70

tricycle, 71

effect on loading passengers, 26

Landing gear design, 389-392

Landing gears, types of, 389-390

Landing gear warning signals, 28

Landing gear weight, 3

tricycle, 16

conventional, 14

Landing loads, 70

items influencing, 72

Least work, principle of, 142

Lift coefficient, 49

Lift force, where applied, 61

on wing, 48

total, 49

Limitation of control surface size, 48

Limit elevator load, balancing, 64

maneuvering, 65

Limiting center of gravity, 40

Limit load factor, 47

Limit load on ailerons, 68

Limit loads, on horizontal surfaces, 64

on vertical surfaces, 67

Linear accelerations, 59

Load, ultimate, on circular cylinders, 311

useful, definition, 3

effect of balance on, 23

weight of, 21

weight per passenger, 4

Load criteria, 78

Load distribution, on ailerons, 68

in incomplete tension-field beams, 245

on wing flaps, 69

- Load distribution, on vertical surfaces, 67
 - Load factor, net, 60
 - tail, 63
 - Load factors, Army and Navy regulations, 46
 - design, 47
 - determined by performance, 42
 - Civil Aeronautics Authority requirements, 42
 - flight, gust, 46
 - maneuvering, 46
 - landing, 46
 - limit, 47
 - wing, 45
 - Loading and unloading, 26
 - Load in sheet stiffener combinations, 210
 - Loads, balancing, on fixed tail surfaces, 64
 - beam, sign convention for, 93
 - external, on airplane, 59
 - fictitious, 139
 - in web stiffeners of thin-webbed beams, 255
 - on control-surface tabs, 69
 - on stiffeners, in plates under pressure, 297
 - torsional, in fuselages, 373
 - unsymmetrical, in fuselage frames, 384
 - Long column, definition of, 154
 - Lubricating system, weight of, 3
- M
- Maintenance, 27
 - of wings, 365
 - Maneuverability, 48
 - load factors affected by, 48
 - Maneuvering elevator load, 65
 - Maneuvering load factors, 46
 - Maneuvering loads, on ailerons, 68
 - on vertical tail surfaces, 67
 - Manufacturing methods for fittings, 393
 - Margin of safety, 76
 - for castings, 77
 - for fittings, 77
 - for parts subjected to shock, 77
 - for reversed stress bearings, 77
 - Material properties, correction of test results for, 220, 227-229
 - Maxwell's reciprocal theorem, 134
 - applied to moments, 136
 - Mean aerodynamic chord, 45
 - Membrane analogy for torsion, 117
 - Membrane analysis of thin plates, 288
 - Military aircraft, mock-up for, 7
 - specifications for, 2
 - Military airplanes, load factors for, 46
 - Misfits in truss analysis, 147
 - Mock-up, 6
 - Modulus of elasticity, definition of, 85
 - limits on, 92
 - reduced, 156
 - Mohr's circle, 82
 - Moment, wing, where applied, 61
 - torsional, in hollow thin-walled cylinders, 120
 - for solid circular cylinders, 115
 - for solid elliptical cylinders, 115
 - for solid rectangular cylinders, 118
 - for *T*-section bars, 119
 - Moment coefficients, 49, 50
 - Moment of inertia, definition of, 96
 - for channel section, 113
 - of stiffeners in plates under pressure, 298, 300, 302, 304
 - polar, 115
 - Moments, hinge, 66
 - in thick plates under pressure, 284
 - of inertia in wing sections, 357-358
 - tail surfaces, 72
 - torsional, in wing sections, 360
 - wing, 72, 74
 - Monocoque structure, 164
- N
- Nacelle moments, effect on balance of, 63
 - Nacelles, weight of, 16
 - Navigator, equipment for, 30
 - Negative high angle of attack condition, 56
 - Negative low angle of attack condition, 56
 - Neutral axis of a beam, 96
 - Neutral axis shift in beams, 98
 - Neutral equilibrium, 155
 - Newton's first law, 47
 - Noise level, 23, 26
 - Nosing-over landing condition, 71
 - Notation, for columns, 154
 - for cylinder analysis, 345
 - for curved beam analysis, 391

Notation, for deflection of stiffened rectangular panels, 303
 for frame analysis, 377
 for oblique web stiffeners in Wagner beams, 237
 for plates under pressure, 283
 for stiffened panels under normal pressure, 296
 for stiffened rectangular panels, 302
 for stiffened square panels, 296
 for torsional column failure, 196
 for vertical web stiffeners in Wagner beam, 236
 for wing analysis, 356

O

Oil, weight per gallon, 37
 Omega corrugations, 267
 and flat sheet, 275
 One-engine operation, effect on vertical control surfaces of, 67, 68
 effect on ailerons of, 68

P

Panel instability, in stiffened cylinders, 330
 Panel resonance, 24
 Panels, stiffened, under
 normal pressure, 296-307
 rectangular plates, 301
 square plates, 298
 Panel tests, stiffened, use of, 220
 Parabolic equation, Johnson, 159
 Parasite drag, where applied, 61
 Passengers, accommodations for, 30
 vision of, 25
 weight of, 37
 Performance, calculations of, 4
 characteristics needed for design, 4
 effect on load factors of, 42
 wind tunnel tests for, 5
 Permanent elongation, 90
 Permanent unit strain, 90
 Pilot, equipment for, 28
 location of, 27
 vision for, 25
 Pilot force, limits on, 64, 65, 66, 67, 68, 69
 Pin-connected trusses, 124
 Pin-ended columns, 156

Pitch-depth ratio of corrugations, strength effect of, 264
 Planes of symmetry in beams, 98
 Plane stress pattern, 83
 Plane trusses, 125
 Plastic deformation, in a buckled plate, 205
 in columns, 156
 Plates, buckled, energy in, 167
 curved, ultimate strength of, 317-322
 under compression, 312-322
 thick, under normal pressure, 284
 thin, analysis of, deflections, 293
 limits on, 290-292
 stresses, 294-295
 buckling of, 164-173
 under shearing stresses, 172, 234
 effective width of, 203
 loaded above buckling load, 203-282
 loaded in own plane, differential equation for, 166
 loaded uniformly, 285
 stiffened, under compression, 208-234, 259-280
 under shear, 234-258
 with elastically restrained edges, 168-171
 stress distribution of, beyond buckling, 203
 under normal pressure, 290-296
 under shear, ultimate strength of, 234-258
 under normal pressure, 283-307
 Plate stiffeners, effect of bending rigidity of, 170
 effect of torsional rigidity of, 169
 Poisson's ratio, 86, 87
 Polar moment of inertia, 115
 Positive high angle of attack condition, 52
 modified, 53
 Positive low angle of attack condition, 55
 modified, 55
 Power loading, design, 45
 Power plant equipment, 31
 weight of, 3, 16
 Pressure, internal, in cylinders, 307
 normal, on plates, 283-307
 Pressurized cabins, plate analysis, 290
 stresses in, 307

Prestrained trusses, 147
 Principle of least work, 142
 Propeller axes, effect of location on vertical tail surface, 67
 effect of location on ailerons, 68
 Propeller efficiency, 61
 Propeller location and clearance, 23
 Propellers, weight of, 3
 Propeller thrust, 61
 where applied, 61
 Proportional limit, definition of, 89, 90
 effect on column failure, 175
 Pure bending in beams, 94

R

Radio operator, equipment for, 30
 Radius, of curvature, 97
 in beams, 95
 of deformation, 134
 of gyration for sheet stiffeners, effective, 214
 Rated horsepower, 44
 Reaction forces in landing, 71
 Reactions, beam, 100
 redundant, 139
 Reciprocal theorem, Maxwell's, 134
 Redistribution of stress due to buckling, 165
 Reduced modulus curve in column failure, 156, 179
 Redundancies, multiple, 143
 Refueling, order of, effect on center of gravity position, 35
 Resolution of forces in trusses, 126
 Resultant air forces, direction of, 59
 Resultant force coefficient, 49
 Resultant shear stress in torsion, 115
 Rib air load, 362
 Ribs, elevator, design criteria for, 66
 weight breakdown, 9
 wing, 361
 types of, 363
 Rigidity, torsional, of plate stiffeners, 169
 of sheet stiffeners, 218
 Rivet analysis for fittings, 394
 Rivet correction factor in tension-field beams, 242
 Rivet load in incomplete tension-field beams, 248

Rivets, inaccessible, 343
 failure of sheets between, 211
 Rivet spacing, effect of, on stiffened panels, 230
 in wing design, 365
 optimum, 233
 Rods, circular, torsion in, 115
 slender, as columns, 154
 Rubber, behavior under load, 85, 86
 Rudder design, 366

S

Safety features, 27
 Safety locks, 28
 Seating arrangements, effect on center of gravity location, 37
 Secant equation for eccentrically loaded columns, 164
 Secondary bending stresses in beam flanges, 257
 Secondary loads in trusses, 124
 Self-strain, in indeterminate structures, 128
 Semi-monocoque structure, 164
 Shear, flat panels under, 234-258
 torsional, 114-123
 wing, material resisting, 9
 Shear analysis of wing, 348-352
 Shear carried by beam web, 241
 Shear-carrying members in wings, 343
 Shear center, of channel section, 113
 of open sections, 195
 of unsymmetrical sections, 113
 of wing, 360
 of wing structure, 350
 Shear curve, wing, 73
 Shear deflections in beams, 108
 Shear distribution, in channel sections, 110-113
 in thin-walled cylinder, 345
 Shear flow, 122
 Shear flux, 122
 Shear force, 79
 Shear in beams, 94
 sign convention for, 93
 Shear in corrugated sheet, 352
 Shearing deformation, 88
 Shearing strain, 85
 in torsion, 115

- Shearing stress, due to torsion, in hollow, thin-walled sections, 122
 in solid circular cylinders, 116
 in solid elliptical cylinders, 116
 in solid rectangular cylinders, 118
 in *T*-section bars, 119
 lines of, in torsion problem, 114
 Shearing stresses, beam, distribution of, 105-109
 in *I*-beams, 107
 maximum value of, 107
 Shear lag, 165
 in wings, 356
 Shear loading of thin plates above buckling, 235
 Shear modulus, 86, 87
 effective, 258
 Shear rigidity, effect on shear analysis, 350
 Shears, in thick plates under pressure, 284
 tail surface, 72
 wing, 72
 Shear stiffness, of corrugated sheet, 352
 of tension-field beam, 351
 Shear strain energy, 131
 Shear stress, 79
 angle for zero, 82
 Shear stresses, in fuselages, 371
 maximum, 82
 wing, due to torsion, 76
 Sheet buckling between rivets, 230-234
 Sheets, stiffened, buckling of, 169
 effect of rivet spacing on, 230
 Sheet stiffener combinations, 169, 171
 column curves for, 211-220
 corrugations in, 259-280
 load in, 210
 Sheet stiffeners, center of rotation of, 195
 Sheet structures, flat, ultimate strength of, 165
 thin, buckling of, 164-173
 edge supported in, 165
 Shock load margins of safety, 77
 Short column analysis, 157-164
 Sign convention, for balancing loads, 61
 for bending moment, 94
 Sign convention, for loads, 93
 for shear, 93
 for stresses, 80, 87
 Slope of beam deflection curve, 102-104
 Space trusses, 125
 Spars, tension-field, 165
 wing, 343
 Specifications, and the designer, 2
 commercial airplane, 1
 company, 2
 military airplane, 2
 Speed, design gliding, 43
 design level speed, 42
 design maneuvering, 43
 indicated, 42, 43
 stalling, 43
 Split flaps, loads on, 69
 Soap film for torsion problem, 118
 Stable cross sections as columns, 154
 Stability of a truss, 124
 Stability range, 35, 59
 Stabilizer, deflection in, 101
 Stabilizer design, 366
 Stabilizer load, balancing distribution of, 64
 Stainless steel corrugations, 265
 and flat sheet, 279
 design curves for, 269, 270
 Stainless steel sections, as columns, 188-193
 Stainless steel stiffened sheets, 216, 217
 Stalling speed, 43
 Starting systems, weight of, 3
 Static tests of wing structures, 355
 Stewardess, weight of, 37
 Stiffener failure in incomplete tension-field beams, 249
 Stiffener loads in plates under pressure, 297
 Stiffeners, center of rotation when attached to sheet, 195
 oblique, in complete tension-field beams, 243
 plate, effect of bending rigidity of, 170
 effect of torsional rigidity of, 169
 web, in thin-webbed beams, 236
 Stiffener sections, general, 183
 Straight line equation for columns, 160
 Strain, definition of, 85

- Strain, normal, 85
 - shear, 85
 - unit, 85
 - Strain energy, derivative of, 137
 - general theorems of, 133
 - in beams, 149
 - in thin-walled cylinders, 122
 - minimum, 142
 - of bending, 130
 - of direct load, 129
 - of shear and torsion, 131
 - Strength, of aircraft elements, ANC-5, 77, 81
 - Strength-weight ratio of wing spars, 344
 - Stress, critical buckling, 167
 - compression, 79
 - non-uniform, equilibrium equations for, 84
 - normal, definition of, 78
 - shear, 79
 - sign convention for, 80
 - tension, 79
 - uniform, equilibrium equations for, 79
 - ultimate, definition of, 89, 90
 - Stress analysis by Mohr's circle, 83
 - Stress axes, 80
 - transfer of, 81
 - Stress directions, principal, 82
 - Stress distribution, affected by buckling, 165
 - in buckled thin plates, 204
 - in stiffened cylinders, 322-329
 - in stiffened flat sheet, 208-209
 - in thick-webbed beam, 235
 - in thin-webbed beams, 236
 - Stresses, causing buckling, 165
 - definition of, 78, 80
 - in membranes, 288, 289
 - in pressurized cabins, 307
 - in thick plates, 284, 286
 - in thin plates under normal pressure, 294, 295
 - principal, 82
 - three-dimensional, 85
 - two-dimensional, 81, 84
 - Stress-strain curves, soft iron, 89
 - steel and aluminum alloys, 91
 - Stress-strain relationships, 86, 89
 - Structures, redundant, 128
 - Surface controls, weight, 19
 - Superposition, principle of, 133
- T
- Tab, load distribution of, 66
 - warning signals, 28
 - Tabs, ailerons, 69
 - control surface, loads on, 69
 - effects on elevator loads, 65
 - rudder, 68
 - Tail, weight, 3
 - Tail force, where applied, 61
 - Tail load, 59
 - Tail load distribution, tabs aiding pilot, 66
 - Tail load factor, net, 63
 - Tail load factor moments, 61
 - Tail loads, balancing, 60
 - distribution of, 64
 - maneuvering, distribution of, 65
 - limits on, 65
 - Tail surface, tension on, 72
 - Tail surface loads, effect of horizontal ground gusts on, 69
 - Tail surface moments, 72
 - Tail surfaces, balancing load, 59
 - Tail surface shears, 72
 - Tail surface weight, breakdown, 12
 - average trends, 12
 - Tail wheel, weight, 3
 - Take-off horsepower, 44
 - Tangent modulus curve in column analysis, 158
 - Temperature effects on redundant trusses, 147
 - Tensor, stress, 79
 - Tension-field angle, 243
 - Tension-field beams, 236-240, 242
 - diagonal, 234-258
 - incomplete, 241-258
 - calculations for typical, 244
 - inclined web stiffeners in, 253
 - load distribution in, 245
 - loads in web stiffeners of, 255
 - loads on flange rivets of, 248
 - oblique stiffeners in, 243
 - rivet correction factor for, 242
 - shear carried by flanges in, 241
 - stiffener failure criteria for, 249
 - stresses in beam flanges of, 255

Tension-field beams, incomplete, tapered
 flanges in, 258
 web buckling in, 243
 Tension-field web, 165
 Tension stress, diagonal, in Wagner
 beam, 236
 Tension tests, effect of using for com-
 pression allowables, 229
 Terminal velocity, 43
 Tests of stiffened panels, analysis of, 220
 Thrust, propeller, where applied, 61
 Torque, work due to, 132
 Torsion, bars with solid cross section, 114
 boundary conditions in, 114
 in doubly connected sections, 123
 in hollow thin-walled sections, 121
 in solid elliptical cylinders, 116
 in solid rectangular cylinders, 117
 in *T*-section bars, 119
 lines of shearing stress in, 114
 of thin cylinders, 338-340
 Torsion bending constant for columns,
 195
 Torsion free bending, 349
 Torsion material in wing sections, 359
 Torsion problem, 114-123
 assumptions in, 114
 membrane analogy for, 117
 Torsion strain energy, 132
 Transfer of stress axes, 81
 Truss, definition of, 124
 joint rigidity in, 124
 Truss analysis, 124-147
 Bow's notation in, 126
 by cut sections, 126, 128
 by resolution of joint forces, 125, 126
 Castigliano's second theorem, 140
 fictitious loads in, 139
 graphical, 125, 126, 127
 intentional misfits in, 147
 Maxwell's reciprocal theorem applied
 to, 134
 multiple redundancies in, 143
 notation for, 127
 joint displacement in, 134
 principle of superposition applied to,
 133
 redundant reactions in, 139
 strain energy in, 129
 temperature effects in, 147

Trusses, external loads on, 124
 plane, 125
 secondary loads in, 124
 statically determinate, 124
 statically indeterminate, 124
 space, 125
 Truss-type spars, 344
T-section column curve, 185
T-sections, torsion in, 119
 Tubes, barrel-shaped, as columns, 161,
 163
 rectangular, as columns, 161, 163
 with thin walls as columns, 179
 square, with thin walls as columns,
 179
 Twisting moment of lift forces, 50

U

Unit deformation, normal, 85, 88
 shearing, 86, 88
 Unit strain, 85

V

Vertical tail surfaces, aspect ratio, 68
 gust loads, 67
 maneuvering loads, 67
 Vibration, damping, 24
 sources of, 24
 Vibrations, 130
 Vision, passengers', 25
 pilot's, 25
 Vierendeel truss, 238
 Vierendeel truss ribs, 364

W

Wagner beams, 236-240
 Warning signals, 28
 Warping of thin-walled column struc-
 tures, 196
 Web-buckling angle, 236
 Weight and balance, 32
 Weight and balance log, 34
 Weight breakdown, preliminary, 3
 second, 7
 Weight, buffet supplies, 38
 communicating equipment, 4, 20
 crew, 37
 de-icer, 4, 21
 design, 44
 electrical equipment, 21

- Weight, engine accessories, 3
 - engines, 3
 - fuel per gallon, 37
 - fuel system, 3, 17
 - fuel tanks, 18
 - furnishings, 4, 20
 - fuselage, 13
 - gross, design breakdown of, 3
 - instrument, 4, 18
 - landing gear, 14, 16
 - lubricating system, 3
 - minimum, 44
 - design, 58
 - nacelles, 16
 - oil, per gallon, 37
 - passengers', 37
 - passengers' baggage, 37
 - power plant, 3, 16
 - power plant controls, 3
 - propeller, 3
 - residual fuel and oil, 4
 - ribs, 9
 - starting system, 3
 - stewardess', 37
 - surface controls, 4, 19
 - tail surface, 12
 - tricycle gear, 3
 - useful load, 4, 21
 - wing, 8
 - Windshield arrangement, 25
 - Wind tunnel tests, 5
 - accuracy and validity of, 5
 - effect of power, 5
 - to determine moment coefficient, 63
 - Wing, lifting force on, 48
 - sweeping, to adjust center of gravity location, 41
 - Wing analysis, bending material, 354-359
 - effective width use in, 359
 - torsion material in, 359
 - Wing area, effective, 44
 - Wing down loads, 54
 - Wing drag, where applied, 61
 - Wing fittings, 365
 - Wing flaps, 69
 - Wing lift, where applied, 61
 - Wing load distribution, 72
 - Wing load factor, 45, 58
 - Wing loading, 61
 - design, 44
 - Wing moments, 72
 - where applied, 61
 - Wing position, effect on fuselage weight of, 41
 - Wing ribs, 361
 - types of, 363
 - Wings, design considerations, 342-366
 - design of, as affected by cutouts, 343
 - shear-carrying members, 343
 - shear analysis, 348-352
 - Wing section, torsion in, 123
 - Wing shears, 72
 - Wing spars, 343
 - Wing structures, types of, 354
 - typical, 353
 - Wing weight, 3
 - dead, non-structural, 10
 - structural, 10
 - distribution of, 8
 - effect of span on, 11
 - equations for determining, 8
 - items influencing the, 7
 - Lipp analysis of, 8
 - loads affecting, 8
 - material breakdown of, 8
 - Wing weight factor, 11
 - Work, due to bending, 130
 - due to loading, 129
 - internal and external, 130
- Y
- Yield point, correction to standard value of, 227
 - definition of, 89, 91
 - Yield point stress, as a design criterion, 77
 - in buckled structures, 165
 - Young's modulus, 87
 - correction to standard value of, 227
 - definition of, 85
 - limits on, 92
- Z
- Z-sections as columns, 174, 188
 - Z-section column curves, 184, 185

DATE OF ISSUE

This book must be returned within 3, 7, 14 days of its issue. A fine of ONE ANNA per day will be charged if the book is overdue.

--	--	--

